COMPLETED

BEST COPY AVAILABLE

NASA Conference Publication 2330

Uranus and Neptune

Jay T. Bergstralh, *Editor*
Jet Propulsion Laboratory
Pasadena, California

Proceedings of a workshop held in
Pasadena, California
February 6-8, 1984

NASA
National Aeronautics
and Space Administration

**Scientific and Technical
Information Branch**

1984

I

BLANK PAGE

PREFACE

On February 6-8, 1984, a workshop sponsored by the Voyager project was held in Pasadena. The goal of the workshop was to establish a scientific framework within which to plan the Voyager encounters with Uranus and Neptune. Specific objectives were: (a) to assess the current state of knowledge of Uranus and Neptune, their magnetospheres, and their respective systems of satellites and rings (if any), (b) to identify important scientific issues that can be addressed effectively by Voyager, and (c) to provide an opportunity for Voyager investigators to interact with other scientists knowledgeable in the field of physical studies of the Uranian and Neptunian systems. This volume contains the papers presented at the workshop. Their number, diversity, and quality attests to our maturing understanding of the physical properties of the outermost parts of the solar system.

The scientific program was organized by Jay Bergstralh with advice from Edward Stone, Charles Stembridge, and the Voyager Science Steering Group. Patricia Cates and Ellis Miner handled local arrangements and logistics. We wish to express our thanks to the individuals who chaired the sessions and to the invited speakers for the high quality of their presentations. Also, sincere thanks to Alleen Piumpunyalerd for her unfailingly cheerful helpfulness.

BLANK PAGE

TABLE OF CONTENTS

PART I

Origin and Evolution of Uranus and Neptune

The Origin and Evolution of Uranus and Neptune
John S. Lewis 3

PART II

Atmospheres of Uranus and Neptune

Atmospheres of Uranus and Neptune
Donald M. Hunten 27

Aeronomy
S. K. Atreya 55

Temperature Structures and Infrared-Derived Properties of the Atmospheres of Uranus and Neptune
Glenn S. Orton and John F. Appleby 89

Ultraviolet Observations of Uranus and Neptune Below 3000 Å
John Caldwell, Richard Wagener, Tobias Owen, Michel Combes, and Therese Encrenaz 157

Properties of the Upper Tropospheres of Uranus and Neptune Derived from Observations at "Visible" to Near-Infrared Wavelengths
Jay T. Bergstralh and Kevin H. Baines 179

Near Infrared Imaging of Uranus and Neptune
Bradford A. Smith 213

A Review of the Millimeter and Centimeter Observations of Uranus
Samuel Gulkis and Imke de Pater 225

Atmospheric Dynamics of Uranus and Neptune: Theoretical Considerations
Andrew P. Ingersoll 263

The Possibility of Detection and Measurement of Cloud Structure in the Atmosphere of Uranus
Reta F. Beebe 271

Variability of Neptune
Dale P. Cruikshank 279

PART III

Interior Structures of Uranus and Neptune

Interior Structure of Uranus
W. B. Hubbard 291

Rotational Properties of Uranus and Neptune
Michael J. S. Belton and Richard Terrile 327

Oblatenesses of Uranus and Neptune
Richard G. French 347

Physical Properties of Neptune and Triton Inferred from the Orbit of Triton
A. W. Harris 357

PART IV

Satellite Systems

Origin and Evolution of the Uranian and Neptunian Satellites: Some Dynamical Considerations
Stanley F. Dermott 377

Composition, Structure and Evolution of Uranian and Neptunian Satellites
David J. Stevenson 405

Physical Properties of the Satellites of Neptune
Dale P. Cruikshank 425

Physical Properties of the Uranian Satellites
Robert Hamilton Brown 437

Satellite Masses in the Uranus and Neptune Systems
Richard Greenberg 463

Seasonal Variations in Triton's Atmospheric Mass and Composition
L. M. Trafton 481

PART V

Magnetospheres and Solar Wind

Magnetospheric Structures: Uranus and Neptune
T. W. Hill 497

PART V (Continued)

The Solar Wind at 20-30 AU
Aaron Barnes and Paul R. Gazis 527

Magnetosphere, Rings, and Moons of Uranus
Andrew F. Cheng 541

Do the Satellites of Uranus Control Its Magnetosphere?
A. F. Cheng and T. W. Hill 557

Lyman-Alpha Aurora
Samuel T. Durrance and John T. Clarke 559

PART VI

Ring Systems

The Structure of the Uranian Rings and the Search for Rings Around Neptune
James L. Elliot 575

Infrared Images of the Uranian Rings
Philip D. Nicholson 589

Dynamics of the Uranian Rings
Stanley F. Dermott 609

PART I

Origin And Evolution Of Uranus And Neptune

BLANK PAGE

2.

The Origin and Evolution
# of Uranus and Neptune

John S. Lewis

Department of Planetary Sciences
University of Arizona
Tucson, Arizona 85721

Abstract

The present state of our understanding of the origin and evolution of the planets Uranus and Neptune is briefly reviewed. Emphasis is placed on the need for improved physical and compositional data on both planets, particularly those data needed to resolve certain major inconsistencies in the present data set.

INTRODUCTION

Two wholly different classes of observational data have major influence on our ideas about the bulk composition, mode of origin, and evolutionary history of Uranus and Neptune. The first of these, measurement of the infrared and microwave brightness, can be conveniently subdivided into near infrared molecular spectroscopy, thermal infrared radiometry, and microwave radiometry. The second is the determination of the structure of the gravitational field of each planet by tracking the motions of natural satellites or spacecraft. The latter data can then be combined with information on the mass, rotational period, and figure of the planet to provide a description of the radial distribution of mass within the planets' interiors.

Both of these roads of attack fall prey to severe interpretive problems. A detailed and realistic optical model of the atmosphere is required before the spectroscopic data can be interpreted usefully. The harmonics of the gravitational field and the rotation period must be reliably established before the internal density structure can be deduced. These observational necessities are among the list of features of Uranus and Neptune that are either highly moot, or have undergone major recent revision.

It may seem that we could derive great benefit from the comparative study of Uranus and Neptune in the context of the Saturn and Jupiter systems. Indeed, if our cosmogonic ideas about Jupiter and Saturn had fully converged, we would hasten to apply these same theories to Uranus and Neptune. But in truth there is still active debate concerning the formation of these two better- studied systems.

Cosmogonic theories for the giant planets have historically been polarized by two extreme schools of thought, and recent advances in understanding can be thought of as resulting from the attempt to fill in the "mixing line" between these two "endmembers". The cosmogonic theories of Safronov (1972) have emphasized the slow accumulation of "solid" planetary cores from a planetesimal swarm of small bodies in heliocentric orbit, which were left behind by the dissipation of the solar nebula. These small bodies were assumed to have adopted a velocity distribution determined by gravitational "stirring" by the largest bodies embedded in this planetesimal swarm. More precisely, it was assumed that the mean encounter velocities were given approximately by the escape velocities of the largest bodies present. After all, it is these bodies that are most effective in stirring the swarm. Subject to these assumptions, and modeling accretion in a statistical way rather than by means of numerical simulations, Safronov concluded that the accretion time scales for the giant planets increased enormously with heliocentric distance: where the spatial density of solids was lowest, and the synodic periods longest, accretion of planets (Uranus and Neptune) should have taken an incredibly long time; perhaps even much longer than the age of the solar system. This followed directly from the presumed velocity distribution, since bodies were commonly encountering one another at such high speeds that their gravitational cross-sections were little larger than their geometrical cross-sections. Of course, accretion of solid planetary cores in a gas-free medium also has the difficulty that planetary compositions rich in hydrogen and helium cannot be explained in any simple manner.

A logical response to this dilemma was to suppose that the major planets formed in such a way that the presence of gas was mandatory, rather than forbidden. The purest example of such ideas was the suggestion that gasdynamic instabilities in the solar nebula itself were responsible for forming the giant planets (see, for example, Cameron, 1978; Bodenheimer, 1976). However, it has become generally accepted that gravitational instability of the nebular gas in the presence of solid planetary nuclei is a more plausible method of triggering hydrodynamic collapse (Perri and Cameron, 1974; Mizuno, 1980; Stevenson, 1982). Thus the onus for the successful accretion of the major planets once again rests upon the existence of some mechanism for rapid accretion of solids. The problem is particularly severe, however, since these models generally require that solid cores with masses tens of times that of the Earth were accumulated at great distances from the Sun while the nebula was still present. It is not clear that this is easy to accomplish.

URANUS: RECENT PROGRESS

We shall here briefly summarize the present state of the observational evidence regarding the atmospheric composition (as determined by both infrared spectroscopy and thermal modeling), the rotational period of the planet, the value of the J2 and J4 coefficients in the spherical harmonic expansion of the gravitational field, and the atmospheric density profiles deduced from internal models constrained by the newest value of J2, the oblateness of the disk, and the two current determinations of the rotational period of Uranus. No detailed critical analysis will be attempted in this general review. The reader is referred to the accompanying papers by Hunten, Hubbard, Belton and Terrile, and French for detailed critical reviews of these areas.

The infrared spectroscopic observations deal principally with the abundace of methane, usually reported in terms of the C:H ratio. One recent review (Trafton, 1981) cites only determinations in which the C:H ratio lies within a factor of six of the solar C:H ratio. However, other spectroscopic studies in which the vertical distribution of methane and of aerosols are treated in a more satisfactory (but not necessarily correct!) manner yield a methane mixing ratio as high as 0.045+/-0.025, corresponding to a C:H ratio near 0.02 (see, for example, Baines, 1983).

A partially independent estimate of the tropospheric methane abundance has been derived from radiative/convective thermal models of the atmosphere, constrained by spectroscopic and radiometric data in the visible, near and thermal infrared, and microwave regions. In this approach a methane mixing ratio in the range 0.01 to 0.1 is needed to fit the observations (Wallace, 1980).

Another important compositional parameter, which is a potential indicator of large additions of hydrogen-bearing ices to the planet, is the D:H ratio. Although the measurement is difficult, both Macy and Smith (1978) and Trafton and Ramsay (1980) report D:H ratios that are only slightly larger than the cosmic D:H ratio. If very large proportions of ice-rich solids were present, and if these solids were isotopically equilibrated with hydrogen at very low temperatures characteristic of the outer solar nebula, we would expect the D:H ratio to be much larger, and hence easily measured. This problem can be avoided if isotopic equilibration between ices and hydrogen took place at higher temperatures in the nebula, or if radial mixing of

Uranus' interior is severely inhibited (Hubbard and MacFarlane, 1980b).

The rotation period of the planet is the subject of an active debate. Nearly a dozen different determinations have been published in the last seven years. Four of these favor rotation periods near 24 hours, while five are closely clustered around 16 hours. The estimated errors on both sets of determinations are typically 0.3 to 4 hours, leaving the two sets of results fully separated by a rotation period interval of several hours.

The discovery of the rings of Uranus has made available to us a much more sensitive probe of the gravitational field of the planet. Recent determinations of J2 cluster closely around 0.00335, with J4 close to 3x10(-5) (Elliot, et al., 1981; Nicholson, et al., 1982). These fully supercede earlier, less precise estimates based on the orbital motions of the Uranian satellites. Estimates of the rotation period based on the new value of J2 and on the oblateness of the disk lie close to 16 hours (Franklin, et al., 1980; Elliot, et al., 1981).

The bulk composition of Uranus, as deduced from internal models that are constrained to fit the newer value of J2, includes 24% rocky core material, 65% icy mantle, and 11% hydrogen- and helium-rich atmosphere by mass (Hubbard and MacFarlane, 1980a). For comparison, the corresponding mass percentages for Neptune were estimated by the same authors as 25% rock, 68% ice, and 6%

gases. Two-layer models (Zharkov and Trubitsyn, 1978), in which the ice and rock components are merged homogeneously, would yield a J2 of about 0.0045 for acceptable values of the oblateness, near 0.023 (Franklin, et al., 1980; Elliot, et al, 1981). The three- layer model described above would, for the same oblateness, give a J2 near 0.0027. These models have rather similar overall composition. The most recent revision of the three-layer model (MacFarlane and Hubbard, 1982), which takes into account the latest observational constraints, gives reasons to favor the 16 hour rotation period. They further find that the Zharkov and Trubitsyn two-layer model, if updated to take into account recent improvements in the equation of state of water ice, gives a good fit to both J2 and the optical oblateness simultaneously. The 1982 revision of the Hubbard and MacFarlane three-layer model differs from their earlier model in that the rotational moment of inertia of the planet has been increased by placing sufficient methane in the atmosphere to account for 40 to 50% of the total atmospheric mass. They favor this model over that of Zharkov and Trubitsyn because the latter assumes that a homogeneous mixture of ices and rock is stable. If, more reasonably, the rock and ice are allowed to separate according to density (i. e., the solubility of rock in supercritical water is not too high), then the value of J2 will fall so low that methane must be brought from the mantle into the atmosphere to restore agreement with observation. A rotation period of 16 hours, combined with a mantle composition with a solar rock:ice ratio of about 2.4 (methane uncondensed, so that the ice is nearly pure water), gives a very good fit to the observational constraints (Podolak and Reynolds, 1981; MacFarlane and Hubbard, 1982).

Two-layer models also have the drawback that, assuming a rotation period of 16 hours, the predicted value of J4 will be too large to reconcile with the observed value (Podolak and Reynolds, 1983). Note that we have here arrived at an interesting dilemma. If the icy component of Uranus is sufficiently well isolated from the atmosphere so that the deuterium abundance in the atmosphere is not increased far above the cosmic D:H ratio, then how can there be sufficiently good communication between the ice layer and the atmosphere so that methane could partition so readily into the atmosphere? What are the ramifications of mantle-atmosphere interaction for the atmospheric ammonia and water vapor content?

This is an appropriate place to remind ourselves of the marked deficiency of ammonia above the ~200K level in the troposphere of Uranus (Gulkis, et al., 1978). This may be attributed to chemical reactions precipitating ammonia quantitatively from a tropospheric upwelling gas in which the hydrogen sulfide abundance equals or surpasses the ammonia abundance: the solid salt ammonium hydrosulfide should precipitate at temperatures a little above 200K. Since the solar S:N ratio is only about 0.2, a substantial enrichment of sulfur is required. However, there is no evidence for any significant excess of hydrogen sulfide over ammonia. In fact, the upper limit on the hydrogen sulfide content of the atmosphere of Uranus above the cloud tops is less than the solar S:H ratio (Fink and Larson, 1979). Thus any addition of large amounts of sulfur for the purpose of precipitating ammonia would have to be carried out with the precision of a laboratory titration. If ammonia is enriched by a factor of 20 relative to hydrogen, then exact removal of this ammonia by reaction with hydrogen sulfide would require that the latter gas be enriched by a factor of 100 with a precision of 1%!

PLANETARY RAW MATERIALS

Three principal chemical scenarios for the condensation of preplanetary solids have been explored for the temperature regime of interest in the outer solar system (<200K). The first of these is the case of direct chemical equilibrium between a solar composition nebula and the condensate (Lewis, 1972). In this case, the dominant carbon compound at low temperatures (<600K) is methane, and the dominant nitrogen-bearing species below ~330K is ammonia. Condensation during cooling follows the sequence:

1. water ice (to exhaustion of water vapor) 2. ammonia monohydrate (to exhaustion of ammonia vapor)
3. methane clathrate hydrate (to exhaustion of water ice)
4. solid methane (to exhaustion of gaseous methane).

Other compounds of the major volatile elements (HCNOS) are unimportant in this temperature range: molecular nitrogen, carbon monoxide, and carbon dioxide are very rare at equilibrium at low temperatures, while sulfur is fully sequestered as the mineral troilite (FeS), which saturates at 690K, and is thus absent from the gas phase at temperatures appropriate for ice condensation. Note that this reaction sequence requires that solids, once formed, remain in intimate chemical interaction with the gas. This we call the equilibrium condensation process.

A second type of condensation behavior occurs when condensed solids, once formed, are quickly isolated from the cooling gas. In this case, products that can only be made by reactions between nebular gas and condensates already present are forbidden. The most likely circumstances to produce this kind of behavior are those in which accretion of solids occurs on a much shorter time scale than does the cooling of the nebula. The large accreted bodies of recent condensate have negligible surface:volume ratios, and are effectively inert to reactions with the remaining gas. Similar behavior also occurs in any approximately adiabatic atmosphere of solar composition, in which sedimentation of cloud particles prevents condensed solids from experiencing conditions much colder than those at their point of condensation. An example illustrative of the difference between this and simple equilibrium condensation would be the behavior of sulfur. With rapid accretion, an early condensate of iron-nickel metal would be accreted, buried, and fully isolated from the gas long before temperatures fall low enough for FeS to become stable. As a result, sulfur remains in the gas phase (as hydrogen sulfide) down to very low temperatures, where it will react with ammonia. This class of behavior can be variously described as rapid accretion, heterogeneous accumulation, or disequilibrium condensation (Barshay and Lewis, 1976).

The third major variant of low-temperature condensation behavior arises from consideration of the kinetics of gas-phase reactions within the solar nebula or within a protoplanetary nebula. In typical models of the solar nebula, ammonia is the most stable nitrogen-bearing gas below about 330K, while molecular nitrogen is more abundant at higher temperatures. For an adiabatic nebular structure, this is equivalent to saying that the inner nebula, from the Sun out to the asteroid belt, would contain ample molecular nitrogen, while the nebula from the heart of the Belt outward would be rich in ammonia at chemical equilibrium. However, the nebula was surely turbulent. Imagine a parcel of gas moving from the 400K region outward to where the nebular temperature was 300K. The time taken to move through this temperature interval may be 1000 years, but the time needed for gas-phase reactions to convert the molecular nitrogen in that gas parcel into ammonia may be 100 million years. Clearly the conversion of nitrogen to ammonia will be so sluggish that chemical equilibrium cannot be closely attained, and high-temperature gas compositions will be found in the outer, cooler regions as well. The situation regarding methane formation is closely similar to that of ammonia. In both cases, reasonable estimates of the rate of homogeneous and heterogeneously catalysed reactions capable of reducing carbon monoxide and nitrogen to methane and ammonia suggest that chemical reaction time scales will be longer than nebular mixing time scales at all temperatures below about 1000K. It therefore seems likely that nitrogen and CO are everywhere abundant in the nebula, while the low-temperature gases ammonia, methane and carbon dioxide are of minor importance, probably accounting for only a few percent of the total inventories of N and C. In planetary subnebulae, with their much higher densities at each temperature, the formation of these gases is much easier (Lewis and Prinn, 1980; Prinn and Fegley, 1981). We refer to the nebular case as the kinetic inhibition scenario.

The condensation behavior for these three models is compared in Figure 1 (from Lewis and Prinn, 1984). It is clear from this Figure that the very identity of the major condensates can be substantially altered by nebular processes such as radial turbulent mixing and accretion. Water is the only ubiquitous ice component.

PLANETARY ACCRETION

Two very recent, and as yet unpublished, contributions appear to be of great importance for understanding the formation of Uranus and Neptune. The first of these concerns the discovery by Greenberg, et al. (1983) that Safronov's (1972) treatment of accretion in the outer solar system is in error in its assumption of very high relative velocities of planetesimals: the eccentricities and inclinations of the orbits of the smaller planetesimals simply do not build up fast enough to stay close to the escape velocities of the largest planetesimals. This means that Safronov has markedly underestimated the gravitational cross- sections of the larger bodies, and correspondingly overestimated the accretion times of planet-sized bodies. With this correction, accretion times for solid planetary cores near the present orbits of Uranus and Neptune become comparable to accretion times in the inner solar system.

However, the formation of a planet with a large amount of captured nebular hydrogen and helium in its envelope requires not only rapid accretion of solids (before the dissipation of the nebula) but also, according to the published models of Perri and Cameron (1974), Mizuno (1980), and Stevenson (1982), these solid bodies need to have masses of 10 to 40 Earths. However, even very small ("lunar-sized") bodies are capable of retaining significant masses of captured gas if the environmental conditions are favorable. These conditions are optimized if the nebular background temperature is low and if the gas capture onto the solid body is strongly subadiabatic. If, as is reasonable, the temporary atmosphere about a Ganymede-sized ice ball embedded in the nebula is rapidly swept clear of dust opacity by sedimentation and accretion, and molecular sources of thermal infrared opacity (water vapor, ammonia, etc.) are largely condensed, then the dominant form of opacity may be collision-induced absorption by molecular hydrogen (Lewis and Prinn, 1984; Stevenson, 1984). Gas capture then occurs grossly isothermally until pressures near the surface approach one bar.

Simple compressional heating of the near-surface atmosphere by further gas capture leads to melting and boiling of surface material (Lewis and Prinn, 1984; Stevenson, 1984). The power of this description lies in the realization by Stevenson that the process of vaporizing surface water causes the atmosphere to behave as if it had an extremely large heat capacity. By analogy with instabilities that arise in the interiors of self-gravitating hydrogen Gazkugeln when central conditions are favorable for the thermal dissociation or ionization of hydrogen, the latent heat of the reaction tends to thermostat the deep interior. Adding mass, and hence deepening the gravitational potential well, is not effectively balanced by a rise in the thermal pressure in the core, and, if the ratio of specific heats falls below 4/3, runaway collapse can result. Note that the "heat capacity" of the gas, defined operationally in a suitable way, includes the latent heat of any chemical reactions or phase changes that occur.

It is clear that this model, in order to be effective, must allow as much water as possible to evaporate into the atmosphere. Since the hydrogen-upon-ice initial structure has stable density stratification, and since the evaporation of ice depends on the downward transport of heat, one might fairly be skeptical of the importance of this mechanism. However, it is my suspicion that non-spherically symmetric gas capture, accretion of gas with some mismatch of the angular momentum vectors, and accretion of solid bodies in almost any form will easily provide the mixing and oistening of the atmosphere required for this model to work.

The contributions of Stevenson and of Greenberg, et al. may point the way to a credible scenario for the formation of Uranus and Neptune.

MIXING MODELS FOR URANUS AND NEPTUNE

It is easy, and probably justified at our present level of ignorance, to regard Uranus and Neptune as having been made of two components, one condensed, and the other gaseous. The principal problem in designing a satisfactory two-component model lies in identifying the composition of the condensed component. Above, in our summary of the chemistry of planetary raw materials, we presented three important composition types, each corresponding to a particular physical environment. It should be clear that, in a dense circumplanetary nebula in the intermediate to late stages of assembly of a planet, thorough equilibration of gases and infalling solids should occur. Recently, Podolak and Reynolds (1983) have criticised Lewis and Prinn (1980) for using the kinetic inhibition model to generate preplanetary solids that went into making Uranus and Neptune. They also present certain kinetic arguments that suggest that methane (not ammonia) formation should have been rapid in the proto-Uranian nebula. They appear to have overlooked the extension of the theory of Lewis and Prinn to protoplanetary nebulae by Fegley and Prinn (1981), which reached its conclusions by means of much more plausible kinetic arguments.

Podolak and Reynolds (1983) point out that, in a protoplanetary setting for the origin of Uranus or Neptune, nitrogen may exist as essentially uncondensable molecular nitrogen gas in the cold gaseous envelope of the protoplanet. Thus it may be lost by turbulent exchange of gas with the surrounding solar nebula. (The detailed kinetic study of the Jovian subnebula by Prinn and Fegley (1981), however, suggests that even in this relatively warm nebula the ammonia abundance will still remain comparable to the abundance of molecular nitrogen. Conditions in the Uranian or Neptunian subnebula should be much more favorable to ammonia.) A similar phenomenon allows deuterium to be depleted as well: thermal isotopic reequilibration of primordial ices with dense, hot hydrogen in the protoplanet removes the large D enrichment that should have been associated with the low-temperature ice condensates. The D partitions back into HD at high temperatures, and this gas may, like nitrogen, be lost by gas exchange with the nebula.

Stevenson (1982) addressed the problem of the severe depletion of ammonia in the upper atmosphere not by discarding nitrogen into the solar nebula, but rather by sequestering the highly soluble ammonia molecule in a dense "ocean". The vapor composition in equilibrium with such an ocean depends sensitively upon the surface temperature and total atmospheric pressure. Available laboratory results at normal pressures cover most of the compositional range of interest (approximately solar proportions of ammonia, water, and hydrogen sulfide), and reveal several general features that bear on the Uranus ammonia problem (Leyko, 1964). First, for solar-composition solutions of ammonia and hydrogen sulfide in water, the dominant component of the gas at any temperature in the range below 500K is likely to be ammonia. For all ocean surface temperatures below 450K the ammonia:hydrogen sulfide ratio in the gas is greater than the solar N:S abundance ratio. Absolute pressures of ammonia, hydrogen sulfide, and water vapor at 400K above a solar-proportion solution would be 3325, 452, and 1604 mm Hg respectively. For a 300K surface temperature the respective partial pressures are 100, 5.07, and 21.6 mm Hg. These ammonia pressures would provide a solar N:H ratio under hydrogen total pressures of 200kb (400K surface) or 6kb (300K surface). Of course, such total pressures are so high that the low-pressure laboratory data are no longer applicable; nor could plausible Uranus atmospheric models provide such high pressures at those temperature levels in an even approximately adiabatic atmosphere. Thus any "shallow" oceanic surface on Uranus would almost certainly be in equilibrium with a gas phase that contains a large excess of ammonia over hydrogen sulfide (and water!), and of both gases over solar abundances relative to hydrogen. The most general conclusion seems to be that the weak acid hydrogen sulfide is so soluble in basic ammoniacal solutions that such oceans would generally tend to increase the atmospheric N:S ratio. Removal of ammonia from the visible upper troposphere would require either a very cold ocean, possibly near the ternary eutectic temperature of the water-ammonia-hydrogen sulfide system, which would have a negligible vapor pressure of all these species, or a very hot surface, probably over 500K, under very great hydrogen pressure, where there is a possibility that the vapor would contain an S:N ratio larger than in solar material, but still less than unity.

The deuterium problem and the ammonia problem could be solved if there is not (and never has been) intimate chemical exchange between the icy component and the atmosphere. This seems to be an unlikely state of affairs, but we cannot be certain. It is also quite possible that the enrichment of D in low-temperature condensates estimated from equilibrium theory is a substantial overestimate. A careful reanalysis of this problem may help ease some of the constraints on the vertical mixing history of Uranus and Neptune.

CONCLUSIONS

The central cosmogonic problems of Uranus and Neptune remain unsolved, although substantial observational and theoretical progress have been made in recent years. Very accurate measurements of J2 and J4 by spacecraft flybys or orbiters may not provide much new insight into the internal structure and evolution. Accurate measurements of the global heat flow would be of interest, and further work on the D:H ratio on both Uranus and Neptune is very desirable. Accurate determination of the rotation period is clearly needed. We remain, however, in the same situation we were in ten years ago: the most crucial questions that we need to answer can best be addressed by suitably instrumented deep-entry probes.

REFERENCES

Baines, K. H. (1983) Icarus 56, 543-559.

Barshay, S. S. and J. S. Lewis (1976) Ann. Rev. Astron. Astrophys. 14, 81-96.

Bodenheimer, P. (1976) Icarus 29, 165-171.

Cameron, A. G. W. (1978) Moon and Planets 18, 5-40.

Elliot, J. L., et al. (1981) Astron. J. 86, 444-455.

Franklin, F. A., et al. (1980) Astrophys. J. 236, 1031-1034.

Greenberg, R. J., et al. (1983) Preprint.

Gulkis, S., et al. (1978) Icarus 34, 10-19.

Hubbard, W. B., and J. J. MacFarlane (1980a) Icarus 44, 676-681.

Hubbard, W. B., and J. J. MacFarlane (1980b) J. Geophys. Res. 85, 225-234.

Lewis, J. S. (1972) Icarus 16, 241-252.

Lewis, J. S., and R. G. Prinn (1980) Astrophys. J. 238, 357-364.

Lewis, J. S., and R. G. Prinn (1984) Planets and their Atmospheres: Origin and Evolution. Academic Press, N. Y., 25-34.

Leyko, J. (1964) Bull. Acad. Polon. Sci., Ser. Sci. Chim. 12, 275-276.

MacFarlane, J. J., and W. B. Hubbard (1982) in: Uranus and the Outer Planets, G. Hunt, ed., Cambridge U. Press, 111-124.

Macy, W., Jr., and W. H. Smith (1978) Astrophys. J. 222, L73-L75.

Mizuno, H. (1980) Progr. Theor. Phys. 64, 544-557.

Nicholson, P. D., et al. (1982) Astron. J. 87, 433-447.

Perri, F., and A. G. W. Cameron (1974) Icarus 22, 416-425.

Podolak, M., and R. T. Reynolds (1981) Icarus 46, 40-50.

Podolak, M., and R. T. Reynolds (1983) Preprint.

Prinn, R. G., and M. B. Fegley, Jr. (1981) Astrophys. J. 249, 308-317.

Safronov, V. S. (1972) Evolution of the Protoplanetary Cloud and Formation of the Earth and Planets. Israel Program for Scientific Translation, Jerusalem.

Stevenson, D. J. (1982) Planet Space Sci. 30, 755-775.

Stevenson, D. J. (1984) Preprint.

Trafton, L. M. (1981) Rev. Geophys. Space Phys. 19, 43-89.

Trafton, L. M., and D. A. Ramsay (1980) Icarus 41, 423-429.

Wallace, L. (1980) Icarus 43, 231-259.

Zharkov, V. N., and Trubitsyn, V. P. (1978) Physics of Planetary Interiors (W. B. Hubbard, transl.) Pachart, Tucson, AZ.

Figure 1

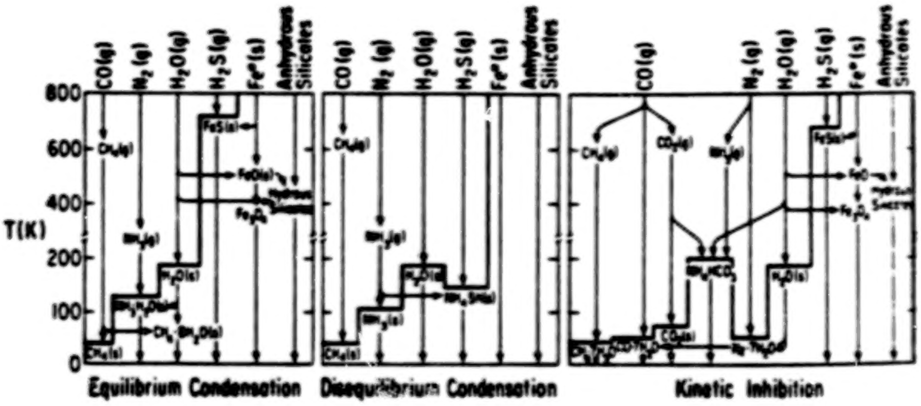
CO(g)
N_2 (g)
H_2O(g)
H_2S(g)
Fe°(s)
Anhydrous Silicates
800
600
400
T(K)
200
100
0
CH_4(g)
FeS(s)
FeO(s)
Hydrous Silicates
Fe_3O_4
NH_3(g)
H_2O(s)
$NH_3 \cdot H_2O$(s)
$CH_4 \cdot 6H_2O$(s)
CH_4(s)
NH_4SH(s)
NH_3(s)
CO_2(g)
NH_4HCO_3
CO_2(s)
Equilibrium Condensation
Disequilibrium Condensation
Kinetic Inhibition

Fig. 1. Low-temperature condensation flowcharts for compounds of H, C, N, O and S. The equilibrium and disequilibrium (rapid accretion) sequences are from Lewis (1972) and from Barshay and Lewis (1976); the sequence for kinetically inhibited formation of ammonia and methane is adapted from Lewis and Prinn (1980). The heavy line separates gases (above) from condensates (below). The relative masses of condensates cannot be read from these diagrams. After Lewis and Prinn (1984).

PART II

Atmospheres Of Uranus And Neptune

BLANK PAGE

ATMOSPHERES OF URANUS AND NEPTUNE

Donald M. Hunten
Lunar and Planetary Laboratory
The University of Arizona
Tucson, Arizona 85721

Abstract

Current knowledge of the atmospheric compositions and structures are surveyed. Although the two planets are similar in some ways, they are strikingly different in a number of others. The similarities include mass, size, and effective temperature. There are differences in heat flow, stratospheric thermal structure and composition, and spectral appearance. Presumably these are traceable to some combination of Uranus' unusual obliquity and smaller distance from the sun, but most of the details are obscure.

INTRODUCTION

This overview is intended to set a context for the more specialized papers on the atmospheres to follow. Details may also be found in the excellent review by Trafton (1981) and, for Uranus, in the bicentennial volume edited by Hunt (1982). This review focuses on work that has appeared since Trafton's. An earlier Uranus workshop volume edited by Hunten (1974) can safely be left in the archives; all the worthwhile material in it has been revised and published in journals. A group of papers by members of the MJU-SAC (Mariner-Jupiter-Uranus Science Advisory Committee) was published in Icarus, v. 24 (1975). Although we all wish that MJU were on its way with the improved (or Modified) IRIS, we can at least celebrate the health of Voyager 2 and wish continued health and prosperity to spacecraft and experimenters. This is a good time to remember Bob Danielson, who was many years ahead of most of us in thinking about these remote planets and was always an inspiration.

Although thermal structure and composition must be considered together in the real world, especially the remote-sensing part of it, they are treated separately here. The remaining sections discuss clouds and some miscellaneous topics, ionospheres, aurora, and rotational periods.

THERMAL STRUCTURE

Temperature profiles are determined mainly by heat balance under the influence of solar and internal heat, and the transfer processes of thermal radiation and convection. The internal heat fluxes are one thing in which Uranus and Neptune are very different, as illustrated in Table 1. The value for Uranus is known to be less than a quarter of that for Neptune. Hubbard's estimate refers to the remaining primordial heat, while that of Danielson is for

Table 1. Estimates of internal heat fluxes (mW m^{-2} or erg cm^{-2} s^{-2})

Uranus	Neptune
<250 observed	1000
100 (Hubbard 1978)	
>10 Danielson (1977)	

radioactive heating in a reasonable quantity of Earth-like material in a core.

Wallace (1980) has considered a range of internal fluxes in Uranus models, and they should apply reasonably well to Neptune. A flux of 100 mW m^{-2} seems to be just enough to maintain an adiabatic temperature gradient at all depths below the usual radiative-convective boundary at 700 mb or so. With smaller fluxes there may be another radiative region between 5 and 20 bars, unless solar radiation penetrates considerably deeper than expected. The effect on the temperature profile is not very obvious, because the radiative lapse rate is only slightly less than the convective. Some of Wallace's profiles are shown in Fig. 1, bottom panel. The breaks in some of these profiles are due to a totally different effect, condensation of methane and the corresponding influence of latent heat on the lapse rate. The curves showing the biggest effect are for a methane mole fraction of 10%, considerably larger than is likely. A possible analogous effect of water vapor is discussed below.

Another problem in modelling concerns the ortho-para (o-p) ratio for H_2, whose behavior affects the specific heat and therefore the dry adiabatic lapse rate (Massie and Hunten, 1982). Wallace adopted the "intermediate" prescription of Trafton (1967), in which the o-p ratio is taken as being in equilibrium with the local temperature, but is not allowed to change during convective motions. Although this procedure seems to give reasonable results for the Jovian planets, it has no theoretical justification. It is the best we can do for the present, but is unlikely to be correct.

Wallace's models are constrained by the visible and near-IR spectrum and albedo.

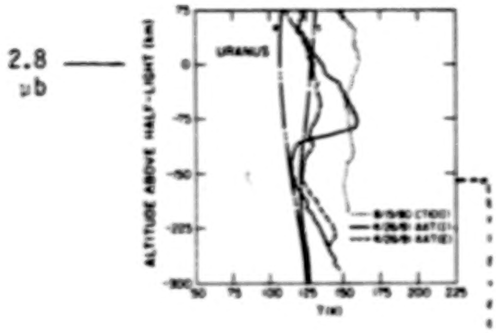

FIG. 7. Temperature profiles of the Uranian stratosphere obtained by numerical inversion of the lightcurves in Figs. 2, 4, and 5. The profiles are aligned in altitude at the point corresponding to the half-light time obtained from an isothermal fit to the data. This corresponds roughly to a number density of 1.2×10^{14} cm^{-3} and a pressure of 2.8 μb. Because of the uncertainties in the initial condition and the choice of baselines used for the inversion, the overall placement of the temperature profiles is uncertain by about 15°K. Also shown are Appleby's (1980) model profiles c and e, corresponding to extreme cases regarding relaxation rates and their temperature dependences. The upper stratosphere is considerably warmer than the warmest of Appleby's extreme models.

(French et al., 1983)

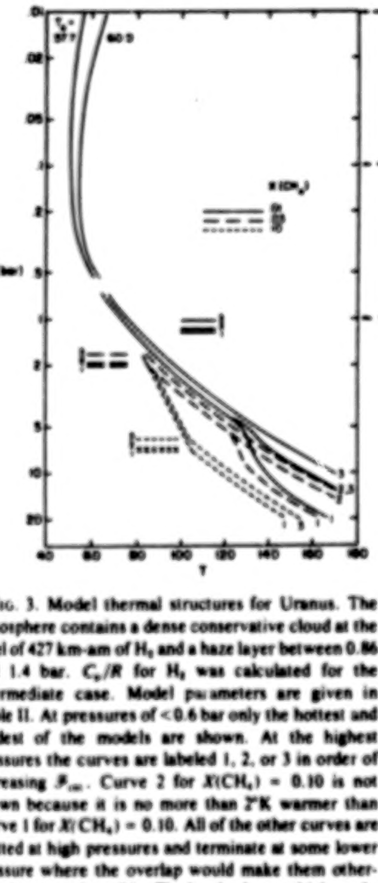

FIG. 3. Model thermal structures for Uranus. The atmosphere contains a dense conservative cloud at the level of 427 km-am of H_2 and a haze layer between 0.86 and 1.4 bar. C_p/R for H_2 was calculated for the intermediate case. Model parameters are given in Table II. At pressures of <0.6 bar only the hottest and coldest of the models are shown. At the highest pressures the curves are labeled 1, 2, or 3 in order of increasing $\mathcal{P}_{(m)}$. Curve 2 for $X(CH_4) = 0.10$ is not shown because it is no more than 2°K warmer than Curve 1 for $X(CH_4) = 0.10$. All of the other curves are plotted at high pressures and terminate at some lower pressure where the overlap would make them otherwise incomprehensible. The levels above which methane condenses are indicated by horizontal bars in the same coding as the thermal structure curves.

(Wallace, 1980)

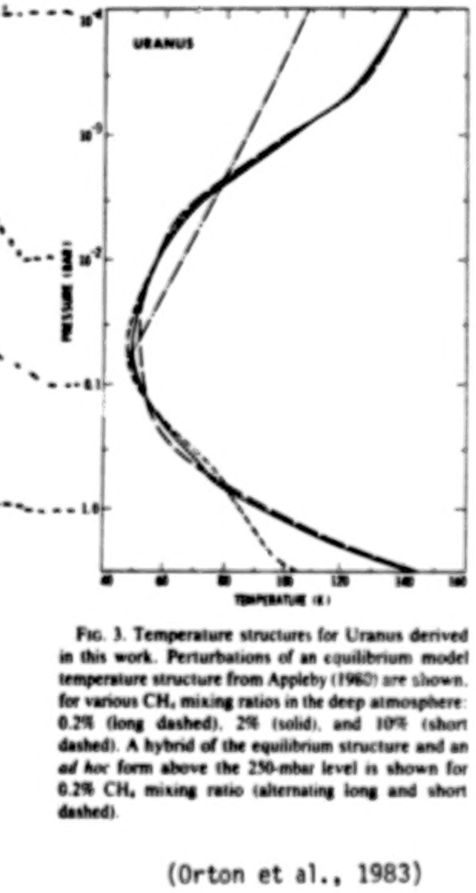

FIG. 3. Temperature structures for Uranus derived in this work. Perturbations of an equilibrium model temperature structure from Appleby (1980) are shown, for various CH_4 mixing ratios in the deep atmosphere: 0.2% (long dashed), 2% (solid), and 10% (short dashed). A hybrid of the equilibrium structure and an *ad hoc* form above the 250-mbar level is shown for 0.2% CH_4 mixing ratio (alternating long and short dashed).

(Orton et al., 1983)

Fig. 1. Temperature profiles for Uranus.

The center panel of Fig. 1, and the lower one of Fig. 2 for Neptune, are obtained by inversion of thermal IR data, shown in Figs. 3 and 4. A number of important measurements with the NASA-Hawaii IRTF have been reported by OTC (Orton et al., 1983), the source of all these figures, and by TOC (Tokunaga et al., 1983). The principal point of TOC is to establish the existence of a substantial temperature inversion in Uranus's lower stratosphere, so that the profile is not very different from that of Neptune. This was done by a careful comparison of measurements of 17.8 and 19.6 μm; the points can be seen in Figs. 3 and 4. Though the differences are small, especially for Uranus, they appear to be significant. The issue arises because of the absence of ethane emission at 12 μm, highly visible in Neptune's spectrum (see again Figs. 3 and 4). Previously it had been widely assumed that the difference was in the temperature profiles (Gautier and Courtin, 1979). OTC argue that it must be in the hydrocarbon abundances; they find that ethane must be 1% as abundant in Uranus's stratosphere as in Neptune's (3×10^{-8} vs. 3×10^{-6}). There is a corresponding difference for methane, undoubtedly the source of the ethane: on Uranus the cold trap at the tropopause seems to be effective, while on Neptune it is not. In fact, the suggested mixing ratio of 1-4 % requires that there be essentially no cold-trapping at all. The simplest way to achieve this effect is to have enough strong updrafts to carry the precipitated methane crystals right through the temperature minimum to a warmer altitude where they can re-evaporate. trapping on Uranus is also discussed by Atreya and Ponthieu (1983), who find major depletions similar to those inferred from observations.

The highest altitudes in Figs. 1 and 2 are represented by data from stellar occultations (French et al., 1983; Sicardy et al., 1982). Generally speaking, SICARDY ET AL. (1982)

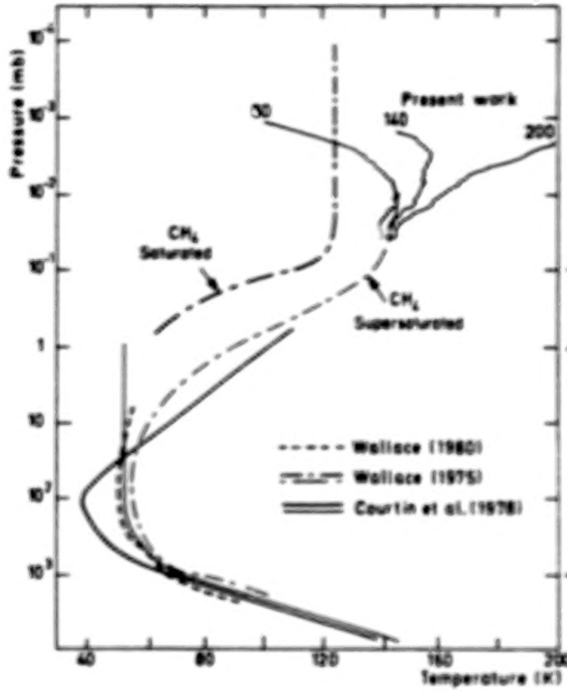

FIG. 10. Comparison of temperature profiles. Here we show the profiles derived from Wallace's (1975) models, the Courtin *et al.* (1978) retrieved profiles from infrared measurements, and the results of the present work (with three different boundary conditions, see Fig. 7).

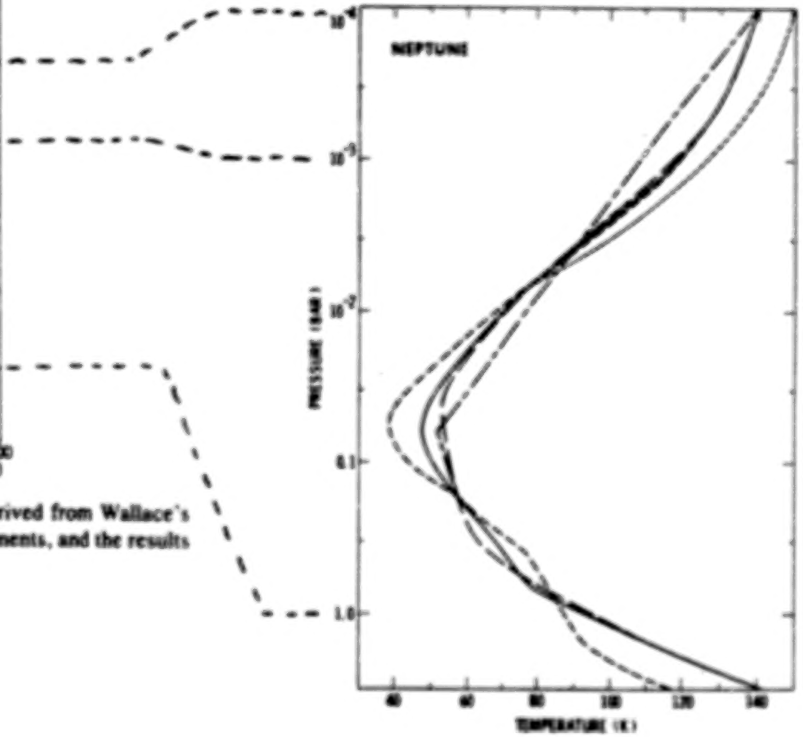

FIG. 7. Temperature structure for Neptune derived in this work. Perturbations of an equilibrium model temperature structure from Appleby (1980) are shown for various mixing ratios of CH_4 assumed in the deep atmosphere in the same way as Fig. 3. A hybrid of the equilibrium structure and an ad hoc form above the 200-mbar level is also shown for a 0.2% CH_4 mixing ratio, also denoted as in Fig. 3. A warm upper stratosphere alternative to the perturbed equilibrium model is shown by the short dashed line for pressures less than 10 mbar.

(Orton et al., 1983)

Fig. 2. Temperature profiles for Neptune.

ORTON, TOKUNAGA, AND CALDWELL (1983)

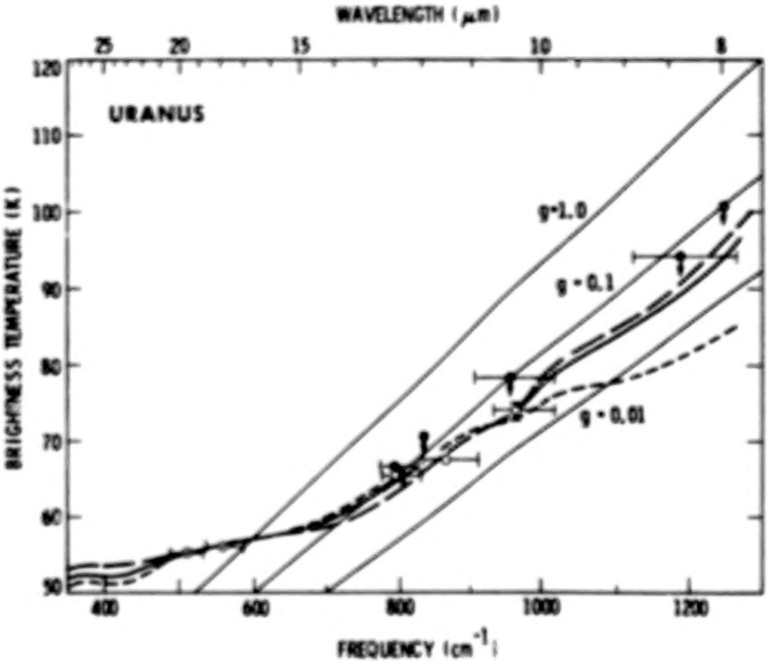

FIG. 2. Brightness temperature spectrum of Uranus from 8 to 20 μm. Filled circles represent 3σ upper detection limits of Gillett and Rieke (1977). Circles with central point represent data of Tokunaga *et al.* (1982). Open circles represent data reported here. Vertical bars represent 1σ uncertainties when larger than the circles. Horizontal bars are schematic representations of the FWHM of interference filters. Model spectra, considering H_2 opacity alone, are represented by curves for various volume mixing ratios of CH_4 in the deep atmosphere: 0.2% (long dashed), 2% (solid), and 10% (short dashed). Thin solid lines represent the apparent brightness temperatures corresponding to values of geometric albedo, g, as marked.

Fig. 3. Uranus brightness temperatures.

BEST COPY AVAILABLE

ORTON, TOKUNAGA, AND CALDWELL (1983)

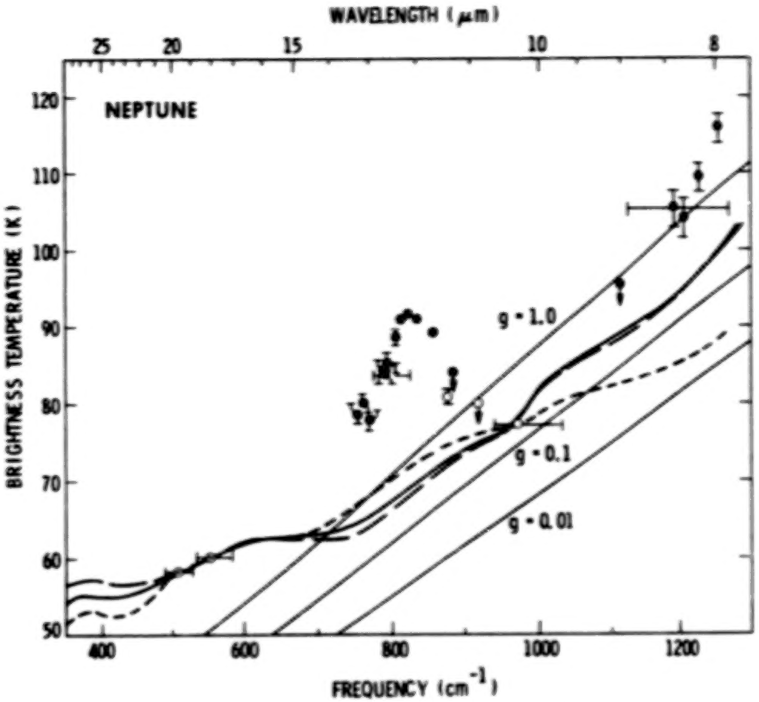

FIG. 6. Brightness temperature spectrum of Neptune from 8 to 20 μm. Filled circles represent data of Gillett and Rieke (1977). Symbols have the same meaning as in Fig. 2, with upper detection limits representing 3σ noise levels and model spectra considering H_2 opacity alone with various tropospheric volume mixing ratios for CH_4: 0.2% (long dashed), 2% (solid), and 10% (short dashed). Thin solid lines represent the apparent brightness temperature corresponding to values of geometric albedo, g, as marked.

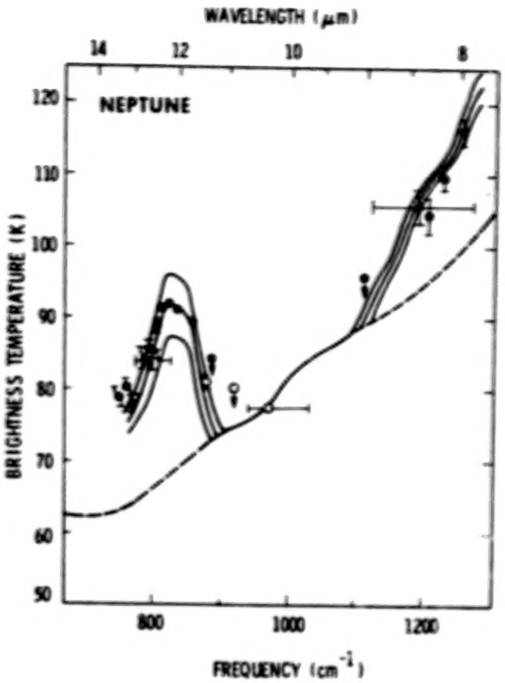

FIG. 8. Model spectra for Neptune in the 8- to 14-μm region for the perturbed equilibrium model with warm upper stratosphere. Models for a tropospheric CH_4 volume mixing ratio of 0.2% are shown. Solid curves represent model spectra (1.5% resolution) for various maximum mixing ratios of stratospheric C_2H_6: 1×10^{-5}, 3×10^{-6}, and 1×10^{-6} (upper to lower) and stratospheric CH_4: 1×10^{-1}, 4×10^{-2}, and 2×10^{-2}. The dotted curve represents the spectrum in the absence of C_2H_6 or CH_4.

Fig. 4. Neptune brightness temperatures.

they represent a reasonable continuation of the infrared data. Similar structure is probably present at all altitudes above the tropopause, but it cannot be resolved in infrared soundings. As noted in the caption for Fig. 1, the thermal models of Appleby (1980) predict temperatures rather lower than observed.

The stratospheric thermal emissions are not the only area where striking differences are found between Uranus and Neptune. Figure 5 shows a collection of near-IR spectra by Fink and Larson (1979). The bottom two panels show the absorptions in the Earth's atmosphere and in a laboratory cell containing methane. Although both planets show very strong methane absorption, the shapes in the bottoms of the bands are very different. Uranus gives flat, almost black, bottoms, resembling the laboratory spectrum more than any other atmosphere. Neptune's bands are almost pointed in the middle, and the best match in Fig. 5 is with Titan. For shorter wavelengths, 0.8-1 μm, a similar difference is seen (Trafton 1981, Fig. 10). A quantitative analysis is still not possible, because we do not have adequate laboratory data and because models combining radiative transfer and band models are not sufficiently developed (see Wallace and Hunten, 1978). But empirical comparisons may not be out of place. The resemblance of Neptune's and Titan's spectra suggests that Neptune's atmosphere may contain an extended, somewhat absorbing, haze. Similarly, the resemblance of Uranus's spectrum to that of the laboratory cell suggests a relatively clear atmosphere with a discrete reflecting cloud layer at the bottom. Such a cloud is needed in the models of Wallace (1980), although he also has some haze at higher altitudes. These models are further discussed below.

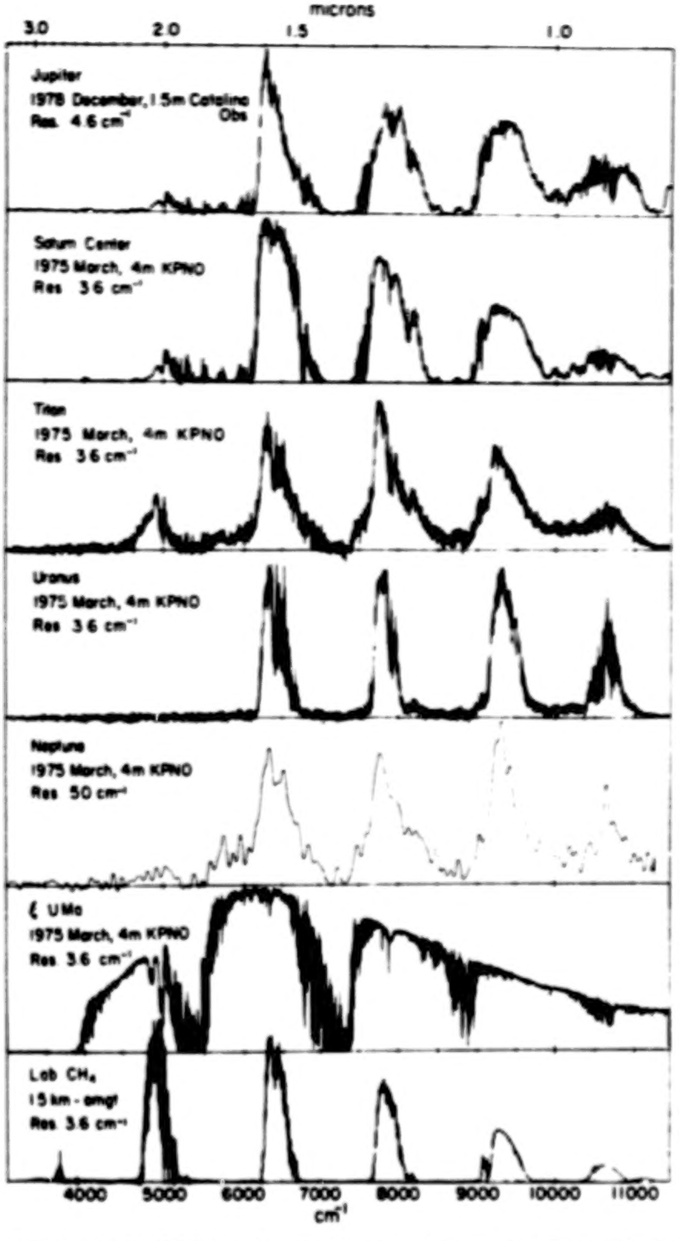

FIG. 1.—Overview of the infrared spectra of Jupiter, Saturn, Uranus, Neptune, and Titan. The G0 V comparison star ξ UMa provides the instrumental response and the strength of the telluric absorptions. A comparison laboratory methane spectrum is also included at the bottom. The noise level is exemplified by the region of zero signal below 4000 cm^{-1}.

(Fink and Larson, 1979)

Fig. 5. Near-infrared spectra.

The remarkable temporal change in Uranus's microwave emission is discussed below. Briggs and Andrew (1980) have suggested that it might be linked to a seasonal behavior of the tropospheric convection, such that the composition is very different in the polar regions and low latitudes. Wallace (1983) took up the challenge of modeling this effect with a series of time-dependent radiative-convective models for the poles. The behavior is very complex, with most of the internal heat coming out during the winter, and interleaved layers of radiative and convective control at various seasons. However, nothing was found to suggest a major effect on the composition.

COMPOSITION AND CLOUD

An excellent summary of the compositions is given by Trafton (1981), whose Table 6 is reproduced here as Table 2. There is really no empirical information on the helium abundance, but in view of the difficulty of finding any mechanism for separating it from hydrogen, a solar abundance for the planet as a whole is highly probable. Gravitational segregation as on Saturn also seems unlikely. Not included in Table 2 is the study by Wallace (1980), who attempted to deduce the methane abundance in the deep atmosphere by analysis of spectra in the visible and near IR. This work extends an earlier treatment by Trafton (1976). The methane partial pressure was constrained to remain at or below the vapor pressure. The sets of curves in Fig. 1 are for mole fractions X of 1%, 3%, and 10%. The leverage from the spectral data is not very strong, because the differences occur at depths that are barely reached by visible radiation. Nevertheless, Wallace is able to conclude that X is between 1% and 10%, with a reasonable fit at 3%. The smaller figures in Table 2 are not inconsistent, as

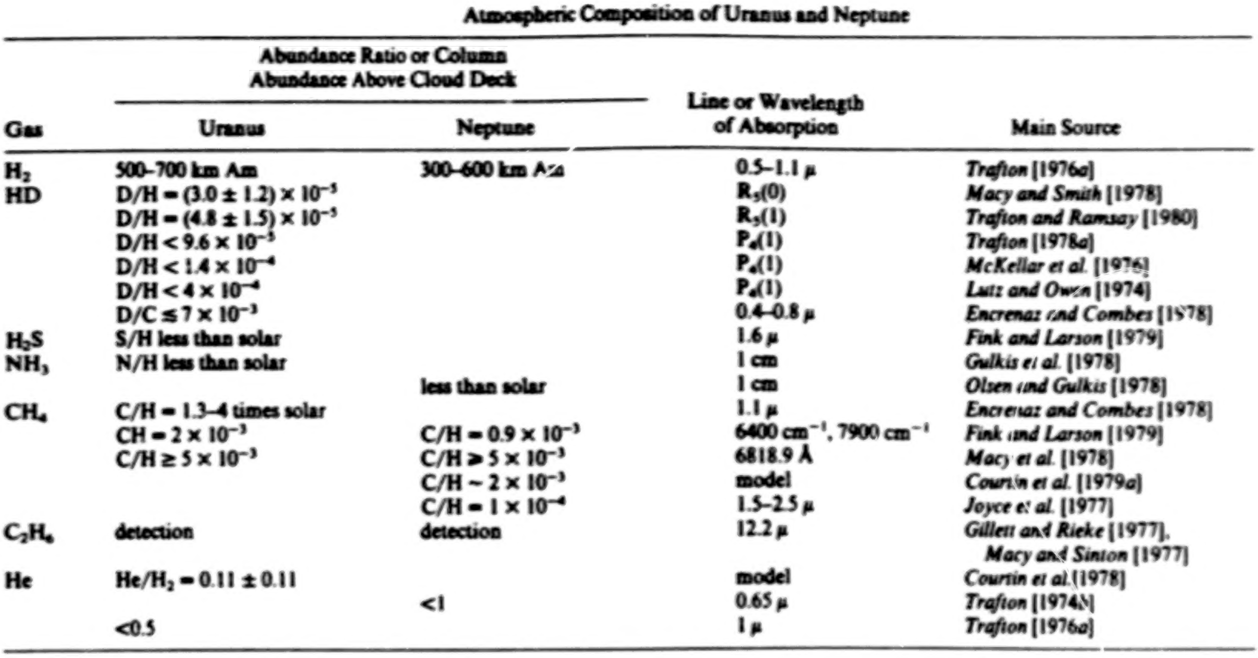

Atmospheric Composition of Uranus and Neptune

Gas	Abundance Ratio or Column Abundance Above Cloud Deck: Uranus	Abundance Ratio or Column Abundance Above Cloud Deck: Neptune	Line or Wavelength of Absorption	Main Source
H_2	500–700 km Am	300–600 km Am	0.5–1.1 μ	*Trafton* [1976a]
HD	$D/H = (3.0 \pm 1.2) \times 10^{-5}$		$R_5(0)$	*Macy and Smith* [1978]
	$D/H = (4.8 \pm 1.5) \times 10^{-5}$		$R_5(1)$	*Trafton and Ramsay* [1980]
	$D/H < 9.6 \times 10^{-5}$		$P_4(1)$	*Trafton* [1978a]
	$D/H < 1.4 \times 10^{-4}$		$P_4(1)$	*McKellar et al.* [1976]
	$D/H < 4 \times 10^{-4}$		$P_4(1)$	*Lutz and Owen* [1974]
	$D/C \leq 7 \times 10^{-3}$		0.4–0.8 μ	*Encrenaz and Combes* [1978]
H_2S	S/H less than solar		1.6 μ	*Fink and Larson* [1979]
NH_3	N/H less than solar		1 cm	*Gulkis et al.* [1978]
		less than solar	1 cm	*Olsen and Gulkis* [1978]
CH_4	C/H = 1.3–4 times solar		1.1 μ	*Encrenaz and Combes* [1978]
	$CH = 2 \times 10^{-3}$	$C/H = 0.9 \times 10^{-3}$	6400 cm^{-1}, 7900 cm^{-1}	*Fink and Larson* [1979]
	$C/H \geq 5 \times 10^{-3}$	$C/H \geq 5 \times 10^{-3}$	6818.9 Å	*Macy et al.* [1978]
		$C/H \sim 2 \times 10^{-3}$	model	*Courtin et al.* [1979a]
		$C/H = 1 \times 10^{-4}$	1.5–2.5 μ	*Joyce et al.* [1977]
C_2H_6	detection	detection	12.2 μ	*Gillett and Rieke* [1977], *Macy and Sinton* [1977]
He	$He/H_2 = 0.11 \pm 0.11$		model	*Courtin et al.* [1978]
		<1	0.65 μ	*Trafton* [1974b]
	<0.5		1 μ	*Trafton* [1976a]

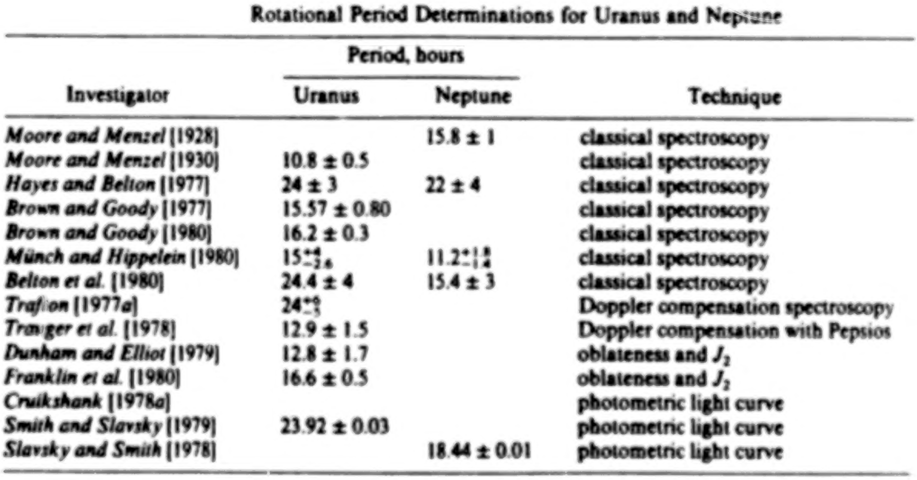

Rotational Period Determinations for Uranus and Neptune

Investigator	Period, hours: Uranus	Period, hours: Neptune	Technique
Moore and Menzel [1928]		15.8 ± 1	classical spectroscopy
Moore and Menzel [1930]	10.8 ± 0.5		classical spectroscopy
Hayes and Belton [1977]	24 ± 3	22 ± 4	classical spectroscopy
Brown and Goody [1977]	15.57 ± 0.80		classical spectroscopy
Brown and Goody [1980]	16.2 ± 0.3		classical spectroscopy
Münch and Hippelein [1980]	$15^{+4}_{-2.6}$	$11.2^{+1.8}_{-1.4}$	classical spectroscopy
Belton et al. [1980]	24.4 ± 4	15.4 ± 3	classical spectroscopy
Trafton [1977a]	24^{+0}_{-3}		Doppler compensation spectroscopy
Trauger et al. [1978]	12.9 ± 1.5		Doppler compensation with Pepsios
Dunham and Elliot [1979]	12.8 ± 1.7		oblateness and J_2
Franklin et al. [1980]	16.6 ± 0.5		oblateness and J_2
Cruikshank [1978a]			photometric light curve
Smith and Slavsky [1979]	23.92 ± 0.03		photometric light curve
Slavsky and Smith [1978]		18.44 ± 0.01	photometric light curve

Table 2 (above): Compositions.

Table 3 (below): Rotation

from Trafton (1981)

they refer to higher levels where most of the methane has been frozen out. A similar comment applies to the 0.3% found by Teifel (1983).

The papers of Baines et al. (1983) and Baines (1983) arrived after this paper had been written. The methane abundance, (4.5±2.5)% is consistent with Wallace's conclusion.

The stratospheric abundances of methane and ethane deduced by OTC have been mentioned above. Macy (1980) has also obtained an acetylene abundance of 10^{-8} for Neptune.

Ammonia is of course totally invisible at optical wavelengths because of the cold temperatures of the visible atmosphere, but as on all the giant planets it can be probed with microwaves. In Jupiter and Saturn the abundance is found to be close to solar, probably slightly above (Gulkis and Poynter, 1972). The behavior of Uranus is strikingly different (Gulkis et al., 1978; Gulkis et al., 1983; see Fig. 6). The brightness temperature in the centimeter range is considerably higher than expected for solar abundance, as illustrated in the first panel of Fig. 6. This effect cannot be explained by changing the temperature profile from the assumed adiabat, because it is impossible to have warmer temperatures at a given depth. Cooler temperatures would be in the wrong direction. The only reasonable explanation seems to be a depletion of ammonia, which is explored in detail by Gulkis et al. (1978). The models shown in Fig. 6 (which is also their Fig. 6) do not really fit the data; if a mole fraction had to be chosen, it would be about 3×10^{-7}. A better fit is found if it assumed that ammonia is removed from the vapor phase by reaction with hydrogen sulfide

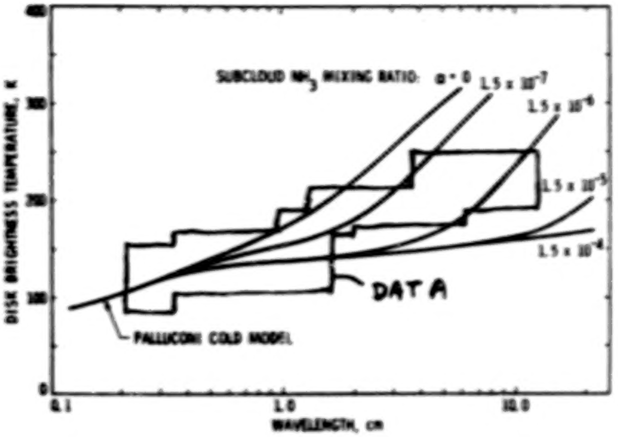

FIG. 6. Theoretical spectra based on the Palluconi cold model incorporating a modified NH_3 abundance. We investigate the possibility that the abundance of NH_3 is simply lower than the solar value. We see that H_2 absorption alone can account for the spectrum at wavelengths less than 8 mm if the cold model is employed; however, another absorber must be present at deeper levels in order to explain the spectrum at longer wavelengths. No value of the NH_3 mixing ratio is acceptable if this absorber is uniformly mixed. Observe that in order to fit the microwave data around 2 cm, the NH_3 mixing ratio in the region immediately below the saturation level must be reduced by at least three orders of magnitude.

(Gulkis et al., 1978)

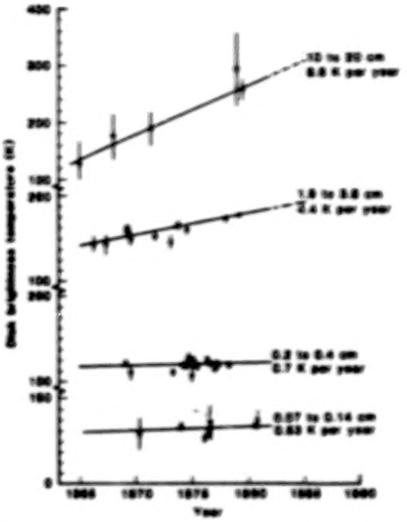

Fig. 1. Variations in the observed disk temperatures of Uranus for four wavelength intervals. The weighted least-squares fit to a linear variation in time is shown for each interval.

(Gulkis et al., 1983)

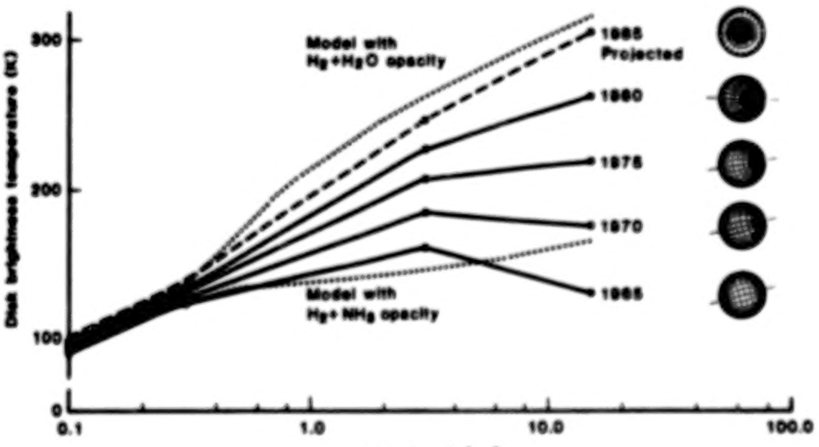

Fig. 2. Schematic evolutionary spectra for Uranus. The dotted lines are theoretical spectra for which it is assumed (upper curve) that water vapor and H_2 are the only sources of the microwave opacity and (lower curve) that the only sources are NH_3 and H_2. The dashed line is a linear extrapolation of the variation to 1985, the next time at which the polar heating will reach a maximum.

S. GULKIS
E. T. OLSEN
M. J. KLEIN
Jet Propulsion Laboratory,
California Institute of Technology,
Pasadena 91109
T. J. THOMPSON (1983)

Ball Aerospace Systems
Division, Western Laboratories,
Huntington Beach, California 92647

Fig. 6. Microwave brightness of Uranus.

and condensation into cloud. A fivefold enhancement of S relative to solar would be required. In view of the strong enhancement of C, such an effect seems more plausible than the huge reduction of N otherwise required, quite apart from the better fit to the data. Much less information is available for Neptune, but it is reported to resemble Uranus (Olsen and Gulkis, 1978).

Even more surprising is the behavior of Uranus as a function of time. The announcement by Klein and Turegano (1978) has been amply borne out by more recent results, conveniently summarized by Gulkis et al. (1983), the source of the two right-hand panels of Fig. 6. Essentially no increase is seen at millimeter wavelengths, where the main opacity is that of H_2. In the centimeter region there has been a marked increase. As suggested in the bottom panel of Fig. 6, the aspect of Uranus has been changing from equatorial to polar over the time of observation, and the depletion of ammonia may be confined to the polar region. Some doubt seems to be cast on the relevance of the earlier data set considered by Gulkis et al. (1978), and the conclusions drawn from it, particularly the role of hydrogen sulfide. The current suggestion is that saturated ammonia dominates the opacity at low latitudes, but that it is essentially absent at the poles and water vapor dominates instead.

Apart from the very indirect inference just mentioned, and the equally indirect inference from the mean density, there is no empirical evidence on the H_2O abundance. Even if it is abundant in the planet as a whole, it may have been segregated into the core during formation (as may also be true for ammonia). An alternative worth exploring is that there may be as much water vapor belo some cloud level as there is methane below its cloud level, 3% following Wallace

(1980). The resulting temperature profile has been calculated (see the Appendix), and is shown in Fig. 7. The H_2O wet adiabat begins to depart noticeably from the dry at about 100 bars, and the cloud base for the 3% mole fraction is at about 550 bars. The temperature at this level is 42 K cooler than it would be for the dry atmosphere. The 8% difference would be reflected at all deeper levels. Figure 7 includes a set of other curves for smaller H_2O abundances; for example, with 1% the cloud base is at 200 bars.

Such a cloud is far too deep in the atmosphere for optical probing. As far as radio frequencies are concerned, the speculations of Gulkis et al. (1983) have been mentioned above. These arguments, even if confirmed, relate to the top of the putative cloud, and do not tell us anything about the mole fraction deep in the atmosphere. Much better information for the higher levels is available from the work of Wallace (1980). His best fits to the spectral data are for an optically dense cloud at about 4 bars and a slightly absorbing haze between 0.5 and 1.4 bars; its optical thickness is 0.3 at 6435 A. These pressure levels are approximate because they were actually specified in terms of the column density (or partial pressure) of H_2. In addition, there is small amount of pure absorption distributed in proportion to the gas density. The dense cloud is roughly in the methane condensation region. The haze occurs at far too low a temperature to be a condensate, and must therefore be a photochemical smog, or Axel-Danielson dust (Axel, 1972), of the type now familiar on Titan.

Even less is known about cloudiness on Neptune, although there is one major difference: On Neptune there are enough distinct clouds to show up in images (Smith et al., 1979; Belton et al, 1981) and to permit estimates of the rotation

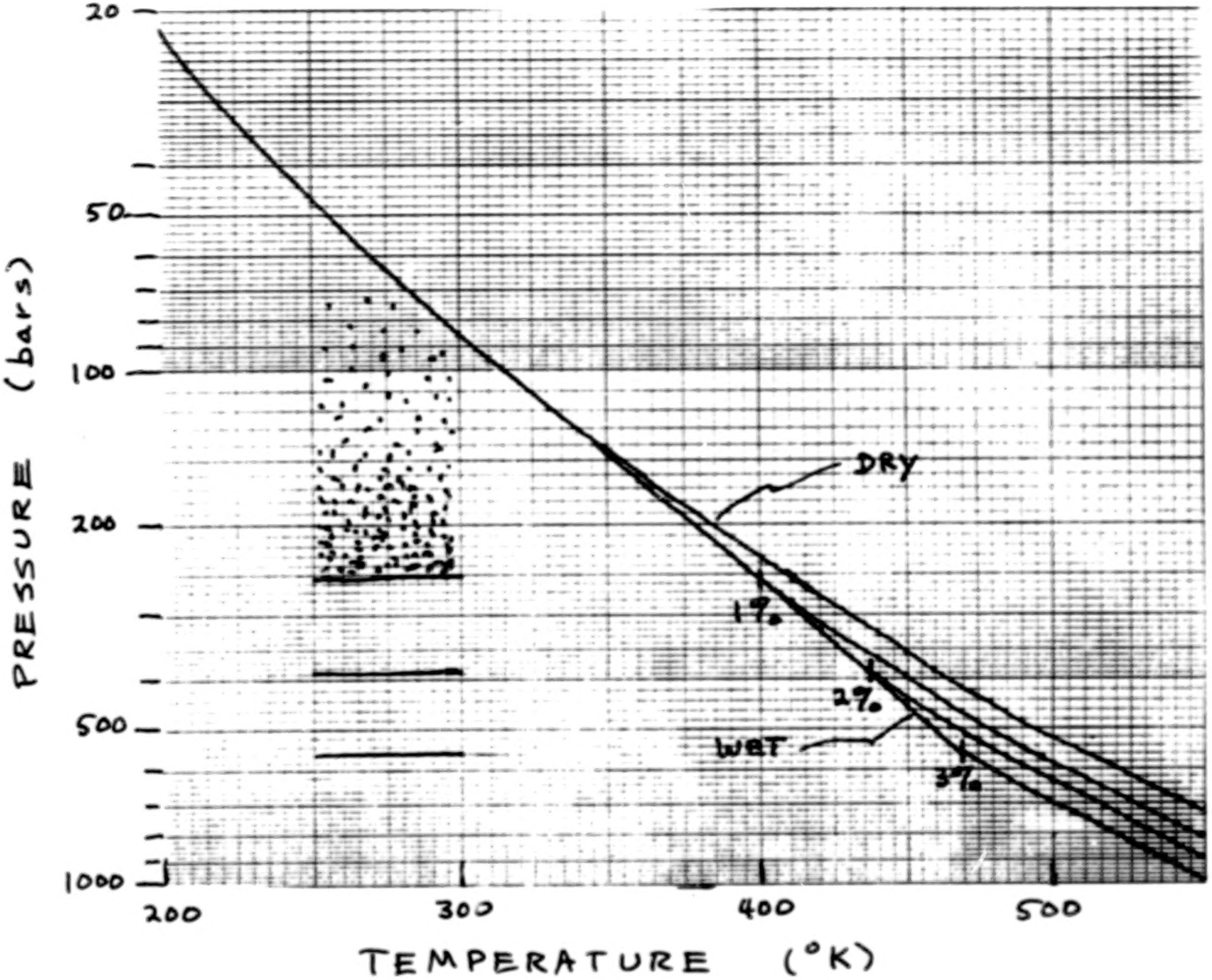

Fig. 7. The deep atmosphere of Uranus and possible H_2O clouds. Temperature profiles and cloud bases are shown for mole fractions 1, 2, 3%.

rate (discussed below). Such work is done at wavelengths strongly absorbed by methane, to suppress light scattered by the enormous amount of hydrogen in the atmosphere. It is assumed that the clouds in question must be at high altitudes, perhaps even stratospheric, to be made visible in this way.

OTHER AREAS

Aurora. Two groups have detected Uranian Lyman-alpha emission with the IUE (Durrance and Moos, 1982; Clarke, 1982). Figure 8 illustrates these results, which require subtraction of the geocoronal intensity (at left) from the total (middle) to get the planetary emission (on the right). By itself, such a detection does not prove the presence of aurora; the important point is that the intensity varies from measurement to measurement over a range from 427 to 1600 Rayleighs (disk-averaged). In turn, the presence of aurora is strong evidence for the presence of a magnetosphere on Uranus, something that has long been a matter of faith, reinforced somewhat by dynamo theory. For Neptune we are still left with faith.

In principle, the observed flux from Uranus could be explained by Rayleigh scattering of solar radiation with an albedo of 0.5; the variation might stem from the difficulty of accurately subtracting the geocorona, which is 3-4 times brighter. This was pointed out by D.E. Shemansky in a recent conversation. The entire stratosphere would have to be essentially empty of methane, which seems unlikely but not much less likely than the depletion already established. The formulation of Carlson and Judge (1971) for Jupiter is directly applicable and the required mole fraction is found to be 6×10^{-9}.

Intense Lyα emission from Uranus

Samuel T. Durrance & H. Warren Moos (1982)

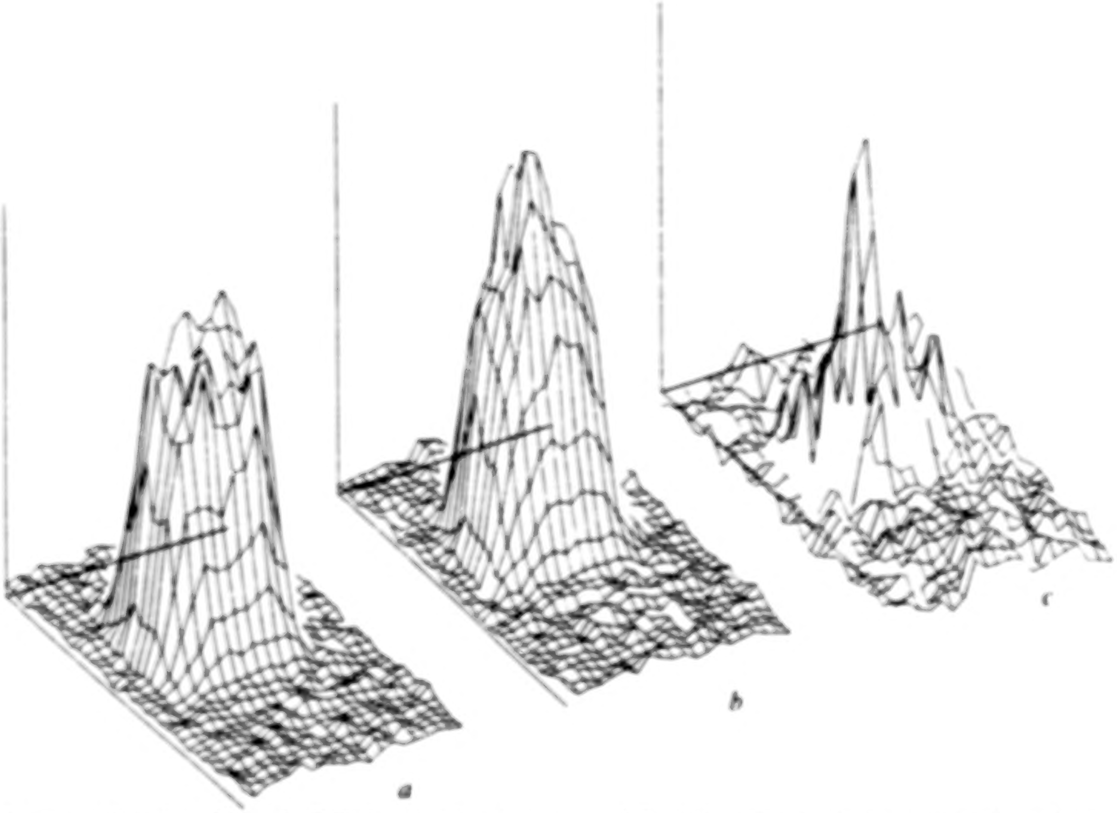

Fig. 1 Projection of the Lyα flux in the IUE short wavelength spectrograph focal plane showing the Lyα emission from Uranus. *a*, Sum of three exposures with geocorona only normalized to *b*; *b*, sum of two 2-h exposures with Uranus at the centre of the large entrance aperture; *c*, the uranian Lyα emission obtained by subtracting the geocoronal contribution from *b* and multiplying the result by 3. The long dimension of the aperture is approximately parallel to the axes pointing upward and to the right. The dispersion direction is approximately parallel to the axes pointing downward and to the right.

Fig. 8. Aurora on Uranus.

BEST COPY AVAILABLE

Ionospheres. Atreya and Ponthieu (1983) have computed an ionosphere for Uranus, taking into account the cold-trapping of hydrocarbons in the stratosphere. On Jupiter, Saturn, and Titan such molecules play a major role by reaction to produce rapidly-recombining ions. On Uranus they are predicted to be much less important. The electron density at the peak is expected to be (2-3) x 10^4 cm^{-3}, but it is suggested that the actual value may be lower, perhaps 5 x 10^3 cm^{-3}, as found on Jupiter and Saturn. If the hydrocarbons are much more abundant in the upper atmosphere of Neptune, the densities could be further reduced, quite apart from the smaller flux of solar UV.

Rotation. Excellent surveys have been published by Trafton (1981) and, fo Uranus, by Goody (1982). Table 3, from Trafton's paper, hardly needs comment, but more recent papers on Neptune have been published by Belton et al. (1980, 1981) and R. H. Brown et al. (1981). Photometric periods are found at 17.73, 18.56, and 18.29 h. The suggestion of Belton et al. is that the true period is 18.2 h, with the others due to amplitude modulation or winds up to 102 m s^{-1}.

Our knowledge of Uranus has increased enormously in the last decade, and some very puzzling facts have also been revealed. The stage is well set for Voyager and for further Earth-based studies.

APPENDIX

The dry and wet adiabats in Fig. 7 were calculated as follows. The adiabatic law is

$$-\beta = \frac{d \ln T}{d \ln p} = \frac{R}{Cp} \quad , \tag{1}$$

where R is the gas constant and Cp the molar specific heat, which is somewhat temperature dependent for H_2. A curve fit to the tabulation of Trafton and Stone (1974) for a He-H_2 mixture gives

$$-\beta = \frac{T}{a+bT} \tag{2}$$

with a = 9.77° K, b = 0.2589. A small allowance has been made for the specific heat of 3% methane. The integral of (2) is

$$P \text{ (bars)} = \left(\frac{a+bT}{a+bT_1}\right)^{1/b} \quad , \tag{3}$$

where T_1 is the temperature at 1 bar. In the present case, T_1 is taken as 69° K to fit the curve given by Wallace (1980), shown in Fig. 1 (155° K at 10 bars). The temperature at 1 bar is therefore somewhat higher than T_1.

For the wet adiabat, the vapor pressure of liquid water is

$$Pv = 1.159 \times 10^6 \exp(-5211/T) \text{ bars.} \tag{4}$$

According to Lasker (1963),

$$-\beta = \frac{1 + X(1+\alpha)}{(Cp/R) + X\alpha(1+\alpha)} \quad , \tag{5}$$

BEST COPY AVAILABLE

with $\alpha = 5211/T$ and $X = Pv/P$, the H_2O mole fraction. If T is used as the independent variable, (1) can be integrated downward in steps until the assumed final value of X is reached. The curve then reverts to the dry adiabat. In view of all the uncertainties, (Cp/R) was taken constant at 3.3 in solution of (5).

REFERENCES

Appleby, J.F. (1980). Atmospheric structures of the giant planets. Ph.D. thesis, State Univ. of New York at Stony Brook.

Atreya, S.K., and J.J. Ponthieu (1983). Photolysis of methane and the ionosphere of Uranus. Planet. Space Sci., 31, 939-944.

Axel, L. (1972). Inhomogeneous models of the atmosphere of Jupiter. Astrophys. J., 173, 451-468.

Baines, K.H., W.V. Schempp, and W.H. Smith (1983). High-resolution observations of the 6815-A band of methane in the major planets. Icarus, 56, 534-542.

Baines, K.H. (1983). Interpretation of the 6618.9-A methane feature observed on Jupiter, Saturn, and Uranus. Icarus, 56, 543-559.

Belton, M.J.S., L. Wallace, and S. Howard (1981). The periods of Neptune: Evidence for atmospheric motions. Icarus, 46, 263-274.

Briggs, F.H. and B.H. Andrew (1980). Microwave radiometry and interferometry of Uranus. Icarus, 41, 269-277.

Brown, R.A., and R.M. Goody (1977). The rotation of Uranus, I. Astrophys. J., 217, 680-687.

Brown, R.A., and R.M. Goody (1980). The rotation of Uranus, II, Astrophys. J., 235, 1066-1070.

Brown, R.H., D.P. Cruikshank, and A.T. Tokunaga (1981). The rotation period of Neptune's upper atmosphere. Icarus, 47, 159-165.

Carlson, R.W., and D.L. Judge (1971). The extreme ultraviolet dayglow of Jupiter. Planet. Space Sci., 19, 327-343.

Clarke, J.T. (1982). Detection of auroral hydrogen Lyman-Alpha emission from Uranus. Astrophys. J., 263, 105-109.

Courtin, R., D. Gautier, and A. Lacombe (1978). On the thermal structure of Uranus from infrared measurements. *Astron. Astrophys.*, *61*, 97-101.

Courtin, R., D. Gautier, and A. Lacombe (1979a). Indications of super-saturated stratospheric methane on Neptune from its atmospheric thermal profile. *Icarus*, *37*, 236-248.

Cruikshank, D.P. (1978a). On the rotation period of Neptune. *Astrophys. J.*, *220*, L57-L59.

Danielson, R.E. (1977). The structure of the atmosphere of Uranus. *Icarus*, *30*, 462-478.

Dunham, E. and J.L. Elliot (1979). The rotation period of Uranus. *Bull. Am. Astron. Soc.*, *11*, 568.

Durrance, S.T. and H.W. Moos (1982). Intense Lyα emission from Uranus. *Nature*, *299*, 428-429.

Encrenaz, T., and M. Combes (1978). On the D/C ratio in the atmosphere of Uranus. *Bull. Am. Astron. Soc.*, *10*, 567-577.

Fink, U., and H.P. Larson (1979). The infrared spectra of Uranus, Neptune, and Titan from 0.8 to 2.5 microns. *Astrophys. J.*, *233*, 1021-1040.

Franklin, F.A., C.C. Avis, G. Colombo, and I.I. Shapiro (1980). The geometric oblateness of Uranus. *Astrophys. J.*, *236*, 1031-1034.

French, R.G., J.L. Elliot, E.W. Dunham, D.A. Allen, J.H. Elias, J.A. Frogel, and W. Liller (1983). The thermal structure and energy balance of the Uranian upper atmosphere. *Icarus*, *53*, 399-414.

Gautier, D., and R. Courtin (1979). Atmospheric thermal structures of the giant planets. *Icarus*, *39*, 28-45.

Gillett, F.C., and G.H. Rieke (1977). 5-20 micron observations of Uranus and Neptune. *Astrophys. J.*, *218*, L141-L144.

Goody, R.M. (1982). The rotation of Uranus. In Uranus and the Outer Planets (G. Hunt, Ed.), pp. 143-153. Cambridge Univ. Press, Cambridge, England.

Gulkis, S. and R. Poynter (1972). Thermal radio emission from Jupiter and Saturn. Phys. Earth Planet. Interiors, 6, 36-43.

Gulkis, S., M.A. Janssen, and F.T. Olsen (1978). Evidence for the depletion of ammonia in the Uranus atmosphere. Icarus, 34, 10-19.

Gulkis, S., E.T. Olsen, and M.J. Klein (1983). Uranus: Variability of the microwave spectrum. Science, 221, 453-454.

Hayes, S.H., and M.J.S. Belton (1977). The rotational periods of Uranus and Neptune. Icarus, 32, 383-401.

Hubbard, W.B. (1978). Comparative thermal evolution of Uranus and Neptune. Icarus, 35, 177-181.

Hunt, G.E. (1982). Meteorology of the outer planets. In Uranus and the Outer Planets (G.E. Hunt, Ed.), pp. 181-191. Cambridge Univ. Press, Cambridge, England.

Hunten, D.M. (1974). (Ed.) The atmosphere of Uranus, NASA Proc. of Workshop at Ames Research Center, Moffett Field, Calif.

Joyce, R.R., C.B. Pilcher, D.P. Cruikshank, and D. Morrison (1977). Evidence for weather on Neptune, I. Astrophys. J., 214, 657-662.

Klein, M.J., and J.A. Turegano (1978). Evidence of an increase in the microwave brightness temperature of Uranus. Astrophys. J., 224, L31-L34.

Lasker, B. (1963). Wet adiabatic model atmospheres for Jupiter. Astrophys. J., 138, 709-719.

Lutz, B.L., and T. Owen (1974). The search for HD in the spectrum of Uranus: An upper limit to [D/H]. Astrophys. J., 190, 731-734.

Macy, W.W., Jr., and W.M. Sinton (1977). Detection of methane and ethane emission on Neptune but not on Uranus. Astrophys. J., 218, L79-L81.

Macy, W.W., Jr., and W.H. Smith (1978). Detection of HD on Saturn and Uranus, and the D/H ratio. Astrophys. J., 222, L73-L75.

Macy, W.W., Jr., J. Gelfand, and W.H. Smith (1978). Interpretation of the 6818.9 A methane line in terms of inhomogeneous scattering models for Uranus and Neptune. Icarus, 34, 20-27.

Macy, W., Jr. (1980). Mixing ratios of methane, ethane, and acetylene in Neptune's stratosphere. Icarus, 41, 153-158.

McKellar, A.R.W., W. Goetz, and D.A. Ramsay (1976). The rotation-vibration spectra of HD: Wavelength and intensity measurements of the 3-0, 4-0, 5-0, and 6-0 electric dipole bands. Astrophys. J., 207, 663-670.

Moore, J.H., and D.H. Menzel (1928). Preliminary results of spectroscopic observations for rotation of Neptune. Publ. Astron. Soc. Pac., 40, 234-238.

Moore, J.H., and D.H. Menzel (1930). The rotation of Uranus. Publ. Astron. Soc. Pac., 42, 330-335.

Munch, G., and H. Hippelein (1980). The effects of seeing on the reflected spectrum of Uranus and Neptune. Astron. Astrophys., 81, 189-197.

Olsen, E.T., and S. Gulkis (1978). A preliminary investigation of Neptune's atmosphere via its microwave continuum emission. Bull. Am. Astron. Soc., 10, 577.

Orton, G.S., A.T. Tokunaga, and J. Caldwell (1983). Observational constraints on the atmospheres of Uranus and Neptune from new measurements near 10 μm. Icarus, 56, 147-164.

Sicardy, B., M. Combes, A. Brahic, P. Bouchet, C. Perrier, and R. Courtin (1982). The 15 August 1980 occultation by the Uranian system: Structure of the rings and temperature of the upper atmosphere. Icarus, 52, 454-472.

Slavsky, D.B., and H.J. Smith (1978). The rotation period of Neptune. Astrophys. J., 226, L49-L52.

Smith, B.A., H.J. Reitsema, and S.M. Larson (1979). Discrete cloud features on Neptune. Bull. Am. Astron. Soc., 11, 570-

Smith, H.J., and D.B. Slavsky (1979). Rotation period of Uranus. Bull. Am. Astron. Soc., 11, 568.

Teifel, V.G. (1983). Methane abundance in the atmosphere of Uranus. Icarus, 53, 389-398.

Tokunaga, A.T., G.S. Orton, and J. Caldwell (1983). New observational constraints on the temperature inversions of Uranus and Neptune. Icarus, 53, 141-146.

Trafton, L.M. (1974b). Neptune: Observations of the H_2 quadrupole lines in the (4-0) band. In Exploration of the Solar System, IAU Symp. 65, (A. Woszczyk and C. Iwaniszewska, Eds.), pp. 497-511. D. Reidel, Hingham, Mass.

Trafton, L.M., and P.H. Stone (1974). Radiative-dynamical equilibrium states for Jupiter. Astrophys. J., 188, 649-655.

Trafton, L.M. (1976a). The aerosol distribution in Uranus' atmosphere: Interpretation of the hydrogen spectrum. Astrophys. J., 207, 1007-1024.

Trafton, L.M. (1977a). Uranus' rotational period. Icarus, 32, 402-412.

Trafton, L.M. (1978a). On the deuterium-to-hydrogen ratio in the atmosphere of Uranus. Astrophys. J., 222, 740-743.

Trafton, L.M. and D.A. Ramsay (1980). The D/H ratio in the atmosphere of Uranus: Detection of the $R_5(1)$ line of HD. Icarus, 41, 423-429.

Trafton, L. (1981). The atmospheres of the outer planets and satellites. Rev. Geophys. Space Phys., 19, 43-89.

Trauger, J.T., F.L. Roesler, and G. Munch (1978). A redetermination of the

Uranus rotation period. Astrophys. J., 219, 1079-1083.

Wallace, L., and D.M. Hunten (1978). The Jovian spectrum in the region 0.4-1.1 μm: The C/H ratio. Rev. Geophys. and Space Physics, 16, 289-319.

Wallace, L. (1980). The structure of the Uranus atmosphere. Icarus, 43, 231-259.

Wallace, L. (1983). The seasonal variation of the thermal structure of the atmosphere of Uranus. Icarus, 54, 110-132.

AERONOMY

S. K. Atreya

The University of Michigan
Department of Atmospheric and Oceanic Science
Space Research Building
Ann Arbor, MI 48109-2143

Abstract

From the known composition (H_2, CH_4, C_2H_2(?), NH_3(?) at Uranus, and H_2, CH_4, C_2H_6 at Neptune) and the inversion and photolysis region temperatures, reasonable theoretical models for the upper atmospheric distribution of the neutral and ionospheric species can be constructed on the basis of the expected physical and chemical processes. The models indicate that C_2H_2 would condense over an extensive height range on Uranus. The extent of the haze is expected to be smaller and deeper in the polar region. Some ethane is also expected to condense, mostly in the vicinity of the temperature inversion. The behavior of the acetylene condensation with latitude and time appears to be consistent with its apparent abundance variation (detected by IUE), and the brightening of Uranus observed in ground-based imaging. Neptune's polar region, on the other hand is expected to be more 'hazy' or 'cloudy' than the equatorial region. Ionospheric calculations indicate peak electron concentrations in the 3000-5000 cm^{-3} range, with an upper limit of 2×10^4 cm^{-3} at Uranus. The maximum atomic hydrogen abundance is calculated to be 2×10^{16} cm^{-2}, including flux from the ionosphere; it is a factor of 10 lower than required to explain the observed Lyα from Uranus by resonance scattering of the solar Lyα photons. The 'apparent' depletion of NH_3 on Uranus results from its loss in the aqueous-ammonia cloud.

INTRODUCTION

The aeronomy of Uranus differs from that of Jupiter and Saturn because of the peculiar inclination of its equator to the orbital plane, lack of internal heat, and the greater heliocentric distance (Table 1). All these physical characteristics have a definite effect on atmospheric thermal structure, thermodynamics, photochemistry, energy transfer and distribution, eddy mixing and the neutral and ion composition. Neptune, on the other hand, has its spin axis orientation similar to Saturn, it possesses an internal heat source, and has a warmer inversion layer than Uranus. The aeronomy of Neptune, however is not expected to be radically different from the aeronomy of Uranus, only that it is modified due to Neptune's greater distance from the Sun.

Table 1

Physical Characteristics

Property	Uranus	Neptune	Jupiter	Saturn
Equatorial radius (km)	25,400	24,300	71,398	60,330
Ellipticity	0.024(?)	0.0266	0.0637	0.102
Mean density (gm cm^{-3})	1.19	1.66	1.314	0.69
Equatorial surface gravity (cm s^{-2})	777(?)	1100(?)	2288	905
Equatorial rotation period (hrs)	15.5	15.8	9.84	10.23
Inclination of equator to orbit	98°	28°.8	3°	29°
Internal heat (Emitted Thermal/ Absorbed Solar)	<1.05(?)	~2(?)	1.668	1.78
Average surface dipole field (Gauss)	1(?)	?	4.2	0.2

This paper is a discussion of the aspects most germane to the upper atmospheric physics and chemistry -- i.e., distribution of the neutral and charged particle constituents. The emphasis is on Uranus, some relevant digression to Neptune is included when warranted by some novel data. Various assumptions used in the theoretical models of this paper are discussed below.

THERMAL STRUCTURE

Radiative-convective models, such as those of Wallace (1980)[1] and Courtin, et al. (1978)[2] yield thermal structure up to about the 1 mbar level.

Infrared measurements at 17.8μm and 19.6μm (Tokunaga, et al., 1983)[3] give the inversion level temperature, while the ground-based stellar occultation data yield temperatures in the 0.3μb - 30μb region (French, et al., 1983)[4]. Only preliminary theoretical models of Appleby (1980)[5] are avilable for thermal structure in the 'middle atmosphere' -- ~1 mb to ~1μb region. The range of temperature gradients in these models is large, and there is no clear indication of their validity to Uranus -- which is entirely reasonable considering the uncertainties in the composition of Uranus atmosphere. For Jupiter and Saturn, a linear interpolation between the tropopause temperatures and the homopause temperatures was found to be a reasonable assumption (see Atreya, et al., 1981,[6] and Festou and Atreya, 1982)[7]. A temperature profile as shown in Fig. 1 is adopted for the purpose of calculations presented in this paper. The temperature at the inversion level is approximately 55K (after data of Tokunaga, et al., 1983)[3] where the atmospheric pressure is ~100mbar. Some of the models give ~50K for the tropopause temperature; its effect on the calculations will be discussed. The temperature at the ~1μb level is between 95 and 154K (after the stellar occultation data). It should be emphasized that the photochemistry calculations are mostly sensitive only to the temperature around the 1μbar level, and not to the thermal structure in the 1 mbar - 1 μbar region. However, if condensation occurs in the middle atmosphere, the density and extent of the condensate become strong functions of the thermal structure. Finally, no handle on the exospheric temperature of Uranus or Neptune can be obtained from the available observations. On Jupiter and Saturn, the exospheric temperatures appear to be controlled by the power deposited in the auroral latitudes (Atreya, et al., 1981[6]; Atreya, et al., 1984)[8].

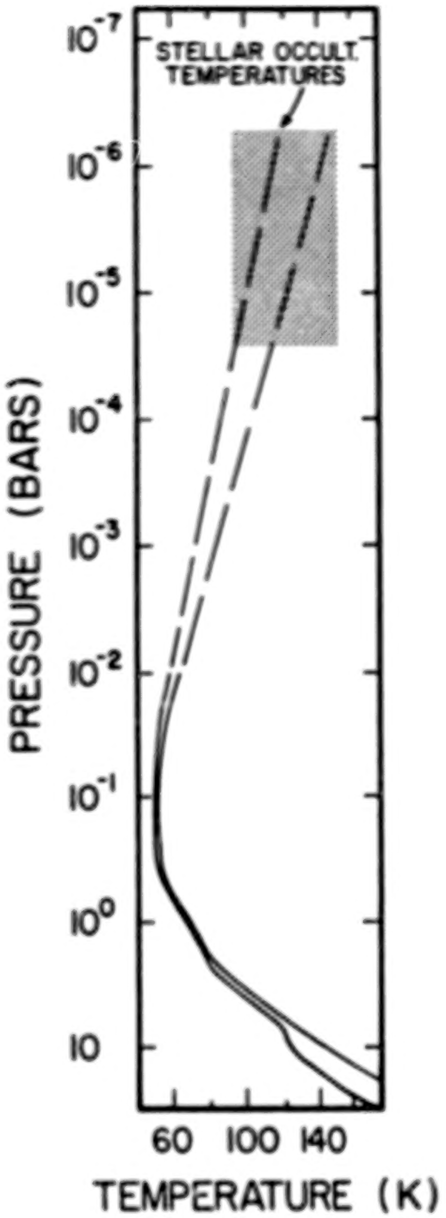

Figure 1. Uranus temperature profile adapted from Wallace (1980)[1], solid lines, and French, et al. (1983)[4], stellar occultation data. The solid lines correspond to $CH_4/H_2=0.03$, and internal heat of 10 erg cm^{-2} s^{-1} (inner curve) and 100 erg cm^{-2} s^{-1}. The Wallace models are extrapolated linearly above the 100 mb level, and they fall within the range of the stellar occultation data shown by the shaded area. This is a 'working model' of temperature for aeronomical studies -- see chapter by Orton and Appleby for physically more realistic stratospheric thermal profiles.

A crude estimate of the power deposited in Uranus' auroral latitudes may be obtained from consideration of the Lyman-alpha intensity measured by the IUE (Clarke, 1982[9]; Durrance and Moos, 1982)[10]. The range, 400-1600R, itself is quite large. It is not at all clear if the range represents real difference or is simply the result of data reduction and interpretation. It should be pointed out that the angular size of Uranus, 4 arc sec, is much smaller than the IUE aperture. Furthermore, Lyman-alpha intensity at Uranus may be quite different from the value measured by IUE at 1 AU due to possible interplanetary absorption of the solar and planetary Lyman-alpha. Assuming that the size of the Uranus auroral region is equal to the size of Uranus, and that the interplanetary absorption is negligible, one can calculate the power dissipated into the auroral region of Uranus to be ~10^{11} Watts (Atreya and Ponthieu, 1983[11]; J. Clarke, personal comm., 1983). The Lyman-alpha intensity in the aurora was assumed to be 400R. A further assumption that the auroral energy is spread uniformly over the planet with 100% efficiency by thermospheric circulation would yield an energy flux of 0.02 erg $cm^{-2} s^{-1}$. Solution of a simple one-dimensional heat conduction equation:

$$K \frac{dT}{dZ} = F$$

where K = conductivity, F = energy flux

yields 100 to 150K rise in temperature above the homopause value. In other words, exospheric temperature in the range of 200-300K on Uranus is conceivable. No sensible guess for Neptune can be made at this time.

ATMOSPHERIC MODEL

The species detected so far on Uranus and Neptune are listed in Table 2.

Table 2

Composition of Uranus and Neptune Atmospheres

	Abundance		
Constituent	Uranus	Neptune	Reference
H_2(0.5-1.1μm)	500-700 km am	300-600 km am	Trafton (1976)[12]
HD ($R_5(0)$; $R_5(1)$; $P_4(1)$)	$1.8\times10^{-5}<D/H<4\times10^{-4}$	?	Macy & Smith (1978)[13]; Trafton & Ramsey (1980)[14]; Trafton (1978)[15]; Lutz & Owen (1974)[16]
NH_3 (microwave)	$N/H<10^{-6}$ in 150-200K range	less than solar	Gulkis, et al. (1978)[17]; Gulkis, et al. (1983)[18]; Olsen & Gulkis (1978)[19]
CH_4(1.1μm, 1.5-2.5μm; 6400 cm^{-1}; 7900 cm^{-1}; 6819Å)	1.3-4 times solar	$1\times10^{-4}<C/H<5\times10^{-3}$	Encrenaz & Combes (1978)[20]; Fink & Larson (1979)[21]; Courtin, et al. (1979)[22]; Joyce, et al. (1977)[23]
C_2H_6(12.2μm)		Detection	Macy & Sinton (1977)[24]
C_2H_2 (IUE, >1600ÅUV)	Variable	?	Encrenaz (1983, personal comm.; Caldwell, 1984 -- this book)
H(IUE, 1216Å)	Lyα=400-1600R	<200R	Fricke & Darius (1982)[25]; Clarke (1982)[9]; Durrance & Moos (1982)[10] J.Clarke, person. comm., 1984

Figs. 2a and 2b show the structure of the major cloud layers in the Uranus atmosphere for the 'solar' and '10x solar' ratios of the elements (Atreya and Romani, 1984)[26]. It is apparent from these figures that H_2O, NH_3 and H_2S (as NH_4SH) are condensed out deep in the troposphere. 70-95% of NH_3 is lost in the aqueous clouds, depending upon the choice of thermal structure. The apparent depletion of NH_3 (in the 150-200K range) detected in the microwave is caused by its solution in the aqueous-NH_3 cloud. CH_4 clouds are expected to form around the 1 bar pressure level. With CH_4 mixing ratio of 3%, CH_4 clouds are formed around the 3-bar level. The only constituent likely to undergo photolysis is CH_4 since its saturation mixing ratio even at the Uranus cold trap is large enough that the unit optical depth in CH_4 occurs nearly 400 to 500 km above the tropopause.

Table 3

Ammonia Mixing Ratios on Uranus (from Atreya and Romani, 1984)[26]

	COLD			WARM	
T	Solar	10 x Solar	10 x H_2O	Solar	10 x Solar
125	$1.2x10^{-7}$	0	0	$3.3x10^{-7}$	$1.4x10^{-7}$
150	$4.0x10^{-6}$	0	0	$9.2x10^{-6}$	$1.4x10^{-7}$
175	$4.0x10^{-6}$	$3.6x10^{-11}$	$1.0x10^{-10}$	$9.2x10^{-6}$	$2.0x10^{-7}$
200	$4.2x10^{-6}$	$3.2x10^{-8}$	$9.4x10^{-8}$	$1.0x10^{-5}$	$3.0x10^{-6}$
225	$1.5x10^{-5}$	$6.2x10^{-6}$	$8.9x10^{-7}$	$2.2x10^{-5}$	$4.4x10^{-5}$

Notes COLD model has T = 450K at P = 670 bars
WARM model has T = 450K at P = 250 bars

'Solar' case has O/H, C/H, N/H and S/H in the solar ratios of the elements

'10 x Solar' case has O/H, C/H, N/H and S/H in 10 x Solar ratios of the elements. Because of the large density of Uranus, volatile abundances may be enhanced.

'10 x H_2O' case has only O/H = 10 x Solar; C/H, N/H and S/H are in the solar ratios. This case is for illustration purposes only, and should not be construed to imply author's prejudice.

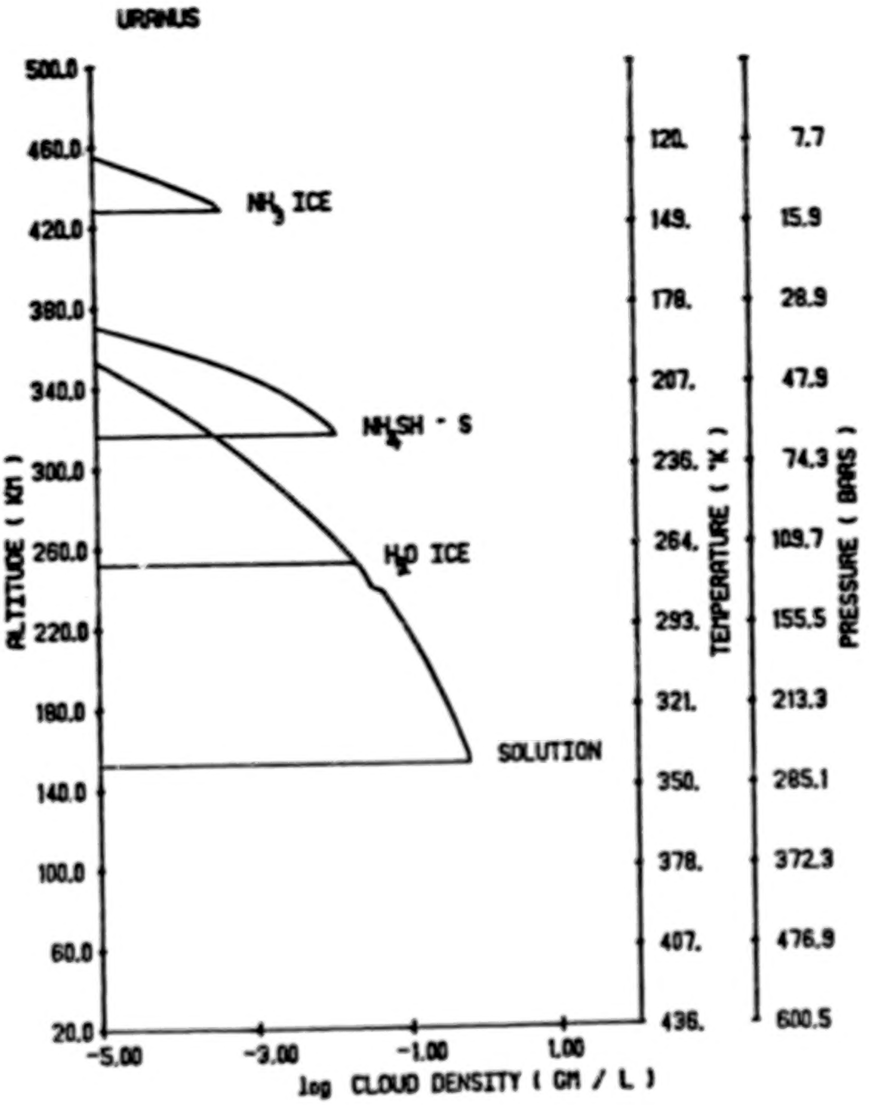

Figure 2a. Cloud structure of "cold" (T = 450 K at P = 670 bars base level), solar composition Uranus. The NH_4SH cloud is composed of solid particles. Altitudes are relative from the base level, cloud densities are log base 10, g = 900 cm sec^{-2}, and the average lapse rate is 0.72 K km^{-1}. (Atreya and Romani, 1984)[26].

BEST COPY AVAILABLE.

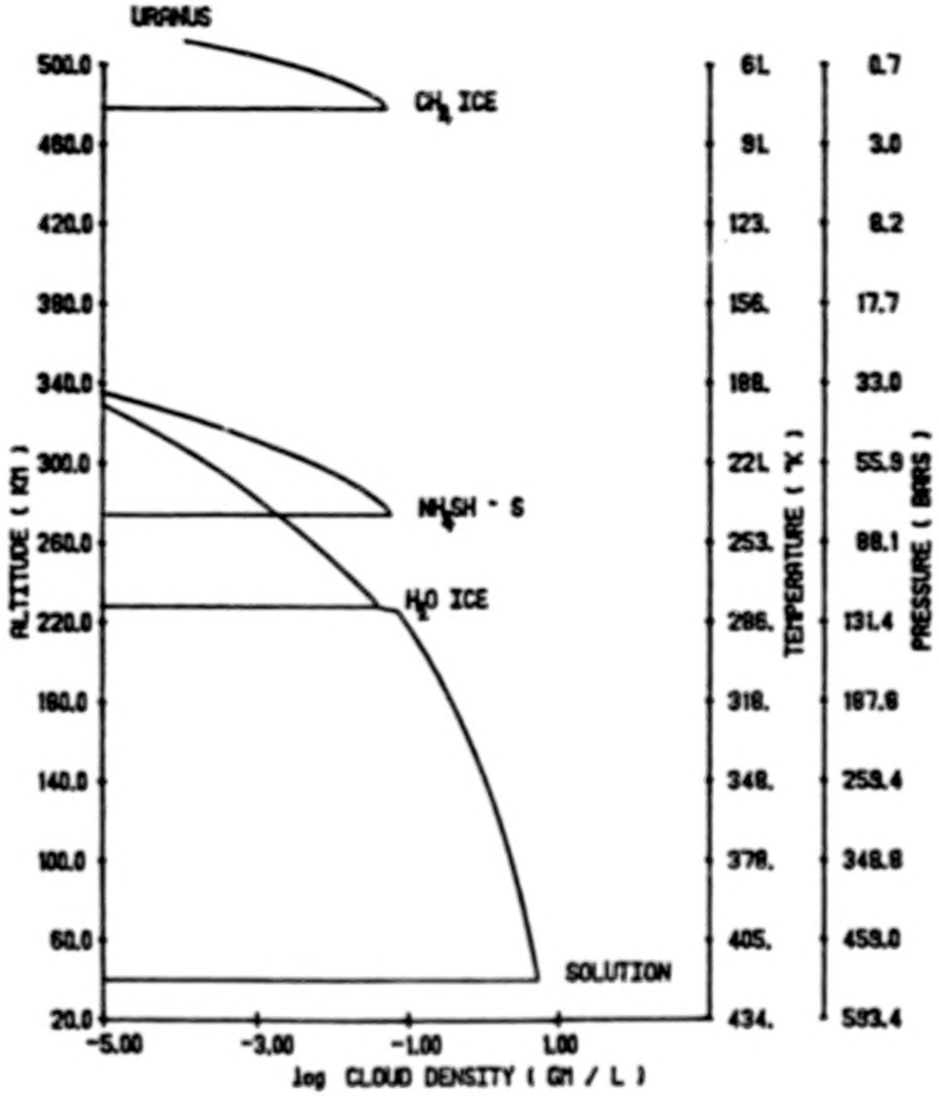

Figure 2b. Cloud structure of "cold" Uranus with NH_3, H_2O, CH_4, and H_2S in 10 x solar amounts. The other parameters are same as in Figure 2a. (Atreya and Romani, 1984)[26].

BEST COPY AVAILABLE

The CH_4 mixing ratios above the tropopause is dictated by the vertical eddy mixing coefficient and the photolysis rate. The relevant atmospheric models for Uranus and Neptune are summarized in Table 4.

Table 4

Thermal Structure and Methane Mixing Ratios

	Uranus	Neptune
He/H_2(assumed solar)	11%	11%
Inversion/Tropopause temperature	50-55K	60-63K*
CH_4 saturation vapor pressure at the tropopause (mbar)	2.4×10^{-3}(50K) 2.2×10^{-2}(55K)	1.4×10^{-1}(60K)* 3.6×10^{-1}(63K)*
Inversion level pressure	~100mbar	~100mbar*
Temperature at 1μbar	95-154K	140K*
Exospheric temperature	200-300K	?

---

* Thermal structure for Neptune from Tokunaga, et al. (1983)[3], Orton, et al. (1984)[27], Gillet and Rieke (1977)[28], and Sicardy, et al. (1983)[29].

VERTICAL MIXING AND SOLAR FLUX

Considering that Uranus does not possess an internal heat source, that it receives only 1/400 of the solar energy incident at 1AU, and the fact that its globally averaged auroral energy input is small would imply a relatively sluggish turbulence in its atmosphere. On the other hand, little is known about the relation of these factors to the homopause value of the eddy diffusion coefficient, K_h. In the present calculations, therefore, a value similar to that at the homopause of Jupiter and Earth, 10^6 cm^2 s^{-1}, is considered to be nominal and effects of lower value are discussed. Presented in Table 5 is a comparison between the values of K_h for the various planets. The solar flux at Uranus is appropriately reduced, by approximately a factor of 400 from that at 1AU, to account for its 20AU distance from the Sun at the time of the Voyager encounter. Since the Voyager encounter is to occur in 1986, which is the time of the solar minimum, the fluxes measured at the last solar cycle minimum (Hinteregger, 1981)[30] are used.

PHOTOCHEMISTRY

As discussed earlier, only CH_4 can undergo photolysis on Uranus and Neptune. Subsequent to the CH_4 photodecomposition, the products C_2H_2, C_2H_4 and C_2H_6 can also be photolyzed. Due to the relatively cold temperatures in the photochemical regime, however, these latter constituents are likely to condense over an extensive height range. We show in Fig. 3 chemical scheme for the CH_4 photolysis. The pathways for the CH_4-photochemistry are explained in Table 6.

A set of coupled partial differential equations is solved to determine the distribution of CH_4 and its principal photolysis products, C_2H_2, C_2H_6 and C_2H_4. Both molecular and eddy diffusion are taken into consideration, and all species are initially assumed to be in the gaseous phase (with CH_4 mixing ratio at the lower boundary, 100mb, fixed by its saturation vapor pressure). Fig. 4 shows the distribution of CH_4 for the various scenarios of eddy diffusion coefficient, tropopause temperature, and the latitude.

Table 5

Eddy Diffusion Coefficient and Temperature (from Atreya, *et al.*, 1984)[8]

	K_h ($cm^2\ s^{-1}$)	Density at Homopause[1] (cm^{-3})	Altitude of Homopause[2] (km)	Atmospheric Pressure at Homopause (bars)	Photolysis Region Temperature[3] (K)	References
Uranus	10^4-10^6 expected	?	?	10^{-6} to 10^{-7}	~100	Atreya & Ponthieu (1983);[11] French, *et al.* (1983)[4]
Saturn	$1.7(+4.3,-1.0)\times10^8$ $8.0(+4.0,-4.0)\times10^7$	1.2×10^{11}	1110	4×10^{-9}	140	Atreya (1982);[31] Sandel, *et al.* (1982)[32]
Jupiter	$1.4(+0.8,-0.7)\times10^6$	1.4×10^{13}	440	10^{-6}	170	Atreya, *et al.* (1981);[6] McConnell, *et al.* (1982)[33]
Earth	10^6	10^{13}	100	3×10^{-7}		Hunten (1975)[34]

---

[1] Density: H_2 for Jupiter, Saturn and Uranus; atmospheric for others. Densities at the homopause correspond to the central values of K_h.

[2] Altitude: For Jupiter and Saturn, the altitudes are above the 1-bar atmospheric pressure level in the equatorial region; some previous publications had the cloud-tops or the 10^{19} cm^{-3} level as the reference. For Earth, the altitudes are above the surface.

[3] Temperature: Average temperature in the middle atmosphere photochemical regime is given. See text for temperature profile near the NH_3 and CH_4 clouds.

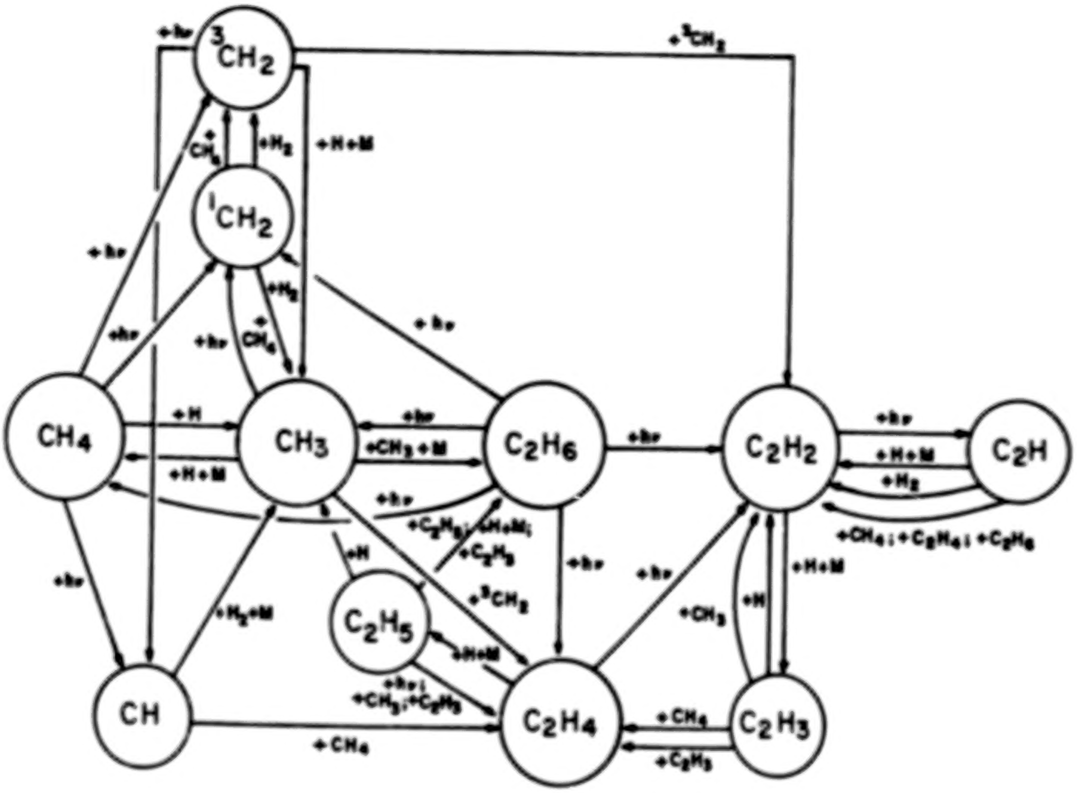
+hν
$^3CH_2$
$+^3CH_2$
+CH_4
+H_2
+H+M
$^1CH_2$
+hν
+hν
+hν
+H_2
+CH_4
+hν
CH_4
+H
CH_3
+H+M
+hν
+CH_3+M
C_2H_6
+hν
C_2H_2
+hν
+H+M
+H_2
C_2H
+CH_4; +C_2H_4; +C_2H_6
+hν
+C_2H_3; +H+M;
+C_2H_5
+H
+hν
+hν
+H+M
+hν
+H_2+M
C_2H_5
+$^3CH_2$
+CH_3
+H
+H+M
+hν;
+CH_3; +C_2H_5
CH
C_2H_4
+CH_4
C_2H_3
+CH_4
+C_2H_3

Figure 3. Photochemical scheme for CH_4 (from Atreya and Romani, 1984).[26]

Table 6

CH_4 Photochemistry (adapted from Gladstone, 1982)[35]

1. CH_4 is photolyzed in the upper layers (max. J at Ly α) and C_2H_4 is eventually produced (10% of all photons by CH_4 produce C_2H_4)

		Reaction Number
	$CH_4 + h\nu \longrightarrow {}^3CH_2 + 2H$	(R6.1)
	$CH_4 + h\nu \longrightarrow {}^1CH_2 + H_2$	(R6.2)
	${}^1CH_2 + H_2 \longrightarrow CH_3 + H$	(R6.3)
	$CH_3 + {}^3CH_2 \longrightarrow C_2H_4 + H$	(R6.4)
Net	$2(CH_4 + h\nu) \longrightarrow C_2H_4 + 4H$	(R6.5)
And		
	$CH_4 + h\nu \longrightarrow CH + H + H_2$	(R6.6)
	$CH + CH_4 \longrightarrow C_2H_4 + H$	(R6.7)
Net	$2CH_4 + h\nu \longrightarrow C_2H_4 + 2H + H_2$	(R6.8)

2. C_2H_4 is quickly lost by photolysis to C_2H_2, or by recycling to CH_4.

	$C_2H_4 + h\nu \longrightarrow C_2H_2 + H_2$	(R6.9)
	$C_2H_4 + h\nu \longrightarrow C_2H_2 + 2H$	(R6.10)
Net	$2(C_2H_4 + h\nu) \longrightarrow 2C_2H_2 + H_2 + 2H$	(R6.11)
And		
	$C_2H_4 + H + M \longrightarrow C_2H_5 + M$	(R6.12)
	$C_2H_5 + H \longrightarrow 2CH_3$	(R6.13)
	$2(CH_3 + H + M \longrightarrow CH_4 + M)$	(R6.14)
Net	$C_2H_4 + 4H \longrightarrow 2CH_4$	(R6.15)

3. Dissociation of CH_4 also leads to the formation of C_2H_6 (20% of all photons absorbed by CH_4 produce C_2H_6)

$2(CH_4 + h\nu \longrightarrow {}^1CH_2 + H_2)$ (R6.16)
$2({}^1CH_2 + H_2 \longrightarrow CH_3 + H)$ (R6.17)
$2CH_3 + M \longrightarrow C_2H_6 + M$ (R6.18)

Net $2(CH_4 + h\nu \longrightarrow C_2H_6 + H)$

4. C_2H_6 is also lost by conversion to C_2H_2 or by recycling to CH_4, as is the case with C_2H_4

$C_2H_6 + h\nu \longrightarrow C_2H_2 + 2H_2$ (R6.20)
$C_2H_6 + h\nu \longrightarrow C_2H_4 + H_2$ (R6.21)
$C_2H_6 + h\nu \longrightarrow C_2H_4 + 2H$ (R6.22)

Followed by
$C_2H_4 + h\nu \longrightarrow C_2H_2 + H_2$ (R6.23)
$C_2H_4 + h\nu \longrightarrow C_2H_2 + 2H$ (R6.24)

Net $3C_2H_6 + h\nu \longrightarrow 3(C_2H_2) + 4H_2 + 4H$ (R6.25)
And

$C_2H_6 + h\nu \longrightarrow C_2H_4 + H_2$ (R6.26)
$\longrightarrow C_2H_4 + 2H$

Followed by
$C_2H_4 \longrightarrow CH_4$ Conversion, (R6.15) (R6.27)

$J_{C_2H_6} \leq 1/10\ J_{C_2H_4}$ so that C_2H_6 is stable in the upper atmosphere and is lost by diffusion to the lower altitudes.

5. Once produced in the above manner, C_2H_2 is highly stable; it undergoes the following reactions

$H + C_2H_2 + M \longrightarrow C_2H_3 + M$ (R6.28)
$C_2H_3 + H \longrightarrow C_2H_2 + H_2$ (R6.29)

Net $2H \longrightarrow H_2$ (R6.30)
And

$$\begin{array}{llcll} 6. & C_2H_2 + h\nu & \longrightarrow & C_2H + H & (R6.31) \\ & C_2H + H_2 & \longrightarrow & C_2H_2 + H & (R6.32) \\ \hline \text{Net} & H_2 & \longrightarrow & 2H & (R6.33) \end{array}$$

C_2H_2 is therefore long-lived and its concentration builds up until its production is balanced by diffusive flux to the lower boundary. In the lower atmosphere also C_2H_2 is photolyzed and immediately recycled in the upper layer.

$$\begin{array}{llcll} & C_2H_2 + h\nu & \longrightarrow & C_2H + H & (R6.34) \\ & C_2H + CH_4 & \longrightarrow & C_2H_2 + CH_3 & (R6.35) \\ \hline \text{Net} & CH_4 + h\nu & \longrightarrow & CH_3 + H & (R6.36) \end{array}$$

This is an indirect manner in which CH_4 can be 'dissociated' to give $CH_3 + H$. The reaction $CH_4 + h\nu \rightarrow CH_3 + H$ is not permitted (Slanger, 1982).[36] CH_3 so produced, however, is either recycled to methane ($CH_3 + H + M \rightarrow CH_4 + M$) 65% of the time, or converted to ethane ($CH_3 + CH_3 + M \rightarrow C_2H_6 + M$) 35% of the time. Finally, higher order hydrocarbons, such as propane (C_3H_8), methylacetylene (C_3H_4), butane (C_4H_{10}), etc. are formed by reactions of the following nature:

$$\begin{array}{ll} C_2H_5 + CH_3 + M \rightarrow C_3H_8 + M & (R6.37) \\ C_3H_7 + CH_3 + M \rightarrow C_4H_{10} + M & (R6.38) \end{array}$$

The heavier hydrocarbons diffuse down, some condense and snow out of the atmosphere. Once in the high pressure, high temperature interior of Jupiter and Saturn, they undergo pyrolysis and are decomposed to give CH_4. Methane is thus recycled, and it convects to the upper atmosphere.

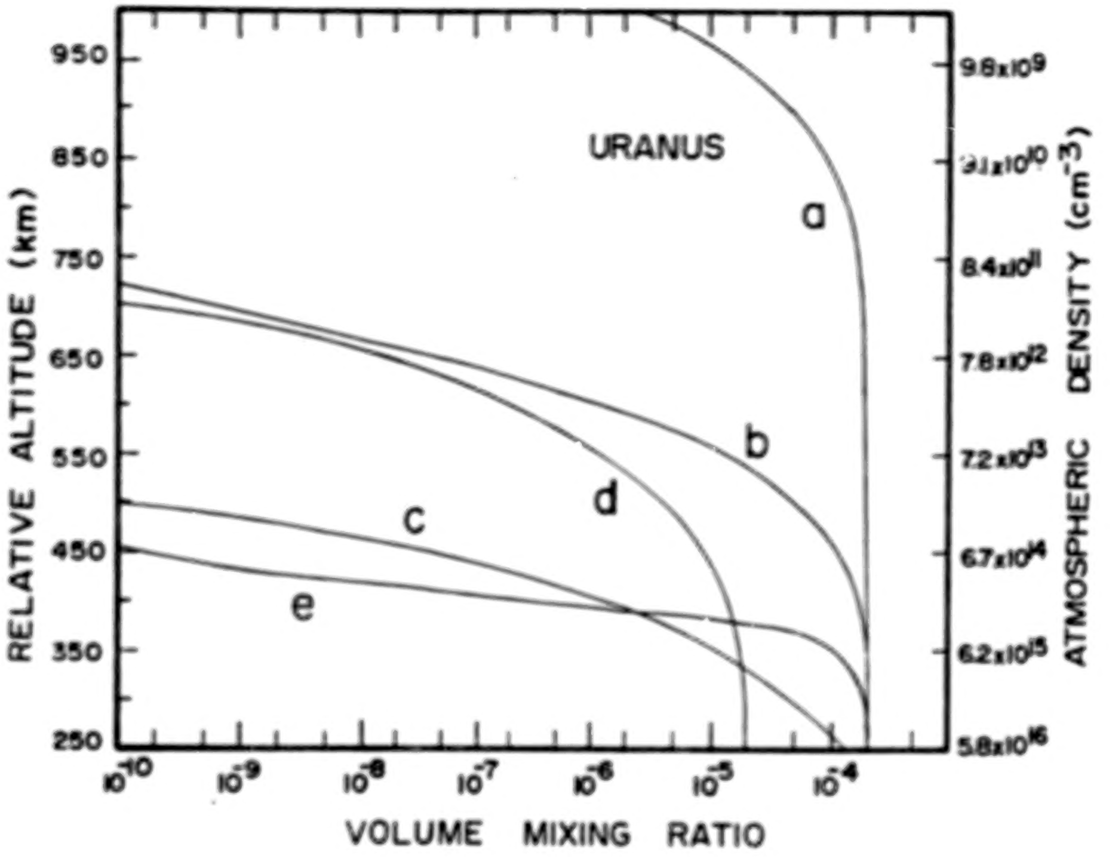

Figure 4. Variation of CH_4 volume mixing ratio on Uranus with: (i) K_h: curves 'a', 'b', and 'c', where K_h = $1.3x10^{10}$ cm^2 s^{-1}, $1.4x10^6$ cm^2 s^{-1}, and $1.3x10^4$ cm^2 s^{-1} respectively. Curves 'a', 'b', and 'c' have inversion temperature, T_{inv}=55K (P=100 mb; $CH_4/H_2=2.4x10^{-4}$), photolysis region temperature T_{photo}=95K, and latitude 2°. Curve 'b' is termed as the 'nominal' case; (ii) T_{inv}: curve 'd', where T_{inv}=50K so that $[CH_4]/[H_2]=2.2x10^{-5}$ at the 100 mb level. Other parameters are same as in curve 'b'; and (iii) latitude: curve 'e', where the latitude is 82° which represents the sub-solar point; the North-pole is pointing almost directly at the Sun in this geometry, and other parameters are same as in curve 'b'. The atmospheric densities shown on the right ordinate correspond to the altitudes on the left. Altitudes are referenced to the 100 mb (inversion layer) level. Add approximately 100 km to obtain altitudes above the 1-bar level (after Atreya and Ponthieu, 1983).[11]

The curves 'a', 'b' and 'c' show the effect of changing K, which is assumed to vary inversely as the square root of the atmospheric number density. Curve 'b' is for the nominal value of K_h ($\sim 10^6$ cm^2 s^{-1}), while 'a' ($K_h \simeq 10^{10}$ cm^2 s^{-1}), and 'c' ($K_h \simeq 10^4$ cm^2 s^{-1}) represent the two extremes. Neither of the extremes have ever been encountered in a planetary atmosphere. The curves 'd' and 'e' show respectively variations of the nominal case with the tropopause temperature and the latitude. Reducing the inversion level temperature to 50K from 55K (curve 'd') has little effect on the CH_4 distribution in the photochemical regime ($z \geq 550$ km), while below it, the CH_4 mixing ratio is dictated by its lower saturation vapor pressure. A much more dramatic effect is seen if the latitude is changed from equatorial to 82°N (comparing curve 'e' to curve 'b'). This is due to the availability of substantially greater solar flux along with a reduced mass path to attenuate it, in the high laitudes. This gives rise to the photolysis of CH_4 at greater depths in a narrow height region. If the photolysis region temperature were changed to 154K from 95K, one finds that the CH_4 mixing ratio decreases by a factor of 2 at the atmospheric density level of 6×10^{15} cm^{-3}, and by a factor of 10 at the 3×10^{14} cm^{-3} density level (Atreya and Ponthieu, 1983).[11]

The calculated distributions of CH_4, C_2H_6 and C_2H_6 for the nominal case (T_{inv} = 55K; T_{photo} = 95K; K_h = 10^6 cm^2 s^{-1}) are shown in Fig. 5. These are assumed to be gas-phase distributions. The mixing ratios near the 100 mbar (z=0 km) are quite similar to the values at 350 km in this figure.

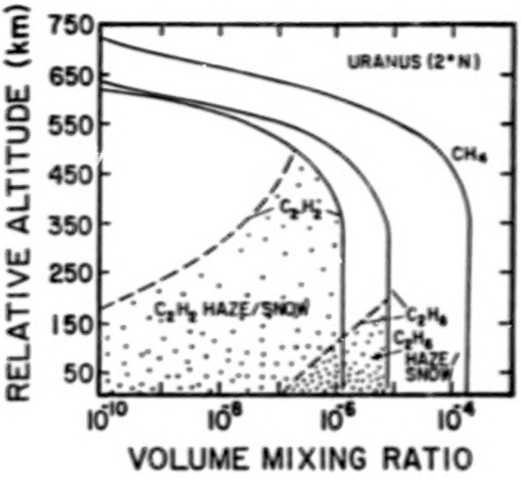

Figure 5. Volume mixing ratios of CH_4, C_2H_2 and C_2H_6 as a function of altitude (left ordinate) for the 'nominal' case. Here, eddy mixing coefficient at the tropopause, $K_o=10^3$ cm^2 s^{-1}; at the homopause, $K_h=1.4\times10^6$ cm^2 s^{-1}; temperature at the inversion level, $T_{inv}=55K$, in the photolysis regime, $T_{photo}=95K$; latitiude=2°; and solar minimum flux. Broken line curves represent saturation vapor mixing ratios corresponding to the thermal structure in Fig. 1. Altitude scale is same as in Fig. 4.

A comparison of the calculated and the saturation vapor mixing ratios of C_2H_2, C_2H_6 and CH_4 at the 100 mb (55K) level given in Table 7 is quite illustrative of the hydrocarbon condensation scenario on Uranus.

Table 7

Partial and Saturation Vapor Pressures (mbar) of C_nH_m at the 100 mbar level on Uranus

	Partial(calculated)	Saturated
CH_4	1 (Wallace, 1980)^1	2×10^{-2} (55K)
	7×10^{-2} (solar)	2×10^{-3} (50K)
C_2H_6	$\sim10^{-3}$	$\sim10^{-5}$ (55K)
		$\sim10^{-6}$ (50K)
C_2H_2	$\sim10^{-4}$	$<10^{-12}$ (50 or 55K)

A comparison of the partial and saturated vapor pressures in Table 7 reveals that condensation of all major photolysis products is a distinct possibility near the inversion layer of Uranus. The calculated C_2H_4 abundance is found to be too low for it to condense anywhere on Uranus. Relatively high concentration CH_4 clouds are expected to be formed around the 1 bar level, if the CH_4 is indeed as enhanced over its solar value as suggested by Wallace (1980).[1] An extensive regime of C_2H_2 condensation is expected in the equatorial region of Uranus. The C_2H_6 condensation, however, is limited to within 100 km above the temeprature inversion. A warmer inversion temperature at Neptune would virtually render C_2H_6 condensation improbable, although C_2H_2 condensation is still a good possibility. Indeed, C_2H_6 has been detected in the IR spectrum at 12.2 μm at Neptune, but not Uranus (Macy and Sinton, 1977).[24] There is some indication of the C_2H_2 detection on Uranus at wavelengths greater than 1600Å in the IUE spectrum (T. Encrenaz, personal comm., 1983; J. Caldwell, this book). It is also found that the C_2H_2 abundance has 'decreased' from 1979 to 1983 on Uranus. Most IUE spectra were taken using the large aperture, 10"x20". These results, to the first order, appear to be consistent with the models just presented. First, in order to be able to detect C_2H_2 in the u.v., its vertical optical depth should approach unity around 1600Å. In the nominal equatorial model of C_2H_2, Fig. 5, this occurs around 330 km where the temperature is approximately 70K. The corresponding C_2H_2 vapor density at 70K is $\sim 10^{10}$ cm^{-3}, i.e. very close to the value needed for $\tau_{C_2H_2} = 1$. Thus detection of C_2H_2 in the equatorial region of Uranus at wavelengths ~1600Å is feasible. The IUE observation of the apparent variation in the C_2H_2

abundance with time is equivalent to seeing a latitudinal change since the N-pole is beginning to point toward the Sun. We can therefore turn to the 82° latitude case, Fig. 4, curve 'e', and find that the unit optical depth in CH_4 (or C_2H_2) would occur much deeper in the atmosphere, assuming that the calculated C_2H_2 is 'all' in the gas phase. Actually, it is found to occur, for C_2H_2, at an altitude where the temperature is ~50K.

The corresponding C_2H_2 vapor density (at ~50K; is much less than 10^{10} cm^{-3}, and thus much smaller, if any C_2H_2, can be detected at the 82° latitude.

The situation with IUE observations is somewhere in between the two extremes (equatorial and polar) just discussed. However, the conclusion remains unaltered.

Returning to the analysis of the CH_4 distributions in the equatorial and polar regions (curves 'b' and 'e', Fig. 4) of Uranus, one discovers possibility of some interesting phenomena. The corresponding C_2H_2 and C_2H_6 distributions also show similar behavior, i.e. a much compressed distribution in the polar region. This implies that the condensation regime (mostly of C_2H_2, and some C_2H_6) in the polar region would be much narrower, raising the possibility that the sunlight would be able to penetrate deeper. This means that as the N-pole begins to point toward the Sun, the sunlight would be able to penetrate deeper and deeper, and the appearance of Uranus should become brighter and brighter due to both scattering off the relatively thick CH_4-ice cloud, and the haze of C_2H_2 and C_2H_6. In fact, ground-based imaging observations by B. A. Smith (personal comm., 1983) done over the last decade, seem to bear this out. The atmospheric haze, or the CH_4 clouds do not necessarily preclude

BEST COPY AVAILABLE

6800Å photons from penetrating to several bars of atmospheric pressure. Seeing to any depth is a function of size and number distribution of the particles and their rate of falling out of the cloud.

Although thorough analysis is lacking, it can be stated with some confidence that the photochemical models for Neptune would reveal a behavior nearly opposite to that of Uranus. That is to say, the polar regions would be 'more' cloudy and hazy than the equatorial ones than the corresponding regions on Uranus. This is on account of Neptune's equator-orbit inclinia-tion. Also, UV detection of C_2H_2 at Neptune should be possible with Voyager/UVS, if not with IUE.

In the CH_4 photochemistry, hydrogen atoms are also produced. Another major source of the H-atoms is the downward flux from the ionosphere. The latter results from the photodissociation and dissociative photoionization of H_2 (see ionospheric section). A chemical scheme for the H-production in the ionosphere is shown in Fig. 6. The pathway involving He contributes less than 10% to the total H abundance. The abundance of H-atoms above the level of unit optical depth in methane ($\tau_{CH_4}=1$) is given in Table 8.

Table 8

Uranus [H] Abundances (cm^{-2}) above $\tau_{CH_4}=1$

Equator	Mid Lat	High Lat (82°)
1.5×10^{15}	3.0×10^{15}	2.3×10^{16}
$\tau_{CH_4}=1$ Level at N(cm^{-3})		
4.3×10^{14}	2.6×10^{15}	3.5×10^{15}

$K_h = 10^6\ cm^2\ s^{-1}$; $T_{trop} = 55K$; $T_{photo} = 95K$

K = atmospheric density

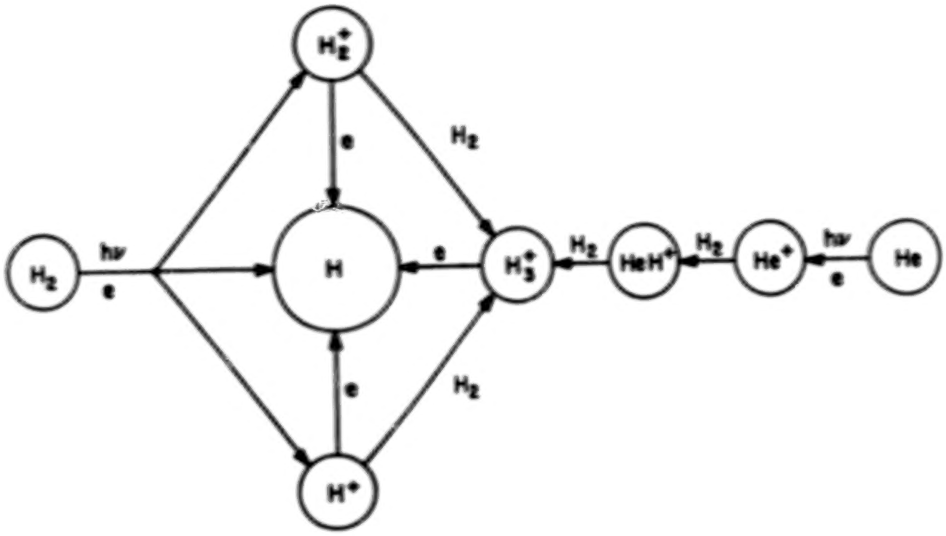
H_2^+
e
H_2
H_2
hν
e
H
e
H_3^+
H_2
HeH^+
H_2
He^+
hν
e
He
e
H_2
H^+

Figure 6. Photochemical scheme of atomic hydrogen

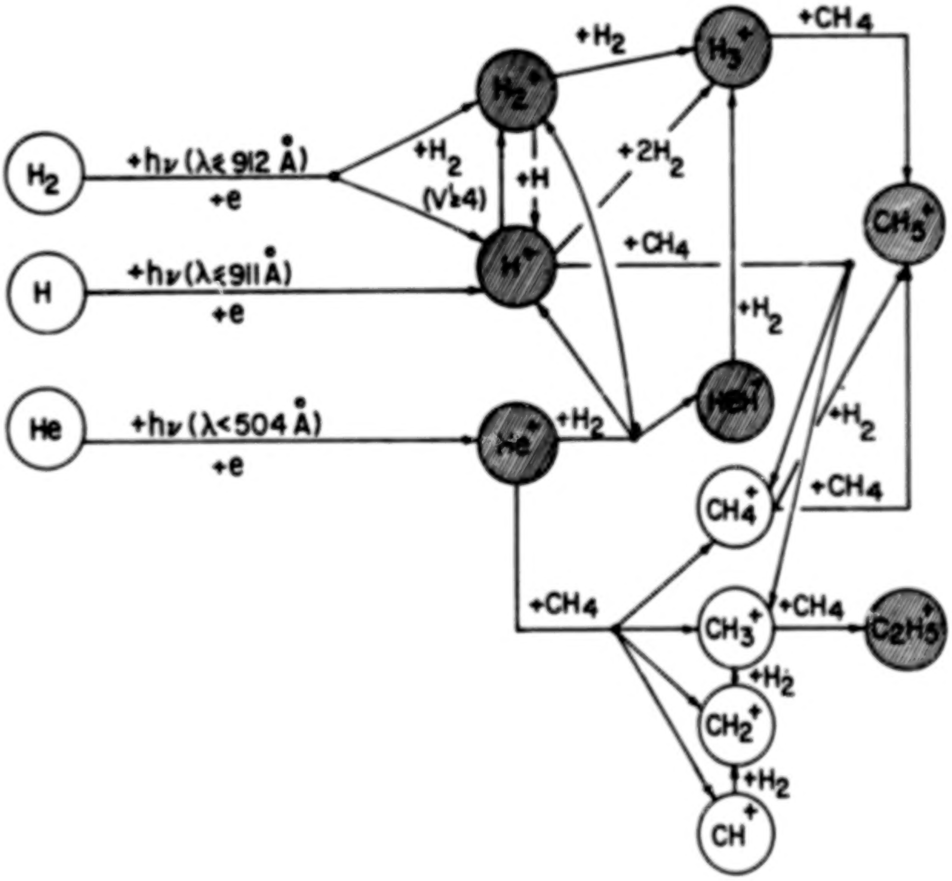
$+H_2$
H_3^+
$+CH_4$
H_2^+
H_2
$+h\nu(\lambda \leq 912\,Å)$
$+e$
$+H_2$
$(V \geq 4)$
$+H$
$+2H_2$
CH_5^+
$+CH_4$
H
$+h\nu(\lambda \leq 911\,Å)$
$+e$
H^+
$+H_2$
He
$+h\nu(\lambda < 504\,Å)$
$+e$
He^+
$+H_2$
HeH^+
$+H_2$
CH_4^+
$+CH_4$
$+CH_4$
CH_3^+
$+CH_4$
$C_2H_5^+$
$+H_2$
CH_2^+
$+H_2$
CH^+

Figure 7. Ionospheric scheme (Atreya and Donahue, 1983)[37]

The entries include the ionospheric flux of hydrogen atoms. The maximum H-abundance, 2.3×10^{16} cm^{-2}, occurs for the situation in which the N-pole is pointing at the Sun (this is the orientation Uranus will have at the time of Voyager 2 encounter in 1986, and is close to the present orientation). In order to account for the 400-800R of Lyα observed by IUE on the basis of resonance scattering of the solar Lyα photons, one needs on the order of 10^{17} to 10^{18} cm^{-2} (Clarke, 1982)[9] column abundance of H. The calculated H-abundance is nowhere close to the value required for interpreting the Lyα observations. The discrepancy between the calculated and the required H-abundance is perhaps even greater since the observations represent at least hemispherically averaged Lyα as the slit size is far greater than the angular dimension of Uranus. The implication is then that the source of Lyα and H-atoms may lie in something other than resonance scattering and photochemistry respectively. Because of the pole-on magnetospheric geometry, there is a strong possibility of solar wind particle deposition in the high latitudes, causing both an aurora and particle dissociation of H_2. Additional H-atoms can be produced by the latter process, and resonance scattering of the solar Lyα photon could still account for the observed Lyα. Unit optical depth for Rayleigh scattering of Lyα by H_2 occurs around 10^{24} cm^{-2} H_2 column abundance. This is well below the level for $\tau=1$ at Lyα for CH_4. Therefore, Rayleigh scattering cannot account for the observed Lyα emission.

IONOSPHERE

Except for the relatively high latitudes where particle precipitation may occur, the ionospheric profile at Uranus is expected to be dominated by the solar EUV ionization of H_2, H, and He. The chemical scheme for the major ion production, atom/molecule-ion interchange, and ion loss is shown in Fig. 7. Further details are given in Atreya and Ponthieu (1983)[11]; Atreya and Donahue (1975a[37], 1975b[39], 1976[40]) and Atreya, et al. (1984)[8]. The terminal ion in the topside is expected to be H^+, although the possibility of a molecular ion, such as H_3^+, in the auroral latitudes exists due to reaction of H^+ with vibrationally excited H_2. In the middle ionosphere H^+ and H_3^+ mixture is likely, while the lower ionosphere experiences the emergence of low concentrations of several hydrocarbon ions. All terminal ions are presumed to be eventually lost by electronic recombination. The Voyager radio occultation measurements of the ionosphere are planned near the terminator at latitudes of 2°N (entry) and 6°N (exit) (L. Tyler and D. Hinson, personal comm., 1983). Because of the 98° inclination of the Uranus equator to its orbit, all latitudes northward of 8°N will be in perpetual daylight, while latitudes southward of 8°S will be in perpetual darkness. Latitudes between 8°N and 8°S will have a 'diurnal' cycle -- which is a useful information for choosing the solar flux, but does not cause a diurnal cycle in the ionosphere. This is because the major ion, H^+, has a lifetime of $\sim 10^7$ s, which is considerably greater than the length of a Uranian night. On the other hand, if the topside ion were converted to a molecular ion, as discussed earlier, the lifetime of the terminal ion would be extremely short. Again, this possibility applies only to the auroral latitudes.

The ionospheric structure calculated for the latitudes of Voyager radio occultations is shown in Fig. 8. The peak electron concentration for the entry and exit occultations is calculated to be $\sim 2\times10^4$ cm^{-3}.

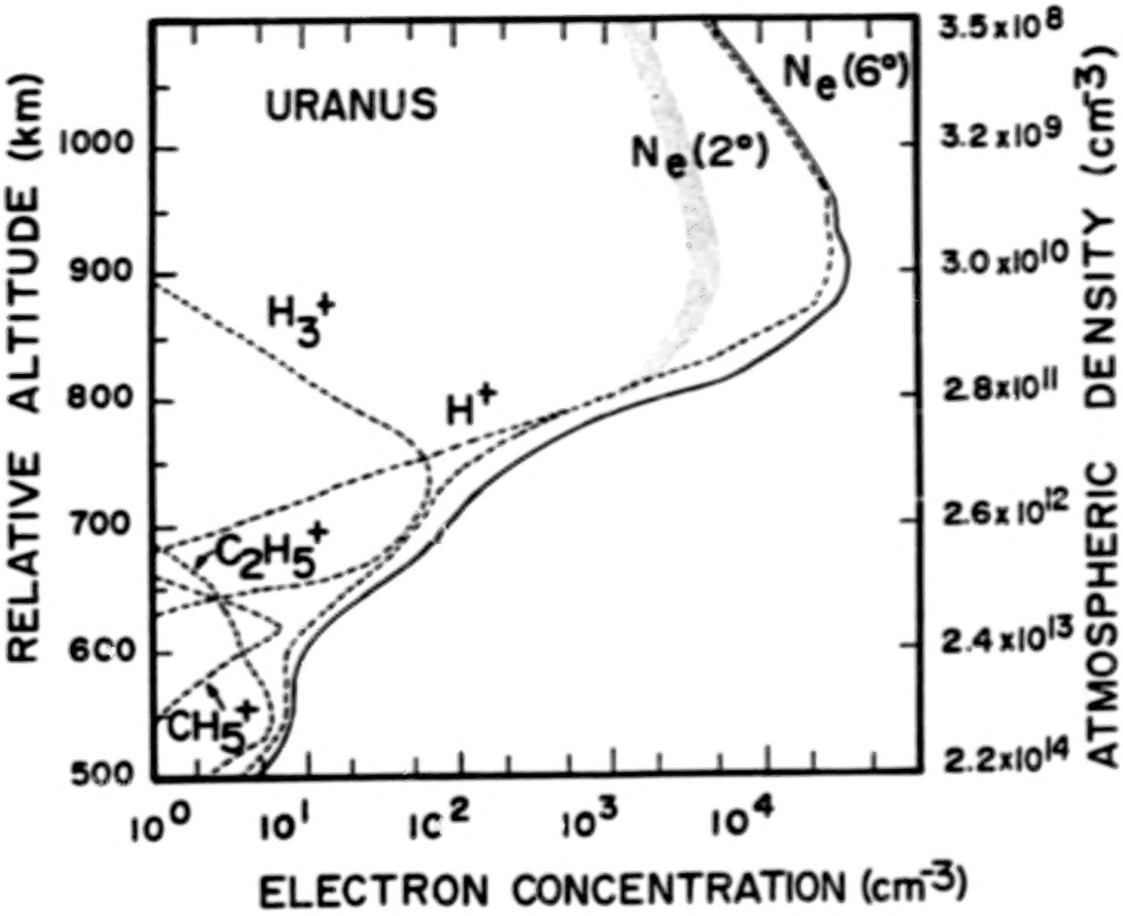

Figure 8. Photochemical equilibrium electron and ion concentrations for the Voyager/Uranus radio occultation points at 2°N and 6°N. The atmospheric model is same as in Figure 4 ('nominal' case). Hydrocarbon ion concentrations are shown only for the 2°N case (from Atreya and Ponthieu, 1983).[11] The peak electron concentration is, in fact an upper limit. The effect of plasma diffusion, ion drifts, and thermospheric dynamics is to reduce the peak concentration to 3000 to 5000 electrons cm^{-3}, as shown by the shaded area which also takes into account possible 200-300K exospheric temperature.

It should be emphasized that it is the photochemical equilibrium peak, and represents an upper limit to the peak concentration. The actual electron concentration at the peak is expected to be lower due to effects of ion drift, plasma diffusion and thermospheric dynamics, in general. Experience with Voyager/Jupiter and Saturn would indicate peak electron concentrations at Uranus to be $(3\text{-}5)\times10^{3}$ cm^{-3}, i.e. about a factor of 5 smaller than the chemical equilibrium peak. The hydrocarbon ion concentrations are small -- less than 100 cm^{-3}. The topside plasma scale height, i.e. above ~900 km could be greater by a factor of 2 to 3 than shown in Fig. 8, if the exospheric temperature in the equatorial region turned out to be 200-300K, as discussed previously. A very crude calculation of the auroral region ionosphere at Uranus is shown in Fig. 9. The power input is assumed to be 10^{11}W, principally through the deposition of energetic electrons.

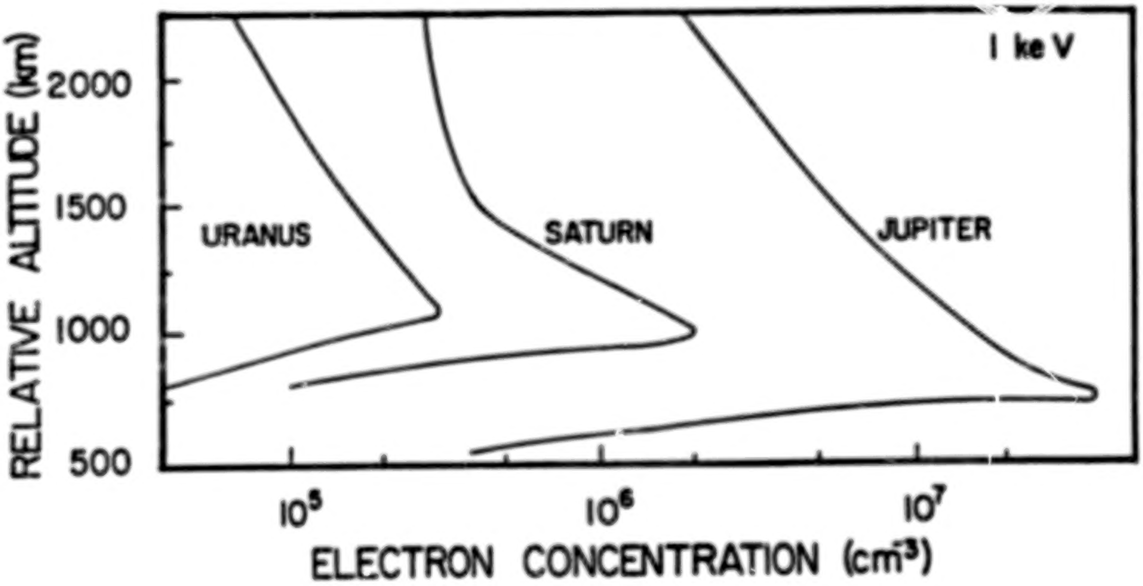

Figure 9. Calculated electron concentration profiles due to impact of 1 keV electrons in the polar regions of Jupiter, Saturn and Uranus. Altitudes are above the 1-bar level.

BEST COPY AVAILABLE

Since virtually nothing is known with certainty about the magnetic field strength, and the energy and number flux of the incoming particles, one should regard this profile to be correct to no more than a factor of 10. For the sake of illustration, the conductivities in the ionospheres of Jupiter, Saturn and Uranus are given in Table 9.

Table 9

Height Integrated Pedersen Conductivities

		Jupiter	Saturn	Uranus	
	σ_P(mho)*	0.02-10	20-58	0.5	5-10(Auroral)
Assumptions	Peak N_e (cm^{-3})	10^6	10^5	5×10^3	$5\times10^4-10^5$
	B (Gauss)	10	0.2	1	1

*1 mho m^{-1} = 9×10^9 s^{-1}

At Neptune, one can only make some speculative guesses regarding the ionospheric structure. I would not venture to make predictions about the auroral (?) region. However, in the equatorial to midlatitude regions, the solar EUV ionization would still dominate. One can expect peak electron concentrations between 1000 to 3000 cm^{-3} because of approximately 1/2 rate of ion production at Neptune compared to Uranus, and due to its 29° equator-orbit inclination. The thin, dark rings of Uranus are not expected to modify the ionosphere by any ring-shadowing effect. Material ejected from Uranus, perhaps on account of energetic particle sputtering could conceivably diffuse into the Uranus atmosphere. This cannot, however have significant influence on the atmospheric and ionospheric structure. Even in the case of Saturn whose atmosphere has a much greater potential of receiving material from its vast ring system, no clear indication of atmospheric/ionospheric modification has been found.

CONCLUDING REMARKS

Theoretical considerations indicate that extensive region of C_2H_2 and C_2H_6 haze should exist in the equatorial region of Uranus. The extent of the haze should be substantially reduced in the polar regions, perhaps giving them a brighter appearance. The latitudinal distribution of the haze should show opposite behavior at Neptune. The calculations need to be extended to take into consideration (i) actual temperature structure in the middle atmosphere, (ii) irreversible pseudo-adiabatic processes in which part of the condensate drops out as snow from the cloud. The ionospheric calculations indicate that the peak electron concentrations in the equatorial region should be around 3000-5000 cm^{-3} at Uranus, and 1000-3000 cm^{-3} at Neptune, the upper limit at Uranus is 2×10^4 cm^{-3}. Exospheric temperatures on the order of 200-300K are possible. The aeronomical calculations and results presented in this paper are preliminary, and substantial improvements are needed before one truly understands the upper atmospheric processes at Uranus and Neptune. Certain fundamental measurements can help; they are listed below.

(1) Thermal structure -- from troposphere through exosphere (possible techniques Voyager/RSS, UVS, IR)

(2) Vertical Eddy Diffusion -- Voyager/UVS

(3) Lyman-alpha airglow and aurora 'at' the planet-Voyager/UVS, ISS

(4) Haze/Aerosol distribution -- Voyager/PPS, ISS

(5) NH_3 abundance to the 5-bar level -- Voyager/RSS

(6) He/H_2 ratio -- Voyager/IRIS, RSS

(7) Tropospheric and upper atmospheric composition, in general -- Voyager/IRIS(?), UVS

(8) Internal Heat -- Voyager/IRIS

(9) Planetary Magnetic Field -- Voyager/Magnetometers

(10) Magnetospheric Interaction with the Atmosphere -- Voyager/Particle and Fields and PRA

(11) Ionospheric Structure - RSS

ACKNOWLEDGMENT

This work was supported by the NASA Planetary Atmospheres Program and the NASA/JPL Voyager Project.

REFERENCES

1. Wallace L (1980) The structure of the Uranus atmosphere. Icarus 43:231-259.

2. Courtin R, Gautier D, Lacombe A (1978) On the thermal structure of Uranus from infrared measurements. Astron Astrophys 63:97-101.

3. Tokunaga AT, Orton GS, Caldwell J (1983) New observational constraints on the temperature inversions of Uranus and Neptune. Icarus 530:141-146.
4. French RG, Elliot JL, Dunham EW, Allen DA, Elias JH, Frogel JA, Liller W (1983) The thermal structure and energy balance of the Uranus upper atmosphere. Icarus 53:399-414.
5. Appleby J (1980) Ph.D. Thesis. SUNY at Stony Brook, New York.
6. Atreya SK, Donahue TM, Festou MC (1981) Jupiter: structure and composition of the upper atmosphere. Astrophys J Lett 247:43-47.
7. Festou MC, Atreya SK (1982) Voyager ultraviolet stellar occultation measurements of the composition and thermal profiles of the Saturnian upper atmosphere. Geophys Res Lett 9:1147-1150.
8. Atreya SK, Waite JH Jr, Donahue TM, Nagy AF, McConnell JC (1984) Theory, measurements and models of the upper atmosphere and ionosphere of Saturn. In: Gehrels T (ed) Saturn. University of Arizona Press.
9. Clarke JT (1982) Detection of auroral H Lyα emission from Uranus. Astrophys J 263:105.
10. Durrance ST, Moos HW (1982) Intense Lyman α emission from Uranus. Nature, to be published.
11. Atreya SK, Ponthieu JJ (1983) Photolysis of methane and the ionosphere of Uranus. Planet Space Sci 33:939-944.
12. Trafton LM (1976) The aerosol distribution in Uranus' atmosphere: interpretation of the hydrogen spectrum. Astrophys J 207:1007-1024.
13. Macy WW Jr, Smith WM (1978) Detection of HD on Saturn and Uranus, and the D/H ratio. Astrophys J 222:L73-L75.

14. Trafton LM, Ramsay DA (1980) The D/H ratio in the atmosphere of Uranus: detection of the $R_5(1)$ line of HD. Icarus 41:423-429.

15. Trafton LM (1978) On the deuterium-to-hydrogen ratio in the atmosphere of Uranus. Astrophys J 222:740-743.

16. Lutz BL, Owen T (1974) The search for HD in the spectrum of Uranus: an upper limit to [D/H]. Astrophys J 190:731-734.

17. Gulkis S, Janssen MA, Olsen ET (1978) Evidence for the detection of ammonia in the Uranus atmosphere. Icarus 34:10-19.

18. Gulkis S, Olsen ET, Klein JM, Thompson TJ (1983) Uranus: variability of the microwave spectrum. Science 221:453-454.

19. Olsen ET, Gulkis S (1978) A preliminary investigation of Neptune's atmosphere via its microwave continuum emission. Bull Am Astron Soc 10:577.

20. Encrenaz T, Combes M (1978) On the D/C ratio in the atmosphere of Uranus. Bull Am Soc 10:567-577.

21. Fink U, Larson HP (1979) The infrared spectra of Uranus, Neptune and Titan from 0.8 to 2.5 microns. Astrophys J 233:1021-1040.

22. Courtin R, Gautier D, Lacombe A (1979) Indications of supersaturated stratospheric methane on Neptune from its atmospheric thermal profile. Icarus 37:236-248.

23. Joyce RR, Pilcher CB, Cruikshank DP, Morrison D (1977) Evidence for weather on Neptune, I. Astrophys J 214:657-662.

24. Macy WW Jr, Sinton WM (1977) Detection of methane and ethane emission on Neptune but not on Uranus. Astrophys J 218:L79-L81.

25. Fricke KH, Darius J (1982) Proceedings of the Third European Conference. ESA SP-176.

26. Atreya SK, Romani PN (1984) Photochemistry and clouds of Jupiter, Saturn and Uranus. In: Hunt GE (ed) Planetary Meteorology. Cambridge University Press.

27. Orton GS, Tokunaga AT, Caldwell JJ (1984) Physical constraints on the atmospheres of Uranus and Neptune from observations near 10μm. Icarus, to be published.

28. Gillet FC, Rieke GH (1977) 5-10 micron observations of Uranus and Neptune. Astrophys J 218:L141-L144.

29. Sicardy B, Maillard JP, Cruikshank DP (1983) Stratospheric temperature of Neptune from stellar occultation. Bull Am Astron Soc 15:858.

30. Hinteregger HE (1981) Representations of solar EUV fluxes for aeronomical applications. Adv Space Res 1:39-52.

31. Atreya SK (1982) Eddy mixing coefficient on Saturn. Planet and Space Sci 30:849-854.

32. Sandel BR, McConnell JC, Strobel DF (1982) Eddy diffusion at Saturn's homopause. Geophys Res Lett 9:1077-1080.

33. McConnell JC, Holberg JB, Smith GR, Sandel B, Shemansky D, Broadfoot AL (1982) A new look at the ionosphere of Saturn in light of the UVS occultation results. Planet Space Sci 31:151-167.

34. Hunten DM (1975) Vertical transport in atmosphere. In: McCormac BM (ed) Atmosphere of earth and planets. D Reidel, Dordrecht, Netherlands, pp 59-72.

35. Gladstone GR (1982) Radiative transfer and photochemistry in the upper atmosphere of Jupiter. Ph.D. Thesis, California Institute of Technology.

36. Slanger TG (1982) 1216Å photodissociation of H_2O, NH_3 and CH_4. Abstracts, 4th Ann Meeting of Planet Atmos Princ Investigators, Ann Arbor, 21-23 April, pp 129-131.

37. Atreya SK, Donahue TM (1982) The atmosphere and ionosphere of Jupiter. Vistas in Astron 25:315-335.

38. Atreya SK, Donahue TM (1975a) Ionospheric models of Saturn, Uranus and Neptune. Icarus 24:358-362.

39. Atreya SK, Donahue TM (1975b) The role of hydrocarbon in the ionosphere of the outer planets. Icarus 25:335-396.

40. Atreya SK, Donahue TM (1976) Model ionospheres of Jupiter. In Gehrels T (ed) Jupiter. University of Arizona Press, Tucson, pp 304-318.

TEMPERATURE STRUCTURES AND INFRARED-DERIVED PROPERTIES OF THE ATMOSPHERES OF URANUS AND NEPTUNE

Glenn S. Orton and John F. Appleby

M. S. 183-301
Earth and Space Sciences Division
Jet Propulsion Laboratory
California Institute of Technology
4800 Oak Grove Drive
Pasadena, California 91109 USA

Abstract

Temperature structures of Uranus and Neptune are currently derivable from a combination of stellar occultation and thermal radiance observations. The globally-averaged temperatures of Uranus and Neptune appear quite similar in their convective regions, reaching temperatures near 75 K at 1 bar and 150 K near 10 bar. Temperature minima near 200 mbar are also similar, near 53 - 55 K. The temperature in the stratosphere of Neptune rises much more steeply with altitude than for Uranus in the range of 0.1 to 100 mbar. Above this level, near 1 μbar, both atmospheres reach temperatures of 120 - 160 K. The bolometric radiant energy output is equivalent to the output of a blackbody at 58.3 ± 2.0 K for Uranus and 60.3 ± 2.0 for Neptune. These values imply approximate equilibrium with absorbed sunlight for Uranus but an internal energy source 1.9 to 2.6 times the absorbed sunlight for Neptune. The implication of the thermal spectra is that while the bulk composition may be consistent with a solar mixture of H_2 and He, the mixing ratio of CH_4 is probably about 2% in the deep atmosheres of both planets. Observations near 10 μm are also consistent with clouds at the CH_4 condensation level in Uranus. Stratospheric clouds (of CH_4 and other hydrocarbons) are implied for Neptune, with CH_4 transported (convectively) through the cold trap. Such vigorous convection is consistent with the variability of the stratospheric cloud reflectivity, the large internal heat source, and the strongly inhomogeneous visual appearance of the planet.

INTRODUCTION

We are at a notable stage in our acquisition of knowledge about the atmospheres of Uranus and Neptune. A great deal of the quantifiable information we have about these planets, much of it derived from remote sensing data at infrared wavelengths, clearly differentiates them from Jupiter and Saturn as well as from one another. Uranus and Neptune can no longer be viewed as discrete points in a more-or-less continuous variation of properties beginning at

Jupiter and proceeding outward. The planets are both alike and different in distinct, unexpected and often baffling ways.

We believe that we have surpassed the "exploratory" stage decribed not so long ago by Belton[1], particularly in regard to achieving a satisfactory first-order picture of temperature structure. Similarly, work from several different approaches is converging on a rough but self-consistent picture of composition and cloud properties. On the other hand, we are not yet able to quantify all of the properties, such as compositional details, which form the context of a meaningful comparison of atmospheric properties. Such a context is the basis for understanding the origin and evolution of the outer solar system. It also makes possible the generalization of physical theories for processes such as cloud formation, planetary circulation, and climate.

Knowledge of the temperature structure is important for determining the vertical distribution of various physical processes which are taking place in the atmosphere. The need for such information ranges from comparisons, such as those between cloud layers and the temperatures associated with condensation of various gaseous constituents, to sine qua non requirements, such as the retrieval of vertically variable physical properties from thermal emission data.

Remote sensing information on temperature is derived from several sources. One of these is the analysis of stellar radiation occulted by the atmosphere; this has been particularly effective in determining temperatures for the 0.1- through 10-μbar levels of Uranus and Neptune. Other sources of information on temperature structure come from sampling thermal emission emerging from the atmosphere. Infrared data can also provide information on composition and cloud properties. However, these have not yet been explored very thoroughly, largely owing to the weak thermal emission associated with both planets and the often superhuman efforts which sometimes seems to be required to extract meaningful measurements with tolerable noise levels.

This state of affairs will soon change. Even before the Voyager 2 encounters with Uranus and Neptune, the development of new detector and cryogenic technologies and the use of new observational facilities is expected to strengthen the empirical constraints on atmospheric conditions. To some extent this has already taken place since the last major reviews of the atmospheres of these planets[1,2]. We will review these very recent data, along with potential future developments and suggest profitable directions of future efforts.

DATA

Infrared Observations - The wavelength interval between 4.5 µm and 3 mm roughly defines the spectral domain relevant to our discussion here. (These upper and lower wavelength boundaries are not to be construed as meaningful in any sense except that of our own convenience and mutual agreement among the reviewers.) One measure of the primitive state of our globally-averaged characterization of Uranus and Neptune is that nearly all the observations which have been reported between 4.5 µm and 3 mm could be summarized on a single page.

The shortest wavelengths are covered the most sparsely, since most of the near infrared spectra of Uranus and Neptune are overwhelmed by saturated CH_4 absorption bands. One exception is the 5-µm region which has been measured by Gillett and Rieke[3], Macy et al.[4], and most recently by Brown et al.[5], using filtered radiometery (Table 1). Only Brown et al. detected Neptune at this wavelength, and they implied that the brightness variation which they observed was correlated with the periodic variability which they detected in the difference between the 1.25- and 2.2-µm brightnesses. A glance at Table 1 shows that the Brown et al. observations are, in fact, characterized by a higher overall

Table 1

Summary of 5-μm Observations of Uranus and Neptune

Date	Planet	Filter λ; $\Delta\lambda$(μm)	Brightness (W cm^{-2} μm^{-1} ster.$^{-1}$)	Geometric Albedo, P	T_B(K)	Reference
1975, 1976	U	5.0; 1.0	$1.5 \pm 1.0 \times 10^{-9*}$	$0.003 \pm 0.002^*$	133 ± 4	3
1978 June	U	5.2; 0.7	$< 8.2 \pm 3.5 \times 10^{-9*}$	$< 0.019 \pm 0.008^*$	$< 140 \pm 3$	4
1978 June	U	4.8; 0.5	$6.4 \pm 3.4 \times 10^{-10*}$	$0.0015 \pm 0.0008^*$	132 ± 3	4
1980 Aug. 8	U	4.8; 0.5	$7.2 \pm 1.8 \times 10^{-10*}$	0.0018 ± 0.0006	$133 \pm 2^*$	5
1975, 1976	N	5.0; 1.0	$< 5.2 \times 10^{-9}$	$< 0.03^*$	< 141	3
1978 June	N	5.2; 0.7	$< 2.4 \pm 0.9 \times 10^{-8*}$	$< 0.13 \pm 0.05^*$	$< 148 \pm 3$	4
1978 June	N	4.8; 0.5	$< 1.7 \pm 0.8 \times 10^{-9*}$	$< 0.010 \pm 0.004^*$	$< 138 \pm 3$	4
1980 Aug. 8	N	4.8; 0.5	$1.9 \pm 0.4 \times 10^{-9*}$	0.011 ± 0.003	$139 \, ^{+1*}_{-2}$	5
1980 Aug. 9	N	4.8; 0.5	$< 1.4 \times 10^{-9}$ $(3\sigma)^*$	< 0.008	$< 137^*$	5
1980 Aug. 19	N	4.8; 0.5	$1.5 \pm 0.3 \times 10^{-9*}$	0.009 ± 0.003	$137 \, ^{+1*}_{-2}$	5

* derived from planetary radius and solar irradiance values given in Ref. 5

signal-to-noise ratio than the other measurements. The low reflectivity for Uranus was interpreted[4,5] as implying gaseous absorption in this spectral region, but no higher resolution studies have been made to confirm this or to identify the absorbers. Brown et al. further interpreted the lower albedo of Uranus as consistent with the "generally hazier atmosphere" of Neptune, as implied by the spectrum at shorter wavelengths. They interpreted the radiation as reflected sunlight, rather than thermal emission. It is likely that this is the correct interpretation, because the reflectivity requirements are easily met. In comparison, rather high temperatures are required to explain a purely thermal origin.

Indisputable differences between the atmospheres of Uranus and Neptune were first revealed in the 8- to 14-μm spectral observations of Gillett and Rieke[3] and Macy and Sinton[7]. Emission features were apparent in the spectrum of Neptune near 7 μm and near 12 μm, respectively corresponding to the features of methane and ethane also seen in emission in the spectra of Jupiter, Saturn and Titan. Nothing of the kind was remotely apparent for Uranus. In fact, Uranus remained undetected until the recent 10.3- to 12.6-μm observations of Orton et al.[8], who also extended the 12-μm observations of Neptune down to 10.3 μm. Most groups generally assumed that the observed radiation was thermal in origin, with the continuum due to emission from a cloud or from the collision-induced opacity of H_2. Alternatively, Orton et al.[8] suggested that a substantial portion of Uranus' outgoing flux in this region and of Neptune's outgoing flux between the emission bands at 7 and 12 μm could also be reflected sunlight. Such an interpretation would mitigate inconsistencies between the brightness observed in this region and at longer wavelengths. Data in this spectral region are displayed in Fig. 1.

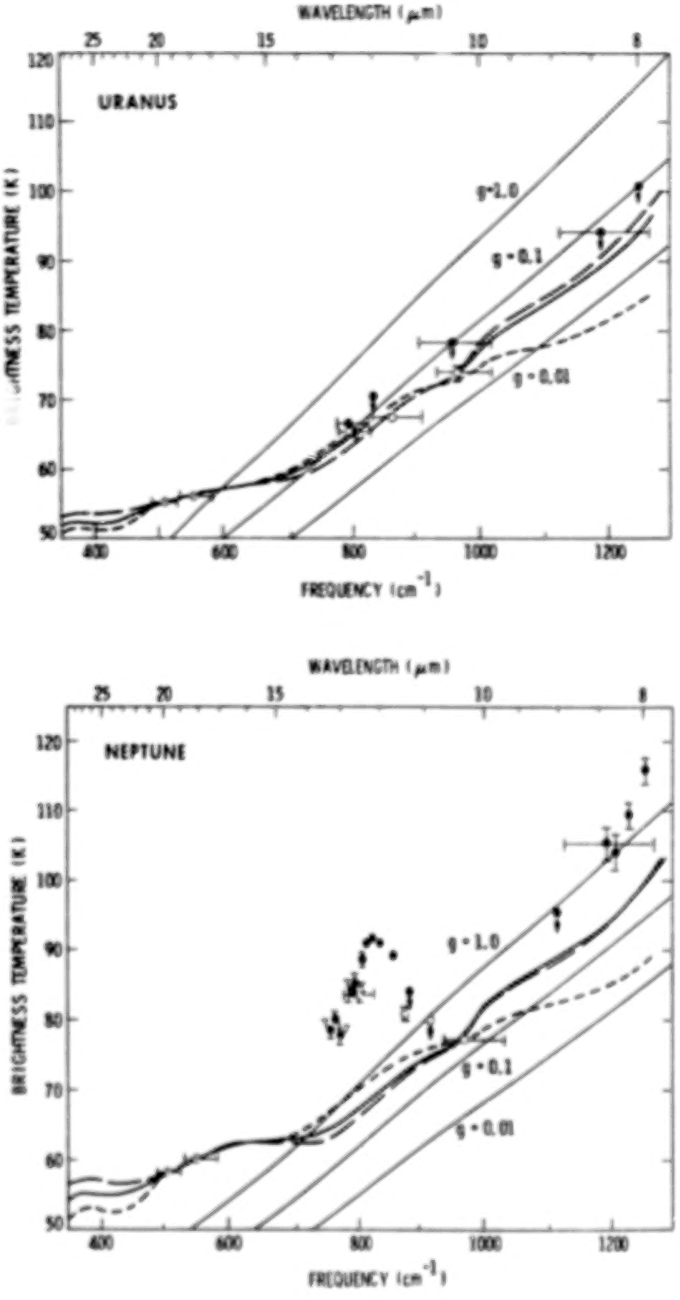

Figure 1. Brightness temperature spectra of Uranus (top) and Neptune (bottom) from ref. 8. Filled circles represent 3σ detection limits of Gillett and Rieke[3]. Circles with central point represent data of Tokunaga et al.[22] with their original calibration; open circles represent data of Orton et al[8]. Vertical bars represent 1σ uncertainties, horizontal bares FWHM of filters. Model spectra consider H_2 opacity and thermal emission alone for 0.2% (long-dashed), 2% (solid), and 10% (short-dashed) tropospheric CH_4 mixing ratios. Thin solid lines represent apparent brightness temperatures corresponding to values of geometric albedo, g, as shown.

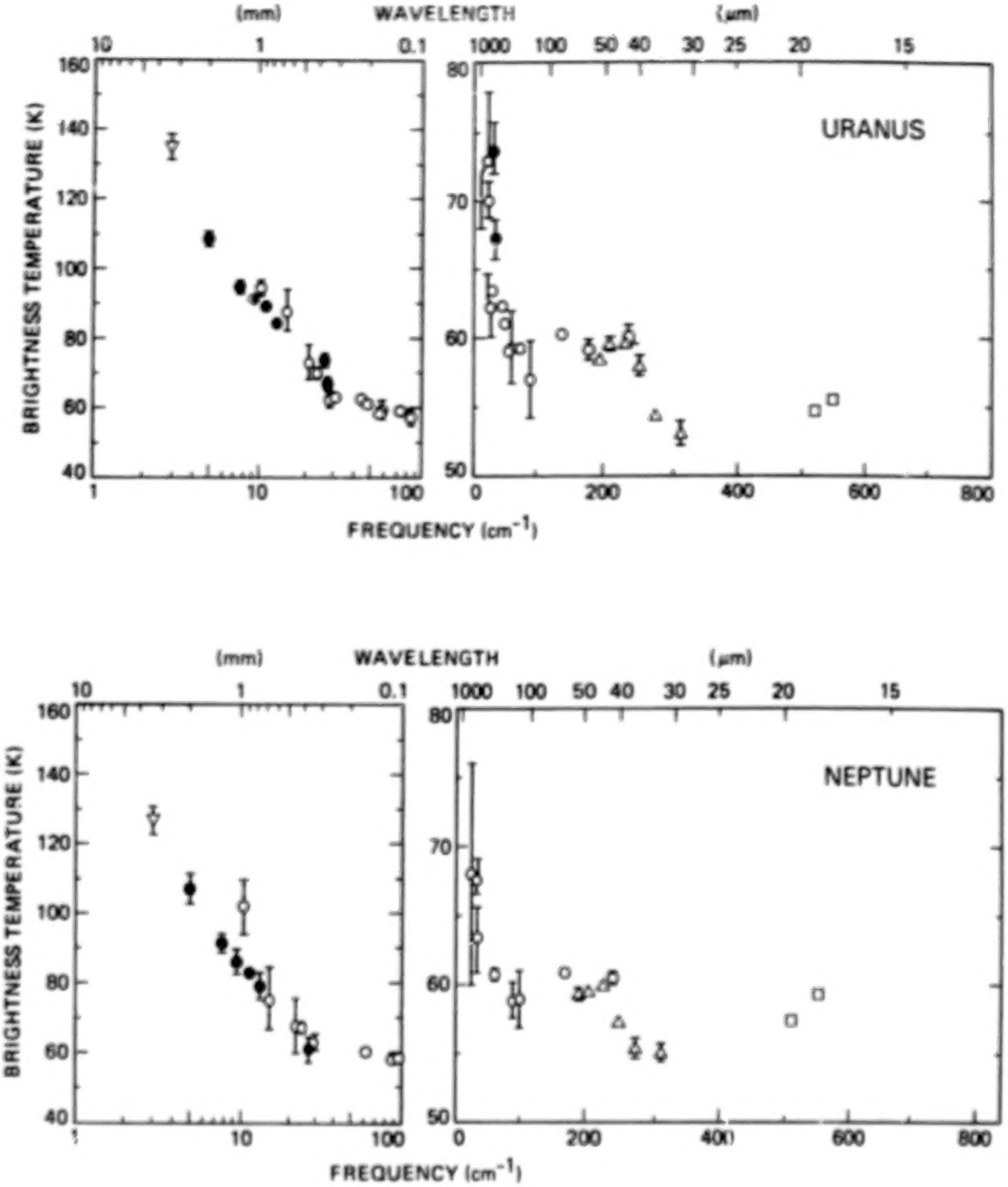

Fig. 2. Brightness temperature spectra of Uranus (top) and Neptune (bottom). The data include those of Tokunaga et al.[23] (squares), Moseley et al.[26] (inverted triangles), Hildebrand et al.[27] (open circles), Nolt et al.[28] (filled circles), and Ulich[25] (triangle). Representation of the FWHM of discrete filters is omitted for clarity. Where larger than the symbols, vertical bars represent 1σ internal errors only, except for 3.3-mm data [25] where the absolute uncertainty is represented. The absolute flux uncertainty of the 32-μm to 2-mm data is estimated as about 10%[26,27,28].

At wavelengths between 17 μm and 3 mm, the historical record is somewhat larger[3,9-22] but also of questionable utility. While these early and often heroic efforts should not go without recognition, the large internal errors and the dispersion in data quality prompts us to delete these older data from detailed quantitative discussion here. There are other reasons, as well. Often observations were made with filters whose spectral response is impossible to reconstruct. Analysis of this collection of data is extremely difficult simply because many of the data are quite inconsistent with one another. This is a much less serious problem in the more recent data set which we will discuss. Finally, while it is a classic canard in discussion of poor data, we are genuinely concerned about the possible variability of outgoing radiation with time. This is especially true for Uranus, where changes in the microwave spectrum, first documented by Klein and Turegano[19], may extend down to 3mm (see the chapter by Gulkis and de Pater).

The data we would like to consider are all taken or are consistent with data taken after 1978, providing a convenient and well-defined epoch. The spectral functions associated with filtered radiometry are known and reconstructable, to the extent that the optical path of water vapor is known (often the most difficult variable to establish, when it is important). Their calibration scales are known, if not absolutely consistent with one another. Such knowledge includes information about the assumed flux of the object used for the calibration and the assumed angular size of the planet. Here, we have adjusted the angular size of the planet as appropriate to the effective emitting radius, taken at the 1-bar level. This adjustment was necessary for the data of Tokunaga et al.[23] (where a new calibration scale[24] was also applied) and Ulich[25] but was already adopted by Moseley et al.[26], Hildebrand et al.[27] and Nolt et

Table 2

Summary of Stellar Occultation Observations of Uranus and Neptune

Date	Planet	Star	Event	Suboccultation Latitude	Observatory	Mean Isothermal Temperature (K)[1]	Reference
1977/3/10	U	SAO 158687	I	+5°	Kuiper Airbone Obs.	106	30
			E	-18°		88	
			I	+7°	Capetown	88	
			E	-21°		95	
1979/6/10	U	KM 9	I	+25°	Las Campanas	136	in preparation
			E	-29°		123	
1980/8/15-16	U	KM 12	I	-26°	Las Campanas	145 (I)[2]	31, 33
			E	+18°	European Southern Obs.	143 (I)[2]	32, 34
					Cierro Tololo	151 (I)[2]	in preparation
						156 (E)[2]	33
1981/4/26	U	KME 13	I	+8°	Anglo-Austrailian	129	31
			E	-19°	Telescope	131	
1982/4/22	U	KME 14	I	-15°			
			E	-3°	European Southern Obs.		34
			I	-11°	Pic-du-Midi		
			E	+8°			
"	"	"			Las Campanas		in preparation
					Cierro Tololo		in preparation
1968/4/7	N	BD-17°4388	(not given)		Tokyo Astronomical Obs. Mt. Stromlo Obs.	40 ± 10[3]	35, 36, 37
1981/5/10	N	MKE 28			Anglo-Australian Telescope	133 (I)[4]	in preparation
					Mt. Stromlo Obs.	165 (E)	in preparation
1981/5/24	N	uncatalogued	I	-56°	Cierro Tololo	145	38
			E	-16°		157	
1983/6/15	N	MKE 30					39 and several others in preparation

[1] where available
[2] from ref. 32; Las Campanas values are 138 K (I) and 110 K (E)
[3] for 90% H_2 and 10% He atmosphere by volume
[4] Mt. Stromlo data only

al.[28]. These four sources form the entire set of data which we will discuss, and they are displayed in Fig. 2. In the analysis of this spectral region, we have chosen between the earth-based submillimeter data of Hildebrand et al.[27] and those of Nolt et al.[28] in favor of the latter on the basis of much smaller internal errors and consistency with a smooth extrapolation to the 3.3-mm data of Ulich[25]. An important point worth special attention is that the data of Ulich span several years between 1975 and 1980, and they indicate that, within the ± 1.3 K uncertainties of the observations, the 3.3-mm fluxes of Uranus and Neptune are constant. As we will discuss in greater detail, the atmospheric opacity over this entire spectral region is probably dominated by the collision-induced opacity of H_2, as first suggested by Trafton[29].

Stellar Occultations - The stellar occultation method of determining temperature structures in the upper atmospheres of Uranus and Neptune is responsible for all our information on the 0.1- to 10-μbar region, which is otherwise observationally inaccessible, at least from the earth. The availablilty of an astonishing number of suitable stars, in spite of the very small apparent disks subtended by these planets, is aided by the planetary spectra. Where the planetary spectra are extremely dim owing to strong CH_4 absorption (i.e. at nearly any wavelength between 0.7 and 2.5 μm), stars need not be extremely bright. Table 2 summarizes the occultations for both planets which have produced published results to date (or work in progress) on the temperature structure.

The temperature structures can be determined from occultation data far more directly than is the case with infrared data. Samples of the reduced results of these occultations are shown in Figs. 3 through 5. The refractivity vs. altitude curve can be transformed into a gas density vs. altitude curve

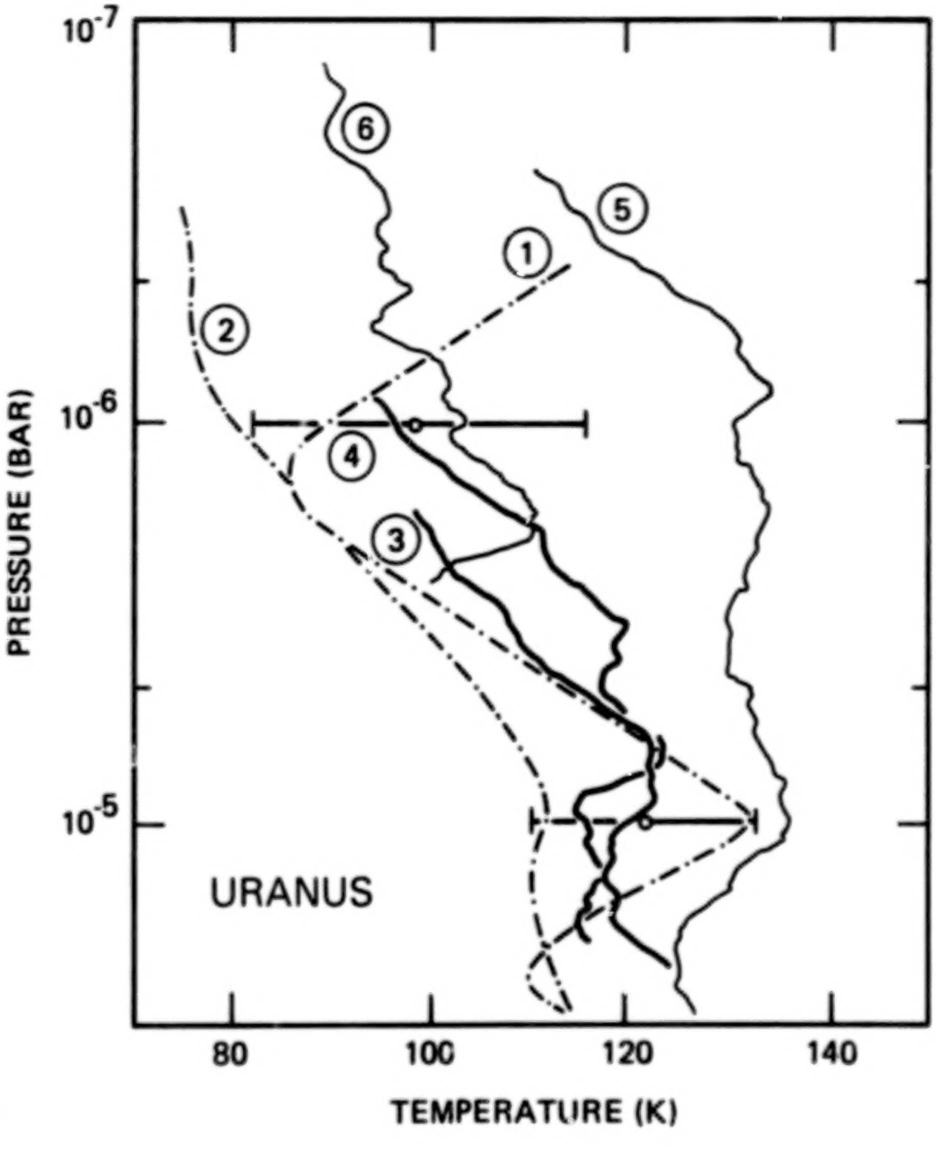

Fig. 3. Summary of stellar occultation results for Uranus for six events, compiled by P. Nicholson. Events are coded as follows: 1977 March (Kuiper) ingress [1], egress [2]; 1979 June (Las Campanas) ingress [3], egress [4]; 1980 August (Las Campanas: reduced by P. Nicholson) ingress [5], egress [6]. Open circles with vertical bars represent mean temperature and associated uncertainty at 10^{-5}- and 10^{-6}-bar levels.

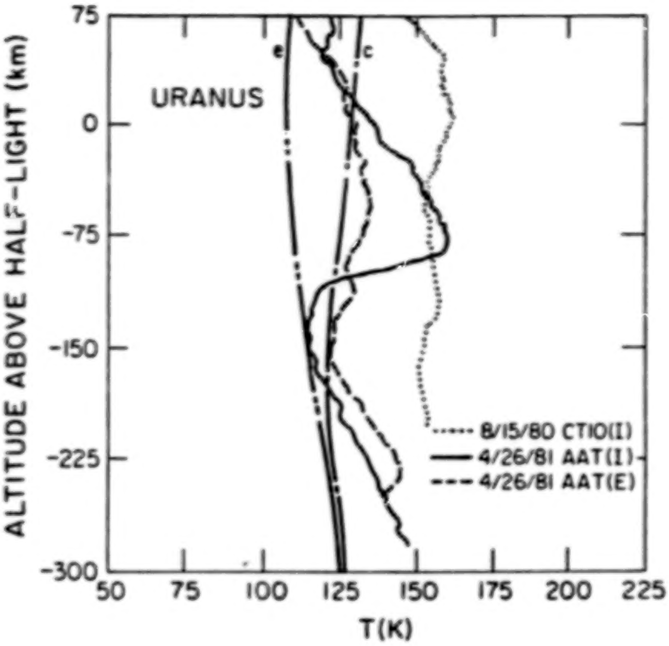

Fig. 4. Summary of stellar occultation results for Uranus for three events, from ref. 31. The pressure at the zero of altitude is 2.5 μbar.

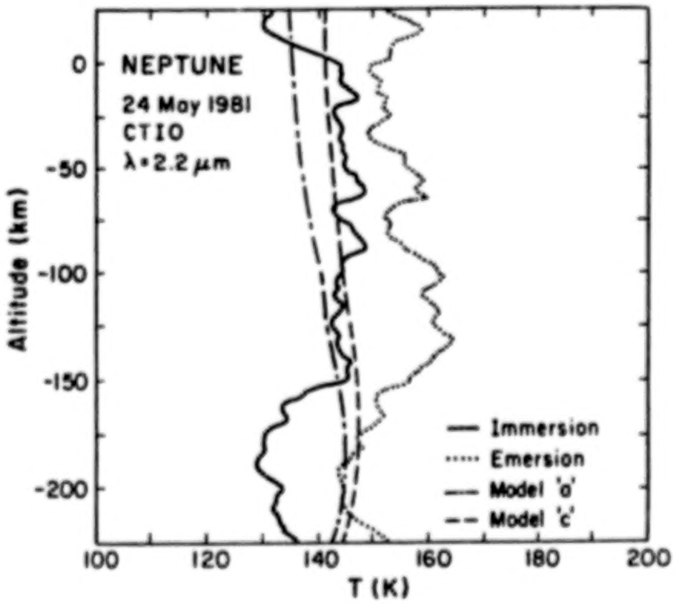

Fig. 5. Results of the 1981 May stellar occultation events reported by French *et al.*[38]. The pressure at the zero of altitude is 1 μbar. The temperature profile of two models by Appleby[66] are shown for comparison.

for a given assumption about the mean molecular weight (a value of 2.2 was used for each of the curves shown, corresponding to a bulk composition of 90% H_2 and 10% He by volume). Temperatures and total pressures are subsequently derivable via the gas law and the hydrostatic equation. More thorough descriptions of the technique itself, its limitations, and its reliability are available elsewhere[32,40-42].

All the results clearly indicate temperatures well above the minimum values (near 50 K) deeper in the atmospheres, and they thus establish that both planets possess "inverted" stratospheres where the temperature lapse rate is negative. In comparing several of the Uranian occultations over time, French _et_ _al_.[31] reported a possible temperature change of about 15 K per year. However, they cautiously advised acquiring more data to determine whether the trend is merely, in their words, "fortuitous groupings of data points". Uncertainties in the zero level of the lightcurves alone are likely to produce uncertainties on the order of 10 K in absolute temperature. While small features and the general shape of the curves are far better known, the absolute temperatures should thus be regarded as uncertain to at least 10 - 15 K when comparing data from different observers and results from somewhat different data analysis approaches (_cf_. Fig. 7 of ref. 32). Sicardy _et_ _al_.[34] reported their examination of recent results which they felt indicated a definite latitudinal dependence, with the warmest regions centered near the equator. Such trends are not readily apparent in the previous data. On the other hand, their effort has the significant advantage of data taken with similar instrumentation and analyzed by the same techniques. This would tend to remove bias from the relative temperature results to a greater extent than can be achieved when comparing data from completely independent groups.

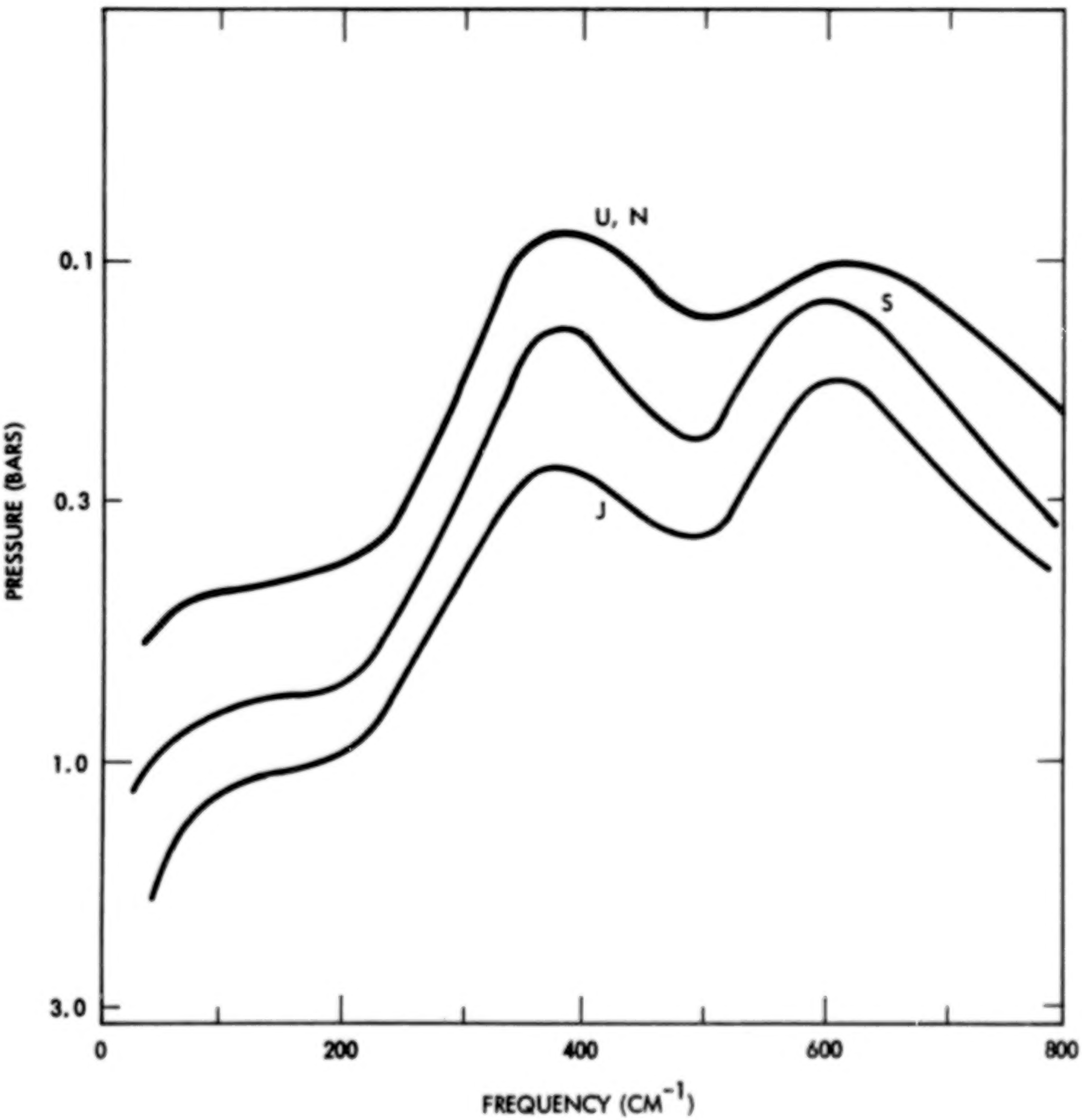

Fig. 6. Pressure at which unit optical depth is reached in the atmospheres of the giant planets owing to the opacity of the collision-induced H_2 dipole alone. A molar mixing ratio of 90% H_2 and 10% He is assumed.

ANALYSIS OF INFRARED RADIATION

Methods - Analyses of thermal radiance observations of Uranus and Neptune contrast in several respects with the relatively straightforward determinations of temperature structure from stellar occultation lightcurves. On the other hand, in principle such observations can be made at any time without reliance on special circumstances (beyond the weather and the disposition of a telescope time allocation committee). Another difference is that, when obtained from the earth, such information is global and average in representation.

One of the primary goals of both approaches is to retrieve the temperature structure, but this is not the only type of information which can be derived from thermal infrared measurements. The spectrum between 5 µm and 3 mm is replete with information about a variety of atmospheric properties. In fact, questions of atmospheric structure and chemical composition as constrained by infrared data must be addressed simultaneously. The objective is to extract information about (1) temperatures, (2) gas composition, and (3) clouds and aerosols while minimizing the dependence of the results on one another.

Of necessity, the approach is iterative. Consider the determination of temperatures. Fig. 6 shows the location of unit optical depth for all the outer planets as determined by the opacity of the collision-induced H_2 dipole, a gas which should be abundant and uniformly mixed in the atmospheres of Uranus and Neptune. An extra advantage is that the spectral region shown in Fig. 6 encompasses the bulk of thermal flux emitted by the planet: if we want signal-this is where to find it! Therefore, radiation sampled between 17 µm and 3 mm should be sensitive to the temperatures between about 100 mbar and 6 bars, if the molar fraction of H_2 is about 90%.

However, several problems arise at the outset. Much of this spectral region is inaccessible from the ground, owing to strong telluric water vapor absorption. Even the maximum thermal flux corresponds to a very low signal when considering brightness temperatures on the order of 55 - 60 K. We must assure ourselves that H_2 is, in fact, providing the bulk of the gaseous opacity. We then want to determine the molar fraction of H_2 (as well He and CH_4) and the ratio of ortho- to para-H_2. Finally, we want to assess the influence of cloud particles or other atmospheric aerosols on the outgoing thermal radiance and to correct for it.

There are two quite distinct approaches to the problem. Direct "inversion" of the radiance data can be employed to determine temperature structures, similar to the approach used to determine terrestrial atmospheric structure from meteorological satellite radiance data. This has been used by Courtin _et al._[43] for Uranus and Courtin _et_ _al_.[44] for Neptune. Alternatively, the older of the two approaches began essentially with Trafton's[29] pioneering work on the temperature structures of the outer planets. This kind of modeling establishes temperature conditions under which radiative and convective energy transport mechanisms achieve equilibrium between (1) the incoming insolation from outside the atmosphere together with infrared radiation upwelling from the deep atmosphere and (2) the outgoing energy radiated at each level of the atmosphere. Such models have been produced by Danielson[45], Danielson _et_ _al_.[46], Wallace[47,48,49] for Uranus, by Macy and Trafton[50] for Neptune, and by Appleby[51] for both planets.

The direct inversion approach (also known as temperature sounding) is quite flexible. It can provide information which might not be evident through the modeling approach, and it has been used to obtain information besides temperature[52,53,54] by minimizing residuals to the data. On the other hand, it can depend on the form of the initial guess in an iterative solution, it has difficulty in temperature minimum regions, its intrinsic vertical resolution is often poor, results can depend critically on boundary conditions, and there is no mathematical guarantee of uniqueness in the solutions. A casual approach to the technique thus has the potential for producing spurious results with alarming speed, and its use must be tempered with considerable caution and numerical testing.

Radiative-convective (R-C) modeling has the advantage of being rigorously based on physical processes at work in the atmosphere. Such techniques form the basis for terrestrial climatological studies, for example, and they have proved their worth in the interpretation of planetary data. On the other hand, observational data do not provide adequate constraints for some important components of R-C equilibrium models, such as the vertical distribution of aerosols or gases which absorb sunlight. Other processes must be omitted from these models altogether, such as the role of atmospheric circulation in redistributing energy. The merits of each approach are in many ways complementary, and recently our colleagues have been successfully persuaded to use a hybrid approach[8,22,26,27] in which results from equilibrium models are combined with temperature sounding. Moseley et al.[24] have also combined approaches in analysis of their airborne spectral data. One should keep in mind that both approaches are subject to the uncertainties associated with unknown gaseous composition and poorly-understood cloud influences cited earlier.

Fundamental Properties and Assumptions - Before discussing the details of the models, it would be useful to obtain a first-order picture of the empirical bounds which can be placed on the atmosphere or which must be assumed prior to any modeling work.

The bolometric flux emitted by the atmosphere is one of the most fundamental characterizations of the atmosphere. It is one of the major constraints on equilibrium models. In concert with visual reflectivity data, the bolometric flux value places a constraint on the presence and size of any source of internal heat, such as both Jupiter and Saturn possess. From the earth, our view of both planets is somewhat restricted and far short of the 4π steradian sampling of planetary emission which represents the ultimate ideal.

The data sets summarized in Fig. 2 provide a good basis for determining the bolometric output of the apparent disks. Represented as a "planetary effective temperature", the integrated spectra yield values of 58.6 ± 2.0 K for Uranus and 60.3 ± 2.0 K for Neptune[27,28]. The value for Uranus is consistent with previous estimates by Steir _et al._[11], Fazio _et al._[12], and Loewenstein _et al._[14]. The value for Neptune is larger than that derived by Loewenstein _et al._[57] but quite close to that derived by Steir _et al._[11]. The uncertainties quoted here include an absolute calibration uncertainty estimated as 10%. The fact that the absolute calibrations for the most relevant observations is based on a fairly unsophisticated model for the thermophysical properties of the planet Mars[55,56] is cause for some concern. We believe that further work is required before we know whether this estimate of the uncertainty is reasonable or joyously optimistic.

Internal energy estimates can be made from these results. Estimates of the Bond albedo of Uranus in 1961 and 1981 by Lockwood _et al._[58] imply equilibrium temperatures of about 57.0 ± 0.8 K and 55.8 ± 1.0 K, respectively. An estimate of the Bond albedo of Neptune by Murphy and Trafton[59] implies an equilibrium temperature of about 45 K. Recent measurements of the phase curves of Uranus and Neptune using the Voyager ISS experiment reported by Wenkert and Danielson[60] would support equilibrium temperatures revised upward by as much as 7% (equivalent to 30% increase in flux). If these revisions are correct, then Uranus almost certainly has no internal heat source. For Neptune, the estimate of internal heat ranges from 2.56 to 1.90 times the amount of absorbed solar energy, depending on the estimate of the phase integral chosen[59,60].

The bulk composition of the atmosphere is an important constraint on the interior structure and formation history. For lack of information to the contrary, it is usually assumed to be approximately solar-like or Jovian-like[52], with mixing ratios of 90% for H_2 and 10% for He. Hunten[61] has argued that abundances of He which are enriched with respect to the solar value are implausible by any process operating on a planetary scale, although devising mechanisms for He depletion is relatively easy. However, D. Stevenson (unpub. communication) believes that an enchancement of He is possible if substantial amounts of H_2 are mixed with H_2O in a liquid phase deep in the interior. The extant data do not strongly favor any particular value, nor are they inconsistent with the solar value. The technique formalized by Gautier and Grossman[62], used successfully as a part of the Voyager IRIS analysis of Jupiter[52] and Saturn[53] spectra, takes advantage of changes in the H_2 collision-induced dipole spectrum under the influence of He collisions to produce an optimized fit to the data. Unfortunately, for the data sets displayed in Fig. 2, the technique yields rather inconclusive results.

For the interim, the solar values apprently will not get us into any great trouble. In regard to the different species of H_2, a popular assumption is that ortho-H_2 and para-H_2 are mixed according to equilibrium at the ambient temperature. This presents no contradictions with any current data set, although there may be problems associated with understanding how these conditions are established, as discussed later. Estimates of the opacity of the atmospheres at infrared wavelengths from the H_2 collision-induced dipole are estimated from the recent multi-thermal laboratory observations of Dore et al.[63] for pure H_2, Cohen et al.[64] for H_2-He collisions and ongoing revisions to a preliminary estimate shown by Orton et al.[8] for H_2-CH_4 collisions. Efforts are underway to improve the reliability of our quantitative estimates of those absorptions, especially at low temperatures. Collaborative work with G. Birnbaum (National Bureau of Standards) and L. Frommhold (Univ. of Texas) is making headway on this problem by (1) fitting semi-empirical models to laboratory data, and (2) assembling a detailed ab initio quantum theory for the H_2 molecule and using it to predict the absorption at any frequency and temperature.

The abundance of CH_4 in the atmosphere is an important quantity for analysis of infrared radiation because of the intrinsically greater strength of the H_2 dipole induced by collisions with CH_4, compared with those induced by collisions with H_2 or He. This is especially true in the spectral regions beyond 200 µm or less than 14 µm, where the H_2-H_2 or H_2-He absorption spectra are very weak. Obviously, the CH_4 mixing ratio in the deep atmosphere is also important for internal structure and cosmogony as a general indicator of the abundances of heavier elements. Historically, CH_4 abundances determined spectroscopically have implied mixing ratios as low as about $2 - 4 \times 10^{-3}$ [65]. More recent research on visual and near infrared measurements (cf. Wallace[48] or the chapter in this volume by Bergstralh and Baines) imply values an order of magnitude higher. Current thermal infrared data can place better constraints on these values but not without some model dependency, as we will show.

The effect of clouds and other atmospheric aerosols on infrared radiances is poorly understood. For the wavelengths under discussion, stratospheric particles in the submicron size range are unlikely to be important. On the other hand, the CH_4 condensate cloud expected to form near the 1-bar level in both planets may influence upwelling thermal infrared radiances for particles on the order of microns in size. In a questionable extension of Occam's razor, such effects have been ignored because (almost all) the data can be fitted reasonably well without invoking clouds. The exception involves the possible contribution of reflected solar radiation near 10 µm[8].

Direct Sounding Models - The only models based purely on direct inversion of infrared Radiance data are those of Courtin *et al.*[43] for Uranus and Courtin *et al.*[44] for Neptune. These models assumed an adiabatic lapse rate in the portion of the atmosphere below the level where direct sounding was possible (near 3 bars total pressure) and a constant value for the change in temperature with pressure logarithm above the highest level sounded (about 150 mbar total pressure). Both efforts labored under the handicaps imposed by the infrared data set extant at the time, which sometimes required making educated guesses among contradictory measurements. For Uranus, an isothermal lapse rate above the 150 mbar level fitted the overall data best, although a mildly inverted lapse rate was used to fit the 24- and 22.5-µm data of Gillett and Rieke[3] (Fig. 7). For Neptune, the model which Courtin *et al.*[44] considered to fit the entire suite of data most successfully was one in which the CH_4 mixing ratio, assumed to be 2×10^{-3}, was uniform throughout the atmosphere. The level of "supersaturation" which their model required at some levels was necessary to explain the strong CH_4 7-µm emission feature.

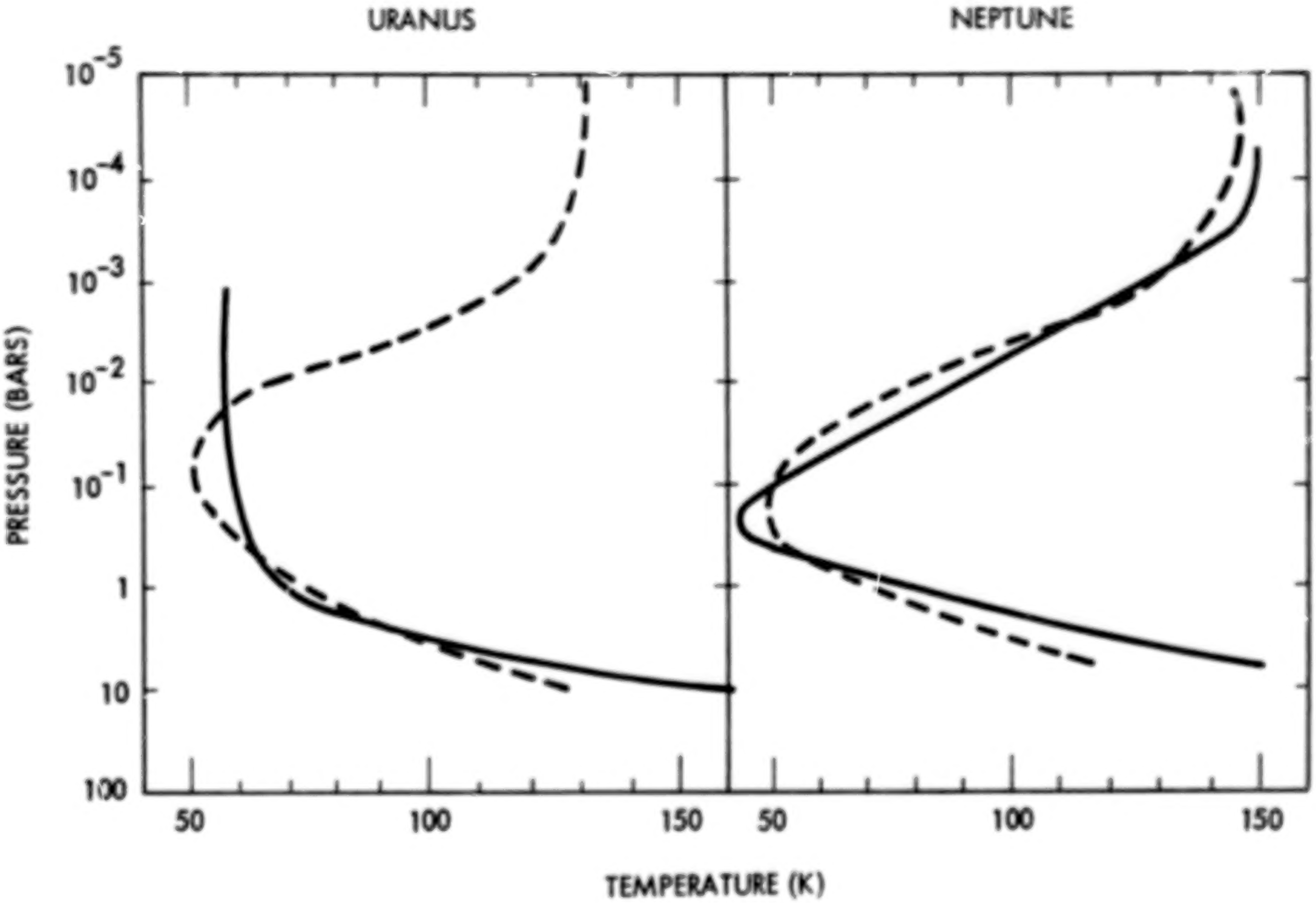

Fig. 7. Temperature structures for Uranus and Neptune. The direct inversion results of Courtin *et al.*[43] (Model I) and Courtin *et al.*[44] (Model N) are respectively shown for Uranus and Neptune in solid lines. Results of Appleby's[51] models are shown as dashed lines.

Radiative-Convective Equilibrium Models - The models of Danielson[45], Danielson *et al.*[46] and Wallace[47], clearly the most prominent among the early equilibrium models of Uranus, are now known to be incorrect. They were the casualties of an increasingly constraining data base, and they were forced to invoke somewhat ad hoc assumptions in order to match the constraints existing at the time. Danielson's models used arbitrary functions to represent deposition of solar flux, and the millimeter spectra predicted by the models turned out to be colder than is observed. Wallace's models, concentrating on the stratosphere, considered a constant (i.e. "supersaturation") CH_4 mixing ratio as well as a CH_4 distribution consistent with saturation equilibrium. The former model predicted 7-µm emission which proved to be much higher than upper limits observed, by Gillett and Rieke[4] and Macy and Sinton[7] and the latter model was much colder than observations at longer wavelengths.

In later models, Wallace[48] concentrated his attention on the troposphere of Uranus and deleted the CH_4 supersaturation effects present in his earlier models. He presented evidence that the CH_4 mixing ratio in the deep atmosphere was between 1 and 10%, by calculating the adiabatic temperature gradient under the influence of condensation by various amounts of CH_4 and constraining these models with millimeter observations. He presented profiles for equilibrium H_2 and for the case in which the molar fractions of para-H_2 and ortho-H_2 replicated those in the equilibrium state, but the specific heat was simply the weighted sum of each species (as in Trafton's[29] original study). He called this state "intermediate" between equilibrium H_2 and normal H_2. Not to be accused of incompleteness, Wallace also calculated first-order cloud effects on the deposition of solar energy, using models for the clouds from a variety of observational constraints in the visible and near infrared spectrum. He also calculated the structure of the deeper atmosphere. Both of these areas are treated in other chapters of this volume.

Wallace followed this work with an examination of the time and spatial dependence of the temperature variations and convective flux activity likely in the Uranian troposphere[48]. Beyond mixing-length theory, considerations of dynamics were excluded from the calculations. Even with this potential equilibrating force excluded, the amplitude of temperature variations throughout the Uranian year was only 5 K at the poles and less at lower latitudes. The minimum local effective temperature was found to occur at the end of the period when a given latitude is in darkness, and the size of the convective flow was found to depend critically on the vertical distribution of CH_4 assumed, i.e. whether or not it is limited to the saturated vapor pressure (assuming a mixing ratio of 3% in the deep atmosphere). Observational tests of this model will be difficult to achieve until the advent of spatially-resolved measurements covering several latitudes. Wallace's[48] work is also reviewed elsewhere in this volume.

The most recent radiative-convective models for Uranus are those of Appleby[51], who emphasized the examination of the atmosphere above the 1-bar level, with particular attention to the stratopshere. The simplest of his models which matched the available data was one with a characteristic effective temperature of 58 K. The stratosphere of this model was heated radiatively by (1) residual CH_4 above the cold trap and (2) aerosols which were uniformly distributed and absorb about 15% of the incident insolation. While the mixing ratio of CH_4 was assumed to be 2% in the deep atmosphere, the heating rate in the stratosphere was largely independent of this assumption, owing to the predominance of control by the saturation vapor pressure at the temperature minimum.

This model (Figs. 8 and 9) demonstrated that the observational constraints could reasonably be satisfied by a model with no extraordinary or ad hoc assumptions about the distribution of CH_4 or insolation-absorbing aerosols in the stratosphere. Associated models also demonstrated that small changes in the vertical distribution of the stratospheric aerosols could produce large changes in the temperature structure (Fig. 10) while still remaining more or less consistent with the observational constraints. By implication, we might expect detectable changes in stratospheric temperatures as a function of insolation history.

Since Trafton[29], there have been few detailed examinations of the structure of the atmosphere of Neptune from the purely radiative-convective equilibrium standpoint. Somewhat cursory models were demonstrated by Danielson[45] and Wallace[47]. Macy and Trafton[50] also explored models with arbitrary solar energy deposition functions, similar to those of Danielson[45] and Danielson _et al._[46]. More recently, Appleby[51] examined Neptune along with Uranus. As for the atmosphere of Uranus, his examination concentrated on the atmosphere above the 1-bar level, particularly the stratosphere, and he assumed a 2% mixing ratio for CH_4 in the deep atmosphere. A model was developed which appears to fit the observational constraints, including the maximum value of 5% insolation absorbed by the stratosphere. In order for the stratosphere to be heated sufficiently to explain the observed level of 7-μm CH_4 emission, more CH_4 was required to be present above the temperature minimum than is consistent with the saturation vapor pressure at the temperature minimum. Rather than stipulate the _ad hoc_ requirement that CH_4 to be "supersaturated" everywhere, as did Courtin _et_ al.[44], Appleby extended remarks originally made by Hunten[61]. He formulated a quantitative model of local saturation equilibrium, in which the partial pressure of CH_4

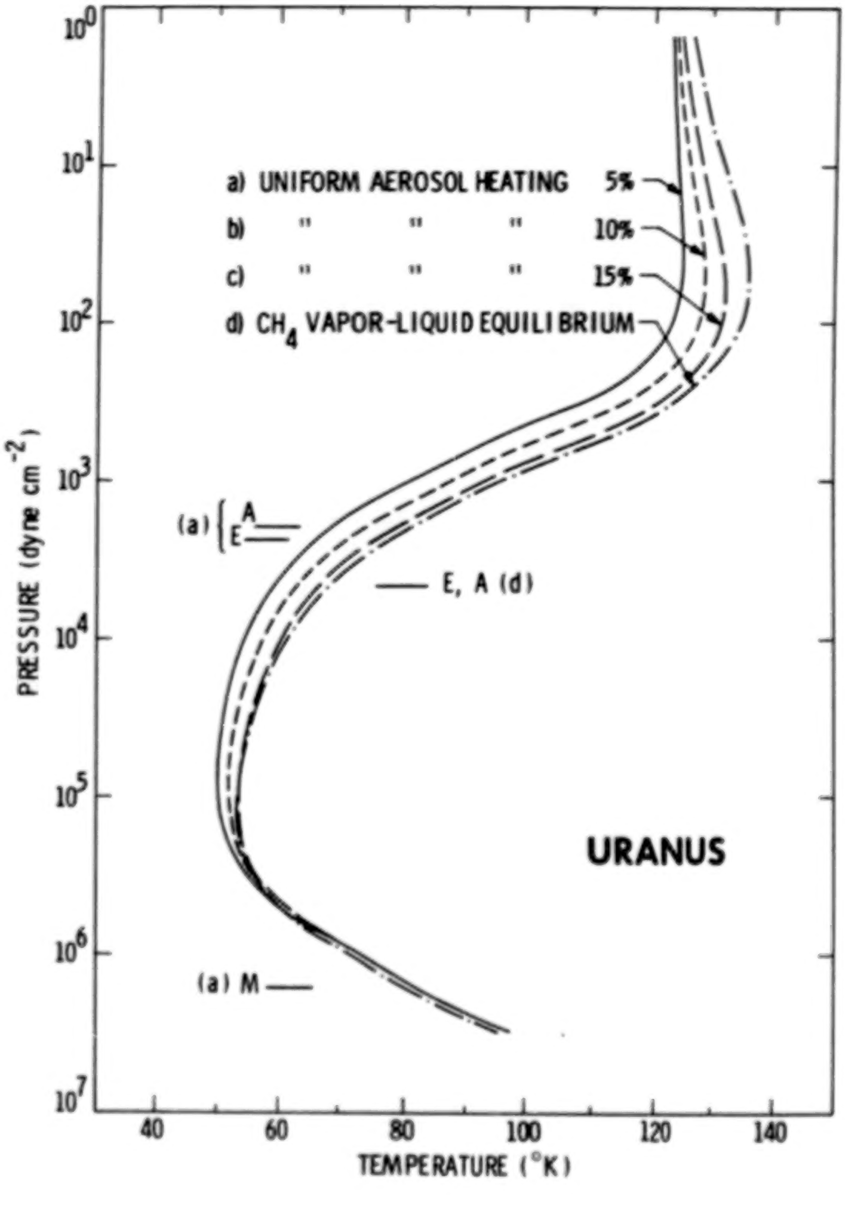

Fig. 8. Results of Appleby's[51] radiative-convective equilibrium models for Uranus. The temperature inversion is supported by heating due to CH_4, which is constrained by saturation equilibrium, and by insolation-absorbing aerosols uniformly distributed above the top of the convective zone. The 15% uniform aerosol heating model fits the infrared constraints best. The locations of the condensation levels corresponding to CH_4 (M), C_2H_2 (A), and C_2H_6 (E) are indicated for models (a) and (d).

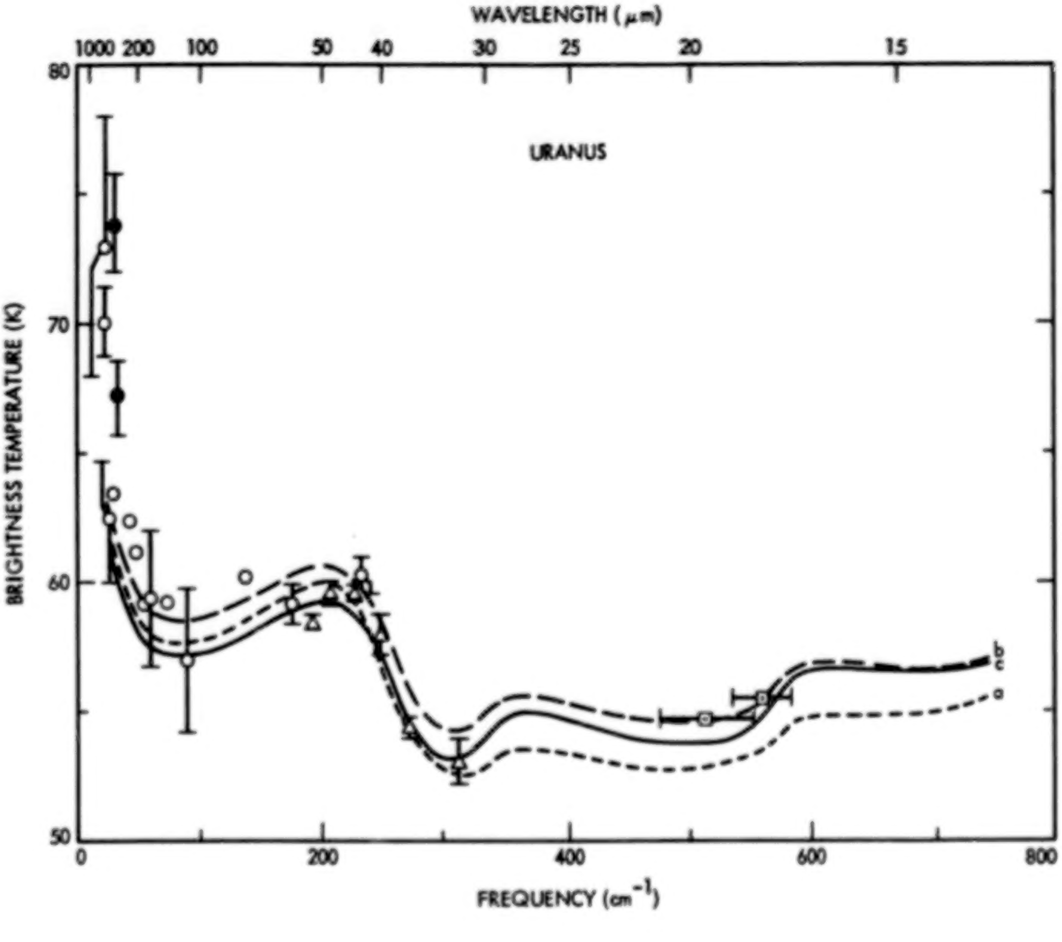

Fig. 9. Spectra for three radiative-convective equilibrium models of Uranus compared with observational data shown in Figure 2. Spectra (a) and (b) correspond, respectively to the 10% and 15% uniform aerosol heating models presented in Figure 8 above. Model (c) assumes 5% uniform aerosol heating, with the mean insolation twice as large as that in models (a) and (b) (which employ the usual diurnal average factor of 1/2). The temperature profile for model (c) is presented with the same label in Figure 21 below.

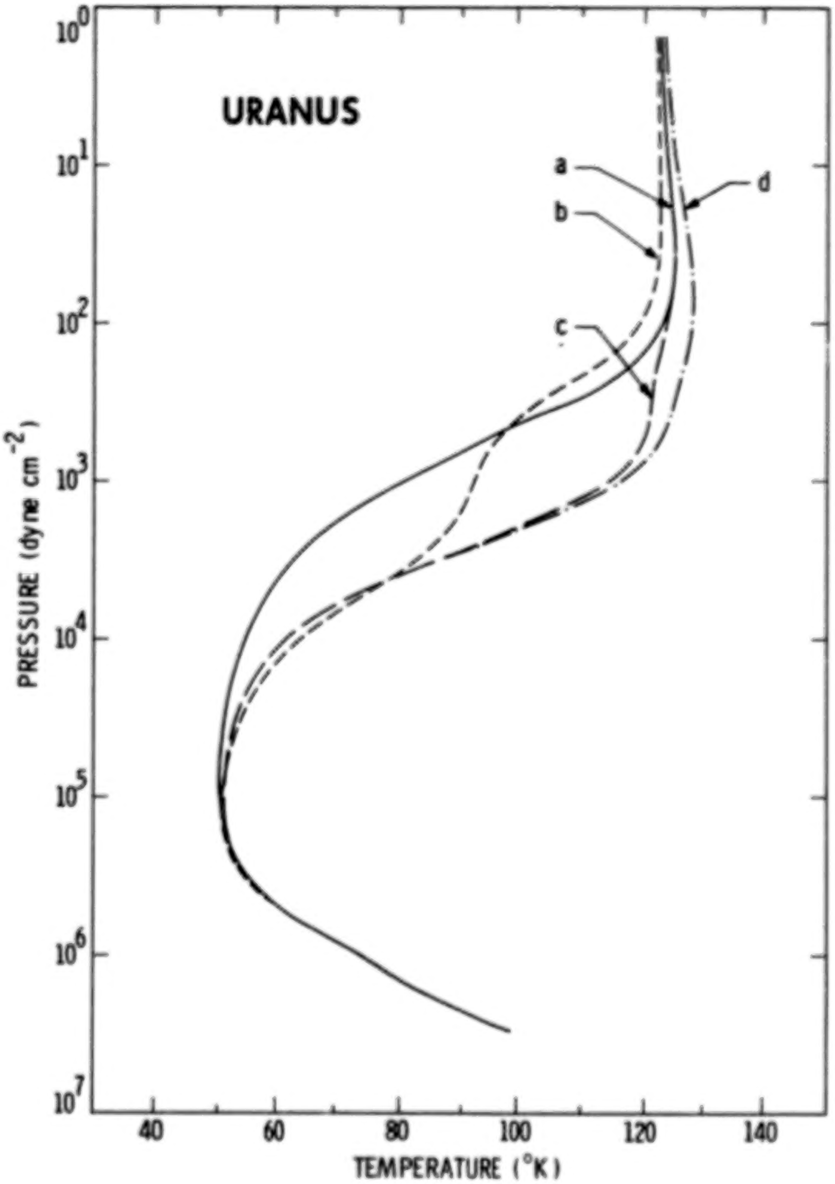

Fig. 10. Temperature profiles for Appleby's[51] models of radiative-convective equilibrium in Uranus under a variety of assumptions for the distributions of stratospheric insolation-absorbing aerosols.

was set equal to the vapor pressure (unless exceeding a 2% maximum mixing ratio) in the stratosphere as well as the troposphere. This was called the "convective penetration" model, focusing on the most likely mechanism for transport of methane from the troposphere into the stratosphere. While this admittedly left open the question about why this mechanism would work for Neptune and not for Uranus, this model is preferable to the full supersaturated-CH_4 model (see further discussion below). The comparison of the model with stellar occultation results and the thermal emission data are respectively displayed in Figs. 11 and 12. Just as for Uranus, small changes in the stratospheric aerosols could produce substantial differences in the temperature structure (Fig. 10).

Appleby[66] further developed a model for non-local thermodynamic equilibrium (non-LTE) for CH_4 emission in the stratospheres of the outer planets, based on the thermalization of solar energy absorbed in the CH_4 band groups centered at 1.7, 2.3 and 3.3 µm. These all show large departures from LTE at pressures below 0.01 mbar, and their potential influence on the stratospheric temperatures of Uranus and Neptune is on the order of 10 to 15 K (Fig. 13). Substantial variations on the equilibrium temperatures of the stratospheres of Uranus and Neptune result from various assumptions about relaxation rates which cannot be resolved at this time in the absence of relevant low-temperature laboratory data.

Several recent authors have used results from equilibrium models in concert with direct inversion to provide some greater sense of physical reality to an otherwise poorly-constrained mathematical environment. The measurements of Tokunaga et al.[23] confirmed with high precision the implications of earlier signal-poor data of Gillett and Rieke[3]. Not only Neptune, but also Uranus, possesses a measureable temperature inversion in the lower stratosphere (50-100

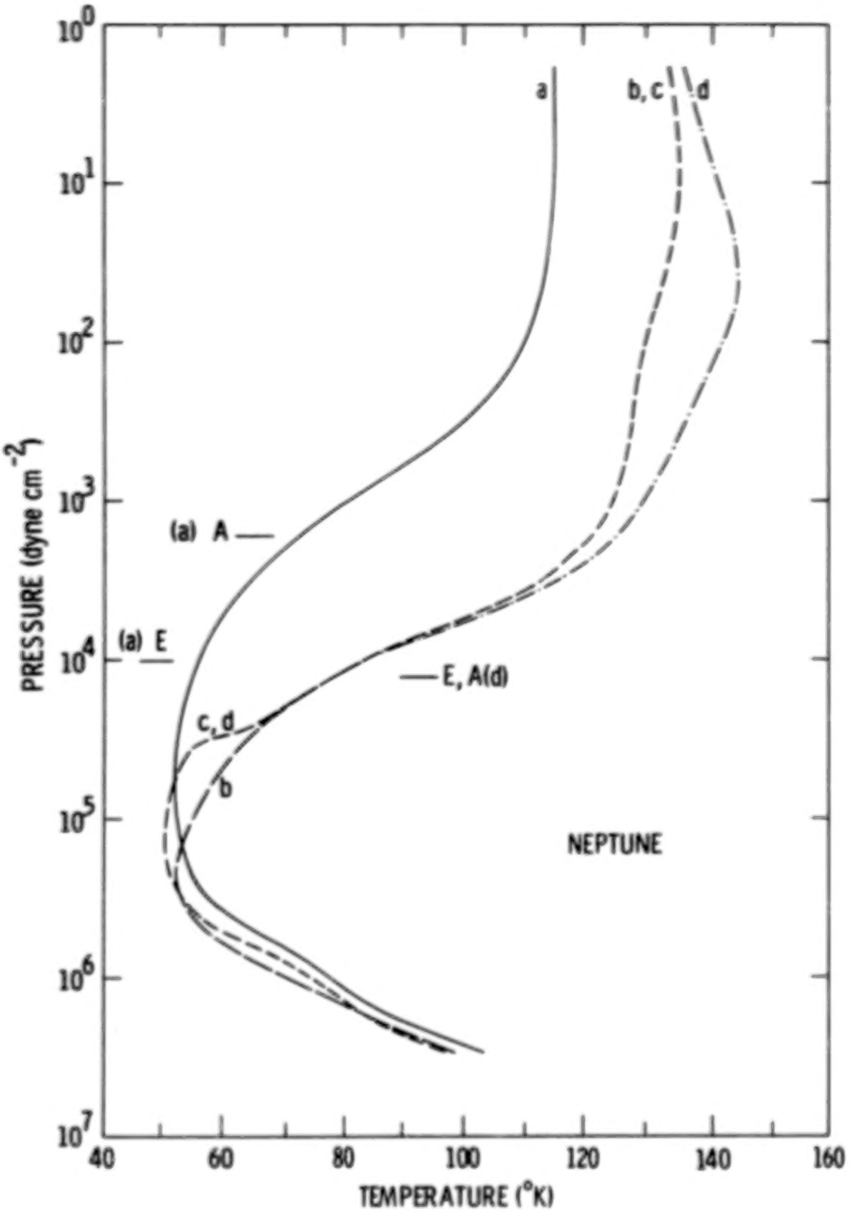

Fig. 11. Results of Appleby's[51] radiative-convective equilibrium models for Neptune. In models (b), (c), and (d), there is deposition of 5% of the insolation in the stratosphere via aerosol absorption. Model (a) employs twice as much aerosol heating but CH_4 is distributed according to saturation equilibrium from below (as in the Uranus models). In model (b) CH_4 is distributed uniformly (with a 2% mixing ratio) at all levels (therefore, CH_4 is supersaturated by large factors at levels near 100 mbar). In model (c) CH_4 is distributed according to the local saturation vapor pressure, even in the stratosphere. Model (d) is similar to model (c), but the distribution of insolation-absorbing aerosols has been changed to provide warmer temperatures in the upper stratosphere.

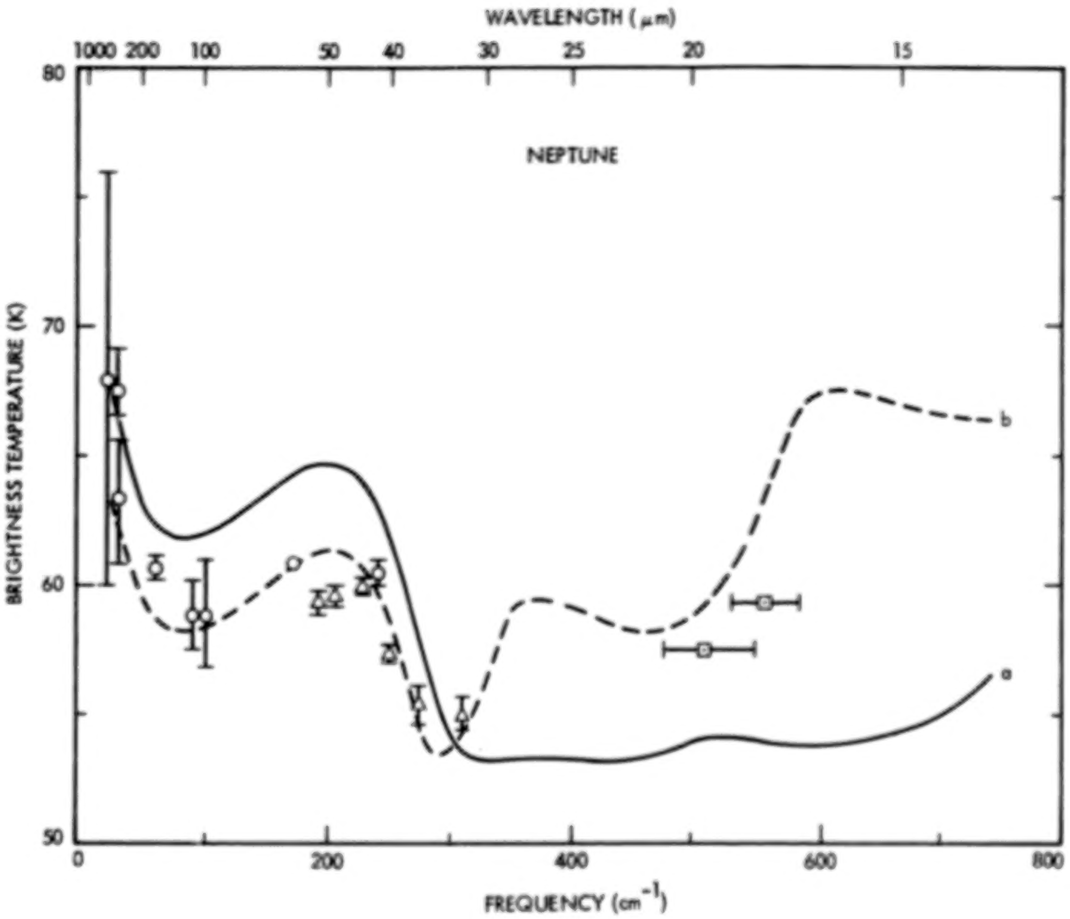

Fig. 12. Spectra for two radiative-convective equilibrium models of Neptune compared with observational data shown in Figure 2. Spectrum (a) corresponds to the 10% uniform aerosol heating model, shown as (a) in Figure 11. T_e = 62.3 K for this model. The stratosphere, where $[CH_4]/[H_2] \sim 10^{-4}$, is much too cold, as evidenced by measurements between 8 and 20 μm. By contrast, model (b) is a "convective penetration" model in which $[CH_4]/[H_2]$ = 0.02 above and below the CH_4 condensation region. T_e = 59.8 K in this case and the temperature profile is given by model (c) in Figure 11. The 8 to 13-μm emission for this model is consistent with observation, although the 18-μm flux is somewhat too high.

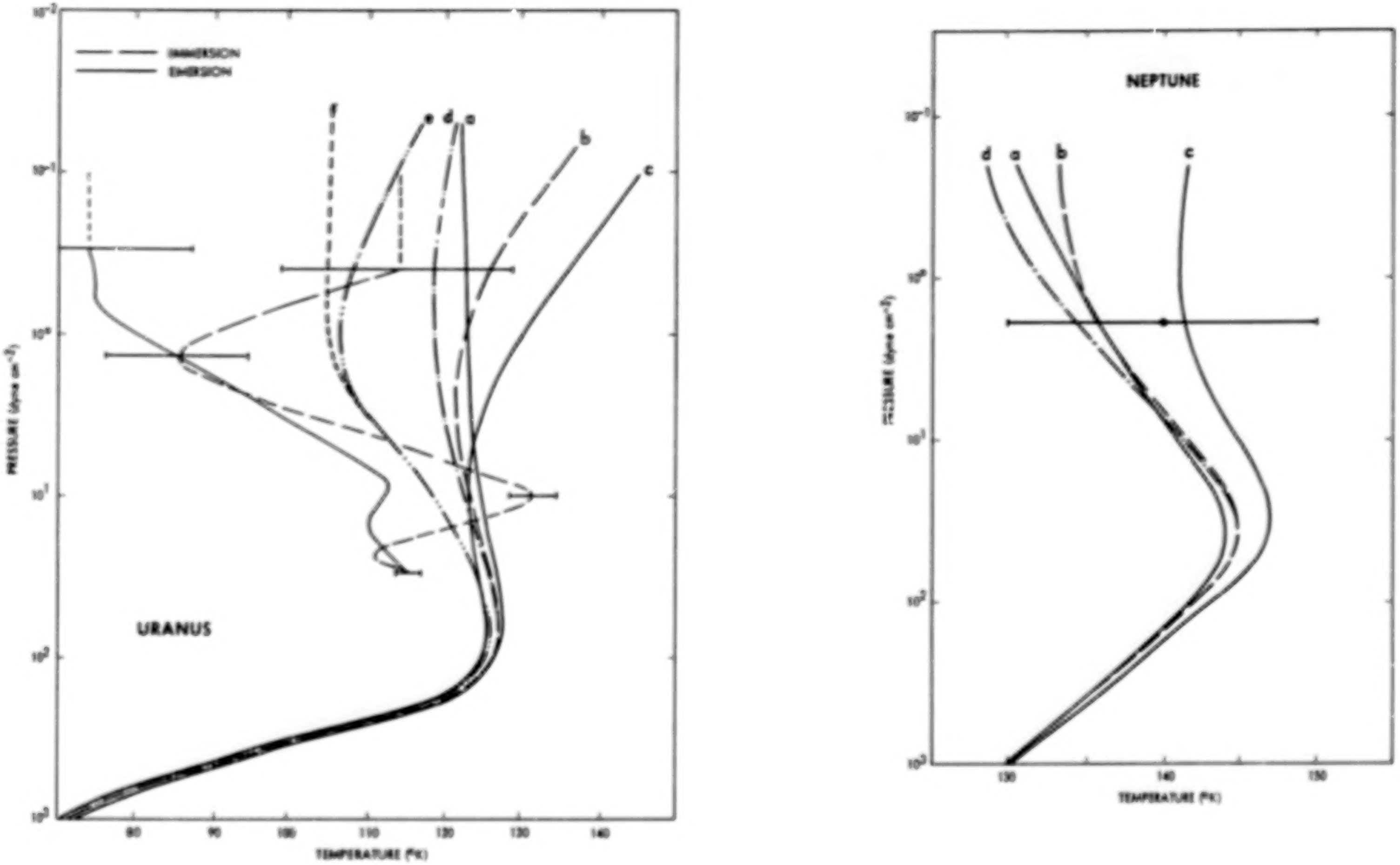

Fig. 13. Summary of CH_4 non-LTE models for Uranus (left) and Neptune (right) from Appleby[66]. The temperature profiles of Dunham et al.[30] for Uranus are shown for comparison. Curves (a) are the LTE control. Curves (b) and (c) are the nominal and "extreme" VT vibrational models. Curves (d) are the nominal VV relaxation models, and curve (e) and (f) for Uranus are "extreme" VV relaxation models.

mbar). However, with only two newly measured spectral points per planet, constraints on a wider vertical range were required. The models of Appleby[51] (then taken from Appleby's thesis results) were perturbed in the stratosphere until a best fit was achieved to the new data. Fig. 14 demonstrates these perturbations together with a constant lapse rate model, similar to the assumptions of Courtin _et al._[43,44]. One must realize that the constant lapse rate models are able to fit the data just as well as those based on a perturbation of Appleby's models. This figure shows that such perturbations were quite small for Uranus but somewhat larger for Neptune.

Newer data in the 10-μm region by Orton _et al._[8] were originally interpreted as indicative of a continuum determined by the high-frequency wing of the collision-induced dipole of H_2 (cf. the model spectra shown in Fig. 1). Temperature sounding, starting with an initial model given by the earlier work of Tokunaga _et al._[23], determined that if the data were so interpreted, then a steep temperature gradient in the troposphere was implied which contradicted measurements at longer wavelengths (unless the He mixing ratio were on the order of 40% or more by volume). Rejecting this interpretation, Orton _et al._ postulated that, in the absence of systematic errors in the measurements (such as undetectable leaks in the interference filters), there was an additional contribution from reflected solar radiation. The required atmospheric reflectivities were modelled simply as Lambert surfaces, characterized by an albedo which was taken as a free parameter. For Uranus, a 450-mbar surface (which could simulate a cloud top near the radiative-convective boundary) would be required to have a reflectivity of 0.82 to contribute sufficient sunlight (together with the overlying thermal emission) to match the observations at 10.3 μm. If the cloud were deeper, the reflectivity would be required to be higher. For Neptune, a unit

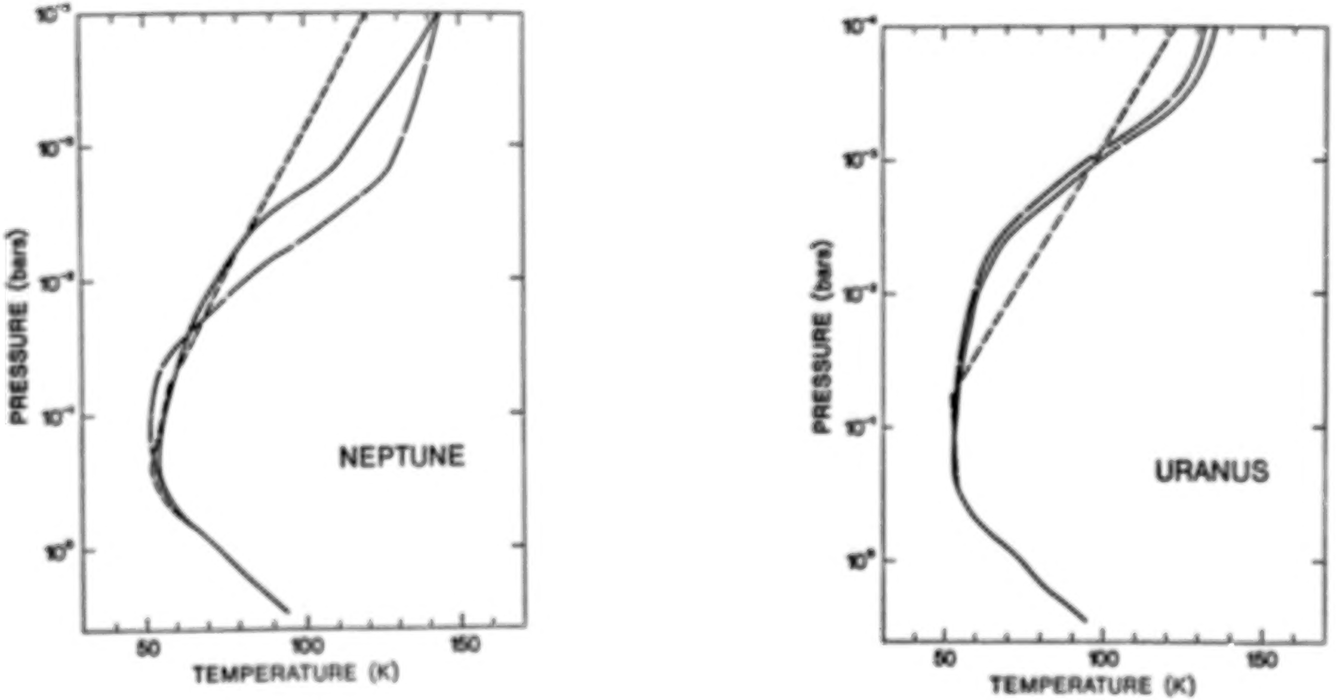

Fig. 14. Temperature structures of Uranus (left) and Neptune (right) derived by Tokunaga *et al.*[23]. Perturbations of Appleby's[51] models (long-dashed line) are shown as solid lines. The short-dashed lines respresent a simple stratospheric temperature structure equally consistent with their data.

reflectivity surface at this level would not contribute sufficient radiance to match the observations at 10.3 µm. However, a surface at 100 mbar would require reflectivity of only 0.70 to meet the same constraint. The pressure level could similarly be adjusted with appropriate changes in the reflectivity. Looking at the spectrum carefully, one realizes that, for Uranus at least, such a "gray" surface model does not fit the 11.6- or 12.2-µm observations simultaneously with the one at 10.3 µm (Fig. 15). The lack of optical constants for CH_4 ice, the most likely candidate to form such cloud tops, prevented a more thorough examination as to whether this was a physically reasonable explanation.

The spectra were also studied in order to estimate the abundances of C_2H_6 and CH_4 from features at 12 µm and 7 µm, respectively. For Uranus, depletion of CH_4 in the upper troposphere and lower stratosphere following the saturation vapor pressure was found to produce an absorption feature at 7 µm which fell well below current limits of detectability (Fig. 16); this indicated that greater abundances of CH_4 might, in fact, be possible. The maximum permissible mixing ratio for C_2H_6 was determined to be on the order of 3×10^{-8}. For Neptune, the emission feature of CH_4 was found to be consistent with a maximum mixing ratio (limited by local vapor pressure) on the order of 1 - 4% (Fig. 16), provided that the temperature structure in the 0.1 to 10 mbar region could be made slightly warmer than in the Tokunaga et al. model. Such a change at these low pressures did not significantly affect the fit to the 17.8- and 19.6-µm data. With this temperature structure, a similar fit for the C_2H_6 maximum mixing ratio (again limited by the vapor pressure equation) was found to be about 3×10^{-6}. Similar values for the C_2H_6 mixing ratio were given in an analysis by Macy[67], who also suggested a value of about 10^{-8} for the mixing ratio of C_2H_2, but in arguments which relied on the model assumptions of Courtin et al.[44].

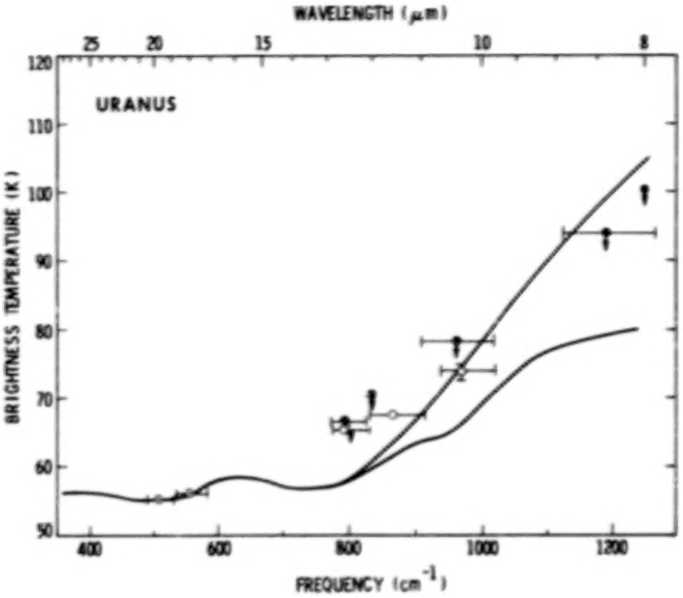

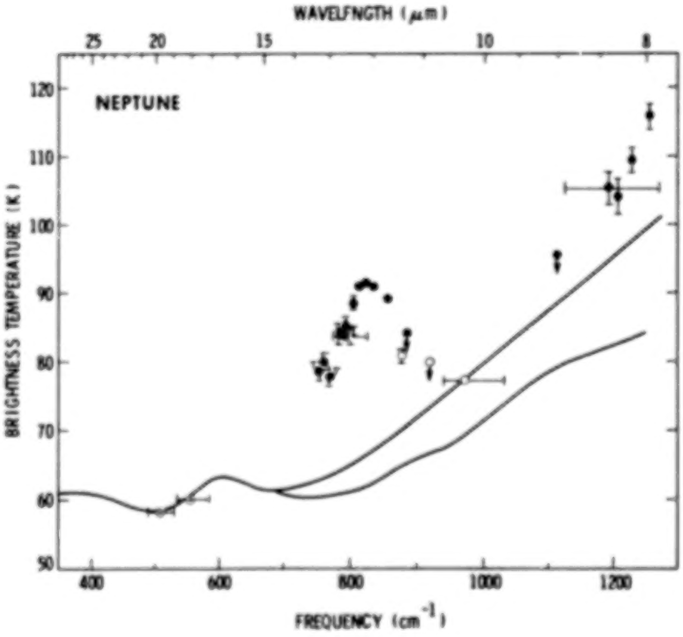

Fig. 15. Brightness temperature spectra of Uranus (top) and Neptune (bottom). Data are depicted as in Fig. 1. The lower curves represent model spectra from thermal emission alone, assuming the perturbed equilibrium temperature profiles of Tokunaga _et al._[23] (Fig. 14). The upper curve represents the spectrum from combined thermal emission and reflected sunlight from models with lower boundaries characterized by emissivities as described in the text. Both model spectra assume atmospheric opacity due only to H_2.

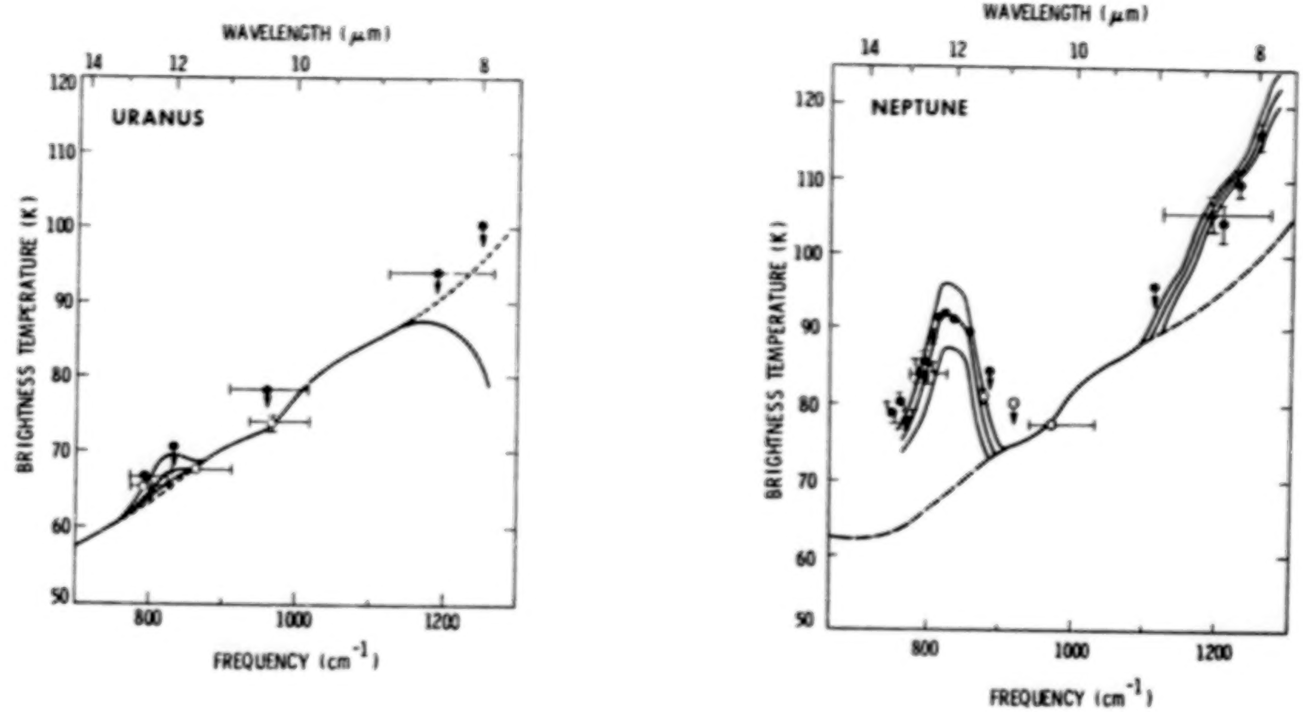

Fig. 16. Spectra of Uranus (left) and Neptune (right) for models with thermal emission only matching the 10-μm fluxes. Dashed curves represent the spectra considering H_2 opacity alone. Solid curves for Uranus represent emission for stratospheric C_2H_6 with mixing ratios of 3×10^{-8}, 1×10^{-8}, and 3×10^{-9} (lower to upper) and absorption of 0.2% CH_4 in the troposphere. For Neptuine they represent C_2H_6 emission from maximum stratospheric mixing ratios of 1×10^{-5}, 3×10^{-6} and 1×10^{-6} and CH_4 emission for maximum stratospheric mixing ratios of 1×10^{-1}, 4×10^{-2}, and 2×10^{-2}. Both constituents obey local saturation equilibrium vapor pressures in the stratosphere of Neptune.

The mixing ratio suggested for CH_4, corresponding to some cold-trap penetration model for CH_4 vertical transport, implies equilibrium with the resevoir of CH_4 available in the deep atmosphere. This indicates that a mechanism is involved which is at least as fast as the precipitation rate.

Moseley et al.[26] obtained data (Fig. 2) which are consistent with the assumption that the collision-induced H_2 dipole dominates the opacity in the middle through far infrared planetary spectrum. Using their own data between 30 and 50 μm, they derived a temperature structure between 100 and 600 mbar for both Uranus and Neptune, assuming an adiabatic extrapolation at higher pressures and Wallace's[47] temperature structures at lower pressures. The results for this inversion and for one in which the data of Tokunaga et al.[23] were included are shown in Fig. 17 and a portion of the predicted spectra in Fig. 18. A satisfactory fit to their own data and those of Tokunaga et al. simultaneously was not possible, although recalibration[24] of the Tokunaga et al. data[23] (down 0.6 K for Uranus and 0.8 K for Neptune for both filters) reduces this discrepancy. We suspect that this arises from an inconsistency in the two calibration systems used as well as the errors intrinsic in the measurements.

Recent observations by Hildebrand et al.[27] and Nolt et al.[28] provided a great increase in our understanding of both planets in the 30-μm through 2-mm range. Both reports discuss similar techniques and address overlapping spectral ranges. We will concentrate on the perspective of the Nolt et al. results because (1) in the submillimeter region where their two data sets overlap, the results of Nolt et al. appear to be characterized by less intrinsic noise, and (2) Nolt et al. included consideration of the measurements of Ulich[25] and Moseley et al.[26] (the latter was not available for Hildebrand et al. in final form).

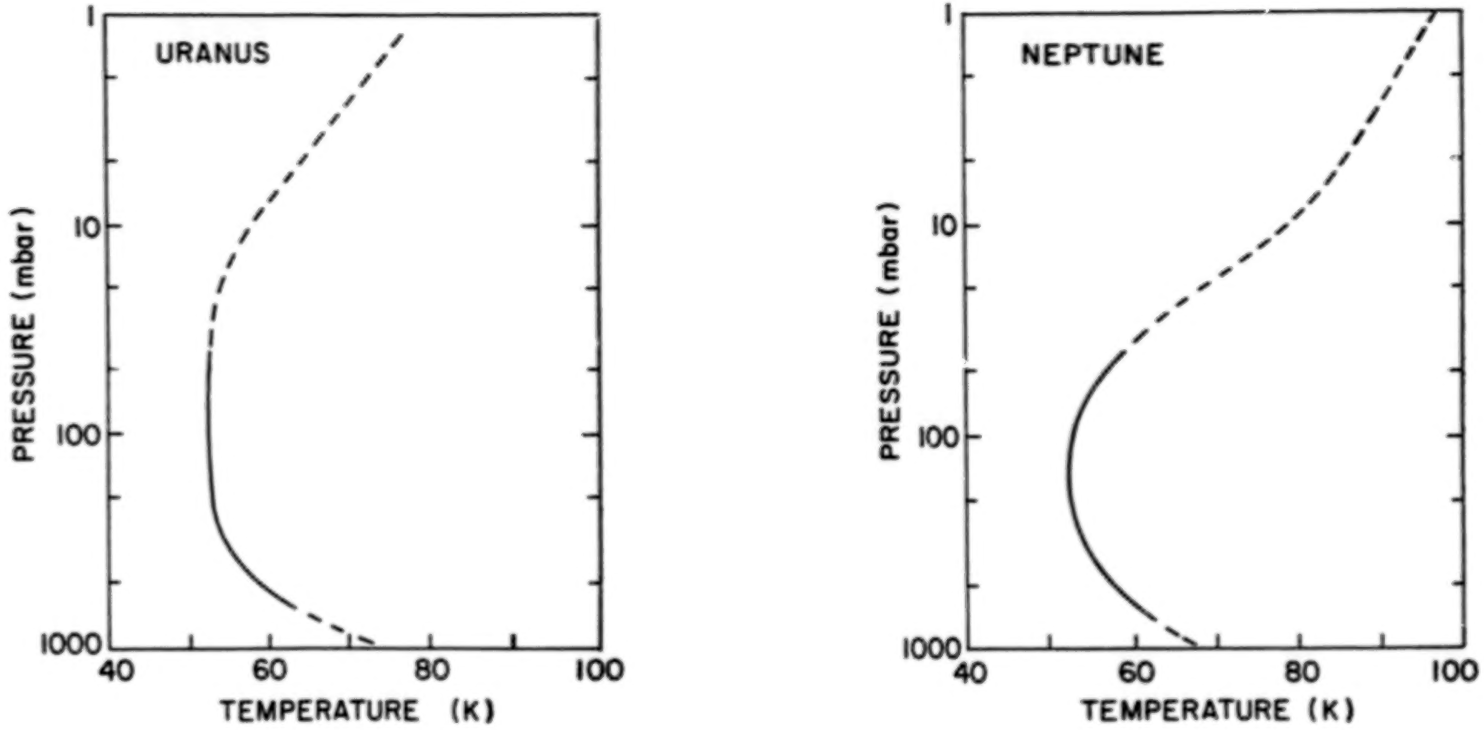

Fig. 17. Vertical temperature profiles for Uranus (left) and Neptune (right), derived by Moseley *et al.*[26]. The solid curves represent the region of maximum information content for their measurements and the broken line their extrapolation outside this region.

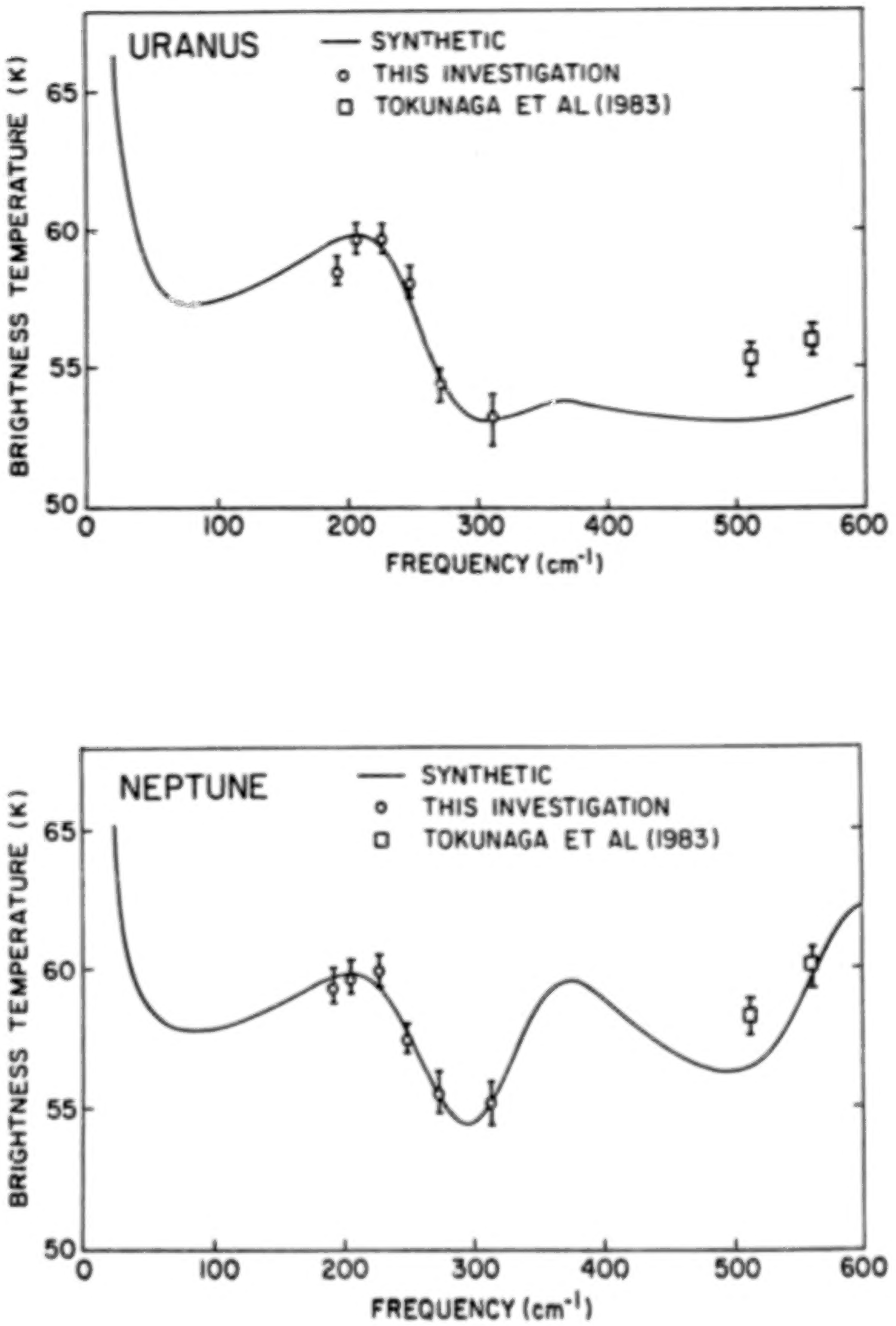

Fig. 18. Brightness temperature spectra of Uranus (top) and Neptune (bottom) for the temperature profiles of Moseley et al[26] shown in Fig. 17. Error bars represent only statistical errors of the measurements. The measurements of Tokunaga et al.[23] are shown as squares.

As a set, these data are sensitive to temperatures in a vertical range from the 200-mbar level down nearly as deep as the 6-bar level. The initial temperature structures were taken from Tokunaga et al.[23] for Uranus and Orton et al.[8] for Neptune, both derived from the models of Appleby[51]. Small changes in the stratospheric temperature structures were made, similar to (but much smaller than) those made by Tokunaga et al.[23] in Appleby's original models. This procedure was performed to reduce the residuals of the temperature sounding fit even further. A few data were omitted from consideration, in order to discriminate againt broad-banded filters. Narrower filters were preferred in order to reduce as much as possible the vertical range of temperatures to which each would be sensitive. The derived temperature structures are shown in Fig. 19 and their associated spectra in Fig. 20.

As part of the background for their analysis, but unreported by Nolt et al.[28], GSO attempted to determine the mixing ratios of He in Uranus and Neptune by assuming various values and minimizing the residuals to the fit[62]. As intimated earlier, these results were quite inconclusive. Formal errors for the derived value of the mixing ratio of He were in the range of 20 to 35%. The formal results of these "optimized" fits were not considered significant. Furthermore, we believe that the current data sets (Fig. 2) are not yet capable of determining a meaningful value of the He mixing ratio unless some discrimination between the thermal and reflected solar components of the 10-μm spectrum were to become possible. Nolt et al.[28] then simply assumed molar mixing ratios of 90% H_2, 8% He and 2% CH_4 (in the deep atmospheres and in the Neptune stratosphere). The assumption of CH_4 mixing ratios of 0.2% or 4% in the deep atmosphere perturbed these results, owing to the change in the H_2-CH_4 collision-induced dipole opacity, only by about 2.5 K.

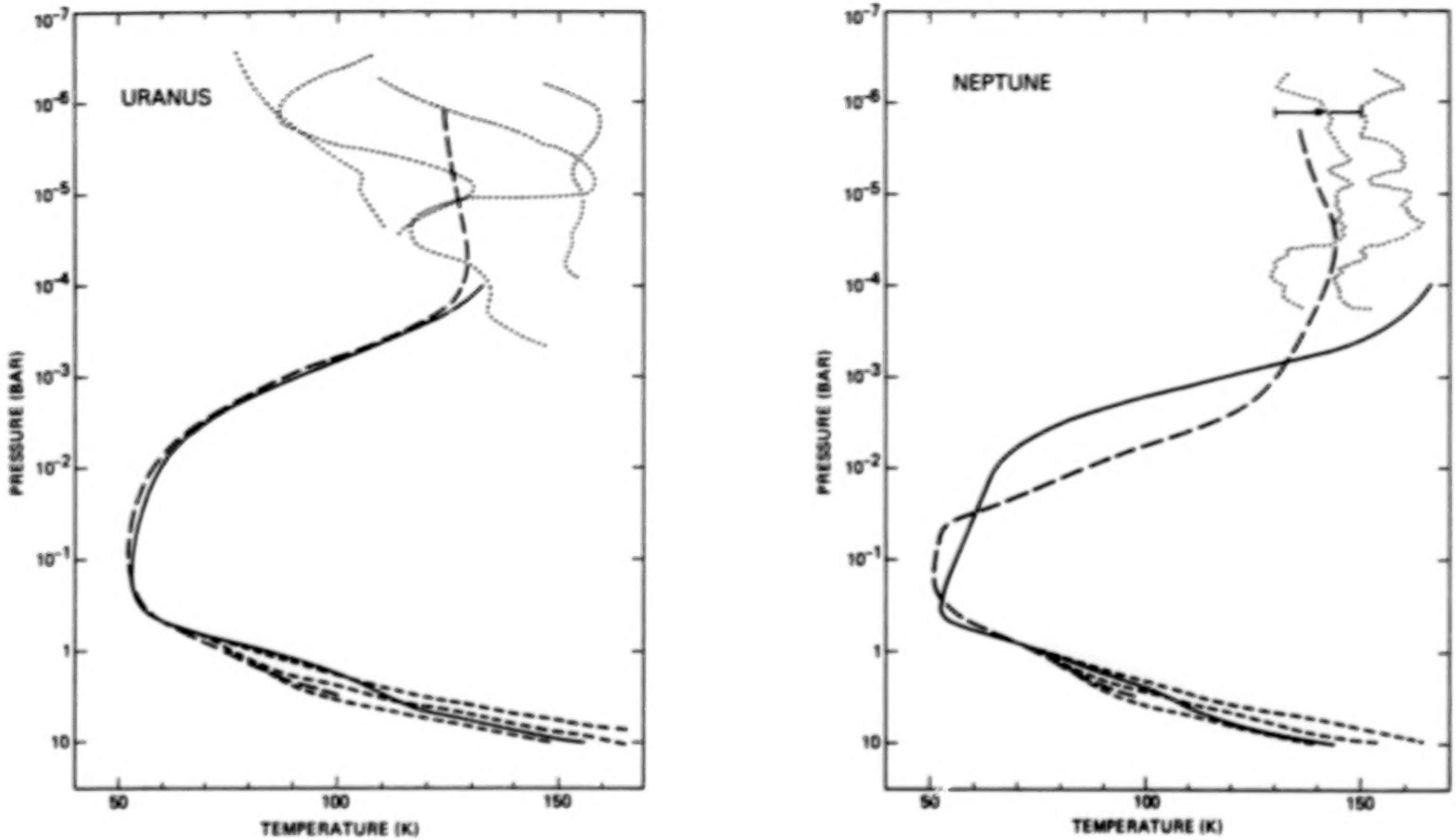

Fig. 19. Temperature profiles for Uranus (left) and Neptune (right) derived by Nolt *et al.*[28]. Solid and short-dashed curves respectively represent results from full temperature sounding and temperature sounding with adiabatic extrapolation to pressures greater than 400 mbar. The upper through lower short-dashed curves represent the results assuming CH_4 mixing ratios of 0.2, 2 and 4%, respectively, in the deep atmosphere. Long-dashed curves represent the models of Appleby[51]. Extremes of stellar occultation results are represented (somewhat schematically) by the dotted curves[30,31,38] and the horizontal bar[37].

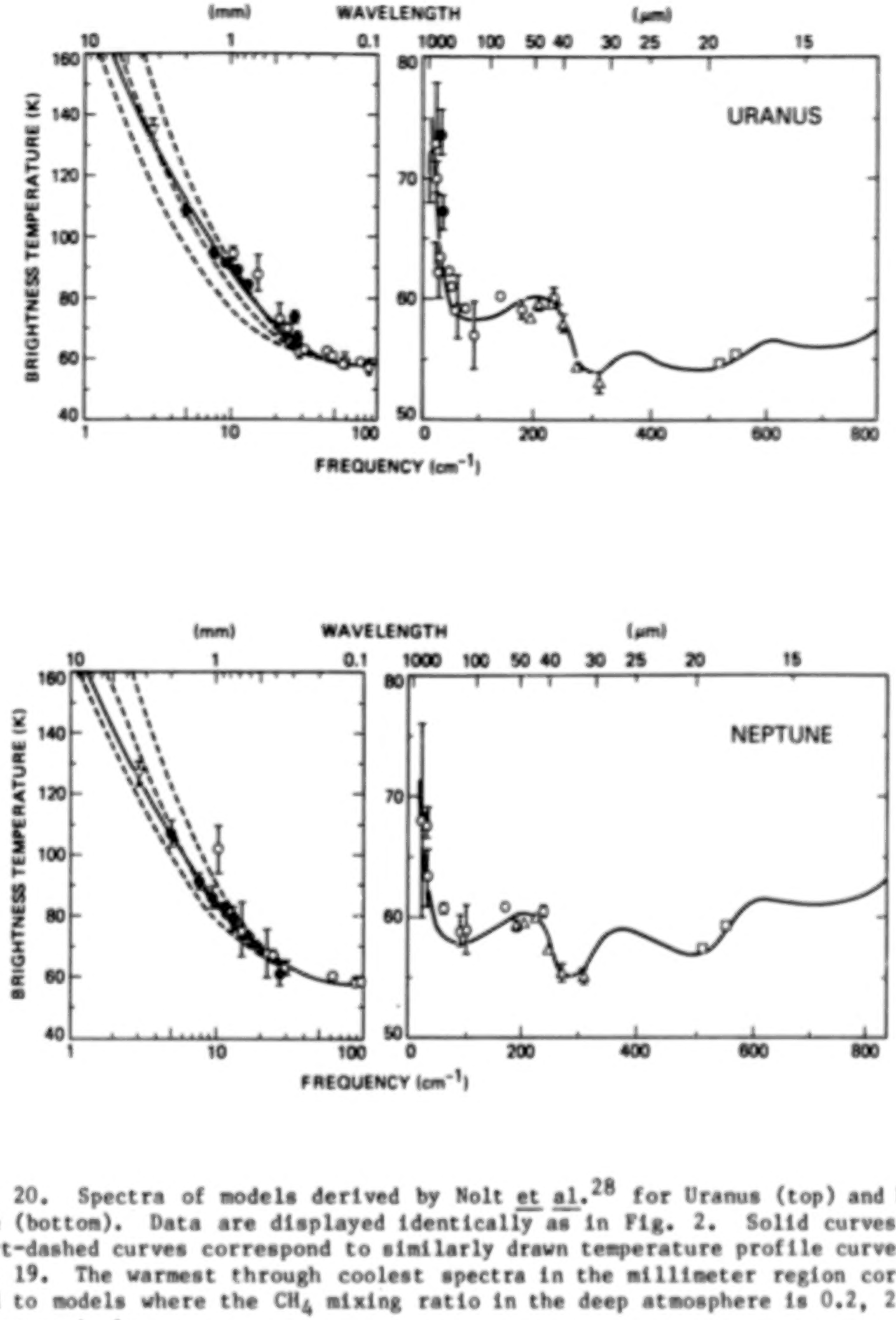

Fig. 20. Spectra of models derived by Nolt et al.[28] for Uranus (top) and Neptune (bottom). Data are displayed identically as in Fig. 2. Solid curves and short-dashed curves correspond to similarly drawn temperature profile curves in Fig. 19. The warmest through coolest spectra in the millimeter region correspond to models where the CH_4 mixing ratio in the deep atmosphere is 0.2, 2 and 4% respectively.

The small temperature gradients in the relevant levels of the Uranus and Neptune atmospheres, compared with their counterparts in the atmospheres of Jupiter or Saturn, dim the prospects for acquiring a very precise fitting using the infrared technique[62]. On the other hand, the comparison of the Voyager Radio Science Subsystem results with those of IRIS to determine consistent temperature and mean molecular weight values may likely lead to much greater accuracies, so long as the influence of heavier molecules is not important or can be understood independently.

A variation of this approach was used (the only one, in fact, adopted by Hildebrand _et al._[27]) by limiting the vertical region of direct temperature retrieval to no deeper than 400 mbar and substituting an adiabatic extrapolation for these deeper levels. A variety of assumptions about the physical conditions in the upper troposphere were then tested against the measurements. The bottom line of such comparisons is that the conditions which are most consistent with the data are given by an equilibrium-like mixture of H_2 para and ortho states with an effective specific heat equal to the weighted sum of both species (i.e. Wallace's[46] "intermediate" H_2), rather than equal to the equilibrating mixture, and a CH_4 mixing ratio of about 2% (Fig. 20). Normal H_2 does poorly; even the limited 16 - 30 μm data discriminate against this possibility. Equilibrium H_2, including the heat of conversion term, also does poorly as a result of the shallow lapse rate which is predicted, even if the He mixing ratio is raised to 50% in an attempt to compensate. The temperature structures (Fig. 19) and associated spectra (Fig. 20) are shown for the "intermediate" [illegible] models with CH_4 mixing ratios of 0.2, 2 and 4% in the deep atmosphere.

The results are not inconsistent with the range of stellar occultation results for each planet which are denoted schematically in Fig. 19. There is still (Fig. 20) difficulty in matching th 17.8- and 19.6-μm measurements of Tokunaga _et al._[23] and the 30-μm measurements of Moseley _et al._[26] simultaneously. A further problem with the results for Uranus is that the models do not fit the details of the data in the submillimeter region, especially the narrow filtered results and wider filtered results located, respectively, at 350 μm and 370 μm in the Nolt _et al._[28] measurements. These suggest that spectral features are present which the model does not take into consideration. The "usual" molecules which have strong rotational spectra in this region such as NH_3 or PH_3 are saturated at these low temperatures. A likely possibility involves ordinarily weak transitions in CH_4: (1) the pure rotation lines arising from the permanent dipole moment caused by centrifugal distortion[67] or (2) the vibrational and rotational transitions associated with CH_4 dimers, which might be expected at low temperatures on the basis of both laboratory measurements and _ab initio_ molecular quantum mechanics[68]. Unfortunately, at this time little can be said about CH_4 dimers, given the dearth of relevant laboratory data. Until these possibilities are clarified quantitatively, conclusions based on this portion of the spectrum must be considered provisional. If weak transitions of CH_4 are the cause of the suspected features, then their presence in the Neptune spectrum is simply disguised by the relatively larger amount of noise associated with the measurements of Neptune relative to those of Uranus. Alternatively, a volatile with strong rotational transitions, such as CO, may simply be very abundant in the atmosphere of Uranus but not Neptune.

SUMMARY AND DISCUSSION

The Emerging Picture: Uranus (mostly) - The stratosphere of Uranus is inverted, and it is probably supported by insolation absorbed by visible and near infrared bands of CH_4, a small amount of which remains above the temperature minimum. Additional heating is required, indicating possible absorption of some 10 - 15% of sunlight in the stratosphere by aerosols. There are no inconsistencies between temperature structures based on or constrained by infrared data and those derived from stellar occultation data. This is heartening, not only for the prospect of a consistent first-order picture of the temperature structure but also for the choice of the 90% H_2 and 10% He composition in the stratosphere. A bulk composition with 25% He by volume, for example, would change a 150 K result to 170 K and produce poorer agreement between these two independent approaches. This same observation can be applied to the results of comparisons between the (largely) infrared-based model structures and the limited stellar occultation results for Neptune.

Radiative transport phenomena are obviously important in the upper stratosphere, including consideration of CH_4 non-LTE effects[66]. Observations by Sicardy *et al.*[34], suggest that a temperature maximum occurs near the equator, while French *et al.*[31] suggest that the close agreement of immersion and emersion temperatures supports the idea of active meridional transport in the stratosphere. Also, French *et al.* found that no significant radiative cooling occurred at points in the atmosphere which had been in darkness more than 1/2 of a terrestrial year. They conclude that molecular and eddy diffusion and atmospheric dynamics are probably just as important as radiation among the competing energy transport mechanisms in the upper stratosphere.

There is still considerable uncertainty in the detailed structure of the lower and middle stratosphere because the infrared data do not provide adequate constraints. For example, these data together with observed geometric albedos (which roughly constrain the total aerosol energy input) give rise to several possible temperature profiles based on localized aerosol heating.

Deeper in the atmosphere, at pressures of 100 mbar to about 6 bars, the average temperature structure is now reasonsbly well constrained (within the uncertainties associated with the bulk composition). The boundary between predominantly radiative and predominantly convective control of the atmosphere is in the vicinity of 400 to 500 mbar. At higher pressures, temperature sounding results are not inconsistent with the assumption of a wet adiabat asociated with about 2% CH_4 by volume in the deep atmosphere and "intermediate" H_2[48]. These conclusions also appear to be true for Neptune. There is not yet a good consensus for how both Uranus and Neptune produce physical conditions which result in this mixture of H_2 species. Opposing explanations for the state of H_2 in outer planet atmospheres are offered by Massie and Hunten[70] and by Conrath and Gierasch[71]. For Uranus, at least, these conclusions are subject to the uncertainty associated with confusion by possible discrete features in the spectrum. These features might well originate from the pure rotation or dimer transitions of CH_4.

Wallace[47] indicates that maximum temperature variations of 5 K are expected in the atmosphere over an annual insolation cycle. These small variations may further be suppressed by the equilibrating effects of convection. As a whole, the conclusions for Uranus so far are consistent with a stable atmosphere, but one in which convection is the dominant energy transport mechanism at pressures higher than about 400 - 500 mbar. To first order, the effects of clouds, which are expected in the vicinity of the CH_4 saturation level, are not apparent. The only infrared evidence for their existence is from somewhat model-dependent interpretations of 10-µm radiance observations; CH_4 condensate clouds at 450 mbar could be consistent with these data as well as with indications from analysis of shorter wavelength data. Radiances observed at 5 µm are probably reflected sunlight which is strongly attenuated by as yet unknown atmospheric absorbers. Otherwise, there is no evidence in the 5-µm to 3-mm spectral range for the presence of deeper clouds in either atmosphere.

Neptune - Neptune's stratosphere is more strongly inverted than Uranus' in the 10 - 100 mbar range, but similar temperatures are achieved in the 1-bar region. The temperature structure is consistent with radiative support by (aerosol) absorption of 5% of the incident insolation together with strong absorption by CH_4 gas in the stratosphere. CH_4 is probably mixed at ratios which appear to be in the same range as those in the deep troposphere (i.e., about 2%). These conclusions are discussed in detail by Appleby[51]. For example, as long as the total aerosol energy input to the atmosphere is about 5 to 10% of the insolation, then aerosol heating cannot power Neptune's thermal inversion regardless of the vertical aerosol distribution.

This implies that CH_4 is actively being transported through the cold trap near 100 mbar. Several mechanisms could accomplish this, some originally suggested by Hunten[61]. (1) Convective activity could be sufficiently strong in some places in the atmosphere that it "overshoots" the regular radiative-convective boundary and delivers CH_4 gas to the stratosphere on a time scale shorter than the time scale for precipitation. (2) Very small particles of CH_4 ice could be updrafted to the stratosphere where they resublimate at warmer temperatures. (3) The atmosphere could be so stable and density variations or other nucleation sites could be so rare that CH_4 remains in a supercooled state on a global scale in the temperature minimum region and passes from the troposphere to the stratosphere in a gaseous state. (4) There are sufficient areas in the planet where the temperature minimum is so warm that the cold trap ceases to exist, i.e. on a global scale the cold trap has "leaks".

We tend to favor (1), which Appleby[51] has called the "convective penetration" model (by analogy with this well-known effect in terrestrial dynamics). We think that there is persuasive evidence for vigorous dynamics in the atmosphere of Neptune. Neptune could have one of the largest internal energy sources (relative to incoming solar energy) among the outer planets. Visible images (reported in another chapter in this volume) show unmistakable evidence for horizontal inhomogeneities. Joyce _et al._[72] report "weather", non-secular changes in atmospheric reflectivities, estimating the transient cloud top location to be in the neighborhood of about 50 mbar[73]. Such a picture is also consistent with the appearance of diurnal variations in the 1- to 2-μm range (J and K filters) and possibly at 4.8 μm (M filter). It could also be consistent with the requirement for the atmosphere to be reflective near or above the 100 mbar level to match the 10.3-μm observation of Orton _et al._[8]. Appleby[51] also pointed out that condensation of CH_4 photolysis products, such as ethane and acetylene, would also occur near the base of the stratosphere (Fig. 11).

Similar to Saturn, Titan and even Jupiter, we might expect considerable differences between the stratospheric temperature structures associated with the polar regions in different seasons, owing to substantial differences in insolation history. At the time of the Voyager 2 encounter with Neptune in 1989, we expect that the northern hemisphere will be in middle to late winter. At that time, the south polar region should be perceptibly warmer than the north if the radiative adjustment time in the middle stratosphere (where hydrocarbon emission features originate) is comparable to or shorter than a Neptunian season (about 40 years).

In the deeper atmosphere, the average temperature structure is reasonably well constrained. As for Uranus, the radiative-convective boundary lies in the region near 400 - 500 mbar, and a correspondence between the direct sounding and adiabatic temperature structure exists, assuming a composition of about 2% CH_4 by volume in the deep atmosphere and an "intermediate" para-H_2 vs. ortho-H_2 mixture. The corresopndence between the mixing ratios of CH_4 in the deep atmosphere and the stratosphere implies an active and efficient transport system between the two.

It is uncertain at this point whether there is a substantive difference between the spectra of Uranus and Neptune in the far infrared and submillimeter with respect to the existence of discrete spectral features. Obviously if they are due to CH_4, then they should appear in the spectra of both atmospheres, but the existing data for Neptune (Fig. 2) are too noisy to resolve this question. Further, if they are due to CH_4 transitions, then current poor spectral resolution would be unable to distinguish between a spectral continuum and absorption features with emission centers in Neptune's spectrum.

Clouds would be expected near the 400-mbar to 1-bar range, owing to saturation of CH_4 gas, but there is no direct evidence for them at infrared wavelengths beyond 4.8 µm nor is there any evidence for any deeper cloud layers.

Problems and Future Prospects - A potentially serious problem in analysis of stellar occultation results is the uncertainty associated with the location of the homopause, the atmospheric level where diffusive separation of H_2 and He becomes important. Uncertain knowledge of the molecular weight, including its variation with height, precludes a straightforward interpretation of the data to determine temperatures. Even worse, spatial inhomogeneities in the location of this level would violate the fundamental requirement of spheroidal symmetry for the results of the technique to be valid. Depending on the eddy diffusion coefficient, the number density at this level is expected to be 10^{11} to 10^{13} cm^{-3}, corresponding to atmospheric pressures of 0.01 to 1 μbar. Independent determinations of its location would be even more useful.

Several processes of energy transport in the upper stratosphere are not modeled on a reliable quantitative basis. Rates for vibration-to-vibration (VV) and vibration-to-translation and rotation (VT) transitions for CH_4 are poorly known at low temperatures[64]. Owing to the important role of these rates in non-LTE effects for CH_4, estimates for radiative equilibrium temperatures can differ by some 10 - 15 K. These rates should be measured, and eventually some estimate should be made of the adequacy of the simple two-level model used by Appleby[66] to estimate the relevant CH_4 non-LTE radiative effects. Other energy transport mechanisms, cited by French et al.[31] may be as important as radiation at these μbar levels in the atmosphere. However, it is difficult to examine these processes quantitatively until some independent estimate is made for the eddy viscosity of the stratosphere and its variation with height. This might be possible via interpretation of the CH_4 abundance profile[74]. The CH_4 profile might be determined from the atmospheric ultraviolet absorption of sunlight or starlight, similar to the Voyager 2 UVS observations of the occultation of α Leo (Regulus)[75]. Finally, the contribution of energy associated with chemical reactions, especially photochemistry of CH_4, and its interaction with the ambient thermal energy resevoir should be estimated.

Appleby's[51] models for both Uranus and Neptune have shown that insolation-absorbing material in these stratospheres can significantly infleunce the temperature structure (Fig. 10), which leads us to seek further constraints on this effect. One approach could be to tighten the constraints available from the reflectivity models in the amount of solar energy absorbed or, if possible, in determination of its vertical structure. This might be possible from Voyager PPS or ISS results at ultraviolet wavelengths, using the advantage of sampling the angular dependence of reflected ultraviolet radiation.

Another approach would devise strategies for extending upward the region capable of thermal sampling. This could be accomplished by obtaining measurements closer to the rotational line centers, especially near 27 µm (370 cm^{-1}). S. H. Moseley (NASA Goddard Space Flight Center) plans to attempt this soon in the 25- to 60-µm range from the Kuiper Airborne Observatory; additional measurements are possible from ground-based observatories. If there is sufficient signal, spacecraft observations, such as Voyager IRIS, could also observe at this wavelength with some added advantage of high emission angle measurements near the limb. For Neptune, the numerical stability and information content of temperature sounding via the 7-µm CH_4 band in the context of the convective penetration model might also be explored.

Some theoretical effort should and can be invested to extend Appleby's[51] work in the stratosphere to determine the variability of the temperature structure as a function of insolation and insolation history. Appleby presented first-order, time-independent exploratory calculations showing the magnitude of such effects (Fig. 21) if meridional transport were negligible; however, French et al.[31] have argued that it may be very efficient, at least near the 1 µbar level. Clearly, rigorous time-dependent studies are needed to establish res-

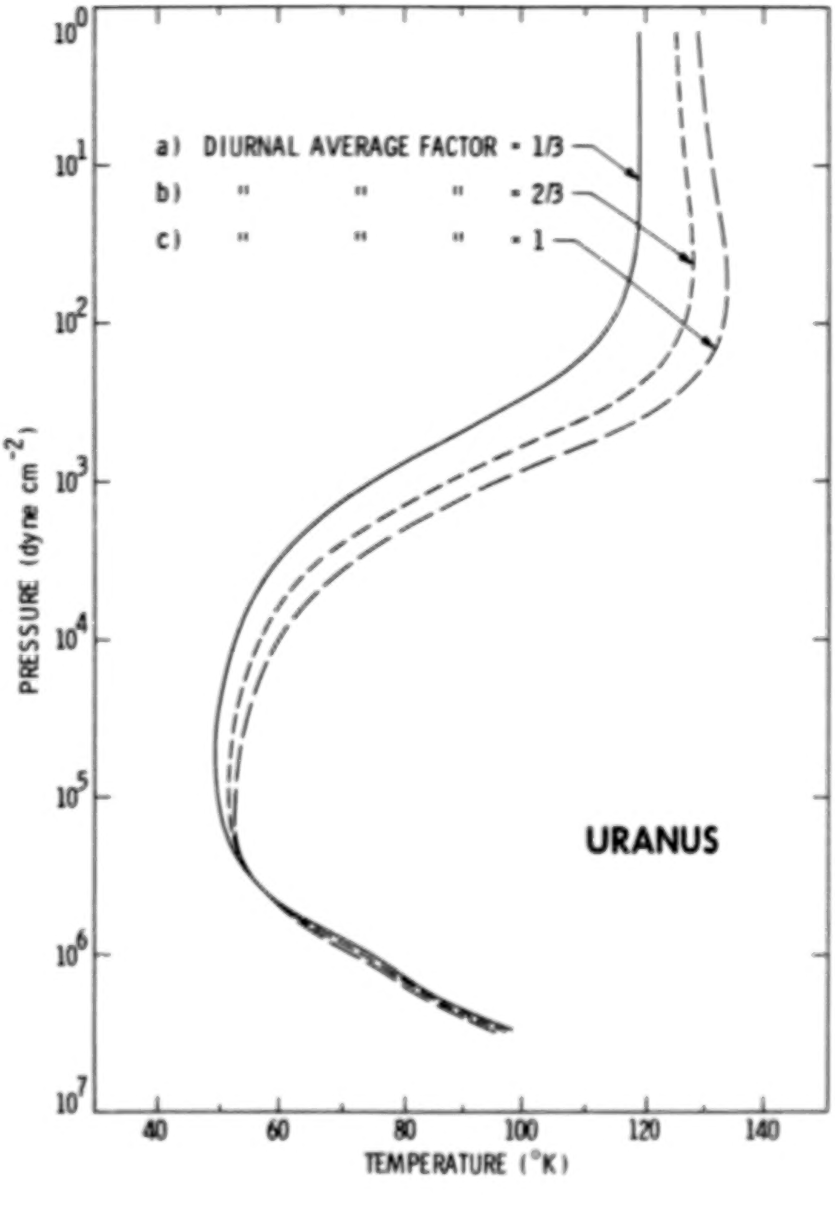

Fig. 21. Appleby's[51] exploratory models for Uranus, showing the response of the atmosphere to variations in the effective insolation. A "diurnal average factor" of 1/2 is usually employed to achieve a day-night mean solar flux. Curve (c) represents a pole-on configuration (which occurs in 1987). The magnitude of these differences would be expected in the absence of meridional heat transfer in the stratosphere.

ponse times of the atmosphere to a variety of possible insolation histories. While such models are universally regarded as awesome sinks of computer resources, they are not beyond current expertise, viz. Wallace's work in the troposphere of Uranus[49]. Additional work for the stratosphere of Neptune might determine (1) the dependence of the radiative equilibrium temperature structure on slightly higher amounts of CH_4 than the 2% in Appleby's models (tropospheric values might conceivably be as high as 4%) and (2) the maximum possible heating of the atmosphere at the 100-mbar level to evaluate quantitatively the potential for creating "leaks" in the cold trap from radiative heating effects.

The calibration of absolute infrared fluxes is a pervasive uncertainty, especially troublesome in comparisons between data sets based on different calibration systems (e.g. Tokunaga *et al.*[24] and Moseley *et al.*[26]). The fundamental uncertainty of absolute infrared flux calibrations remains as the primary uncertainty in the determination of the bolometric thermal flux from Uranus and Neptune. A program in which GSO is involved is underway to measure Uranus and Neptune at 30 μm from the ground, based on a calibration other than the "standard" Mars model[55,56] in order to cross-calibrate with the data of Moseley *et al.*[26]. An improvement in the absolute flux may also be forthcoming from Infrared Astronomy Satellite observations of Uranus and Neptune, using a comparison with their calibration system which involves both stellar and solar system objects. In terms of the Voyager contribution, while the IRIS experiment will not be expected to sample a large portion of the spectrum, its excellent calibration might establish another benchmark to cross-calibrate other sets of earth-based observations. This latter possibility can only be realized technically, however, if observations of the whole disk (or simulations of the whole disk) are made which are relevant to the geometry observable from the earth.

Improvements in measurements of the bolometric thermal output can be made with certainty by sampling the full latitude range. The unique Voyager encounter with Uranus actually helps fulfill this requirement to a much greater extent than for the nearly equatorial trajectories of the other Voyager planetary encounters. However, in practice, the restricted spectral grasp of the IRIS experiment may limit the extent to which this is possible by direct observations. Nonetheless, IRIS may be able to retrieve sufficient spectral information to form reliable physical models on which the full spectra and thermal flux output may be based. Future spacecraft missions in which determination of the temperature profile, for example, is a science goal must be able to observe much longer wavelengths than the 50-µm limit of the IRIS experiment.

The nearly vanishing constraints on the mixing ratio of He in the atmosphere can be improved prior to the Voyager encounter by better data longward of the 50-µm limit of Moseley _et al._[26]. Where possible, such continuous measurements may be more helpful than the broader-band filtered radiometric measurements of Hildebrand _et al._[27], for example. To provide a truly useful lever on the spectral shape, such measurements should extend out to 100 µm. Measurements in the 10-µm region would provide another lever, were it not for confusion with possible reflected solar radiation. On the other hand, the most definitive measurements of this ratio will probably best come from a coordinated examination of IRIS spectra of the region characterized by the RSS occultation experiment, as for Jupiter[52] and Saturn[53]. However, for both Uranus and Neptune the mean molecular weight may vary significantly with altitude and make a proper transformation of the refractivity profile to the temperature profile rather challenging. The presence or absence of 2% CH_4 in gaseous form changes the mean molecular weight by 12%. A failure to consider changes in the level-by-level partial pressure of CH_4 could therefore produce systematic errors of 8 K or more in temperature. Furthermore, the possible presence of heavier gases such as N_2 or Ar must also be considered.

Uncertainty about the origin of the putative far infrared and submillimeter features may best be resolved by direct spectroscopic observations. Such observations will be attempted for Uranus by I. Nolt (U. Oregon) and P. A. R. Ade (Queen Mary College, London) and their colleagues in the near future, using a Fabry-Perot spectrometer in the 350-µm through 2-mm region. If successful (and if features are actually detected) then it may be possible to detect and identify new atmospheric species for lines not due to CH_4 absorption. If CH_4 is the source of the features, then a more accurate determination of the CH_4 mixing ratio may be possible, providing sufficient molecular spectroscopic information.

Similarly, spectroscopy should be performed in the 5-µm region, even at low resolution, to determine to first order whether the low flux from this region is due to discrete gaseous absorption. Measurements at sufficiently high resolution could lead to improved quantitative information about the abundances of minor constituents, provided that the cloud continuum reflecting properties can be characterized adequately.

More observations in general, even those which appear to duplicate previous efforts could be quite useful. This could be particularly true if a new approach were to be used and the data compared with older results (e.g. spectral radiometry compared with older filtered radiometry). The perversity of infrared photons is not to be denied. Independent judgements are strongly encouraged which might help to determine whether filtered radiometric observations in regions of weak thermal flux, such as those of Tokunaga et al.[23] or Orton et al.[8], have been influenced by small (but potentially devastating) shorter or longer wavelength leaks.

The mechanisms for producing an adiabatic lapse rate consistent with the specific heat characterized by "intermediate" H_2 is not unquestionably established. Massie and Hunten[70] explain the existence of such a state by suggesting that the most efficient conversion process involves catalytic reactions between free-radical surface sites on aerosol particles and H_2 molecules. Equilibrating collisions (on aerosol surfaces) change the para- and ortho-H_2 ratios and redistribute the rotational levels among and between even and odd quantum number levels. Other bimolecular collisions simply redistribute rotational levels among even-only and odd-only levels. If the number of equilibrating collisions is much less than the number of binary collisions, an equilibrium-like para-ortho ratio results with a specific heat nearly equal to the weighted sum of the para- and ortho-H_2 molecules present. Significant amounts of equilibrated H_2 can be produced near the 1-bar level, they estimate, if the efficiency of conversion per collision is between 10^{-8} and 10^{-9} and the effective eddy mixing coefficient is 10^4 cm^2/sec.

On the other hand, Conrath and Gierasch[71], reviewing the variability of the Jovian para-ortho ratio as a function of position on the planet, show evidence that the Jovian atmosphere is not characterized by "intermediate" H_2, as might be inferred from Massie and Hunten's report. Furthermore, they suggest that H_2-H_2 collisions, not aerosol surface catalytic reactions, are the dominant means for para-ortho conversion with a characteristic conversion time scale of 10^9 sec; this is much longer than suggested by Massie and Hunten. They argue that the para-ortho variations in the Jovian atmosphere are quite uncorrelated with first-order estimates of the presence of clouds, further diminishing the strength of Massie and Hunten's picture of the conversion process in Jupiter. Conrath and Gierasch do, in fact, predict close equilibration of ortho- to para-H_2 for the atmospheres of Uranus and Neptune. However, they expect a strong influence of the conversion process on the convection overturning rate and they would have expected the lapse rate characteristic of equilibrating H_2.

Infrared data for both planets suggest that the atmospheres are best characterized by "intermediate" H_2. We could be confused by different signatures from strongly inhomogeneous atmospheres characterized by strong vertical updrafts and downdrafts, creating different mixtures of species we are attributing to a single state. But that would only be creative (i.e. laminar) handwaving, because the dynamical regimes of Uranus and Nepture appear to be very different. The issue involves two distinct problems. One is the proper estimation of catalysis reaction rates on the surface of NH_3 and CH_4 ices for which Conrath and Gierrasch[70] suggest that more laboratory information is needed. The other concerns the effects of the energy of conversion of ortho- and para-H_2. In the views of Conrath and Gierasch (personal communications) the presence of "intermediate" H_2, i.e. significant amounts of converted H_2 remaining in the vicinity of the same temperatures where conversion took place, would seem to imply that parcels of gas cyclically traverse the same temperature fields on a planet-wide basis. More thought should be given to the possibility that more efficient energetic pathways exist. Other tests of the Conrath and Gierasch view[71] will develop from examining the depth dependence of the para-ortho ratio in the atmospheres of Jupiter and possibly Saturn.

Another problem lurking in the troposphere is the presence of clouds and their potential influence on outgoing radiation. More information on clouds is available from the visible and near infrared spectral region. However, extrapolation of heuristically-determined cloud properties over a decade or more in wavelength is not wise. Probably the best approach is to test specific physical cloud models by studying their influence on synthetic infrared spectra. Such work has been done for NH_3 ice clouds for Jupiter[76,77] and should be attempted for CH_4 condensates in the atmospheres of Uranus and Neptune. This, of course, requires the determination of indices of refraction for CH_4 ice from absorption and reflection measurements in the laboratory. These do not yet exist in a set covering a wide spectral range, but provisional values may be determinable for a narrower range. Further complications will also arise, similar to those for NH_3 ice as a candidate cloud constituent in the atmospheres of Jupiter and Saturn, in estimating the scattering properties of non-spherical particles of unknown shape. Nevertheless, even rudimentary estimates would help determine whether such "model clouds" (1) are responsible for the reflection of solar radiation at 5 µm, (2) are capable of providing the "additional" flux at 10 µm to be consistent with observations, or (3) influence the outgoing thermal flux at longer wavelengths. Some additional work in constraining the particle size would also follow from a study of various characteristic size and time scales associated with cloud formation along the lines pursued by Rossow[78] for the Earth, Venus, Mars and Jupiter. Further observational work might strengthen the link between 10-µm flux and clouds in Neptune by suggesting a correlation of the flux with the established diurnal variability of the planet at shorter wavelengths[5].

For the deeper atmosphere, a test of Wallace's model[49] for the time-dependence of convective and radiative flux as a function of planetary position must be made by spacecraft observations or by imaging the planet at millimeter wavelengths. Voyager IRIS results may shed some light on this by searching for temperature variations of the kind predicted by the model near 450-mbar (the level to which 50-μm radiation is sensitive). For information about deeper atmospheric levels, only future missions equipped with far infrared through millimeter detection capability (or several direct probes) would be able to provide answers in sufficient detail.

In summary, the Voyager mission should be able to provide some answers - even if only provisional ones, for the remaining problems in the characterization of the atmospheres of Uranus and Neptune. Other answers may be forthcoming through further earth-based observations. In fact, the prospect of acquiring new and useful information about Uranus and Neptune from ground-based and airborne observatories is still quite exciting. This will certainly be true with the development of millimeter (and submillimeter) synthetic imaging arrays, similar to the capability of the VLA in the microwave region (cf. Gulkis and de Pater's chapter in this volume). Further theoretical work needs to be done on several fronts, as outlined above. The cross-comparison of results among several planets will be an especially fruitful approach in general. Additional cross-comparisons may also be useful between different approaches to a spectral problem, involving efforts to understand information from several different spectral regions, following Wallace's[48] example.

However, any information about spatial variability of temperatures or any other infrared-derived properties in a wide variety of locations across the planet must rely on spacecraft experiments. Future considerations of relevant spacecraft experiments must consider the hardware requirements involving observations of much colder thermal sources and much longer wavelengths than has been the case for previous missions.

ACKOWLEDGEMENTS

We express our sincere gratitude to all those who have, by their voluntary release of data prior to publication, personal discussion, insightful comment and critical review of a preliminary version of this review, contributed to it in some way. Our special thanks should be mentioned specifically for the following people: Kevin Baines, Jay Bergstralh, Michael Combes, Barney Conrath, Peter Gierasch, Roger Hildebrand, Bill Hubbard, Bob Lowenstein, Harvey Moseley, Ira Nolt, Bruno Sicardy, and Alan Tokunaga. The resources required by this review and much of the work cited herein was sponsored by the Planetary Atmospheres discipline of the Earth and Planetary Exploration Division of NASA through contract NAS 7-100 to the Jet Propulsion Laboratory, California Institute of Technology.

REFERENCES

1. M. J. S. Belton. 1982. An introductory review of our present understanding of the structure and composition of Uranus' atmosphere. In Uranus and the Outer Planets. (G. E. Hunt, Ed.) Cambridge Univ. Press. Cambridge. pp. 155-172.

2. L. Trafton. 1981. The atmospheres of the outer planets and satellites. Rev. Geophys. Space Phys. 19, 43-89.

3. F. C. Gillett and G. H. Rieke. 1977. 5 - 20 micron observations of Uranus and Neptune. Astrophys. J. 218, L141-L144.

4. W. W. Macy, W. M. Sinton and C. A. Beichman. 1980. Five-micrometer measurements of Uranus and Neptune. Icarus 42, 68-70.

5. R. H. Brown, D. P. Cruikshank, and A. T. Tokunaga. 1981. The rotation period of Neptune's upper atmosphere. Icarus 47, 159-165.

6. U. Fink and H. P. Larson. 1979. The infrared spectra of Uranus, Neptune and Titan from 0.8 to 2.5 microns. Astrophys. J. 233, 1021-1040.

7. W. W. Macy and W. M. Sinton. 1977. Detection of methane and ethane emission on Neptune but not on Uranus. Astrophys. J. 218, L79-L81.

8. G. S. Orton, A. T. Tokunaga, and J. Caldwell. 1983. Observational constraints on the atmospheres of Uranus and Neptune from new measurements at 10 μm. Icarus 56, 147-164.

9. D. Morrison and D. P. Cruikshank. 1973. Temperatures of Uranus and Neptune at 24 microns. Astrophys. J. 179, 329-331.

10. G. H. Rieke and F. J. Low. 1974. Infrared measurements of Uranus and Neptune. Astrophys. J. 193, L147-L149.

11. M. T. Steir, W. A. Traub, G. G. Fazio, E. L. Wright, and F. J. Low. 1978. Far-infrared observations of Uranus, Neptune, and Ceres. Astrophys. J. 226, 347-349.

12. G. G. Fazio, W. A. Traub, E. L. Wright, F. J. Low, and L. Trafton. 1976. The effective temperature of Uranus. Astrophys. J. 209, 663-637.

13. D. A. Harper, F. J. Low, G. H. Rieke, and K. R. Armstrong. 1972. Observations of planets, nebulae, and galaxies at 350 microns. Astrophys. J. 177, L21-L35.

14. R. F. Loewenstein, D. A. Harper, S. H. Moseley, C. M. Telesco, and H. A. Thronson. 1977. Far-infrared and submillimeter observations of the planets. Icarus 31, 315-324.

15. S. E. Whitcomb, R. H. Hildebrand, J. Keene, R. F. Stiening, and D. A. Harper. 1979. Submillimeter brightness temperatures of Venus, Jupiter, Uranus and Neptune. Icarus 38, 75-80.

16. C. T. Cunningham, P. A. R. Ade, E. J. Robson, I. G. Nolt, and J. Radostitz. 1981. The submillimeter spectra of the planets: Narrow-band photomtery. Icarus 48, 127-139.

17. R. Courtin, N. Coron, T. Encrenaz, R. Gispert, P. Bruston, J. Leblanc, G. Dambier, and A. Vidal-Madjar. 1977. Observations of the giant planets at 1.4 mm and consequences on the effective temperatures. Astron. Astrophys. 60, 115-123.

18. W. M. Werner, G. Neugebauer, D. R. Houck and M. G. Hauser. 1978. One-millimeter brightness temperatures of the planets. Icarus 35, 289-296.

19. B. L. Ulich 1974. Absolute brightness temperature measurements at 2.1-mm wavelength. Icarus 21, 254-261.

20. B. L. Ulich and E. R. Conklin. 1976. Observations of Ganymede, Callisto, Ceres, Uranus and Neptune at 3.33 mm Wavelength. Icarus 27, 183-189.

21. E. E. Epstein, M. M. Dworetsky, J. W. Montgomery and W. G. Fogarty. 1970. Mars, Jupiter, Saturn, and Uranus: 3.3-mm brightness temperatures and a search for variations with time or phase angle. Icarus 13, 276-281.

22. M. J. Klein and J. A. Turegano. 1978. Evidence of an increase in the microwave brightness temperature of Uranus. Astrophys. J. 224, L31-L34.

23. A. T. Tokunaga, G. S. Orton and J. Caldwell. 1983. New observational constraints on the temperature inversions of Uranus and Neptune. Icarus 53, 141-146.

24. A. T. Tokunaga. 1984. A re-evalutation of the 20-μm magnitude system. Astron. J. In press.

25. B. K. Ulich. 1981. Millimeter-wavelength continuum calibration sources. Astron. J. 86, 1619-1626; unpublished communication.

26. S. H. Moseley, B. J. Conrath, and R. F. Silverberg. 1984. Atmospheric temperature profiles of Uranus and Neptune. Submitted.

27. R. H. Hildebrand, R. F. Loewenstein, D. A. Harper, G. S. Orton, J. B. Keene, and S. E. Whitcomb. 1984. Far infrared and submillimeter brightness temperatures of the giant planets at 38 - 968 μm. Submitted.

28. I. Nolt, J. Radostitz, G. Orton, P. Ade, C. Cunningham, M. Griffin, and E. Robson. 1984. Submillimeter and millimeter observations of Uranus and Neptune. Submitted.

29. L. Trafton. 1967. Model atmospheres of the major planets. Astrophys. J. 147, 765-781.

30. E. Dunham, J. L. Elliot, and P. J. Gierasch. 1980. The upper atmosphere of Uranus: Mean temperature and temperature variations. Astrophys. J. 235, 279-284.

31. R. G. French, J. L. Elliot, E. W. Dunham, D. A. Allen, J. M. Elias, J. A. Frogel, and W. Liller. 1983. The thermal structure and energy balance of the Uranian upper atmosphere. Icarus 53, 399-414.

32. B. Sicardy, M. Combes, A. Brahic, P. Bouchet, C. Perrier, and R. Courtin. 1982. The 15 August 1980 occultation by the Uranian system: Structure of the rings and temperature of the upper atmosphere. Icarus 52, 454-472.

33. R. G. French, J. L. Elliot, B. Sicardy, P. Nicholson, and K. Matthews. 1982. The upper atmosphere of Uranus: A critical test of isotropic turbulence models. Icarus 51, 491-508.

34. B. Sicardy, M. Combes, J. Lecacheux, P. Bouchet, A. Brahic, P. Laques, C. Perrier, L. Vapillon, and Y. Zeau. 1984. Variations of the stratospheric temperature profile along the limb of Uranus: Results of the 22 April 1982 stellar occultation. Submitted.

35. J. Kovalevsky and F. Link. 1969. Diamètre aplatissement et propriétés optiques de la haute atmosphère de Neptune d'après l'occultation de l'étoile BD 17°4388. Astron. Astrophys. 2, 98-412.

36. K. C. Freeman and G. Lyngå. 1970. Data for Neptune from occultation observations. Astrophys. J. 160, 767-780.

37. L. Wallace. 1975. On the occultation of BD-17°4388 by Neptune. Astrophys. J. 197, 257-261.

38. R. G. French, J. H. Elias, D. J. Mink, and J. L. Elliot. 1983. The structure of Neptune's upper atmosphere: The stellar occultation of 24 May 1981. Icarus 55, 332-336.

39. B. Sicardy, J. P. Maillard, and D. P. Cruikshank. 1983. Stratospheric temperatures of Neptune from stellar occultation. Bull. Amer. Astron. Soc. 15, 858.

40. J. L. Elliot. 1979. Stellar occultation studies of the solar system. Ann. Rev. Astron. Astrophys. 17, 445-475.

41. R. G. French, J. L. Elliot, and P. J. Gierasch. 1978. Analysis of stellar occultation data: Effects of photon noise and initial conditions. Icarus 33, 186-202.

42. R. G. French, and R. V. E. Lovelace. 1983. Strong turbulence and atmospheric waves in stellar occultations. Icarus 56, 122-126.

43. R. Courtin, D. Gautier, and A. Lacombe. 1978. On the thermal structure of Uranus from infrared measurements. Astron. Astrophys. 63, 97-101.

44. R. Courtin, D. Gautier, and A. Lacombe. 1979. Indications of supersaturated stratospheric methane in Neptune from its atmospheric thermal profile. Icarus 37, 236-248.

45. R. E. Danielson. 1977. The structure of the atmosphere of Uranus. Icarus 30, 462-478.

46. R. E. Danielson, W. D. Cochran, P. G. Wannier, and E. S. Light. 1977. A saturation model of the atmosphere of Uranus. Icarus 31, 97-109.

47. L. Wallace. 1975. On the thermal structure of Uranus. Icarus 25, 538-544.

48. L. Wallace. 1980. The structure of the Uranus atmosphere. Icarus 43, 231-259.

49. L. Wallace. 1983. The seasonal variation of the thermal structure of the atmosphere of Uranus. Icarus 54, 110-132.

50. W. Macy and L. Trafton. 1975. Neptune's atmosphere: The source of the thermal inversion. Icarus 26, 428-436.

51. J. F. Appleby. 1984. Radiative-convective equilibrium models of Uranus and Neptune. Submitted.

52. D. Gautier, B. Conrath, M. Flasar, R. Hanel, V. Kunde, A. Chedin, and N. Scott. 1981. The helium abundance of Jupiter from Voyager. J. Geophpys. Res. 86, 8713-8720.

53. D. Gautier, B. Conrath, M. Flasar, R. Hanel, V. Kunde, A. Chedin, and N. Scott. 1983. The helium abundance of Saturn from Voyager. Astrophys. J. In press.

54. D. Gautier, B. Bezard, A. Marten, J. P. Baluteau, N. Scott, A. Chedin, V. Kunde, and R. Hanel. 1982. The C/H ratio in Jupiter from the Voyager infrared investigations. Astrophys. J. 257, 901-912.

55. E. L. Wright. 1977. Recalibration of the far infrared brightness temperatures of the planets. Astrophys. J. 210, 250-253.

56. E. L. Wright and S. Odenwald. 1980. Brightness temperatures of Mars 1979-1983. Bull. Amer. Astron. Soc. 12, 456.

57. R. L. Loewenstein, D. A. Harper, and S. H. Moseley. 1977. The effective temperature of Neptune. Astrophys. J. 218, L145-L146.

58. G. W. Lockwood, B. L. Lutz, D. T. Thompson, and A. Warnock. 1983. The albedo of Uranus. Astrophys. J. 266, 402-414.

59. R. E. Murphy and L. M. Trafton. 1974. Evidence for an internal heat source in Neptune. Astrophys. J. 193, 253-255.

60. D. Wenkert and G. E. Danielson. 1982. The visible phase curves of Uranus and Neptune from Voyager. Bull. Amer. Astron. Soc. 14, 760.

61. D. H. Hunten. 1972. Introduction and summary. In The atmosphere of Uranus: Proceedings of a workshop held at Ames Research Center Sept 30, 1974. (D. M. Hunten, Ed.), pp. 1-13.

62. D. Gautier and K. Grossman. 1972. A new method for determining the mixing ratio hydrogen to helium in the giant planets. J. Atmos. Sci. 29, 788-792.

63. P. Dore, L. Nencini, and G. Birnbaum. 1983. Far infrared absorption in normal H_2 from 77K to 298K. J. Quant. Spectrosc. Radiat. Transf. 30, 245-254.

64. E. R. Cohen, L. Frommhold, and G. Birnbaum. 1983. Analysis of the far infrared H_2-He spectrum. J. Chem. Phys. 77, 4933-4941.

65. U. Fink and H. P. Larson. 1979. The infrared spectra of Uranus, Neptune, and Titan from 0.8 to 2.5 micron. Astrophys. J. 233, 1021-1040.

66. J. F. Appleby. 1984. CH_4 non-LTE in the atmospheres of the outer planets. Submitted.

67. W. W. Macy. 1980. Mixing ratios of methane, ethane and acetylene in Neptune's stratosphere. Icarus 41, 153-158.

68. A. Rosenberg, I. Ozier, and A. K. Kudian. 1972. Pure rotational spectrum of CH_4. J. Chem. Phys. 57, 568-569.

69. G. Birnbaum, L. Frommhold, L. Nencinni, and H. Sutter. 1983. The collision-induced far-infrared absorption band of gaseous methane in the region 30 - 900 cm^{-1}. Chem. Phys. Lett. 100, 292-296.

70. S. T. Massie and D. M. Hunten. 1982. Conversion of para and ortho hydrogen in the Jovian planets. Icarus 49, 213-226.

71. B. J. Conrath and P. J. Gierasch. 1984. Global variation of the para hydrogen fraction in Jupiter's atmopsphere and implications for dynamics in the outer planets. Icarus. In press.

72. R. R. Joyce, C. B. Pilcher, D. P. Cruikshank, and D. Morrison. 1977. Evidence for weather on Neptune I. Astrophys. J. 214, 657-662.

73. C. B. Pilcher. 1977. Evidence for weather on Neptune II. Astrophys. J. 214, 663-666.

74. S. K. Atreya and J. H. Ponthieu. 1983. Photolysis of methane and the ionosphere of Uranus. Planet. Space Sci. 31, 939-944.

75. M. C. Festou, S. K. Atreya, T. M. Donahue, B. R. Sandel, D. E. Shemansky, and A. L. Broadfoot. 1981. Composition and thermal profiles of the Jovian upper atmosphere determined by the Voyager ultraviolet stellar occultation experiment. J. Geophys. Res. 86, 5715-5725.

76. A. Marten, D. Rouan, J.-P. Baluteau, D. Gautier, B. J. Conrath, R. Hanel, V. Kunde, R. Samuelson, A. Chedin, and N. Scott. 1981. Study of the ammonia

ice cloud layer in the equatorial region of Jupiter from the infrared interferometric experiment on Voyager. Icarus 46, 233-248.

77. G. S. Orton, J. F. Appleby, and J. V. Martonchik. 1982. The effect of ammonia ice on the outgoing thermal radiance from the atmosphere of Jupiter. Icarus 52, 94-116.

78. W. Rossow. 1978. Cloud microphysics: Analysis of the clouds of Earth, Venus, Mars, and Jupiter. Icarus 36, 1-50.

BLANK PAGE

ULTRAVIOLET OBSERVATIONS OF URANUS AND NEPTUNE BELOW 3000 Å

John Caldwell, Richard Wagener and Tobias Owen

Department of Earth and Space Science
State University of New York
Stony Brook, New York 11794, USA

Michel Combes and Therese Encrenaz

Observatoire de Paris
Meudon 92190, France

Abstract

From 2000 to 3000 Å, both Uranus and Neptune have albedos that are about two times higher than Jupiter or Saturn's, implying that the outer giants have stratospheres that are relatively free of aerosol absorption. Uncertainties in the absolute calibration procedure allow discrepancies of order 15% between conservative models and the observations. A small amount of aerosol absorption is therefore possible. Below 2000 Å the derived albedo is highly dependent on the solar spectrum source used in the data reduction. The most recent result for Uranus, first reported here, is consistent with a secular change in C_2H_2 mixing ratio from ~ $3 \cdot 10^{-8}$ in 1980 to $\lesssim 10^{-9}$ in 1983. These values are ~ 2 orders of magnitude less than the mixing ratios of this gas on Saturn, and comparable to the amount on Jupiter.

INTRODUCTION

This review of ultraviolet observations includes critical discussion of published work from three earth-orbiting satellites and also presentation of new results from the International Ultraviolet Explorer satellite (IUE) not previously published. The first two authors are responsible for writing this review. The others participated in the observing phase of the new results, but because of the deadline for preparing this manuscript, they unfortunately could not be included in the writing.

Between 2000 and 3000 Å, data reduction is quite straightforward. Broadband photometry and intermediate resolution spectrophotometry of Uranus and Neptune in this spectral region from 3 satellites are presented. The data clearly show that the albedos for both planets are higher than the corresponding albedos for Jupiter and Saturn. The implication is that the outer two giant's stratospheres have much less aerosol absorption than do the inner two. As will be discussed, existing observations cannot conclusively distinguish between the possibilities of nearly-conservative aerosol scattering and no aerosol scattering. The Voyager PPS experiment may resolve this issue with its wide phase angle coverage at the 1986 Uranus encounter.

Below 2000 Å, where many interesting gases in trace amounts could produce significant absorption, derived albedos are extremely sensitive to the method used to determine the solar spectrum. This has resulted in a diversity of opinion on whether or not such absorption actually exists on Uranus. One gas which is known or suspected to be present on the other three giant planets, C_2H_2, is modelled and compared to recent IUE observations of Uranus. Our results are consistent with a variable abundance of C_2H_2 there, but this result is critically dependent on corresponding, published solar variability. A Voyager UVS solar occultation experiment would clarify this question.

The unique observing geometry that will be achieved by Voyager therefore has the potential to improve our understanding of stratospheric ultraviolet absorbers in several aspects.

OBSERVATIONS BEFORE IUE

In addition to studies with the International Ultraviolet Explorer satellite, which is still active, there have been UV observations of both Uranus and

Neptune by two other satellites: the Orbiting Astronomical Observatory - A2 (OAO-A2) and the Netherlands Astronomical Satellite (ANS)[1,2,3]. In each case, the earlier satellites produced broad-band photometry which together covered the range 1800 to 4300 Å. The resulting geometric albedos are summarized in Table I. In each case, the greater absolute brightness of Uranus led to the formal quotation of an albedo one filter shorter than was done for Neptune, but these short wavelength values have much greater uncertainties than the other Uranus data. With the exception of the questionable OAO-A2 point at 2110 Å, there is very good agreement between the two satellites in their region of spectral overlap. This agreement is certainly helped by the common data reduction procedures, which involves comparison of planetary and G star photometry. This technique avoids all instrumental calibration errors.

For the region 2000 to 3000 Å, the numbers in Table I indicate that the albedos of both planets are very near 0.5. As a class, these two planets are distinctly different from Jupiter and Saturn, where the geometric albedos are approximately a factor of 2 lower.[2,4] The strong implication is that the stratospheres of both Uranus and Neptune are relatively much clearer than those of Jupiter and Saturn, where the appreciable ultraviolet absorption is usually attributed to absorption by hypothetical aerosols. The aerosols are thought to be the result of some chemical disequilibrating agent such as solar ultraviolet photons or high energy particles, acting primarily on stratospheric CH_4.

The atmospheres of Uranus and Neptune are sufficiently cold that much of their CH_4 must be frozen in their tropospheres, with a consequent severe depletion of CH_4 in their stratospheres relative to Jupiter and Saturn. The relatively high albedos in Table I are completely consistent with there being a reduced

Table I. BROADBAND GEOMETRIC ALBEDOS

a) URANUS

OAO-A2		ANS	
Effective Wavelength (Å)	Geometric Albedo	Channel (Å)	Geometric Albedo
4300	0.54	-	-
3360	0.49	3300	0.48
3075	0.50	-	-
2590	0.49	2500	0.54
2110	0.70*	2200	0.51
-	-	1800	0.39**

*extremely uncertain

**uncertain

b) NEPTUNE

OAO-A2		ANS	
Effective Wavelength (Å)	Geometric Albedo	Channel (Å)	Geometric Albedo
4300	0.58	-	-
3360	0.54	3300	0.51
3075	0.50	-	-
2590	0.59	2500	0.56
-	-	2200	0.57

amount of raw material, CH_4, at high enough altitudes to be affected by the disequilibrating agent(s).

Savage et al. (1980)[1] found that there was still some indication of aerosol scattering in their data, however. They compared their results with a semi-infinite, Rayleigh-Raman scattering H_2 atmosphere, including effects of almost conservative aerosol scattering. They concluded that the case of no aerosol scattering could be ruled out, and that for both planets, a wavelength independent, homogeneously distributed aerosol extinction, with single scattering albedo $\omega = 0.97$ and extinction optical depth set equal to Rayleigh scattering optical depth at 2500 Å, matched their data well.

Because their shortest wavelength point for Uranus was less certain than the other ones, they merely pointed out that a decrease in albedo below 2000 Å would be consistent with absorption by trace amounts of H_2S, CS_2 or PH_3, for example. They did not claim that their data constituted firm evidence for such absorption, however. As will be seen in the following discussion, this point remains unsettled even with the best available evidence today.

INITIAL OBSERVATIONS WITH THE IUE

Caldwell et al. (1981)[3] presented IUE spectrophotometry of Uranus and Neptune (and Titan) mostly above 2000 Å. The effective resolution was ~ 10 Å, so that there was in principle much more information than in the broad band photometry previously discussed. However, no narrow absorption features were seen for either planet. The upper limit for equivalent widths was approximately 2 Å. There were problems with the absolute scale of the data, so to determine continuum reflectivities, 50 Å running averages were normalized to the OAO-A2

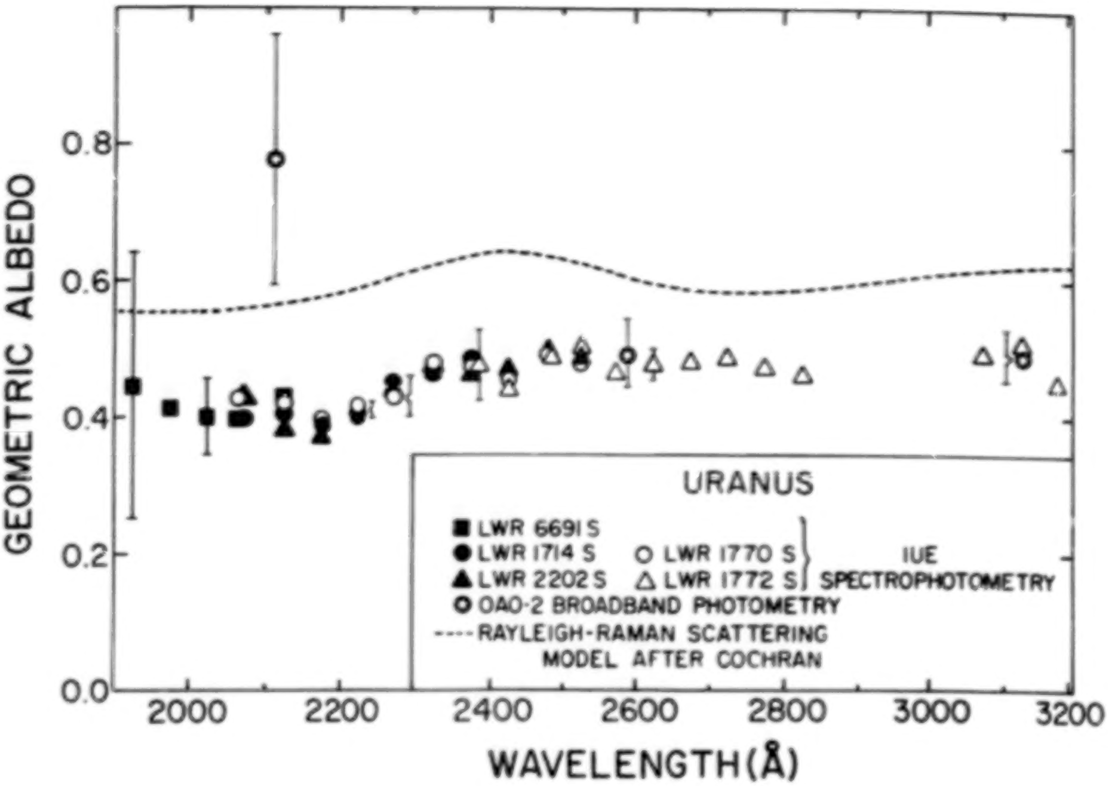

Figure 1: IUE spectrophotometry of Uranus, combining five separate exposures. The photometry point at 2100 Å has been disregarded. The other photometry points have been used to normalize the IUE data. IUE error bars increase toward shorter wavelengths in each exposure as the declining absolute planetary signal merges with the background.

photometry. In the normalization, the shortest wavelength point for each planet was given low weight. The results are shown here as figures 1 and 2 reproduced from Caldwell et al.[3]. Also included is the Rayleigh - Raman scattering curve calculated by W.D. Cochran (1978, private communication). This curve is not as high as would be the case for Rayleigh scattering only, because Raman scattering includes a shift in photon wavelength, which simulates an absorption.

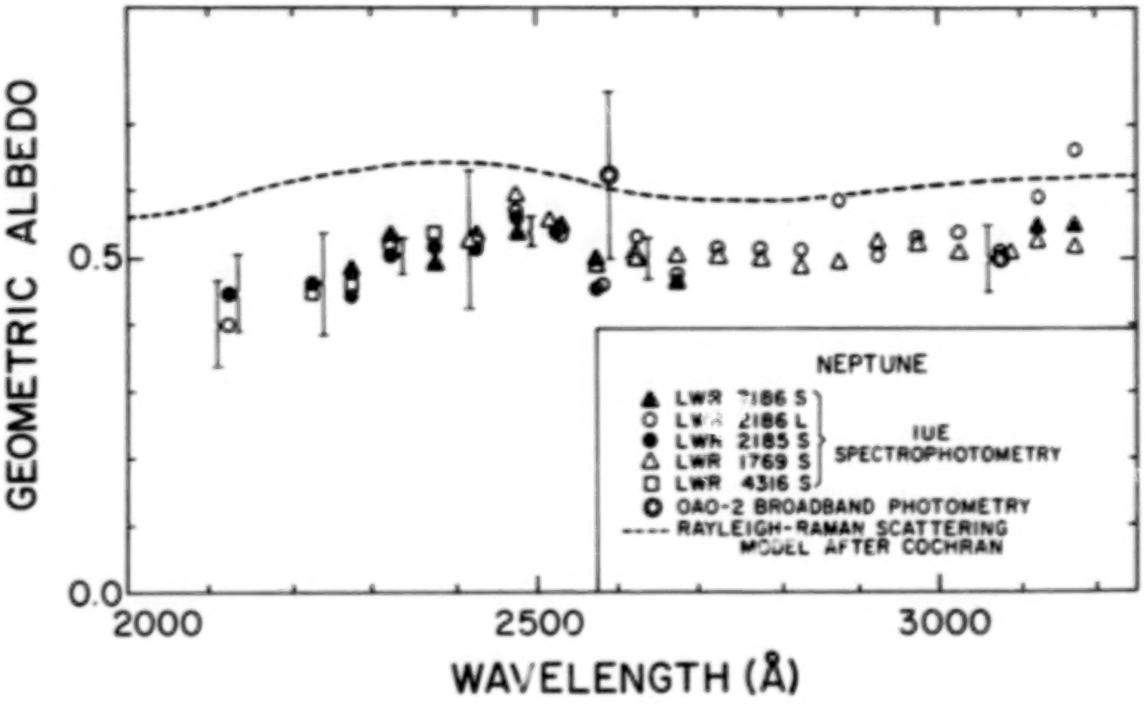

Figure 2: IUE spectrophotometry of Neptune. In normalizing the IUE data, the photometric point at 2600 Å has been given relatively low weight.

Consistent with the conclusions of Savage et al. (1980)[1], the observed albedo curves are somewhat lower than the model curves for both planets. This is what led Savage et al. to conclude that there was some high-altitude aerosol absorption on both.

However, Caldwell et al. (1981)[3] were persuaded to a different conclusion. They noted that the shapes of the observed albedo curves both agreed very well with the model, and that they were both lower by approximately the same amount. Coupled with the knowledge that the stratospheres of these planets are known to be very different in many aspects, as is discussed elsewhere in this volume, this led Caldwell et al.[3] to speculate that there might be a common systematic error in the data reduction, and that both stratospheres might indeed exhibit conservative Rayleigh - Raman scattering.

Caldwell et al.[3] further suggested that a plausible systematic error was the choice of solar V and B magnitudes implicit in the reductions by both Savage and Caldwell (1974)[2] and Savage et al. (1980)[1]. Arguing that if the Sun were fainter and redder than assumed in the earlier reductions, but within plausible limits, Caldwell et al.[3] concluded that the observational curves in figures 1 and 2 could indeed be consistent with the total absence of aerosol absorption in the upper few km-atm of H_2 on both planets.

As a result of experience gained, it is now possible to do a better normalization with IUE data alone than was done previously. A proposal has been submitted to the IUE Observatory to do this for Uranus. It was motivated in part by the possibility that such information could be uniquely useful to the Voyager PPS experiment for absolute calibration. It is also possible that the Voyager PPS could contribute significantly to the aerosol problem on Uranus by taking advantage of its wide range of observable phase angles, to distinguish polarimetrically between aerosol and Rayleigh scattering.

If the PPS should determine that Uranus is in fact clear at those altitudes sampled by 2000 to 3000 Å reflected photons, then at those wavelengths Uranus would be a unique standard for which the reflectivity can be calculated from first principles, as Cochran has done. Spectrophotometry of the Sun could then be accomplished accurately by conventional astronomical facilities, such as Space Telescope, using Uranus as a known reflector. It may even be possible to determine the B and V colors of the Sun by this means, indirectly but more accurately than has been done otherwise.

Caldwell et al. (1981)[3] also made a preliminary attempt to push the IUE range below 2000 Å. Using the photographic spectrum of Kjeldseth-Moe et al. (1976)[10], Caldwell et al.[3] concluded that the reflectivity of Uranus below 2000 Å was flat down to 1800 Å, contrary to the result of Savage et al. (1980)[1]. Caldwell et al.[3] suggested that the difference might be due to the choice of the specific G star (18 Sco) used by Savage et al.[1] to represent the Sun. As will be discussed below, however, the problems with establishing the solar spectrum below 2000 Å are still far from resolved, and the possibility of sub 2000 Å molecular absorption on Uranus continues to be open.

SOLAR SPECTRA BELOW 2000 Å

To derive a planetary albedo, one must know the solar spectrum accurately. The IUE has routinely extended the accessible ultraviolet region of Uranus below 2000 Å. There, the Sun is highly variable[5], so that its output must be monitored regularly. Because of the importance of this calibration, and the difficulties of making the solar measurements, we describe our data sources in some detail.

The full-disk solar irradiance between about 1150 and 3170 Å has been measured by Mount and Rottman in 4 rocket flights in 1979[6], 1980[7], 1982[8] and 1983[9]. There were some problems with the 1979 and 1983 data, but within their uncertainties they were similar to the 1980 and 1982 spectra respectively. There is, however, a significant decrease of the flux shortward of 1900 Å from the near solar maximum data of 1980 to those of 1982. In the following discussion, the 1980 spectrum of Mount and Rottman is assumed to be representative of the Sun for the solar maximum years 1979 and 1980, and the 1982 spectrum for 1982 and 1983. We will denote them as MR1980 and MR1982 respectively.

Their instrument consisted of two scanning spectrometers covering the wavelength regions from 1150 to 1900 Å and 1600 to 3170 Å respectively. To improve the wavelength-scale, we compared the two spectra to higher resolution photographic spectra[10,11], that we convolved to the resolution of Mount and Rottman's spectrometers (about 2.1 Å). We measured shifts of about 100 solar absorption and emission lines. The largest shifts were 10 Å for MR1980 and 5 Å for MR1982. We adjusted the wavelength-scales of Mount and Rottman to agree with the photographic spectra. In so doing, we improved the feature to feature agreement between MR1980 and MR1982 and also between their solar spectra and our IUE spectra.

In addition to the wavelength shifts, we also suspect problems in the intensity values of both spectra of Mount and Rottman over very limited spectral ranges, where the scans from the two spectrometers have been joined together. MR1980 shows a sharp discontinuity near 1780 Å that is clearly instrumental, not physical. The data are qualitatively different on each side of the discontinuity. This discontinuity is illustrated in figure 3, which is a ratio of MR1980 to the solar spectrum of Kjeldseth-Moe et al. (1976)[10]. The latter is a high resolution photographic spectrum of a quiet region on the Sun combined from data taken during two rocket flights in 1973 and 1974 near solar minimum. Figure 4, which is a ratio of MR1982 to the same quiet region solar spectrum also shows a discontinuous interval between 1820 and 1870 Å. We applied subjective, empirical corrections to the two spectra of Mount and

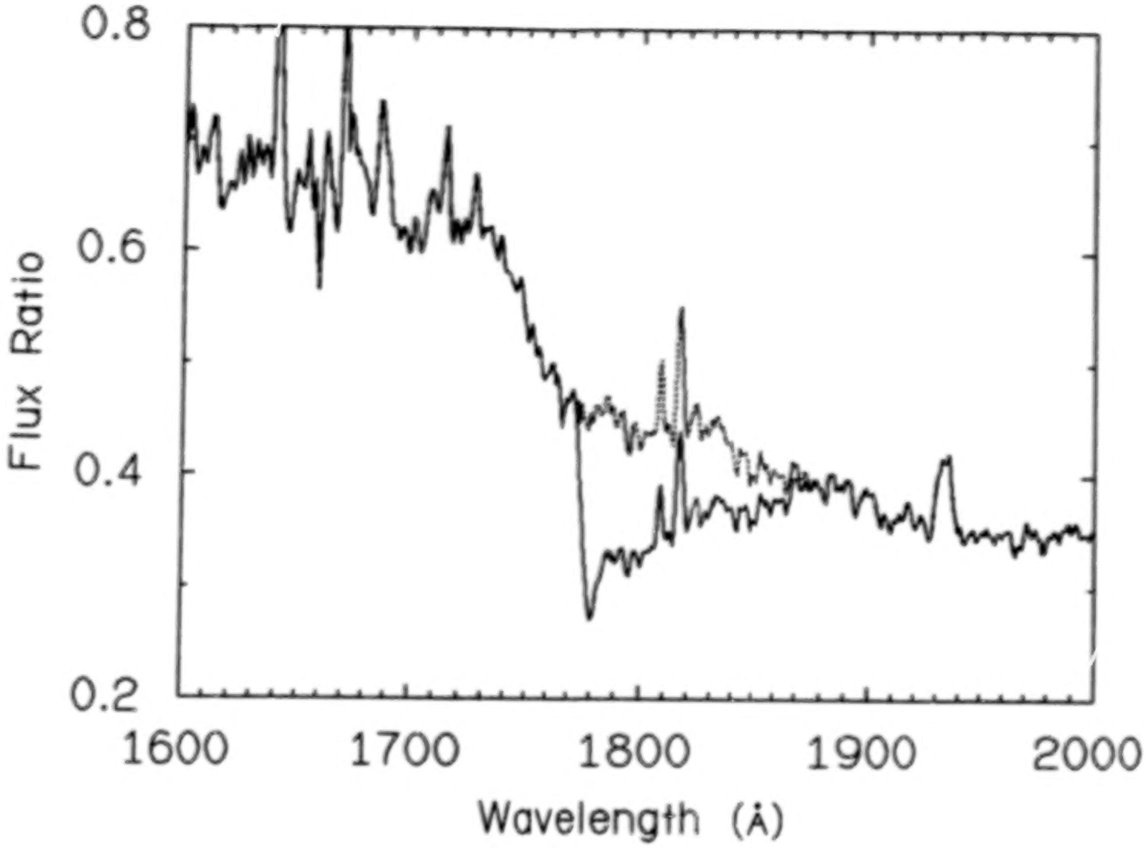

Figure 3: Ratio of MR1980[7] to the high resolution spectrum of Kjeldseth-Moe et al.[10] convolved to the same resolution 2.1 Å. The broken line shows the same ratio after a subjective correction to MR1980 has been applied to remove the discontinuity at ~1780 Å.

Rottman, as shown by the broken lines in figures 3 and 4, to restore continuity. The corrections were the smallest possible ones that would render the ratio spectra continuous throughout the range 1700 - 2000 Å, which is the region of primary interest for planetary studies. In figure 5, we show the resulting ratio of MR1980 to MR1982. The error bars are from Mount and Rottman, except where we have increased them between 1780 and 1870 Å because of our empirical adjustments.

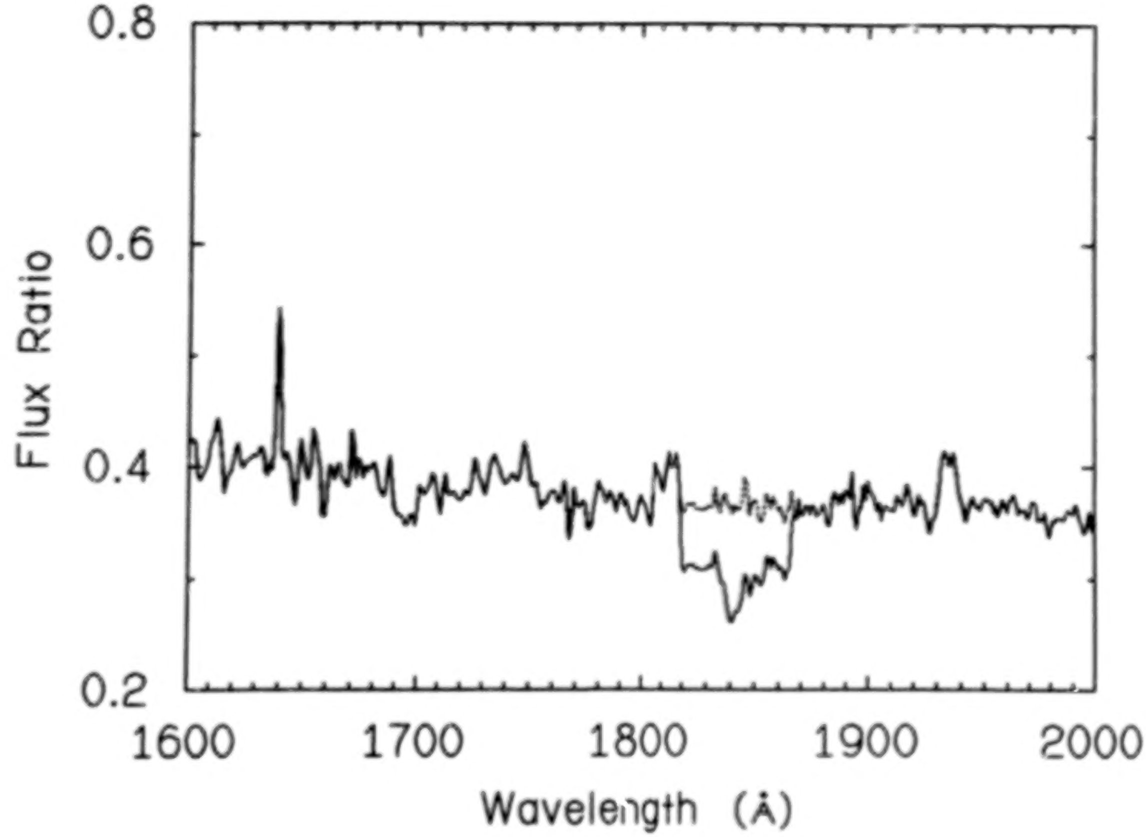

Figure 4: Similar to figure 3 except for MR1982[*]. In this case there are two discontinuities at two different wavelength.

While the data of Mount and Rottman are imperfect, they appear to be the best available for our needs. The problems described above illustrate the great difficulty in obtaining absolute solar spectra in this region. We hope that continued efforts will be made to monitor solar variations in the ultraviolet in order to improve planetary data reduction, as well as for their intrinsic merit.

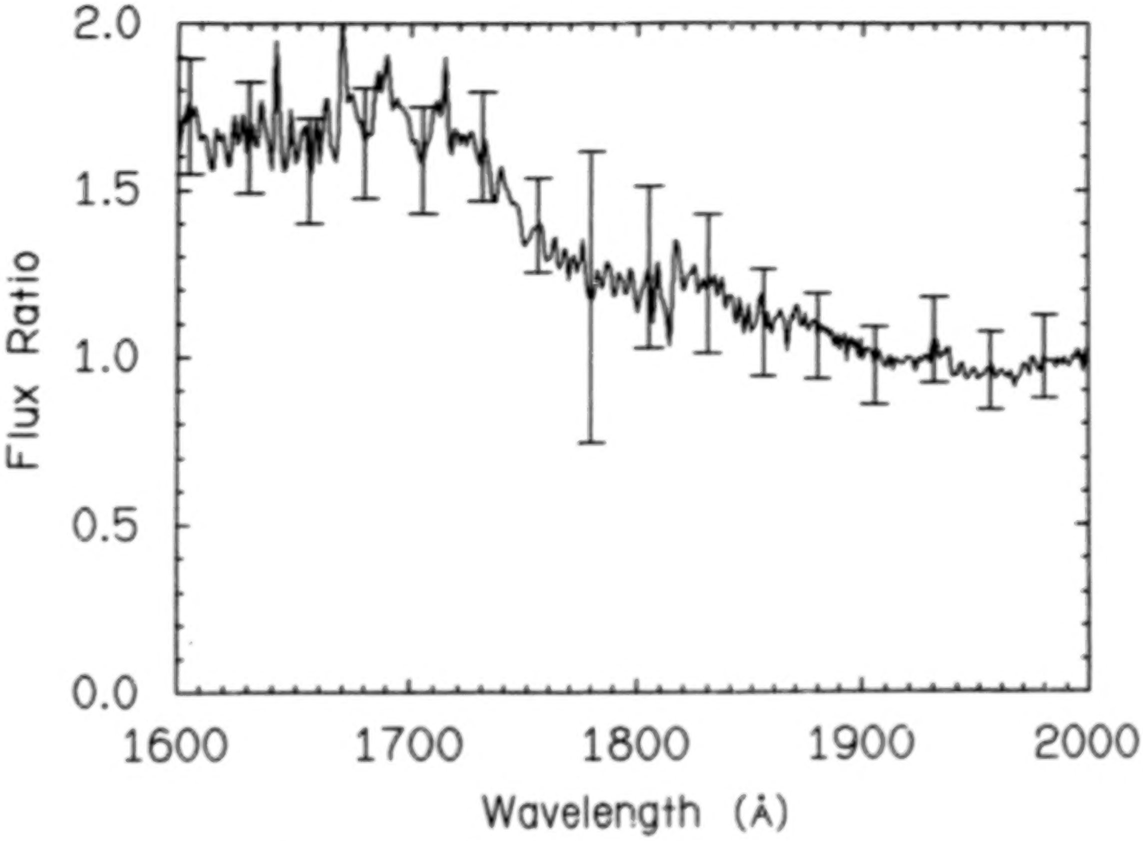

Figure 5: Ratio of MR1980 to MR1982 after the corrections have been applied. The error bars are the ones given by Mount and Rottman[7,8], except in the regions where corrections have been applied. At these wavelengths the errors have been increased to show the uncertainties due to the corrections.

IUE SPECTRA OF URANUS BELOW 2000 Å

Medium resolution (10 Å) spectrometric observations of Uranus shortward of 2000 Å have first been made possible with the launch of the IUE satellite in 1978. The characterictics of the instruments have been described elsewhere[12]. In the following, only the limitations specific to planetary observations will be discussed:

1. Solar Variability: The solar spectrum shortward of 1900 Å is highly variable, as discussed in detail in the previous section.

Table II. 1980 small aperture Uranus spectra

Image number	date	exposure time (h)	normalization factor
SWP 7679	17 Jan. 80	2	0.972
SWP 7680	17 Jan. 80	5	1.089
SWP 8765	16 Apr. 80	6.5	0.975
SWP 9478	9 Jul. 80	14	0.964

Table III. 1983 large aperture Uranus spectra

Image number	date	exposure time (h)	normalization factor
SWP 20501	21 Jul. 83	1	1.145
SWP 20502	22 Jul. 83	3.5	1.042
SWP 20503	22 Jul. 83	6.42	0.897
SWP 20504	22 Jul. 83	0.83	0.855
SWP 20505	23 Jul. 83	13.2	1.135
SWP 20737	20 Aug. 83	6.25	0.927

2. Low dynamic range of the IUE: Over the IUE spectral range from 3000 Å to 1200 Å the continuum solar fluxes and hence planetary fluxes decrease by more than 5 orders of magnitude. The dynamic range of the IUE cameras, on the other hand, is only about 25, which means that a number of individual exposures with a wide range of exposure times must be combined to achieve maximum wavelength coverage. We obtained two such sets of spectra, one in 1980 with the small (3 arcsec) circular aperture (see Table II) and the other one in 1983 with the large (10 X 20 arcsec) aperture (see Table III).

During an 8 - 9 hour period every day, the IUE spacecraft in its elliptical, quasi-geostationary orbit passes through the outer radiation belts. This greatly increases the overall camera background level due to Cerenkov radiation from high energy electrons. The remaining 16 hours of low background are divided between the ESA, controlling the spacecraft from a groundstation near Madrid during the eastern most part of the orbit, and NASA (GSFC). Fortunately, exposures started in Europe can be continued without interruption, in the United States, thus allowing us to obtain exposures as long as 14 hours. In the case of Uranus this yields spectral information down to about 1700 Å. Any attempt to obtain longer exposures would be defeated by instrument saturation due to the high background in the remaining part of the orbit.

3. Scattered light in the SWP: The Short Wavelength Primary (SWP) camera, designed to measure the spectral range from 1200 to 1980 Å, is also sensitive to scattered light from longer wavelengths up to 3500 Å. In most cases this is negligible, but in solar type spectra, with steeply increasing fluxes toward longer wavelengths, even a small amount of scattering along the dispersion direction introduces a significant amount of contamination in the SWP camera.

We adopted a wavelength-independent intensity correction, which is determined empirically by the observed flux between 1250 and 1500 Å, where the true flux from Uranus should be negligible.

After being calibrated, individual spectra are normalized to the same level in regions of overlap with the factors indicated in Tables II and III, and then combined using a weighted average. The errors were estimated from the standard deviations of the background on either side of the dispersion line. The combined spectra are converted to photon flux and convolved with a 6 Å gaussian filter to smooth the data and then divided by the solar spectra MR1980 and MR1982 respectively after they have been convolved to 10 Å FWHM resolution. These ratios are scaled to geometric albedos (p) with the relation:

$$p = \frac{F_u}{F_o} \cdot \frac{\pi}{\Omega}$$

F_u = Uranian flux at 1 AU

F_o = Solar flux at 1 AU

$$\Omega = \begin{cases} 1.62 \cdot 10^{-10} \text{ steradians for sm.ap.} \\ 2.10 \cdot 10^{-10} \text{ steradians for lg.ap.} \end{cases}$$

(solid angle of Uranus)

In the case of the small aperture, which covers only the central 3 arcsec of the 3.4 arcsec disk of Uranus, the true geometric albedo will be somewhat smaller due to limb darkening. But no correction for that has been made, because it is estimated from our models (see below) to be a reduction of less than 10%, which is less than the uncertainties in our data. The results are plotted in figures 6 and 7. The places where the curves are interrupted are

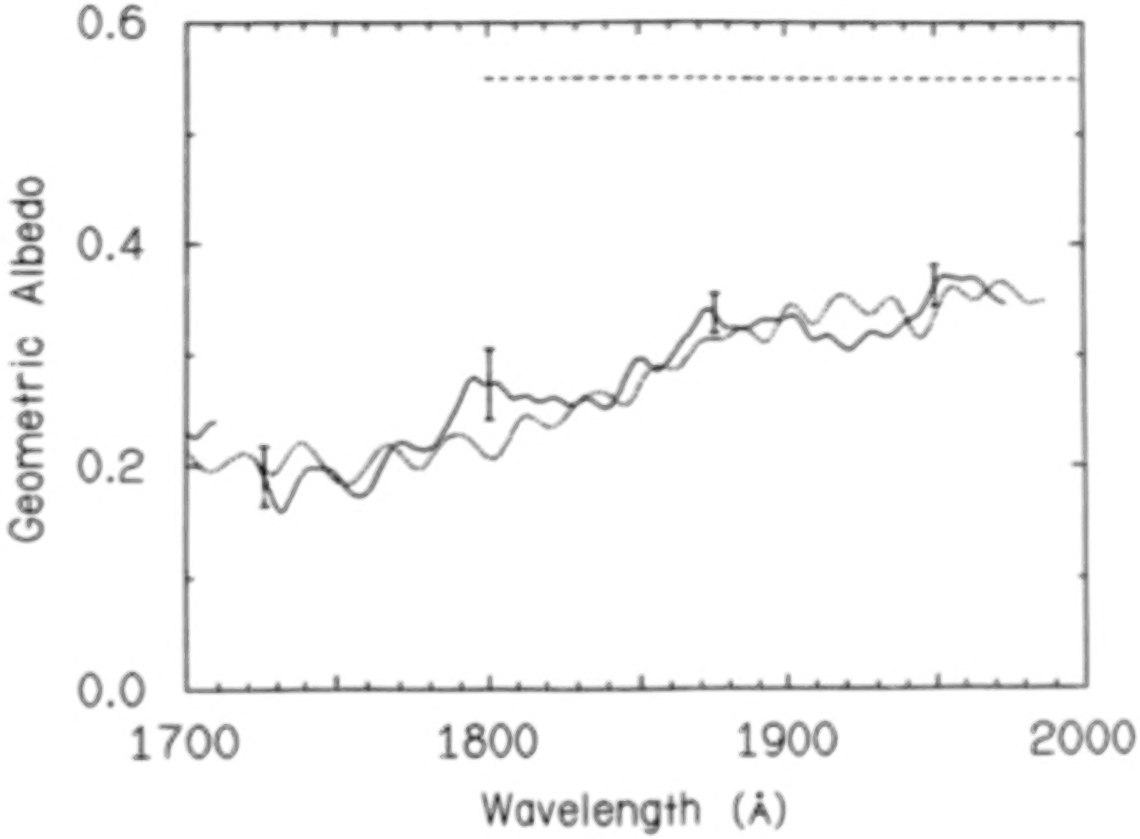

Figure 6: 1980 geometric albedo of Uranus from 4 small aperture spectra. The straight dashed line is the Rayleigh-Raman scattering model of W.D. Cochran. The broken line is a semi-infinite Rayleigh scattering model with C_2H_2 homogeneously mixed at a mixing ratio of $3 \cdot 10^{-8}$.

the positions of reseau marks, points on the faceplate of the camera used to determine the wavelength scale. The error bars indicate the combined errors of the IUE spectra and the solar spectra as discussed above. The IUE errors do not include possible systematic errors due to guiding errors or defocusing. These effects have been observed to vary the exposure levels of point sources in the small aperture by up to 50%, but they are negligible for extended sources like Jupiter and should be intermediate for Uranus, which with a

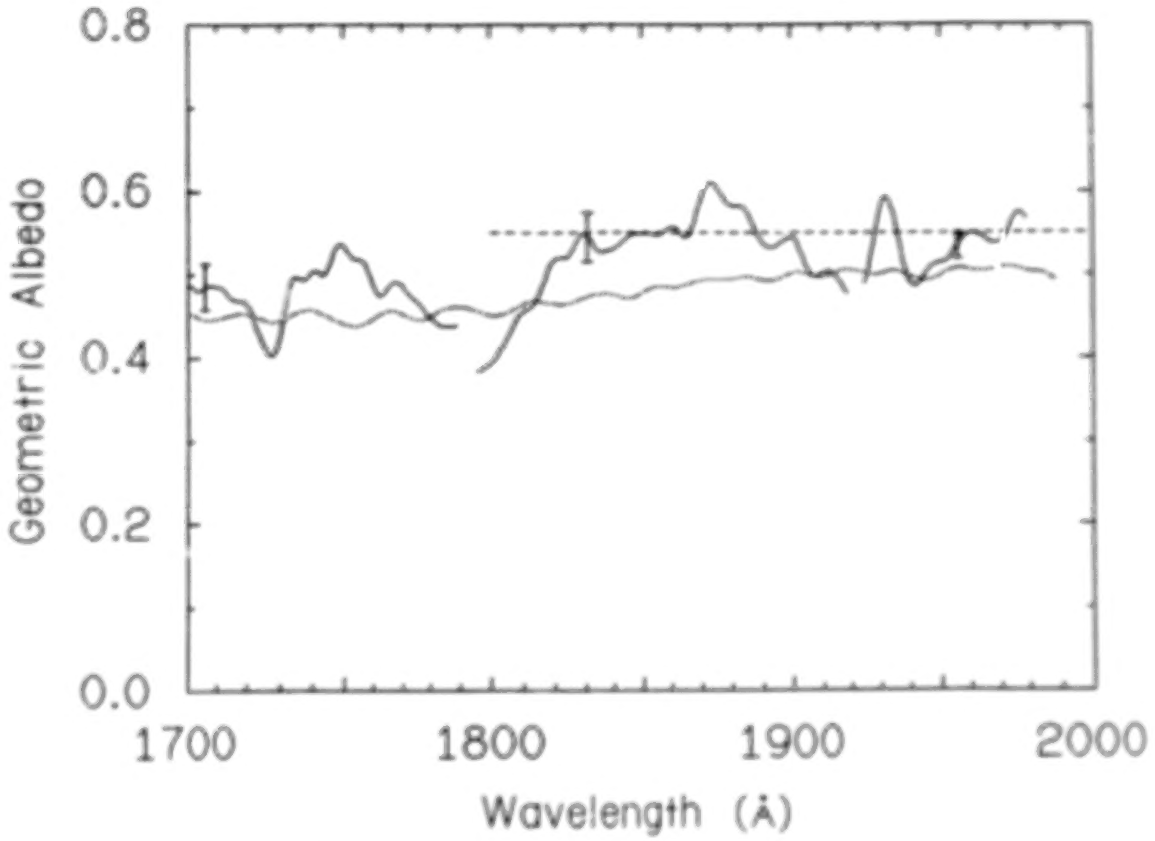

Figure 7: 1983 geometric albedo of Uranus from 6 large aperture spectra. The straight dashed line is the Rayleigh-Raman scattering model (see figure 6). The broken line is a semi-infinite Rayleigh scattering model with C_2H_2 at a mixing ratio of 10^{-9}.

diameter of 3.4 arcsec slightly overfills the small aperture. An indication of a good photometric repeatability are the rather small deviations (<10%) of the normalization factors in table II.

The geometric albedo of Uranus appears to have decreased from 1980 to 1983, although there are large uncertainties due to the variability of the Sun and the calibration of the small aperture. Below, we model this change as an affect of variable C_2H_2 abundance on Uranus.

MODELS

We computed one layer models of Rayleigh scattering, semi-infinite H_2 atmospheres with no particle absorption, which we normalized to the Rayleigh-Raman scattering model of Cochran. We then added some C_2H_2 to match the slope of the albedo curves in figures 6 and 7. We could not reliably identify any of the C_2H_2 spectral features, because of noise in our data. Nor were we trying to fit the absolute level of the 1980 small aperture albedo curve in figure 6, because of the relatively large uncertainty of the absolute calibration of the small aperture. A C_2H_2 mixing ratio of $3 \cdot 10^{-8}$ happens to fit both the slope and the nominal absolute level of the 1980 data quite well. The curve for 1983 is much flatter and is consistent, both in slope and absolute level, with C_2H_2 mixing ratios $\lesssim 10^{-9}$.

The change of the Uranian albedo from 1980 to 1983 can thus be modelled with a change of C_2H_2 abundance. We should point out that C_2H_2 may not be the only absorber in this wavelength region, and the fit is not unique, because of the non-detection of C_2H_2 bands. On the other hand, C_2H_2 is a plausible candidate, because it has been detected on Jupiter and Saturn and is suspected to occur on Neptune. On Jupiter[13,14] and Saturn[15,16] C_2H_2 band features have been detected with the IUE, with model abundances as high as or even higher than the ones reported here.

Further IUE observations of Uranus have been proposed to clarify the structure and possible temporal variation of its stratosphere.

ACKNOWLEDGEMENT

The new work reported here was supported in part by NASA grant NSG 5250 at Stony Brook.

REFERENCES

1. Savage, B.D., Cochran, W.D., and Wesselius, P. (1980). Ultraviolet albedos of Uranus and Neptune. Astrophys.J. **237**, 627-632.
2. Savage, B.D. and Caldwell, J.J. (1974). Ultraviolet photometry from the Orbiting Astronomical Observatory. XIII. The albedos of Jupiter, Uranus and Neptune. Astrophys.J. **187**, 197-208.
3. Caldwell, J., Owen, T., Rivolo, A.R., Moore, V., Hunt, G.E. and Butterworth, P.S. (1981). Observations of Uranus, Neptune and Titan by the International Ultraviolet Explorer. Astron.J. **86**, 298-305.
4. Caldwell, J., (1977). Ultraviolet observations of Mars and Saturn by the TD1A and by the OAO-A2 satellites. Icarus **32**, 190-209.
5. Brueckner, G.E., (1981). The variability of the Sun's ultraviolet radiation. Adv. Space Res. **1**, 101-116.
6. Mount, G., Rottman, G. and Timothy, J.G. (1980). The solar spectral Irradiance 1200 - 2550 Å at solar maximum. J.Geophys.Res. **85**, 4271-4274.
7. Mount, G. and Rottman, G. (1981). The solar spectral irradiance 1200 - 3184 Å near solar maximum: July 15, 1980. J.Geophys.Res. **86**, 9193-9198.
8. Mount, G. and Rottman, G. (1983). The solar absolute spectral irradiance 1150 - 3173 Å, May 17, 1982. J.Geophys.Res. **88**, 5403-5410.
9. Mount, G. and Rottman, G. (1983). The solar absolute spectral irradiance at 1216 Å and 1800 - 3173 Å: January 12, 1983. J.Geophys.Res. **88**, 6807-6811.
10. Kjeldseth-Moe, O., VanHoosier, M.E., Bartoe, J.-D.F. and Brueckner, G.E. (1976). A Spectral Atlas of the Sun Between 1175 and 2100 Angstroms. Naval Research Laboratory Report #8056.

11. Brinkmann, R.T., Green, A.E.S., Barth, C.A. (1966). JPL Tech. Rept., No. 32-951.

12. Boggess, A. et al. (1978): The IUE spacecraft and instrumentation. Nature **275**, 372-377 and 377-385.

13. Owen, T., Caldwell, J., Rivolo, A.R., Moore, V., Lane, A.L., Sagan, C., Hunt, G. and Ponnamperuma, C. (1980). Observations of the Spectrum of Jupiter from 1500 to 2000 Å with the IUE. Astrophys.J. **236**, L39-L42.

14. Wagener, R. et al. (1984). Ultraviolet observations of Jupiter with the IUE. In preparation.

15. Moos, H.W. and Clarke, J.T. (1979). Detection of acetylene in the Saturnian atmosphere using the IUE satellite. Astrophys.J. **229**, L107-L108.

16. Winkelstein, P., Caldwell, J., Kim, S.J., Combes, M., Hunt, G.E. and Moore, V. (1983). A Determination of the Composition of the Saturnian Stratosphere Using the IUE. Icarus **54**, 309-318.

BLANK PAGE

PROPERTIES OF THE UPPER TROPOSPHERES OF URANUS AND NEPTUNE DERIVED FROM OBSERVATIONS AT "VISIBLE" TO NEAR-INFRARED WAVELENGTHS

Jay T. Bergstralh and Kevin H. Baines
Jet Propulsion Laboratory
California Institute of Technology
Pasadena, CA 91109

Photons at wavelengths between 0.3 and 4.5 μm penetrate the atmospheres of Uranus and Neptune to pressures between about 0.01 bar and 10 bars. This pressure range brackets the radiative-convective boundary in both atmospheres and is therefore designated "upper troposphere." Physical processes which govern the transfer of radiation in Uranus's and Neptune's atmospheres at these wavelengths include Rayleigh/Raman scattering by hydrogen, scattering and broadband absorption by suspended aerosol particles and absorption in discrete bands and lines by methane and hydrogen. Consequently, tropospheric properties constrained by observations at these wavelengths include optical properties and distribution of aerosol particles, methane/hydrogen ratio, and ortho/para hydrogen ratio. Recent observations of Uranus and Neptune in this spectral range, including unpublished work by the authors, are reviewed and compared with predictions based on models of the atmospheric structures. Significant results for Uranus include the presence of an opaque lower boundary to the visible atmosphere very near the level corresponding to 2 bars pressure, and consequently a methane/hydrogen ratio no less than 3 percent.

I. INTRODUCTION

This paper reviews what is known about the atmospheres of Uranus and Neptune from spectroscopic and spectrophotometric observations at wavelengths between 0.3 μm and 2.5 μm. This interval is dominated by reflected solar radiation and is easily accessible to ground-based observation. Consequently, it is associated with a long history of observations. James Keeler may have taken the earliest photographic spectrograms of Uranus and Neptune late in the nineteenth century. Between 1905 and 1931, V. M. Slipher detected and reported all of the major molecular absorption bands which characterize the spectra of the outer planets, out to nearly 1 μm wavelength (Figure 1). In 1931, Rupert Wildt identified most of these bands as rotational-vibrational overtones of methane. In 1952, Gerhard Herzberg identified a feature in Uranus's spectrum, detected by Gerard Kuiper, as a collision-induced dipole transition of hydrogen and thereby

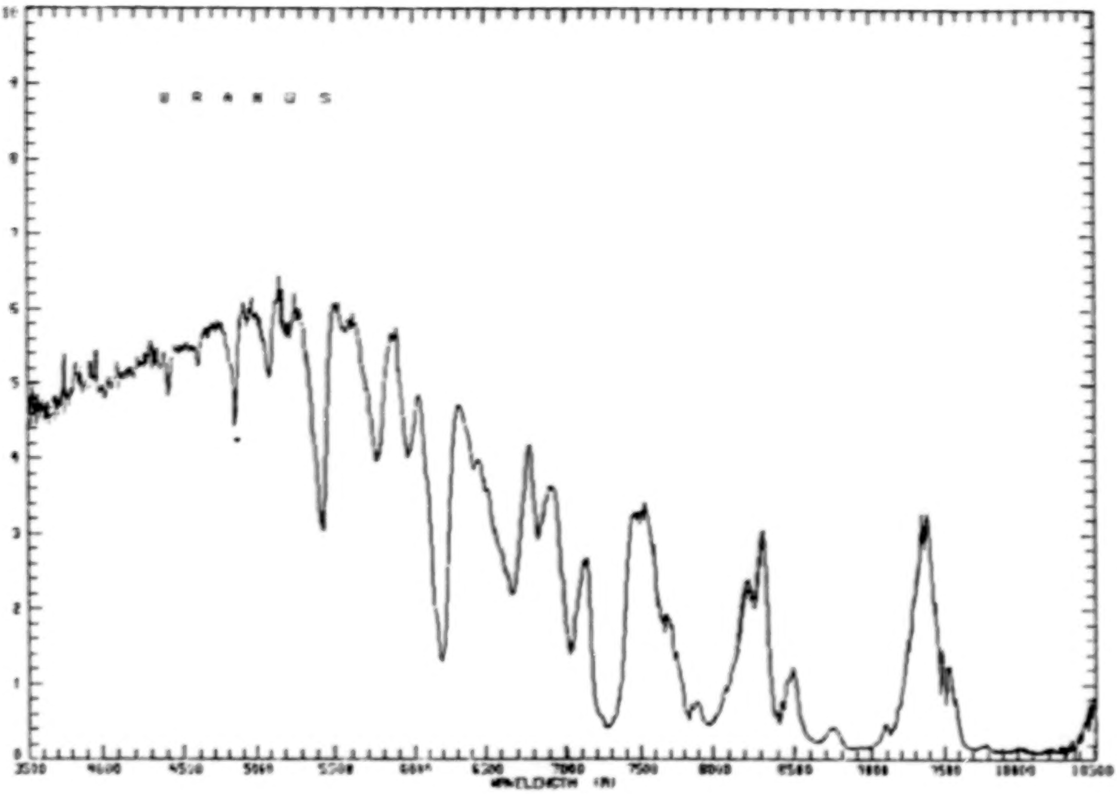

1a. Geometric albedo spectrum of Uranus from 0.35 µm to 1.05 µm at spectral resolution 6.6 A. Data are from Ref. 5.

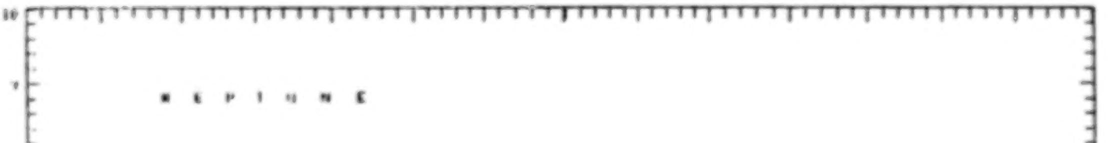

1b. Same as for 1a, but for Neptune.

confirmed what had long been inferred: that hydrogen is a major constituent of the atmospheres of the giant planets.

Photons at these wavelengths probe the atmospheres of Uranus and Neptune at depths corresponding to pressures between about 10 millibars and 10 bars. This pressure range brackets the expected level of the radiative-convective boundary in the atmospheres of both planets, and, consequently, we designate this region as the "upper troposphere." Belton[1] has noted that this part of the atmosphere is in "most effective radiative contact with space."

Three physical processes dominate transfer of radiation in this wavelength and pressure range and therefore govern the character of the spectra of Uranus and Neptune: (1) Rayleigh and Raman scattering by hydrogen and other atmospheric gases, (2) scattering and broadband absorption by aerosol particles suspended in the atmospheres, and (3) absorption in discrete bands and lines by methane and by quadrupole and collision induced dipole transitions of hydrogen. Tropospheric properties that can be constrained by such observations therefore include (1) optical properties and distribution of suspended aerosols, (2) methane/hydrogen ratio, and (3) ortho/para hydrogen ratio. All of these properties have significant influence on atmospheric structure. Aerosols and the distribution of methane affect the pressure-temperature structures in the radiative layers of the atmospheres because they affect the deposition of incident solar radiation in these layers. The methane/hydrogen and ortho/para hydrogen ratios affect the temperature lapse rates in the convective layers of the atmospheres through their influence on specific heat. Scattering by aerosols modifies the transfer of radiation within discrete molecular absorption features and, therefore, affects the interpretation of methane and hydrogen abundances.

Several comprehensive reviews[1,2,3,4] have summarized observations and analy-

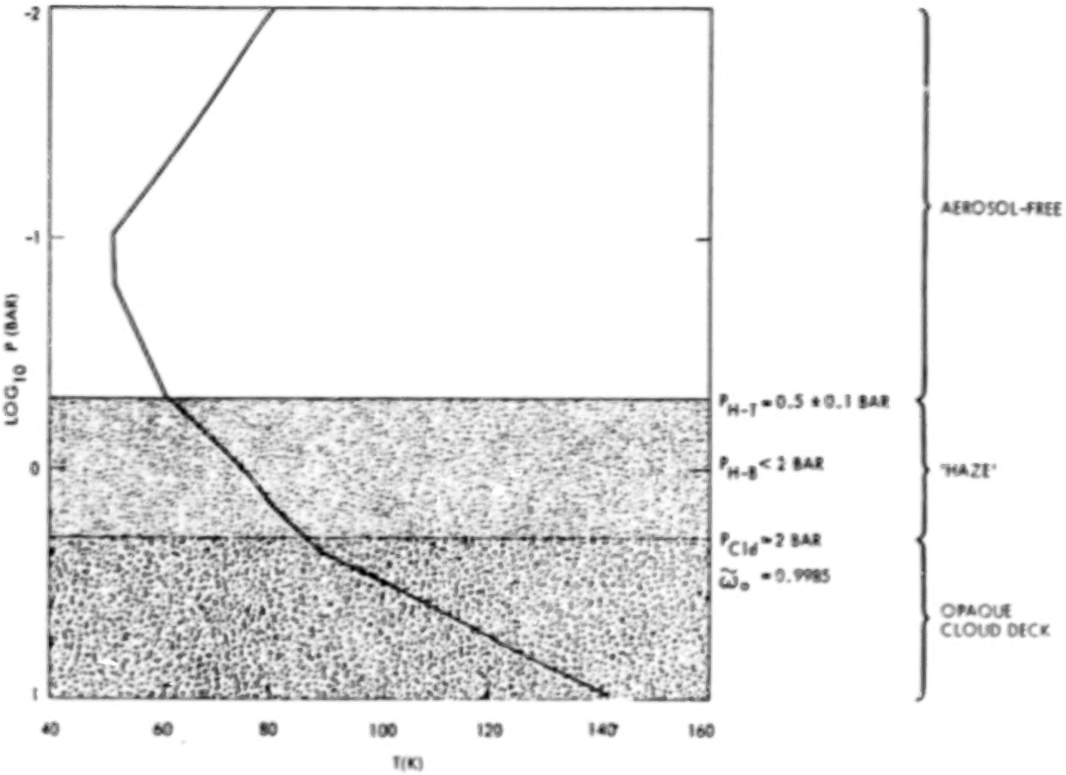

2a. Schematic of Uranus model atmosphere, illustrating pressure-temperature structure (Appleby, private communication) and aerosol parameters to be constrained.

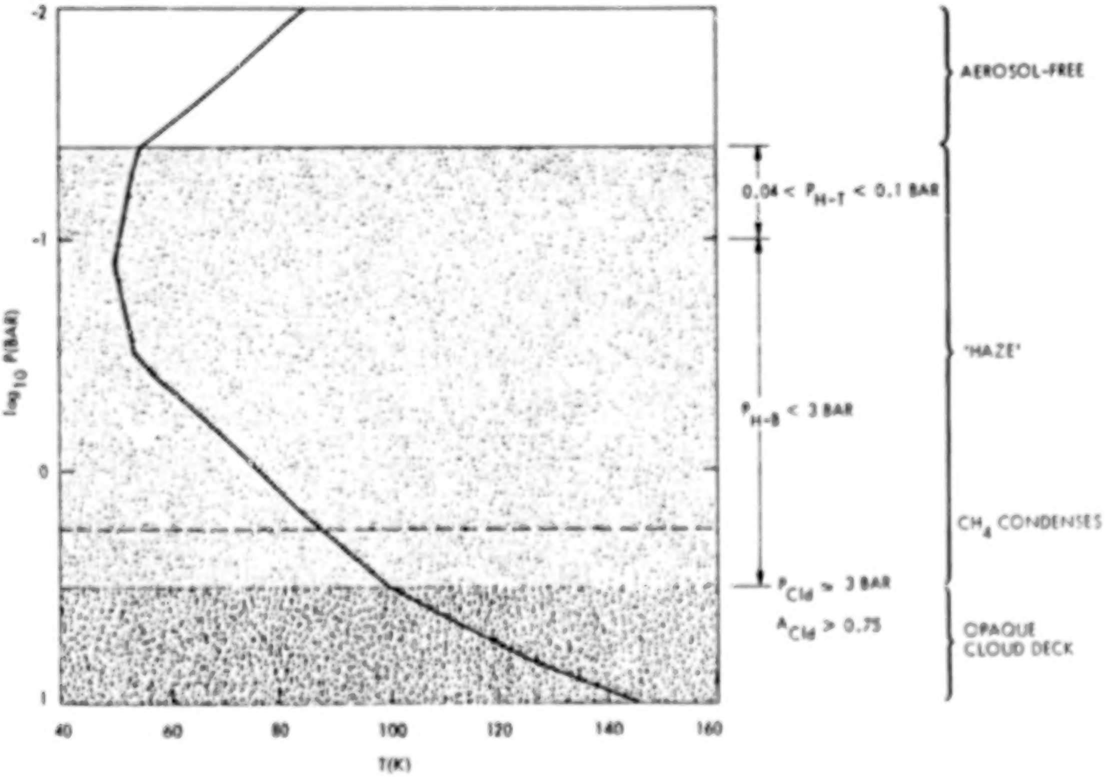

2b. Same as 2a, but for Neptune.

ses of Uranus and Neptune in this spectral interval prior to about 1980. We will focus on analysis of very recent observations[5,6].

II. SPECTROPHOTOMETRY

A. UV - Blue Continuum

Scattering processes dominate the spectra of Uranus and Neptune between 0.35 and 0.45 µm. The effects of scattering are most evident within this spectral interval, although they are non-negligible at several other wavelengths. The characteristics of the planetary spectra in this interval (Figure 3) lead immediately to two semi-quantitative conclusions about the structures of the atmospheres.

First, nonconservative scattering aerosols are suspended in the upper tropospheres of Uranus and Neptune. If Rayleigh scattering were the only source of opacity within this spectral interval, then the geometric albedos of both planets would be about 0.75--significantly higher than the measured values (cf. Figure 3). Belton, McElroy and Price[7] demonstrated that Raman scattering by hydrogen must reduce the UV continuum albedo of Uranus owing the the nearly exponential fall-off of solar flux towards shorter wavelengths. An improved analysis published by Wallace[8] reached the same conclusion qualitatively but demonstrated quantitatively that the albedo of a deep aerosol-free hydrogen atmosphere still would be higher than the observed values for Uranus and Neptune. Cochran and Trafton[9] published the most physically realistic and presumably the most accurate predictions of the effects of Raman scattering on the spectra of aerosol-free hydrogen atmospheres. Their model I--an aerosol-free hydrogen atmosphere deep enough to be semi-infinite in Rayleigh scattering--is represented by the dashed curves in Figure 3. Their results agreed quantitatively with Wallace's

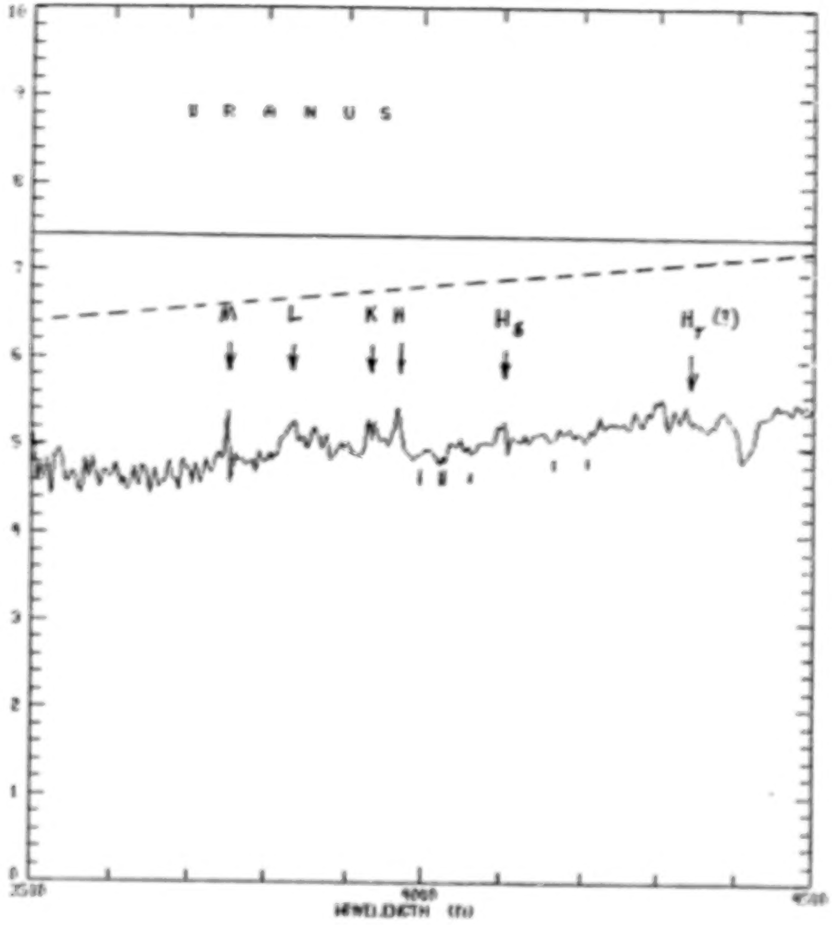

3a. Geometric albedo spectrum of Uranus between 0.35 and 0.45 μm on expanded scale (same source of data as Fig. 1), showing signature of Raman scattering. Apparent emission peaks labelled with capital letters are strong Fraunhofer absorption lines, partially filled in by Raman scattering in the planetary spectrum (cf. Refs. 5, 11).

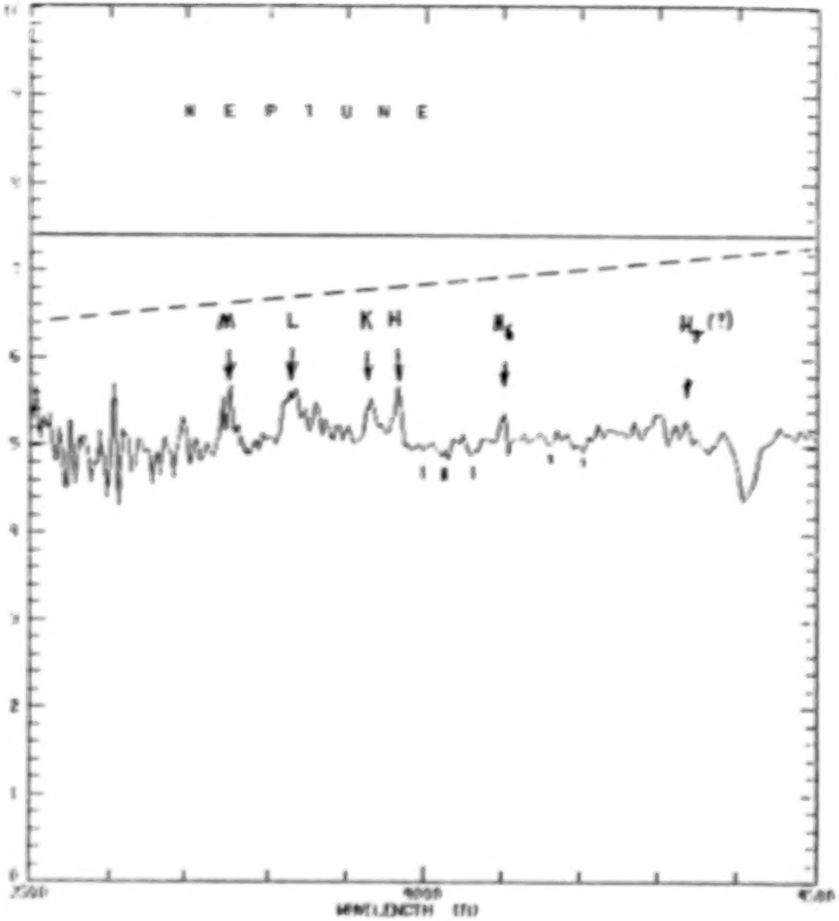

3b. Same as 3a, but for Neptune.

"best" model; the geometric albedo predicted for a deep aerosol-free hydrogen atmosphere is significantly higher than the observed albedos of Uranus and Neptune even when Raman scattering is taken into account. An additional source of broad-band UV opacity must be present in the atmospheres. The most likely source of such opacity is nonconservative scattering by aerosols.

Second, while nonconservative scattering aerosols are suspended in the atmospheres of Uranus and Neptune, the aerosols are tenuous or essentially absent from the uppermost 100 to 200 km amagat of hydrogen. Evidence for this conclusion stems from the high spatial frequency features in Figure 3. These features are not statistical noise (Figure 4); they are further manifestations of Raman scattering. Their origin has been discussed in several papers[9,10,11,12]. Their significance here is simply that they are visible. Cochran and Trafton[9] estimated that the cores of the Fraunhofer H and K lines should appear about twice as high as the neighboring continuum in their model I. The presence of nonconservative aerosols decreases the proportion of photons that are Raman-scattered and thus rapidly decreases the contrast of these features. Belton, Wallace and Price[11] detected the Fraunhofer "H" line in "emission" and the negative S(0) and S(1) Stokes "ghosts" of Fraunhofer H and K in the spectrum of Uranus, with amplitudes significantly lower than those expected for a deep, aerosol-free hydrogen atmosphere. Price[10] estimated from the observed amplitudes that the volume scattering coefficient for aerosols in Uranus's upper atmosphere could be no more than an order of magnitude larger than the volume coefficient for Rayleigh scattering, if the aerosols are uniformly mixed with the atmospheric gases. An alternate interpretation is that the observed amplitudes "are consistent with any H_2 column density greater than 200 km-amagat," and

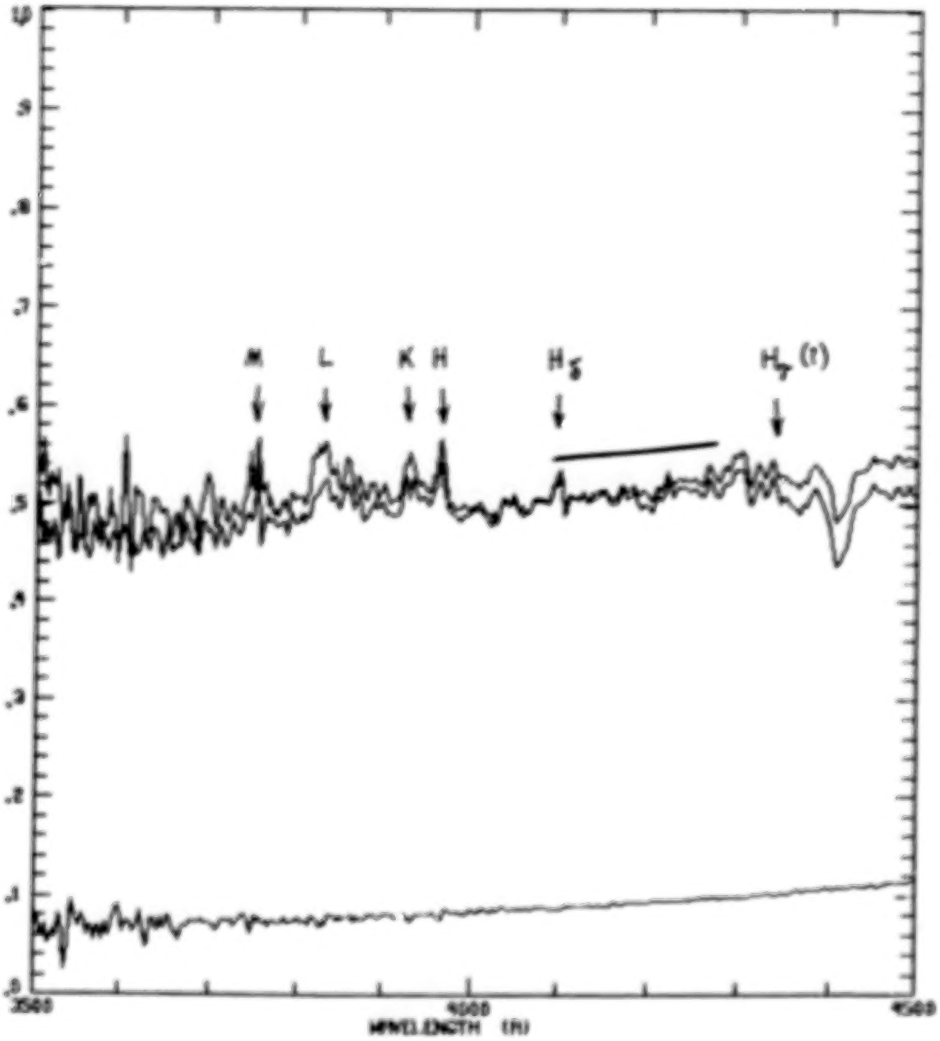

4. Geometric albedo spectra of Uranus, Neptune and Titan superimposed. Note correlated high-spatial-frequency features present in spectra of Uranus and Neptune but absent from that of Titan.

consequently the uppermost 200 km-amagat of hydrogen may be free of aerosols.

To our knowledge, the data presented in Figure 3 represent the most complete and detailed picture to date of Raman scattering in Uranus's spectrum and the first reported detection of Raman scattering in Neptune's spectrum. The amplitudes of the Fraunhofer H and K features in Uranus's spectrum are comparable with those reported by Belton, Wallace and Price[11] and therefore they lead to the same conclusions[10] regarding aerosols. By inspection, the amplitudes of the Raman features in Neptune's spectrum are comparable with those in Uranus's, so the same conclusions apply to Neptune.

B. 'Blue' Methane Bands

Molecular absorption first becomes evident in the spectra of Uranus and Neptune with the weak methane band at 4410 A. Progressively stronger methane bands appear at longer wavelengths until, in the visible and near-infrared, they dominate the spectra. Longward of about 5000 A, the wings of neighboring methane bands overlap so absorption dominates the spectra even in the intervals between the strong bands. The spectral interval between 4500 A and 5500 A can be characterized as a "transition" region, from dominance by scattering processes to dominance by molecular absorption bands.

The relatively weak methane bands at 4410, 4590, 4860, 5020 and 5210 A are conventionally designated the "blue" bands. Even in the deep atmospheres of Uranus and Neptune, absorption by these bands should be unsaturated. Consequently, in the absence of scattering, photons at these wavelengths should penetrate to the deep convectively-mixed layers of the atmospheres. The blue bands are therefore sensitive to the abundance of methane in the line of sight and should give us our best estimate of methane/hydrogen ratio[13].

Lutz, Owen and Cess[14] employed empirical curves of growth, a semi-empirical band model and a reflecting layer radiative transfer model to derive methane column abundances of 5.8 (+0.4, -1.0) km-amagat for Uranus and 7.6 (+0.6, -0.4) km amagat for Neptune from the measured equivalent widths of the 4410, 4860, 5430 and 5760 A bands. They adopted a hydrogen column abundance of 450 km amagat for both planets, from which they derived average methane/hydrogen ratios in the range (1.3-1.7) × 10^{-2} for the visible layers of the atmospheres. Higher values of the ratio are implied for the deep, warm, convectively-mixed layers.

Figure 5 illustrates our best current effort to model the blue methane bands in the spectrum of Uranus. The significance of this model is that its methane/hydrogen ratio is 3 percent in the convectively-mixed part of the atmosphere, consistent with the results of Lutz, et al.[14]. As we shall see in subsequent discussion, the hydrogen quadrupole and collision-induced dipole features in Uranus's spectrum imply the existence of an opaque boundary to the visible part of the atmosphere at a level corresponding to 2 bars total pressure. Consequently, we can not decrease methane/hydrogen and increase the visible depth of the atmosphere to keep the methane column abundance constant. Furthermore, methane becomes saturated very near the 2 bar level for a methane/hydrogen ratio of 3 percent. The saturation level moves deeper for higher values of the ratio, to levels that are invisible according to the evidence of the hydrogen absorption features. The methane column abundance in the visible layers of Uranus's atmosphere is insensitive to CH_4 molar fraction greater than 3 percent in the deep atmosphere. Therefore, our data imply a lower limit of 3 percent to the methane/hydrogen ratio.

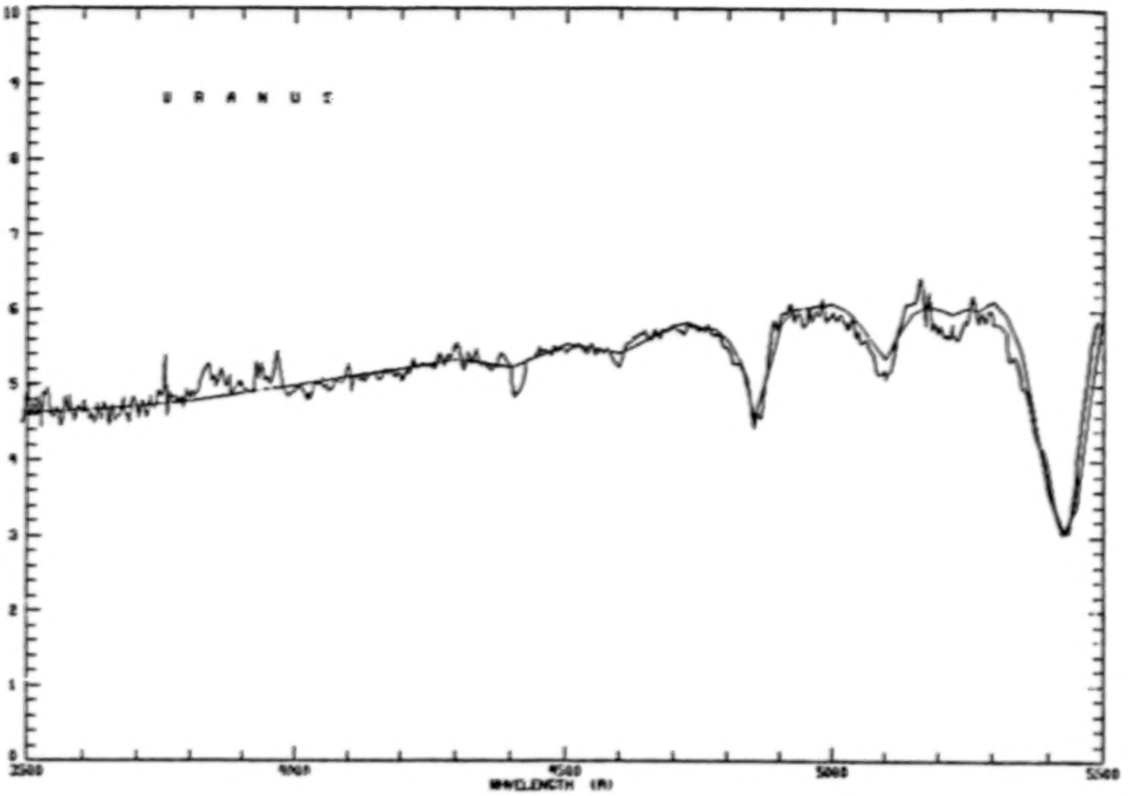

5a. Best current attempt to model UV continuum and "blue" methane bands in spectrum of Uranus. $P_h = 0.35$bar, T_N 0.15, $P_{cld} = 2.67$ bar.

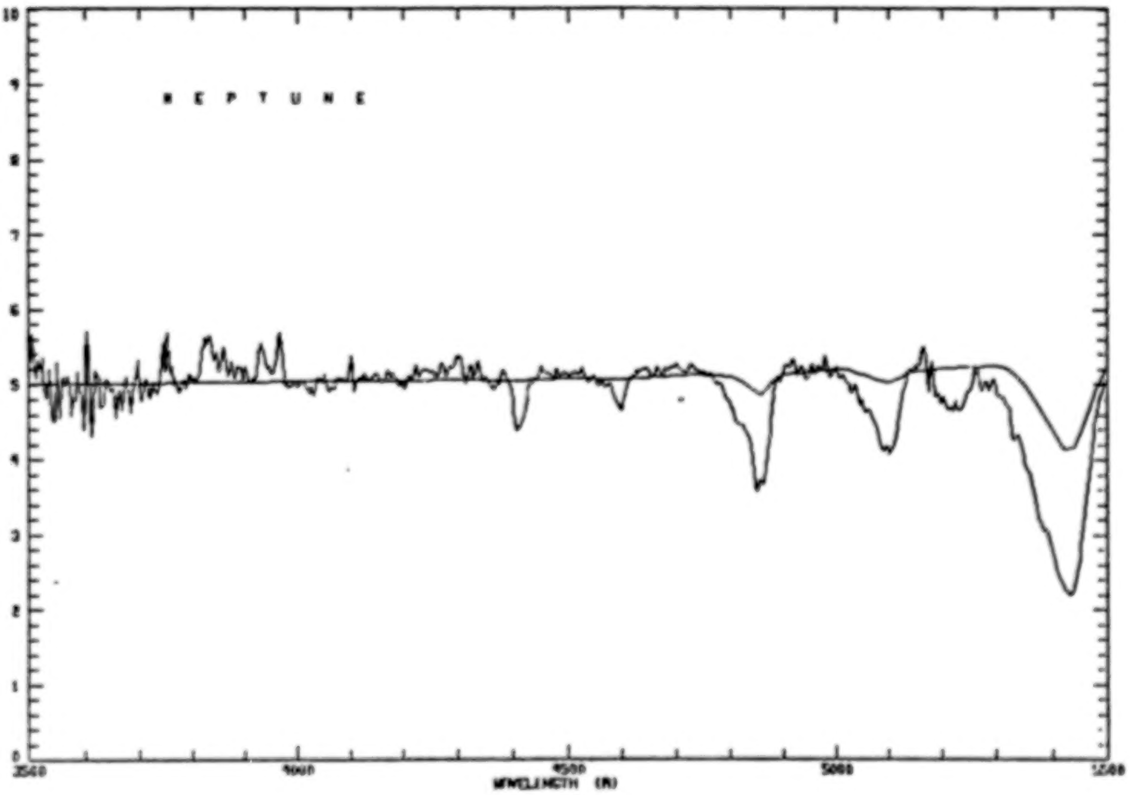

5b. "Best" model for Neptune. $P_h = 0.17$ bar, $T_N = 10$, $P_{cld} = 3$ bar (cf. Fig. 2).

C. Hydrogen Collision-Induced Dipole Absorption

Because the hydrogen molecule has no permanent dipole moment, its spectrum is ordinarily confined to weak quadrupole transitions (to be discussed in Section III). However, collisions with other molecules temporarily induce a dipole moment, so hydrogen can have a dipole spectrum under proper density conditions. Indeed, the induced rotational-translational spectrum of hydrogen is the principal source of thermal infrared opacity in the atmospheres of the giant planets[15]. The induced $S_3(0)$ rotational-vibrational overtone feature at 8270 A was the first hydrogen feature identified in the spectrum of Uranus.

Belton and Spinrad[16] published the earliest quantitative analysis of the $S_3(0)$ induced feature in the spectrum of Uranus. They found that an aerosol-free atmosphere model predicted geometric albedos that were significantly lower than measured values. They achieved reasonable fits to their data only with models that incorporated aerosols in some form. Two extreme cases of models which produced acceptable fits were (1) a semi-infinite homogeneous scattering model, incorporating a Rayleigh scattering aerosol mixed uniformly with atmospheric gases (modelled by doubling the volume coefficient for Rayleigh scattering by hydrogen) and (2) a finite reflecting-layer model with 300 to 400 km-amagat of hydrogen overlying an opaque cloud deck with surface reflectivity $A = 1$.

Figure 6 presents our data in the interval 8000-8500 A, with our best current attempts to model these data. The important feature of these models is that they are insensitive to all parameters except the pressure P_c at which we place an opaque cloud deck. By inspection, P_c is not much greater than 2 bars for Uranus and 3 bars for Neptune, corresponding to hydrogen column abundances of 230 and 300 km amagat, respectively. In the case of

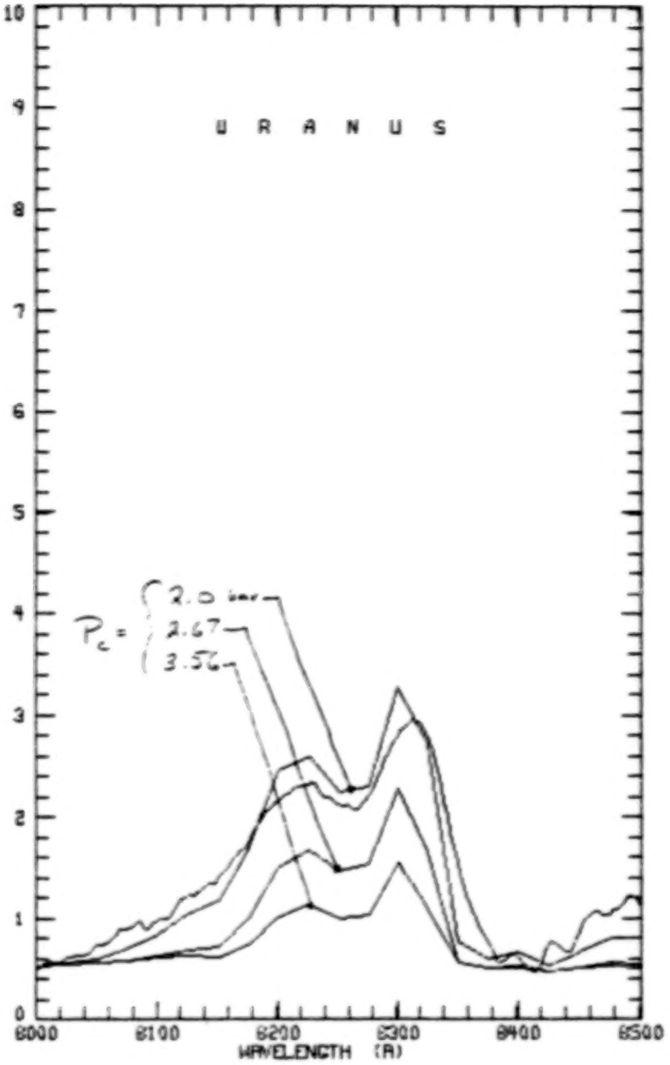

6a. Geometric albedo spectrum of Uranus between 8000 A and 8500 A (same data as Fig. 1, on expanded scale). Fitted models correspond to $P_h = 0.3$ bar, $\tau_h = 0.15$, various values of P_{cld}.

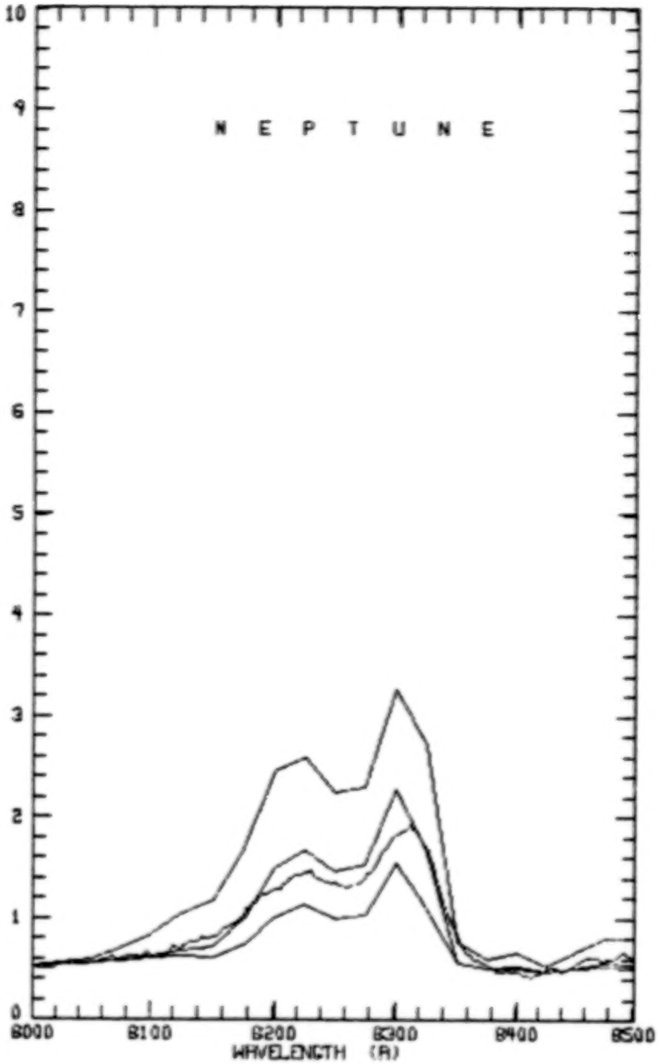

6b. Same as 6a, but with Neptune data substituted for Uranus.

Uranus, this is significantly less than Belton and Spinrad's column abundance for a similar model. The difference stems principally from the systematically higher geometric albedos we measured in the vicinity of $S_3(0)$. This difference may reflect a real secular or seasonal variation in Uranus's brightness. Belton and Spinrad employed Younkin's[17] spectrophotometry of Uranus to calibrate their spectrum scans photometrically. Younkin made his observations in 1961-1963, when the subsolar latitude on Uranus was nearly equatorial. Our observations were made in 1981, when the subsolar and subearth latitudes were greater than 70 degrees. Recent imaging observations of the planet indicate that a bright region is present around the visible pole. This may be a manifestation of a higher concentration of aerosols suspended in the circumpolar atmosphere and consequently a smaller scattering mean free path, averaged over the visible hemisphere.

Another significant result incorporated in Figure 6 is that the ortho/para hydrogen ratio evidently follows the equilibrium distribution at the local temperature in the atmospheres of both planets. Models in which the ortho/para ratio is set equal to the "normal" value of 3 fail to reproduce the $S_3(0)$ dip which is clearly evident at 8260 A in the spectra of both planets.

D. Methane Red and Near-Infrared Bands

The methane bands longward of 6000 A are saturated quite high in the atmospheres of Uranus and Neptune. Their strengths are, therefore, insensitive to methane column abundance and methane/hydrogen ratio. With one exception, they are not sensitive to any of the free parameters in our models.

In the absence of scattering, the residual intensities in the cores of the methane bands longward of 8000 A would be sensibly zero. The residual intensities are observed to be significantly greater than zero in the spectra of Uranus and Neptune, which indicates that scattering is significant at quite high altitudes in these atmospheres[18,19]. The residual intensities of the near-IR methane bands in Uranus's spectrum can be modelled successfully with Rayleigh scattering by a column density of approximately 70 km amagat of hydrogen, provided that (1) conservative aerosol scattering is absent and (2) methane is depleted (i.e., the methane partial pressure follows the saturation vapor pressure) in the uppermost atmospheric layers[18,19]. The residual intensities of the near-infrared methane bands in Neptune's spectrum are significantly higher than in Uranus's. They strongly suggest the presence of a scattering aerosol, with approximately 1/λ dependence of scattering cross section, at a depth no greater than 50 km-amagat of hydrogen (approximately 0.6 bars total pressure)[19].

Another manifestation of scattering in the cores of the near-infrared methane bands is the presence of Raman "ghosts." Cochran and Trafton[9] calculated the contribution of Raman scattering to the residual intensity of the 9000 A methane band for two variants on their deep hydrogen model atmosphere: model Ia in which methane is uniformly mixed with hydrogen at a ratio of 0.005 at all levels of the atmosphere (i.e., methane is supersaturated in the stratosphere) and model Ib in which the methane partial pressure follows the saturation vapor pressure curve throughout the visible atmosphere. The result is two "ghost" features: S(0) at about 8500 A and S(1) at approximately 8700 A. The predicted ghosts reproduce features evident in our spectrophotometric data (Figure 7), which appear to favor model Ib.

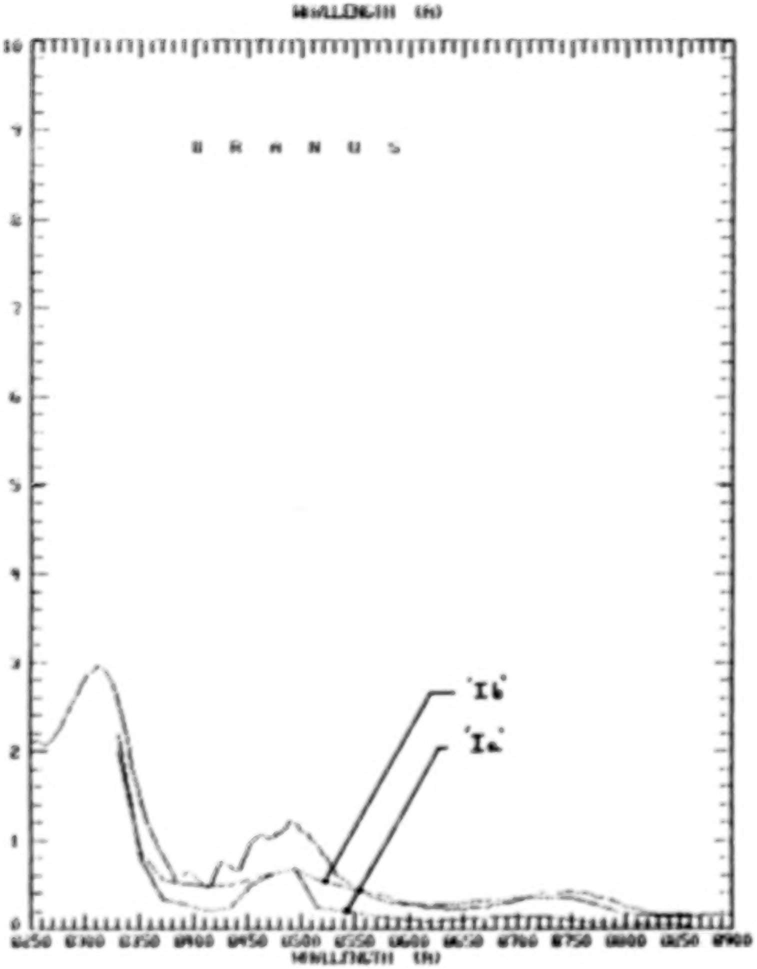

7a. Geometric albedo spectrum of Uranus between 8250 A and 8900 A (same data as Fig. 1, but on expanded scale). Cochran and Trafton's[9] models Ia and Ib are superimposed on the data.

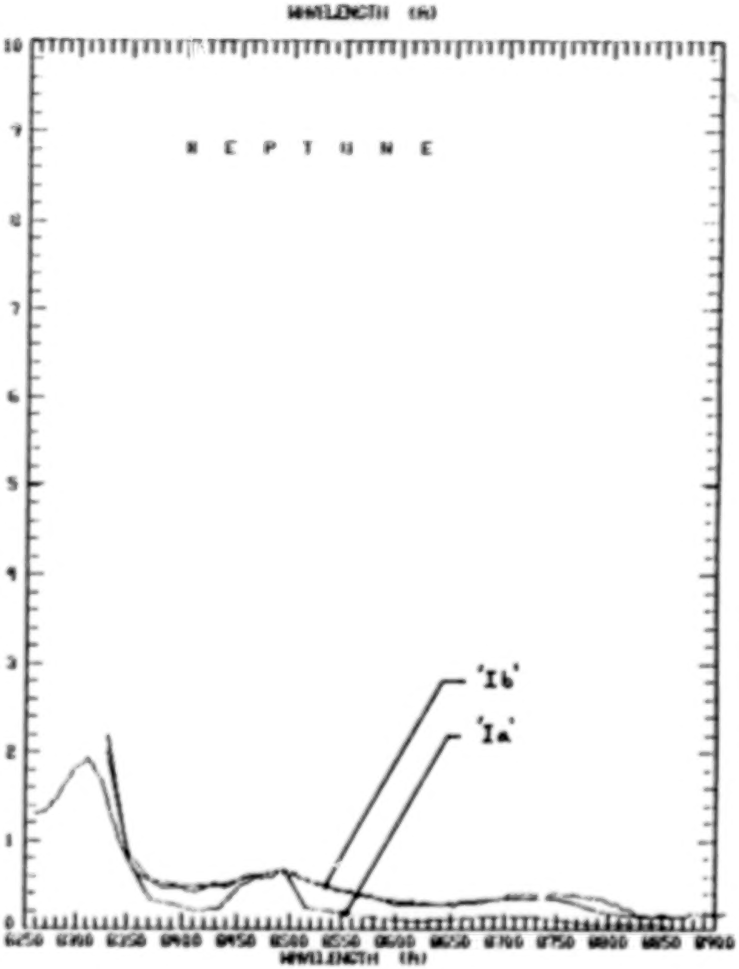

7b. Same as 7a, but with Neptune data substituted for Uranus.

E. Limitations and Caveats

While low-resolution observations yield much useful information about the structures of planetary atmospheres, they have limitations which restrict their interpretation. Their principal limitation is imposed by the unknown temperature behavior of the unresolved methane bands. There are good compilations of room temperature methane absorption coefficients[20,21], but there has been no effective investigation of their temperature behavior. Yet, since the population distribution of rotational levels in the ground vibrational state--which determines the strengths of individual lines comprising the unresolved bands--is a strong function of temperature, it is unlikely that the behavior of these bands is not strongly temperature dependent. Specifically, since the temperatures in the visible regions of Uranus and Neptune are significantly lower than room temperature (50-100 K compared with 300 K), we expect spectral regions dominated by lines of low rotational quantum number ($J < 5$) to show markedly enhanced absorption in Uranus and Neptune while spectral regions dominated by high-J lines should show decreased absorption.

Another limitation is imposed by differing radiative transfer properties within individual transitions comprising an absorption band. Scattering by gases and aerosols generally enhances absorption in intrinsically weak lines relative to absorption in strong ones. This is because scattering preferentially increases the mean atmospheric path lengths of photons in weak absorptions so that such photons have a greater chance of being absorbed. By contrast, photons in strong absorptions are likely to be absorbed regardless of the presence of scatterers.

Further limitations arise from pressure effects in unresolved bands. Pressure generally broadens and desaturates isolated spectral lines. As pressure increases, absorption within isolated lines increases beyond what is expected in the absence of broadening. In bands, however, neighboring lines increasingly influence the absorption experienced by photons near each other's intrinsic wavelengths as pressure increases. Consequently, a spectral interval which has a high density of strong lines may show little increase in absorption with pressure because the interval is virtually saturated at all pressures.

III. HIGH-RESOLUTION SPECTROSCOPY

Analyses of high-resolution observations of isolated spectral lines can potentially overcome these shortcomings. The temperature and pressure behaviors of the lines must be known accurately. For a spectral interval containing methane lines, this reduces to knowing the rotational quantum number and the room-temperature intensity, and pressure-broadening coefficient for each line as functions of temperature. Owing to the pressure effects discussed earlier, accurate analysis also requires knowing the behavior of lines whose intrinsic wavelengths may be quite far from the interval under analysis. There are few regions of the optical spectrum where these conditions are even partially met. While room temperature line strengths and pressure-broadening characteristics have been determined for a few specific methane features (e.g. the 6818.9 A line), rotational quantum numbers have never been determined theoretically or experimentally for any methane line in the visible to near-IR. This parameter is critical because the populations of rotational state (and, consequently, the line intensities) are quite sensitive to it. For example, lines corresponding to rotational quantum number $J = 4$ have intensities in Uranus's atmosphere which are essentially identical to their intensities measured experimentally at room temperature. By contrast, lines with $J = 0$ are more than an order of magnitude more intense at temperatures corresponding to the visible part of Uranus's atmosphere than at room temperature. Earlier investigations have resorted to (1) assuming temperature-independent line intensities[22], (2) an assumed rotational quantum number assignment[23], or (3) deriving rotational quantum number assignments from observations of planets whose atmospheric structures are (presumably) known[24]. None of these methods is above reproach. Atmospheric properties derived from analyses of isolated methane lines will be no more accurate than those derived from analyses of unresolved bands until the rotational quantum numbers of the isolated lines can be determined. However, we expect this situation to improve markedly in the near future, as low-temperature high-resolution techniques are applied to the problem.

A number of investigators have acquired high-resolution observations of isolated spectral features in Uranus and Neptune over the past two decades. Owing to the relatively low temperatures and large methane path lengths in these atmospheres, useful observations have been restricted principally to the S(0) and S(1) lines of the (3-0), (4-0), and, for Uranus, (5-0) hydrogen quadrupole overtones and isolated lines in the 6815 A methane band. Tables 1 through 4 summarize all high-resolution observations of which we are aware. The apparition, equivalent width, and instrumental resolution are listed for each observation.

A. Hydrogen Quadrupole Lines

Herzberg[25] first suggested the possibility of detecting hydrogen quadrupole lines in the spectra of the hydrogen-rich giant planets. Only a few features are available for study, but they are valuable because their temperature and pressure behaviors are well known from quantum mechanical theory and from experimental measurements.

TABLE I

Uranus: Summary of H_2 (3-0) and (4-0) Quadrupole Line Equivalent Widths

		(3-0)		(4-0)		Res.
Year	Ref.	S(0)	S(1)	S(0)	S(1)	(mA)
1964	26			30+8	41+15	160
1971	29	95+25	114+15			250
1972	30			62+19	58+13	260
1973	31			30^{+4}_{-3}	29^{+6}_{-3}	40
1970	18	122^{+21}_{-9}	121^{+21}_{-9}			470
1971	18	131+28	157+27		4+5	370
1972	18	146+15	157+11	27+3	31+5	430,270
1973	18	138+4	119+6	29+4	31+2	290,160
1974	18	141+4	114+6	29+3	31+2	290,160
1975	18	137+4	119+6	28+1	31+1	290,160
1975	32				21.5+1.6	35
1976	33			22+4	21+3	75-85
1981	6			23.4+1	22.5+1	30
1983	34		107+10		18.6+3	80

Additional Observations:

Encrenaz and Owen[31] report <1 mA for (4-0) S(2).
Trafton[35] reports 6.7+1.5 mA for (5-0) S(0) and 4.9(+0.6,-0.3) mA for (5-0) S(1).

TABLE II

Neptune: Summary of H_2 Quadrupole Line Equivalent Width Observations

		(3-0)		Res.
Year(s)	Ref.	S(0)	S(1)	(mA)
1973	27	28+4	31+4	150
1976-78	33	22+6	19+2	75-80
1983	34		19+3	80

Giver and Spinrad[26] reported the earliest quantitatively useful measurements of the (4-0) equivalent widths in Uranus. A number of other investigators have subsequently measured quadrupole lines in the (3-0) and (5-0) overtones. For Neptune, only the (4-0) overtone has been measured[27]. Specifically, no measurements of the (3-0) overtone have been reported for this planet.

The (4-0) S(0) and S(1) lines are especially useful because they are relatively free of interference from other planetary and telluric spectral features (by contrast, the lines of the (3-0) overtone are clearly contaminated by planetary lines in the strong 8000 A and 8400 A methane bands and by telluric lines in the "z" band of water vapor). Nonetheless, there is considerable dispersion in the equivalent widths reported for the (4-0) lines. This probably reflects systematic differences among observers in estimating the continuum level and in accounting for residual contamination by neighboring methane features. Smith, et al.[28] emphasized this when they noted that the equivalent widths they measured during the 1976-1978 apparitions were 1/3 smaller than the values reported by Trafton[18]. It is extremely unlikely that Uranus and Neptune simultaneously underwent global atmospheric changes of this magnitude between the 1975 and 1976-1978 apparitions. Thus, no temporal variations can be ascertained conclusively from the published measurements. However, the most recent measurement of (4-0) S(1) by Smith[34] suggest that temporal variations may be detectable.

For Uranus, the highest resolution observations reported to date are by Trauger and Bergstralh[6]. They report the first detection of asymmetry in the (4-0) quadrupole line profiles which is readily explained as a manifestation of the pressure dependence of the central line frequency. Figure 8 shows recent models by Bergstralh et al.[36] compared to the observed (4-0)

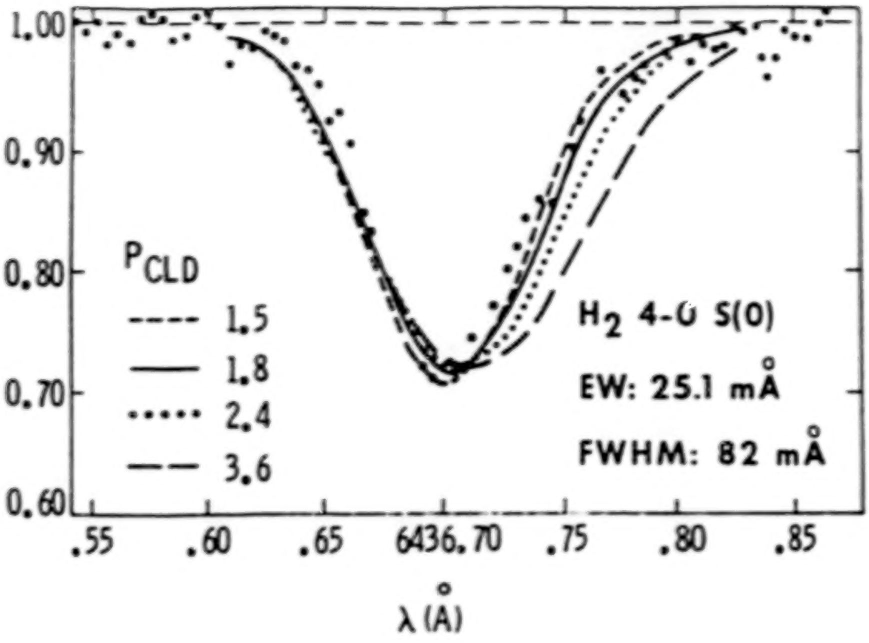

8. Modelled 4-0 S(0) line profiles for various cloud-top pressures, P_{cld}, vs the observations of Trauger and Bergstralh (1981). Breadth of line and line position restrict $P_{cld} < 2.4$ bars. Depth of line satisfied by line strength $S = 0.000030\ cm^{-1}\ (km\text{-}am)^{-1}$, assuming $\tau_H = 0.3$.

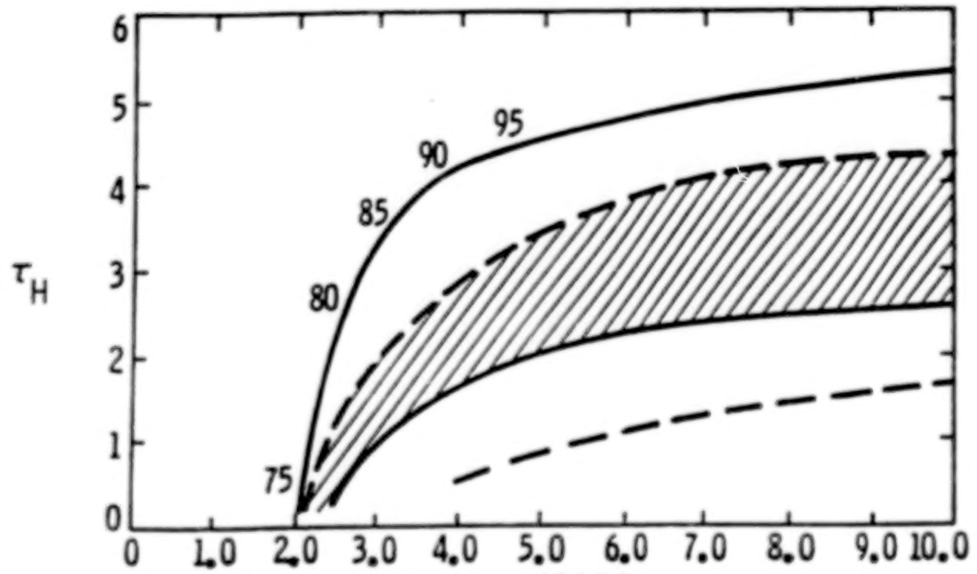

9. τ_H vs P_{cld} constraint diagram which satisfies equivalent widths and continuum continuum albedos for 4-0 S(0) (dashed) and 4-0 S(1) (solid) simultaneously (cross-hatched area). Line strengths of Bragg et al (1982) and an equilibrium distribution of ortho/para states for H_2 are assumed. Constraints impose a limit of $\tau_H < 1.3$. Additional constraints imposed by shape of line profile, e.g. the full-width at half-maximum (numbers, in mÅ), restrict solutions to $\tau_H < 0.3$ $P_{cld} < 2.5$ bars.

BEST COPY AVAILABLE

S(0) line profile. The analysis reveals that a model incorporating the nominal haze parameters and an optically thick cloud top at about 2 bars satisfies both the line width and frequency shift of the peak absorption. The absorption peak itself is modelled well with a room-temperature line strength of 3×10^{-5} cm^{-1} $(km\text{-}amagat)^{-1}$ (i.e., midway between the theoretical value, 3.7×10^{-4}, and the value 2.2×10^{-4} measured experimentally by Bragg et al.[37]). The identical model fits the profile of the S(1) feature well if a line intensity within the uncertainties of the Bragg, et al. measurements is adopted. An equilibrium distribution of ortho-para states is assumed for these models. The "normal" ortho/para ratio, 3:1, is qualitatively incompatible with the observed near-equality of the equivalent widths of the S(0) and S(1) lines.

It should be noted that Cochran and Smith[38] previously predicted the existence of a base at 2 bars pressure for the visible part of Uranus's atmosphere from the equivalent width measurements of Smith et al.[33]. Their conclusions were essentially correct because they adopted the Bragg et al.[37] line intensities for their analysis. They would have inferred the presence of a base nearly twice as deep in hydrogen column abundance if they had adopted the weaker experimental line strengths reported by Mickelson et al.[39] and Bergstralh et al.[40]. Our analysis relies principally on the half-widths and pressure shifts of the quadrupole lines, and, therefore, is independent of the values adopted for the line intensities. Indeed, we have utilized the model we have derived for the atmosphere of Uranus to constrain the quadrupole line intensities.

Figure 9 shows the range of haze optical depth vs. cloud-top pressure which satisfies both the observed equivalent widths and geometric albedos for the S(0) and S(1) lines simultaneously, if we adopt the line intensities reported by Bragg et al.[37]. Not surprisingly, as the haze optical depth increases, the cloud-top pressure also must increase to compensate for the increasing proportion of photons reflected by the haze. Owing to pressure-shift effects, this mechanism preserves the equivalent width of the line by increasing its width rather than its depth. The observations of Trauger and Bergstralh[6] impose a tight constraint on the width of the profile, so that we are restricted to the lower left hand region on the diagram (i.e., 2 bars and $0.15 < \tau_H < 0.30$).

Relatively little modelling of hydrogen quadrupole features has been performed for Neptune. The most thorough analysis to date is by Smith et al.[33] who report a hydrogen column abundance greater than 200 km-amagat (corresponding to pressure greater than 2 bars at the visible base), based on the similarity of the observed equivalent widths to those observed for Uranus and adopting a helium molar fraction of about 10 percent. The observed enhancement of high altitude aerosols in Neptune implies that the base of the visible atmosphere lies deeper than on Uranus, to compensate for the greater proportion of photons scattered out of Neptune's atmosphere at high altitudes.

B. The 6818.9 A Methane Line

As far as we know, the weak band at 6815 A is the only methane feature in the spectra of Uranus and Neptune which has been resolved into individual rotational lines. Detailed analyses have concentrated on the most prominent feature in the band--the line at 6818.9 A. There is notable agreement among the equivalent widths reported by various observers over the past decade (Tables III and IV), suggesting (1) that there is little temporal change in the atmospheres of these planets, on a global scale, and

TABLE III

Uranus: Summary of 6818.9 A Methane Line Equivalent Width Observations

Year	Ref.	W (mA)	Res. (mA)
1966	43	detection	1500
1973	23	155	150
1974	44	150	300
1975	22	150	280
1980	42	150+10	100

TABLE IV

Neptune: Summary of 6818.9 A Methane Line Equivalent Width Observations

Year	Ref.	W (mA)	Res. (mA)
1975	22	140	280
1980	42	130+10	100

(2) there is little systematic difference among observers in determining the continuum level.

Baines[41] has utilized the highest resolution observations of this feature[42] to model the line profile. He found that the halfwidth rather than the equivalent width of the line is diagnostic of the methane column abundance, owing to saturation effects. Assuming the value J = 0 for the rotational quantum number of the line, he derived a methane molar fraction of 3-4% for a 2.4 bar atmospheric base--essentially in agreement with the results of the analysis of broadband spectrophotometry described earlier in this paper. An optical depth of 2.4 was derived for the tropospheric haze from the residual intensity at the bottom of the 6818.9 A feature. This is a factor of 16 greater than the value we derived earlier from the broadband data. We note that we adopted absorption coefficients measured experimentally at room temperature for the weak methane bands used to constrain the haze optical depth. It is possible that our analysis under estimated the haze optical depth if the peak absorption coefficients increase with decreasing temperature. Nevertheless, an optically thick haze disagrees with the results of our hydrogen quadrupole analysis: Figure 9 shows that the permitted range of optical depths does not overlap that derived by Baines[41], τ_H being restricted to values less than 0.75 for cloud-top pressures less than 10 bars.

As in the case of the hydrogen quadrupole features, comparatively little modelling has been performed for the 6818.9 A methane line in Neptune's spectrum. Macy, et al.[22] determined pressures approximately 0.4 bars less than the values they found for Uranus from a rather qualitative analysis of their measured line width (i.e., they found an effective pressure in the range 1.9-3.5 bars vs. 2.3-3.8 bars). However, their value is suspect because they did not account for line saturation effects or for the broadening effects of scattering. Baines[41] performed a cursory evaluation which demonstrated that a Uranus haze model satisfies the observed line profile[30] with the exception that $t_H = 3.0$. However, he noted that if Neptune's stratosphere is supersaturated with methane, as postulated by Macy and Trafton[45] to account for the ν_4 emissions at 7.7 µm, then the aerosol content could be considerably greater.

IV. CONCLUSIONS

Table V summarizes the atmospheric model parameters derived for Uranus from analyses of visible to near-infrared observations.

ACKNOWLEDGEMENTS

The research described in this paper was performed by the Jet Propulsion Laboratory, California Institute of Technology, under contract with the National Aeronautics and Space Administration.

TABLE V

Uranus: Summary of Derived Parameters

Parameter	Range	Observational Constraints
Haze:*		
τ_h	0.15-0.3	Weak methane bands, (4-0) S(0), S(1) peak absorption
$\tilde{\omega}_h(\lambda)$	$W_a = 0.24$; $W_b = 4.56$ $W_a = 0.90$; $W_b = 4.37$	Blue continuum
Haze-top pressure pressure P_{H-T}	0.5±0.1 bar	Blue continuum, residual intensities in strong CH_4 bands
Haze bottom pressure P_{H-B}	< 2 bars	CH_4 molar fraction from weak CH_4 bands, 6818.9 A line equiv. width; saturation vapor pressure
Cloud:		
$\tilde{\omega}_{cld}$	0.9985	Peak geometric albedo (5150 A)
Cloud-top pressure P_{cld}	2 bars	(4-0) quadrupole widths, peak absorption, freq. shifts; (3-0) PIA dipole peak absorption
CH_4:		
Molar fraction	> 3%	Weak CH_4 bands, 6818.9 A line width
Distribution	Depleted in upper troposphere and stratosphere	Residual intensities in strong CH_4 bands; limb brightening in strong CH_4 bands (Ref. 46)
H_2:		
Ortho/para ratio	Equilibrium distribution	(4-0) quadrupole S(0) and S(1) equiv. widths; (3-0) PIA
(4-0) S(1) line strength	Theoretical	Peak absorption in (4-0) S(1) quadrupole line

* Wavelength-dependent haze optical properties parameterized as:

$$\tilde{\omega}_h(\lambda) = [1 + W_a(3500/\lambda)^{W_b}]^{-1}$$

$$\tau_h(\lambda) = \tau_H\ (6435/\lambda)^4$$

Wallace's[47] parameterization of Trafton's[18] haze properties satisfied by $W_a = 0.02$, $W_b = 4$, $T = 1$.

TABLE VI

Neptune: Summary of Derived Parameters

Parameter	Range	Observational Constraints
Haze:		
Optical depth (5000 A)	$0.032 < \tau_H < 0.1$	Blue continuum*
Cloud:		
Cloud-top pressure	$P_{cld} = 3$ bars	(3-0) PIA dipole peak absorption
Surface albedo	$A_{cld} > 0.75$	Blue continuum*
CH_4:		
Molar fraction	$0.01 < f\ CH_4 < 0.03$	CH_4 bands*
H_2:		
Ortho/para ratio	Equilibrium	(3-0) PIA dipole peak absorption

---

* From Reference 48.

REFERENCES

1. Belton, M. J. S. (1982). An introductory review of our present understanding of the structure and composition of Uranus' atmosphere. In Uranus and the Outer Planets, ed. Hunt, G. E. (Cambridge, University Press), 155-171.

2. Trafton, L. M. (1981). The atmospheres of the outer planets and satellites. Rev. Geophys. Space Phys., 19, 43-89.

3. Trafton, L. M. (1977). Recent observational studies of the outer planets. Proceedings, Symposium on Planetary Atmospheres, ed. Jones, A. V. (Ottawa, Roy. Soc. of Canada, 19th Symposium), 111-116.

4. Trafton, L. M. (1974). Spectroscopic data. In The Atmosphere of Uranus, ed. Hunten, D. M. (proceedings of workshop held at NASA-Ames Research Center), 80-85.

5. Neff, J. S., Humm, D. C., Bergstralh, J. T., Cochran, A. L. Cochran, W. D., Barker, E. S. and Tull, R. G. (1984). Absolute spectrophotometry of Uranus, Neptune and Titan: 3500 A - 10500 A. Icarus, in press.

6. Trauger, J. T. and Bergstralh, J. T. (1981). Asymmetrical profiles of the H_2 (4-0) quadrupole lines in the spectrum of Uranus. Bull. Amer. Astron. Soc., 13, 732.

7. Belton, M. J. S., McElroy, M. B., and Price, M. J. (1971). The atmosphere of Uranus. Astrophys. J., 164, 191-209.

8. Wallace, L. (1972). Rayleigh and Raman scattering by H_2 in a planetary atmospere. Astrophys. J., 176, 249-257.

9. Cochran, W. and Trafton, L. M. (1978). Raman scattering in the atmospheres of the major planets. Astrophys. J., 219, 756-762.

10. Price, M. J. (1977). On probing the outer planets with the Raman effect. Rev. Geophys. and Space Phys., 15, 227-234.

11. Belton, M. J. S., Wallace, L. and Price, M. J. (1973). Observation of the Raman effect in the spectrum of Uranus. Astrophys. J. (Lett.), 184, L143-L146.

12. Cochran, W. D. (1981). Raman scattering as a probe of planetary atmospheres. Advances in Space Research, 1, 143-153.

13. Encrenaz, T., Hardorp, J., Owen, T. and Woodman, J. H. (1974). Observational constraints on model atmospheres for Uranus and Neptune. In Exploration of the Planetary System, ed. Wosczcyk and Iwaniszewska (IAU), 487-496.

14. Lutz, B. L., Owen, T. and Cess, R. D. (1976). Laboratory band strengths of methane and their application to the atmospheres of Jupiter, Saturn, Uranus, Neptune and Titan. Astrophys. J., 203, 541-551.

15. Trafton, L. M. (1967). Model atmospheres of the major planets. Astrophys. J., 147, 765-781.

16. Belton, M. J. S. and Spinrad, H. (1973). H_2 pressure induced lines in the spectra of the major planets. Astrophys. J., 185, 363-372.

17. Younkin, R. L. (1970). Spectrophotometry of the Moon, Mars, and Uranus. Unpublished doctoral dissertation, University of California Los Angeles.

18. Trafton, L. M. (1976). The aerosol distribution in Uranus' atmosphere: interpretation of the hydrogen spectrum. Astrophys. J., 207, 1007-1024.

19. Fink, U. and Larson, H. P. (1979). The infrared spectra of Uranus, Neptune and Titan from 0.8 to 2.5 microns. Astrophys. J., 233, 1021-1040.

20. Fink, U., Benner, D. C. and Dick, K. A. (1977). Band model analysis of laboratory absorption spectra from 4500 to 10500 A. J. Quant. Spectrosc. Radiat. Transfer, 18, 447-457.

21. Giver, L. P. (1978). Intensity measurements of the CH_4 bands in the region of 4350 to 10600 A. J. Quant. Spectrosc. Radiat. Transfer, 19, 311-322.

22. Macy, W., Gelfand, J. and Smith, W. H. (1978). Interpretation of the 6818.9 A methane line in terms of inhomogeneous scattering models for Uranus and Neptune. Icarus, 34, 20-27.

23. Bergstralh, J. T. (1975). Uranian methane abundance, rotational temperature, and effective pressure from the 6800 A band. Astrophys. J., 202, 832-838.

24. Baines, K. H. (1983). Interpretation of th 6818.9 A methane feature observed on Jupiter, Saturn and Uranus. Icarus, 56, 549-559.

25. Herzberg, G. (1938). On the possibility of detecting molecular hydrogen and nitrogen in planetary and stellar atmospheres by their rotation-vibration spectra. Astrophys. J., 87, 428.

26. Giver, L. P. and Spinrad, H. (1966). Molecular hydrogen features in the spectra of Saturn and Uranus. Icarus, 5, 586-589.

27. Trafton, L. M. (1976). Neptune: Observations of the H_2 quadrupole lines in the (4-0) band. In Exploration of the Planetary System, ed. Wosczcyk and Iwaniszewska (Dordrecht, D. Reidel), 497.

28. Smith, W. H., Macy, W. and Pilcher, C. B. (1980). Measurements of the H_2 (4-0) quadrupole bands of Uranus and Neptune. Icarus, 43, 153-160.

29. Lutz, B. L. (1973). Molecular hydrogen on Uranus. Observations of the (3-0) quadrupole band. Astrophys. J., 182, 989-998.

30. Price, M. J. (1973). The scattering mena free path in the Uranian atmosphere. Icarus, 20, 455-464.

31. Encrenaz, T. and Owen, T. (1973). New observations of the hydrogen quadrupole lines in Saturn and Uranus. Astron. Astrophys., 28, 119-124.

32. Trauger, J. T., Roesler, F. L. and Munch, G. (1978). A redetermination of the Uranus rotation period. Astrophys. J., 219, 1079-1083.

33. Smith, W. H., Macy, W. and Pilcher, C. B. (1980). Measurements of the H_2 (4-0) quadrupole bands of Uranus and Neptune. Icarus, 43, 153-160.

34. Smith, W. H. (1984). Private communication.

35. Trafton, L. M. (1978). Detection of H_2 quadrupole lines belonging to the (5-0) overtone band in the spectrum of Uranus. Astrophys. J., 223, 339-343.

36. Bergstralh, J. T., Baines, K. H., Trauger, J. T. and Apt, J. (1983). The structure of the Uranus atmosphere: Constraints of contemporary broadband absolute spectrophotometry and high-resolution observations of the H_2 (4-0), S(0) and S(1) features. Bull. Amer. Astron. Soc., 15, 859.

37. Bragg, S. L., Brault, J. W. and Smith, W. H. (1982). Line positions and strengths in the H_2 quadrupole spectrum. Astrophys. J., 263, 999-1004.

38. Cochran, W. D. and Smith, W. H. (1983). The desaturation of H_2 quadrupole lines in the atmospheres of the outer planets. Astrophys. J., 271, 859-864.

39. Mickelson, M. E., Larson, L. E. and Trauger, J. T. (1977). Laboratory measurements of the hydrogen (3-0) and (4-0) S(1) quadrupole lines. Bull. Amer. Astron. Soc., 9, 515.

40. Bergstralh, J. T., Margolis, J. S. and Brault, J. W. (1978). Intensity and pressure shifts of the H_2 (4-0), S(1) quadrupole lines. Astrophys. J. (Lett.), 224, L39-41.

41. Baines, K. H. (1982). Interpretation of the 6815 A band of methane observed in the major planets. Unpublished Ph.D. dissertation (St. Louis, Washington University).

42. Baines, K. H., Schempp, W. V. and Smith, W. H. (1983). High resolution observations of the 6815 A band of methane in the major planets. Icarus, 56, 534-542.

43. Owen, T. (1966). An identification of the 6800 A methane band in the spectrum of Uranus and a determination of atmospheric temperature. Astrophys. J., 146, 611-613.

44. Belton, M. J. S. and Hayes, S. H. (1975). An estimate of the temperature and abundance of CH_4 and other molecules in the atmosphere of Uranus. Icarus, 24, 348-357.

45. Macy, W. and Trafton, L. (1975). Neptune's atmosphere: the source of the thermal inversion. Icarus, 26, 428-436.

46. Pilcher, C. B., Morgan, J. S., Macy, W. and Kunkle, D. (1979). Methane band limb-brightening in Uranus. Icarus, 39, 54-64.

47. Wallace, L. (1980). The structure of the Uranus atmosphere. Icarus, 43, 231-259.

48. Bergstralh, J. T. and Neff. J. H. (1983). Absolute spectrophotometry of Neptune: 3390 to 7800 A. Icarus, 55, 40-49.

NEAR INFRARED IMAGING OF URANUS AND NEPTUNE

Bradford A. Smith

Lunar and Planetary Laboratory
University of Arizona
Tucson, AZ 85721

Abstract

Imaging of Uranus and Neptune in the deep methane absorption band at 890nm has been used to detect high-altitude atmospheric hazes and to search for possible undiscovered close-in satellites. The appearances of Uranus and Neptune are very different from one another and Uranus seems to be changing with time. The Neptune images show rotation in the direct sense. No new satellites have been found to date.

INTRODUCTION

The remoteness of Uranus and Neptune is the single-most important factor in our lack of knowledge of these distant systems. Although their true diameters fall somewhere between those of the giant planets, Jupiter and Saturn, and those of the terrestrial bodies, the size of their disks in the focal plane of a groundbased telescope is exceedingly small. The image of Uranus (3.9 arcsec) would almost fit within the image of the Great Red Spot of Jupiter, while that of Neptune (2.3 arcsec) is scarcely larger than the disk of Ganymede. Furthermore, the feeble solar illumination in the outer solar system, 370 and 900 times less than at the earth for Uranus and Neptune, respectively, causes the surface brightness of the tiny disks to be lower than that of many planetary nebulae. Thus, the longer integration times required to overcome the low surface brightness further compounds the difficulty of observing these distant bodies. Earlier attempts to record cloud structure on Uranus, by the Stratoscope project and by the writer while at New Mexico State

University, have been unsuccessful. Within the limited spatial resolution, the disk of Uranus in the visible region of the spectrum seems to be featureless, not unlike a visible image of Venus. However, this lack of detail is not due to remoteness alone; the 45 arcsec disk of Jupiter, reduced to 3.9 arcsec, would still reveal the familiar banded pattern. The contrast of any large-scale cloud structure on Uranus (and, presumably, Neptune as well) in visible light must be less than that of the clouds on Jupiter.

Since the mid 70s, the writer (and, more recently, with R.J. Terrile of JPL) has renewed an attempt to image cloud structure in the atmospheres of Uranus and Neptune and to search for small nearby satellites of both planets. Because the atmospheres of both planets contain relatively large amounts of methane, the strong absorption in the methane bands in the far red and near infrared create very low geometrical albedoes, approximately 0.01 for both Uranus and Neptune. Thus, imaging within these deep methane bands subdues reflected light from the planetary atmospheres and provides the best opportunity to detect high altitude atmospheric hazes and to search for nearby faint objects. The deepest of these optical methane bands, at 890 and 1000 nm, became easily reachable only with the advent of scientific quality CCDs in the mid 70s.

EARLY OBSERVATIONS

Among the first astronomical results obtained with CCDs were a series of Uranus images taken in the 890 nm methane band in April 1976 with the 1.5 m Catalina reflector at the University of Arizona. The images (see Fig. 1) showed a dark disk with limb brightening that was asymmetrically stronger toward the pole. A search for undiscovered satellites in these and later images revealed no new objects to m = 19. However, a marginal detection of the Epsilon ring[1] suggested a ring albedo of 0.01-0.02. In 1979 the CCD camera was successful in recording discrete clouds in the atmosphere of Neptune[2]. The clouds, probably thin, high-altitude patches of methane ice or photochemically produced particulates, were observed to rotate with Neptune (Fig. 2). Although the temporal coverage was inadequate to provide an optical rotation period, the sense of the rotation was determined to be direct, not retrograde, i.e., not in the same direction as the revolution of Triton.

As the CCD has greatly improved our ability to study Uranus and Neptune, so also has the development of a long-forgotten instrument, the coronagraph. First used by Lyot[3] in the 1930s, the coronagraph was reintroduced by Whitaker[4] in the early 70's. Based on the principle of using an exit pupil mask to remove diffraction producing edges, the coronagraph effectively eliminates diffraction created at the edges of the primary telescope mirror, the secondary mirror cell and the secondary mirror support system. Scattered (diffracted) light from mirror dust and microscratches and from atmospheric inhomogeneities (seeing) remain, but the total amount of diffracted light around a stellar image is dramatically reduced. The use of a coronagraph thereby improves the recorded contrast of features on extended objects and greatly increases the detectability of faint objects close to very bright ones.

RECENT OBSERVATIONS

In 1982 and 1983, R.J. Terrile and the writer observed Uranus and Neptune with the 2.5-m du Pont telescope of the Las Campanas Observatory (Chile) using a CCD camera system provided by the Space Telescope Wide Field/Planetary Camera Instrument Development Team and two coronagraphs designed and fabricated at the Lunar and Planetary Laboratory. Because of optical constraints, the first Arizona coronagraph operated in a reducing mode only. Consequently, during 1982, we were able only to conduct satellite searches; no direct imaging of either Uranus or Neptune was possible. In 1983 a second Arizona coronagraph was used, allowing both continued satellite searching at a reduced focal ratio of f/2.8 (wider field of view) and direct imaging at f/7.5.

The direct images of Uranus and Neptune were taken with the coronagraph through a 890nm filter, 40nm wide and centered on the methane absorption band. Exposure times of one minute were typical. The Uranus images (Fig. 3) appeared to be very different from those obtained in the mid to late 70s. No pronounced limb brightening is seen in the unprocessed images, although careful processing (yet to be attempted) may show detail not visible in the raw images. It appears likely that real changes have taken place on Uranus. Neptune, on the other hand, shows a cloud pattern (Fig. 4) very similar to that seen in 1979. The Las Campanas images, unlike those obtained in 1979, were collected over a five-day interval and thus present an opportunity for determining an optical rotation period. Terrile reports on those results elsewhere in these Proceedings.

The 1983 Neptune images are characterized by several patches of haze located at the mid-latitudes in both northern and southern hemispheres. Because the earth's declination on Neptune is presently at -24^0, the southern hemispheric features are most clearly seen. Neptune appears to show less limb brightening in the 890-nm methane band than did Uranus during the mid to late 70s, but this may be due in part to the preliminary processing; Neptune appears to have cloud structure with inherently higher contrast and the images, therefore, are not as strongly enhanced during processing.

If the rotation period of Neptune is established, allowing geometrical solutions for the changing air mass over the bright clouds, it may be possible to solve for the columnar depth of methane over the clouds and thereby derive their pressure height in the Neptune atmosphere.

The search for faint new satellites around Uranus and Neptune has continued through 1982-83. The survey includes images taken in both the direct and reducing coronagraph modes and both with and without focal plane masks. The focal plane mask is a small (0.5 to 0.7mm) opaque disk, supported in the focal plane of the telescope by silk monofiliments and centered on the planetary disk. While the mask tends to further reduce scattered light by blocking the image of the relatively bright planetary disk, it is always chosen to be somewhat larger than the planetary disk itself and, therefore, does not permit searching close to the planetary limb. The limiting magnitude of the search reaches $m_I \sim 23$ at distances well away from Uranus and Neptune and decreases with decreasing distance from the limbs. The search limit, expressed as the radius of a satellite having a geometrical albedo of 0.2, is shown in Fig. 5 as a function of distance from each planet. To date only a cursory search has been completed; the current limit is a radius several times greater than that indicated in Fig. 5. No new satellites have been found to date.

Analysis of the direct and satellite search images is continuing; new observational data will be collected in April 1984.

REFERENCES

1. Methane-band detection of the Uranian ring system, B.A. Smith, H.J. Reitsema and D.E. Weistrop, Bull. Am. Astron. Soc. 9, 499, 1977.

2. Discrete cloud features on Neptune, B.A. Smith, H.J. Reitsema and S.M. Larson, Bull. Am. Astron. Soc. 11, 570, 1979.

3. A Study of the Solar Corona and Prominences without Eclipses, B. Lyot, Monthly Notices of R.A.S., 99, 580, 1939.

4. Eccentricity and Inclination of Miranda's Orbit, E. Whitaker and R. Greenberg, Comm Lunar and Planetary Lab, 10, 70, 1973.

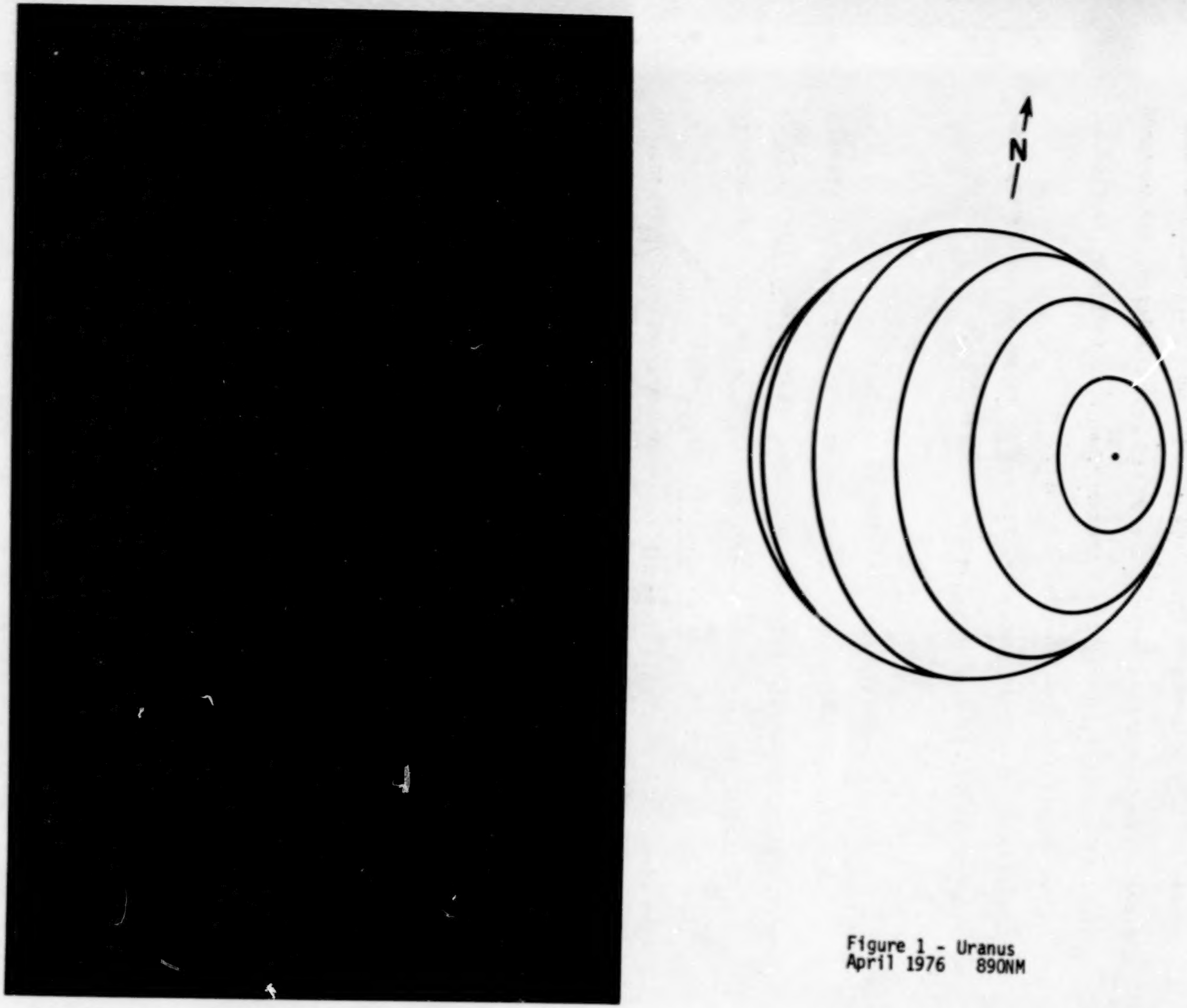

Figure 1 - Uranus
April 1976 890NM

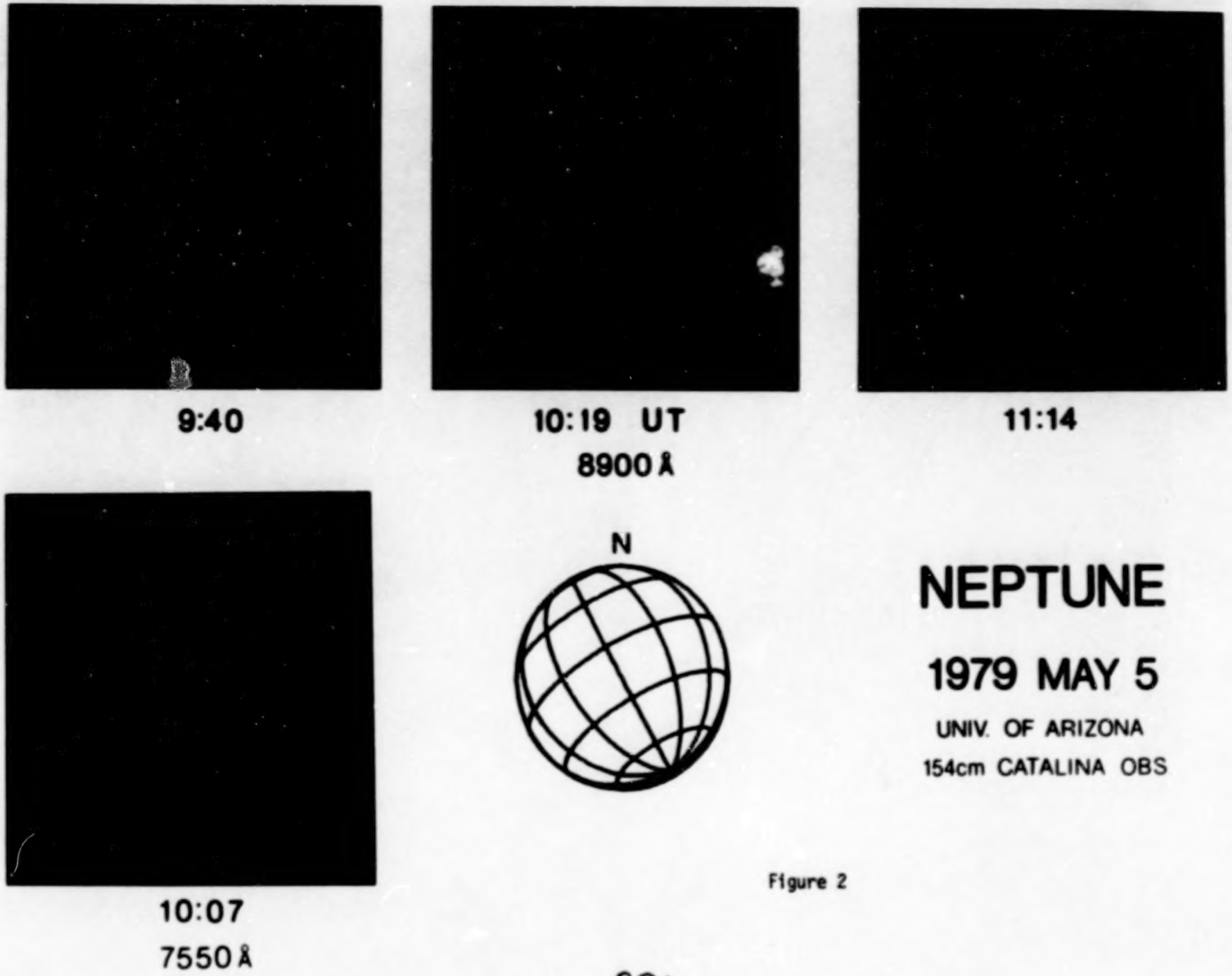
9:40
10:19 UT
8900 Å
11:14
10:07
7550 Å
N
NEPTUNE
1979 MAY 5
UNIV. OF ARIZONA
154cm CATALINA OBS

Figure 2

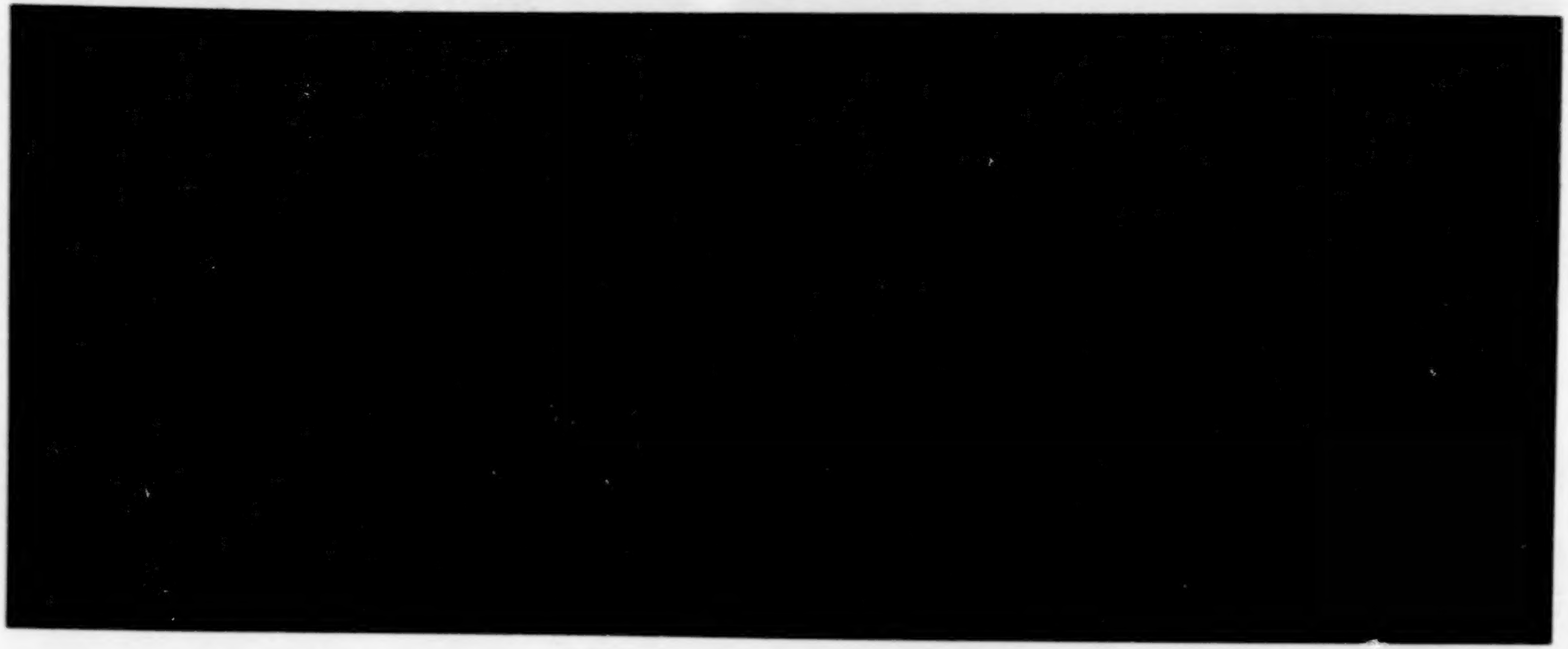

Figure 3 - Uranus
May, 1983 - 890 NM

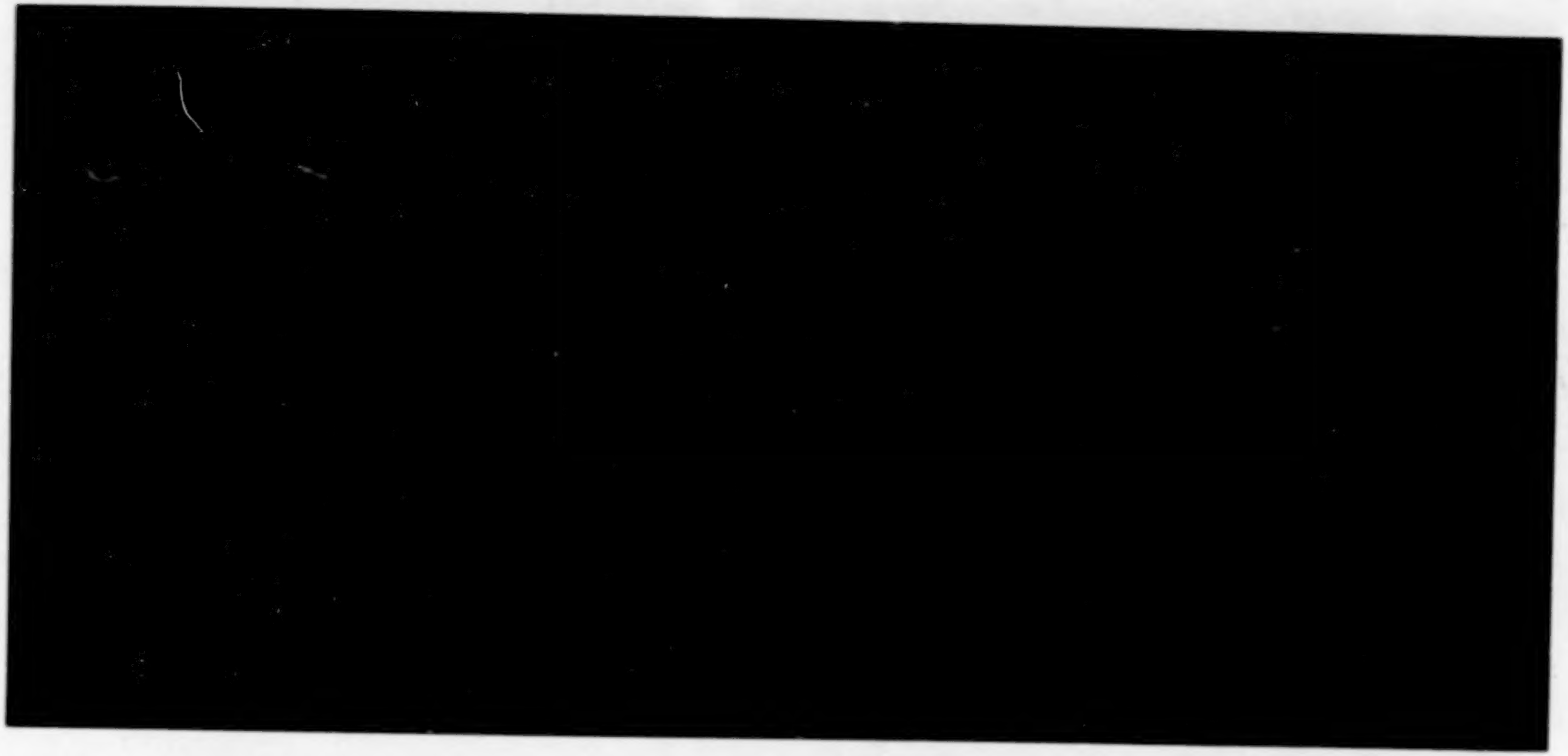

Figure 4 - Neptune
May, 1983 - 890 NM

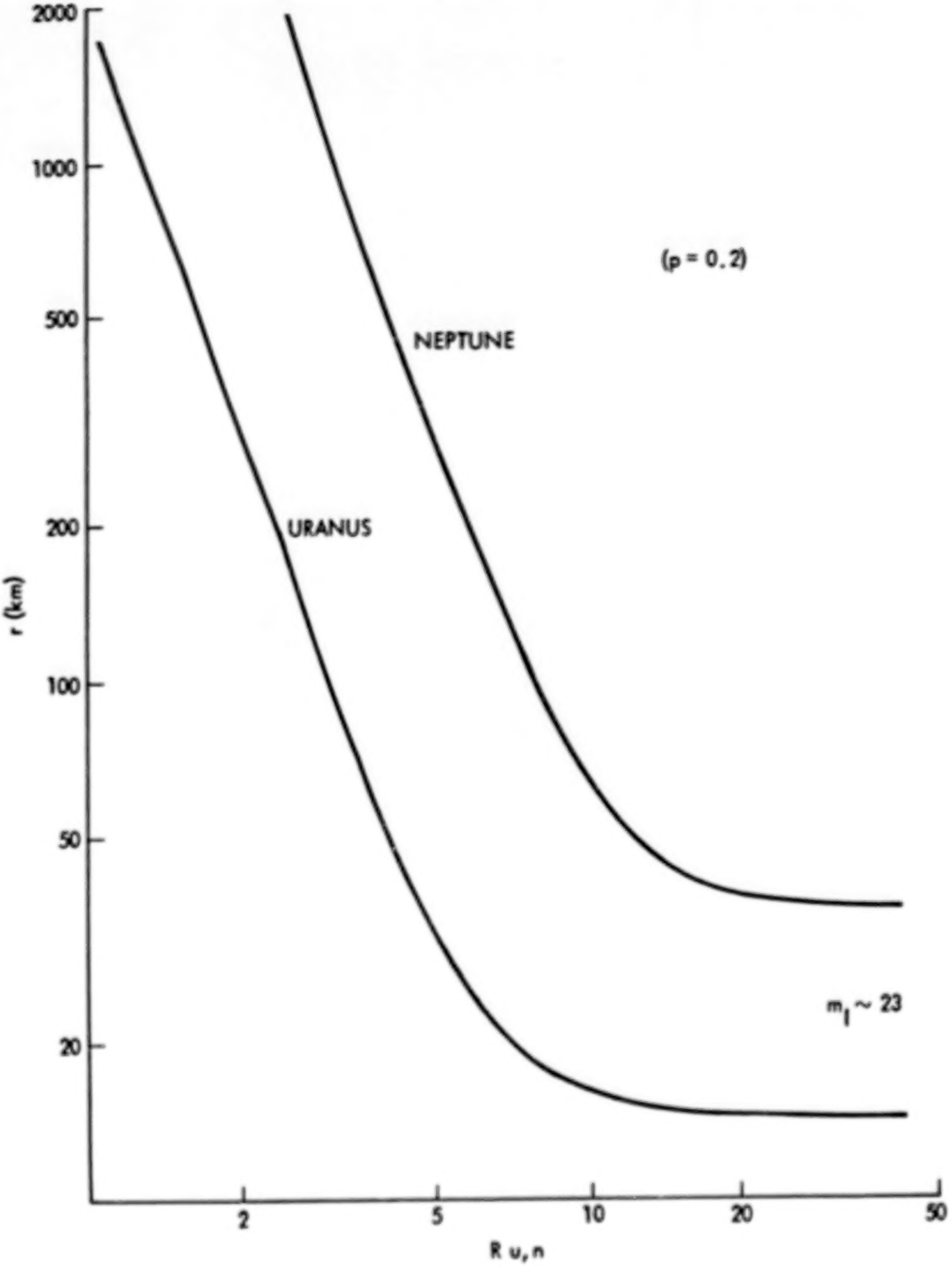

Figure 5. Limiting Radius for Satellite Search

A REVIEW OF THE MILLIMETER AND CENTIMETER OBSERVATIONS OF URANUS

Samuel Gulkis

Jet Propulsion Laboratory
California Institute of Technology
4800 Oak Grove Drive
Pasadena, California 91109

Imke de Pater

Astronomy Department
University of California
Berkeley, California 94720

Abstract

Millimeter and centimeter wave astronomical data of Uranus are presented and discussed. Some recent observations of the brightness distribution across the disk at 2 cm and 6 cm wavelength are reported. Data which relate to the variability of the microwave spectrum are reanalysed taking into account the strong variation of temperature with wavelength, and including up-to-date data. The results indicate that the brightness temperatures of Uranus have probably reached their maximum values. The evidence for the depletion of ammonia in the upper atmosphere is discussed.

INTRODUCTION

The angular diameter of Uranus subtends an angle of less than 4 arc seconds at the earth's distance and until quite recently, the only radio measurements of Uranus were of the unresolved disk. Nevertheless, the total flux density measurements when combined with the best estimates of the planet's radius are sufficient to show that the upper atmosphere of Uranus is distinctly different from those of Jupiter and Saturn. Despite its greater distance from the sun, Uranus is as warm as, or warmer than both Jupiter and Saturn at centimeter wavelengths. The spectrum rises sharply with wavelength between 1 and 10 centimeters, although a "flat" spectrum is expected due to the high pressure at which an ammonia cloud would form on Uranus. The higher temperatures on Uranus are believed to be related to a relatively lower atmospheric opacity thereby allowing higher temperatures to be sensed. Modelling studies have shown that Uranus must be severely depleted of ammonia compared to the solar abundance in the 150 K to 200 K temperature range of the atmosphere (Gulkis et al., 1978). This corresponds roughly to the pressure range 7 to 20 atmospheres. No such dramatic depletion is indicated from the microwave observations of Jupiter and Saturn. Another observation, apparently unique to Uranus, is that its spectrum at centimeter wavelengths is changing with time. This effect is unexplained at the present time.

Since 1978, a number of important new measurements of Uranus have been achieved. Most notable are the short millimeter wavelength flux density measurements which have been made with the NASA Infrared Telescope Facility (IRTF) and the 12 m NRAO telescopes, and the high angular resolution measurements which have been made with the NRAO Very Large Array (VLA) telescope. These later measurements have sufficient resolution to resolve the disk, thereby opening up an entirely new class of observations.

In this review, we summarize both the disk integrated flux density measurements and the resolved disk measurements. We review the principal inferences which have been drawn from the data and reexamine these using the up-to-date data base and current models of the atmosphere. Many of the newer measurements are unpublished and consequently undocumented. In the spirit of the workshop, we discuss the unpublished data where we have the permission of the original researchers. However, we caution the readers that unpublished data are preliminary and that firm conclusions based on these data should await publication by the original researchers.

OBSERVATIONS

Average Disk Brightness Temperatures - Most of the existing radio measurements of Uranus have insufficient resolution to resolve the disk. Consequently, most disk brightness temperatures reported are not measured directly. The fundamental measurement which leads to the disk brightness temperatures is the integrated (over the solid angle of the planet) flux density (S) at a given frequency (f), bandwidth (df), and time (t). The fractional bandwidth (df/f) covered in a single observation is generally small and the measured average flux density over the bandwidth is assumed to be the flux density at the center frequency of the measurement. Flux density is usually expressed in units of Janskys (Jy) where 1 Jy = 10^{-26} wm^{-2} Hz^{-1}.

Table I gives a list of the reported flux densities, but adjusted such that they refer to a common calibration scale and an earth-Uranus distance of 19 AU. The disk temperatures corresponding to the adjusted flux densities are given in column 6. Figure 1 shows the disk brightness temperatures as a function of wavelength. These were calculated using the Planck radiation

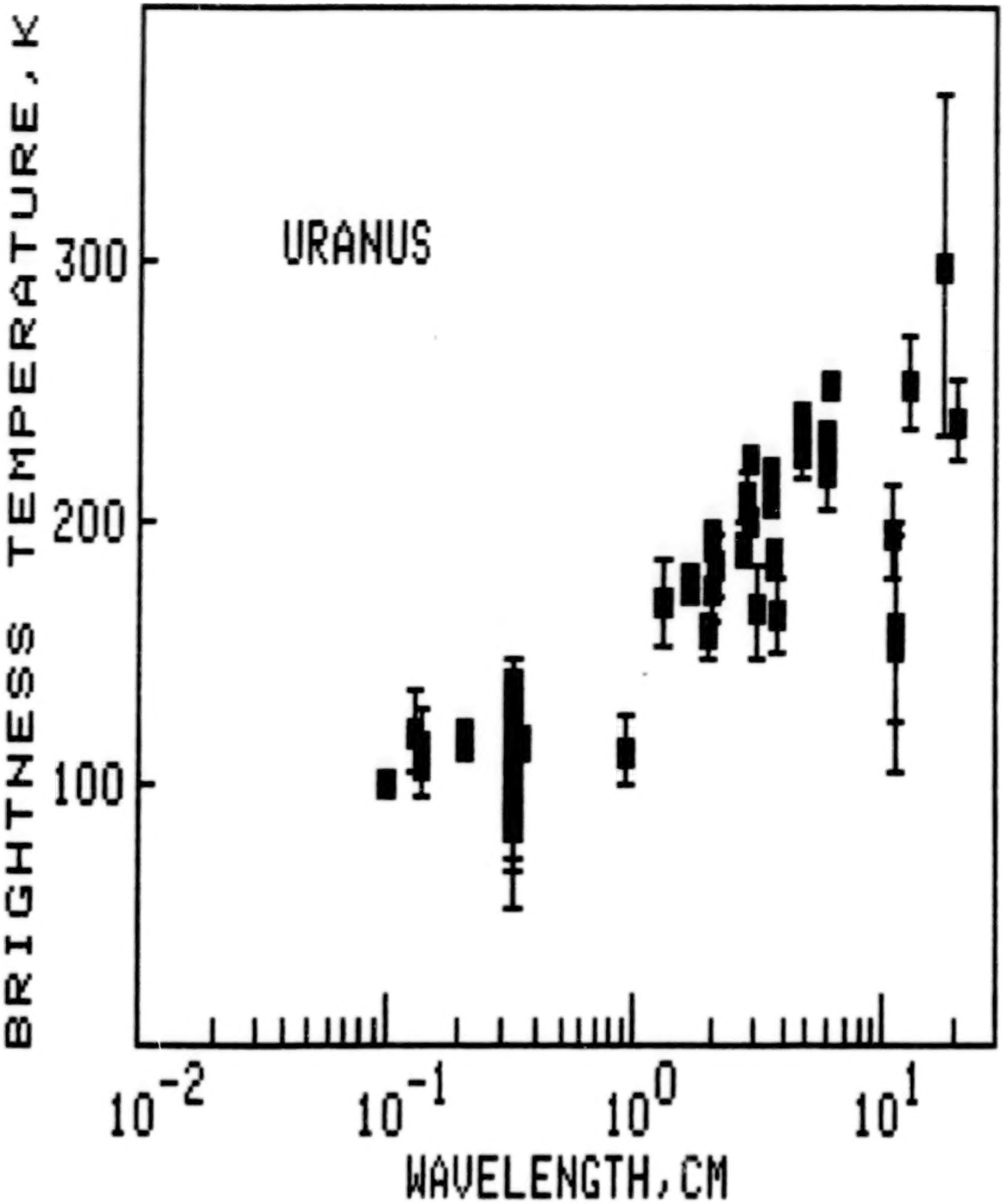

Figure 1 - Microwave spectrum for Uranus. The data shown are from Table I.

law. We assumed Uranus to be an oblate disk with an equatorial diameter(ED) of 51300 km and a polar diameter(PD) of 50274 km. The solid angle subtended by the planet is assumed to be given by $(\pi/4)(PD)(ED)$. This assumption introduces a small systematic error due to the large inclination of the rotation axis. When observed pole on, the solid angle of Uranus should be $(\pi/4)(ED)(ED)$, which is 2 % larger than the solid angle assumed. Consequently, the disk temperatures given in column 6 may be too high by up to 2 %. This is particularly true for the recent measurements in which Uranus was viewed nearly pole on.

In column 3 of Table I, we give the original value of the published disk temperature. Note in some cases, the very large discrepancy between the adjusted temperatures given in column 6 and the original values. This is primarilly due to the adoption of a different solid angle for Uranus.

High Resolution Spatially Resolved Radio Maps - Various VLA observations of Uranus have been made over the past few years, in 1980 and 1981 by Jaffe and co-workers and in 1982 and 1983 by de Pater and co-workers. Neither set of maps has yet been published. The de Pater et al. maps were made at wavelengths of 1.3, 2.0, 6.1, and 20.5 centimeters. Figures 2 and 3 show the preliminary high resolution maps obtained by de Pater et al. in 1982 at 6 and 2 cm wavelengths respectively. These maps have an angular resolution of 0.65 arc secs at both wavelengths. (We did not show the 20.5 cm maps because they do not resolve the disk nor the 1.3 cm maps which are of overall lower quality than the others.) The pole and the sub-earth points are indicated by a cross and a dot respectively on both maps, at the time of the observations. Both maps clearly show the brightness distribution to be slightly asymmetric.

TABLE I

EPOCH	WAVELENGTH (CM)	PUBLISHED DISC TEMP (K)	NORMALIZED FLUX DENSITY (JY)	ESTIMATED RMS ERROR (%)	NORMALIZED DISC TEMP (K)	REFERENCE
1982.45	20.463	240.0	4.051E-03	8.0	244.8	De PATER (P.C.)
1978.92	18.002	291.0	6.388E-03	21.9	299.1	CONWAY (1980)
1979.45	13.100	255.0	1.026E-02	7.1	254.3	BATTY et al. (1981)
1965.00	11.300	130.0	8.361E-03	30.8	154.3	KELLERMAN (1966)
1968.10	11.132	180.0	8.965E-03	22.2	160.5	GERARD (1969)
1971.40	11.100	195.0	1.108E-02	8.9	197.2	WEBSTER et al. (1972)
1978.07	6.148	259.0	4.653E-02	1.5	254.1	BRIGGS&ANDREW (1980)
1969.70	6.000	210.0	4.247E-02	6.3	220.9	MAYER&McCULLOUGH (1971)
1982.45	6.141	231.0	4.329E-02	3.5	235.6	De PATER (P.C.)
1978.20	4.815	243.0	7.119E-02	3.7	238.6	BRIGGS&ANDREW (1980)
1977.17	4.769	230.0	6.884E-02	3.9	226.3	BRIGGS&ANDREW (1980)
1966.20	3.750	165.0	8.123E-02	8.5	165.2	KLEIN&SELING (1966)
1971.40	3.710	189.0	9.364E-02	3.9	186.4	WEBSTER et al. (1972)
1977.24	3.560	212.0	1.155E-01	3.8	211.6	KLEIN&TUREGANO (1978)
1977.73	3.560	217.0	1.180E-01	4.6	216.2	KLEIN&TUREGANO (1978)
1978.33	3.560	217.0	1.182E-01	3.2	216.6	KLEIN&TUREGANO (1978)
1967.33	3.126	158.0	1.180E-01	10.4	166.8	BERGE (1968)
1978.25	2.921	228.0	1.820E-01	.9	224.6	BRIGGS&ANDREW (1980)
1977.22	2.863	203.0	1.692E-01	2.0	200.5	BRIGGS&ANDREW (1980)
1973.33	2.852	202.0	1.794E-01	4.0	211.0	BRIGGS&ANDREW (1980)
1969.70	2.700	212.0	1.825E-01	3.9	192.5	MAYER&McCULLOUGH (1971)
1972.70	2.069	178.7	2.980E-01	7.0	184.6	GARY (1974)
1974.40	2.030	201.1	3.259E-01	3.6	194.3	GARY (P.C.)
1982.54	2.005	176.0	3.110E-01	6.8	179.5	DePATER (P.C.)
1969.29	1.950	181.0	2.860E-01	5.7	157.5	PTOTH&KELLERMANN (1970)
1969.70	1.650	201.0	4.501E-01	4.2	177.4	MAYER&McCULLOUGH (1971)
1982.54	1.333	176.0	6.863E-01	10.8	173.4	De PATER (P.C.)
1969.29	.950	125.0	8.676E-01	11.8	113.9	PTOTH&KELLERMANN (1970)
1969.29	.350	111.0	6.460E+00	5.3	116.3	PTOTH&KELLERMANN (1970)
1969.22	.330	100.0	6.092E+00	27.0	98.0	EPSTEIN et al. (1970)
1969.46	.330	85.0	5.164E+00	36.5	83.4	EPSTEIN et al. (1970)
1970.01	.330	97.0	5.910E+00	27.8	95.1	EPSTEIN et al. (1970)
1970.13	.330	125.0	7.617E+00	17.6	122.0	EPSTEIN et al. (1970)
1974.28	.330	132.0	8.076E+00	15.3	129.2	ULICH (P.C.)
1974.50	.330	125.0	6.885E+00	5.4	110.5	ULICH&CONKLIN (1976)
1974.87	.330	133.2	8.127E+00	5.3	130.0	ULICH (P.C.)
1975.30	.330	138.0	8.392E+00	2.7	134.2	ULICH (P.C.)
1975.56	.330	125.7	7.686E+00	4.3	123.1	ULICH (P.C.)
1976.37	.330	143.5	8.730E+00	3.1	139.5	ULICH (P.C.)
1976.66	.330	133.8	8.146E+00	3.1	130.3	ULICH (P.C.)
1977.09	.330	130.8	8.315E+00	2.2	133.0	ULICH (P.C.)
1977.30	.330	134.5	8.550E+00	5.1	136.7	ULICH (P.C.)
1978.34	.330	130.8	8.315E+00	4.7	133.0	ULICH (P.C.)
1979.17	.330	135.4	8.608E+00	2.3	137.6	ULICH (P.C.)
1980.01	.330	134.1	8.525E+00	4.6	136.3	ULICH (P.C.)
1973.40	.214	122.0	1.730E+01	6.8	117.8	COGDELL et al. (1975)
1975.25	.140	105.0	3.614E+01	10.5	10774	COURTIN et al. (1978)
1974.03	.139	113.0	3.990E+01	11.5	116.4	COURTIN et al. (1978)
1980.50	.131	117.0	4.663E+01	13.2	121.0	ORTON (P.C.)
1983.50	.137	101.0	3.850E+01	3.0	103.0	ULICH et al. (1984)
1980.50	.100	97.0	6.546E+01	3.0	101.6	ORTON (P.C.)

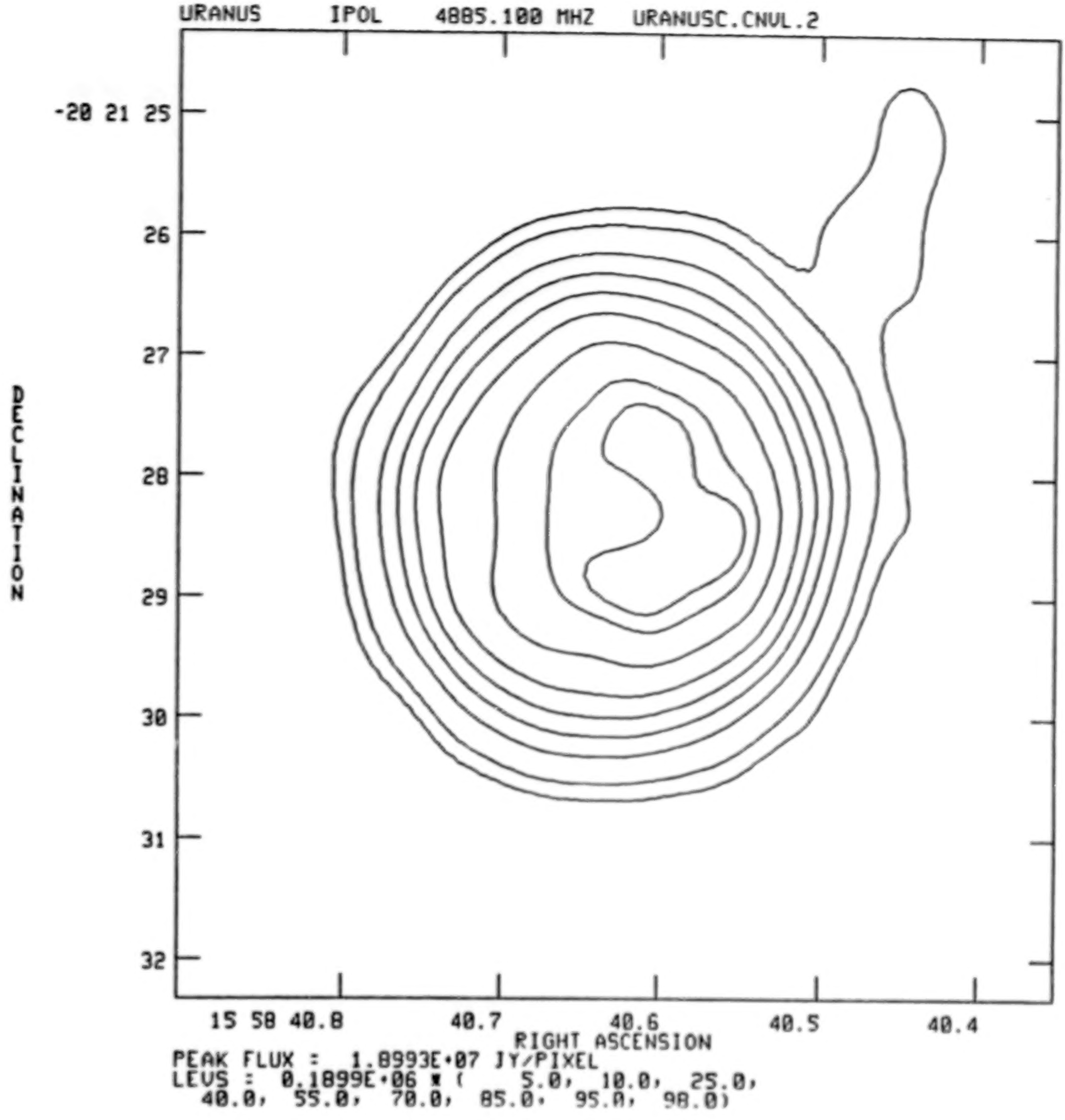

Figure 2 - Preliminary high resolution map of Uranus at 6 cm. The contours indicated are at 5, 10, 25, 40, 55, 70, 85, 95, and 98% of the peak flux density in the map. The integrated flux density is 48.5 mJy. The cross and the dot indicate the position of the pole and the sub-earth point respectively at the time of the observation. The data were taken on June 15-17, 1982.

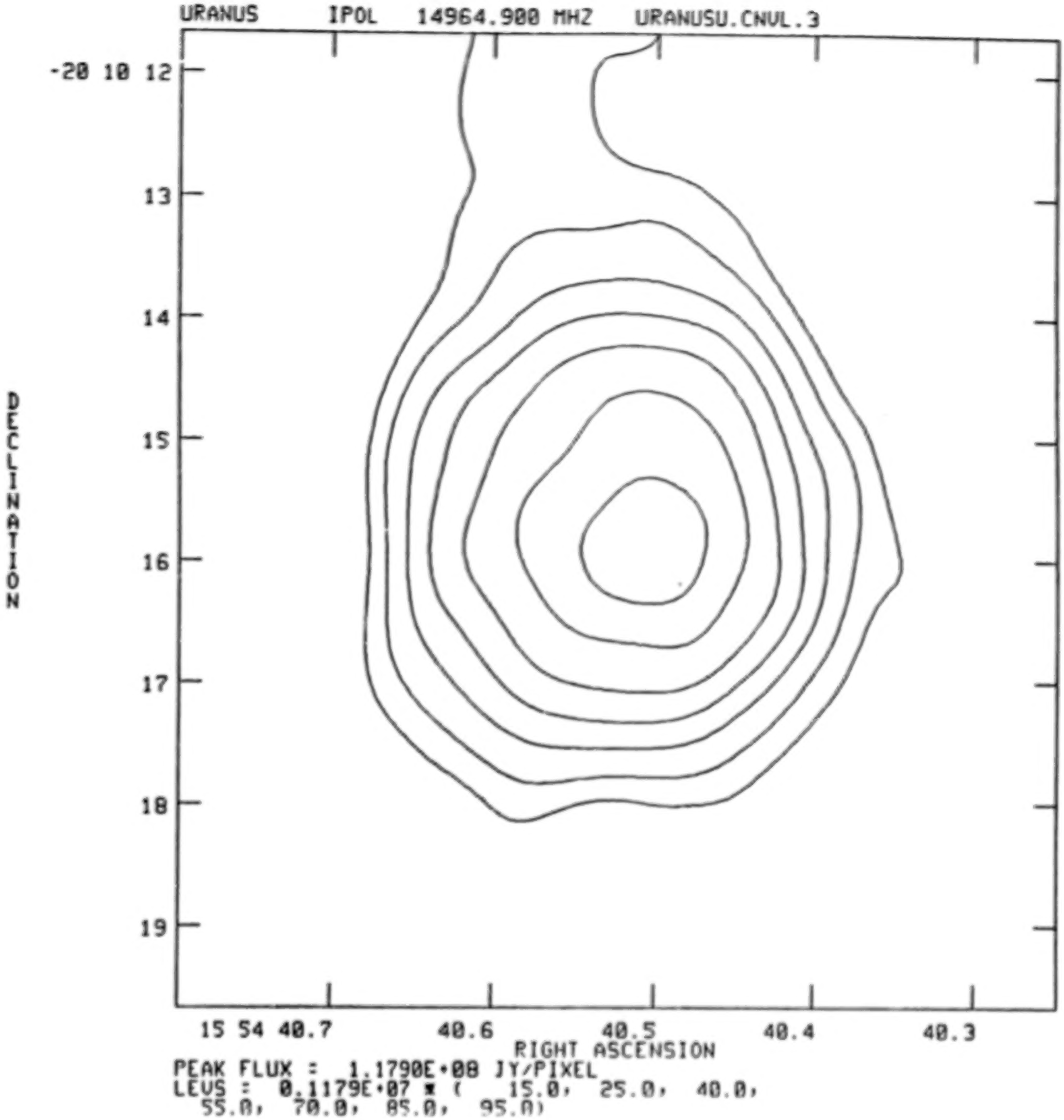

Figure 3 - Preliminary high resolution map of Uranus at 2 cm. The contours indicated are at 15, 25, 40, 50, 75, 85, and 95% of the peak flux density in the map. The integrated flux density is 336 mJy. The cross and the dot indicate the position of the pole and sub-earth point respectively at the time of the observation. The data were taken on July 18-20, 1982.

The peak brightness is shifted toward the pole. At 6 cm, the brightest point on the map nearly coincides with the position of the pole; at 2 cm it is half-way between the sub-earth point and the position of the pole.

DISCUSSION

Thermal emission from a deep atmosphere whose temperature increases with depth appears to explain the microwave spectra of Jupiter and Saturn, and is believed (by us) to be the prime candidate model for explaining the spectrum of Uranus. The recent VLA observations show convincingly that the vast majority of the emission originates from the vicinity of the optical disk, thereby ruling out the possibility of any major extended source of emission (in the 2 to 20 cm wavelength range) including synchrotron emission or emission from rings. No extreme limb brightening is observed thereby ruling out thermal emission from a hot ionosphere as discussed by Gulkis et al. (1978). A remaining possibility, is that there is a localized source of emission centered near the pole. As an example, a super dense polar ionosphere, possibly induced by charged particle dumping at the poles, could explain the high brightness temperatures.

The most widely used method of calculating the disk brightness temperature is to integrate the brightness temperature over the the entire disk assuming spherical symmetry of the disk. This approximation makes the angle between the line of sight to the observer and the normal to the "surface" easy to compute. Because the oblateness of Uranus is only .02(+/-.01) this approximation is not expected to introduce a large error. The brightness temperature is calculated by integrating the equation of radiative transfer through a model atmosphere in which the pressure, temperature, and absorption coefficient are defined at every point.

A serious concern is the lack of good experimental data on the absorption coefficients of the various gases which are likely to be responsible for the microwave opacity. The problems anticipated are associated with the line shapes produced by foreign gas broadening at high pressures over the wide range of temperatures and pressures which are encountered. In particular, the absorption coefficient of ammonia under the conditions in the Uranus atmosphere has never been measured, while the calculation requires a large extrapolation from the meagre laboratory data which are available. de Pater and Massie (1984) show that a comparison of the spectra of all four Jovian planets with model atmosphere calculations indicates that the line shape profile may lie closer to the Van vleck Weiskopf profile than the Ben Reuven profile which has generally been used. An alternative explanation to the one given by dePater and Massie, is that the pressure-broadened line widths and coupling elements (i.e. Berge and Gulkis, 1976) used in the Ben Reuven line shape are incorrect. In particular, a reduction in the magnitude of the coupling element will move the Ben Reuven line shape closer to the Van vleck Weiskopf while maintaining the principal features of the line shape.

Gulkis et al. (1978) considered a wide variety of atmospheric models and compared them with the available data. They assumed that the major sources of microwave opacity were due to hydrogen, ammonia vapor, and water vapor. They showed that collision-induced absorption due to hydrogen provided the major source of opacity at short millimeter wavelengths, while absorption due to the inversion transitions in ammonia dominates the spectrum at wavelengths longer than about 3 mm. They showed that if ammonia is uniformly mixed throughout the atmosphere with a mixing ratio of ~2 parts in 10000, and follows the vapor pressure relationship for pure ammonia in the upper atmosphere, then the expected spectrum for Uranus is nearly flat (temperature is constant) from 3 mm to 10 cm. The observations show a sharp rise in temperature which starts at about 1 cm and extends to 10 cm or longer. They showed that the mixing ratio must be reduced by two orders of magnitude inorder to explain the high brightness temperatures in the vicinity of 2 cm. Figure 4 shows their calculations of the microwave spectra for Jupiter, Saturn, and Uranus along with the data available in 1978. Klein and Turegano (1978) later discovered that between 1966 and 1978 the flux density of Uranus was increasing in the wavelength range from 2 to 3.6 cm.

Both the depletion of ammonia and the variability are of paramount importance to the understanding of the atmosphere. Therefore, it seems worthwhile to re-examine these results using the most up-to-date data bases available to us. In particular, we will examine the following three areas below: a) the variability of the spectrum, b)theoretical spectra based on up-to-date models of the atmosphere, and c)implications of the high resolution Uranus maps.

A. Variability-The data base for variability studies spans the years 1965 to 1982.45. Published studies (Klein and Turegano, 1978; Batty et al., 1981; Gulkis et al., 1983) have examined the variability by subdividing the data into narrow wavelength intervals as shown in Figure 5. A potential source of error with this analysis arises from the gradient of temperature across the wavelength interval. An alternative means of illustrating the variability, which is independent of this source of error, is shown in Figure 6. In that figure, we show the entire data set using crosses for data taken before 1973 and rectangles for data taken after 1973. The trend of the early data showing that Uranus was cooler prior to 1973 is evident. The variability appears to start at a wavelength at least as short as three millimeters and extend to longer wavelengths.

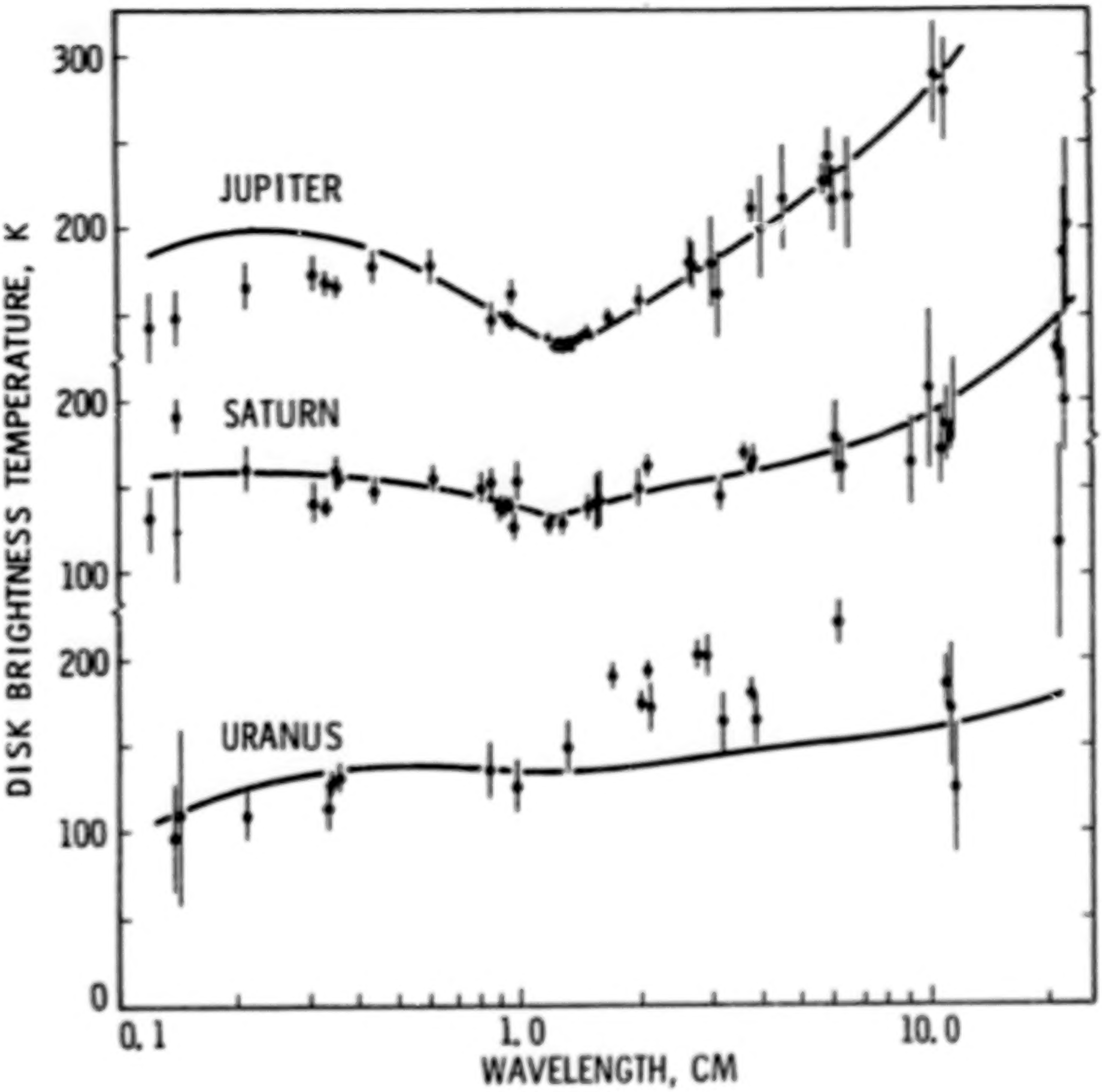

Figure 4 - Microwave spectra for Jupiter, Saturn, and Uranus (after Gulkis et al., 1978). Progressing from Jupiter to Saturn to Uranus the model calculations show that the temperature-wavelength dependence becomes less steep due to pressure broadening. The poor fit of the data in the vicinity of 2 cm wavelength provide evidence that ammonia must be depleted on Uranus.

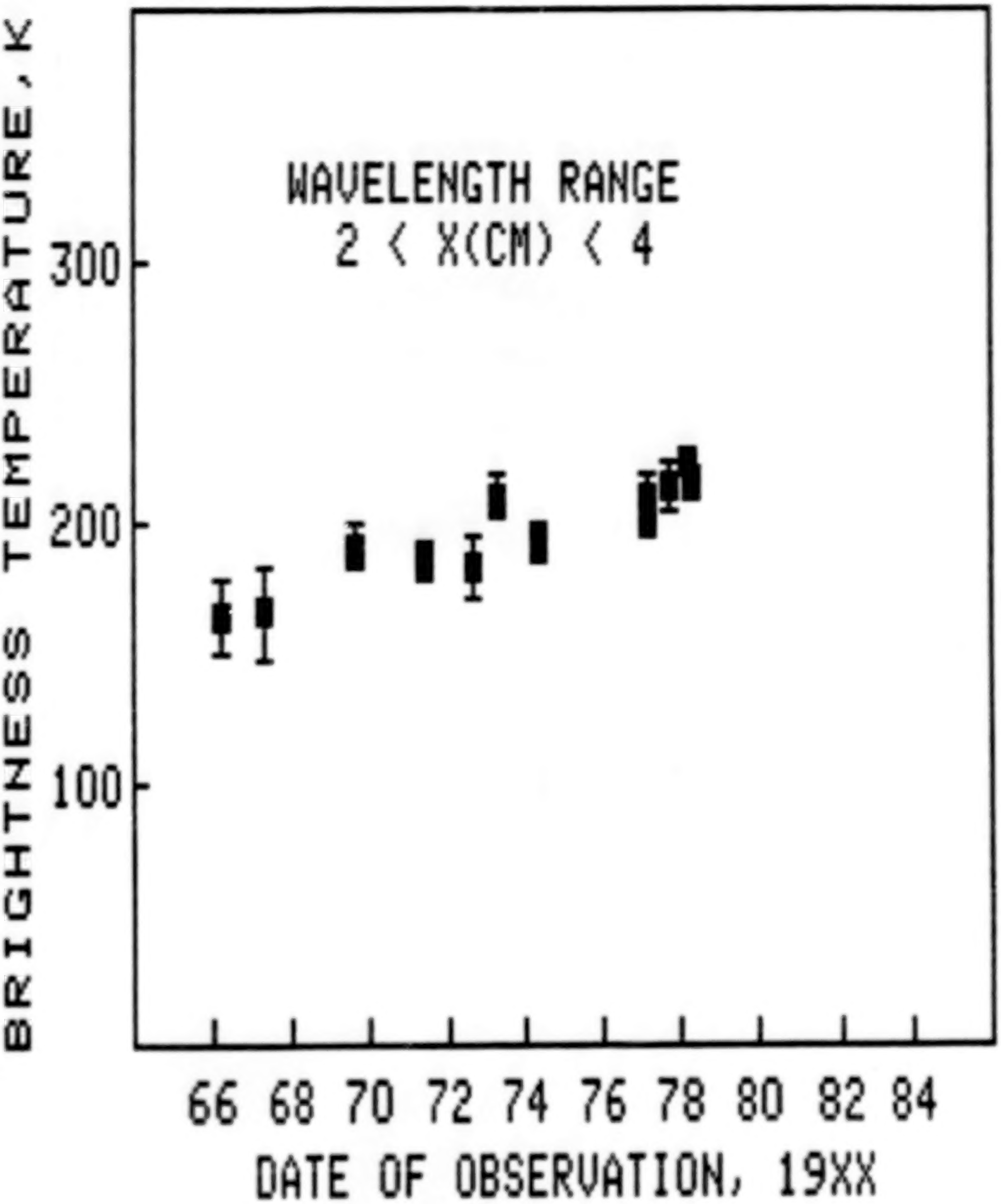

Figure 5 - The disk temperatures of Uranus plotted against the date of observation. The wave length interval 2cm to 4cm is the same interval used by Klein and Turegano (1978) in their "discovery" paper.

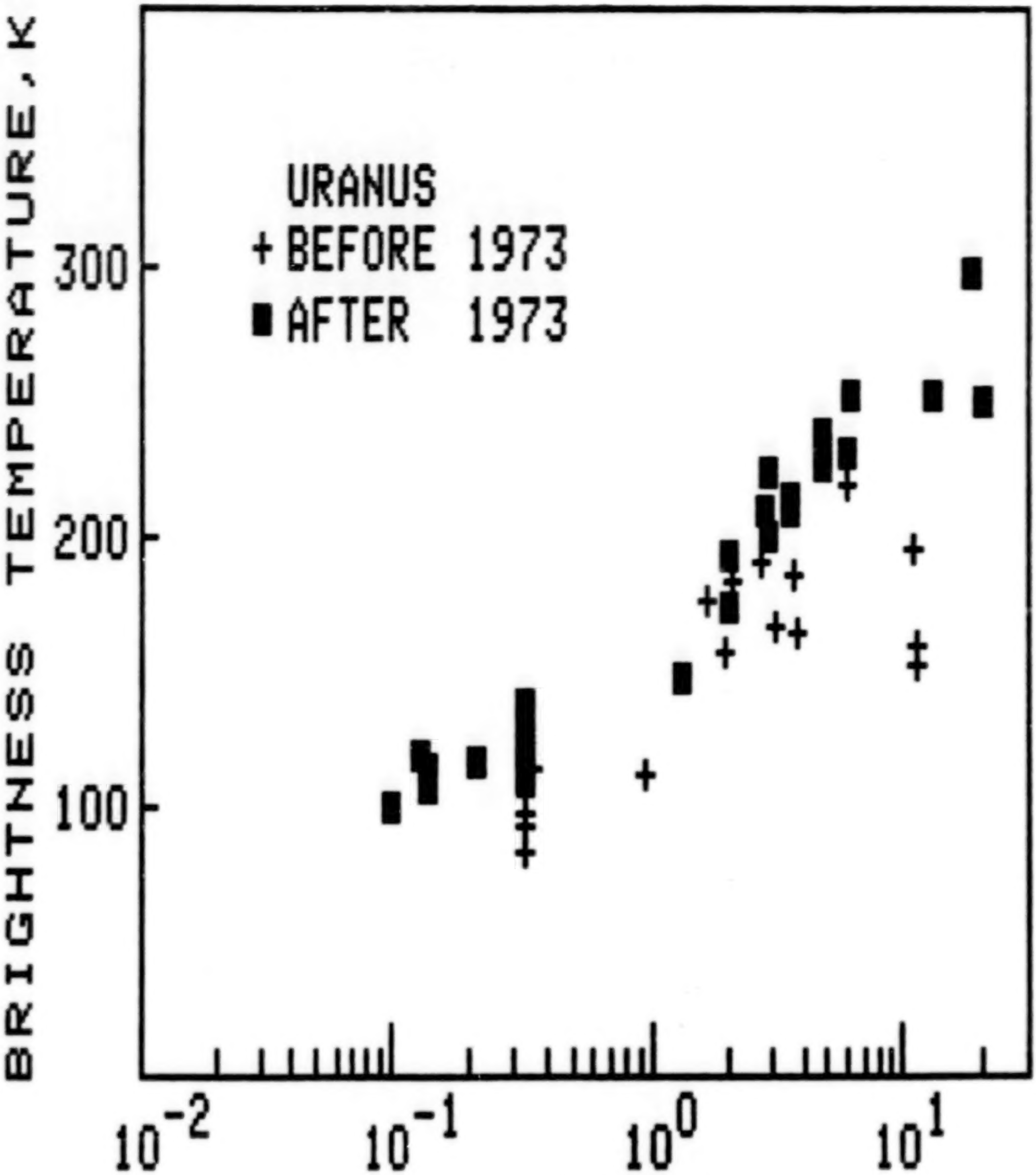

Figure 6 - The microwave spectrum of Uranus plotted using cross symbols for the data taken before 1973 and rectangles for data taken after 1973. The early data are seen to be systematically lower than the later data.

While dividing the data into two groups is useful to illustrate the presence of variability, it is less useful as a tool to determine the form of the variability. To investigate the form, we divided the data set up into wavelength intervals and applied a correction for the temperature variation across the interval.

The solid line superimposed on the data in Figure 7 gives a reasonable representation of the temperature gradient between 1.5 and 10 cm. The gradient between 10 and 20 cm is ill defined at the present time because of the sparsity of data at long wavelengths.

The analytic expression of the solid line in Figure 7 is

$$T = 175\ \mathrm{LOG(WAVELENGTH,CM)} + 115\ \mathrm{K} \quad .$$

From this relationship, we estimate the temperature gradient across the wavelength interval dl to be

$$dT = 76\ dl/l \quad .$$

Since dl/l was approximately unity in previous studies, the temperature gradient potentially introduces an error of up to 76 K. Klein and Turegano (1978) measured a total variation of approximately 60 K which is comparable to the magnitude of this error. Consequently, the temperature gradient could have a dramatic effect on the interpretation of the data.

In Figure 8, we show the same data set as in Figure 5, but with a "correction factor" for the temperature gradient applied to each data point.

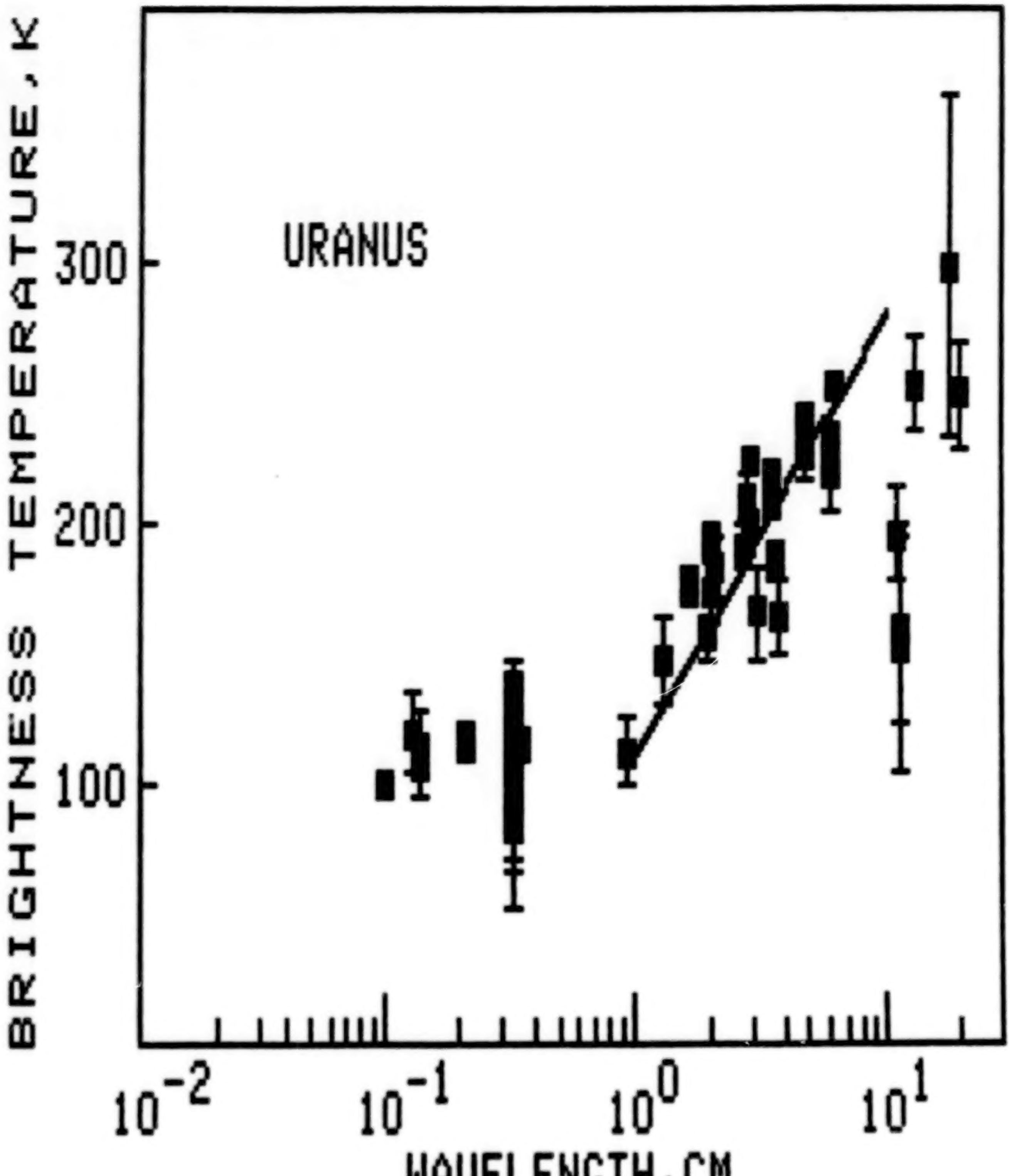

Figure 7 - The disk temperatures of Uranus are shown with a solid line representing the temperature gradient between 1 cm and 10 cm. The equation of the solid line is T = 175 log (wavelength, cm) + 115.

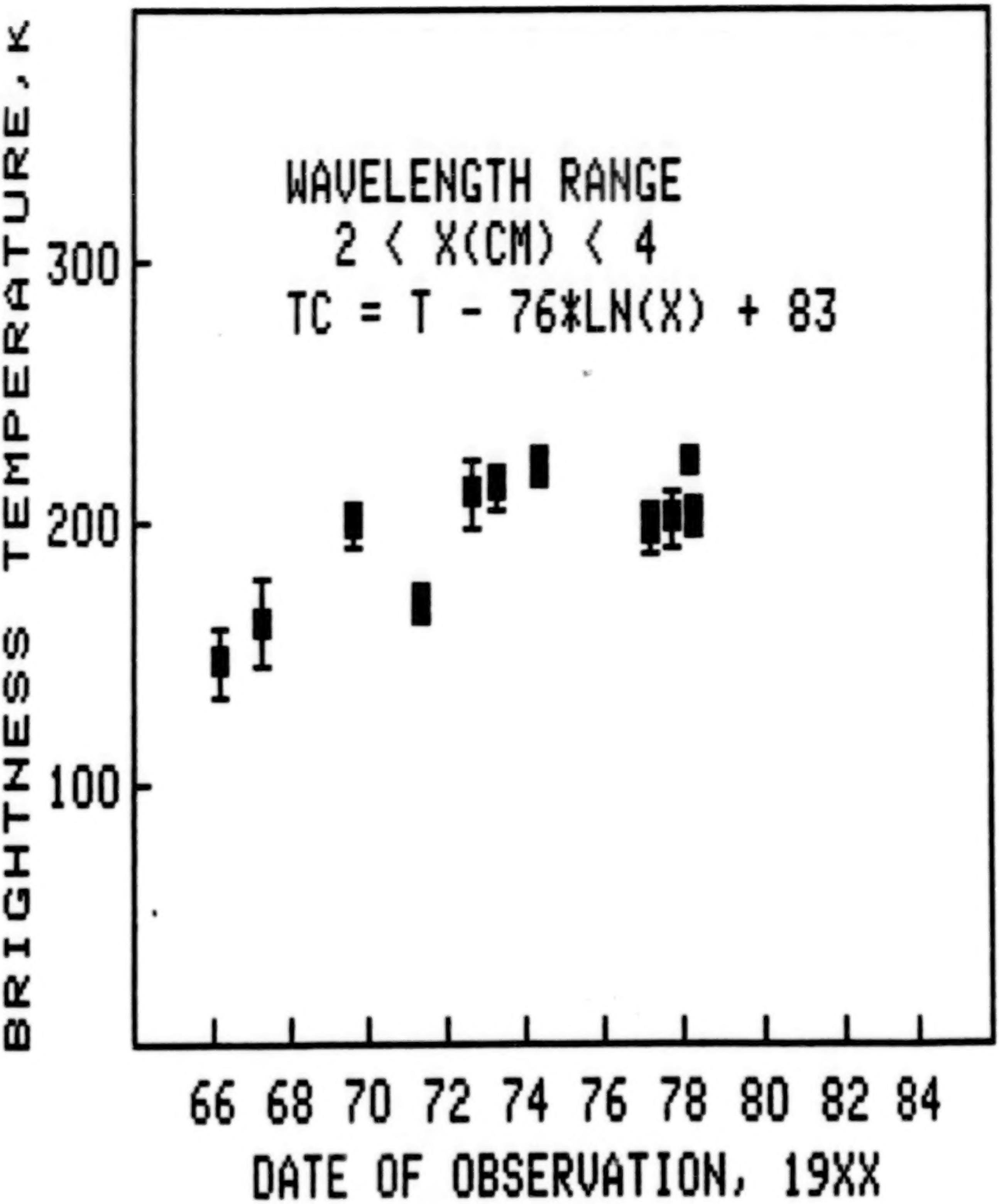

Figure 8 - The disk temperatures of Uranus plotted against the date of observation. The wave length interval is 2 to 4 cm as in Figure 5. The figure differs from Figure 5 in that each data point has been adjusted to account for the gradient across the wavelength interval as explained in the text.

The algorithm used to adjust the data was

$$T(adj) = T - 175 \log(\text{wavelength,cm}) + 83$$

This algorithm leaves the 3 cm data unperturbed, adds up to 30 K to the 2-3 cm data, and subtracts up to 22 K from the 3-4 cm data. The principal difference between the data trends suggested by the adjusted data in Figure 7 and the raw data in Figure 5 is that the raw data show a steady increase in temperature from 1966 to 1978 whereas the adjusted data suggest an increase between 1966 and 1971 with a leveling off at later years.

The 10 to 20 cm wavelength range has previously been analysed in the same manner as the 2 to 4 cm data (Batty et al., 1982; Gulkis et al., 1983). In this wavelength range, the temperature variation is about twice as large as that seen at 2 to 4 cm. Thus we expect that an adjustment for the temperature gradient between 10 and 20 cm will have a smaller effect than at the shorter wavelength interval. It is difficult to estimate the temperature gradient between 10 and 20 cm. Current measurements suggest that the gradient is rather small. We are suspicious that the error bars on the early 10-20 cm data are too small; confusion from background radio sources makes these measurements difficult to carry out with a single dish antenna. Figures 9 and 10 show the 10 to 20 cm data plotted in the same manner as Figures 5 and 7. The temperature variation is clearly present in both cases. As expected, the adjusted data do not differ significantly from the raw data.

Gulkis et al. (1983) had previously reported a small variation in the 2 to 4 mm wavelength range which appeared to them not to be statistically significant. They estimated a temperature drift rate of 0.7 K/year with an

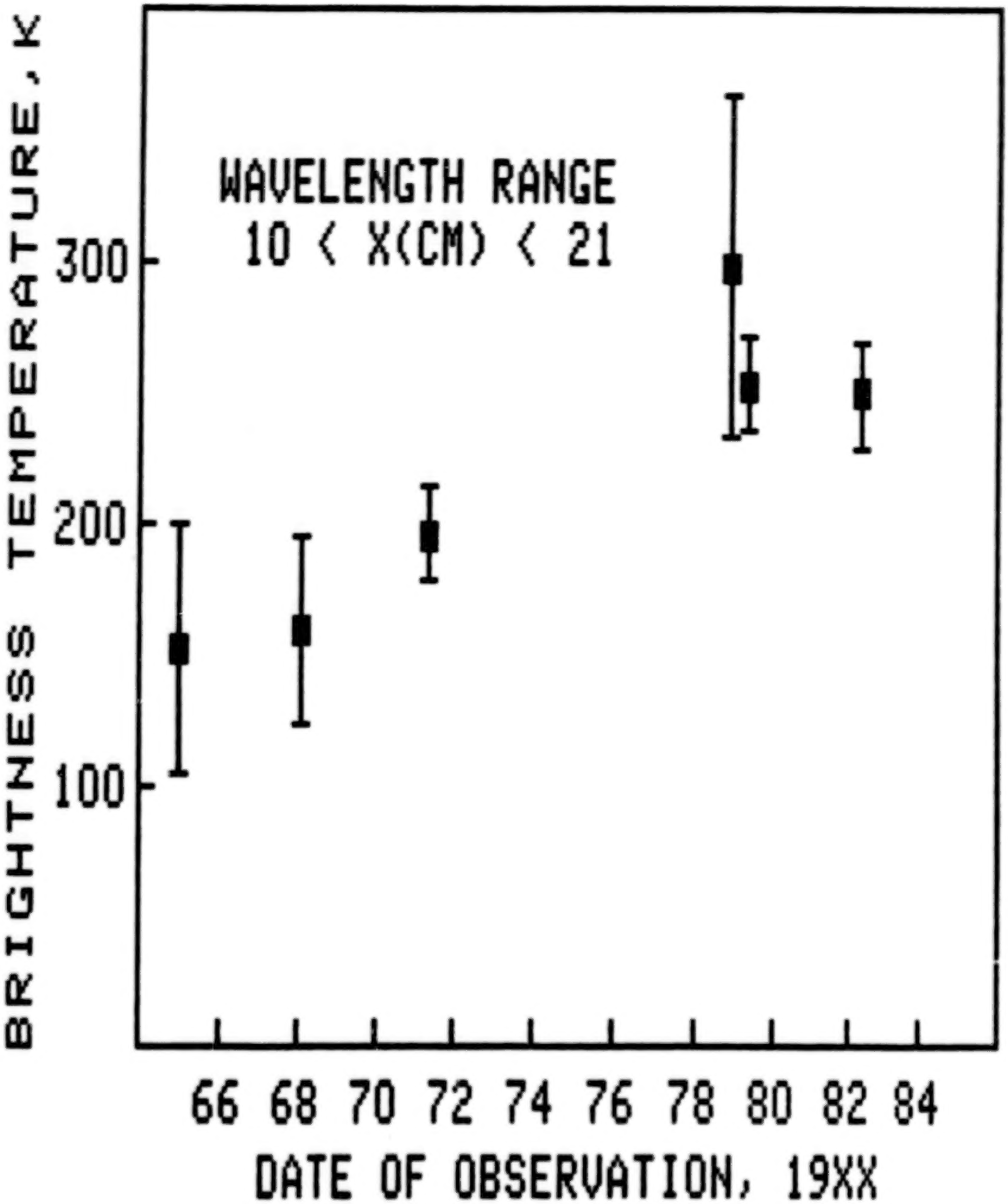

Figure 9 - The disk temperatures of Uranus plotted against the date of observation. The wave length interval is 10 to 20 cm.

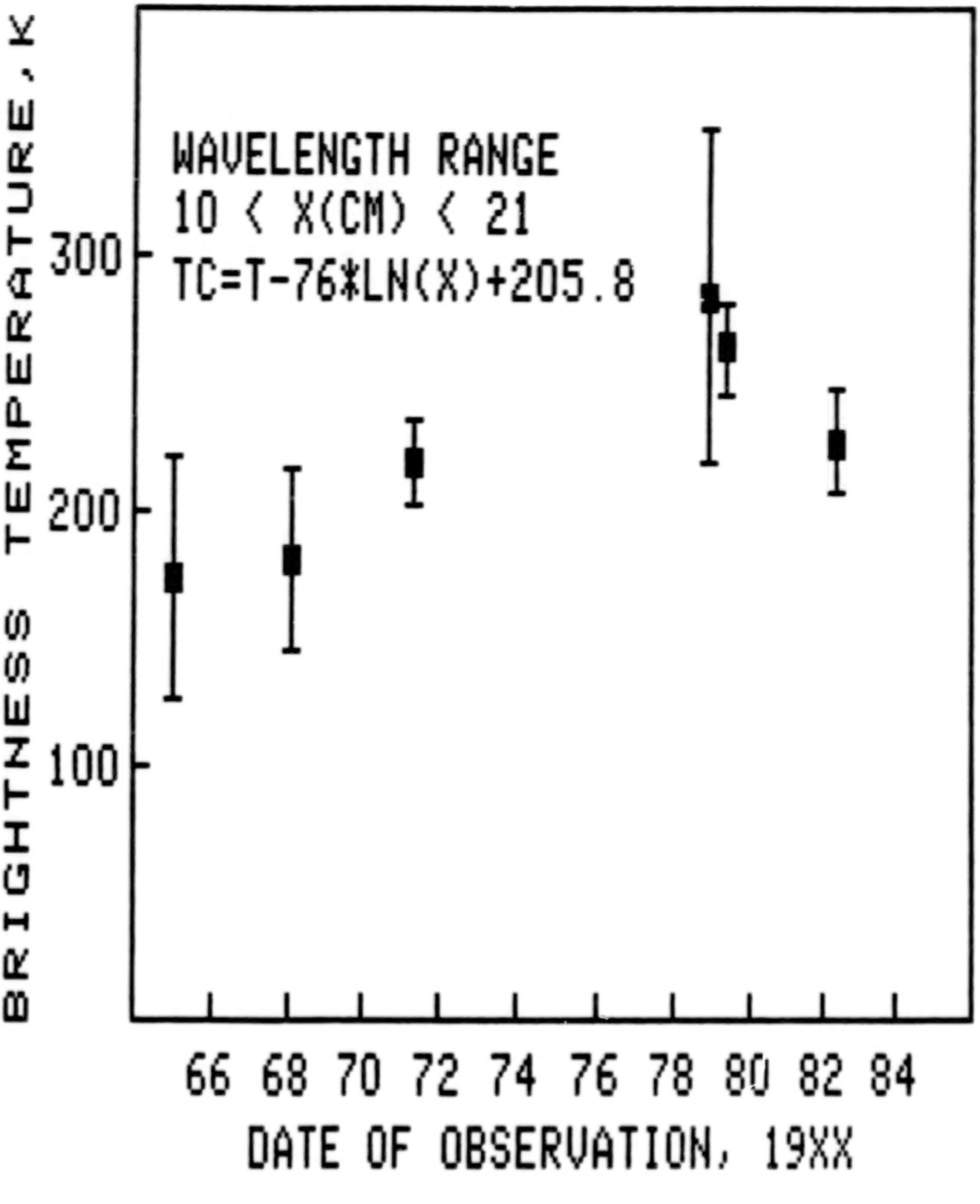

Figure 10 - The disk temperatures of Uranus plotted against the date of observation. The wave length interval is 10 to 20 cm as in Figure 9. The figure differs from Figure 9 in that each data point has been adjusted to account for the gradient across the wavelength interval as explained in the text.

uncertainty of (+/-)1 K /year on the drift rate. Figure 6 prompted us to re-examine this result. Figure 11 shows the brightness temperature data in the 3 to 4 mm wavelength range. It is evident that there is little evidence of variability after 1972; however in prior years there is a clear trend to be cooler. This did not show up as significant in the earlier analysis because the authors searched for a linear dependence in time and because the early data were excessively noisy. No correction for the temperature gradient need be applied to this data because the spectrum is flat in this wavelength range. A further result of a non-linear variation in time is that we no longer can be sure that the spectrum at 1 mm is not variable since few measurements were available before 1975. Gulkis et al. (1983) have mentioned that the nonvariability of the short millimeter wave data implies that the pressure-temperature profile is not changing dramatically.

B. Theoretical spectra - Theoretical microwave spectra (here defined as the frequency range from 1 GHz to 300 GHz) depend both on the temperature-pressure structure of the atmosphere and on the distribution of the opacity in the atmosphere. The sources of opacity in the Uranus atmosphere are not well known although it seems certain that they consist of non-resonant, collision induced absorption in hydrogen, and probably resonant absorption due to ammonia, water, and/or hydrogen sulfide. Slightly broadened pressure lines can in principal be used to measure the temperature, pressure, and mixing ratio of an absorber. However, at the high pressures encountered in the Uranus atmosphere, resonant spectral lines are collisionally broadened into a continuum making it impossible to unambiguously separate the pressure-temperature profile from the opacity distribution. Probably the greatest leverage provided by the microwave observations is in testing model atmospheres which have been derived from a broad set of considerations such

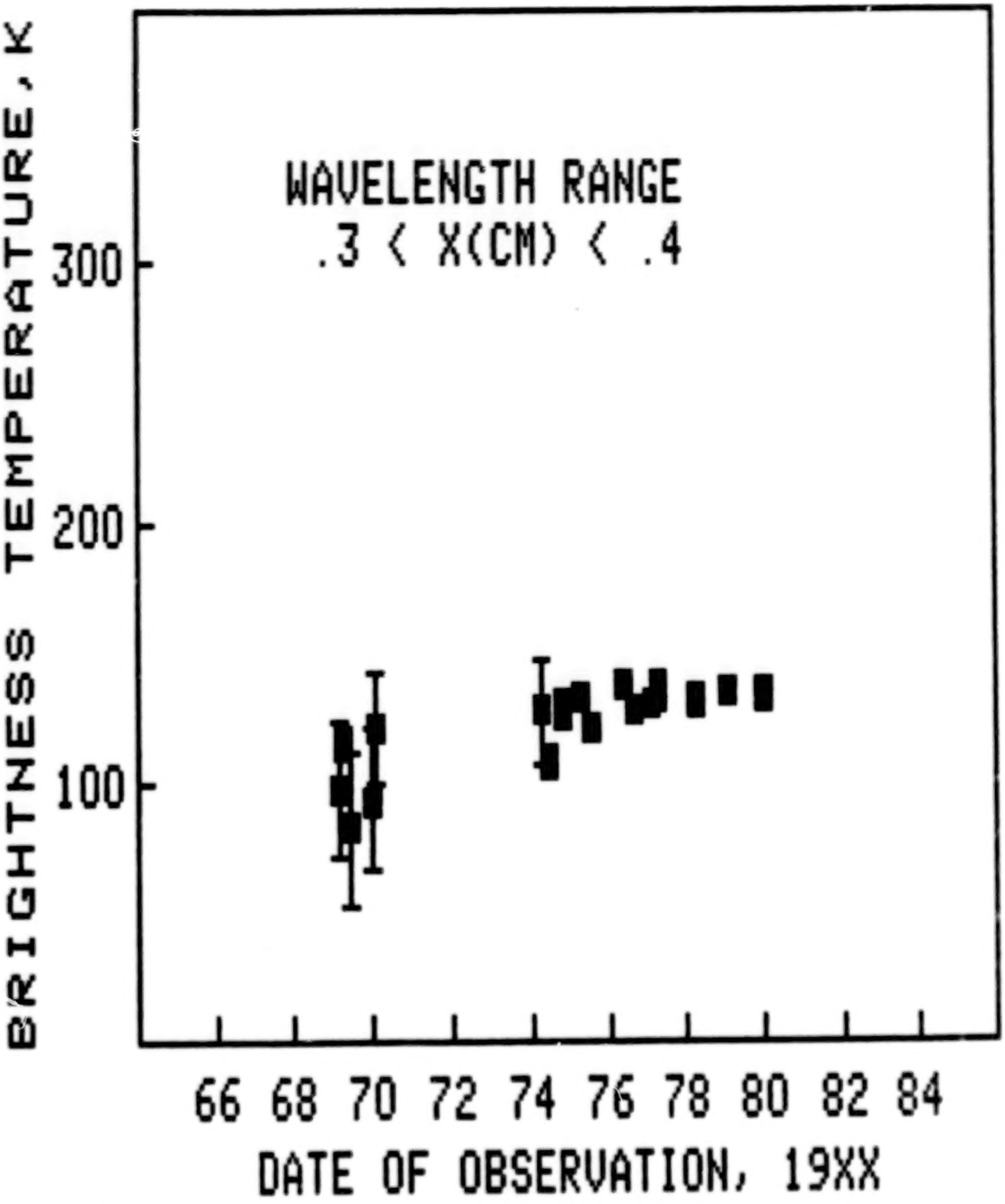

Figure 11 - The disk temperatures of Uranus plotted against the date of observation. The wavelength interval is 3 to 4 mm.

as composition, solar heat input, infrared flux, etc. A number of such models have been generated including those of Wallace (1980), Appleby (1980), and Orton (1983).

In order to re-examine the evidence for the depletion of ammonia in the Uranus atmosphere, we chose the temperature-pressure profile of Orton (1983) to represent Uranus' atmospheric structure and superimposed a number of ammonia distributions. Theoretical spectra were then calculated using the methods described in Gulkis et al. (1978). Figure 12 shows the pressure-temperature profile we used and Figure 13 shows the up-to-date spectra with various model calculations superimposed. For all curves we used the following concentrations by number: Hydrogen, 90%; helium, 7%; methane, 3%; water, 1×10^{-4}%. Curve 1 is for the case in which ammonia is uniformly mixed with a ratio of 1.5×10^{-4} below the saturation level (9.5 atm and 160 K) and follows the saturation vapor pressure law for ammonia at higher altitudes. Curve 2 is for an atmosphere with an ammonia abundance which is strongly depleted 1.0×10^{-6} compared to the solar value of 1.5×10^{-4}. Curve 3 is for an atmosphere in which the only absorption is due to hydrogen. Curve 1 shows a good fit to the millimeter data, but is much too cold compared to the centimeter wave data. Curve 2 provides a much better fit over the spectral range from 1 mm to 10 cm but predicts a higher temperature than is observed at 20 cm. Curve 3, a model in which no absorption due to ammonia is included, shows that the short millimeter spectrum is controlled by the hydrogen opacity. This implies that the millimeter wave brightness temperatures provide a direct constraint on the pressure temperature profiles. Courtin et al. (1978) have used this argument to rule out methane rich models which are too cold in the convective regions to explain the observations.

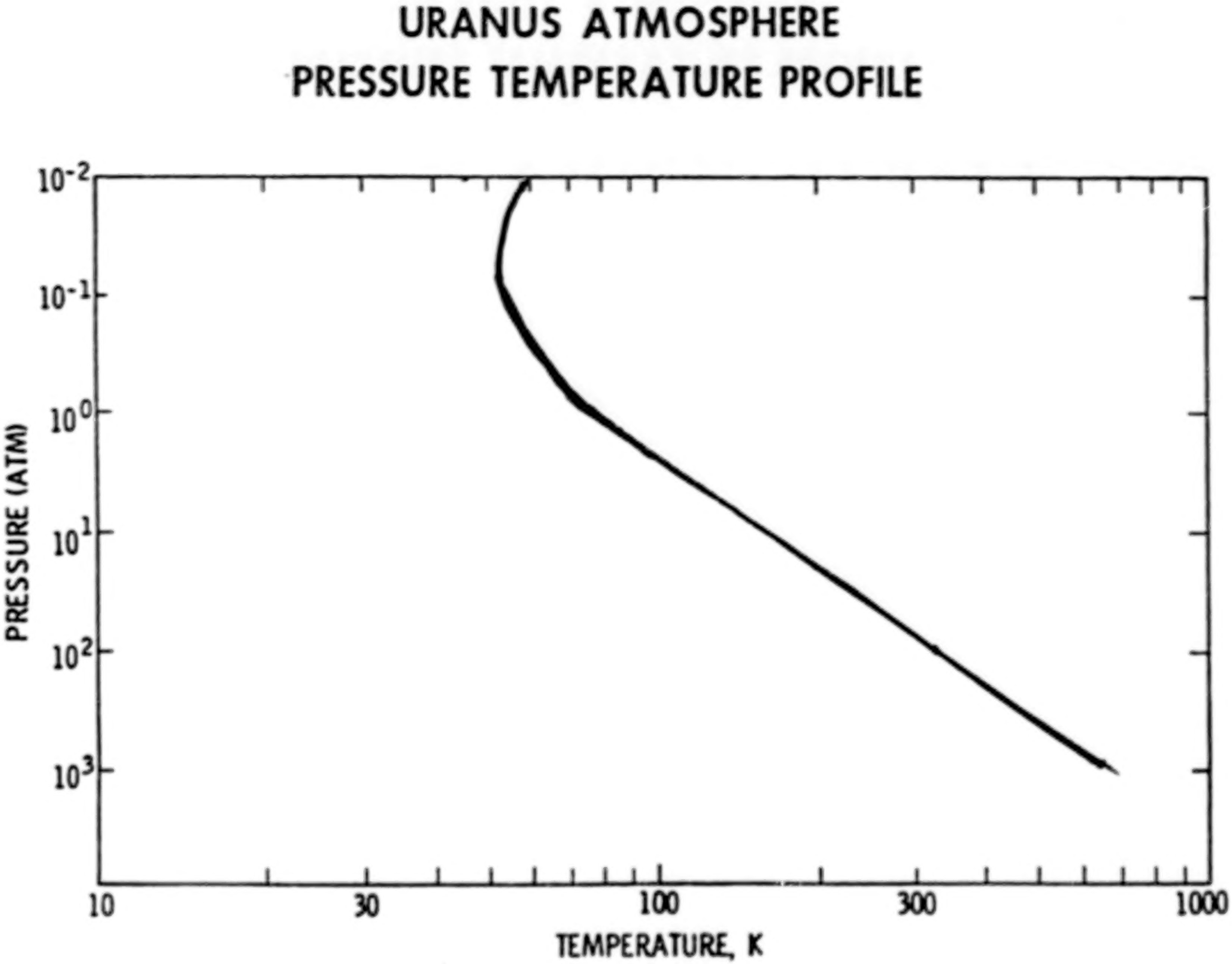

Figure 12 - The pressure-temperature profile of Uranus (after Orton) used in the brightness temperature calculation.

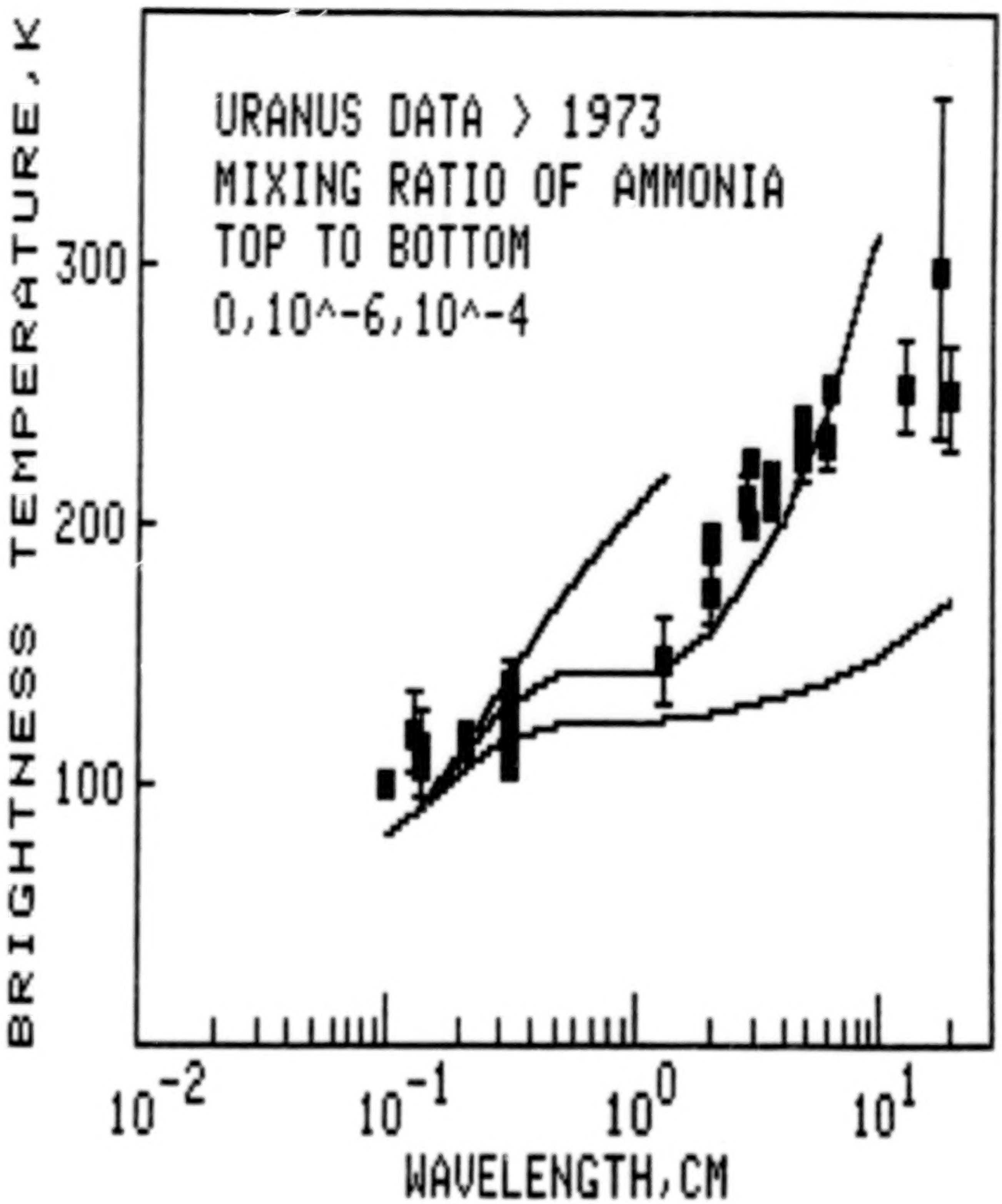

Figure 13 - Theoretical microwave spectra for Uranus based on an Orton model atmosphere with various concentrations of ammonia.

In order to match a theoretical brightness temperature model to all of the microwave data using the Orton (1983) pressure-temperature profile, it is necessary that the ammonia be depleted only in the upper levels of the atmosphere. (This is true of all adiabatic convective atmosphere models we have tried.) Atreya and Romani (1984) have proposed that a plausible mechanism for selective alititude depletion is loss of ammonia in the aqueous ammonia cloud. This mechanism does not require an enrichment of volatiles over solar values however a slight enrichment of the volatiles (O,C,N,S) enhances the depletion. This mechanism for depletion appears more reasonable than selective enrichment of sulfur as was suggested by Gulkis et al.(1978).

The evidence for depletion of ammonia is based on the assumption that the atmosphere is in adiabatic convective equilibrium. Small changes to the adiabatic lapse rate will not change this conclusion. However if the atmosphere should become superadiabic or isothermal the spectrum could be dominated more by the lapse rate than the mixing ratio of ammonia. de Pater and Massie (1984) considered a model in which the upper atmosphere is in convective equilibrium while at deep levels the atmosphere becomes isothermal. This model has the effect of flattening the spectrum at long wavelengths.

C. Radio Maps - The radio maps shown in Figures 2 and 3 provide quantitative data on the brightness distribution across the disk. We have already remarked on the apparent asymmetry of the distributions, with the tendency for the peak brightness to be shifted toward the pole. A symmetrical limb darkened planet would show a peak brightness at the sub-earth point rather than at the pole. Here we will make some quantitative, but preliminary estimates of the limb darkening/brightening distributions.

We have calculated the limb darkening for several plausible atmospheric models for Uranus at 10 GHz and 22 GHz. These models include microwave absorption due to H_2 alone, a model in which the ammonia concentration is very low (less than 10e-7), and a model in which the ammonia is depleted in the upper atmosphere but present at the solar abundance value at depth. In the first case, the limb darkening is very severe whereas in the latter case the limb darkening is very slight. We indicate these two extreme cases in Figure 14. Figure 15 shows the center-to-limb variation on a uniform and limb darkened (case 1) Uranus model, after the planet was convolved with a Gaussian shape beam which matched the VLA beam. The half-power beam width was 0.65 arc sec.

Superimposed on Figure 15, we show the normalized brightness temperatures measured from the 6 cm radio map. The data were measured along a longitude line on Uranus which intercepted the sub-earth point (and the pole). Data measured from the sub-earth point toward the sunlit pole are indicated by filled dots; data measured from the sub-earth point in the opposite direction are indicated by crosses. The asymmetry in the brightness distribution causes these two curves to diverge. The curve which passes through the pole reaches a shallow maximum away from the sub-earth point and then decreases falling between the two model limb darkening curves. The measured brightness in the opposite direction falls off faster than the severely limb darkened model. We believe that these results cannot be explained by limb darkening alone and must respresent a true temperature variation across the disk.

If the brightness temperature distribution across the disk is modeled by a spherical harmonic series expansion,symmetric about the rotation axis, and warm at the sunlit pole, then the first two terms of the series are that of a constant and a dipole of the form

$$T = T(0) + (T(p) - T(eq)) \cos(1)$$

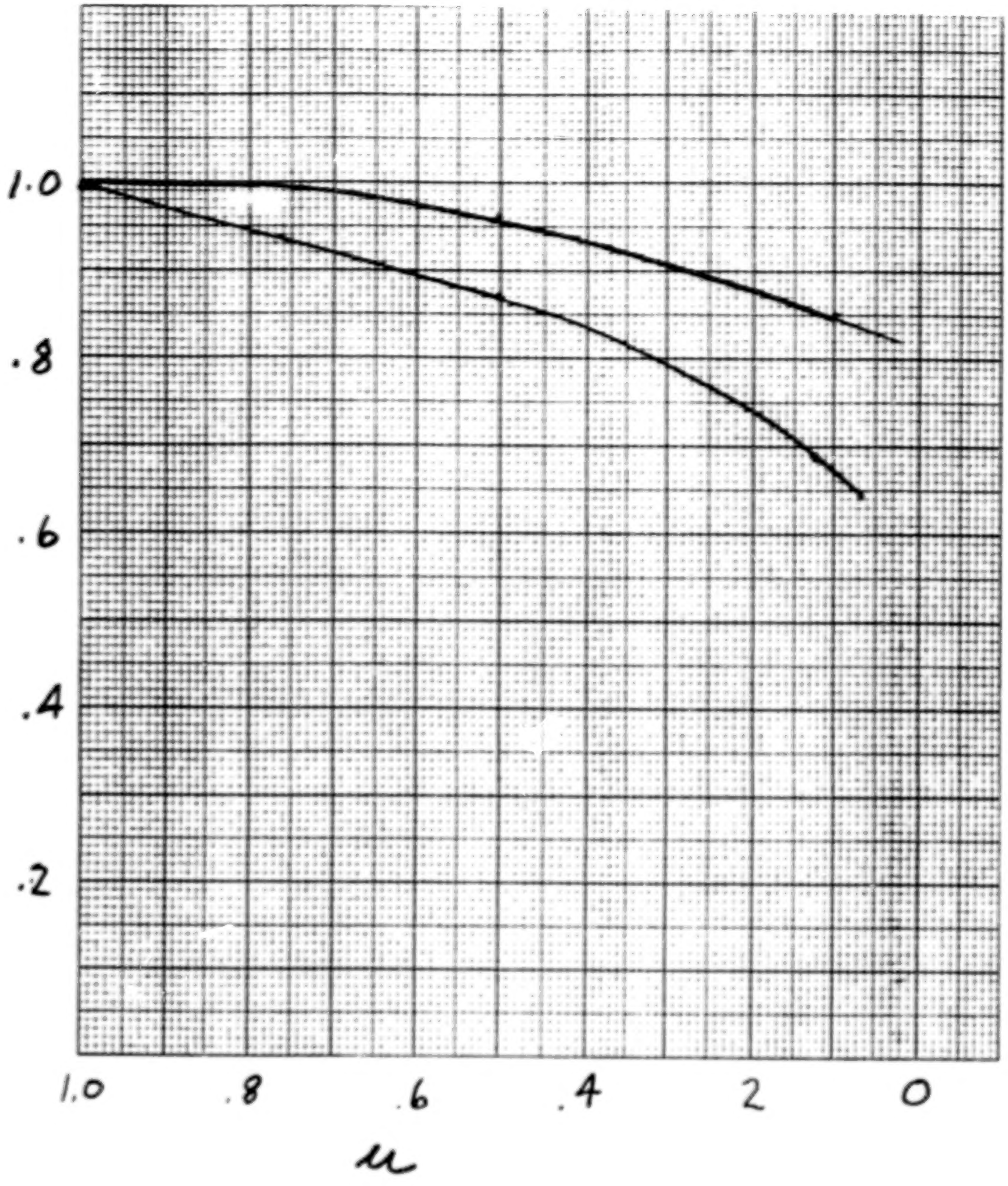

Figure 14 - Limb darkening model calculations for Uranus at 10.7 GHz to illustrate a range of possibilities. Curve A is for a case in which ammonia is severely depleted above the 200 K level and has a mixing ratio of 10e-4 below that level. Curve B is for a case in which the absorption is due to H2 alone. The curves are normalized to the center of the disk and plotted versus the cosine of the emission angle, μ.

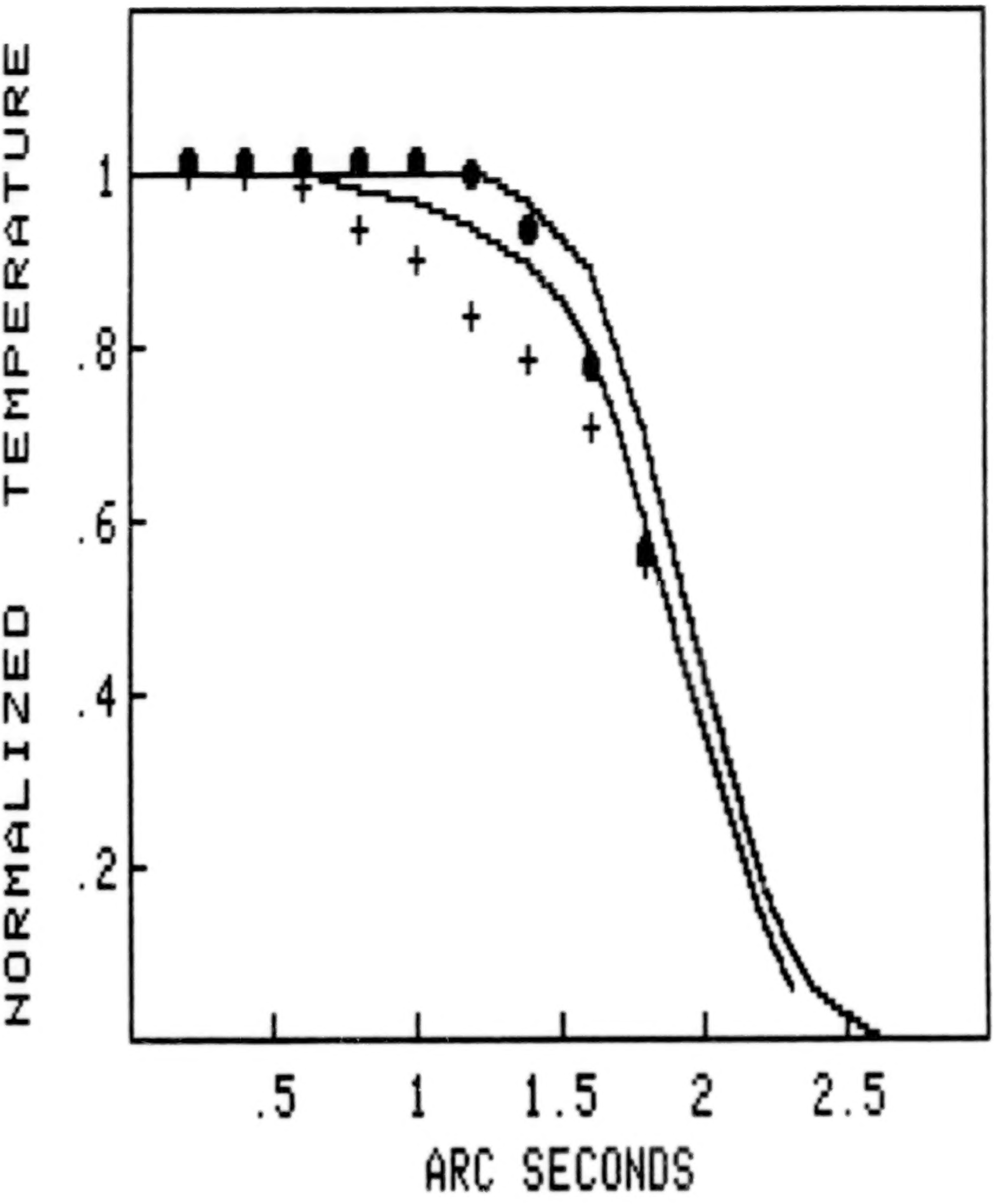

Figure 15 - The solid curves show a uniform disk (upper curve) and a severely (curve B from Figure 14) limb darkened disk (lower curve) with the angular dimensions of Uranus convolved with a 0.65 arc sec Gausssian beam. The filled dots are measurements from the 6 cm map measured along a strip from the sub-earth point toward the sunlit pole. The crosses are measurements along a strip from the sub-earth point and away from the sunlit pole. Note that the crosses lie considerably below the severely limb darkened model.

where 1 is the colatitude of the sub-earth point, T(0) is a constant term, T(p) is the temperature at the pole, and T(eq) is the temperature at the equator. The solid curves in Figure 16 show the expected limb darkening for a planet with this brightness distribution and using the parameters T(0) = 200 K and (T(p)-T(eq)) = 100 K. The curves were generated by convolving the model whose angular dimensions matched Uranus (1.97 arc sec radius) at the time of the observations with a Gaussian beam (HPBW = 0.65 arc sec). No limb darkening other than that produced by the model itself was included. These curves give a very striking resemblance to the data which are indicated (as in Figure 15) by crosses and filled dots.

It is interesting to speculate whether a permanent temperature distribution of this form and magnitude might explain the variability which was discussed earlier. A straight forward calculation of the disk brightness temperature for this model shows that it will vary as

$$T = T(0) + .66\,(T(p)-T(eq))\cos(1)$$

provided that the temperature distribution itself is not time variable. The variation of this function with epoch is shown in Figure 17. The cos(1) dependence in this equation causes the greatest variation to occur between 1965 and 1976. Qualitatively, the adjusted data showed this same trend. We show in Figure 17 all data in the 2.0 to 10 cm wavelength range, adjusted for the temperature gradient and centered on 6 cm wavelength, plotted versus the epoch of the measurement. The 2.0 to 10 cm range is a very wide range to consider since the amplitude of the variations appears to be wavelength dependent. However, since the time history of 6 cm measurements is incomplete,

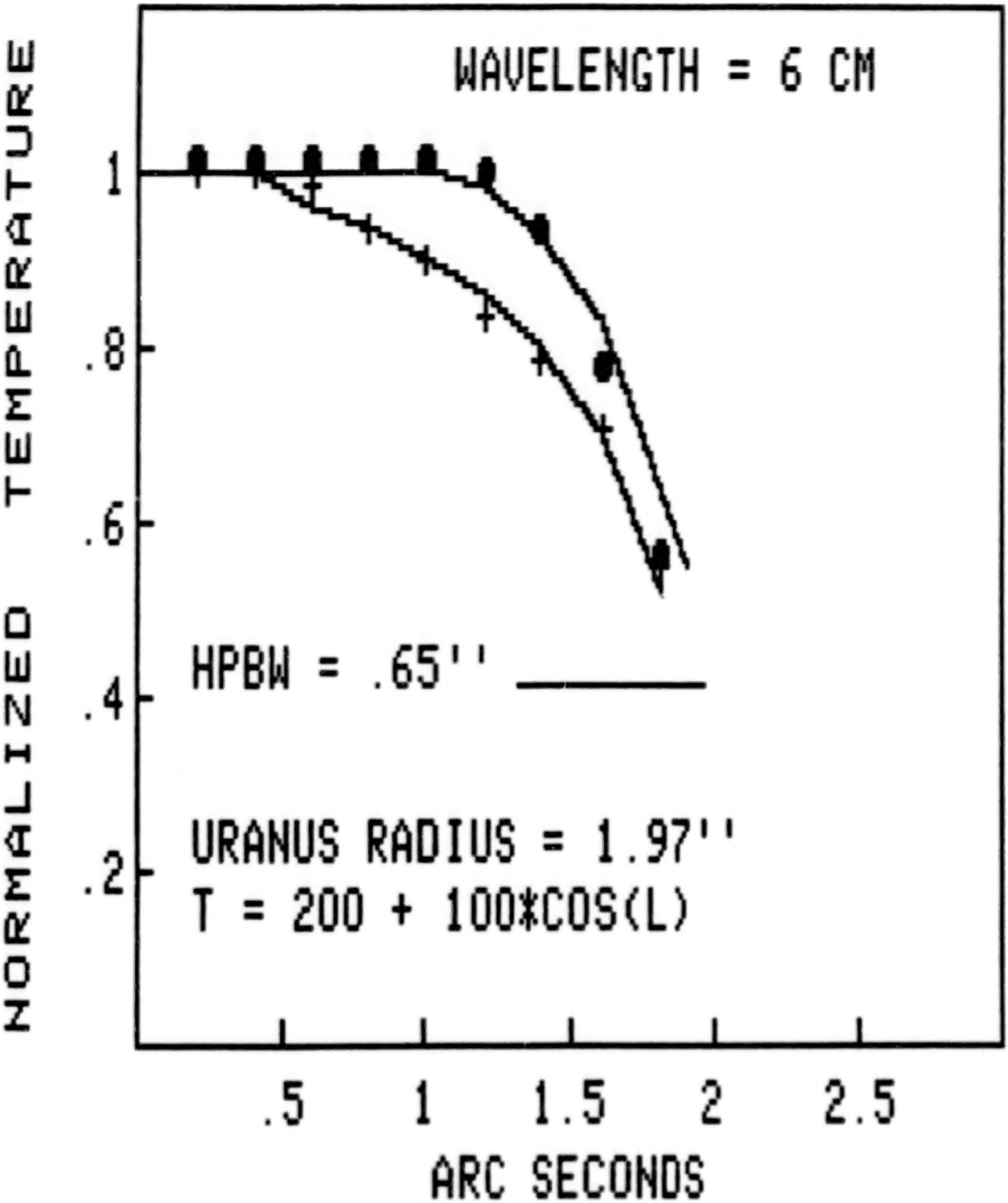

Figure 16 - The solid curves show the expected limb darkening for the model described in the paper along a strip which passes through the pole and sub-earth point. The filled dots are measurements from the 6 cm data measured along a strip from the sub-earth point toward the sunlit pole. The crosses are measurements along a strip from the sub-earth point and away from the sunlit pole. The radius of Uranus was 1.97 arc sec at the time of the observations.

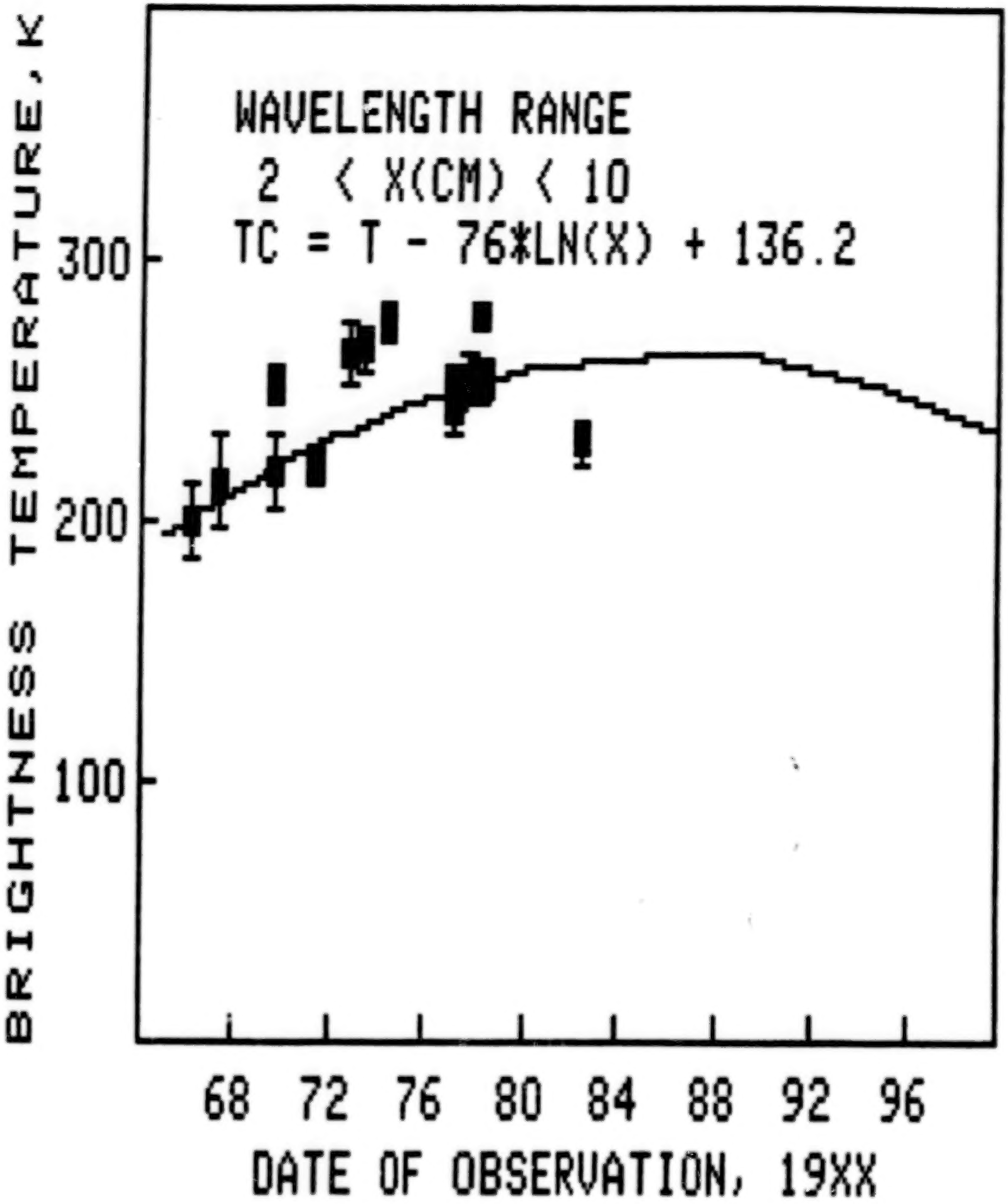

Figure 17 - The disk temperatures of Uranus in the wavelength range 2 to 10 cm corrected for the gradient across the wavelength interval. The solid line shows the expected variation of the brightness temperature for the model described in the text.

we have used the wide window to establish the trend. The solid curve is seen to be in qualitative agreement with the observed variations.

This comparison suggests that the observed time variability of the Uranus centimeter brightness temperatures is due to a gradient in the brightness temperature across the planet. The temperature distribution can either be caused by a true temperature variation or by a variation in the opacity of the atmosphere or both. It seems unlikely that the major effect is due to a true temperature change since the heat capacity of the atmosphere is so large. It seems most likely to us that the variation is due to an opacity difference between the pole and equator. If the brightness temperature distribution is that of a dipole, with the sun-lit pole being the warmest, the pole to equator temperature difference would have to be about 100K. A least square fit to the data has not been attempted at this time.

To be certain, we do not believe this preliminary analysis of the 6 cm data proves that the variability is tied to the brightness distribution and changing aspect of the planet. It may however point the way for more detailed analysis and assist in the planning of spacecraft experiments. In particular, we note that the brightest point on the 2 cm map (Figure 3) is not at the pole, nor at the sub-earth point, but somewhere in between. The 2 cm map shows a brightness variation across the disk, but somewhat different than that at 6 cm.

SUMMARY

The principal conclusions we have reached on re-examining the Uranus brightness temperature data and on carrying out a preliminary analysis of a high resolution 6 cm map of Uranus are as follows:

1) The brightness temperatures of Uranus are variable throughout the centimeter wavelength range (2 to 20 cm) with some evidence of variability at wavelengths as short as 3 mm. The data near 1 mm wavelength are too incomplete to allow one to draw firm conclusions about variability. The brightness temperature variation was greatest between 1965 and 1971 and appears to have leveled off since then.

2) The Uranus upper atmosphere is depleted in ammonia by a factor of the order of 100 below the solar values at temperatures less than 200K. The temperature pressure profiles derived by Appleby (1980), Orton (1984) and Wallace (1980) are consistent with the microwave observations. The principal constraint to the profiles is from the millimeter observations which sets limits on how hot or cold the atmosphere can be. If the thermal structure of Uranus is not in adiabatic-convective equilibrium, conclusions based on modelling studies may need to be revised.

3) The high angular resolution 6 cm map of Uranus shows an asymmetric brightness distribution. The peak brightness is near the sunlit pole. This spatially variable brightness distribution may be responsible for the observed variability of the microwave spectrum.

Acknowledgement

This work was partly supported by NSF grant ASF-8405358 to the University of California. This paper presents the results of one phase of research carried out at the Jet Propulsion Laboratory, California Institute of Technology, under Contract NAS7-100.

REFERENCES

Appleby, J.F., 1980. Thesis, State University of New York at Stony Brook.

Atreya, S.K. and P.N. Romani, 1984. Photochemistry and Clouds of Jupiter, Saturn, and Uranus. A Chapter in Planetary Meteorology (Ed. G.E. Hunt) Cambridge University Press.

Batty, M.J., Jauncey, D.L., Rayner, P.T. and S. Gulkis, 1980. Planetary Observations with the Tidbinbilla Interferometer. Proc. Astron. Soc. of Aust. 4, 72-73.

Batty, M.J., Jauncey, D.L., Rayner, P.T. and S. Gulkis, 1981. Evidence For Changes in the Microwave Brightness Temperature and Spectrum of Uranus. Astrophys. J. 243, 1058-1061.

Berge, G.L., 1968. Recent Observations of Saturn, Uranus, and Neptune at 3.12 cm. Astrophys. J. 2, 127-131.

Berge, G.L. and S. Gulkis, 1976. Earth-based radio observations of Jupiter: Millimeter to meter wavelengths, in Jupiter, Ed. T. Gehrels, University of Arizonia Press, 621-692.

Briggs, F.H., and B.H. Andrew, 1980. Microwave Radiometry and Interferometry of Uranus. Icarus 41, 269-277.

Conway, R.G., 1980. Decimetric radio observations of Saturn and Uranus. Mon. Not. R. Astr. Soc. 190, 169-176.

Cogdell, J. R., Davis, J. H. Ulrich, B. T. and B. J. Wills, 1975, Ap. J. 196, 363-368.

Courtin, R., Coron, N., Encrenaz, Th., Gispert, R., Bruston, P., Leblanc, J., Danbien, G., and A. Vidal-Madjar, 1977. Astron. and Astro. 60, 115-123.

Courtin, R.D., Gautier, D., and A. Lacombe, 1978. On the Thermal Structure of Uranus from Infrared Measurements. Astron. Astrophys. 63, 97-101.

de Pater, I. (private communications)

de Pater, I., and S.T. Massie, 1984. A Comparison of Jovian Spectra at millimeter-centimeter Wavelengths. Paper in preparation.

Epstein, E.E., Dworetsky, M.M., Montgomery, J.W., Fogarty, W.G. and R. A. Schorn, 1970. Mars, Jupiter, Saturn, and Uranus: 3.3-mm brightness temperatures and a search for variation with time and phase angle. Icarus 13, 276-281.

Gary, B.L. (private communication).

Gary, B.L., 1974. Jupiter, Saturn, and Uranus disk temperature measurements at 2.07 and 3.56 cm. Astron. J. 79, 318-320.

Gerard, E., 1969. Observations of Saturn, Uranus, and Neptune at 11.13 cm. Astro. and Astrophys. 2, 246-248.

Gulkis, S., Janssen, M.J., and E.T. Olsen, 1978. Evidence for the Depletion of Ammonia in the Uranus Atmosphere. Icarus 34, 10-19.

Gulkis, S., Olsen, E.T., Klein, M.J. and T.J. Thompson, 1983. Uranus: Variability of the Microwave Spectrum. Science 221, 453-455.

Kellermann, K.I., 1966. The Thermal radio emission from Mercury, Venus, Mars, Saturn, and Uranus. Icarus 5, 478-490.

Klein, M.J. and T.V. Seling, 1966. RAdio Emission from Uranus at 8 Gc/s. Astrophys, J. 146, 599-602.

Klein, M.J. and J.A. Turegano, 1978. Evidence of an Increase in the Microwave Brightness Temperature of Uranus. Astrophys. J. 224, L31-L34.

Mayer, C.H. and T.P. McCullough, 1971. Microwave Radiation From Uranus and Neptune. Icarus 14, 187-191.

Orton, G. (private communication)

Pauliny-Toth, I.K. and Kellermann, K.I., 1970. Millimeter Wavelength measurements of Uranus and Neptune. Astrophys. Lett. 6, 185-187.

Ulich B.L. (private communication)

Ulich, B.L. and E.K. Conklin, 1976. Observations of Ganymede, Callisto, Ceres, Uranus, and Neptune at 3.33-mm wavelength. Icarus 27, 183-189.

Ulich, B. L., Dickel, J. R., and I. de Pater, 1984. 1.3 mm Observations of Planetary Bodies. Icarus, submitted.

Wallace, L., 1980. The Structure of the Uranus Atmosphere. Icarus 43, 231-259.

Webster, W.J., Webster, A.C., and G.T. Webster, 1972. Interferometer Observations of Uranus, Neptune, and Pluto at Wavelenghts of 11.1 and 3.7 cm. Astrophys. J. 174, 679-684.

ATMOSPHERIC DYNAMICS OF URANUS

AND NEPTUNE: THEORETICAL CONSIDERATIONS

Andrew P. Ingersoll
Division of Geological and Planetary Sciences
California Institute of Technology
Pasadena, California 91125

Abstract

Uranus, because of its pole-on orientation and low internal heat source, is in a dynamically different atmospheric regime from Jupiter and Saturn. Neptune resembles Jupiter and Saturn in orientation and internal heating, but its extremely long radiative time constant puts Neptune in a different class. Voyager observations of seasonal temperature gradients, equator-to-pole temperature gradients, infrared emission, Bond albedo, possible cloud structures (bands, spots, eddies), and cloud motions should greatly improve our ability to classify planetary atmospheres according to their dynamical regimes.

The subject of atmospheric dynamics of Uranus and Neptune is short on observational constraints but long on potential impact. The educated layman appreciates that the atmosphere of Uranus, with its pole-on orientation, is driven by sunlight in a way that is different from that of other planets. Predicting the circulation patterns of the clouds is a major challenge. Neptune resembles Jupiter and Saturn as far as orientation is concerned, but its long radiative time constant, as discussed below, puts Neptune in a separate class.

In this paper I will first review models of the seasonal thermal cycles published recently by Wallace (1983).[1] I will then review the internal heat and its role in the meteorology as explained by Ingersoll (1976)[2] and by Ingersoll and Porco (1978)[3]. Stone's (1972, 1975)[4,5] models of the atmospheric heat transport (from pole to equator on Uranus) will then be discussed. Finally, possible Voyager observations that bear on these questions will be mentioned.

SEASONAL THERMAL CYCLE

Wallace (1983)[1] has published a time-dependent, radiative-convective seasonal model for Uranus. Horizontal heat transport is neglected. The height of the convective zone and the temperature profile are allowed to vary over the year. The pressure range is roughly 0.03-10 bars, although most of the seasonal change occurs at $P \leq 1.0$ bars.

Wallace finds that the maximum temperature change over the year occurs at the poles and is about ±2.5 K. The emergent IR flux varies by about ±18%, with the largest flux occurring almost 1/4 Uranian year after the peak solar heating. The results are sensitive to (and diagnostic of) the amount of CH_4 and absorbing haze as well as the latitudinal distribution of internal heat flux.

The important point for dynamics is that the seasonal variation of emergent infrared flux is not as large as that of the absorbed sunlight. The polar atmosphere gains net heat in the summer and loses it in the fall. Moreover, despite the pole's effective temperature being hotter than that of the equator, there is still net energy deposited at the pole on an annual basis and net energy radiated at the equator. This energy must be transported equatorward, and the question arises: at what level (i.e., in the atmosphere or in the interior) does this transport take place? As discussed below, the answer probably depends on the magnitude of the internal heat source.

INTERNAL HEAT AND THE METEOROLOGY

At the May 1975 Tucson Conference on Jupiter, Ingersoll argued that Jupiter's convective interior would short-circuit the atmosphere in transporting heat poleward and upward. As a result the equator-to-pole temperature difference and atmospheric heat transport should be small. The argument was published in the conference special issue by Ingersoll (1976),[2] and detailed models were published by Ingersoll and Porco (1978).[3]

Because of its internal heat, Jupiter's net (emitted infrared minus absorbed solar) irradiance is positive at all latitudes. This fact was established by Pioneer and Voyager infrared and visible observations (Ingersoll et al., 1976; Hanel et al., 1981).[6,7] As a result the upward flux of internal heat must be positive at all latitudes, and the deep atmosphere and interior must be convective at all latitudes. Since convection tends to maintain all fluid particles close to the same adiabat, temperature variations on constant pressure surfaces should be small. This nearly isentropic state of the interior is maintained by convection currents that drive internal heat poleward and upward to balance the latitudinal variation of absorbed sunlight. Within each band of latitude the visible atmosphere receives as much solar and internal energy as it emits to space, so the poleward atmospheric heat transport is zero.

The internal energy sources of Jupiter, Saturn and Neptune all seem to be large enough so that the net irradiance is positive at all latitudes (Gautier and Courtin, 1979).[8] Uranus has a weaker internal energy source.[8] In this respect it is an earth-like planet. Those latitudes (the poles) that receive the most sunlight over the Uranian year must transport energy to other latitudes (the equator). Without a large internal heat source this transport must take place in the visible atmosphere--above the deepest levels to which sunlight penetrates. Using curves for the annual average isolation of Uranus, I calculate that the internal heat source must be at least 27% of the absorbed sunlight before Uranus would no longer be an earth-like planet in this respect.

An interesting possibility is that the extra annual average sunlight at the Uranian poles might completely inhibit the internal heat transport there. The deep atmosphere might be subadiabatic from the poles down to some critical latitude determined by the magnitude of the internal heat source. If the internal heat source were slightly less than 27% of the absorbed sunlight, the subadiabatic polar region would be small. If the internal heat source were much less than the absorbed sunlight the subadiabatic polar region would be large. Within the subadiabatic polar region, the visible layers of the Uranian atmosphere might behave in an earth-like manner, with lateral (equatorward) heat transport by baroclinic eddies in a stably stratified environment. In the equatorial band outside the subadiabatic polar regions the Uranian atmosphere might behave in a more Jovian manner, with strong zonal jets and little evidence of mixing across latitudes.

ESTIMATES OF ATMOSPHERIC HEAT TRANSPORT

Stone (1972, 1973, 1975)[4,9,5] has developed a set of scaling arguments to estimate the equator-to-pole temperature gradient $\partial T/\partial y$, the vertical potential temperature gradient $\partial \theta/\partial z$, the horizontal eddy velocity v, and horizontal eddy length scale L. The estimates are based on several assumptions, first, that the eddies grow to a size where their meridional velocities are comparable to the zonal velocity difference from top to bottom in the baroclinic atmosphere. A second assumption is that the heat transport takes place in the visible atmosphere, with no compensation by the internal heat flux for the latitudinal gradient in incident sunlight. For Jupiter, Saturn and Neptune, this second assumption should lead to an overestimate of the equator-to-pole temperature gradient, for reasons discussed in the preceding section. A third assumption is that the upward and lateral heat transports by eddies are balanced by radiation, which tends to de-stabilize the atmosphere in most of Stone's worked examples. In particular the contribution of small-scale convection to the upward heat transport is neglected.

Subject to these limitations, Stone's formulas provide a classification scheme for the giant planets that complements the classification of the preceding section. The two most important parameters are $\delta = \Omega\tau$ and $\varepsilon = \Omega r/c$, where Ω is the rotation rate of the planet, τ is the radiative time constant of the visible layers, r is the planetary radius, $c \simeq (gH)^{1/2}$ is the speed of sound, g is the acceleration of gravity and H is the pressure scale height. Both δ and ε are larger than unity for the earth and the giant planets. When δ is large the radiative forcing is weak. When ε is large the inhibiting effects of rapid rotation, large horizontal distances, and small buoyancy are strong. Thus planets with very large δ and not-so-large ε tend to have small (<5%) equator-to-pole temperature differences $\Delta T/T$ because radiative forcing is weak and the heat has to be transported over a relatively short distance r. Uranus and Neptune are in this category. Conversely, planets with large ε and not-so-large δ tend to have large (20%) horizontal temperature differences $\Delta T/T$. Jupiter, and to a lesser extent Saturn, would be in this category if their internal heat fluxes were independent of latitude. The earth has modest values of both ε and δ, and has moderately large (10%) values of $\Delta T/T$ according to Stone's formulas.

In other words, Uranus and Neptune, because of their extremely weak radiative forcing (long radiative time constants) are in a class by themselves. Uranus, which seems to have insufficient internal heat to compensate for lateral variations in sunlight, should have small temperature differences ($T_{pole} - T_{equator} < 1$ K), small eddy velocities ($v < 2$ m s^{-1}), and small eddy length scales ($L < 1000$ km). Verifying these scaling relations would help in classifying the different types of atmospheric behavior for the different types of planets.

VOYAGER OBSERVATIONS

Both visible-wavelength imaging at high spatial resolution (better than 100 km per pixel pair) and visible and infrared radiometry at low spatial resolution can yield important information about Uranus and Neptune. The global energy budget and the magnitude of the internal energy source can be inferred from the infrared emission and the spherical Bond albedo. Infrared observations by Voyager must be used with a seasonal temperature model to infer the annual average emission. Visible-wavelength observations by the Voyager IRIS and imaging systems must be used with a scattering model to infer the globally averaged absorbed sunlight. The winter-summer temperature gradient and the associated infrared emission gradient are important for estimating the seasonal cycle. The pole-to-equator temperature gradients (the poles should be hotter) are important for understanding the horizontal atmospheric energy transport. In spite of the featureless appearance of

Uranus from earth, visible-wavelength imaging is still the best means by which Voyager can determine the large-scale cloud structure (bands and spots, should they exist) and motions of small-scale features. Experience of Voyager at Saturn indicates that numerous small-scale features could be present without their having been seen from earth.

REFERENCES

1. Wallace, L. 1983. The Seasonal Variation of the Thermal Structure of the Atmosphere of Uranus, Icarus, **54**, 110.

2. Ingersoll, A.P. 1976. Pioneer 10 and 11 Observations and the Dynamics of Jupiter's Atmosphere, Icarus **29**, 245.

3. Ingersoll, A.P. and Porco, C.C. 1978. Solar Heating and Internal Heat Flow on Jupiter, Icarus **35**, 27.

4. Stone, P.H. 1972. A Simplified Radiative-Dynamical Model for the Static Stability of Rotating Atmospheres, J. Atmos. Sci. **29**, 405.

5. __________ 1975. The Atmosphere of Uranus, Icarus **24**, 292.

6. Ingersoll, A.P., Munch, G., Neugebauer, G., and Orton, G.S. 1976. Results of the Infrared Radiometer Experiment on Pioneers 10 and 11, in Jupiter (ed. T. Gehrels) Univ. of Arizona Press, Tucson.

7. Hanel, R.A., Conrath, B.J., Herath, L.W., Kunde, V.G., and Pirraglia, J.A. 1981. Albedo, Internal Heat, and Energy Balance of Jupiter: Preliminary Results of the Voyager Infrared Investigation, J. Geophys. Res. **86**, 8705.

8. Gautier, D. and Courtin, R. 1979. Atmospheric Thermal Structures of the Giant Planets, Icarus **39**, 28.

9. Stone, P.H. 1972. A Simplified Radiative-Dynamical Model for the Static Stability of Rotating Atmospheres, J. Atmos. Sci. **29**, 405.

BLANK PAGE

THE POSSIBILITY OF DETECTION AND MEASUREMENT OF CLOUD STRUCTURE IN THE ATMOSPHERE OF URANUS

Reta F. Beebe

New Mexico State University
Box 4500
Las Cruces, New Mexico 88003

Abstract

Historical data concerning variability of surface brightness of the visible cloud deck are reviewed. The data do not rule out low contrast small cloud structures of the type measured in the Saturnian Voyager wind measurements. Convective models in which methane can condense suggest similar structure may be present at the level of the visible cloud deck in Uranus' atmosphere. Horizontal space and time scales derived from dynamical considerations lie within the accessible range of the wide- and narrow- angle Voyager cameras. Therefore, Voyager 2 may obtain significant dynamical information about the Uranian atmosphere.

INTRODUCTION

More than two hundred years have passed since 13 March 1781 when William Herschel discovered the planet Uranus. During the intervening period, Uranus has approached perihelion in 1798, 1882, and 1966. At perihelion, we observe the Uranian satellite system almost edge on; thus, if the equatorial plane coincides with the plane of revolution of the satellites we observe Uranus equatorward-on at perihelion and aphelion. This would imply that the most favorable periods of this century for observing a zonal cloud system similar to that on Jupiter and Saturn occurred in 1924 and 1966 when the banded structure would have been parallel to the plane of revolution of the satellites.

The highest resolution data consist of the March 26-27, 1970 Stratoscope II photographs[1]. These data, photographed through a pass band of 380 to 580nm, showed no visible markings with contrasts above 5%. In addition, the observed equatorial and polar limb-darkening could be fit with a conservative Rayleigh layer of optical depth = 0.5 overlying a Lambert surface (albedo = 0.75).

In contrast, in Alexander's review[2] of the history of observations of Uranus, he cites observations by E. M. Antoniadi in 1924 with the 33-in aperture Meudon refractor where he draws two faint dusky belts on each side of a brighter equatorial zone and notes that the observed pattern is in agreement with Laplace's theory.

Alexander also cites earlier work[3] by Young in 1883, and the Henry brothers and Perrotin in 1884 which reported that the south pole was brighter than the north pole and there were two faint belts; however, these belts were reported to be inclined to the line of the satellites.

Belton and Vescelus[4] argue that reports of the existence of markings cannot be dismissed based on the Stratoscope II results. They point out that the pass-band of the Stratoscope data is insensitive to color difference and that these data represent observations on a single night. On the other hand, the fact that the diameter of Uranus is less than four seconds of arc places severe constraints on the visual observer and suggests that a more reliable way to determine the maximum possible cloud contrast would be color dependent integrated disk photometry.

In 1933, Becker published a summary of visual magnitudes of Uranus which is reviewed by Alexander[5]. Becker reported a sinusoidal component with an amplitude of $0\overset{m}{.}29$ and a period of 42 years, as well as fluctuations in brightness of about $0\overset{m}{.}15$. It should be noted that these were visual observations and do not have the accuracy of Lockwood's[6] photoelectric photometry. For data from 1953 to 1966, Lockwood reports a monotonic decrease in brightness of 0.04 magnitudes and for data from 1953 to 1961 no short term variations greater than 0.002 magnitudes were observed. Combining data from 1972 to 1976 with the 1953 to 1966 data, Lockwood proposes a geometrical oblateness of 0.01 in agreement with Danielson et al.[7] and Smith[8] and a south pole 15% brighter than the equator before perihelion and a north pole 20% brighter than the equator after perihelion. Additional searches by Lockwood and Thompson[9] for photometric evidence of a rotational period fail to detect any short term variation above the level of 0.003 magnitudes; therefore, there is little evidence of rapid brightening reported in earlier visual work. Based on these data, Lockwood and Thompson state that this level of variation precludes an albedo feature analogous to Jupiter's Red Spot with an albedo variation of 25%. These observations indicate that variation in cloud structures at visible wavelengths are dominated by polar brightenings; however, Lockwood et al.'s limits on variability do not preclude the presence of small low contrast structure.

ARGUMENTS FOR LOW CONTRAST FEATURES

A review of preliminary zonal wind measurements of Voyager 1 and 2 Saturn images reveals that measurements were made on low contrast features. A comparison of Smith et al.'s[10] figure 1, 3 and 5 illustrate the low contrast detail utilized in the northern hemisphere. Although the southern hemisphere showed far fewer large features and appeared to be more heavily obscured by an overlying haze, figure 2 in Smith et al.'s Voyager 2 review[11] shows bright banding associated with eastward maxima in the zonal winds and a more mottled pattern in regions undergoing westward displacement. Inspection of figure 5 reveals strong hemispheric symmetry in the zonal wind pattern even though large scale albedo contrast was less in the southern hemisphere. It should be noted that the low contrast and small surface area of the individual cloud structures that were used to establish the zonal winds of Saturn would not be detectable as photometric variations; therefore, we should examine the Uranian atmosphere in terms of the possibility of the existence of similar structure.

Modeling by Wallace[12] illustrates the importance of absorption of solar flux by methane in comparison with the magnitude of an internal heat source. He finds that methane condenses throughout a large portion of the atmosphere and agrees with Trafton's model[13] which requires a haze between 1.1 and 1.8 bars of pressure. Wallace points out that methane would condense in the lower portion of Trafton's haze and that the ~225°K brightness temperature at 6cm requires a small internal heat source. With or without an internal heat source his models are convective down to a 15 bar pressure level. These results suggest that convective overshoot could carry material up into a region where methane ice could form markers for displacement measurements similar to those on Saturn.

ADVANTAGES OF THE APPROACH GEOMETRY OF VOYAGER 2.

Two main observing periods[14] allow detailed analysis of single frame series which will contain the whole Uranian image and simplify navigation.

Because the approach path is essentially pole-on, a series of scans of surface brightness at a fixed latitude extending over a longitudinal range up to 360° can be obtained with time spacings that are independent of the rotational period of the planet. Cross-correlations of a series of these scans could yield significant zonal velocities for a major portion of the illuminated hemisphere. If features are ill-defined or if a measurable component of meridional motion is evident, two dimensional cross-correlations and analysis of three-dimensional plots of surface brightness as a function of latitude and longitude are possible if the cloud contrast is similar to that of Saturn.

The period from -10 to -5 days before encounter provides a time period when the narrow-angle camera will produce an image of Uranus with a resolution of 300 to 150 km/line pair. Also the wide-angle camera provides similar resolution over a twenty-four hour period from 1.75 to .75 days before encounter. This second opportunity allows use of a methane filter in the wide-angle camera and selected nested narrow-angle images.

EVIDENCE OF SEASONAL FORMATION OF AEROSOLS

Voyager observations of Saturn and Titan suggest that increases in reflectivity are correlated with increased local insolation. A detailed analysis of ground-based broad pass-band photographs of Saturn by Suggs[15] indicates that the greatest change in the albedo of the belts and zones in the visual region of the spectrum occurs in the interval spanned by the violet Voyager filters centered near 400nm. This is a region where aerosol scattering competes with Rayleigh scattering. Historically, the

South Temperate Region of Saturn shows the largest response to variation of insolation. This can be interpreted in terms of cloud heights in current models and integrated solar insolation.

Because perihelion occurs when the axis of rotation is perpendicular to the incident rays, and the eccentricity of Uranus' orbit is 0.047, the solar illumination was 21% greater in 1966 than at aphelion in 1924, when Antoniadi reported seeing dusky grey equatorial belts. In addition, the axial tilt provides a geometry such that the visible hemisphere receives more insolation per Uranian day at all other times. Based on historical data concerning belt-zone contrast in Saturn's atmosphere, the period when Antoniadi reported a belted aspect to the Uranian Atmosphere was the most likely time to observe its occurance.

Loss of albedo contrast in narrow band CCD methane images* and a systematic change in Lockwood's b-y color index[16] indicate an increase in reflectivity in the northern hemisphere at mid-latitudes in methane images and in the b filter centered at 465nm. These results indicate that aerosol obscuration is increasing in Uranus' northern hemisphere as the subsolar region shifts toward the pole.

CONCLUSIONS

Although the orbital geometry is such that enhanced aerosol concentration eliminates the chance that we will have maximum belted contrasts in 1986, and although we are observing when the solar insolation is near pole-on, we cannot rule out the possibility that we will be able to detect low contrast cloud features such as those we measured in Saturn's atmosphere. Because models predict a convective atmosphere in which methane can condense it is possible that convection may carry material up through the observed cloud deck and fresh methane ice will form and serve as markers. If the size of cloud features and the horizontal winds are of the order of magnitude estimated by Stone[17], the spacial resolution available in the narrow and wide-angle camera frames when Uranus is easily navigated should allow us to identify and characterize the latitudinal dependence of the clouds and the narrow-angle frames for the period from 5 days to 18 hours before encounter should provide adequate resolution (150 to 20 km per line pair) for preliminary classification of cloud morphology.

---

*See Smith, B. A. in this publication.

REFERENCES

1) Danielson, R. E., Tomasko, M. G., and Savage, B. D., "High-Resolution Imagery of Uranus Obtained by Stratoscope II," Astrophys. J., Vol. 178, 1972, pp. 887-900.

2) Alexander, A. F. O'D., "The Planet Uranus, A History of Observation, Theory and Discovery," 1st ed., American Elsevier Publishing Co., New York, 1965, pp. 235.

3) ________ pp. 178-180.

4) Belton, M. J. S. and Vescelus, F. E., "Why Image Uranus?," Icarus, Vol. 24, 1975, pp. 229-310.

5) Alexander, "The Planet Uranus," pp. 252.

6) Lockwood, G. W., "Analysis of Variations of Uranus and Neptune Since 1953," Icarus, Vol. 35, 1978, pp. 79-92.

7) Danielson, "High-Resolution,"

8) Smith, B. A., "Uranus Photography in the 890-nm Absorption Band of Methane," Bull. Amer. Astron. Soc., Vol. 9, pp. 473.

9) Lockwood, G. W. and Thompson, D. T., "A Photometric Test of Rotational Periods for Uranus and Time Variations of Methane-Bank Strengths," Astrophys. J., Vol. 221, 1978, pp. 689-693.

10) Smith, B. A. et al., "Encounter with Saturn: Voyager 1 Imaging Scinece Results," Science, Vol. 212, 1981, pp. 163-191.

11) Smith, B. A. et al., "A New Look at the Saturnian System: The Voyager 2 Images," Science, Vol. 215, 1982, pp. 504-537.

12) Wallace, L., "The Structure of the Uranus Atmosphere," Icarus, Vol. 43, 1980, 231-259.

13) Trafton, L., "The Aerosol Distribution in Uranus' Atmosphere: Interpretation of the Hydrogen Spectrum," Astrophys. J., Vol. 207, 1972, 1007-1024.

14) Bunker, A., private communication, 1983.

15) Suggs, R. M., "Temporal Albedo Variations in Saturn's Atmosphere," Doctoral Dissertation, New Mexico State University, 1983.

16) Lockwood, G. W., private communication, 1983.

17) Stone, P. H., "The Atmosphere of Uranus," Icarus, Vol. 24, 1975, pp. 292-298.

VARIABILITY OF NEPTUNE

Dale P. Cruikshank

Institute for Astronomy
2680 Woodlawn Drive
Honolulu, HI 96822

Abstract

Earth-based observers of Neptune have found that the planet varies in brightness at various wavelengths in ways that suggest that changes occur in the planet's atmosphere on several different time-scales. Global inhomogeneities in high-altitude haze distribution that are stable for several days permit measurements of the planet's rotation period (about 18 hours), but this stability sometimes breaks down, obscuring the diurnal lightcurve. In addition, there is an apparent long-term variability of the brightness of Neptune in anticorrelation with the cycle of solar activity. This slow variability of low amplitude may be punctuated by outbursts of high-altitude condensation of particles in the atmosphere, whose decay time is several months.

INTRODUCTION

A decade of photometric observations at various wavelengths has shown that Neptune varies in brightness with at least four characteristic time-scales. Inasmuch as changes of the optical properties of planet's upper atmosphere are related to the global dynamics of the atmosphere, a review of the observational facts may serve as a useful point of departure for comparisons with theoretical studies. This paper is not intended to be a thorough review of the literature of Neptune observations, but will focus on the crucial results of the last decade in establishing the variability of the planet's brightness as seen at various wavelengths.

1. Diurnal Variation. Because portions of Neptune's spectrum, especially in the near-infrared, are strongly absorbed by methane in the planet's atmosphere, and because some spectral regions are unaffected by methane absorptions, various investigators have sought to define the rotation period of

Neptune from photometric observations using a color index that is defined on the basis of the planet's absorption spectrum. The strongest contrast between spectral regions of absorption and nonabsorption occurs in the near-infrared (1-3 μm), and Cruikshank (1978)[1] showed that Neptune exhibits a brightness change of at least 1 magnitude in the J-K color (1.25-2.2 μm). [One magnitude is a factor of 2.5 in brightness.] Using a set of observations obtained over a 56-day interval in 1977, Cruikshank found a best-fit period of 18.2 hours, but noted an apparent cycle-to-cycle variation superimposed on the presumed diurnal lightcurve (Figure 1).

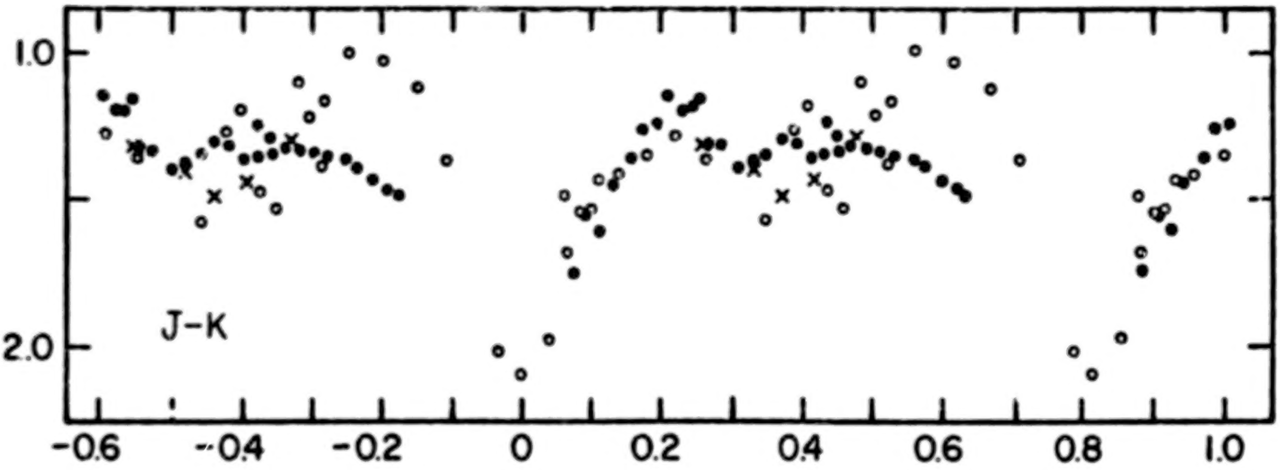

Fig. 1. J-K color of Neptune, 1977, plotted with a best-fit period of 18.2 hours. Crosses are data for period May 31-June 1; open circles, for July 11-14; and filled circles for July 23-25. From Cruikshank (1978),[1] reproduced from The Astrophysical Journal.

The near-infrared photometry was repeated by Brown *et al.* (1981),[2] who found a more uniform lightcurve in a four-day set of observations in 1980. Their lightcurve (Figure 2, upper panel) yields a rotation period of 17.73 ± 0.1 hours. Observing in the same year, Belton *et al.* (1981)[3] found the same

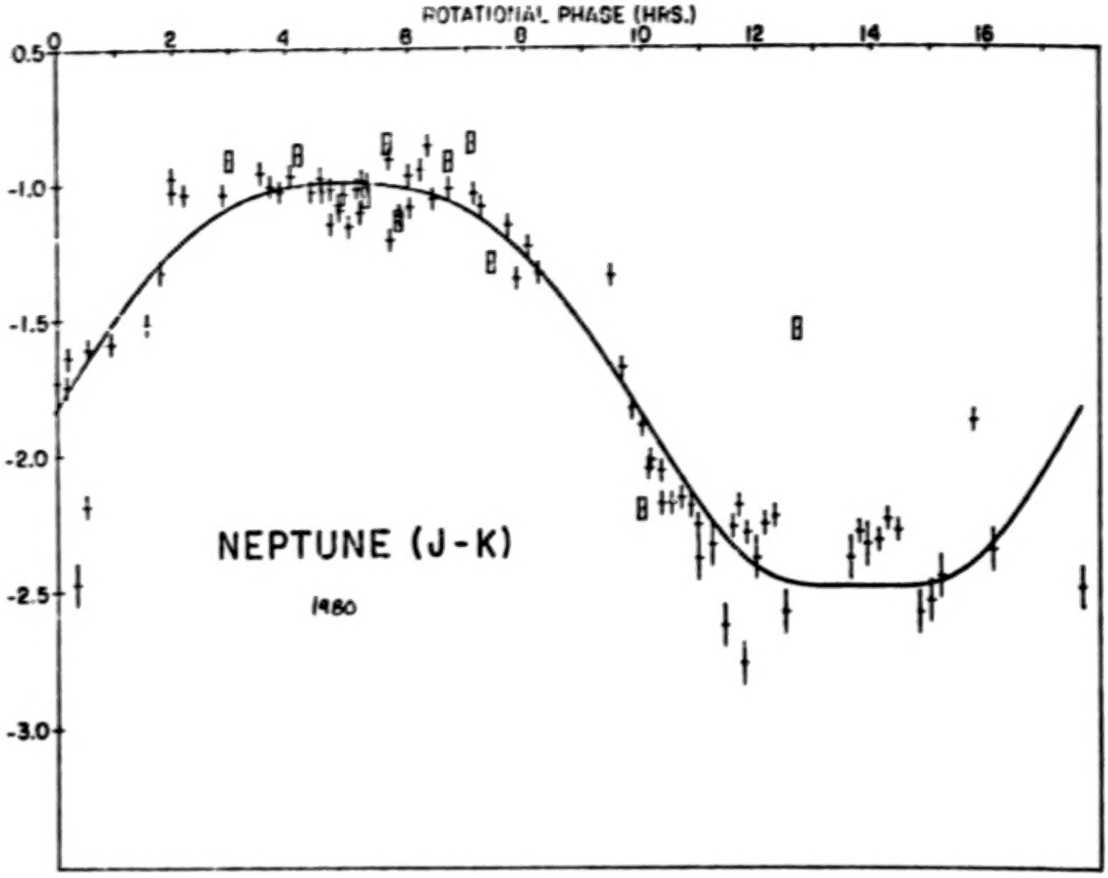
ROTATIONAL PHASE (HRS.)
0
2
4
6
8
10
12
14
16
0.5
-1.0
-1.5
-2.0
-2.5
-3.0
NEPTUNE (J-K)
1980

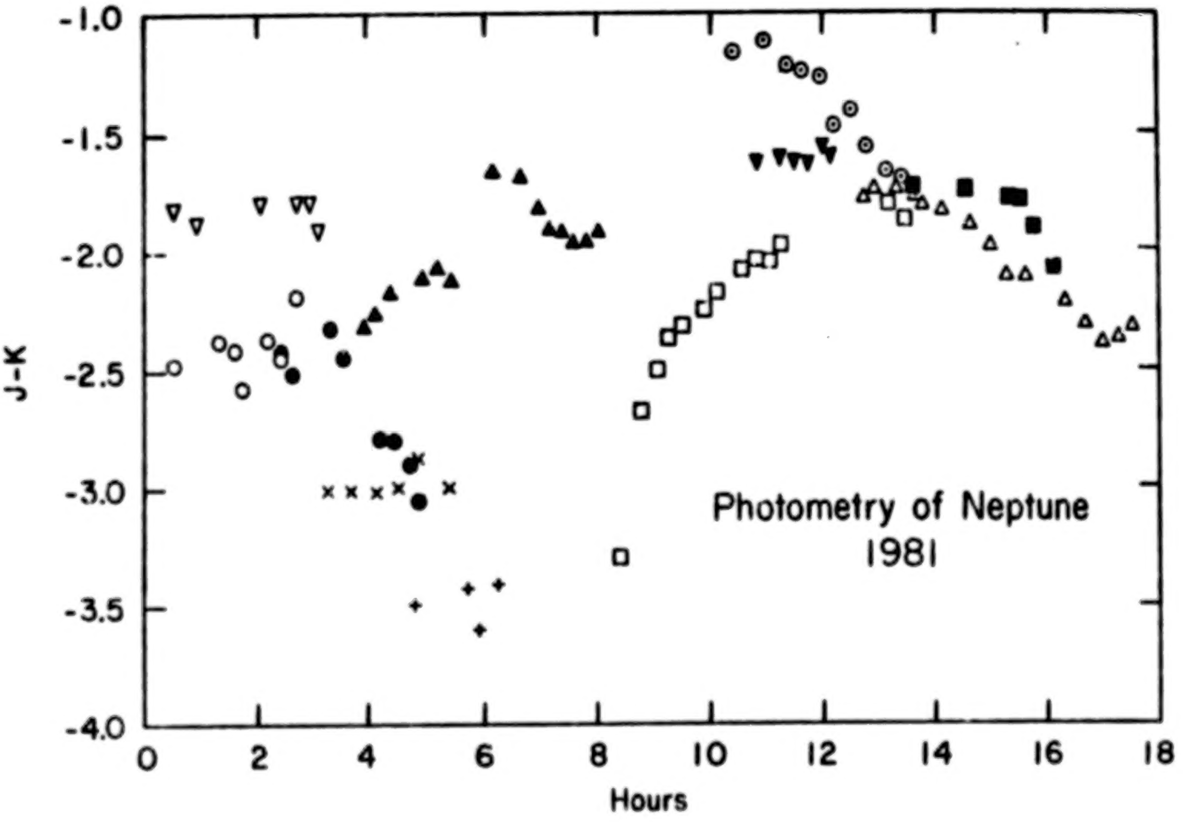
-1.0
-1.5
-2.0
-2.5
-3.0
-3.5
-4.0
J-K
0
2
4
6
8
10
12
14
16
18
Hours
Photometry of Neptune
1981

period, but identified two additional fundamental periods (18.56 and 19.29 hours) in their larger data set (which included the Brown et al. data). Belton et al. suggested that all three fundamental periods are real, and they proposed that they reveal distinct zonal wind systems in Neptune's atmosphere. Golitsyn (1979)[4] had reached a similar conclusion about the presence of two fundamental periods in the 1977 Cruikshank data. With a Jupiter-like model of the zonal wind structure, they deduced a rotation period of 18.2 ± 0.4 hours for the body of the planet. At levels somewhat deeper in the Neptune atmosphere, where the weaker CH_4 bands are formed, the photometrically determined rotation period is 18.44 ± 0.01 hours (Slavsky and Smith 1978).[5]

Thus, planet-wide inhomogeneities in the atmosphere, when stable, permit the observation of Neptune's diurnal period. The stability time for the Brown et al. and Belton et al. observations was on the order of several days.

2. Day-to-Day Variations in the Atmosphere. The observations of Brown et al. (1982)[2] and Belton et al. (1981)[3] cited above succeeded because there was during the observing period an inhomogeneity in Neptune's atmosphere that was stable for several days. It is the inhomogeneity, as modeled by Brown et al. (1981),[2] that gives the lightcurve in the first place, and it probably represents a nonuniform distribution of high-altitude haze.

The atmosphere of Neptune is not always stable in this sense, however, for attempts at further photometric observations in 1981 gave rather different

---

Fig. 2 (previous page). Upper panel: J-K photometry of Neptune, 1980, plotted with a period of 17.73 hours. Solid line is a model fit. From Brown et al. (1981),[2] reproduced from Icarus. Lower panel: J-K photometry of Neptune, 1981, plotted with the same period as the upper panel. Different symbols represent different nights of observations. Observations obtained by Robert R. Howell, Univ. of Hawaii.

results. The lower panel of Figure 2 shows the J-K lightcurve as observed by Robert R. Howell; various symbols represent sequences on various nights in April and June, all plotted with the 17.7-hour period determined from observations in the previous year. The range of variability is greater than in 1980, but the diural lightcurve is completely masked by other variations in brightness of Neptune that appear to be related to activity in the planet's atmosphere. This is the same kind of interruption of the diurnal lightcurve, though to a much greater degree, seen in the original Cruikshank data of 1977.*

3. Variability of Neptune with the Solar Cycle. Neptune has been observed at photovisual wavelengths for a number of years, together with Uranus and Titan, to monitor the stability of the solar flux. In 1979 Lockwood and Thompson[6] reported a significant anticorrelation between solar activity and the brightness of Titan and Neptune in the interval 1972-1978. Neptune brightened by about 4 %, as shown in Figure 3, in apparent synchronism with solar activity. The brightness of Neptune has been monitored since the publication of the original paper, and while it stabilized at approximately the 1978 level until early 1982, there is preliminary evidence that the brightness increased unexpectedly in 1983 (G. W. Lockwood, private communication, 1984).

The anticorrelation of Neptune's brightness with solar activity is not

---

*In the early 1980s, Neptune moved into the galactic plane, where there are countless diffuse and point infrared sources of radiation that are comparable in signal strength to the planet itself. This has increasingly complicated the photometric observations to the extent that after 1981 the project at the University of Hawaii was abandoned for several years until Neptune moves to a less crowded part of the sky. Dr. Howell's 1981 data were taken under these difficult circumstances, and to a small degree may be degraded by the unseen background sources, though every effort was made to ensure the purity of the signal from the planet. It is believed that most of the variations seen in the lower panel of Figure 2 represent the variation of Neptune itself.

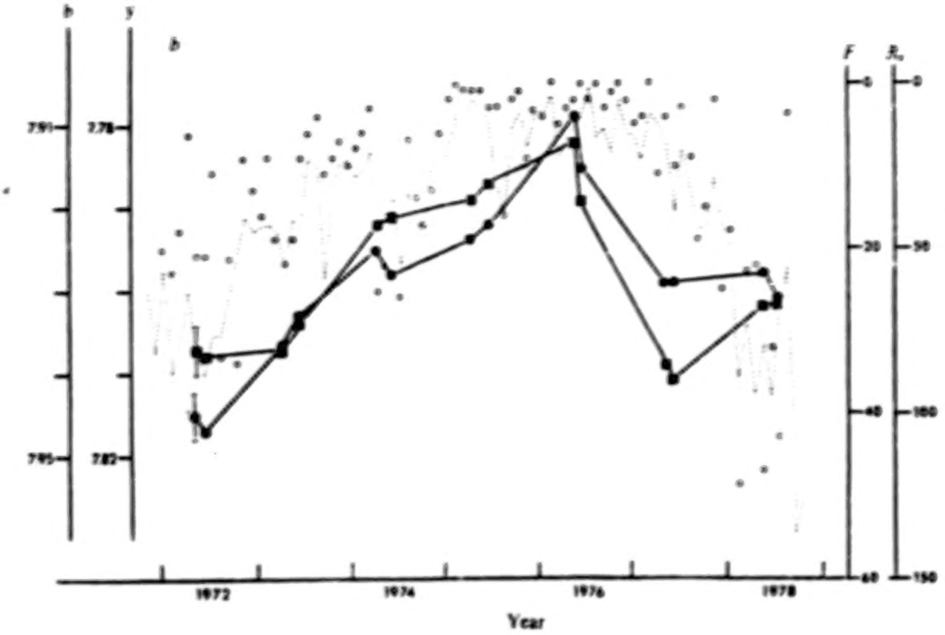

Fig. 3. Brightness of Neptune in the Stromgren b and y filter bands (large points and connecting lines) and indices of solar activity (R_z = monthly mean sunspost number, F = flare index). From Lockwood and Thompson (1979),[6] reproduced from Nature.

proven because of the relatively short interval of precise observations, but continued monitoring will help to establish if the particle or photo output of the sun affects the planet's upper atmosphere. In any event, the variability of Neptune's brightness on a time-scale of about 10 years appears established.

4. Outbursts. In March 1976, Richard Joyce discovered that Neptune was unexpectedly bright in the JHKL near-infrared filter bands in comparison with Uranus and with Neptune's brightness measured a year earlier. Continued monitoring of the photometric brightness showed a steady decrease over the next several months. A near-infrared spectrum of Neptune, the first ever obtained beyond 2.5 μm, showed that at the time of the maximum planetary brightness the

methane absorption bands were at minimum strength. This result is consistent with the interpretation that at the time of maximum brightness there was a haze of global extent in the planet's high atmosphere that limited the penetration depth of solar photons to an extent much greater than that during ambient conditions (Joyce et al.).[7] In a detailed study of the outburst, Pilcher (1977)[8] showed that the data could be satisfactorily accounted for with a model in which a cloud of unit or greater optical depth formed (perhaps by condensation) of particles at least 1 μm in diameter at high altitude in the atmosphere of Neptune. Eventual dissipation of the cloud by the settling of the particles to greater atmospheric depths slowly restored the infrared brightness of Neptune to its normal level. The time history of the photometry of this event is shown in Figure 4. Note, incidentally, that the peak in the Lockwood and Thompson curve correlates quite closely in time with the outburst reported by Joyce et al. The decay times of the two curves are also comparable, though the change in brightness in the photovisual light was only 1%, while that in the infrared was nearly a factor of two. One might speculate that the sudden rise in brightness in 1983 suspected by Lockwood (private communication, 1984) would also show as an infrared outburst, but there is no supporting evidence from the infrared observers.

While there was a suggestion by Apt et al. (1980)[9] that another outburst had been observed in April 1980, it is now thought that the flux of Neptune was contaminated with that of a strong background infrared source (R. N. Clark, private communication, 1982).

In any event, it appears that a major disturbance to the high atmosphere of Neptune has been observed, and that recovery took a few months. There is

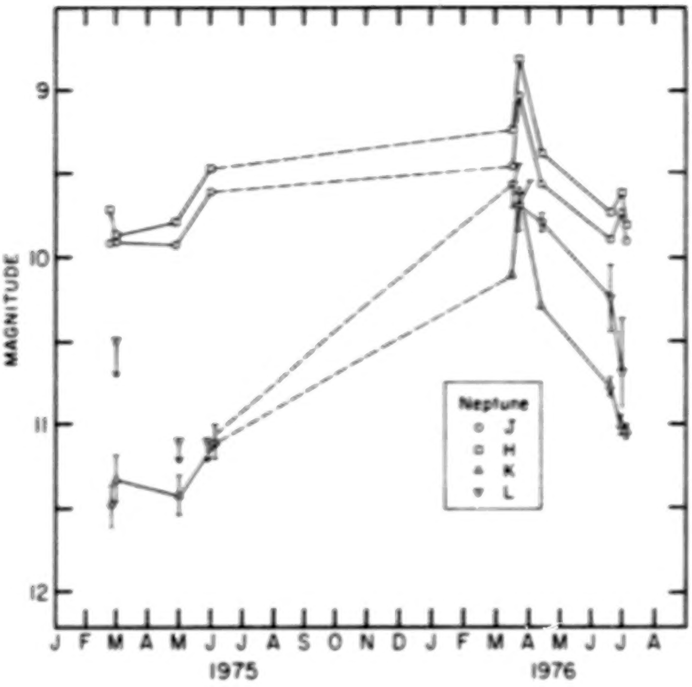

Fig. 4. Photometry of Neptune in the JHKL filter bands. From Joyce et al. (1977),[7] reproduced from The Astrophysical Journal.

no information on the frequency of these events, unless the 1983 photovisual brightening also signaled an infrared outburst, in which case the interval between the two events was seven years.

SUMMARY

The upper atmosphere of Neptune is variable with at least four characteristic time-scales. While stable global inhomogeneities in the high-altitude haze distribution allow the diurnal period to be observed, these inhomogeneities can be unstable on a time-scale of about 10 hours, thus obscuring the lightcurve. There is a long-term brightness change of Neptune that appears to be anticorrelated with solar activity, though only one full cycle has been observed so far. This low-amplitude variability is punctuated by occasional outbursts that have their greatest contrast in the near-infrared.

Theories of the dynamics of the atmosphere of Neptune must account for the observed changes outlined here. It is clear that additional ground-based observations will be useful in improving the definition of the variabilities in Neptune's photometric and spectroscopic properties.

This work was supported in part by NASA grant NGL 12-001-057. I thank Dr. G. W. Lockwood for advance information on his photometry, and Dr. R. R. Howell for permission to show his infrared data.

REFERENCES

1. Cruikshank, D. P. (1978). On the rotation period of Neptune. Astrophys. J. (Lett.) 220, L57-L59.
2. Brown, R. H., D. P. Cruikshank, and A. T. Tokunaga (1981). The rotation period of Neptune's upper atmosphere. Icarus 47, 159-165.
3. Belton, M. J. S., L. Wallace, and S. Howard (1981). The periods of Neptune: Evidence for atmospheric motions. Icarus 46, 263-274.
4. Golitsyn, G. S. (1979). Atmospheric dynamics on the outer planets and some of their satellites. Icarus 38, 333-341.
5. Slavsky, D., and H. J. Smith (1978). The rotation period of Neptune. Astrophys. J. 226, L49-L52.
6. Lockwood, G. W., and D. T. Thompson (1979). A relationship between solar activity and planetary albedos. Nature 280, 43-45.
7. Joyce, R. R., C. B. Pilcher, D. P. Cruikshank, and D. Morrison (1977). Evidence for weather on Neptune. I. Astrophys. J. 214, 657-662.
8. Pilcher, C. B. (1977). Evidence for weather on Neptune. II. Astrophys. J. 214, 663-666.
9. Apt, J., R. N. Clark, and R. B. Singer (1980). Photometric spectra of the elusive Neptune haze. Bull. Amer. Astron. Soc. 12, 705 (Abstract).

BLANK PAGE

288

PART III

Interior Structures Of Uranus And Neptune

BLANK PAGE

INTERIOR STRUCTURE OF URANUS

W. B. Hubbard

Department of Planetary Sciences
Lunar and Planetary Laboratory
University of Arizona
Tucson, Arizona 85721

Abstract

This paper discusses key measurements which are diagnostic of Uranus' interior structure and evolutionary history, and reviews their present status. Typical interior models have chondritic cores, but have the bulk of their mass in an envelope consisting of "ice"-component, principally H_2O. The total amount of free H_2 in the planet cannot exceed ∿ 1-2 earth masses. Measurements of the gravitational moments of Uranus are beginning to be accurate enough to constrain models, but are limited in utility by uncertainty in the rotation period. We discuss evidence that the outermost planetary layers have a gravitationally significant quantity of denser material ("ice"-component?) in addition to H_2 and He. The He/H ratio and the deuterium abundance in the atmosphere may be diagnostic of the planet's previous evolutionary history. It is argued that the planet's interior is likely to now be at a temperature $\sim 10^3$ °K. We compare Uranus' interior with Neptune's in a number of ways, considering heat flow, degree of internal differentiation, and possible magnetic field.

INTRODUCTION

Study of the interior structure of Uranus is still at a preliminary stage. A number of zeroth-order questions about the interior are still only partly answered at best. Such questions include the following:

(a) What is the bulk chemical composition of Uranus? How does it compare with the presumed primordial solar composition?

(b) What is the chemical composition of observable layers of Uranus? What does this tell us about the interior?

(c) To what degree is Uranus differentiated, and how does this compare with the other Jovian planets? What processes could lead to chemical differentiation of Uranus?

(d) What is the value of the globally-averaged heat flux for Uranus? What processes contribute to this heat flux? How are they related to the planet's formation processes? How are they related to the planet's interior and atmospheric dynamics? Does Uranus support a hydromagnetic dynamo?

We review the available answers to these questions in the following sections, and discuss future measurements which would be desirable for the purpose of providing better answers. It will also be useful to compare Uranus with the other Jovian planets in order to better understand the degree to which Uranus' interior can be included in a general conceptual framework. Attempts to construct such a framework have been partially successful, but some unresolved paradoxes still exist.

BULK COMPOSITION

Although the mass and radius of Uranus are now known to satisfactory accuracy for most purposes, these quantities alone only weakly constrain possible interior compositions. The mass of Uranus is taken as 14.51 M_E (M_E = earth mass).[1]

For purposes of modeling the interior, it is customary to define the planetary radius to be the equatorial radius of that level surface which is at a pressure of one bar. This choice is not altogether arbitrary because this portion of the atmosphere probably includes the troposphere and is readily incorporated as an extension of interior models with an adiabatic interior temperature distribution. An accurate measurement of the radius of the 1-bar level cannot be accurately obtained with presently available techniques. On the other hand, the 1-microbar level, which is detected during stellar occultation observed from the earth, is readily measured. Thus it is necessary to employ a model atmosphere to calculate the altitude difference between the two levels. This exercise yields a value of about 480 km, with some uncertainty due to lack of detailed knowledge of atmospheric structure. Applying this correction to the 1-microbar equatorial radius of a' = 26,145 ± 30 km,[2] one obtains an equatorial radius at one bar of a = 25,662 ± 60 km, where the error bars have been doubled to account for the probable uncertainty in atmospheric structure. The value of the polar radius at one bar, b, can be computed using the known oblateness:[2]

$$\varepsilon = (a - b)/a = 0.024 \pm 0.003, \qquad (1)$$

yielding b = 25046 ± 60 km.

Using these values, we can then plot Uranus on a plot of 1-bar equatorial radius vs. mass (Fig. 1), and compare it with the other Jovian planets and with theoretical curves (solid lines) for hydrostatic equilibrium objects having various chemical compositions and interior temperature distributions. The hydrogen-helium curve is computed for a solar-composition fluid mixture having an adiabatic temperature distribution starting at a temperature of 140 °K at 1 bar pressure. The segments marked with rotation periods just above this curve indicate its shifted position after one applies a rotation correction for Saturn and Jupiter respectively.

Corrections due to a finite interior temperature and finite rotation rate are comparable and significant for deducing the bulk composition of Jupiter and Saturn. However, the uncertainty in these corrections plays no role in reaching the conclusion that Uranus and Neptune differ markedly from bulk solar composition. The absence of a large hydrogen-rich envelope seems to be the principal feature of Uranus and Neptune which differentiates them from Jupiter and Saturn.

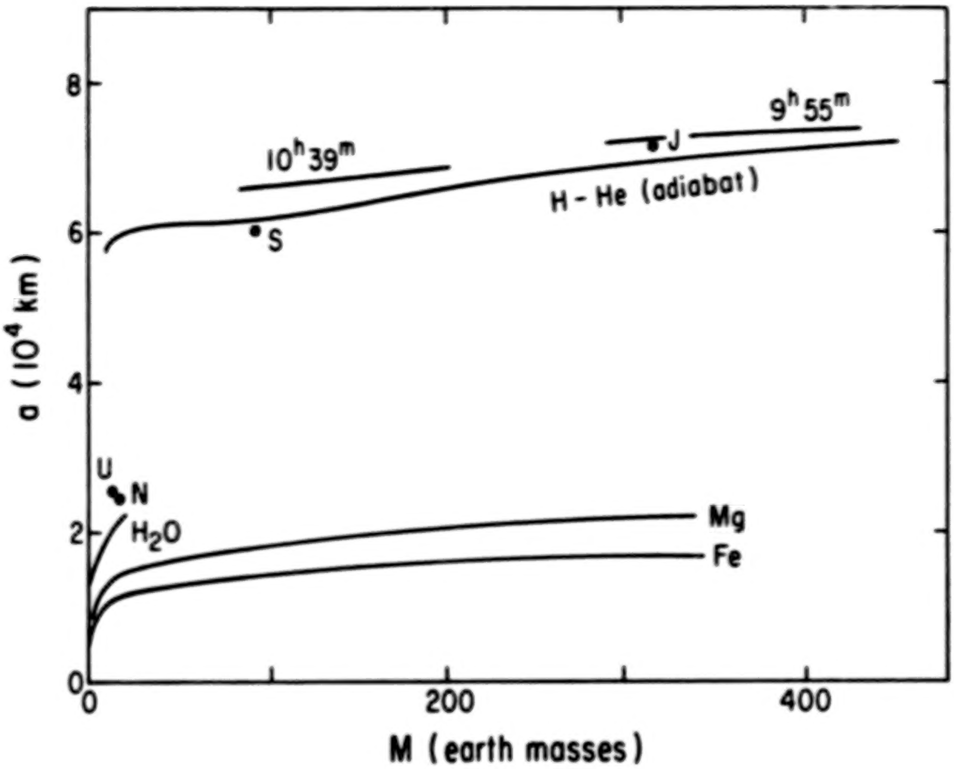

Fig. 1: Plot of equatorial radius at 1 bar pressure vs. planetary mass for the Jovian planets, compared with theoretical curves for a solar composition H-He mixture with an adiabatic temperature distribution, and curves for H_2O, magnesium, and iron.

Fig. 1 shows a radius-mass curve for water which is based on recent data[3] on shock compression of H_2O. The proximity of Uranus to this curve indicates that H_2O is a good candidate for a major chemical constituent of its interior, as would also be expected on the basis of the cosmic abundance of oxygen.

Table 1 presents selected data from a recent compilation of solar abundances (Anders and Ebihara 1982). This table includes those elements whose cosmic abundance is sufficiently large for them to be of potential significance in the bulk composition of Uranus. We also include the principal elements responsible for radioactive heating. One of our main tasks is to determine whether the relative proportions of any of these groups are preserved in Uranus.

TABLE 1

Solar abundances of selected elements

Derived from Cl chondrites and astronomical data*
(from Anders and Ebihara[4])

element	component	number/H	mass fraction
H	G	1	0.744
He	G	0.080	0.237
C	I,G?	4.412E-04	3.912E-03
N	I,G?	9.081E-05	9.389E-04
O	I,G?	7.390E-04	8.725E-03
Ne	G	1.283E-04	1.910E-03
Mg	R	3.934E-05	7.058E-04
Si	R	3.676E-05	7.621E-04
S	I,R?	1.892E-05	4.477E-04
Ar	I?	3.824E-06	1.127E-04
K	R	1.386E-07	4.000E-06
Fe	R	3.310E-05	1.364E-03
Th (present)	R	1.232E-12	2.110E-10
Th (primordial)	R	1.544E-12	2.645E-10
U (present)	R	3.311E-13	5.816E-11
U (primordial)	R	8.761E-13	1.539E-10

*The number of significant figures given is for the sake of numerical consistency and does not necessarily reflect the accuracy of the determination.

The number of independent parameters of a Uranus interior model would greatly exceed the number of constraints if each of the relative abundances in Table 1 were separately adjustable. It is therefore convenient to group the most abundant elements into three main classes: gas (G), ice (I), and chondritic or "rock" (R).[5] These classifications reflect the presumed phase of the component under primordial solar nebula conditions when Uranus was forming, rather than its phase in the present planet. It is a reasonable (but debatable) procedure to assume that solar proportions of elements are preserved in Uranus within each of the three main classes (G,I,R), although not necessarily between the classes. We therefore assume that when Uranus formed, compounds which were in a condensed phase at the ambient temperatures and pressures were more readily incorporated in the primordial planet than those compounds which were still gaseous. Thus the G-group is defined to consist of those compounds which were gaseous at the time that Uranus formed, and which were therefore incorporated in the planet, if at all, only by relatively inefficient capture processes, or by secondary outgassing from condensates. The I-group comprises those compounds whose condensation temperatures lie close to the range of plausible ambient temperatures at the time of Uranus' formation. Relative abundances within this group in the planet would therefore depend somewhat sensitively on details of the planetary formation process, and might be diagnostic of the process. The R-group comprises the remaining compounds, principally magnesium silicates and iron, which would almost certainly have been fully condensed at the time of Uranus' formation.

According to calculations for thermodynamic equilibrium conditions in the presumed primordial solar nebula,[6] the G-component would consist primarily of H_2 and He, while the I-component would consist of H_2O, CH_4, and NH_3. The G-component would never condense under plausible nebular conditions. The I-component condenses over temperatures ranging from about 160 °K to ∿ 60 °K, and the major constituents of the R-component condense in the temperature range ∿1500 - 1400 °K. Since the three components have such widely-separated condensation ranges, the simplest model for the bulk composition of Uranus suggests itself: Let the planet have an undepleted core of R-component, and assume that the I-component is also present in solar proportions. Only the G-component is depleted, and is present as a relatively thin envelope.

The mass ratio of ice to rock (I/R) in Uranus is readily calculated for the above assumptions, using the data of Table 1. The result is $I/R = 3.5$. This is the largest possible value of I/R; smaller values would be expected for plausible formation scenarios which differ from the one assumed above. For example, ammonia and methane are substantially more volatile than H_2O, and could have been primarily in the G-component at the time of planetary formation. If this is so, the planet's bulk composition should correspond to $I/R = 2.0$.

The value of I/R in Uranus could be even lower if a suggestion of Lewis and Prinn[7] proves to be correct. According to the latter, under the low-pressure conditions of the primordial solar nebula, the major carbon-, nitrogen-, and oxygen-bearing species will be CO, N_2, and H_2O at high temperatures, converting to CH_4, N_2, and H_2O at intermediate temperatures, and finally to CH_4, NH_3, and H_2O at low temperatures. But because of kinetic inhibition of reaction rates, the high-temperature species may not reequilibrate at low temperatures, so that the primordial Uranus possibly formed from material containing H_2, He, N_2, and CO in the G-component and H_2O as the only significant member of the I-component. This would have major repercussions on the I/R value since CO then ties considerably up more than half of the available oxygen (see Table 1), greatly reducing the amount of H_2O which can be formed.[8] In this limit, I/R = 0.6.

In summary, the mass and radius of Uranus imply that only a minor amount of G-component is present in the planet. But the I/R ratio is not constrained by the mass and radius alone, and is only weakly constrained by cosmogonical/chemical considerations. In following sections we will present further observational constraints on the relative amounts of G, I, and R in Uranus.

ATMOSPHERIC ABUNDANCES: IMPLICATIONS FOR INTERIOR STRUCTURE

The atmosphere of Uranus seems to be predominantly composed of H_2 gas,[9] and it is customary to assume that this atmosphere corresponds to the same G-component atmosphere that we see in Jupiter and Saturn, i.e., that it represents a captured remnant of the primordial solar nebula, although much reduced in mass. As discussed below, however, some now-unknown fraction of this atmosphere might be of a different origin.

One of the principal puzzles in understanding the abundance of other constituents in Uranus' atmosphere is that the CH_4/H_2 number ratio seems to be substantially enhanced relative to solar composition, while the NH_3/H_2 ratio may be depleted. According to Wallace, the CH_4/H_2 number ratio is between about 10 and 100 times solar.[10] This could be a gravitationally significant enhancement if it extends throughout the hydrogen-rich envelope; it corresponds to a methane mass fraction ranging from about 7% up to about 40%. The latter figure could have implications for the external gravity field. We will consider evidence for this in the following section.

It is not easy to understand why NH_3 is depleted. According to Gulkis et al.,[11] ammonia is depleted in the outer layers of Uranus by at least two orders of magnitude relative to solar abundance. As ammonia is less volatile than methane, this presumably does not reflect an interrupted primordial condensation sequence. Gulkis et al.[11] suggest that ammonia could be depleted by the reaction $NH_3 + H_2S \dashrightarrow NH_4SH$, but as is evident from Table 1, this process requires about a fivefold enhancement of sulfur to begin with if it is to go to completion. However, as pointed out by Lewis and Prinn[7] and further discussed by Podolak and Reynolds,[8] a nonequilibrium solar nebula with most of the nitrogen in the form of N_2 could produce a primordial Uranus with very little NH_3, virtually all of which would be converted into NH_4SH. But this hypothesis has further implications for the bulk I/R ratio in the planet, which we discuss in the following section.

Deuterium abundances in a Jovian planet could in principle be used to confirm bulk I-component abundances in the body of the planet.[12] According to equilibrium chemistry, at temperatures low enough to condense the I-component (< 200°K), the deuterium/hydrogen number ratio in the I-condensate will exceed by at least one order of magnitude the D/H ratio in the primordial solar-composition gas from which the condensate forms. This phenomenon arises because of a rather delicate difference between the binding energy of a deuteron in an HD molecule on the one hand and in an HDO, CH_3D, or NH_2D

molecule on the other. The deuteron is somewhat more tightly bound in the latter than in the former, and the small energy difference becomes thermodynamically significant in the temperature range where the I-component condenses. Thus, if equilibrium can be attained, the I-component in Uranus or Neptune will have a D/H ratio which greatly exceeds the primordial ratio of about 2×10^{-5}. After the deuterium reequilibrates with the thin hydrogen-rich atmosphere (and there is certainly plenty of time available for it to do so), the atmosphere should reflect an enhanced D/H ratio. For an interior with significant amounts of I-component (several earth masses), and an atmosphere with only one or two earth masses of hydrogen (the most permitted by the mean density), one then expects to see an atmospheric D/H ratio greater than $\sim 10^{-4}$. But the observed values in Uranus' atmosphere are[13,14] $(3 \pm 1.2) \times 10^{-5}$ and $(4.8 \pm 1.5) \times 10^{-5}$, not significantly different from values for Jupiter and Saturn.

There are three possible interpretations of the observed deuterium abundance in Uranus' atmosphere. First, it is quite plausible that the deuterium concentration never comes to thermodynamic equilibrium at the low temperatures where the I-component condenses. Second, Uranus may be so inactive that the atmosphere never reequilibrates with the interior (this seems most unlikely). The third possibility is that Uranus may have initially had a hydrogen-rich envelope comparable in mass to that of Jupiter or Saturn, but that most of this envelope was somehow dispersed following formation of an I-rich core.

A definitive, more accurate, measurement of the D/H ratio in the atmosphere of Uranus (and Neptune as well) is needed in order to help resolve the questions outlined above.

As we will discuss below, a definitive measurement of the He/H ratio in Uranus' atmosphere will also be diagnostic of interior structure and evolutionary processes.

DEGREE OF DIFFERENTIATION

A further diagnostic of the bulk chemical composition of Uranus is obtained by considering the relative mass distribution in its interior. This distribution is constrained by the zonal harmonic coefficients of the planet's external gravitational potential:

$$V = (GM/r)[1 - \sum_{\ell=1}^{\infty} J_{2\ell}\,(a_G/r)^{2\ell}\,P_{2\ell}\,(\cos\theta)], \tag{2}$$

where G is the gravitational constant, M is the mass, r is the distance from the planet's center of mass, $J_{2\ell}$ are the dimensionless zonal harmonic coefficients (whose value depends on the choice of normalizing radius a_G), $P_{2\ell}$ $(\cos\theta)$ are the even Legendre polynomials, and θ is the colatitude, or angular distance from the rotation axis. If the planet is in exact hydrostatic equilibrium, probably a valid assumption (at least for the low-degree harmonics) considering Uranus' likely composition and interior temperatures, then the planet's interior structure is characterized by a set of response coefficients:

$$\begin{aligned} J_2 &= \Lambda_{2,0}q + \Lambda_{2,1}q^2 + \ldots, \\ -J_4 &= \Lambda_{4,0}q^2 + \Lambda_{4,1}q^3 + \ldots, \\ &\text{etc.,} \end{aligned} \tag{3}$$

where

$$q = \omega^2 a_G{}^3/GM, \tag{4}$$

and ω is the planet's angular rotation rate.[5] Elliot[2] derives a rotation period of 15.5 ± 1.3 h from Uranus' figure as measured by occultation, while Goody[15] finds a rotation period of 16.31 ± 0.27 h from a weighted mean of all available data. Using the customary choice $a_G = 26{,}200$ km, we obtain $q = 0.0394\ (+0.0075, -0.0059)$ from the former and $q = 0.0355 \pm 0.0011$ from the latter. Elliot[2] finds $J_2 = (3.352 \pm 0.006) \times 10^{-3}$ and $J_4 = (-2.9 \pm 1.3) \times 10^{-5}$ using a_G as defined above, while Nicholson et al.[1] give $J_2 = (3.347 \pm 0.008) \times 10^{-3}$ and $J_4 = (-3.6 \pm 1.2) \times 10^{-5}$. In the absence of a varying rotation rate, we cannot determine all of the coefficients in expansions (3). Assuming that $q \ll 1$, we define Λ_2 to be an estimate of the initial coefficient $\Lambda_{2,0}$, etc. (accurate calculation of interior models takes the full expansion into account):

$$\Lambda_2 \simeq J_2/q \tag{5}$$

and

$$\Lambda_4 \simeq -J_4/q^2, \tag{6}$$

the above results give

$$\Lambda_2 = 0.089 \pm 0.011, \tag{7}$$

and

$$\Lambda_4 \sim 0.03. \tag{8}$$

The value of Λ_2 is related to the dimensionless moment of inertia factor C/Ma^2, where C is the polar moment of inertia, to the extent that the Radau-Darwin approximation is valid. Thus the smaller the value of Λ_2, the more centrally-condensed is the relative planetary density distribution (a uniform-density sphere has $\Lambda_{2,0} = 0.5$, while a polytrope of index one, a good approximation to Jupiter, has $\Lambda_{2,0} = 0.173$). Table 2 gives a summary of values of Λ_2 for the Jovian planets. The value given for Neptune is based upon a new occultation determination of the planet's oblateness[16] and a corresponding determination of Neptune's q = 0.038 ± 0.013 and a rotation period of 13.7 h (+3.2 h, -1.9 h). The value of Neptune's J_2 is also uncertain by about 10%, which contributes to the sizable error bars on Λ_2.

TABLE 2

Approximate second-degree response coefficients for the Jovian planets.

Planet	Λ_2
Jupiter	0.166
Saturn	0.108
Uranus	0.089 ± 0.011
Neptune	0.10 (+0.07,-0.03)

Note that if Neptune's rotation period were taken to be equal to 18 h or greater[17,18,19], the corresponding Λ_2 for Neptune would equal 0.20 or greater, making this planet's interior structure grossly dissimilar to that of Uranus or any other Jovian planet.

According to Table 2, a "typical" second-degree response coefficient for the Jovian planets has a value of about 0.1. Based on our current understanding of the interior structure of Jupiter and Saturn, the relatively large value for Jupiter occurs because about 90-95% of this planet's mass comprises an approximately-solar envelope, whose gradual increase in density toward the center of the planet under self-compression dominates the density profile and corresponding moment of inertia. The Jovian core, while comparable in mass to the entire mass of Uranus or Neptune,[20] plays a subordinate role in this density profile.

In Saturn we find a much more significant core (about 20% of the total planetary mass[20]), which leads to a substantially smaller value of Λ_2. Since Uranus and possibly Neptune have similar values of this parameter, one class of acceptable models for their interior structure would be those with density distributions homologous to Saturn's.

It is suggestive that both Jupiter and Saturn have deduced "core" (i.e., R- and I- component) masses of about 15-30 M_E. This is about the same as the total mass of Uranus or Neptune, and may imply that Jupiter and Saturn can be regarded as objects similar to Uranus or Neptune, but "clothed" with extensive envelopes of G-component material.

Successful models of Jupiter and Saturn can be constructed along the following lines. We start with an inner core of R-component material, and an outer core of I-component. The two components are presumed to be differentiated because of their greatly differing volatilities and melting points at high pressures.[21] Actually, this hardly matters in Jupiter or Saturn because the core structure is not significantly expressed in the external gravity expansion. The composite core is then overlain with an extensive G-component envelope, which may be slightly enriched with CH_4 and possibly H_2O relative to solar composition.

It turns out that such a three-layer model does not work for Uranus.

Such a highly-differentiated structure is too centrally condensed, for it predicts $\Lambda_2 = 0.067$. The point is illustrated in Fig. 2, which exhibits properties of interior models[22] in terms of the two observable parameters J_2 and ϵ. A model with given Λ_2 plots as a straight line on this diagram with slope $(3+\Lambda_2^{-1})/2$. Hydrostatic equilibrium imposes another linear relationship between ϵ and J_2 for a fixed rotation period (dashed lines). The observed value of J_2 and two slightly different values[23,2] of ϵ are indicated on this figure, along with Hubbard and MacFarlane's[24] three-layer model, described above. The figure also shows both Zharkov and Trubitsyn's[5] original two-layer model (Z + T), and a version modified for an improved H_2O equation of state (2-layer). Finally, the figure shows a modified three-layer model "dense atmosphere" in which the I/R ratio remains approximately solar in the inner two layers, but the outermost hydrogenic layer is nearly 50% methane (or some other I-component) by mass.[25] The latter two models are consistent with the observational constraints on oblateness and J_2.

For comparison, Fig. 3 shows a similar plot for Neptune. Two of the models shown (H + M, Z + T), are analogous to the corresponding ones for Uranus. The model marked "no ice" is calculated assuming that Neptune contains only an R-component core and a G-component envelope. It is clearly inconsistent with the data points, which show Neptune's oblateness determined by Hubbard et al.[16] and an earlier result from Kovalevsky and Link.[26]

Data on J_2 and ϵ appear to rule out interior models for both Uranus and Neptune in which the I/R ratio is low compared with chemical-equilibrium cosmic proportions. This result is confirmed by further studies which take into account the weak constraint imposed by the observed value of Uranus' J_4

term. Studies of two- and three-layer Uranus models[8] find that a rotation period of 16 h can be accommodated within other constraints only by a three-layer model analogous to that of Hubbard and MacFarlane[24], but with an I/R ration of ≈ 3.0 (Hubbard and MacFarlane used I/R = 2.7). However, such a model has J_4 near the upper limit of observation: $J_4 = -5 \times 10^{-5}$.

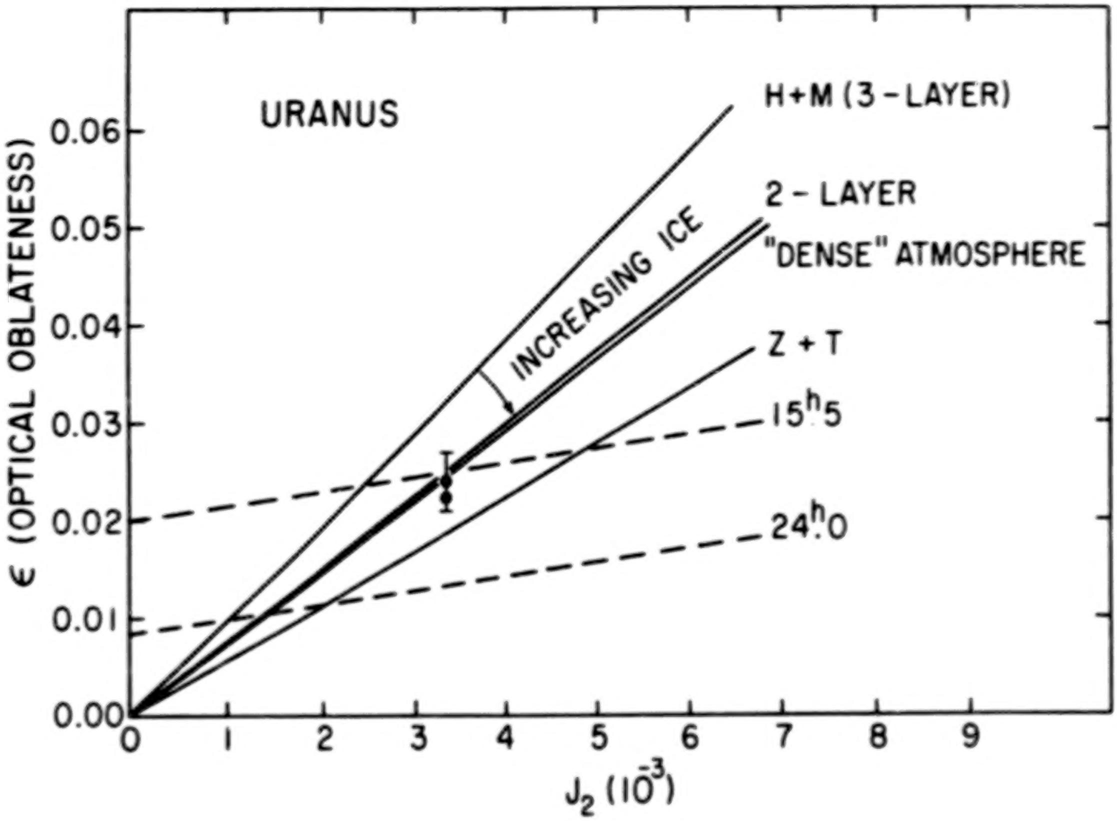

Fig. 2: Oblateness vs. J_2 for several Uranus models (from MacFarlane and Hubbard, "Internal Structure of Uranus", in *Uranus and the Outer Planets* (ed. G. Hunt), Cambridge Univ. Press, 1982.

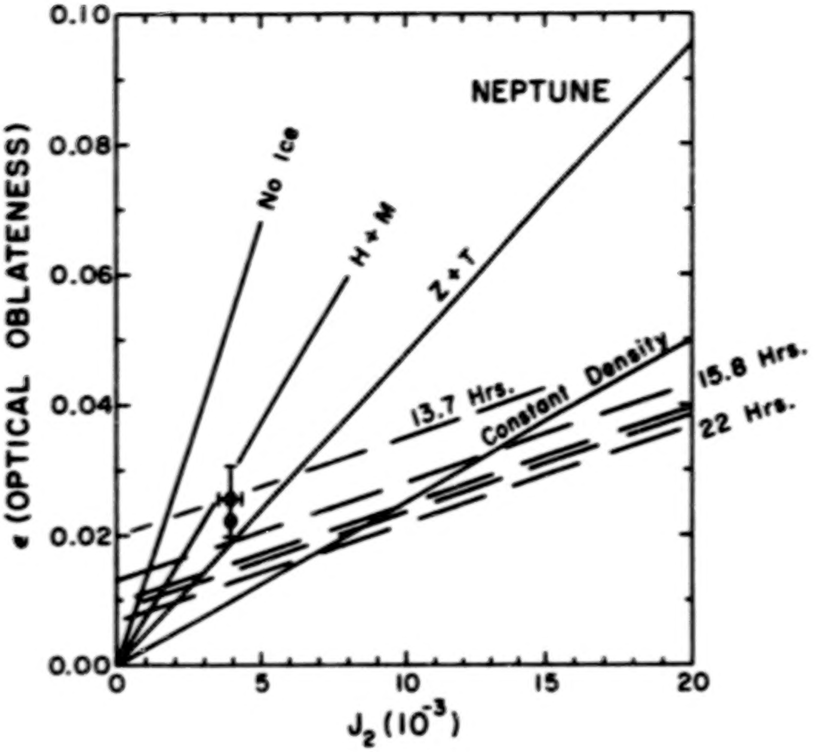

Fig. 3: Oblateness vs. J_2 for Neptune models. The upper data point is from Hubbard *et al.*,[16] while the lower data point is from Kovalevsky and Link.[26]

The most recent study of the problem of Uranus' gravity field[27] has applied an automatic model-fitting procedure[20] to Uranus models. In one class of models, the planet has an R-component core with a fixed pressure-density, and a single envelope with a polytropic equation of state of the form

$$P = K\rho^{\,1+1/n}, \qquad (9)$$

where P is the pressure, ρ is the mass density, and K and n are the polytropic constant and index respectively. The model-fitting procedure adjusts the core mass and K and n in order to obtain agreement with the gravitational constraints.

The results of this study are roughly consistent with those of Podolak and Reynolds.[8] First, with a rotation period of 16.3 h, a converged model is found only if $|J_4|$ is near its upper limit of 5×10^{-5}. Further, the rock core mass is 6.2 M_E (43% of the total mass). The polytropic constant for the envelope is $K = 0.518$ (for P in Mbar and ρ in g/cm^3), and $n = 0.450$. The resulting empirical envelope pressure-density relation is shown in Fig. 4 (solid line), along with the pressure-density relation for one of Hubbard and MacFarlane's three-layer models[24] (dashed lines). The empirical relationship emphasizes the earlier result of MacFarlane and Hubbard:[25] an acceptable model seems to demand that the G- and I-layers in Uranus be mixed together to a considerable extent, which forces the value of Λ_2 to increase. Using the additive volume mixing law, the empirical pressure-density relation shown in Fig. 4 implies that the G-I envelope of Uranus is about two-thirds I-component and about one-third G-component. Thus, very roughly, the overall composition of Uranus would be about 43% R, 38% I, and 19% G, leading to I/R = 0.9.

It should be emphasized that modeling studies of Uranus' interior differentiation via gravitational field constraints do not yet accurately define the bulk value of I/R in the planet. Nevertheless, it appears highly unlikely that this ratio could be substantially smaller than 1.0. There is little evidence that I/R could be as small as 0.6, as would be implied by the nonequilibrium condensation chemistry proposed by Lewis and Prinn.[7,8] There is some evidence that the outermost layers of both Uranus and Neptune have a substantial mass fraction of I-component in addition to pure G-component.

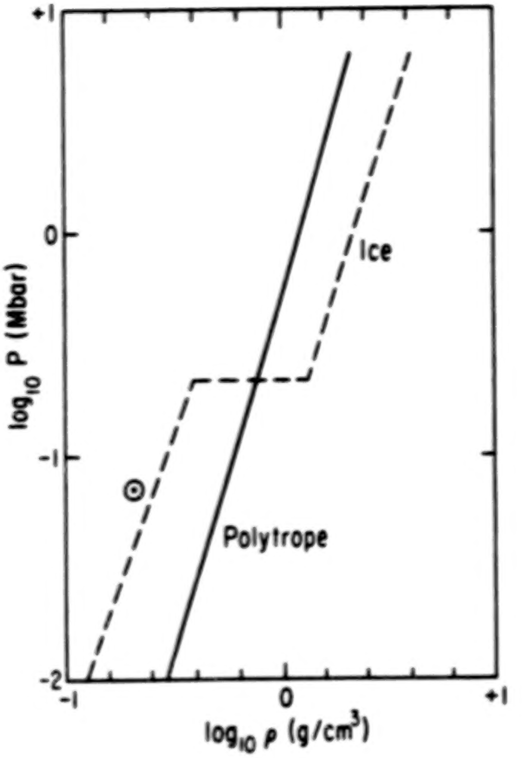

Fig. 4: Pressure-density relations in Uranus' envelope. Dashed curve: pressure-density relation in a model with a deep, adiabatic solar-composition atmosphere over an I-component layer. Solid curve: polytropic relation found by automatic model-fitting procedure.

Although ground-based measurements of Uranus' bulk rotation period now seem to be converging on ∿ 16 h, the uncertainty is still substantial, and is likely to be the limiting factor in applying improved measurements of Uranus' J_4 to constrain interior models (without a correspondingly accurate value of q, an accurate value of J_{2n} is useless). A definitive measurement of the rotation period will therefore greatly enhance the value of future efforts to define Uranus' gravitational multipole moments via studies of ring motions. Experiments on the Voyager flyby which can contribute to this goal are important.

HEAT FLUX

Table 3 presents heat flow data for various solar system objects. In this table, T_e is the observed overall effective temperature of the body, which is the temperature of a blackbody of the same surface area which radiates an equal amount of power integrated over the thermal infrared. T_s is the effective temperature that the object would have were it merely reradiating absorbed solar energy. H_i is the intrinsic surface heat flux, i.e., the total surface heat flux less the contribution from thermalized sunlight. Finally, L_i/M is the specific luminosity of the body, or the average internal power per gram of material.

Several different internal power mechanisms are represented in Table 3. The sun's source of power is thermonuclear fusion; this mechanism cannot be important in any planet. Radioactive heating is important in chondritic material, and its present value is indicated in Table 3. We will consider the possible significance of this source in the R-component core of Uranus. Tidal dissipation appears to be a dominant source of heating in Io, but cannot be significant in Uranus because of the small size of its satellites. Jupiter's heat flow is primarily derived from cooling of its interior.[37,38,39] Much of Saturn's heat flow is likewise derived from such a cooling process, although gravitational unmixing of helium may also be an important contributor.[40,41]

Uranus is the only Jovian planet whose intrinsic heat flow has not yet been detected. We will now review the possible importance in Uranus of the mechanisms listed above, and the implications of the nondetection of a Uranian heat flow for such mechanisms.

TABLE 3

Heat flow parameters for some solar system objects.

Object	T_e (°K)	T_s (°K)	H_i (erg/cm^2/s)	L_i/M (erg/g/s)
Sun[28]	5770		6.2×10^{10}	1.9
carbonaceous chondrite[29]				4×10^{-8}
Earth[30]		246	62	5.3×10^{-8}
Moon[31]		274	17	8.7×10^{-8}
Jupiter[32]	124.4 ± 0.3	109.5 ± 1.6	5400 ± 400	1.7×10^{-6}
Io[33]	106 ± 1	100	1500 ± 300	6.7×10^{-6}
Saturn[34]	95.0 ± 0.4	82.5 ± 1.3	2000 ± 140	1.5×10^{-6}
Uranus[35]	58 ± 2	57	<180	$<2 \times 10^{-7}$
Neptune[36]	55.5 ± 2	46	285	2×10^{-7}

Radioactive heating can have only marginal importance in the energetics of Uranus or Neptune. Assuming chondritic composition for the R-component, the specific luminosity of the rocky core as a function of time t is given very approximately by

$$L_i/M = 3 \times 10^{-7} \exp(-t/\tau) \text{ erg/g/s}, \tag{10}$$

where t is the time since the origin of Uranus and $\tau = 1.88 \times 10^9$ years, which is the decay time constant for ^{40}K, assumed to be the dominant contributor to radioactive heating. Averaging eq. (10) over the age of the solar system and over the entire mass of Uranus, we find that the planet has received an average radioactive heat input of 2.39×10^{21} erg/s, which would correspond to an average surface heat flux $H_i \simeq 30$ erg/cm^2/s, well below the detection threshold given in Table 3. The total amount of radioactive heating over the age of the solar system could have raised the average interior temperature by only a few hundred °K.

Nevertheless, it is likely that the average interior temperature of Uranus (or Neptune) is on the order of several thousand °K. The gravitational binding energy of the planet is on the order of 10^{41} erg. A moderately efficient process of planetary accumulation and heating could transform a significant fraction of this energy into thermal energy, since the average temperature equivalent to the gravitational binding energy would be about 10^5 °K. The collapse of a G-component envelope onto an ice-rock nucleus may also be an important step in the heating of the planet's interior, because adiabatic compression of hydrogen from a pressure of $\sim$ 1 bar and a temperature $\sim$ 80 °K to a pressure $\sim$ 200 Kbar can produce a final temperature $\sim$ 2000 °K.

The simplest "hot" model of the interior of Uranus or Neptune has an adiabatic temperature distribution.[42] This model proceeds by considering the points stated above, and by noting that the thermal diffusivity of "icy" material is so low that very little primordially-stored heat could escape from a Uranus-sized object over the age of the solar system.

It is possible to calculate models for the thermal evolution of Uranus or Neptune if we assume that an adiabatic temperature profile is maintained in the planet as it evolves. Thermal evolution could proceed in this manner if the planet's interior behaves like the interior of Jupiter, that is, if it is liquid and transports heat by efficient convection. However, it should be emphasized that this model is assumed for purposes of convenience, because it short-circuits the need to know interior transport coefficients, and not because it has been justified by fundamental calculations.

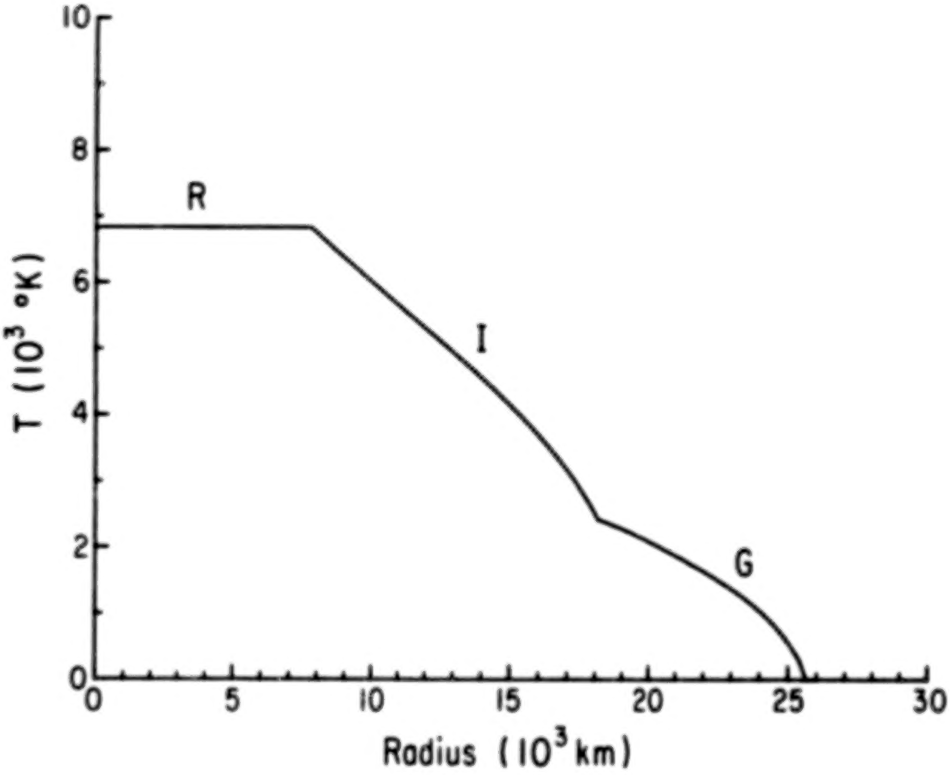

Fig. 5: Temperature distribution in a Uranus interior model. The temperature is assumed to follow an adiabatic lapse rate within the G-component and I-component layers, and to be isothermal in the R-component core.

Fig. 5 shows the present temperature distribution in a three-layer Uranus model, calculated under the assumption that the interior temperature follows a piecewise-continuous adiabat from the one-bar pressure level to the bottom of the "icy" layer. The "rocky" core is assumed to be isothermal. For such a temperature distribution, calculations[21] show that the I-component layer is likely to be liquid. The adiabatic temperature distribution shown in Fig. 5 probably represents an upper limit to temperatures in Uranus' envelope because convection would tend to level out a steeper temperature distribution.

The tidal Q values for Uranus and Neptune are quite large, larger than values $\sim 10^2$ which are frequently associated with solid layers in the terrestrial planets. This provides further evidence that their interiors are largely liquid. The limit is placed on Q by considering the satellite which could have undergone the greatest degree of tidal evolution, and requiring that that satellite be just outside the Roche limit at the time of origin of the solar system.[43] This argument then requires $Q \gtrsim 3 \times 10^5$ for Jupiter (ignoring possible additional constraints imposed by Io's heat flow) and $Q \gtrsim 3 \times 10^4$ for Saturn. The most stringent constraint on Uranus' Q so far comes from its satellite Ariel: $Q \gtrsim 5000$. The lower limit is substantially less than the lower limit for Jupiter or Saturn because of the smallness of Ariel. Interestingly, it may now be possible to place a more stringent limit on Neptune. Because Triton's orbit is retrograde, the existence of this satellite places no limits on Neptune's Q. However, the unconfirmed new satellite 1981N1 may do so if it is in a prograde, regular orbit at a distance of $\sim$ 3 Neptune radii.[44] Taking a mass of $\sim 6 \times 10^{21}$ g for this satellite, the Neptune Q is then constrained to be larger than 36,000.

Once an interior temperature distribution has been specified, it then becomes possible to calculate a Kelvin cooling time for the planet, and to determine whether a cooling model is consistent with observational constraints on the planetary heat flow. Fig. 6 shows results of calculations for three-layer models carried out by Hubbard and MacFarlane,[24] where the interior temperature distribution is assumed to be piecewise isentropic (as in Fig. 5), but where the starting temperature for the adiabat changes as a function of T_e, as specified by a model atmosphere solution for a specified net heat flux (interior + converted solar) through the effective planetary photosphere. At age zero (the present), the value of T_e is constrained to equal the observed value. Two values of T_s are shown for Uranus to demonstrate the sensitivity of the model to this parameter, while the solution for Neptune is less sensitive and uses the value of T_s given in Table 3.

The principal conclusion which we reach from Fig. 6 is that a Kelvin-type model for the heat flows of Uranus and Neptune encounters no apparent difficulties with regard to adequacy of stored thermal energy. That is, if enough I-component is present in the planet, then interior temperatures of several thousand °K correspond to enough thermal energy to allow the planet to radiate interior heat at the present rate (or at a somewhat higher rate in the past) for at least the age of the solar system. If enough I-component is present, that is, if the I/R value is on the order of 2.5 to 3, then primordial values of T_e and corresponding interior temperatures are only modestly higher than present values. This is because, with a relatively low molecular weight, the I-layer can store considerably more thermal energy than the R-layer. The mass of the G-layer is limited to a minor fraction of the total mass because of restrictions on the planetary mean density.

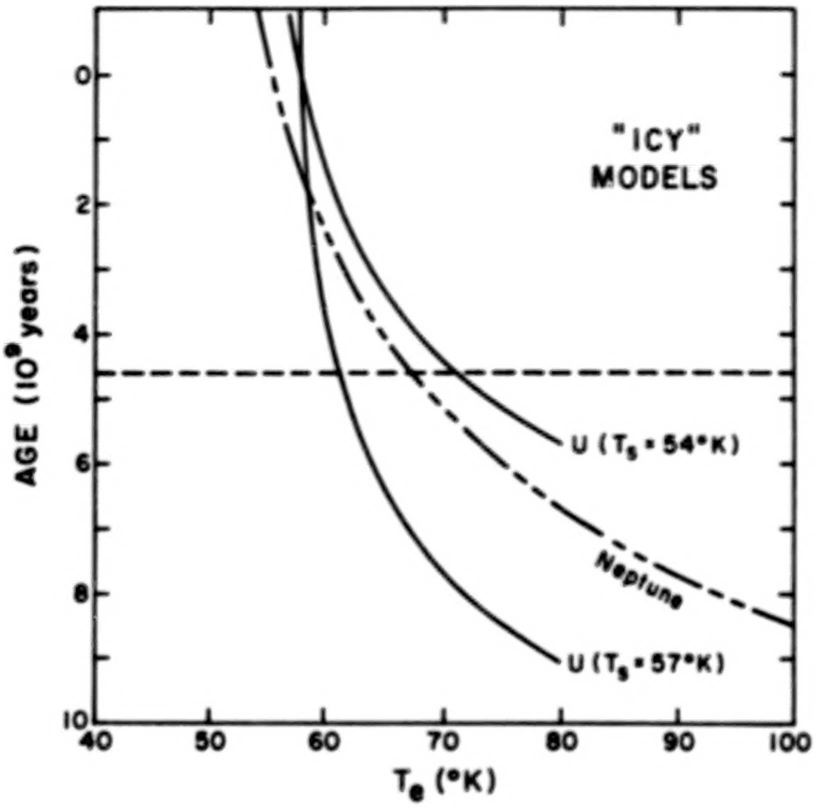

Fig. 6: Thermal histories of Uranus and Neptune models. Age zero is the present, and age 4.6×10^9 years (horizontal dashed line) corresponds to the beginning of evolution; thus models evolve from bottom to top. These are "icy" models, i.e., they contain about 50% H_2O by mass.

According to this model, the low intrinsic heat flux for Uranus compared with Neptune is attributable to Uranus' higher value of T_s. The interior of Uranus cools more slowly than the interior of Neptune, at the same temperature, because the heat delivered to the atmosphere from the interior of Uranus can be smaller and still satisfy the surface boundary condition.

We cannot completely rule out the possibility that Uranus or Neptune were formed at much higher interior temperatures and luminosities. If the mean heat capacity of the planet is reduced by reducing the amount of I-component, the evolutionary curves start out farther to the right, and cross the horizontal dashed line at higher values of T_e. If the I/R ratio in Neptune is reduced below unity, the model does not have enough heat capacity to continue radiating to the present. In this case, the evolutionary curve does not intersect the horizontal dashed line. This serves as an additional piece of evidence that Neptune (and presumably Uranus) contains a substantial mass fraction of I-component. But, by "fine-tuning" the heat capacity of Uranus and Neptune models to marginal values, it is possible to find models which asymptotically approach the horizontal dashed line (going backwards in time). Such models would resemble models for the early evolution of Jupiter[37,39] which postulate an early high-luminosity phase.

Other models for the luminosity of Uranus and Neptune need to be investigated. For example, it is possible that some type of gravitational separation may generate internal heat. According to Ross,[45] CH_4 may be pyrolized in the deep, hot layers of the envelope, producing solid carbon and H_2 gas. If methane is sufficiently abundant, the settling of the carbon might produce an energy source.

The principal evidence for this process comes from reflected shock experiments on initially-liquid methane.[46] At pressures on the order of 900 Kbar, methane seems to have a slightly lower density than would be predicted by a simple model of compressed, intact CH_4 molecules. Ross and Ree interpret this discrepancy as evidence that the methane is converted into molecular hydrogen and elemental carbon at pressures greater than ~ 200 Kbar. A pressure of 200 Kbar corresponds to a temperature of about 2500 °K in an adiabatic model of the G-component envelope of Uranus or Neptune. If the carbon can form macroscopic particles of precipitate (Ross suggests that the precipitate might be in the diamond phase), then an irreversible loss of carbon toward the center of the planet might proceed. Evidence from Uranus' gravity field (see earlier sections) may indicate that methane is concentrated in the outer layers of these planets, if anything, so this mechanism may not be operating. Of course, methane will be much more dilute in a hydrogen-rich envelope, which may result in the equilibrium being driven back toward stability of methane molecules. Quantitative calculations of this process are needed.

If decomposition of methane primarily depends on the temperature being sufficiently high to break the carbon-hydrogen bonds, then formation of precipitate will cost a certain amount of thermal energy. If the planet loses more thermal energy than it gains by formation of sinking precipitate, methane pyrolysis will shut itself off and the temperature will stabilize in the vicinity of the critical temperature. If the opposite is true, conceivably most of the planet's methane would be pyrolized, leaving only a small amount (possibly enriched relative to solar composition, however) in the outermost, cool layers. Interestingly, if a large amount of methane were originally present in Uranus or Neptune (say 3-4 earth masses), then nearly one earth mass of molecular hydrogen could be produced after complete decomposition. Thus a significant portion of the observed atmosphere might be of secondary origin, rather than derived from capture of primordial hydrogen in the solar nebula, as is evidently the case for Jupiter and Saturn. An obvious test of this rather speculative hypothesis can be made: an accurate measurement of the He/H ratio in the atmospheres of Uranus and Neptune would reveal whether their atmospheres have values similar to Jupiter's (in which case the hydrogen is captured), or much smaller (which would indicate secondary origin of the hydrogen). Available information about phase separation processes for hydrogen-helium mixtures[40] indicates that such processes would not occur under the comparatively low pressures in the envelopes of Uranus and Neptune.

Data on the shock compression of water and ammonia[3] indicate that these substances undergo a substantial increase in electrical conductivity at pressures and temperatures comparable to those in the envelopes of Uranus and Neptune ($\sim 10^2$ Kbar, $\sim 10^3$ °K). The conductivity of compressed H_2O appears to level off at a value of about 10 $ohm^{-1}cm^{-1}$ at the highest observed pressures. This number gives a magnetic diffusion coefficient of about 7×10^6 cm^2/s for the interior of Uranus or Neptune. The corresponding magnetic diffusion time for the entire planet is about 10^{11} s. According to conventional ideas about hydromagnetic dynamos in planets,[47] a self-regenerative magnetic dynamo can exist in a planetary interior if the diffusion time is small compared with circulation times for convection and differential rotation. If convective velocities are on the order of 0.1 to 1 cm/s in Uranus or Neptune, the condition might be obeyed. A definitive measurement of the intrinsic heat flow from Uranus (i.e., a measurement of T_e and T_s to an accuracy ∿ 10-100 times the current accuracy), together with a positive identification of an intrinsic magnetic field, would help to confirm the validity of the "hot-interior" model presented here.

CONCLUSION

Because of the remoteness of Uranus, many quantities which are fundamental for understanding its interior structure have not been adequately measured by ground-based techniques. We have listed certain crucial measurements in the above discussion and explained why they are important to issues concerning the planet's interior structure and origin. A successful Voyager encounter should reduce the number of existing major uncertainties.

This work was principally supported by NASA Grant NSG-7045.

ADDENDUM:

The results for Neptune's rotation period and second-degree response coefficient given above[16] are based upon the Neptune pole position given by Gill and Gault[48]. Somewhat different numbers are obtained if we derive the Neptune pole position from Harris' analysis (this volume). Specifically, if the nominal Triton mass is adopted, then we find[16] $q = 0.033 \pm 0.009$, $\Lambda_2 = 0.12\ (+0.06, -0.04)$, and a rotation period equal to 15 h (+3 h, -2 h).

REFERENCES

[1] Nicholson, P.D., Matthews, K., and Goldreich, P., "Radial Widths, Optical Depths, and Eccentricities of the Uranian Rings", Astron. J., vol. 87, 1982, pp. 433-447.

[2] Elliot, J. L., in Uranus and the Outer Planets, ed. by G. Hunt, Cambridge Univ. Press, 1982.

[3] Mitchell, A. C., and Nellis, W. J., "Equation of State and Electrical Conductivity of Water and Ammonia Shocked to the 100 GPa (1 Mbar) Pressure Range", J. Chem. Phys., vol. 76, 1982, pp. 6273-6281.

[4] Anders, E., and Ebihara, M., "Solar-system Abundances of the Elements", Geochim. Cosmochim. Acta, vol. 46, 1982, pp. 2363-2380.

[5] Zharkov, V. N., and Trubitsyn, V. P., Physics of Planetary Interiors, Pachart Publ. House, 1978.

[6] Lewis, J. S., "Low Temperature Condensation from the Solar Nebula", Icarus, vol. 16, 1972, pp. 241-252.

[7] Lewis, J. S., and Prinn, R. G., "Kinetic Inhibition of CO and N_2 Reduction in the Solar Nebula", Astrophys. J., vol. 238, 1980, pp. 357-364.

[8] Podolak, M., and Reynolds, R. T., "Consistency Tests of Cosmogonic Theories from Models of Uranus and Neptune", preprint.

[9] Belton, M. J. S., in Uranus and the Outer Planets, ed. by G. Hunt, Cambridge Univ. Press, 1982.

[10] Wallace, L., "The Structure of the Uranus Atmosphere", Icarus, vol. 43, 1980, pp. 231-259.

[11] Gulkis, S., Janssen, M. A., and Olsen, E. T., "Evidence for Depletion of Ammonia in the Uranus Atmosphere", Icarus, vol. 34, pp. 10-19.

[12] Hubbard, W. B., and MacFarlane, J. J., "Theoretical Predictions of Deuterium Abundances in the Jovian Planets", *Icarus*, vol. 44, 1980, pp. 676-682.

[13] Macy, W., Jr., and Smith, W. H., "Detection of HD on Saturn and Uranus and the D/H Ratio", *Astrophys. J*, vol. 222, 1978, pp. L73-L75.

[14] Trafton, L. M., and Ramsay, D. A., "The D/H Ratio in the Atmosphere of Uranus: Detection of the $R_5(1)$ Line of HD", *Icarus*, vol. 41, 1980, pp. 423-429.

[15] Goody, R. M., in *Uranus and the Outer Planets*, ed. by G. Hunt, Cambridge Univ. Press, 1982.

[16] Hubbard, W. B., Avey, H. P., Carter, B., Frecker, J., Fu, H. H., Gehrels, J.-A., Gehrels, T., Hunten, D. M., Kennedy, H. D., Lebofsky, L. A., Mottram, K., Murphy, T., Nielsen, A., Page, A. A., Reitsema, H. J., Smith, B. A., Tholen, D. J., Varnes, B., Vilas, F., Waterworth, M. D., Wu, H. H., and Zellner, B., "Results from Observations of the 15 June 1983 Occultation by the Neptune System", submitted to *Astron. J.* (1984).

[17] Slavsky, D., and Smith, H. J., "The Rotation Period of Neptune", *Astrophys. J.*, vol. 226, 1978, pp. L49-L52.

[18] Brown, R. H., Cruikshank, D. P., and Tokunaga, A. T., "The Rotation Period of Neptune's Upper Atmosphere", *Icarus*, vol. 47, 1981, pp. 159-165.

[19] Hayes, S. H., and Belton, M. J. S., "The Rotational Periods of Uranus and Neptune", *Icarus*, vol. 32, 1977, pp. 383-401.

[20] Hubbard, W. B., and Horedt, G. P., "Computation of Jupiter Interior Models from Gravitational Inversion Theory", *Icarus*, vol. 54, 1983, pp. 456-465.

[21] Hubbard, W. B., "Constraints on the Origin and Interior Structure of the

Major Planets", *Phil. Trans. R. Soc. Lond. A*, vol. 303, 1981, pp. 315-326.

[22] Podolak, M., "Methane Rich Models of Uranus', *Icarus*, vol. 27, 1976, pp. 473-477.

[23] Franklin, F. A., Avis, C. C., Colombo, G., and Shapiro, I. I., "The Geometric Oblateness of Uranus", *Astrophys. J.*, vol. 236, 1980, pp. 1031-1034.

[24] Hubbard, W. B., and MacFarlane, J. J., "Structure and Evolution of Uranus and Neptune", *J. Geophys. Res.*, vol. 85, 1980, pp. 225-234.

[25] MacFarlane, J. J., and Hubbard, W. B., in *Uranus and the Outer Planets*, ed. by G. Hunt, Cambridge Univ. Press, 1982.

[26] Kovalevsky, J., and Link, F., "Diametre, Aplatissement et Proprietes Optiques de la Haute Atmosphere de Neptune d'apres l'Occultation de l'Etoile BD -17°4388", *Astron. & Astrophys.*, vol. 2, 1969, pp. 398-412.

[27] Horedt, G. P., and Hubbard, W. B., "Two- and Three-layer Models of Uranus", submitted to *Moon & Planets*.

[28] Allen, C. W. *Astrophysical Quantities*. London: Athlone Press, 1973.

[29] Stacey, F. D. *Physics of the earth*. New York: Wiley & Sons, 1969.

[30] *ibid.*, and Zharkov, V. N., and Trubitsyn, V. P. *Physics of Planetary Interiors*. Tucson: Pachart, 1978.

[31] Keihm, S. J., and Langseth, M. G., "Lunar Thermal Regime to 300 km.", *Proc. 8th Lunar Sci. Conf.*, vol. 1, 1977, pp. 371-398.

[32] Hanel, R. A., Conrath, B. J., Herath, L. W., Kunde, V. G., and Pirraglia, J. A., "Albedo, Internal Heat, and Energy Balance of Jupiter: Preliminary Results from the Voyager Infrared Investigation", *J. Geophys. Res.*, vol. 86, 1981, pp. 8705-8712.

[33]Pearl, J. C., and Sinton, W. M. Hot spots of Io. In Satellites of Jupiter (D. Morrison, ed.). Tucson: Univ. of Arizona Press, 1982, pp. 724-755.

[34]Hanel, R. A., Conrath, B. J., Kunde, V. G., Pearl, J. C., and Pirraglia, J. A., "Albedo, Internal Heat Flux, and Energy Balance of Saturn", Icarus, vol. 53, 1983, pp. 262-285.

[35]Fazio, C. G., Traub. W. O., Wright, E. L., Low, F. J., and Trafton, L., "The Effective Temperature of Uranus", Astrophys. J., vol. 209, 1976, pp. 633-637.

[36]Lowenstein, R. F., Harper, D. A., and Moseley, H. The Effective Temperature of Neptune", Astrophys. J., vol. 218, 1977, pp. L145-L146.

[37]Graboske, H. C., Pollack, J. B., Grossman, A. S., and Olness, R. J., "The Structure and Evolution of Jupiter: the Fluid Contraction Phase", Astrophys. J., vol. 199, 1975, pp. 265-281.

[38]Grossman, A. S., Pollack, J. B., Reynolds, R. T., Summers, A. L., and Graboske, H. C., Jr., "The Effect of Dense Cores on the Structure and Evolution of Jupiter and Saturn", Icarus, vol. 42, 1980, pp. 358-379.

[39]Hubbard, W. B., "The Jovian Surface Condition and Cooling Rate", Icarus, vol. 30, 1977, pp. 305-310.

[40]Stevenson, D. J., and Salpeter, E. E., "The Dynamics and Helium Distribution in Hydrogen-helium Fluid Planets", Astrophys. J. Suppl., vol. 35, 1977, pp. 239-261.

[41]Hubbard, W. B., and Stevenson, D. J., "Interior Structure of Saturn", in Saturn, ed. by T. Gehrels, Univ. of Arizona Press, 1984.

[42]Zharkov, V. N., and Trubitsyn, V. P., "Adiabatic Temperatures in Uranus

and Neptune", Izv. Akad. Nauk SSSR Fiz. Zemli, vol. 7, 1972, pp. 120-127.

[43]Goldreich, P., and Soter, S., "Q in the Solar System", Icarus, vol. 5, 1966, pp. 375-389.

[44]Reitsema, H. J., Hubbard, W. B., Lebofsky, L. A., and Tholen, D. J., "Occultation by a Possible Third Satellite of Neptune", Science, vol. 215, 1982, pp. 289-291.

[45]Ross, M., "The Ice Layer in Uranus and Neptune -- Diamonds in the Sky?", Nature, vol. 292, 1981, pp. 435-436.

[46]Ross, M., and Ree, F. H., "Repulsive Forces of Simple Molecules and Mixtures at High Density and Pressure", J. Chem. Phys., vol. 73, 1980, pp. 6146-6152.

[47]Levy, E. H., "Generation of Planetary Magnetic Fields", Ann. Rev. Earth & Planetary Sci., vol. 4, 1976, pp. 159-185.

[48]Gill, J. R., and Gault, B. L., "A New Determination of the Orbit of Triton, Pole of Neptune's Equator, and Mass of Neptune", Astron. J., vol. 73, 1968, p. S95.

BLANK PAGE

ROTATIONAL PROPERTIES OF URANUS AND NEPTUNE

by

Michael J. S. Belton
Kitt Peak National Observatory[1]
Tucson, AZ

and

Richard Terrile[2]
Jet Propulsion Laboratory
California Institute of Technology
Pasadena, CA

Contribution to the Voyager "Uranus-Neptune Workshop", held in Pasadena, February 6-8, 1984.

---

[1] Operated by the Association of Universities for Research in Astronomy, Inc., under contract with the National Science Foundation.

[2] Guest observer of Las Campanas Observatory of the Carnegie Institution of Washington.

ABSTRACT

An assessment of recent research bearing on the rotational properties of Uranus and Neptune is given. We conclude that these properties are best described by the following estimates: URANUS. Direction of pole = α (1950) = $256^{\circ}\!.72$ δ (1950) = $-15^{\circ}\!.04$ with an absolute uncertainty of about $0^{\circ}\!.2$, Period = 15 to 17 hours; Sense of spin = Retrograde; NEPTUNE: α (1950) = $297^{\circ}\!.8$; δ (1950) = $+ 41^{\circ}\!.2$, with an uncertainty of about 4 degrees towards the pole of Triton's orbit, Period = 18.2 ± 0.4 hours, Sense of spin = Prograde. There is a clear signature of large-scale, zonal, atmospheric flows in observations of the atmosphere of Neptune. Wind velocities are at least as great as 109 $\mathrm{m.sec}^{-1}$. There is no evidence pro or con for atmospheric motions in the Uranus case.

INTRODUCTION

Precise knowledge of the rotational properties of a planet is needed if its gravitational moments are to be of some use as probes of its internal structure. In addition the sense and magnitude of a planets spin are important boundary conditions for understanding the nature of observed atmospheric motions as well as for understanding the evolution of the orbits of the planets' satellites through tidal interaction.

Deep within their convective interiors the outer planets are expected to be in solid body rotation although this basic assumption has not been discussed in detail in the published literature. We will refer to the period of this rotation as the "true" or "body" period. In Jupiter and Saturn this is assumed to be the same as the System III period which measures the rotation of the planetary magnetic field and is assumed to be locked to the planet's core.

In the region of their visible atmospheres global scale flows with sufficient velocity occur so that the apparent rotation period may deviate substantially from the true period. These "atmospheric" periods can be greater or less than the true period and a planet may exhibit several depending on how it is observed. Experience shows that (for prograde planets) the major high velocity flows are directed from west to east such that the predominant atmospheric periods are substantially less than the true period of rotation. For example on Jupiter and Saturn the 'atmospheric' periods differ from the 'body' periods by -5 and -25 minutes respectively. An extreme, and probably not too relevant an example for the outer planets, is the case of Venus where the observed atmospheric period is some 240 days shorter than the period of rotation of the planet itself!

Because of their distance, small angular diameter, and bland appearance, the rotational properties of Uranus and Neptune are, at present, poorly defined. Major leaps in their precision are among the more confidently anticipated results of the Voyager-Uranus and -Neptune encounters.

CURRENT STATUS

In table 1 we show a matrix of techniques that have been used to explore the rotational properties of Uranus and Neptune. Two techniques, which have been very successfully used elsewhere, but have not or cannot be used in the case of these planets are radar sounding and the analysis of magnetospheric radio emission for periodic modulation. The latter method may soon be available to Voyager as the spacecraft approaches the vicinity of Uranus. In the case of Neptune this will depend on whether the planet has a developed magnetosphere. Also the exceptional pole orientation of Uranus with respect to the approaching spacecraft may frustrate early results. Nevertheless, using Saturn as a benchmark, we expect that the Voyager PRA experimenters may have a new information on the "true" period of Uranus as early as the beginning of 1985.

1. Direction of Polar axis. URANUS: The observed regularity and apparent stability of its satellite system demands that the individual members all have very small inclinations to the planets equatorial plane. Dunhams' (1971) analysis of satellite motion is the reference most widely favored although it remains unpublished. He finds:

$$\alpha(1950) = 256^{\circ}.72 \pm 0.04;\ \delta(1950) = -15^{\circ}.04 \pm 0.04$$

More recently Elliot et al. (1981) have published an analysis of five stellar occultations behind Uranus' ring system. With the assumption that the mean ring plane is coincident with the planets equatorial plane they find:

$$\alpha(1950) = 256.61 \pm 0.04;\ \delta(1950) + -15.22 \pm 0.05$$

The significance of the small 0.2 degree discrepancy in the two studies is not known. Elliot et al. suspect that their formal errors underestimate the true errors in their determination.

Crude, but nevertheless direct, support for these results come from spectrographic observations of the position angle of the spin axis projected on the plane of the sky. At a time when the position angle of the projected spin axis was expected to be $278\overset{\circ}{.}8$ Hayes and Belton (1977) measured a value of 283° ± 3.5.

NEPTUNE: The unpublished analysis of Tritons' orbital precession between 1887-1958 by Gill and Gault (1968) gives the direction of the pole as:

$$\alpha(1950) = 294\overset{\circ}{.}91; \ \delta(1950) = +40\overset{\circ}{.}53$$

The time span of the observations is only 12 percent of a complete precessional period, formal error estimates are not available, and this study does not take into account the possible substantial effects of the large angular orbital momentum that resides in Triton (Harris, 1984). There is very crude spectroscopic confirmation for this pole in Hayes and Beltons' work. At a time when the direction of the pole projected on the sky was predicted to be at PA = $32\overset{\circ}{.}8$ they measured a PA of 32° ± 11. More recently Harris (1983) has reported the results of a study of Tritons' orbit which based on a data set that extends the observational base to the present day. He reports that the north pole of the invariable plane points in the direction

$$\alpha(1950) = 297^{\circ}\!.813 \pm 1^{\circ}\!.5;\ \delta(1950) = +41^{\circ}\!.185 \pm 1^{\circ}\!.5$$

This is the direction of the planet's pole only if the Mass of Triton is negligible. According to Harris, current estimates of Tritons' mass could lead to a 3.6 degree inclination of the equatorial plane to the invariable plane (Harris, 1981, 1984) in the direction towards Tritons' orbital plane. Ground-based CCD imaging of Neptune (Terrile _et al_., 1984) gives us a sky plane projection of its rotation axis to within 1° ± 8° of the pole of the invariable plane. Our assessment is that the best that can be done is to accept at present the orientation of Harris's invariable plane as Neptunes' spin axis and recognize that uncertainies of as much as four degrees of arc exist. In any event the uncertainties appear to be considerably greater than are implied by the precision of Gill and Gaults' reported numbers.

2. _Sense of rotation_: Spectrographic studies of line tilts have, in our opinion, convincingly and consistently shown that the sense of Uranus' spin is retrograde and that of Neptunes' is prograde. (cf. Hayes and Belton for modern results and a review of earlier work). Imaging studies of the motion of spot like markings on Neptune confirm these results (Smith _et al_., 1979, Terrile and Smith, 1983).

3. Periods and atmospheric motions: There are, at present, no ways to measure the true periods of rotation of Uranus and Neptune with high precision. Given our experience that large-scale zonal atmospheric flows exist with velocities of the order of 100 $m.sec^{-1}$ in the other planets then we can expect that periods deduced by occultation, spectroscopic, imaging, or photometric means will be different to the true rotation period. These differences can be expected to be easily as much as half an hour or so.

The occultation method is based on the expectation that the surface of a rotating planet will be coincident with a surface of constant geopotential, i.e. the atmosphere is in hydrostatic equilibrium. If this is true then the following relationship between the gravitational moment, J_2, the ellipticity or oblateness, e, of the outer surface of the planet and a parameter $m = \omega^2 R^3 (1 - e)/GM$ will be approximately true:

$$J = (2/3)e - (1/3)m \qquad (1)$$

This is correct to the first order in e; to improve the accuracy a further term, equal to $e(-(1/3)e + (2/21)m)$, should be added to the right hand side. This will make it correct to the second order in the ellipticity

(Jeffreys, 1959). In these expressions ω is the spin angular velocity of the surface whose oblateness is measured and is assumed constant on that surface; ($\equiv 2\pi$/period); R, the equatorial radius, G, the gravitational constant; and M, the mass of the planet.

A suitable test of the utility of eq. 1 is an application to Jupiter and Saturn. Using data taken from the recent compilation of Davies et al. (1980) and the 1983 Astronomical Almanac we find that the relationship holds to an accuracy of better than 1 percent for Jupiter, i.e. dP = P(System 1) − P(predict) = +3 minutes. The true period of Jupiter is some 1.3 percent, or 8 minutes longer than the prediction. For Saturn the predicted period is 33 minutes shorter than System 1, a large discrepancy which can be improved by about 12 minutes if the second order terms in e are included. The predicted period is about 46 minutes shorter than the true period measured by Kaiser et al. (1980) a difference that seems to us surprisingly large and which has not, to our knowledge, been noted before. It probably implies that the value for the oblateness (= 0.107; Reese, 1971) is high by about 10 percent and possibly that small adjustments in the dimensions of Saturn are in order. Ingersoll and Beebe (1984) have told us of improved fits to the limb of Saturn when unpublished Voyager data is used to derive a new value for the oblateness.

With the above results it appears that given data of contemporary accuracy on e and J_2, eq. 1 can be used to infer atmospheric rotation periods of Uranus and Neptune to an accuracy of better than 10 percent that refer to the 1-10 μ bar level.

In addition we note that their small sizes, and what turn out to be relatively long rotation periods, lead us to expect that eq. 1 should hold particularly well in their cases (Hubbard, 1984).

There have recently been major advances in our knowledge of Uranus' gravitational moment through the observation and analysis of stellar occultations behind its system of elliptical rings. These rings which are thought to be uniformly precessing in Uranus' spheroidal gravitational field, maintain their geometric integrity through the action of as yet unobserved "shepherding" satellites (Nicholson *et al.*, 1978; Elliot *et al.* 1981). Parallel advances on J_2 have also been made by Veillet (1980) through a detailed analysis of the orbit of Miranda.

For the oblateness Elliot *et al* (1981) have used stellar occultations behind the planet to yield a value of e which agrees with the result of Franklin *et al* (1980) based on a detailed analysis of the high spatial resolution Stratoscope II images. Using eq. 1 Elliot *et al.* find a period for Uranus of 15.5 hours based on their own data. With a slightly different combination of the data Goody (1982) computes a rotation period of 16.7 ± 0.5 hours by this method. Folding in the experience with Jupiter and Saturn related above we believe that the best that can be said is that the atmospheric rotation rate for Uranus most probably falls in the range of 15 to 17 hours and, lacking further evidence, this represents the best estimate of the body rotation of Uranus that can be made at this time.

In the case of Neptune, Hayes and Belton (1977) used published estimates of the rate of precession of Tritons' orbit to estimate J_2 and combined it with a value for the oblateness derived from the analysis of the occultation of BD -17 4388 behind the planet (Freeman and Lynga, 1970; Kovalevsky and Link, 1969). They estimate an atmospheric period of 15.4 hours, however the large formal uncertainties in this estimate (primarily in the estimates for the oblateness) allow a wide range of possible periods. Hayes and Belton find that this period might reasonably lie anywhere between 13.4 and 18.5 hours. An occultation by Neptune of the star MKE 30 in June 1983 was widely reported but no new results on the oblateness, or infered period, have been published to date.

Several modern attempts have been made to measure atmospheric rotation periods for these planets by spectrographic means (cf. the review by Goody (1982) or the compilation of Davies et al. (1980)). In our opinion, the wide discrepancy in the results of these studies indicates that these measurements are susceptable to large, uncontrollable, systematic errors (eg. Munch and Hippelein, 1979, for a discussion of the effects of observational seeing and the dependence on limb darkening). All of the studies are, in our opinion, of high quality and probably the best that can be done with these results is to take the simple, but brutal, step of forming their grand average and view the result as a simple, but crude, check on other methods.

In the case of Uranus such an average yields an atmospheric period near 18 hours (considerable uncertainty is, of course implied by the wide spread of results). This period agrees tollerably well with the range noted above that was based on eq. 1 but, unfortunately, is otherwise not very useful.

For Neptune a period near 13 hours results (there are only two studies). In our opinion, little faith should be placed in this estimate since the true limb darkening of Neptune, which is an important factor in assessing the very large systematic seeing corrections to the observed line tilts (a factor of 2 or more), is not known with adequate precision.

Unlike Uranus' atmosphere, which has an exceedingly bland appearance at all observed wavelengths, that of Neptune has been found to show contrasty, spotlike, markings when imaged in a narrow range of wavelengths centered on the 8900 A methane absorption band (Smith _et al_., 1979). Terrile and Smith (1983) report that these bright features are confined to two latitude regions at ± 30°. Over a period of 7 Neptune rotations these features were used to measure an atmospheric rotation period of 17.83 ± 0.1 hours Terrile _et al_. (1984). Furthermore, no differential rotation greater than about 10 m. sec^{-1} was detected between features at these two latitudes. Figure 1 from Terrile _et al_. (1984) shows an 8900Å image of Neptune recorded on 25 May 1983 from the Las Campanas Observatory. Also shown is the Neptune geometry using the invariable plane to define the pole.

Neptune also shows extreme photometric variability in the near IR (Joyce _et al_., 1977) and similar variability, but at a much lower amplitude, has been found at visible wavelengths by Smith and Slavsky (1980). As a result a number of precise atmospheric rotation periods for Neptune have recently been determined by means of extracting periodicities from extended time-series of photometric observations. Work by Cruikshank (1978), Brown _et al_. (1981), Belton _et al_. (1981), and Smith and Slavsky (1980) have yielded the following periods:

PERIOD (hours)	AUTHORS
17.73	Brown _et al_ (1981)
17.73 18.29 18.56	*Belton _et al_ (1981)
18.44 17.71	Smith and Slavsky (1980)

(*Belton _et al_. believe that the two periods near 18.42 hours could be the manifestation of a single period whose source is undergoing strong amplitude modulation with a time-scale of 100 days.)

Figure 2 from Belton _et al_. shows the near IR photometric data set plotted against the predicted variation. The fact that the predicted curve remains physically reasonable throughout the period covered by the observations (i.e. greater than zero almost everywhere), particularly in the long stretches of time where there are no data to constrain the solution, we consider to be strong support for the reasonablness of their analysis.

The existence of well separated and clearly defined periods at 17.7 and near 18.4 hours leaves no doubt in our minds that wind systems exist on Neptune and that the velocity contrasts are at least 109 m. sec^{-1}. The small differences between Smith and Slavsky's periods and those based on IR photometry can, if believed significant, be explained in terms of a vertical shear in the atmosphere. A modest shear greater than 3 m $\sec^{-1}$ (scale-height)$^{-1}$ is all that is needed. Other explanations such as zonal contrasts are also possible and should be looked for by using speckle imaging techniques at the longer infrared wavelengths to determine the latitude of the contrasts.

Neptune, like Jupiter and Saturn, is in prograde rotation, and so its true period should most likely be identified with the longer of the various observed atmospheric periods. The period cannot be much in excess of 18.5 hours for otherwise there would be conflict with the range of periods allowed by observed values of J_2 and the ellipticity. Belton et al. (1981), using an analogy based on atmospheric periods on Jupiter recommend a value for the true period of Neptune of 18.2 ± 0.4 hours.

For Uranus the only evidence for an atmospheric period is in the unpublished work of Slavsky and Smith (1980). They find a periodicity in a photometric time series near to 24 hours. However this modulation is so weak and so close to the dominant sampling frequency that its credibility has been seriously questioned (Goody, 1982). We also note that in spite of its agreement with the spectrographic work of Trafton (1977) and of Hayes and Belton (1977), it is so far removed from the range of periods allowed by the figure of the planet that we have not considered it further.

In summary the true period of Uranus is poorly determined but probably lies somewhere in the range from 15 to 17 hours; there is no convincing observational evidence either for or against the existence of large scale atmospheric flows in the atmosphere of this planet. For Neptune the true period is estimated at 18.2 + 0.4 hours; the observation of several distinct atmospheric rotation periods indicates that large-scale atmospheric currents with relative zonal velocities of at least 109 m.sec^{-1} exist in its atmosphere.

REFERENCES

Belton, M.J.S., L. Wallace, and S. Howard (1981) *Icarus*, **46**, 263.

Brown, R. H., D. P. Cruikshank, and A. T. Tokunaga (1981), *Icarus*, **47**, 159.

Cruikshank, D. P. (1978), *Ap*. *J*. *Lett*., **220**, L57.

Davies, M. E., V. K. Abalakin, C. A. Cross, R. L. Duncombe, H. Masursky, B. Morando, T. C. Owen, P. K. Seidelmann, A. T. Sinclair, G. A. Wilkins, and Y. S. Tjuflin (1980), *Cel. Mech*., **22**, 205.

Dunham, D. W. (1971) Ph.D Thesis. Yale University.

Elliot, J. L., R. G. French, J. A. Frogel, J. H. Elias, D. J. Mink, and W. Liller (1981) *Astron. J*., **86**, 444.

Franklin, F. A., C. C. Avis, G. Columbo, I. I. Shapiro (1980) *Ap*. *J*., **236**, 1031.

Freeman, K. C., and G. Lynga (1970), *Ap*. *J*., **160**, 767.

Gill, J. R., and B. L. Gault, (1968) *Astron. J*. **73**, 595 (abstract only).

Goody, R. (1982), In "Uranus and the Outer Planets", Cambridge University Press, ed. Garry Hunt.

Harris, A. W. (1984) Private Communication.

__________ (1983) *Bull. A.A.S.*, **15**, 870.

__________ (1981) *Bull. A.A.S.*, **13**, 573.

Hayes, S. H., and M. J. S. Belton (1977), Icarus, **32**, 383.

Hubbard, W. (1984). Personal Communication.

Ingersoll, A. P. and R. Beebe (1984). Private Communications.

Joyce, R. R., C. B. Pilcher, D. P. Cruickshank, and D. Morrison (1977) *Ap. J.*, **214**, 657.

Jeffreys, Sir H. (1959). In "*The Earth*". Cambridge University Press.

Kaiser, M. L., M. D. Desch, J. W. Warick, and J. B. Pearce (1980), *Science*, **209**, 1238.

Kovalevsky, J., and F. Link (1969), *Astron. & Astrophys.*, **2**, 398.

Munch, G., and H. Hippelein (1979) *Astron. and Astrophys*. **81**, 189.

Nicholson, P. D., K. Mathews, and P. Goldreich (1982) *Astron. J.*, **87**, 433.

Smith, B. A., H. J. Reitsema, and S. M. Larson (1979) *Bull. A.A.S.*, **11**, 570.

Smith, H. J. and D. B. Slavsky (1979). *Bull. A.A.S.*, **11**, 568.

____________ (1980), *Bull. A.A.S.*, **12**, 704.

Terrile, R. J. and Smith, B. A. 1983 *Bull. A.A.S.*, **15**, 858.

Terrile, R. J., Smith, B. A. and Avis, C. C. (1984) in preparation.

Trafton, L. (1977), *Icarus*, **32**, 402.

Veillet, C. (1982), *Astron. & Astrophys.*, **118**, 211.

TABLE 1

METHODS USED TO DERIVE ROTATIONAL PROPERTIES OF URANUS AND NEPTUNE

Planet Properties	URANUS	NEPTUNE
Pole direction	1. Geometry of satellite plane	1. Precession of Tritons' orbit
	2. Geometry of ring plane	2. Spectroscopy (plane of sky only)
	3. Spectroscopy. (plane of sky only)	3. CCD Imaging (plane of sky only)
Direction of spin	1. Spectroscopy (line tilts)	1. CCD Imaging
		2. Spectroscopy (line tilts)
Period	1. J_2 and oblateness - Satellite precession - Ring Precession - Stellar occultation - Photography and visual observations,	1. J_2 and oblateness - Satellite precession - Stellar occultation
	2. Spectroscopy - Line tilts - Line shape	2. Spectroscopy - Line tilts
	3. Photometry - visible	3. Photometry - IR colors - visible
		4. CCD Imaging
Atmospheric Motions	---------------	1. CCD Imaging
		2. Photometry

BLANK PAGE

BLANK PAGE

BLANK PAGE

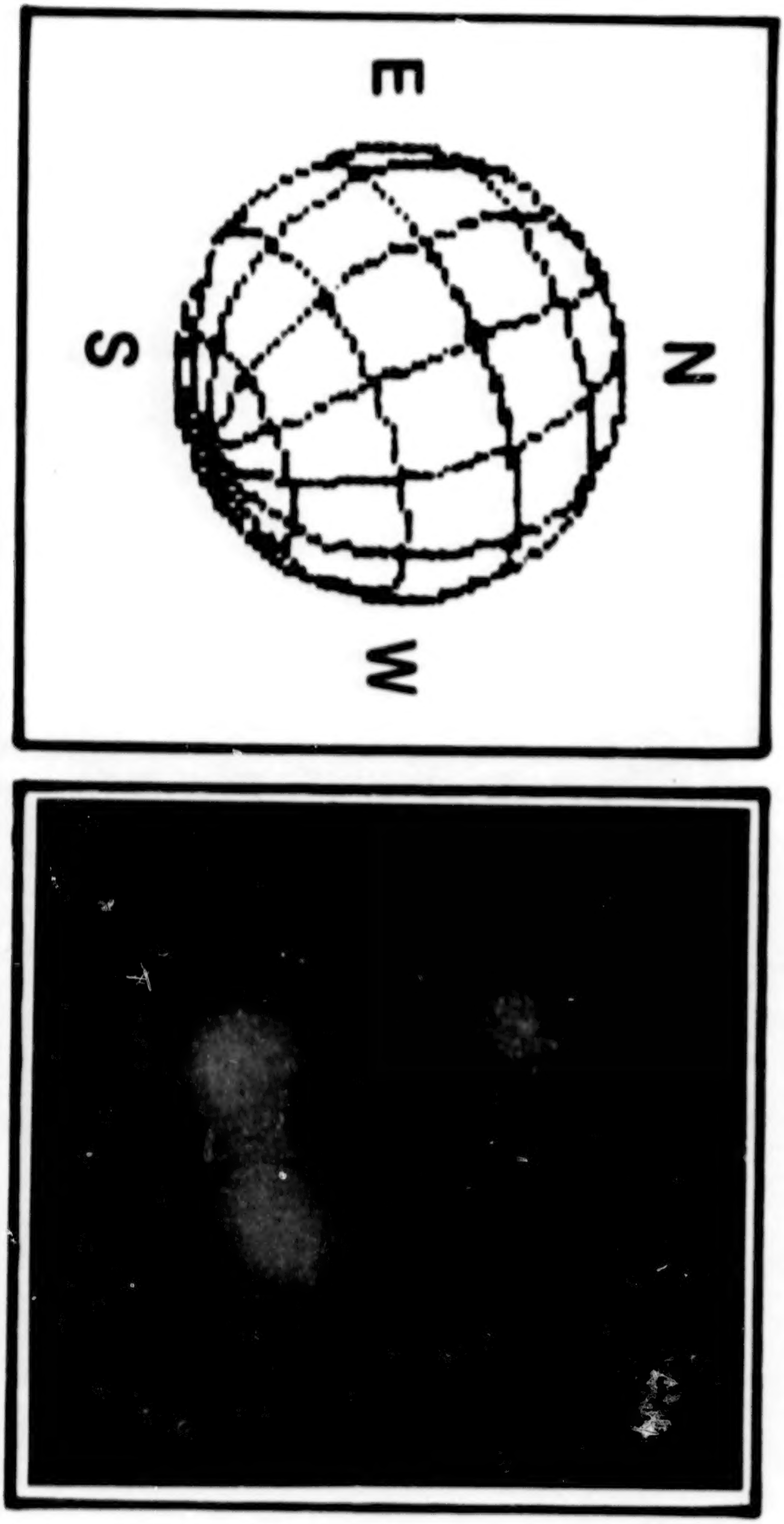
E
S
N
W

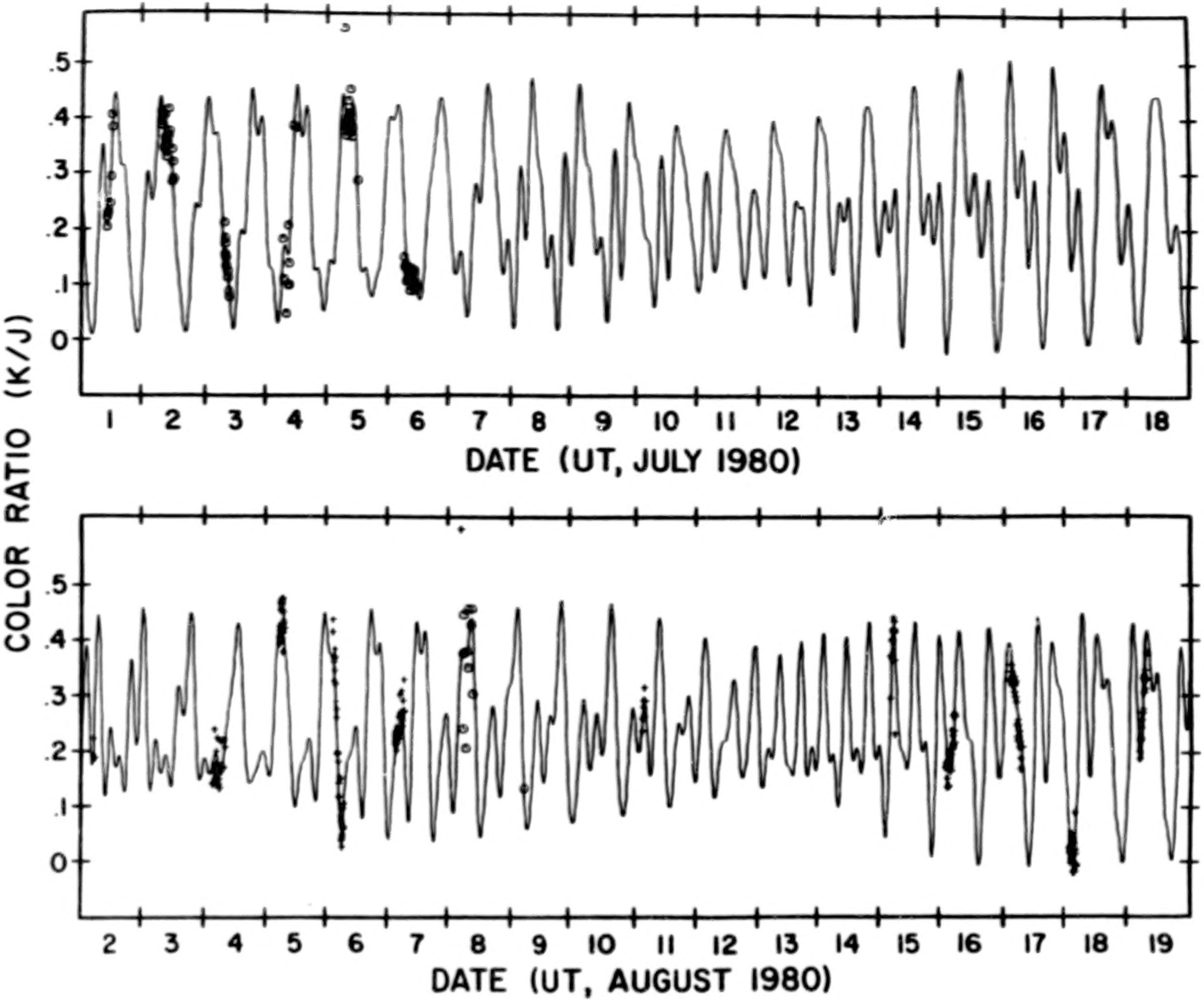
COLOR RATIO (K/J)
.5
.4
.3
.2
.1
0
1
2
3
4
5
6
7
8
9
10
11
12
13
14
15
16
17
18
DATE (UT, JULY 1980)
.5
.4
.3
.2
.1
0
2
3
4
5
6
7
8
9
10
11
12
13
14
15
16
17
18
19
DATE (UT, AUGUST 1980)

BLANK PAGE

OBLATENESSES OF URANUS AND NEPTUNE

Richard G. French
Department of Earth, Atmospheric, and Planetary Sciences
Massachusetts Institute of Technology
Cambridge, MA 02139

Abstract

The oblateness of a planet is closely related to its rotation rate and internal mass distribution, and is therefore an important indicator of gross planetary structure. Analysis of Stratoscope II images of Uranus yields ε 0.022 ± 0.001, and stellar occultation observations yield $\varepsilon = 0.024 \pm 0.003$. Because of the current pole-on aspect of Uranus, it is unlikely that a significantly more accurate value can be determined by stellar occultations before Voyager 2 encounters Uranus in January, 1986. Neptune's oblateness has been determined from stellar occultation observations made in 1968 and 1983. The 1968 observations yield an oblateness of 0.021 ± 0.004. A recent determination of Neptune's oblateness using both the 1968 and 1983 observations is consistent with this value. Space Telescope observations of several stellar occultations by Neptune could provide a significantly more accurate determination of the oblateness before the Voyager 2 encounter in 1990.

INTRODUCTION

The geometric oblateness (also known as ellipticity, or flattening) of a planet is defined as $\varepsilon = 1-R_p/R_e$, where R_p and R_e are the polar and equatorial radii, respectively. For an isolated, slowly rotating fluid body in hydrostatic equilibrium, equipotential surfaces are oblate spheroids, and the oblateness is closely related to the rotation period and the distribution of mass within the planet by the relation:[1]

$$P = 2\pi\left[\frac{R_e^{\,3}(1-\varepsilon)\left(1+\frac{3}{2}J_2\right)}{2GM\left(\varepsilon - \frac{3}{2}J_2 - \frac{5}{8}J_4 - \frac{9}{4}J_2^{\,2}\right)}\right]^{1/2} \tag{1}$$

where P is the rotation period, J_2 and J_4 are the coefficients of the first two even harmonics of the gravitational potential, G is the gravitational constant, and M is the planetary mass. (If the reference radius, R_r, for the harmonic expansion of the gravitational potential does not equal R_e, then one must set $\rho = R_r/R_e$ and substitute $\rho^2 J_2$ for J_2 and $\rho^4 J_4$ for J_4 in Eq. 1.) Elliot and Nicholson have shown that the period predicted by Eq. 1 is quite close to the actual period in those cases where all required quantities are known.[2] For Uranus and Neptune, rotation periods have not yet been agreed upon by all concerned, and accurate measurements of their oblatenesses can provide important indicators of gross planetary structure.

THE OBLATENESS OF URANUS

Because of the small angular diameter of Uranus, direct measurement of its optical flattening from ground-based images is quite difficult. Photographs of Uranus, obtained in 1970 by the Stratoscope II balloon-borne 91 cm telescope, initially yielded a value of $\varepsilon = 0.01 \pm 0.01$ for the oblateness, based on estimates of the polar and equatorial diameters of the images.[3] However, the photographs were recently re-digitized and re-analyzed by Franklin _et al._, using techniques not available at the time of the earlier study. To determine the oblateness, Franklin _et al._ performed least-squares fits of ellipses to a series of isophotes in the annular region, $0.97\ R_e < r < 1.00\ R_e$, of several images. Their final estimate of the oblateness was $\varepsilon = 0.022 \pm 0.001$, where the uncertainty is the standard error, based on the rms scatter of the independent results from 23 exposures. A key assumption of this analysis is that there is no latitude-dependent limb darkening, which would cause the isophotal ellipses to deviate from the true planetary figure. Stated somewhat differently, it must be assumed that the isophotes are gravitational equipotentials if the measured optical flattening is to be identified as ε in Eq. 1.

Stellar occultation observations provide an independent measure of the figure of Uranus. From the measured times of disappearance and reappearance of the occulted star, a chord across the planet can be determined. It has become conventional to define these immersion and emersion times as the time at which the best-fitting isothermal model light curve reaches half-intensity. These are the "half-light" times of the occultation. When chords are combined from several observations, it is possible to perform a least-squares fit to the planetary figure. Generally, corrections in right ascension and declination to the relative positions of the star and planet must be accounted for in the fit. However, the nine rings encircling Uranus provide a reference system which allows the offset between the star and planet to be determined independently with great accuracy, as a by-product of the least-squares solution for the orbital elements of the rings. Once this offset has been measured, even a single chord across the planet can provide useful information about the oblateness, when combined with results from other occultations. Using this technique, Elliot et al. found an oblateness of $\epsilon = 0.024 \pm 0.003$.[5] The inclusion of more recent observations has not significantly improved this value. The reason is that the current pole-on aspect of Uranus restricts the latitude range probed to the equatorial region, which does not provide a strong constraint on the oblateness.

Although the Stratoscope II and stellar occultation oblatenesses agree to within their stated errors, two points should be kept in mind when comparing the two determinations. First, the Stratoscope II measurement refers to a region near the cloud deck, whereas the occultation oblateness refers to a level whose atmospheric pressure is of order 1 μbar, which lies some 500 km above the clouds. If there are significant meridional temperature gradients in the region between these atmospheric levels, the oblateness could vary substantially with height, as was found for Mars.[6] Second, the half-light points used in the occultation method lie on a surface which may differ substantially from an equipotential surface. This is especially true if the atmosphere has strong vertical temperature variations, as Uranus has.[7] The importance of this effect is currently being explored.[8]

THE OBLATENESS OF NEPTUNE

Neptune's angular diameter is so small that direct measurement of ground-based images to determine the oblateness is of little value. However, occultation observations have provided useful measurements of Neptune's figure. In 1968, Neptune occulted BD -17° 4388, and from an analysis of data taken from several sites, Kovalevsky and Link obtained $\epsilon = 0.021 \pm 0.004$.[9] Freeman and Lyngå independently analyzed the same observations, and found $\epsilon = 0.0259 \pm 0.0051$.[10] Data from a 1983 occultation are still being analyzed, and give results that are consistent with the above values, but with significantly smaller errors. These results are being prepared for publication. In the meantime, some comments are in order concerning the results from the 1968 event. First, the observations were recorded on strip charts, introducing a significant uncertainty into the time measurements. Second, since Neptune has no known ring system to provide a well determined reference frame, the relative positions of the star and the planet must be determined as part of the least squares fit to the occultation data. On the other hand, the occultation chords cover a wider range of latitudes on Neptune than on Uranus, so that the oblateness can still be well determined. Third, the main difference between the two determinations concerns the choice of occultation times to use as part of the fit. Kovalevsky and Link used half-light times, where Freeman and Lyngå used times corresponding to 9 percent fading of initial starlight. The results of an ongoing analysis of the 1983 observations give an oblateness within the errors quoted by Kovalevsky and Link, and it is suggested that their value of $\varepsilon = 0.021 \pm 0.004$ be used until the newer findings have been published.

Because of the orientation of Neptune's pole, the full range of latitudes can be probed by upcoming occultations, which could provide a significantly more accurate determination of Neptune's oblateness by the time of the Voyager 2 encounter with Neptune in 1990. A series of occultation observations by the Space Telescope would be especially useful in this regard.

ROTATION PERIODS

The rotation periods of Uranus and Neptune were computed using Eq. 1. The results are given in Table I.[2] The error in the calculated period reflects that introduced by the oblateness.

TABLE I

Rotation Periods of Uranus and Neptune

	Uranus		Neptune	
Oblateness (ϵ)	0.024 ± 0.003[5]	0.022 ± 0.001[4]	0.021 ± 0.004[9]	0.0259 ± 0.0051[10]
Equatorial Radius (R_e, km)	26,145 ± 30[5]	25,600 ± 100[2]	25,225 ± 30[9]	25,265 ± 35[10]
GM × 10^{-3} (km^3 sec^{-2})	5,784 ± 4[11]	5,784 ± 4[11]	6,787 ± 5[12]	6,787 ± 5[12]
$J_2 \times 10^3$	3.349 ± 0.005[5]	3.349 ± 0.005[5]	4.3 ± 0.3[13]	4.3 ± 0.3[13]
$J_4 \times 10^6$	-38 ± 9[5]	-38 ± 9[5]	?	?
Reference Radius (R_r, km)	26,200[5]	26,200[5]	25,225[9]	25,225[9]
Calculated Rotation Period (hr)	15.6 ± 1.4	16.6 ± 0.5	15.6 ± 1.8	13.5 ± 2.2

REFERENCES

[1] Brouwer, D. and Clemence, G.M. (1961). In *The Solar System*, *3*, ed. by G.P. Kuiper and B.M. Middlehurst (Chicago: University of Chicago Press), 31.

[2] Elliot, J.L. and Nicholson, P.D. (1984). In *The Rings of Uranus*, ed. by A. Brahic and R. Greenberg (Tucson: University of Arizona Press), in press.

[3] Danielson, R.E., Tomasko, M.G., and Savage, B.D. (1972). *Ap.J.* *178*, 887.

[4] Franklin, F.A., Avis, C.C., Colombo, G., and Shapiro, I.I. (1980). *Ap.J.* *236*, 1031.

[5] Elliot,J.L., French, R.G., Frogel, J.A., Elias, J.H., Mink, D.M., Liller, W. (1981). *A.J.* *86*, 444.

[6] French, R.G., and Taylor, G.E. (1981). *Icarus* *45*, 577.

[7] French, R.G., Elliot, J.L., Dunham, E.W., Allen, D., Elias, J.H., Frogel, J.A., and Liller, W. (1983). *Icarus* *53*, 399.

[8] Melroy, P. (1984). Master's Thesis, Massachusetts Institute of Technology, in preparation.

[9] Kovalevsky, J., and Link, F. (1969). *Astron.* *&* *Astrophys.* *2*, 398.

[10] Freeman, K.C., and Lyngå, G. (1970). *Ap.J.* *160*, 767.

[11] Dunham, D.W. (1971). Ph.D. Thesis, Yale University.

[12] Gill, J.R. and Gault, B.L. (1968). *A.J.* *73*, 595.

[13] Harris, A.W. (1984). Memorandum.

BLANK PAGE

PHYSICAL PROPERTIES OF NEPTUNE AND TRITON INFERRED FROM THE ORBIT OF TRITON

A.W. Harris

Jet Propulsion Laboratory of
The California Institute of Technology
4800 Oak Grove Drive
Pasadena, California 91109

ABSTRACT

The orbital motion of Triton was redetermined from photographic data spanning the interval 1899-1981. The resulting ephemeris should provide Triton positions with respect to Neptune with an accuracy of ±500 km through the end of the century. The following physical results follow from the orbit solution. The inverse mass of Neptune + Triton is $m_{\odot}/(m_N+m_T) = 19490 \pm 40$. No acceleration of the mean motion nor orbital eccentricity were detected, thus constraining the tidal dissipation factors of Neptune and Triton to $Q_N > 650$ and $Q_T < 10^4$. Tidal heating of Triton is presently insignificant. The gravitational harmonic J_2 of Neptune is 0.0043 ± 0.0003 if Triton is as massive as $m_T/m_N = 0.00128$, and if Neptune's spin is prograde with $P \approx 18^h$, or $J_2 = 0.0037 \pm 0.0002$ if Triton is much less massive. Triton undergoes extreme climatic variations due to the combined motion of it's orbit plane and Neptune's orbital motion. ~10% of Triton's surface is presently hidden from diurnal insolation, which may provide a powerful cold trap for atmospheric volatiles.

INTRODUCTION

The last definitive study of the orbital motion of Triton was that of Eichelberger and Newton[1] in 1926. Gill and Gault[2,3] recomputed the orbit including photographic data from 1939-1942[4,5], however both solutions were dominated by the large number of visual observations compared to photographic. With the availability of photographic data beginning in 1975 from the USNO Flagstaff station,[6,7] it appeared possible to achieve a meaningful improvement in the determination of the orbit, and the upcoming encounter with Neptune by Voyager II makes such a redetermination of timely importance for navigational use. The solution which I present here is based on photographic observations only which can be grouped into three time intervals:

1899-1910	428 observations from the Royal Greenwich Observatory[8], 19 from Pulkovo[1], and 8 from Lick[1].
1939-1942	73 observations from the Yale South Africa station [4,5].
1975-1981	94 observations from the USNO Flagstaff station[6,7].

In the following sections, I will briefly define the theory of motion and solution obtained, and then discuss the physically significant results which can be derived from the motion of Triton (mass of the system, gravitational harmonics, etc.).

ORBIT SOLUTION

The observations were fitted to a theory of uniform motion in a circular inclined orbit processing at a constant rate about an inertially fixed plane. The definitions of the constants required, and their solution values are as follows:

t_o = Jan 1.0 1950 = JD 2433282.5, Epoch

a = 354,290 km = 0.0023683 au = 16.283 arcsec @ 30 au, orbit radius (semi major axis) of Triton

$e \equiv 0$, eccentricity of orbit, assumed zero

n = $61\overset{\circ}{.}2588532$ per day, nodal mean motion

λ_o = $200\overset{\circ}{.}913$, longitude from ascending node through the invariable plane at epoch

i = $158\overset{\circ}{.}996$ = $21\overset{\circ}{.}004$ retrograde, inclination of orbit to the invariable plane

Ω_o = $151^\circ\!.401$, angle from the intersection of invariable plane with the earth's equatorial plane of 1950.0, to the ascending node of the orbit through the invariable plane

$\dot{\Omega}$ = $+0^\circ\!.57806$ per year (T_p = 622.77 years), nodal precision rate

α_p = $297^\circ\!.813$ } 1950.0 Right Ascension and Declination of the

δ_p = $41^\circ\!.185$ } pole of the invariable plane.

The assumption of a circular orbit appears justified by the residuals, which contain no signature above a 1σ level which could be attributed to eccentric motion. Also, tidal dissipation in Triton should have damped any original eccentricity in a very short time compared to the age of the solar system (see PHYSICAL RESULTS section).

To obtain the cartesian state vector of Triton at time t (in days), define $\lambda = \lambda_o + n(t-t_o)$ and $\Omega = \Omega_o + \dot{\Omega}(t-t_o)/365.25$. The state vector is given, in earth equatorial coordinates of 1950.0, by:

$$\vec{r} = R_3(-\alpha_p - \frac{\pi}{2})R_1(\delta_p - \frac{\pi}{2})R_3(-\Omega)R_1(-i)\begin{pmatrix} a\cos\lambda \\ a\sin\lambda \\ 0 \end{pmatrix}, \qquad (1)$$

where $R_i(\theta)$ is the rotation matrix about axis i, e.g.,

$$R_1(\theta) = \begin{pmatrix} 1 & 0 & 0 \\ 0 & \cos\theta & \sin\theta \\ 0 & -\sin\theta & \cos\theta \end{pmatrix}, \qquad (2)$$

and $R_2(\theta)$ and $R_3(\theta)$ can be obtained by permuting subscripts. To obtain the apparent position of Triton relative to Neptune, as seen from the earth, multiply by the following rotation matrices:

$$\begin{pmatrix} x \\ \Delta\alpha \cos\delta \\ \Delta\delta \end{pmatrix} = R_2(-\delta_N)R_3(\alpha_N)\,\frac{\vec{r}}{d}\,, \tag{3}$$

where α_N, δ_N, and d are the RA, Dec, and distance of Neptune at observation time. If r and d are in the same units, the offsets, $\Delta\alpha\cos\delta$ and $\Delta\delta$, will be in radians. Multiply by 206,265 to obtain arcseconds. x is the radial component, positive away from the observer. If α_N, δ_N are 1950.0 coordinates, then the offsets will likewise be 1950.0 coordinates. To obtain offset coordinates of date, either precess the state vector r and then use α_N, δ_N coordinates of date, or precess the 1950 offsets as follows:

$$(\Delta\alpha\cos\delta)_{date} = (\Delta\alpha\cos\delta)_{1950} + \Delta\delta\, N\,\frac{\sin\alpha_m}{\cos\delta_m} \tag{4}$$

$$\Delta\delta_{date} = \Delta\delta_{1950} - (\Delta\alpha\cos\delta)\, N\,\frac{\sin\alpha_m}{\cos\delta_m}\,, \tag{5}$$

where N is the precession constant as defined in the Astronomical Almanac, and α_m, δ_m are 1/2 $(\alpha_{1950} + \alpha_{date})$ and 1/2 $(\delta_{1950} + \delta_{date})$, respectively.

The ephemeris of the orbit normal can be obtained by rotating the unit vector in the z direction (0,0,1) as in equation (1):

$$\vec{r} = R_3(-\alpha_p - \tfrac{\pi}{2})R_1(\delta_p - \tfrac{\pi}{2})R_3(-\Omega)R_1(-i)\begin{pmatrix} 0 \\ 0 \\ 1 \end{pmatrix}. \tag{6}$$

The spin axis of Neptune does not lie exactly in the direction of the pole of the invariable plane (α_p, δ_p), but rather is tipped by an angle ε toward the direction of Triton's orbit normal and co-precesses with it such that the component of Triton's orbital angular momentum which lies in the invariable plane is equal and opposite to the component of Neptune's spin angular momentum in that plane. This is illustrated in Figure 1. Because Neptune's spin and Tritons orbital motion are in opposite directions, the pole is tipped toward the orbit normal, rather than away, as would be the case for spin and orbit motion in the same direction. For nominal values of all factors involved, $\sin \varepsilon = -0.173 \sin i$, or $\varepsilon = -3^{\circ}\!.6$ for $i = 21^{\circ}\!.0$. The uncertainties which affect the determination of this angle are discussed

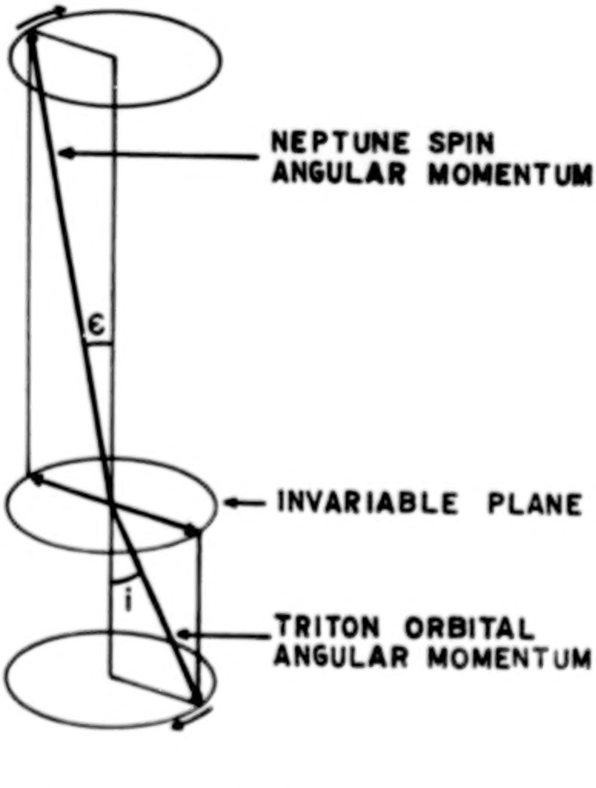

Figure 1. The pole of Neptune is inclined by an angle ε to the pole of the invariable plane such that the component of its spin angular momentum in the invariable plane is equal and opposite to the component of Triton's orbital angular momentum in the invariable plane.

further in the next section. For the present purpose, it suffices to note that the mass of Triton may be much less than the Alden value[5], and thus ε may be much smaller. To obtain the spin axis of Neptune, replace i by $-3\overset{\circ}{.}6$ (or $+3\overset{\circ}{.}6$ for assumed retrograde spin, or a lower value for assumed lower mass of Triton) in the above equation. The apparent positions of the orbit and spin axis can be found by further rotating by the RA and Dec of Neptune, equation (3).

PHYSICAL RESULTS

Some of the solution constants stated in the last section are highly correlated. Thus the error bars which should be assigned for the purpose of deriving physical properties of Neptune or Triton are in some cases much larger than the precision required to generate a fully accurate ephemeris. The orbital constants of physical interest, with appropriate uncertainties, are:

$$a = 0.0023683 \pm 0.0000015 \text{ au}$$

$$n_s = 61\overset{\circ}{.}2572 \pm 0\overset{\circ}{.}0001 \text{ per day}^*$$

$$|\dot{n}| \leq 2 \text{ degrees/century}^2$$

$$e \leq 0.0005$$

$$i = 21\overset{\circ}{.}0 \pm 1\overset{\circ}{.}5$$

$$T_p/\sin i = 1738 \pm 3 \text{ years}$$

The eccentricity, e, and acceleration of the mean motion, $\dot{n}$, were not a part of the formal solution. The post-fit residuals were examined for characteristic signatures of each of these effects. Neither was found at a statistically significant level. The quoted limits correspond to the ability of the data set to yield a 1σ detection.

---

*The above value is the sideral, rather than nodal, mean motion. The large associated error is due to the uncertainties in the inclination and the nodal precession rate.

In addition to the above constants, several auxiliary constants are needed in order to derive physical properties. The equatorial radius of Neptune, r_N, and optical flattening have been determined by stellar occultation[9,10]:

$$r_N = 25,225 \pm 30 \text{ km}$$

$$f = 0.021 \pm 0.004.$$

The orbit radius of Triton in planetary units is thus $a/r_N = 14.10 \pm 0.01$.

The rotation period is best determined by lightcurve variations in the methane absorption bands[11,12]:

$$P_N = 18^{h}\!.2 + 0^{h}\!.4.$$

Both the direction of rotation and the period appear to be confirmed by direct imaging[13].

The mass of Triton has been determined by measuring the barycentric wobble of Neptune against background stars[5]:

$$m_T/m_N = 0.00128 \pm 0.00023 .$$

The difficulty of this measurement, along with the apparently inconsistent radiometrically determined diameter of Triton[14], suggest that Triton may actually be considerably less massive. The possibility of a substantial atmosphere and/or ocean on Triton would considerably alter the thermal balance of Triton[15,16], thus it may be possible to reconcile the observed IR emission with a body as massive as the Alden value and a reasonable density. However, pending a redetermination of Triton's mass, one should keep in mind the possibility that Triton may be less massive than the above value.

Mass of the Neptune Triton system. The mean motion of Triton and the semimajor axis of its orbit determine the combined mass of the two bodies:

$$n_s^2 = \frac{G(m_N + m_T)}{a^3} .$$

Stated in the usual form of inverse solar masses, the result is:

$$\frac{m_\odot}{m_N + m_T} = 19490 + 40.$$

This value is somewhat larger (less mass) than earlier estimates (summarized in references 17,18).

Tidal evolution of Triton's orbit. The limit on the acceleration of the mean motion constrains the tidal effective Q of Neptune as follows:[20]

$$\frac{Q_N}{k_2} = \frac{9}{2} \frac{m_T}{m_N} \left(\frac{r_N}{a} \right)^5 \frac{n_s^2}{\dot{n}_s} .$$

Thus for $n_s < 2^\circ/\text{century}^2$, $Q_N/k_2 > 450$. For a fluid sphere, $k_2 = 5/[1 + 6.25(1-1.5\gamma)^2]-1$ (see ref 19, p. 73), where the moment of inertia factor $\gamma = C/m_N r_N^2$, is a measure of the central condensation of Neptune. γ estimated from a theoretical interior model of Neptune[20] is 0.19[21], thus $k_2 \sim 0.2$, and $Q_N > 2000$. A value this low would result in a very short tidal decay time for Triton ($\sim 3 \times 10^7$ years), and is very much less than the lower limit on Q of Uranus constrained by the limited outward evolution of its satellite system[22], $Q_U > 70{,}000$. It is noteworthy that if $Q_N \sim Q_U$, then the timescale of decay of Triton's orbit is $> 3 \times 10^9$ years.

Tidal decay of the orbital eccentricity. The upper limit on the orbital eccentricity, < 0.005, suggests that it is tidally decayed from a larger value. Neglecting the effect of the planetary tide, the tide raised on the satellite by the planet causes the eccentricity to decay with a time constant of[22]

$$t_o = \frac{2}{21}\left(\frac{m_T}{m_N}\right)\left(\frac{a}{r_s}\right)^5\left(\frac{Q}{k_2}\right)_T n_s^{-1}$$

For the eccentricity to have decayed by at least an order of magnitude, $t_o < 2 \times 10^9$ years, whence $(Q/k_2)_T < 5 \times 10^5$. The value k_2 for Triton is very uncertain, since its size, mass and composition are all somewhat uncertain. A value in the range $10^{-2} - 10^{-1}$ should be appropriate (cf. reference 19,22), hence $Q_T < 10^4$. This is an implausibly high value for any reasonable solid body, hence one could better reverse the argument to show that for any reasonable size, mass, and density of Triton, the tidal decay timescale is very short, $t_o < 10^7$ years. Because of Triton's retrograde orbit, there are no resonances which could have excited an appreciable eccentricuty in the past, thus it is safe to conclude that Triton's orbit is now, and has been for at least 4×10^9 years, very circular. Therefore, it is unlikely that any evidence of tidal heating or tidally induced surface features will be found on Triton.

Gravitational harmonics of Neptune. The second degree harmonic, J_2, causes the precession of the orbit plane about the invariable plane. The torque couple between the equatorial bulge and Triton, and hence the rate of motion of the orbit normal, depends on the inclination of the orbit to Neptunes equator, $i + \varepsilon$. As discussed in the last section (see Figure 1), ε is determined by equating the components of Triton's orbital angular momentum and Neptunes spin angular momentum which lie in the invariable plane:

$$\sin \varepsilon = \frac{m_T a^2 n_s}{\gamma \, m_N r_N^2 \omega_N} \sin i \quad ,$$

where $\omega_N = 2\pi/P_N$ is the rotation frequency of Neptune. Note that for a prograde spin of Neptune (n_s of opposite sign to ω_N), ε has the opposite sign of i, hence the equator is tipped toward the orbit plane of Triton. For $\gamma = 0.19$, $m_T/m_N = 0.00128$, $a/r_N = 14.10$, and $n_s/\omega_N = 0.129$ (corresponding to a rotation period of Neptune of 18.2 hours),

$$\sin \varepsilon = -0.173 \sin i \quad .$$

Thus for the generally accepted prograde rotation of Neptune the total angle between Neptune's equator and Triton's orbit plane is $i + \varepsilon = 17\overset{\circ}{.}4 \pm 1\overset{\circ}{.}2$. However if Neptune spins in a retrograde sense, then $i + \varepsilon = 24\overset{\circ}{.}6 \pm 1\overset{\circ}{.}8$. Furthermore, if Triton is much less massive than claimed, or if Neptune spins more rapidly than claimed, or if γ is larger than 0.19, then ε may be much smaller, thue $i + \varepsilon$ may be $\sim 21^\circ$ regardless of the direction of Neptune's spin. It is clear that the above uncertainties, primarily the mass of Triton, dominate the error budget of $i + \varepsilon$, thus a redetermination of the mass of Triton is of great importance.

The torque felt by Triton in its orbit from the equatorial bulge of Neptune (the J_2 gravitational harmonic) is proportional to $\sin 2(i + \varepsilon)$. The distance traveled by the orbit normal to complete a single precession cycle is proportional to sin i. Hence the precession rate, $\dot{\Omega}$, depends on both angles as follows:

$$\dot{\Omega} = \frac{3}{4} \; \frac{J_2 n_s}{(a/r_N)^2} \; \frac{\sin 2(i+\varepsilon)}{\sin i} \; .$$

This can be rearranged to solve for J_2 in terms of the orbit precession period, T_P, and the orbit period of Triton, T_T:

$$J_2 = \frac{4}{3} \left(\frac{a}{r_N}\right)^2 \; \frac{1}{\sin 2(i+\varepsilon)} \; T_T \; \frac{\sin i}{T_P} \; .$$

The uncertainties in i and T_p are highly correlated, such that $T_p/\sin i = 1738$ years is very precisely determined. Unfortunately, the determination of J_2 is still strongly affected by the uncertainty in the remaining factor sin 2(i+ε). For the above adopted value of $\varepsilon = 3\overset{\circ}{.}6$, $J_2 = 0.0043 \pm 0.0003$ if Neptune's spin is direct, or $J_2 = 0.0032_5 \pm 0.0002$ if it is retrograde. If Triton is much less massive than claimed, then $J_2 = 0.0037 \pm 0.0002$, regardless of the direction of Neptune's spin.

The four quantities, γ, rotation period P_N, optical flattening f, and gravitational harmonic J_2, are related such that if any two are known, the other two can be uniquely inferred. Figure 2, adapted from reference 20 (see also reference 23) summarizes the current status of observational and theoretical determinations of these quantities. The "prograde" and "retrograde" values of J_2 are plotted at the measured value of f, and again on the line of the observed rotation period, $18\overset{h}{.}2$. The associated error bars are indicated. It is likely that either the rotation period or the flattening is in error. If those two values are assumed to be exactly correct, then J_2

would be ~9σ from its computed value, and γ would be ~0.38, which is impossibly high for any reasonable composition of Neptune.

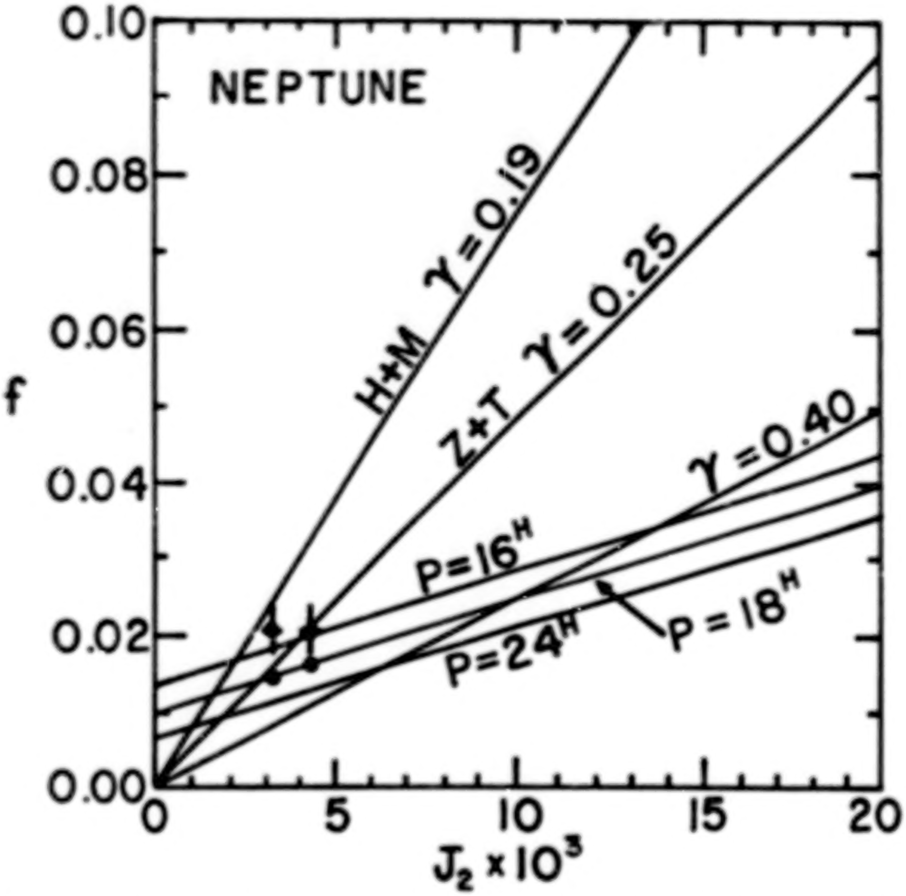

Figure 2. The values of J_2 assuming Alden's value of the mass of Triton are plotted for prograde and retrograde spins of Neptune, at the Kovalevky and Link value of flattening, and along the line of 18 hours rotation period. Formal error bars for J_2 and f are indicated.

The so-called "pear-shape" harmonic, J_3, of Neptune can be constrained by the observed circularity of the orbit of Triton[24]:

$$J_3 < 2J_2 \frac{a}{r_N} \frac{\Delta e}{\sin i} ,$$

where Δe is the maximum deviation from circularity, or 0.0005. Thus $J_3 <$ 0.00014. This is not a very significant constraint, since one would not expect a value even as large as $\sim 10^{-6}$ for a solid planet the size of Neptune.

Climate on Triton. The Cassini state of Triton is inclined ~0°.9 to the orbit normal in a direction away from the pole of the invariable plane. Hence the equator of Triton is inclined ~22° to the invariable plane and precesses about it with a period of 650 ± 40 years. Due to the motion of Neptune in its orbit, the sun appears to circulate along a path inclined ~30° to the invariable plane with a period of 166 years. The combination of these two motions results in a variation of the subsolar latitude on Triton which is quite complex, and can reach an extreme value as large as 52°. Figure 3 is a plot of the subsolar latitude on Triton for 3000 years. At present, the subsolar latitude is at +40° and increasing toward a peak of +52° by the year 2005. Hence ~10% of the total area of Triton surrounding the south pole is hidden from sunlight and will remain so for ~50 years. These extreme variations in insolation may lead to drastic variations in the density and composition of Triton's atmosphere with time[26]. It is noteworthy that Pluto experiences similar (even larger) variations, and is just now passing through equatorial aspect. Thus even if the two bodies are quite similar in size and composition, their present atmospheres may be very different.

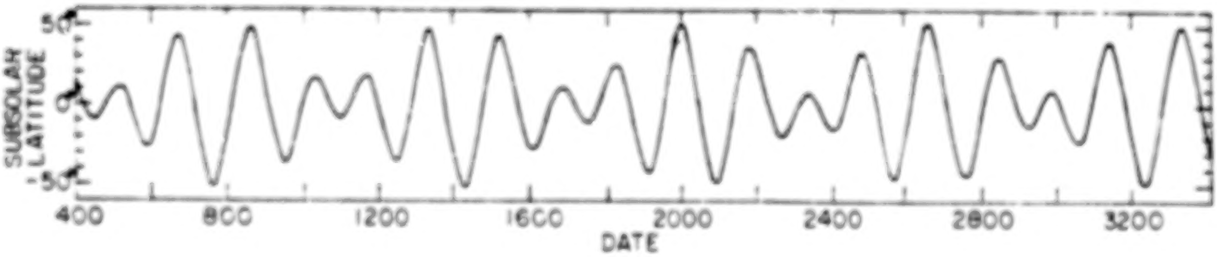

Figure 3. The subsolar latitude on Triton for 3000 years. The present subsolar latitude is indicated by the cross.

SUMMARY: OBSERVATIONAL DESIDERATA

Despite their similarity of appearance, Uranus and Neptune may be very different worlds, much as Jupiter and Saturn have proven to be. Thus it is important to our understanding of the origin and evolution of the solar system to determine the interior structure of Neptune without prejudice from Uranus. To that end, it is important to measure the mass of Triton, optical flattening, period of rotation, and equatorial plane of Neptune unambiguously so that J_2 and γ can be inferred with certainty. The mass of Triton can be redetermined from ground based astrometry. Both the USNO Flagstaff station and the ESO have demonstrated the capability to do this[6,7,18]. Continued observations of stellar occultations by Neptune may improve the determination of flattening somewhat. Voyager imaging should allow a better determination, but will take some care to extract the right answer, as demonstrated by the difficulty in determining the figure of Io. The period of rotation and plane of the equator should be determined in great detail by Voyager. Space Telescope will of course be able to do a superb job in re-determining the mass of Triton, and this should be done if possible before the Voyager encounter. Direct imaging from ST is unlikely to improve meaningfully upon the determination of flattening or the orientation of the equatorial plane.

Triton is emerging as one of the most fascinating bodies in the outer solar sytem. A redetermination of its mass is thus important for physical studies of Triton, in addition to the value for studies of Neptune. A direct measure of the diameter of Triton is of highest priority. Along with the mass determination, these will allow a determination of the mean density. With reflectance photometry, a meaningful albedo can be found. And along with the radiometric brightness, one can begin to construct a model of atmospheric heat transport, or lack of it. A stellar occultation by Triton is the only hope for making an accurate ground-based measurement of the diameter of Triton. Such an event would also yield a direct probe of Triton's atmosphere. Thus the successful observation of a stellar occultation by Triton is perhaps the most scientifically exciting ground-based experiment contemplated for the outer planets.

ACKNOWLEDGEMENT

This work was supported at the Jet Propulsion Laboratory, California Institute of Technology, by contract from the Planetary Program of NASA.

REFERENCES

1. Eichelbreger, W.S., and Newton, A. (1926) The orbit of Neptune's satellite and the pole of Neptune's equator. Astron. Pap. Am. Ephem. 9, 275-337.
2. Gill, J.R., and Gault, B.L. (1968) A new determination of the orbit of Triton, pole of Neptune's equator, and mass of Neptune. Astron. J. 73, 595 (abstract).
3. Gill, J.R. (1959) The motion of Neptune's satellite Triton. PhD dissertation, Yale University, New Haven 59 pp.
4. Alden, H.L. (1942) Observations of the satellite of Neptune. Astron. J. 49, 70-72.
5. Alden, H.L. (1943) Observations of the satellite of Neptune Astron. J. 50, 110-111.
6. Walker, R.L., Christy, J.W., and Harrington, R.S. (1978) Positions of planets and natural satellites. Astron J. 83, 838-844.

7. Harrington, R.S., private communication of USNO observations not yet published.

8. Observations of the satellite of Neptune. Greenwich Observations (1899) 243, (1902) 61, (1903), 99-100, (1904) 151, (1905) 175, (1906) 177-178, (1907) 209, (1908) 193, (1911) C67-C68.

9. Kovalevsky, J. and Link, F. (1969) Diamètre, aplatissement et propriètès optiques de la haute atmosphère de Neptune d'apres l'occulation de l'etoile BD-17^{o}4388. Astron. Astropys. 2, 398-412.

10. French, R. (this volume).

11. Belton, M.J.S., Wallace, L., and Howard, S. (1981) The periods of Neptune: Evidence for atmospheric motions.

12. Belton, M.J.S. and Terrile, R. (this volume).

13. Smith, B. A. (this volume).

14. Lebofsky, L.A., Rieke, G.H., and Lebofsky, M.J. (1982) The radii and albedos of Triton and Pluto. Bul. Amer. Astron. Soc. 14, 766.

15. Cruikshank, D.P., and Brown, R.H. (1984) Outer planet satellites. In Natural Satellites (J. Burns ed.) University of Ariz. Press, Tucson (in press).

16. Cruikshank, D.P. (this volume).

17. Mignard, F. (1981) The mean elements of Nereid. Astron. J. 86, 1728-1729.

18. Veillet, C. (1982) Orbital elements of Nereid from new observations. Astron. Atrophys. 112, 277-280.

19. Kaula. W.M. (1968) An Introduction to Planetary Physics: The Terrestrial Planets, p. 202. Wiley: New York, 490 pp.

20. Hubbard, W.B., and McFarlane, J.J. (1980) Structure and evolution of Uranus and Neptune. J. Geophys. Res. 85, 225-234.

21. Harris, A.W. and Ward, W.R. (1982) Dynamical constraints on the formation and evolution of planetary bodies. _Ann. Rev. Earth Planet Sci. 10_, 61-108.

22. Goldreich, P., and Soter, S. (1966) Q in the solar system, _Icarus 5_, 375-389.

23. Hubbard, W.B. (this volume).

24. Yoder, C.F. (1984) private communication.

25. Trafton, L. (this volume).

BLANK PAGE

PART IV

Satellite System

BLANK PAGE

ORIGIN AND EVOLUTION OF THE URANIAN AND NEPTUNIAN SATELLITES: SOME DYNAMICAL CONSIDERATIONS

Stanley F. Dermott
Center for Radiophysics and Space Research
Cornell University
Ithaca, NY 14853

Abstract

The satellite system of Neptune is so irregular that some formation mechanism or subsequent dynamical evolution that sets it apart from the other, more regular, satellite systems is obviously indicated. McKinnon has argued that satellite capture is the most likely possibility and has shown that tidal circularization of Triton's presumably highly eccentric initial orbit probably resulted in melting of the satellite's interior. The satellite system of Uranus, although somewhat bland, also has a number of special features that indicate an interesting dynamical history. These include the anomalously high orbital inclination of Miranda and the probable coexistence of small satellites and narrow rings inside the planet's Roche limit. I discuss the possibility that orbital evolution due to tidal dissipation is involved in both of these phenomena. Other topics discussed are: the origin of rings; the formation of coorbital satellites; the lack of stable orbit-orbit resonances in the Uranian satellite system; and chaos, tidal heating and the shapes of Miranda and Ariel.

INTRODUCTION

Some of the most interesting recent work on the origin of satellites has focussed on the problems posed by a few special features and processes, particularly those revealed or inspired by spacecraft exploration. The radial density gradient in the Jovian satellite system is a good example, although that was discovered by ground-based methods and only confirmed by spacecraft observations. This gradient can be accounted for if Jupiter was once a giant gaseous protoplanet that went through a phase of high luminosity as it contracted to its present size.[1] The closer views of the Galilean satellites afforded by Voyager have revealed more specific problems. Of these, the one most diagnostic of accretion conditions is probably that of the contrasting surfaces of Ganymede and Callisto.[2] These satellites have almost the same size and mean density and yet their surfaces are quite different, with that of Ganymede appearing to be much younger than that of Callisto.

Measurements of the abundance of methane in Titan's atmosphere, apart from inspiring speculation on the existence of hydrocarbon oceans,[3,4,5] also raise the question of how carbon was incorporated in the satellite. At Saturn's distance from the sun, satellites are composed mostly of silicate rock, water-ice, Ar and compounds containing C, N and O. Lewis and Prinn[6] concluded that CO and CO_2 were the major carriers of carbon in the solar nebula. However, Prinn and Fegley[7] investigated conditions in the Saturnian nebula and showed that the reaction rate of CO to CH_4 was rapid relative to the nebula cooling and radial mixing rates. Thus, it is likely that CH_4 was the major carrier of carbon in the Saturnian nebula and that CH_4 was incorporated in Titan in a CH_4-, Ar-, N_2- (or NH_3) rich clathrate hydrate. The detection of a hydrocarbon ocean by a spaceborne radar reflectometer[4] could confirm ideas on the evolution of Titan's putative ocean and on accretion conditions in the Saturnian nebula.

A new aspect of accretion dynamics raised by Voyager is that of the role of cometary bombardment in the disruption of small satellites.[8] This role could, perhaps, have been anticipated prior to the Voyager encounters. However, spacecraft images showing the surviving small satellites bearing impact craters with diameters comparable to the satellite radii force us to conclude that these satellites have suffered impacts only marginally below the probable disruption level,[9] implying that from time to time more disruptive collisions probably occur. Other important, recent developments include the discovery of numerous coorbital satellites in the Saturnian (but not the Jovian) satellite system and the discovery by Goldreich and Tremaine[10] of the shepherding satellite mechanism.

TABLE 1: Satellites of Neptune

	Radius km	a Planetary Radii	e	I Degrees
Triton	1750 ± 250	14.6	<0.005	158.5
Nereid	(200)	227	0.75	27.6
X	50-500	3 ± 1	--	--

The satellite system of Neptune has a number of special features that suggest obvious points of attack. In fact, the irregularity of the system is the only aspect that is discussed in the literature. The data are shown in Table 1. Since the work of Lyttleton,[11] the origin of Pluto has often been discussed in association with that of the satellites of Neptune, but, as we shall see, it is now considered unlikely that Pluto is an escaped satellite. Pluto, Triton and Nereid are probably remanent planetesimals, two of which (at least) were captured by Neptune, destroying in the process any regular satellite system that the planet may have possessed. The newly discovered satellite of Neptune,[12] satellite X, may be a member of the original satellite system that survived the capture of Triton, possibly because the satellite's orbit is closer to the planet than Triton's initial pericenter distance.

The feature of the Uranian system most often remarked upon is the planet's high obliquity (98°) and the fact that, despite the latter, the satellites are near-equatorial. I have never been much impressed by these arguments. In a qualitative sense, there is little difference between an obliquity of 30° (Earth, Mars, Saturn and Neptune) and one of 90°. Harris and Ward,[13] chiefly following Safronov,[14] have calculated the masses of the largest planetesimals needed to produce the observed obliquities of Saturn and Uranus. These are ~ 10 and ~ 1 Earth masses respectively, making Saturn's obliquity the more startling. Note, however, that these planetesimal masses are completely at odds with the masses needed to account for the orbital eccentricities and inclinations which are a factor ~ 10^{-2} smaller.[13]

TABLE 2: Satellites of Uranus[1]

	a Planetary Radii	e	I degrees	sinI/e
Miranda	5.0	0.0027	4.22	27.2
Ariel	7.3	0.0034	0.31	1.6
Umbriel	10.2	0.0050	0.36	1.3
Titania	16.7	0.0022	0.142	1.1
Oberon	21.7	0.0008	0.101	2.3

[1] Data from Ch. Veillet (Ph.D. Thesis, Paris, 1983).

Dynamical features of the Uranian system that can, at present, be profitably discussed include: the probable coexistence of small satellites and narrow rings within the planet's Roche limit; the high inclination of Miranda's orbit; and the complete lack of stable orbit-orbit resonances. (The Laplace-type resonance involving Miranda, Ariel and Umbriel is not exact and has no special dynamical significance.) The orbital data are shown in Table 2. For all the satellites, except Miranda, and for most of the narrow rings,[15] sinI/e ≈ 1, making the value of 27 for Miranda anomalously high.

One uniting theme of this talk will be tidal evolution of satellite orbits and its observable consequences. Other major topics will be the origin of planetary rings and the origin and evolution of coorbital satellites.

SATELLITE CAPTURE

The idea of an encounter between Pluto, as a satellite of Neptune, and Triton, as proposed by Lyttleton,[11] has been shot down by McKinnon[16] and Lin.[17] Using the presently accepted masses of Triton and Pluto (plus Charon), McKinnon has shown, simply by considering the energy and angular momentum exchanges involved, that any plausible interaction between the two bodies that could have reversed the orbit of Triton would also have resulted in the ejection of Pluto from the solar system. Lin[17] has pointed out that if the Pluto-Charon system was once a double satellite of Neptune, then Pluto and Charon's combined tidal interaction (at the distance of Triton from Neptune) would have driven them to merge with each other within $\sim 10^5$ years.[17,16]

Several other schemes for disrupting the Neptunian system and ejecting Pluto have been proposed.[18,19,20] That of Harrington and Van Flandern[18] is probably the most interesting. They consider the passage of a very large planetesimal (of 2-5 Earth masses) through an initially regular system. (This planetesimal may be still bound to the sun in a distant trans-Neptunian orbit.[18]) Using bullets of this size, spectacular results can be achieved but they are somewhat improbable--the probability of ejecting Pluto into a bound orbit being ~ 0.005. We now know that even if close encounters with Neptune were possible, and even if repeated encounters were allowed, Pluto itself is far too small to disrupt the Neptunian system.[18] It seems probable that Pluto-Charon are remanent planetesimals that were never satellites of Neptune and that Triton and Nereid are planetesimals that were somehow captured by Neptune.

Satellite capture typically involves a dramatic loss of energy during a single encounter and this can only be achieved in special circumstances. Capture through the inner Lagrange point has been suggested, but this can only lead to permanent capture if it is accompanied by significant mass changes, of either the sun or the planet, on the same timescale as that of temporary capture and this is very short (1 to 10^2 years).[21,22,23]

Capture could be most directly achieved by a collision within the planet's Hill's sphere.[24,25] This is the mechanism favored by Stevenson et al.[2] for the origin of the outer, irregular Jovian satellites. The mechanism does have the advantage that it is not tied to a particular model of planet formation. If, however, a planet did pass through a giant gaseous protoplanet phase, then capture due to gas drag is possible. This has now been proposed for the origin of the Moon,[26] Phobos and Deimos,[27] the irregular Jovian satellites,[23] Phoebe and Iapetus,[23] and Triton and Nereid.[23] In the case of the Jovian satellites, Pollack et al.[23] describe a number of features of the two irregular satellite groups that positively support the gas drag hypothesis. The lack of small satellites[29] is particularly significant.

Although the orbit of Triton is now near-circular, this may not have been the case in the past since tidal dissipation in the body of the satellite would have acted to circularize the orbit.[30] If Triton was captured, then the initial orbit may have been highly eccentric.

McKinnon[16] has recently investigated the latter extreme case and has shown that the orbit would have circularized in ~ 4 10^6 Q years, where Q is the tidal dissipation function of Triton and that the heat flow produced by the tidal dissipation would have been sufficient to melt the satellite's interior, releasing to the surface the satellite's inventory of clathrated gases.

ORIGIN OF RINGS

Harris[31] has argued persuasively that ring particles are not primordial. There are a number of processes that operated in the circumplanetary disk of gas and solids out of which the satellites accreted that would have removed particles inside the planet's Roche limit on timescales less than that for planet formation. These processes also acted on particles outside the Roche limit, but, if in that region contact led to coagulation, then accretion timescales were even shorter than the other timescales and satellite growth was rapid. The processes that Harris has considered include viscous spreading, gas drag and the effect of the infall of matter from heliocentric orbits onto the circumplanetary disk.

Viscous dissipation results in spreading on a timescale ~ 10^2 years. This is very short and may be less than the time needed for a planet to collect a substantial disk of material from heliocentric orbits.[31] This may be an acute problem for satellite as well as for ring formation.

Solid particles in a disk rapidly settle to the midplane[32,33], but since they orbit the planet at slightly higher speeds than the surrounding gas, they experience a negative torque which reduces their orbits. The orbital decay timescale for the midplane sheet as a whole is determined by the ratio of the surface mass densities of the surrounding gas and of the solids in the sheet and is 10-10^3 years. Satellites of radius r (in kms) also experience orbital decay due to aerodynamical drag on timescales between 5r years and 10^4r years, depending on their location.[31]

Since the present ring particles are not primordial, Harris considers that they derive from small satellites that were dragged inside the planet's Roche limit at the tail-end of the accretion process due to the infall of heliocentric material. Since the planets are far from rotational instability, Harris argues that the infalling material must have carried very little angular momentum with it.[34] Hence, addition of heliocentric material to the circumplanetary disk must have resulted in drag on both the disk material (and this in itself is an efficient way of removing primordial ring particles) and on any satellites present. This resulted in orbital decay on a timescale related to the accretion rate by

$$\frac{\delta a}{a} \sim - \frac{dm}{m} \qquad (1)$$

where a is the orbital radius and m the mass of the growing satellite. Harris considers that the small satellites brought inside the planet's Roche limit by this process were later disrupted by meteoritic bombardment.

This is a compelling scenario and while agreeing that the ring material was probably stored for some time in small satellites, I would argue that these satellites may have been dragged inside the Roche limit by tidal forces.[35,36] This process may not work for Saturn's rings, since icy satellites of density ~ 1 g cm^{-3} can only form outside Saturn's

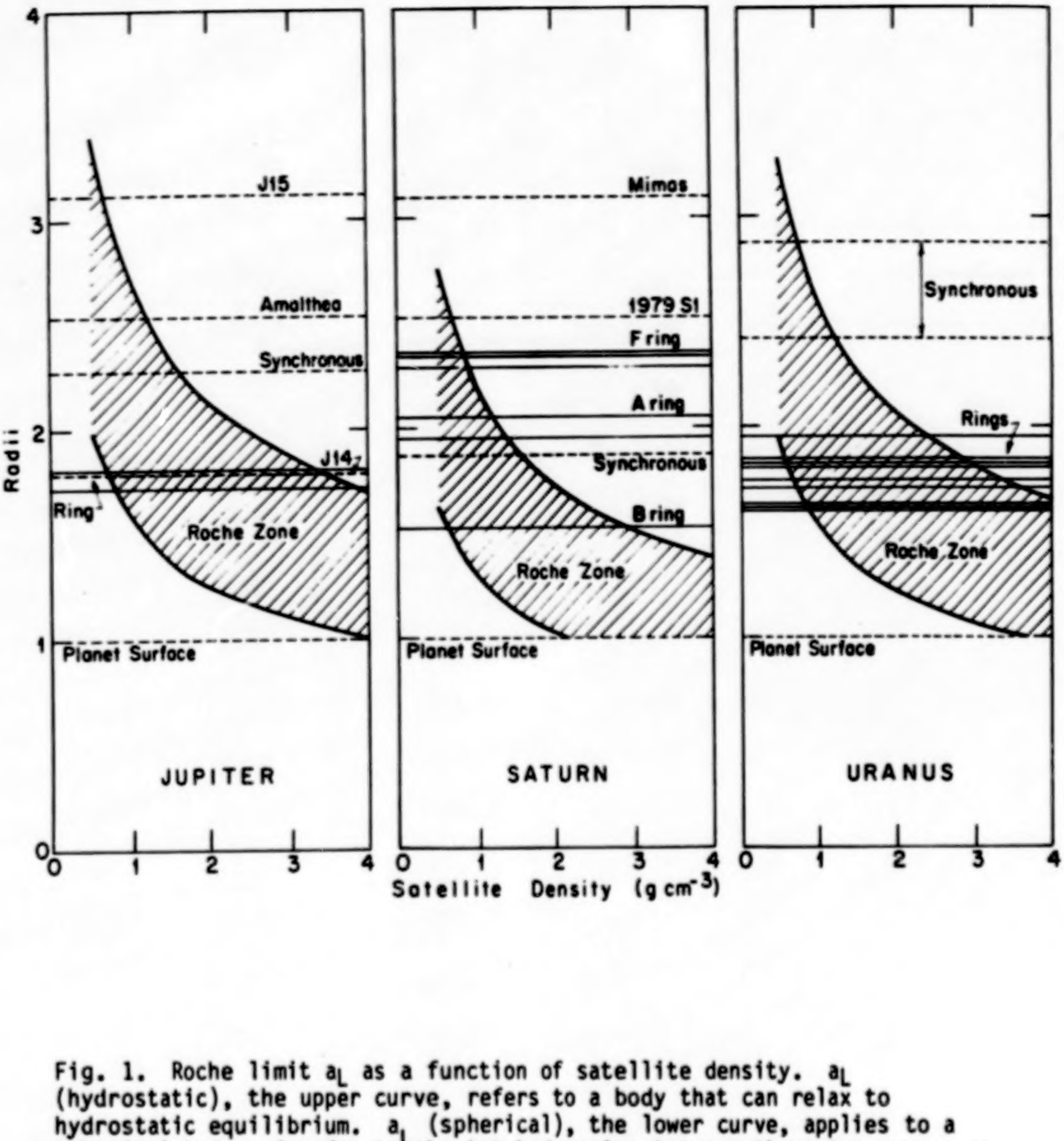

Fig. 1. Roche limit a_L as a function of satellite density. a_L (hydrostatic), the upper curve, refers to a body that can relax to hydrostatic equilibrium. a_L (spherical), the lower curve, applies to a spherical body. I refer to the hatched region between these two curves as the Roche zone. It is in this zone that unconsolidated satellites and ring particles can coexist.[35,36,37] (Copyright of the Royal Society, London.)

synchronous orbit (see Fig. 1). For that system, we may have to invoke Harris' process of accretion drag. For the Jovian and the Uranian systems, however, satellites of density > 2 g cm^{-3} (that is, carbonaceous or rocky rather than icy satellites) can form outside the Roche zone and still be inside the synchronous orbit. Tidal forces on these satellites will then cause their orbits to decay.

For the satellites to be brought inside the Roche zone in times less than the age of the solar system, they need to be as massive as 10^{-8} M, where M is the mass of the planet.[35,36,37] This is probably greater than the mass of the present Uranian ring system (shepherds and sheep) by a factor of ~ 10^2. But if the impact histories of these satellites were as violent and as disruptive as the shapes and the cratering records of some of the surviving small satellites in the solar system indicate, then these satellites were probably at least partially fragmented before entering the Roche zone. On entering the zone and suffering further impacts, these satellites would have dispersed and only those fragments not large enough to have been removed by tidal forces or not small enough to have been removed by the effects of further impacts now survive. It may be that the Uranian and Jovian rings are younger than the Saturnian rings and that only in the former have a few small satellites managed to survive the effects of prolonged meteoritic bombardment.

TIDAL EVOLUTION

Orbital evolution due to tidal dissipation has been discussed in the case of the satellites of the outer planets as a mechanism for the formation of the observed orbit-orbit resonances, in particular, the

Io-Europa-Ganymede, Laplace-type, resonance and the Mimas-Tethys and Enceladus-Dione resonances.[38,39] The major problem with the tidal hypothesis of resonance formation is that we have never been able to identify, with any degree of confidence, an adequate source of energy dissipation despite the fact that the necessary values of the tidal dissipation factor, Q, are extremely high (~ 10^5-10^6). The problem has been alleviated to some extent with the discovery of the tidal heating of Io and with Yoder's work on the Laplace resonance.[40,41] Although we still do not know the source of the dissipation, Yoder and Peale[41] have placed bounds on the tidal dissipation function of Jupiter, Q_J, viz.,

$$6\ 10^4 < Q_J < 2\ 10^6 \qquad (2)$$

where the upper bound is obtained from the observed thermal output of Io and the lower bound from the limited expansion of the satellite orbits. Since we are now confident that significant tidal dissipation probably does occur in the body of Jupiter, it is, perhaps, reasonable to assume that this may be the case for the other major planets. However, since we do not know the nature of the dissipation process, it may be a mistake to oversimplify the problem, as is usually done, and assume that the tidal dissipation function is amplitude, frequency, and time independent. I prefer to write[42]

$$Q = f(P,t)(\text{tidal amplitude})^p(\text{tidal frequency})^f \qquad (3)$$

where f(P,t) is a function of parameters of the planet only and time. We can further assume that the coefficients p and f are ≤ 0. Since the tidal frequency is approximately the same for all satellites, the frequency dependence of Q can be neglected in the first instance and we can write

$$Q = f(P,t)m^p a^{-3p} \qquad (4)$$

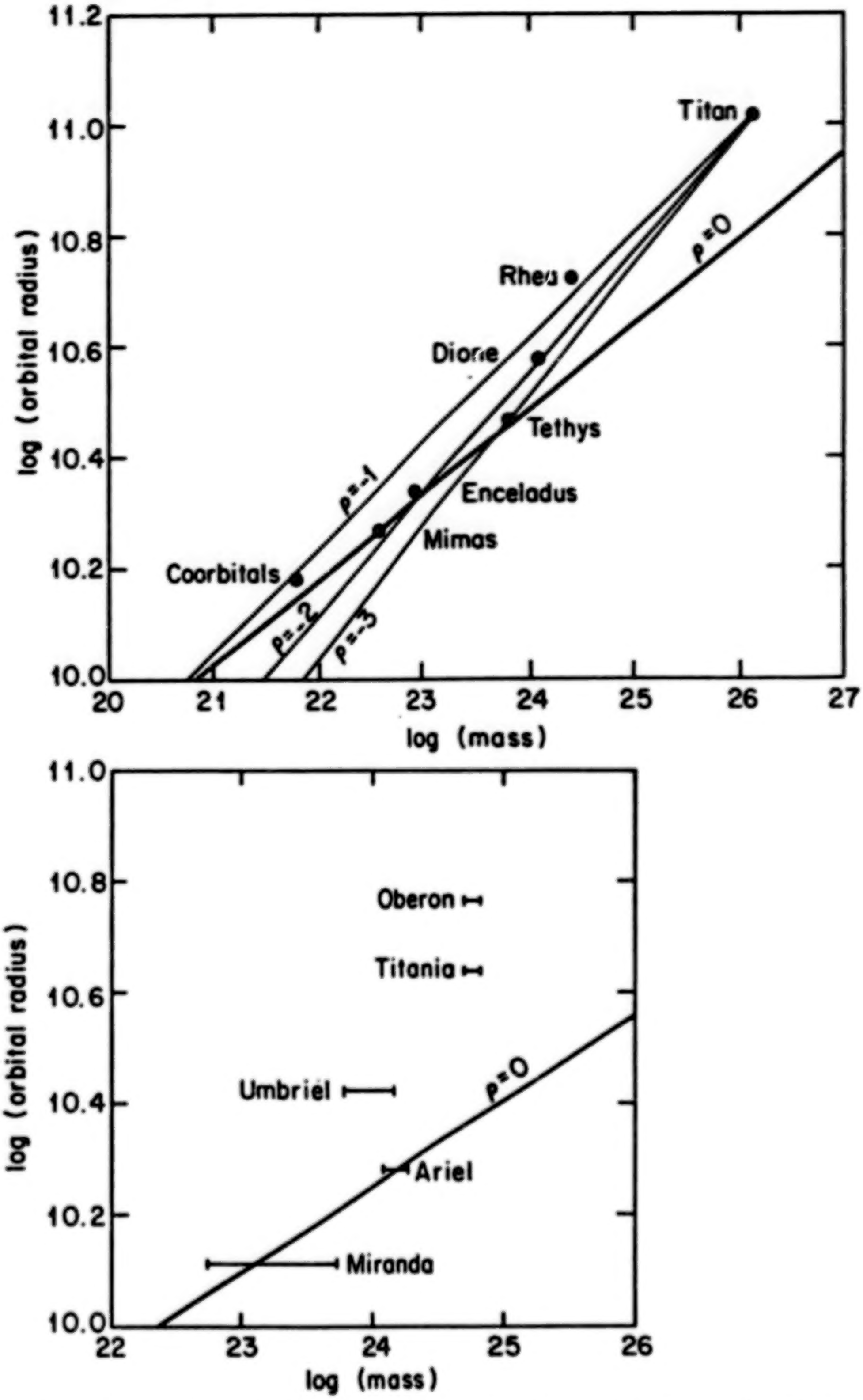

Fig. 2. If orbital evolution has been appreciable, then there should be a linear relation between log a and log m. p describes the amplitude dependence of the tidal dissipation function.

It can then be shown[42] that after appreciable orbital evolution, the orbital radii a of the satellites will be related to their masses m by

$$\log a = \frac{1 - p}{13/2 - p} \log m + \text{constant} \qquad (5)$$

Plots of log a against log m for the satellite systems of Saturn and Uranus are shown in Fig. 2.

There is the possibility that orbital evolution due to tidal dissipation has been the major factor in the structuring of the Saturnian satellite system. A remarkable feature of the latter is the progressive increase in mass with increasing orbital radius. Such a distribution is the only stable outcome of prolonged orbital evolution due to tidal dissipation. If the peculiar mass distribution is not original, then there must have been a major resorting involving orbital evolution, collisions, destruction and reaccretion before the observed distribution was achieved. This could be the reason why there now appears to be no relation between satellite mean density and orbital radius in the Saturnian system.

Such a major resorting, however, could only be achieved if the Saturnian tidal dissipation function Q is (or was!) amplitude dependent with $p \sim -2$ (see Fig. 2). We then have the problem that the stability of the Mimas-Tethys resonance cannot be accounted for.[42] Two statements can be made about this: (a) the analysis is incorrect since tidal dissipation is treated in a linear fashion, whereas if Q is amplitude dependent, then the problem is highly non-linear; (b) there may be more than one source of tidal dissipation and both sources may be time-dependent. Since we know so little about the nature of tidal dissipation, I do not feel at all compelled to accept the simple, constant, amplitude independent Q scenario. We may have to allow that a more complicated dissipation mechanism is the correct one.

Orbital evolution due to tidal dissipation could not possibly have been quite as dramatic in the Uranian as in the Saturnian satellite system. Even if we allow that Q is amplitude dependent, we must conclude that the orbits of the satellites beyond Miranda and Ariel are probably primordial. For Miranda and Ariel, however, even if Q is amplitude independent ($p = 0$), orbital evolution may have been appreciable. After appreciable orbital evolution, the ratio of the orbital radii will satisfy

$$\frac{a'}{a} = \left(\frac{m'}{m}\right)^{(1-p)/(13/2 - p)} \tag{6}$$

Measurement of the satellite masses by Voyager will enable us to estimate the value of p, always assuming, of course, that the orbits are tidally evolved.

RESONANCE OVERLAP AND CHAOS

That the orbits of the Uranian satellites are insignificantly tidally evolved may be an adequate explanation for the complete absence of stable orbit-orbit resonances in that system. However, another and more interesting possibility, which allows significant orbital evolution, involves resonance overlap and chaotic motion.[43]

The magnitudes and the phases of the perturbations of a satellite's near-keplerian orbit are determined by the disturbing potential U of the perturbing satellite. For a satellite moving in a total potential V, one may define U as $U = V - GM/r$, where GM/r is the central potential of the planet at the distance r of the satellite. The classical approach to solar system problems is to expand U in a Fourier-like series. The high-frequency terms in this series are then removed by averaging and the problem is reduced to a study of the equations of motion when only a single term, that associated with some resonant argument ϕ, is retained in the disturbing function. The circumstances under which this approach is not valid are now, to some extent, understood and appear to be well-described by the resonance overlap criterion.[44,45]

Consider the following specific example. At some location where the mean motions of two satellites are close to the ratio (p + q):p, there are an infinite number of possible resonances but most are weak and insignificant. Two of the stronger resonances satisfy the conditions

$$pn_1 - (p + q)n_2 + q\dot{\tilde{\omega}}_1 = 0 \tag{7}$$

or

$$pn_1' - (p + q)n_2 + q\dot{\tilde{\omega}}_2 = 0 \tag{8}$$

where n_1 and n_1' are two possible resonant mean motions of the inner satellite, $\dot{\tilde{\omega}}$ is the rate of motion of a pericenter as determined by the dynamical oblateness of the planet, J_2, the subscripts 1 and 2 refer to the inner and outer satellites, respectively, and p and q are integers. The separation $\delta n(= |n_1 - n_1'|)$ of these resonances is given by

$$\delta n = \frac{3}{2} J_2 n_1 (\frac{B}{a_1})^2 (1 - [p/(p + q)]^{7/3}) \tag{9}$$

$$\leq \frac{3}{2} J_2 n_1 (\frac{B}{a_1})^2 \tag{10}$$

where B is the radius of the planet.

If the inner satellite is trapped in some resonance of strength S, and the libration amplitude of the associated resonant argument ϕ is a maximum, then the range δn_ℓ through which the mean motion n_1 oscillates (or librates) is also a maximum. We have[43]

$$\delta n_\ell = 2(12|S|/a_1^2)^{1/2} \qquad (11)$$

For first-order resonances $q = 1$ and

$$|S|/a_1^2 = n_1^2 \, f(a_1/a_2) \, e \, (m_2/M) \qquad (12)$$

where $f(a_1/a_2)$ is a function of Laplace coefficients and $> 3/4$, and e refers to either of the free eccentricities e_1 or e_2 depending on whether the resonant argument involves $\tilde{\omega}_1$ or $\tilde{\omega}_2$, respectively, although in what follows I do not distinguish between e_1 and e_2.

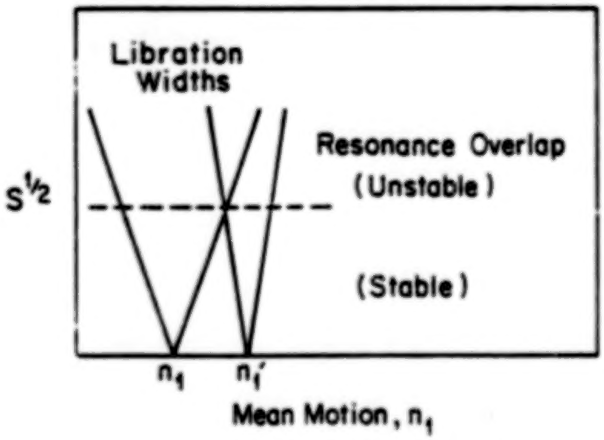

Fig. 3. The libration widths are the V-shaped regions. These represent the maximum range δn_ℓ through which n_1 can oscillate for a particular value of S, the strength of the resonance. For first-order ($q = 1$) resonance, S, and the libration width, increase with the orbital eccentricity e. If the eccentricities are large enough, then the resonances overlap and the resultant motion may be chaotic.

Resonance overlap occurs if the separation of the resonances is less than half the sum of the libration widths, that is, if

$$\delta n < \Sigma \, \frac{1}{2} \, \delta n_\ell \qquad (13)$$

where the sum is taken over both resonances (see Fig. 3). In these circumstances, the motion of the satellite is determined by both resonant terms in the disturbing function and it is a matter of experience that the resultant motion is chaotic. I estimate that for first-order resonance this will occur if

$$e > J_2^2 \left(\frac{B}{a_1}\right)^4 \frac{M}{6m_2} \qquad (14)$$

For the Uranian system, both J_2 and B/a_1 are small and, even for Miranda for which B/a_1 is a maximum, equation (14) is satisfied if $e > 0.0017$. This is less than any of the present free eccentricities (see Table 2).

Thus, it would appear that orbital evolution in the Uranian satellite system could not have resulted in the formation of stable, first-order, orbit-orbit resonances. The satellites Miranda and Ariel, however, may have evolved through a number of these resonances and many higher-order ($q > 1$) resonances. Since we do not know either the exact masses of these satellites or the nature of the tidal dissipation mechanism, we cannot ascertain if the ratio of the mean motions of these satellites was greater or lesser in the past. So, since the present ratio is 1.783, candidate resonances that could have been passed through include the 2:1 and the 3:2 resonances. In addition, the satellites Ariel and Umbriel may have passed through both the 5:3 and the 2:1 resonances.

The tidal evolution of orbits through a resonance in circumstances where the resultant motion is likely to be chaotic is a problem that deserves immediate attention. Particularly if, as in the case of some resonant asteroidal orbits,[46] the chaotic motion results in the excitation of large orbital eccentricities. The very high inclination of Miranda's orbit, which is almost certainly not primordial, and which, unlike any excited orbital eccentricity, would not have been reduced by subsequent tidal dissipation in the satellite,[47] encourages me to speculate that some spectacular changes in the orbital elements may have occurred.

TABLE 3: Eccentricity Damping Timescales, T_e

	V_0	m/M × 10^5	Radius km	Density g cm^{-3}	T_e/Q years
Miranda	16.5	(0.2)[1]	(280)	---	10^6
Ariel	14.4	1.8 ± 0.4	665	1.3 ± 0.5	4 10^5
Umbriel	15.3	1.2 ± 0.5	555	1.4 ± 0.6	8 10^6
Titania	14	6.8 ± 0.8	800	2.7 ± 0.6	2 10^7
Oberon	14.2	6.9 ± 0.8	815	2.6 ± 0.6	1 10^8

[1] Values in parentheses are estimates.

The eccentricity damping timescales, T_e, in Q years, where Q is now the tidal dissipation function of the satellite, are shown in Table 3. In calculating these timescales, I have assumed that the satellites are icy and have rigidities of 4 10^{10} dyne cm^{-2}. The associated tidal heating rates per unit mass, $\dot{E}/m$, are given by

$$\frac{\dot{E}}{m} = \frac{e^2}{T_e}\frac{GM}{2a} = \frac{e^2}{\mu Q\beta} \tag{15}$$

where

$$\beta = \frac{T}{\rho}\left(\frac{a}{M}\right)^2\left(\frac{a}{R}\right)^4 c \tag{16}$$

where c(= $38/63\pi G^2$) is a constant, and ρ, T and R are the density, orbital period and radius, respectively, of the satellite.

In units such that the value of β for Io is unity, the values of β for Miranda and Ariel are ~ 10^3 and it would appear that the heating rates of the inner Uranian satellites are comparatively low. However, there are several reasons why this is probably a pessimistic conclusion. If the satellites are icy, then μQ may be lower than that for a solid, rocky Io by a factor ~ 10^2. Tidal dissipation in icy satellites will be dominated by those parts of the satellite where the temperature is $> 0.5\ T_m$, where T_m is the melting point. Since T_m is particularly low, a small input of heat could lead to a marked drop in both the local Q and the effective rigidity. This special property of icy satellites would make the possibility of melting due to a tidal runaway easier to achieve than in a rocky Io.

The forced eccentricity of Io's orbit is 0.0041 which is comparable with the free eccentricities of Miranda and Ariel (see Table 2). However, passage through resonance may have excited much larger eccentricities than the present values and the subsequent heating events, on both Miranda and Ariel, although these would have occurred at different times, may have been large enough to cause substantial melting and resurfacing. However, much more work is needed on this problem and my comments here, although, perhaps, appropriate for a discussion meeting, should be regarded as preliminary.

If the surfaces of Miranda and Ariel have relaxed to hydrostatic equilibrium, then the shapes of these satellites will be far from spherical and measurements of the tidally and rotationally distorted figures would yield valuable information on their internal structures.[48] I estimate that the difference in the polar and the equatorial diameters of Miranda may be as large as 16 km.

COORBITAL SATELLITES

Some of the smaller satellites in the solar system share their orbits with larger companions. A major puzzle of the distribution of these satellites is that all the known coorbitals are associated with the Saturnian satellites. The Jovian system has been equally well observed but no coorbitals have been discovered. The status of the Uranian system in this respect will probably remain undetermined until the arrival of the Voyager 2 spacecraft in 1986.

The dynamics of coorbital satellite systems have been discussed by Dermott et al.[35,36] Dermott and Murray[49,50] Yoder et al.[51] and Sinclair.[52] Dermott et al. [35,36] pointed out that for two reasons we might expect horseshoe orbits in the solar system to be associated only with very small satellites. First, the ratio of the radial widths of those regions where, respectively, tadpole alone and tadpole and horseshoe orbits are possible is ~ $(m/M)^{1/6}$, where m is the mass of the larger of the two coorbitals and M is the mass of the planet. It follows that the horseshoe region is only dominant if $(m/M)^{1/6} \ll 1$. The second reason obtains from considerations of orbital stability. Dermott et al.[36,49] have suggested that due to perturbations by nearby satellites, the horseshoe paths may be imperfectly periodic and that random changes in the semimajor axes of the satellites of magnitude $\delta a/a \sim \pm m/M$ may occur on each encounter of the coorbitals. The horseshoe configuration would then have a lifetime, $L \sim T(m/M)^{-5/3}$, where T is the orbital period of the satellites (see Fig. 4). For $L > 10^8$ years, we require $m/M < 10^{-7}$. This should be regarded as more of a hypothesis than a definite result. Very little is known about the long-term dynamical stability of the solar system. However, if the above estimate of L is correct, then I would not expect the Uranian satellites to be associated with coorbitals moving in horseshoe paths.

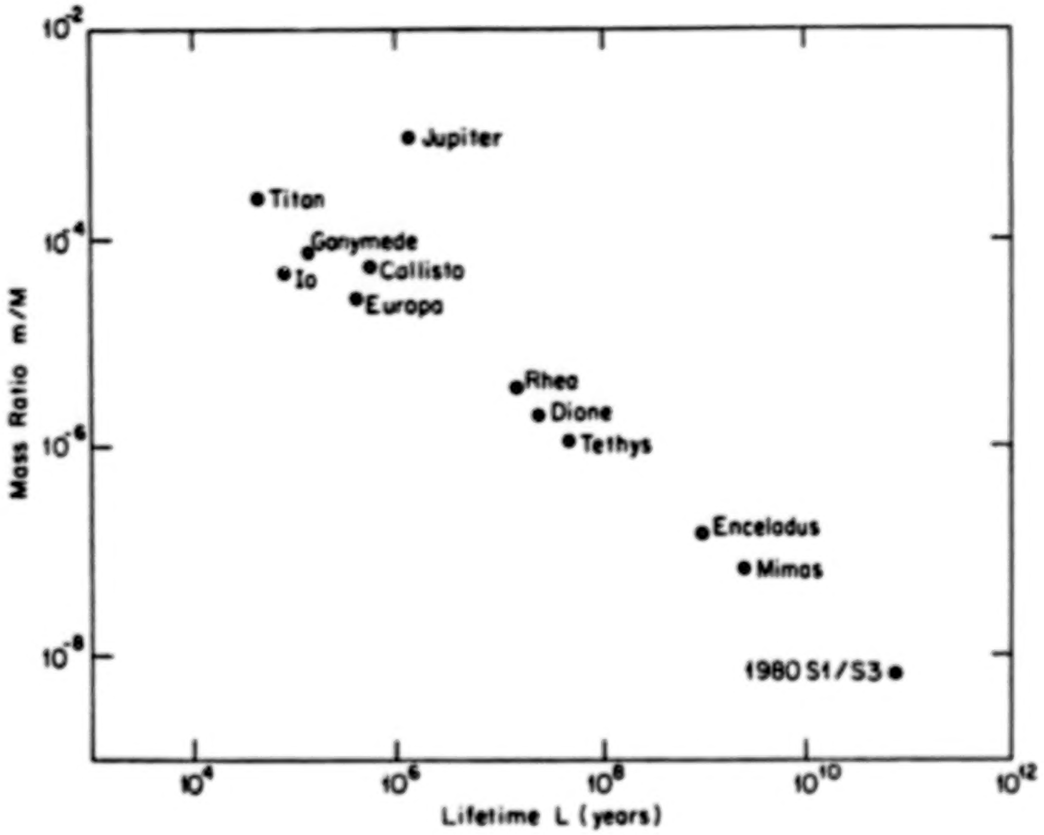

Fig. 4. If the evolution of the semimajor axis of a small satellite moving in a horseshoe orbit due to encounters with a primary or more massive coorbital satellite can be described by a random walk process, then the lifetime L of the small satellite can be estimated from the mass ratio m/M, where m is the mass of the primary satellite and M is the mass of the planet. Horseshoe orbits may be associated only with very small, or young, primary satellites. (Copyright University of Arizona Press).

Small Uranian satellites may exist in tadpole orbits, but I am unable to make any firm predictions. Progress with this problem could probably be made if we had some understanding of why there are no known Jovian coorbitals. It may be that drag forces are a determining factor. These can act to either drive the satellites towards the Lagrangian equilibrium points, L_4 or L_5, or away from those points.[51,53,54] In particular, any force that acts on the larger or the primary satellite to push it away from the planet will almost certainly act to reduce the relative velocity of the coorbital satellites and drive the smaller of the two satellites towards either L_4 or L_5 of the larger satellite. Tidal torques exerted on the satellite by the planet or by a massive ring system would be effective mechanisms. The latter, in particular, may be the one feature that distinguishes Saturn from Jupiter, but ring torques are only significant for those satellites very close to the Saturnian A ring.

It may be that those drag forces that operated during planet and satellite formation acted to disrupt all the primordial coorbital systems. In that case, the Saturnian coorbitals may exist because they are not primordial but the results of later disruptions caused by cometary impacts.[8] That being the case, I would argue that Uranian coorbitals may exist only if the Uranian satellites have suffered disruptions since the time of planet formation. Small satellites, such as Miranda, that are close to the planet, are the most likely candidates.

This research was supported by NASA Grant NAGW-392.

REFERENCES

1. Pollack, J. B. and Fanale, F. (1982). Origin and evolution of the Jupiter satellite system. In Satellites of Jupiter, (ed. Morrison, D.), pp. 872-910, University of Arizona Press.
2. Stevenson, D. J., Harris, A. W. and Lunine, J. I. (1984). Origins of satellites. In Natural Satellites, (eds. Burns, J. A. and Morrison, D.), University of Arizona Press (in press).
3. Samuelson, R. E., Hanel, R. A., Kunde, V. G., and Maguire, W. C. (1981). Mean molecular weight and hydrogen abundance of Titan's atmosphere. Nature 292, 688-693.
4. Sagan, C. and Dermott, S. F. (1982). The tide in the seas of Titan. Nature 300, 731-733.
5. Lunine, J. I., Stevenson, D. J. and Yung, Y. L. (1983). Ethane ocean on Titan. Science 222, 1229-1230.
6. Lewis, J. S., and Prinn, R. G. (1980). Kinetic inhibition of CO and N_2 reduction in the solar nebula. Astrophys. J. 238, 357-364.
7. Prinn, R. G., and Fegley, Jr., B. (1981). Kinetic inhibition of CO and N_2 reduction in circumplanetary nebulae: implications for satellite composition. Astrophys. J. 249, 308-317.
8. Smith, B. A., et al. (1982). A new look at the Saturn system: the Voyager 2 images. Science 215, 504-537.
9. Thomas, P., Veverka, J., and Dermott, S. (1984). Small satellites. In Natural Satellites, (eds. Burns, J. A. and Morrison, D.), University of Arizona Press (in press).

10. Goldreich, P., and Tremaine, S. (1979). Towards a theory for the Uranian rings. Nature 277, 97-99.

11. Lyttleton, R. A. (1936). On the possible results of an encounter of Pluto with the Neptunian system. Mon. Not. Roy. Astron. Soc. 97, 108-115.

12. Reitsema, H. J., Hubbard, W. B., Lebofsky, L. A., and Tholen, D. J. (1982). Occultation by a possible third satellite of Neptune, Science 215, 289-291.

13. Harris, A. W., and Ward, W. R. (1982). Dynamical constraints on the formation and evolution of planetary bodies, Ann. Rev. Earth Planet. Sci. 10, 61-108.

14. Safronov, V. S. (1969). Evolution of the proplanetary cloud and formation of the Earth and planets, Moscow: Nauka. Transl. Israel Program for Scientific Translations, NASA TTF-677.

15. French, R. G., Elliot, J. L., and Allen, D. A. (1982). Inclinations of the Uranian rings. Nature 298, 827-829.

16. McKinnon, W. B. (1984). On the origin of Triton and Pluto. Nature (submitted).

17. Lin, D. N. C. (1981). On the origin of the Pluto-Charon system. Mon. Not. Roy. Astron. Soc. 197, 1081-1085.

18. Harrington, R. S. and Van Flandern, T. C. (1979). The satellites of Neptune and the origin of Pluto. Icarus 39, 131-136.

19. Dormand, J. R. and Woolfson, M. M. (1980). The origin of Pluto. Mon. Not. Roy. Astron. Soc. 193, 171-174.

20. Farinella, P., Milani, A., Nobili, A. M., and Valsecchi, G. B. (1979). Tidal evolution and the Pluto-Charon system. *Moon and Planets* *20*, 415-421.

21. Heppenheimer, T. A., and Porco, C. (1977). New contributions to the problem of capture. *Icarus* *30*, 385-401.

22. Byl, J., and Ovenden, M. W. (1975). On the satellite capture problem. *Mon. Not. Roy. Astron. Soc. 173*, 579-584.

23. Pollack, J. B., Burns, J. A., and Tauber, M. E. (1979). Gas drag in primordial circumplanetary envelopes: a mechanism for satellite capture. *Icarus* *37*, 587-611.

24. Colombo, G., and Franklin, F. A. (1971). On the formation of the outer satellite groups of Jupiter. *Icarus* *15*, 186-191.

25. Ruskol, E. L. (1960). Origin of the Moon I. *Soviet Astronomy--AJ* *4*, 657-668.

27. Hunten, D. M. (1979). Capture of Phobos and Deimos by protatmospheric drag. *Icarus* *37*, 113-123.

28. Kuiper, G. P. (1951). On the origin of the irregular satellites. *Proc. Nat. Acad. Sci.* USA *37*, 717-721.

29. Gehrels, T. (1977). Some interrelations of asteroids, Trojans and satellites. In *Comets, Asteroids, Meteorites: Interrelations, Evolution and Origins* (ed. Delsemme, A.), pp. 323-325, Univ. of Toledo Press.

30. McCord, T. B. (1966). Dynamical evolution of the Neptunian system. *Astron. J*. *71*, 585-590.

31. Harris, A. W. (1984). The origin and evolution of planetary rings. In Planetary Rings (eds. Greenberg, R., and Brahic, A.), University of Arizona Press (in press).

32. Weidenschilling, S. J. (1982). Origin of regular satellites. In The Comparative Study of the Planets (eds. Coradini, A., and Fulchignoni, M.), pp. 49-59, Reidel, Dordrecht.

33. Goldreich, P., and Ward, W. R. (1973). The formation of planetesimals. Astrophys. J. 183, 1051-1061.

34. Harris, A. W. An analytical theory of planetary rotation rates. Icarus 31, 168-174.

35. Dermott, S. F., Gold, T., and Sinclair, A. T. (1979). The rings of Uranus: nature and origin. Astron. J. 84, 1225-1234.

36. Dermott, S. F., Murray, C. D., and Sinclair, A. T. (1980). The narrow rings of Jupiter, Saturn and Uranus. Nature 284, 309-313.

37. Dermott, S. F. (1981). The origin of planetary rings. Phil. Trans. R. Soc. Lond. A303, 261-279.

38. Goldreich, P. (1965). An explanation of the frequent occurrence of commensurable mean motions in the solar system. Mon. Not. Roy. Astron. Soc. 130, 159-181.

39. Peale, S. J. (1976). Orbital resonances in the solar system. Ann. Rev. Astron. Astrophys. 14, 215-246.

40. Yoder, C. F. (1979). How tidal heating in Io drives the Galilean orbital resonance locks. Nature 279, 747-770.

41. Yoder, C. F., and Peale, S. J. (1981). The tides of Io. Icarus 47, 1-35.

42. Dermott, S. F. (1972). Bode's law and the preference for near-commensurability among pairs of orbital periods in the solar system. In The Origin of the Solar System (ed. Reeves, H.), pp. 320-335, C.N.R.S., Paris.

43. Dermott, S. F., and Murray, C. D. (1983). Nature of the Kirkwood gaps in the asteroid belt. Nature 31, 201-205.

44. Chirikov, B. V. (1979). The universal instability of many-dimensional oscillator systems. Phys. Rep. 52, 263-379.

45. Dermott, S. F. (1984). Few-body problem in celestial mechanics. Nuclear Physics A416, 535c-550c.

46. Wisdom, J. (1982). The origin of the Kirkwood gaps: a mapping for asteroidal motion near the 3/1 commensurability. Astron. J. 87, 577-593.

47. Squyres, S. W., Reynolds, R. T., and Lissauer, J. J. (1984). On the tidal evolution of the Uranian satellites. (preprint).

48. Dermott, S. F. (1984). Rotation and the internal structures of the major planets and their inner satellites. Phil. Trans. R. Soc. Lond. A, (in press).

49. Dermott, S. F., and Murray, C. D. (1981). The dynamics of tadpole and horseshoe orbits I. Theory. Icarus 48. 1-11.

50. Dermott, S. F., and Murray, C. D. (1981). The dynamics of tadpole and horseshoe orbits II. The coorbital satellites of Saturn. Icarus 48, 12-22.

51. Yoder, C. F., Colombo, G., Synnott, S. P., and Yoder, K. A. (1983). Theory of motion of Saturn's coorbiting satellites. Icarus 53, 431-443.

52. Sinclair, A. T. (1984). Perturbations on the orbits of companions of the satellites of Saturn. Astron. & Astrophys. (in press).

53. Dermott, S. F. (1984). Dynamics of narrow rings. In Planetary Rings (eds. Greenberg, R. and Brahic, A.), University of Arizona Press (in press).

54. Dermott, S. F., Murray, C. D., and Williams, I. P. (1984). Drag forces in the three-body problem and the formation of coorbital satellites. Icarus (to be submitted).

COMPOSITION, STRUCTURE AND EVOLUTION OF URANIAN AND NEPTUNIAN SATELLITES*

David J. Stevenson

Division of Geological and Planetary Sciences
California Institute of Technology
Pasadena, California 91125

Abstract

Large uncertainties in the current estimated densities of all of these satellites prevent detailed modeling or predictions. Nevertheless, current evidence suggests that at least Titania and Oberon might have ''anomalously'' high densities (2-3 g cm^{-3}), possibly requiring almost ice-free hydrated silicates or formation in a CO-rich environment, implying presence of CO-clathrate and a small ice/rock ratio. Triton and the four largest satellites of Uranus are massive enough to have undergone significant accretional heating and early differentiation; NH_3-H_2O volcanism; partial outgassing of CO, N_2, CH_4; formation of dark surficial deposits of carbon-rich material obtained by UV irradiation of outgassed material; and, at least in the cases of Ariel and Triton, a possibility of weak ongoing icy volcanic activity. Triton may be the largest captured body in the solar system, with an unusual history and composition, including the possibility of substantial liquid or solid nitrogen obtained from either primordial NH_3 photolysis or clathrate decomposition.

INTRODUCTION

Voyager observations at Jupiter and Saturn have yielded a diversity of new worlds for study. The individuality of these satellites leads us to suspect that surprises and further diversity await us in the Uranian and Neptunian systems. Ground-based observations already provide evidence to support this expectation. My goal here is to provide some primarily theoretical arguments, based on very general considerations, which constrain the possible

---

*Contribution number 4042 of the Division of Geological and Planetary Sciences, California Institute of Technology, Pasadena, California 91125.

BEST COPY AVAILABLE

nature of these satellites and provide further indication for their suspected individuality and novelty.

Unfortunately, the existing data (described briefly in the next section and in far greater detail elsewhere in this workshop report) are insufficient for quantitative modeling of individual satellites. For this reason, I discuss generic satellites and avoid, as far as possible, any cosmogonic prejudice. However, a few speculative suggestions are offered about the origin and formation conditions since these factors, while not the primary focus of this report, are crucial for understanding composition and evolution. The issues I consider are these:

1) What range of compositions are conceivable for these satellites?
2) What relationship does the composition have to formation conditions?
3) What was the early evolution of these satellites, including the consequences of accretion?
4) How are the constituents distributed internally? (Are there cores? Are there undifferentiated satellites?)
5) What is the present dynamic state?
6) What implications follow for the surficial appearance?

OBSERVATIONAL CONSTRAINTS AND THEIR IMPLICATIONS

The average density is the most important constraint, yet poorly known in all cases as the Table below indicates. The Uranian satellite masses are taken from Veillet (1983). The radii are from Brown et al. (1982, 1983). The Table also lists central pressures, computed from $p_c = 2\pi G\bar{\rho}^2 R^2/3$, useful for characterizing the nature or phase of the material, and nominal

Table I

	Miranda	Ariel	Umbriel	Titania	Oberon	Triton	Nereid
Mass, M (10^{24} g)	$\lesssim 0.2$	1.6	1.0	5.9	6.0	~100?	?
Radius, R (km)	220 ± 70	660 ± 60	560 ± 50	800 ± 60	815 ± 70	1750 ± 250	~300?
Average density, $\bar{\rho}$(g/cm^3)	$\lesssim 3$?	1.3 ± 0.5	1.4 ± 0.6	2.7 ± 0.6	2.6 ± 0.6	?	?
Central pressure P_c(bars)	~600?	~1000	~1000	~6500	~6500	~2×10^4?	?
Nominal central temperature, T_c (K)	~85	270	210	375	385	(1600)*	?
Nominal maximum accretional temperature rise T_{acc} (K)	~20	~100	~100	~250	~250	~1000	?
Surface	H_2O ice + low albedo material					CH_4 ice, N_2 liquid? H_2O ice?	?

*Triton is too large to be in conductive steady state.

central temperatures $T_c = QR^2/6k$, for a body in conductive steady state ($k = 1 \times 10^5$ cgs), containing an energy source $Q = 3 \times 10^{-8}$ erg/cm^3-s crudely representative of present day radiogenic heat from a 50-50 mixture of chondritic material and ice. This nominal temperature is not a good estimate for the actual central temperature in most cases, but serves as a basis for more careful analysis. The table also includes a maximum conceivable accretional temperature rise $T_{acc} = 3GM/5RC_p$, where $C_p \cong 1 \times 10^7$ erg/g-k is the specific heat.

The estimated average densities allow almost the complete range of conceivable values, from volatile-rich assemblages ($\bar{\rho} < 1$ g cm^{-3}) to rocky, ice-free bodies ($\bar{\rho} \sim 3.5$ g cm^{-3}). The estimates also allow the possibility that all the bodies have similar composition ($\bar{\rho} \sim 2$ g cm^{-3}). The estimated pressures are potentially large enough for high pressure phases of ice to be present in the five largest satellites listed. The nominal central temperatures are large enough in these five bodies to admit the possibility of internal activity (partial melting of NH_3-H_2O, convection, outgassing) but the timing and extent of this activity depends, of course, on the composition. The accretional temperature rises are strictly upper bounds but are again potentially important in the five largest bodies; especially Titania, Oberon and Triton; since they may have caused mobilization of the more volatile phases and perhaps caused transient NH_3-H_2O lakes (Titania, Oberon) or oceans (Triton). The ground-based data on the surfaces are unfortunately not a strong constraint on bulk composition since the materials detected may be minor constituents. The non-detection of CH_4 on the small satellites implies nothing about their nature since CH_4 can rapidly escape and/or undergo UV modification.

COMPOSITIONAL MODELS

The likely ingredients of a satellite can be classified as follows, in order of increasing volatility (Lewis, 1971): ''rock'' (anhydrous or hydrated), water ice, ammonia hydrate ($NH_3 \cdot H_2O$), ice clathrate ($\sim X \cdot 6H_2O$; $X = CH_4$, CO, $N_2 \cdots$), more volatile ices (CH_4, etc). In accordance with the cosmogonic argument that these constituents formed by condensation from the gas phase, it is usually assumed that no member of this list is present in a

Table II. Generic Satellites

	Composition (mass fractions in brackets)	Uncompressed Density ($g\ cm^{-3}$)	Examples
I.	Hydrated ''rock'' (1.0)	~2.5*	Primordial Europa
II.	Rock (0.4) + H_2O ice (0.6)	1.3	Ganymede, Callisto
III.	Rock (0.35) + H_2O ice (0.55) + $NH_3 \cdot H_2O$ ice (0.1)	1.25	Enceladus + ?
IV.	Rock (0.35) + $CH_4 \cdot 7H_2O$ (0.55) + $NH_3 \cdot H_2O$ ice (0.1)	1.25	Iapetus + ? Titan
V.	Rock (0.25) + $CH_4 \cdot 7H_2O$ (0.4) + $NH_3 \cdot H_2O$ (0.1) + CH_4 ice (0.25)	~0.9	Pluto?
VI.	Rock + (CO, N_2)$\cdot 7H_2O$	~1.8	(? Possibly Uranian)

*Somewhat uncertain. This uncertainty propagates systematically through all the subsequent values in this Table.

satellite unless all preceding members on the list are present. This might be wrong if the formation conditions are unusual (e.g. formation from a debris cloud following a large collision). Even if the sequential nature of the list is adhered to, the relative mass fractions can be significantly modified by the chemical nature of the gas phase. The most important factor is the CO/CH_4 ratio. If most of the carbon is in the form of CO, then because carbon is ~60% as abundant as oxygen (Anders and Ebihara, 1982), this reduces the amount of H_2O present. A satellite of rock and H_2O ice forming from a cosmic composition environment is then ~70% rock, 30% ice by mass (average uncompressed density ~1.7 to 1.9 $g\ cm^{-3}$). If carbon is in the form CH_4 then the body which forms is ~40% rock, 60% ice by mass (average uncompressed density ~1.3 $g\ cm^{-3}$). Lewis and Prinn (1980) and Prinn and Fegley (1981) sought to establish the CO/CH_4 ratio in the solar and protoplanetary nebulae, respectively, by a consideration of the kinetics of the summation reaction $CH_4 + H_2O \longleftrightarrow CO + 3H_2$. They found CO-dominance for the solar nebula but a high probability of CH_4-dominance for protoplanetary nebulae. However, this is an oversimplification since much of the gas may have retained its interstellar CO/CH_4 (because it is never heated above $\sim 10^3$ K) and some of the gas may have been heated under conditions substantially different from those assumed (e.g. giant impacts). Similar concerns apply for the N_2/NH_3 ratio.

The generic models considered here encompass most (but not all) possible contingencies. In subsequent sections, I examine the evolution and structure of each model class.

FORMATION AND POST-ACCRETIONAL CONDITIONS

Consider an accreting satellite of instantaneous mass M which forms in an ambient gas-free (or optically thin) environment of temperature T_o. A characteristic accretion time is $\tau = M/(dM/dt)$ and is likely to be of order 10^3-10^4 years (Safronov and Ruskol, 1977), much less than that for planets. A crude estimate for the surface temperature T_s during accretion can be obtained from the energy balance:

$$\sigma(T_s^4 - T_o^4)\cdot 4\pi R^2 = \frac{M}{\tau}\left[\frac{GM}{R} - C_p(T_s - T_o)\right] \qquad (1)$$

where M, R are the instantaneous mass and radius, σ is the Stefan-Boltzmann constant, and C_p is the specific heat of the accreted material. The model assumes that the impact velocity $\simeq$ escape velocity. The solution of this equation is shown in Figure 1 for $T_o = 55$ K, $C_p = 1 \times 10^7$ erg/g and $\tau = 10^4$

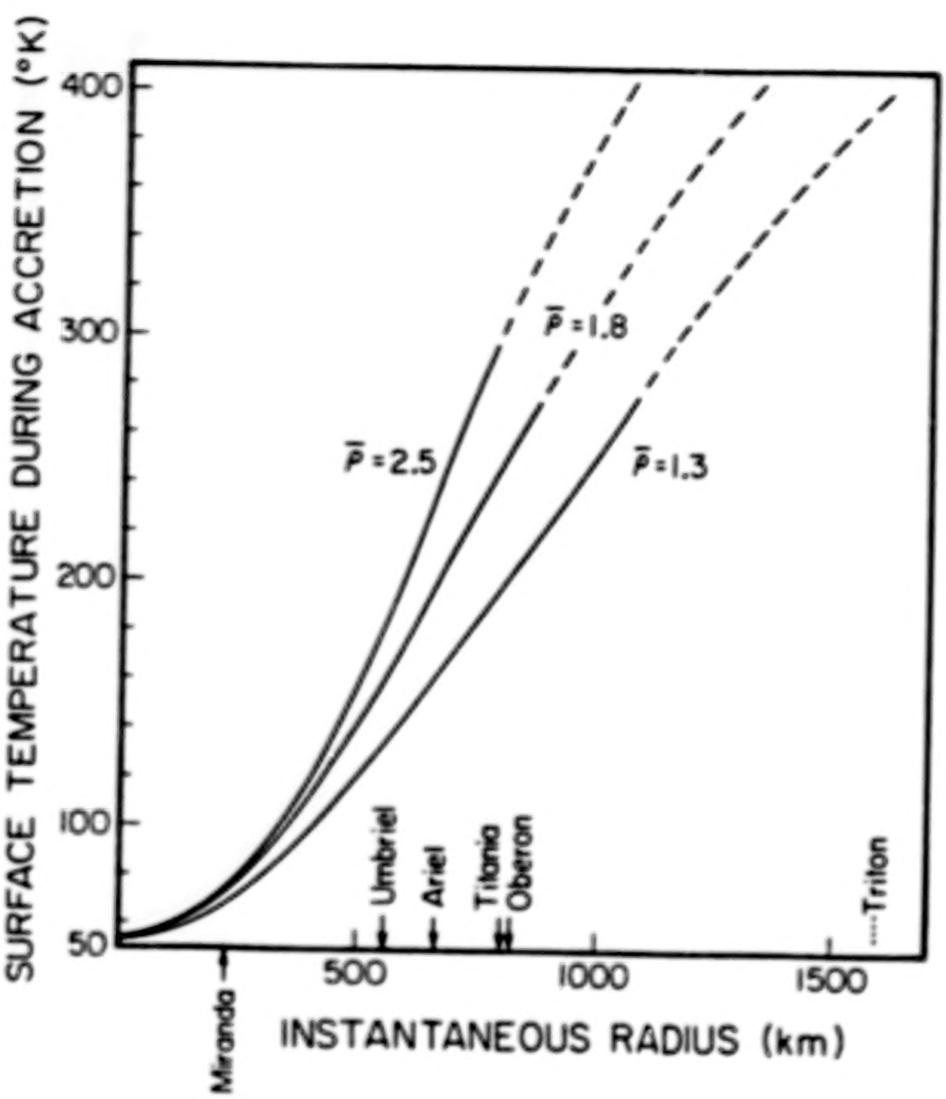

Fig. 1. Surface temperature during accretion, for three choices of average density $\bar{\rho}$.

years. Bodies larger than ~10^3 km are not accurately modeled, primarily because of latent heat effects (which buffer the rise of temperature) but also because of transient (e.g. steam) atmosphere effects. The temperature estimates in Figure 1 may also be somewhat high because of unmodeled effects such as radiative cooling from ejected particulate impact debris immediately after individual impacts. For comparison, the sub-surface temperature is bounded above by the values given in Table I; a more realistic estimate may be $\lesssim$50% of these values since only a fraction of the input energy is deposited below the thermal boundary layer (see Schubert et al., 1981, for a similar calculation applied to the Jovian satellites).

These calculations show that the expected temperature rise during accretion may be sufficient to evaporate the more volatile ices (i.e. CH_4, CO, N_2) even for satellites ~500 km radius. If this material is not effectively buried during individual impacts then it may undergo hydrodynamic blow-off. Even if it is buried, it may be warm enough to melt and migrate immediately to the surface. Clathrates should at least partially survive, however, since hydrostatic pressure helps to stabilize these compounds. (There are several misconceptions in the existing literature concerning clathrates. One is the notion that clathrates gradually decompose, causing outgassing of the satellite. This is not true, in general, unless the temperature is raised by a large amount or the pressure exceeds ~10 kbar. See Lunine and Stevenson, 1984.) In satellites $\gtrsim$800 km in radius, partial melting of H_2O-NH_3 may occur at or near the surface but melting of pure water ice is unlikely until the body becomes about the size of Triton. It is certainly possible that Triton possessed a primordial NH_3-H_2O ocean caused by accretional heating. This can also occur if the accretional environment is optically thick because of the presence of a dense, gas phase (a situation analyzed for the Jovian satellites by Lunine and Stevenson, 1982a).

The accretional and immediate post-accretional states can be summarized for each satellite class in Table II, as follows. Type I (hydrated silicates) undergoes no accretion modification unless the temperature exceeds ~600-800 K; this requires a body $\gtrsim$1500 km in radius, perhaps a body ~ Europa, if the body forms in a cold environment. The consequence is an ice layer overlying the silicates. Type II (rock + H_2O ice) has already been modeled in the Jovian system (Schubert et al., 1981; Lunine and Stevenson, 1982a). It is probable that bodies $\gtrsim$1500 km undergo partial melting and resurfacing although the critical size might even be near the size of Callisto, perhaps explaining the striking surficial dissimilarity of Ganymede and Callisto. Type III ($NH_3 \cdot H_2O$ added) may undergo partial melting and primordial resurfacing at $R \sim 500$-1000 km, a size range which encompasses the four larger Uranian satellites. Type IV (CH_4 clathrate added) would behave similarly, with the addition of some explosive CH_4 release (discussed by Stevenson, 1982) as 'hot' ($\sim$180 K) NH_3-H_2O magma comes into contact with near-surface clathrate. Type V (CH_4 added) should be almost 'explosive' if $R \gtrsim 300$-500 km, with a large fraction of the CH_4 undergoing melting, surface evaporation and rapid escape. Type VI (CH_4 poor; CO as clathrate) may not undergo melting or decomposition during accretion, unless $R \gtrsim 700$-1000 km. Some N_2, CO may migrate to the surface, undergoing escape less rapidly than CH_4 because of the higher molecular weight.

THERMAL HISTORIES

Although a pure ice satellite is conceivable, it is very likely that all satellites contain a sufficient complement of rock to undergo significant radiogenic heating after accretion. Unless the giant planets and their satellites formed very rapidly ($<10^6$ years after the initiation of solar system formation), ^{26}Al should be unimportant, and the heat is derived from long-lived isotopes, primarily ^{40}K, ^{235}U, ^{238}U, and ^{232}Th. The thermal history of a conductive sphere containing heat sources is easy to compute if the conductivity is constant and known (e.g. the asteroid evolutions of Allen and Jacobs, 1956). In the case of icy satellites, this simple approach, using the conductivity of crystalline H_2O ice, leads to the prediction that bodies with R $\lesssim$ 700 km would not even achieve partial melting of NH_3-H_2O (Consolmagno and Lewis, 1978). The problem is that even a relatively thin (~few kilometers), low conductivity regolith layer can dramatically alter the evolution. The presence of $NH_3 \cdot H_2O$ and clathrate substantially lower the thermal conductivity of the interior (Stevenson, 1982). My calculations show that these factors can allow satellites $\gtrsim$300 km in radius to undergo significant partial melting, even assuming that the evolution begins from a cold state. Amorphous ice is also a possible reason for higher temperatures and igneous activity because of its very low conductivity (Smoluchowski, 1978; Klinger, 1982).

A different problem, acting in the opposite sense, is subsolidus convection of ice. This was neglected in earlier work on icy satellites (Consolmagno and Lewis, 1976, 1978) but is unquestionably important in all large, icy satellites (Reynolds and Cassen, 1979), including even satellites with radius ~700 km (Ellsworth and Schubert, 1983). Heat transport by subsolidus creep is sufficiently efficient to prevent melting of pure water ice by radiogenic heating, and probably even prevents melting of the water component of a rock-ice mixture, unless the satellite is about the same size and rock-ice ratio as Ganymede (Friedson and Stevenson, 1983). However, subsolidus creep probably never prevents the partial melting of a satellite containing both H_2O and NH_3. The reason is that the viscosity is likely to be dominated by water ice and is very large at 173 K, the eutectic of H_2O-NH_3. Above this temperature, a cosmic abundance of Nh_3 (~18% mole fraction relative to H_2O) can be incorporated into a eutectic melt (~67% H_2O, 33% NH_3) and migrate upwards by percolation through the porous water ice matrix. The unimportance of convection under these circumstances can be seen from consideration of the Rayleigh number

$$Ra \cong g\alpha\Delta T d^3/\ K \qquad (2)$$

together with a likely viscosity law for water ice (Weertman, 1983)

$$\nu \simeq 10^{15} \exp\left[25\left(\frac{273}{T} - 1\right)\right] \text{ cm}^2/\text{s} \qquad (3)$$

where the pre-exponential constant corresponds to the low deviatoric stresses encountered in icy satellites. At $T = 173$ K, $\nu \gtrsim 10^{21}$ cm^2/s. Substituting $g \simeq 3$ (R/100 km) cm/s^2, R = satellite radius, $d \sim 0.5R$, $\alpha = 10^{-4}$ °K^{-1}, $\Delta T \sim 20$°K, $K = 10^{-2}$ cm^2/s and $\nu = 10^{21}$ cm^2/s yields $Ra \simeq 0.6$ $(R/10^2\ \text{km})^4$. Onset of convection occurs at $Ra \sim 2 \times 10^3$ (since it is likely to be a rigid boundary condition) and requires $R \gtrsim 760$ km at this temperature of 173 K. Even at $R \sim 1500$ km, the enhancement of heat transport relative to conduction is only ~ twofold. As a consequence, generation of $H_2O - NH_3$ melt is not prevented by solid state creep.

Migrating, buoyant water-ammonia magma can cause decomposition of near-surface clathrates (Stevenson, 1982) perhaps leading to explosive venting, resurfacing by magma, ejection of hydroclasts (ice tektites) and formation of transient rings such as the E-ring (Herkenhoff and Stevenson, 1984). However, these are all likely to occur early in the history of the satellite, when the temperature first reaches 173 K. They may not occur at all in large satellites ($R \gtrsim 1500$ km) which undergo extensive melting during accretion and may evolve differently (see the section on Triton below). The generation of melt will, in all cases, cause settling of the dense silicate-rich residue to form a core.

If a large amount of the much more volatile CH_4 ice is present and retained, then there is rapid upward differentiation to form a CH_4 outer shell (cf. Lupo and Lewis, 1982, in their work on Pluto). Subsequent contact between

NH_3 - H_2O magma and CH_4 can cause explosive CH_4 volcanism, since the ~ 180 K water-ammonia magma is capable of causing a hot, buoyantly rising CH_4 plume which expands explosively into a gas. (At one bar pressure and 180 K, CH_4 gas occupies over one hundred times more volume than the same mass of liquid CH_4.) Although the latent heat of vaporization limits the amount of gas produced, events of this kind could be spectacular and might even continue to occur in larger bodies ($R \gtrsim 1000$ km) for which the present day internal temperatures exceed 173 K.

Based on these general comments, it is possible to construct a likely evolution outcome for each of the satellite classes listed in Table II. These qualitative models are shown in Figure 2 and are intended to correspond to satellites in the Uranian size range (500-1000 km radius), rather than the substantially larger (but very poorly constrained) Neptunian moon, Triton. The models are largely self-explanatory; a few additional comments follow:

I. Hydrated rock bodies in this size range do not become hot enough to undergo large scale dehydration. However, impacts can cause local dehydration and a partial or complete layer of water ice.

II. Water ice and rock satellites are likely to show no evidence of endogenic processes (they may look like Callisto).

III., IV. The surficial appearance of these bodies should be similar to Dione, Rhea, etc.

V. This model is only meaningful if significant CH_4 can remain for the age of the solar system. (However, the photochemical residue may remain to darken the surface, even if all the CH_4 escapes.)

VI. The clathrate is stable in the absence of heating events (such as NH_3-H_2O magma). Thus, these bodies may show little evidence for endogenic activity. Differentiation is also unlikely for essentially the same reason (lack of a fluid phase).

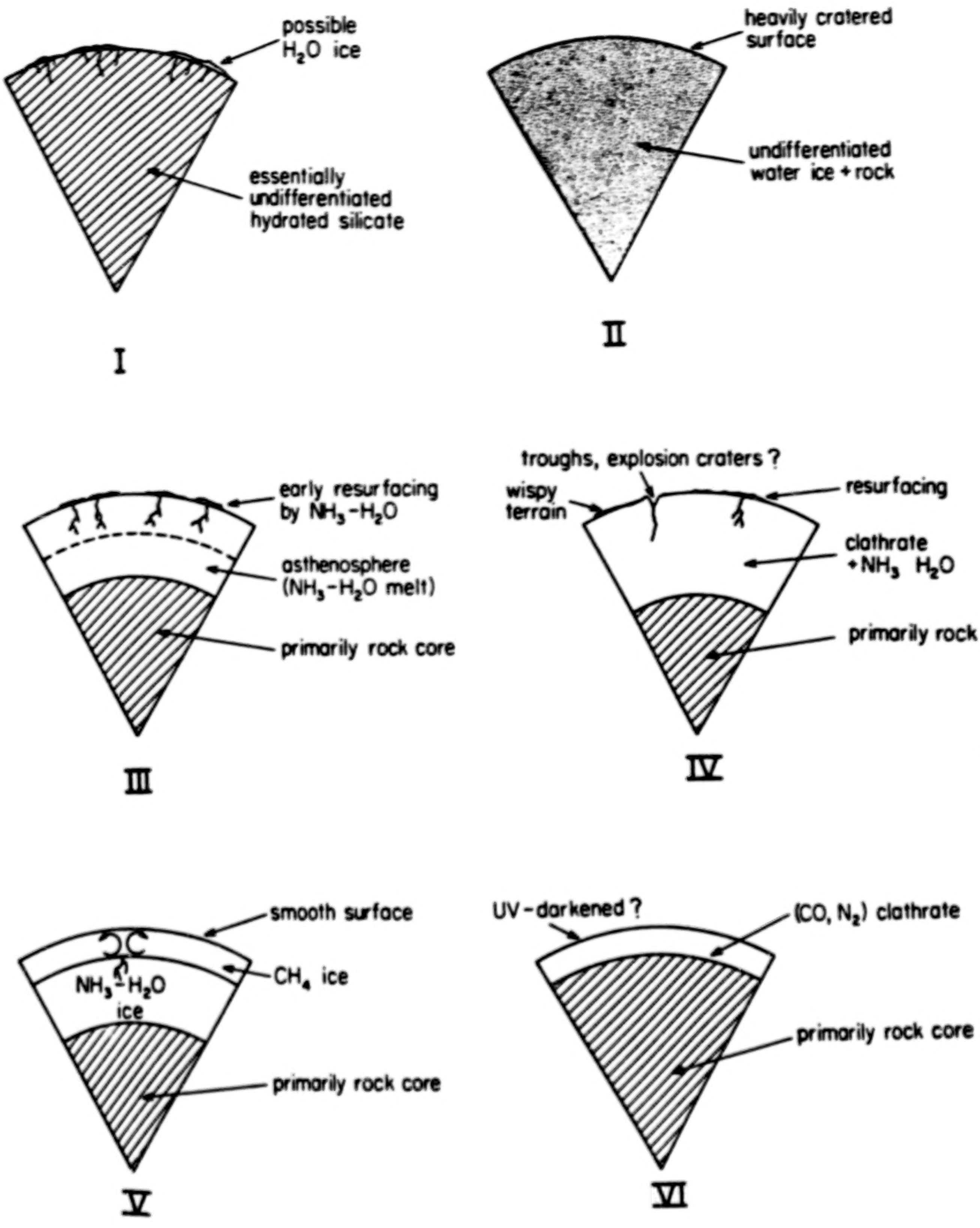

Fig . 2 Pie diagrams for the six classes of generic satellites described in Table II.

possible H_2O ice
essentially undifferentiated hydrated silicate
I
heavily cratered surface
undifferentiated water ice + rock
II
early resurfacing by NH_3-H_2O
asthenosphere (NH_3-H_2O melt)
primarily rock core
III
troughs, explosion craters ?
wispy terrain
resurfacing
clathrate + NH_3 H_2O
primarily rock
IV
smooth surface
CH_4 ice
NH_3-H_2O ice
primarily rock core
V
UV-darkened ?
(CO, N_2) clathrate
primarily rock core
VI

TRITON

In the absence of reliable radius and mass determinations, comments about Triton are necessarily highly speculative. Guided only by the observation of CH_4 frost and the probable detection of liquid N_2 (Cruikshank et al., 1983), it seems possible that Triton has some similarity to Titan, but failed to form a massive atmosphere because of less severe heating during accretion and a lower ambient temperature. Analysis of Titan (Hunten et al., 1984) is partially transferable to Triton and suggest that:

a) CH_4 might come from decomposed clathrate, if the central pressure $\gtrsim$ 10 kbar, or from ''trapped'' CH_4 left at the surface after a primordial H_2O-NH_3 ocean froze over (analogous to the Titan scenario proposed by Lunine and Stevenson, 1982b). It might also be derived from the thermal decomposition of clathrate that occurs if Triton was captured by Neptune and underwent an early, extremely vigorous tidal heating episode (McKinnon, 1983).

b) N_2 might come from photolysis of NH_3 overlying a primordial H_2O-NH_3 ocean, or from impacts, or from clathrate. However, the latter possibility strongly suggests the presence of CO (not yet detected).

c) Ongoing NH_3-H_2O volcanism is marginally possible.

d) A differentiated internal structure is expected, with a liquid H_2O-NH_3 layer at ~ 200 km depth persisting up to the present day, provided significant NH_3 was incorporated.

ORIGIN OF THE URANIAN SATELLITES

I proceed now to some speculative comments, motivated by the possibility (Table I) that the Uranian satellites are more dense on average than would normally be expected, with the outer two satellites (Titania and Oberon) possibly being ice-poor. The following speculation may eventually prove unnecessary, but deserves consideration for the present. Suppose the Uranian satellites formed from a disk that was created immediately after an impact on Uranus by a body of mass ~ one or two earth masses. This impact at ~ 20 km/s could cause the present striking (98°) obliquity of Uranus as well as rendering the equatorial belt of material rotationally unstable (provided the pre-impact Uranus was near rotational instability). The material flows out from this belt into a disk, redistributing angular momentum by eddy diffusion. The outermost material in this disk is likely to be a mixture of shocked atmosphere and ablated projectile. Later, inner additions to the disk are likely to be similar in composition to the present, deep atmosphere of Uranus. The interesting feature of this scenario is that when an H_2-CH_4-H_2O atmosphere is shocked, it quenches into an H_2-CO dominated mixture (possibly including heavier hydrocarbons and even elemental carbon) which contains very little water. This is shown semiquantitatively in Figure 3. The release adiabats in the shock process are clearly in the CO equilibrium field at T ~ 1200 K, a likely quench temperature at the relevant timescale of hours. (See Lewis and Prinn, 1980 for the relevant kinetics and thermodynamics; also Lewis et al. 1982, for a related problem of impact in the earth's atmosphere).

The outer satellites would subsequently form from a nebula which was H_2O-poor, but containing some rock derived from ablated projectile. Some CO and N_2 might be incorporated as clathrate, corresponding to model VI in Table II. If very little water remains, then the satellite might even be almost entirely anhydrous or hydrated silicate (model I in Table II).

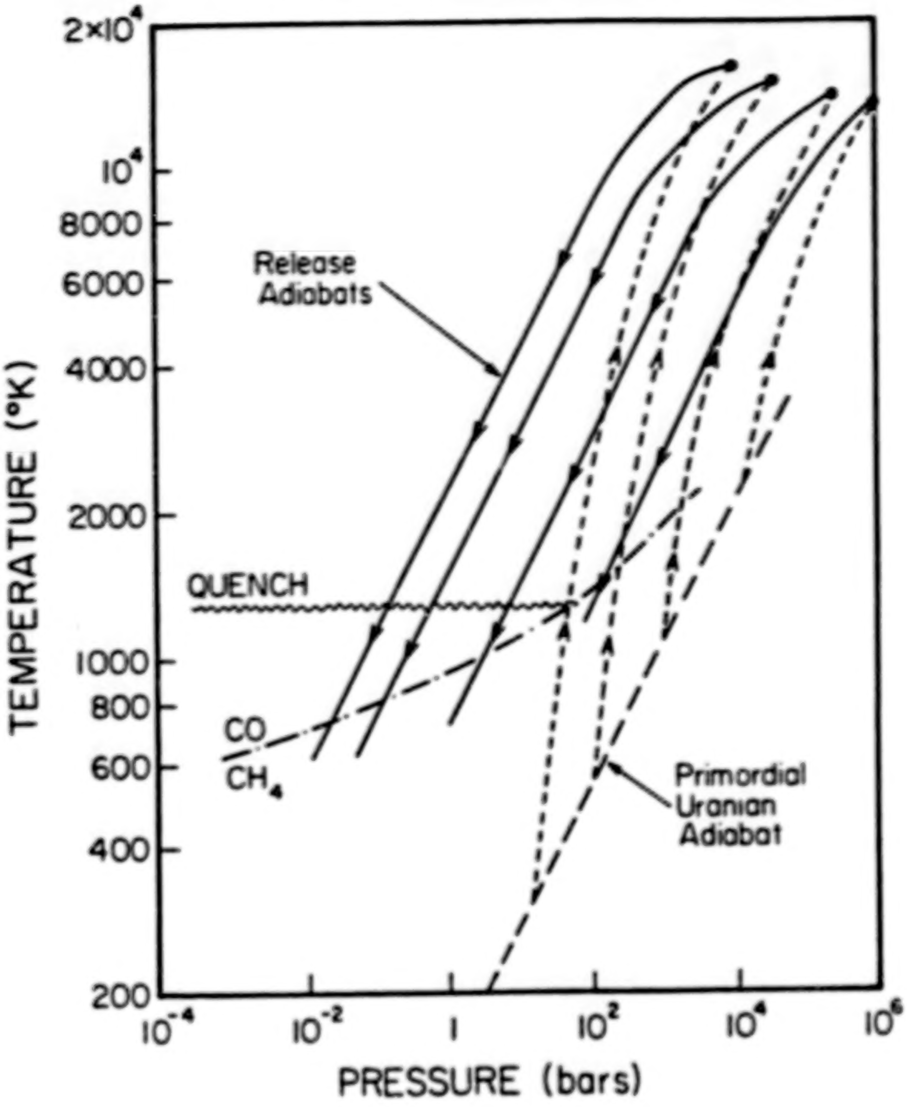

Fig. 3. Consequences of impact into the early Uranian atmosphere. The long dash line is the primordial T-P relation for the Uranian atmosphere assumed in the calculation. The short-dashed lines are the thermodynamic trajectories of this gas as it is shocked. The solid lines are the release adiabats for this shocked gas after impact. The wiggly line represents the approximate temperature below which there is kinetic inhibition and failure to achieve thermodynamic equilibrium. Since most of the release adiabats achieve quench before crossing the CO-CH_4 equilibrium line, the quenched gas will be CO rich (at the expense of H_2O).

CONCLUDING COMMENTS

I have not covered all possible outcomes. For example, there is a slight possibility that Ariel undergoes significant tidal heating (Squyres and Reynolds, 1983) if the reported near resonance configuration is actually an exact resonance or was exact in the recent geologic past. It is also possible that the assemblage of ices in these bodies is more complex than I have considered above, including significant amounts of CO_2, for example. The general impression is of a bewildering range of possibilities and a strong likelihood of interesting, perhaps unexpected, surface appearances and internal properties. The satellites are likely to be one of the highlights of the Voyager encounter of Uranus, and Triton may prove to be the highlight of the Neptune encounter.

ACKNOWLEDGMENT

This work is supported by NASA Planetary Geology grant NAGW-450.

REFERENCES

Allan, D.W. and Jacobs, J.A. (1956) Geochim. Cosmochim. Acta 9, 256.

Anders, E. and Ebihara, M. (1982) Geochim. Cosmochim. Acta 46, 2363.

Brown, R.H., Morrison, D. and Cruikshank, D.P. (1982) Nature, 300, 423.

Brown, R.H. and Clark, R.N. (1983) Bull. Am. Astron. Soc. 15, 856.

Consolmagno, G.J. and Lewis, J.S. (1976) In ''Jupiter,'' ed. T. Gehrels, Un. Arizona Press, p. 1035.

Consolmagno, G.J. and Lewis, J.S. (1970) Icarus 34, 280.

Cruikshank, D.P., Brown, R.H. and Clark, R.N. (1983) Bull. Am. Astron. Soc. 15, 857.

Ellsworth, K. and Schubert, G. (1983) Icarus 54, 490.

Friedson, A.J. and Stevenson, D.J. (1983) Icarus 56, 1.

Herkenhoff, K.E. and Stevenson, D.J. (1984) LPSC XV Abstracts, in press.

Hunten, D.M., Tomasko, M.G., Flasar, F.M., Samuelson, R.E., Strobel, D.F. and Stevenson, D.J. (1984) In ''Saturn'', ed. T. Gehrels, Un. Arizona Press, in press.

Klinger, J. (1982) Nature 299, 41.

Lewis, J.S. (1971) Icarus 15, 175.

Lewis, J.S. and Prinn, R.G. (1980) Astrophys. J. 238, 357.

Lewis,, J.S., Watkins, H.G., Hartman, H. and Prinn, R.G. (1982) G.S.A. Special Paper 190, p. 215.

Lunine, J.I. and Stevenson, D.J. (1982a) Icarus 52, 14.

______________________________ (1982b) Bull. Am. Astron. Soc. 14, 713.

______________________________ (1984) Submitted to Astrophys. J.

Lupo, M.J. and Lewis, J.S. (1980) Icarus 44, 41.

McKinnon, W.B. (1983) Bull. Am. Astron. Soc. 15, 857.

Prinn, R.G. and Fegley, B. (1981) Astrophys. J. 249, 308.

Reynolds, R.T. and Cassen, P.M. (1979) Geophys. Res. Lett. 6, 121.

Schubert, G., Stevenson, D.J. and Ellsworth, K. (1981) Icarus 47, 46.

Smoluchowski, R. (1978) Science 201, 809.

Squyres, S.W. and Reynolds, R.T. (1983) EOS Trans. AGU 64, 746.

Stevenson, D.J. (1982) Nature 298, 142.

Veillet, Ch. (1983) Ph.D., University of Paris.

Weertman, J. (1983) Ann. Rev. Earth Planet. Sci. 11, 215.

BLANK PAGE

PHYSICAL PROPERTIES OF THE SATELLITES OF NEPTUNE

Dale P. Cruikshank

Institute for Astronomy
2680 Woodlawn Drive
Honolulu, HI 96822

Abstract

Spectrophotometric studies of Triton suggest a surface covered in part by solid methane. Nitrogen is suspected on the basis of a single spectral band, but this material, if present, must be in a condensed state. Liquid nitrogen covering part of Triton to a depth of a few tens of centimeter can satisfy the spectral data so far available. If condensed nitrogen occurs on Triton, the satellite has an atmosphere largely of N_2 (pressure ~0.1 bar), with CH_4 as a minor constituent. The reddish hue of Triton's surface may result from photochemical derivatives of the methane and nitrogen, as in the case of Titan. The radius of Triton has been determined by indirect means to be 1750 km, but there may be a large systematic error in this value. If the mean density is ~2-3 g/cm^3, the mass derived from astrometric observations is in error. There is no information on physical properties of Nereid. A third suspected satellite has not been confirmed.

INTRODUCTION

This is a brief review of the physical properties of Triton, Neptune's largest satellite. A portion of this material was prepared for a review chapter on outer planet satellites by Cruikshank and R. H. Brown for a projected book on natural satellites by D. Morrison and J. A. Burns. A summary of this material was presented by IAU Colloquium 77, Ithaca, NY, July 1983.

TRITON

1. The Surface and Atmosphere of Triton. The spectrum of Triton has been explored with relatively low spectral resolution from 0.3 to 2.5 µm. From 0.3 to 0.6 µm, the spectrum is red and without any distinct absorption features, as shown in Figure 1, which combines photographic spectrophotometry (Cruikshank *et al.* 1979)[1] and multifilter photometry (Bell *et al.* 1979)[2]; the data sets are in agreement. Longward of 0.8 µm, absorption bands appear, as shown

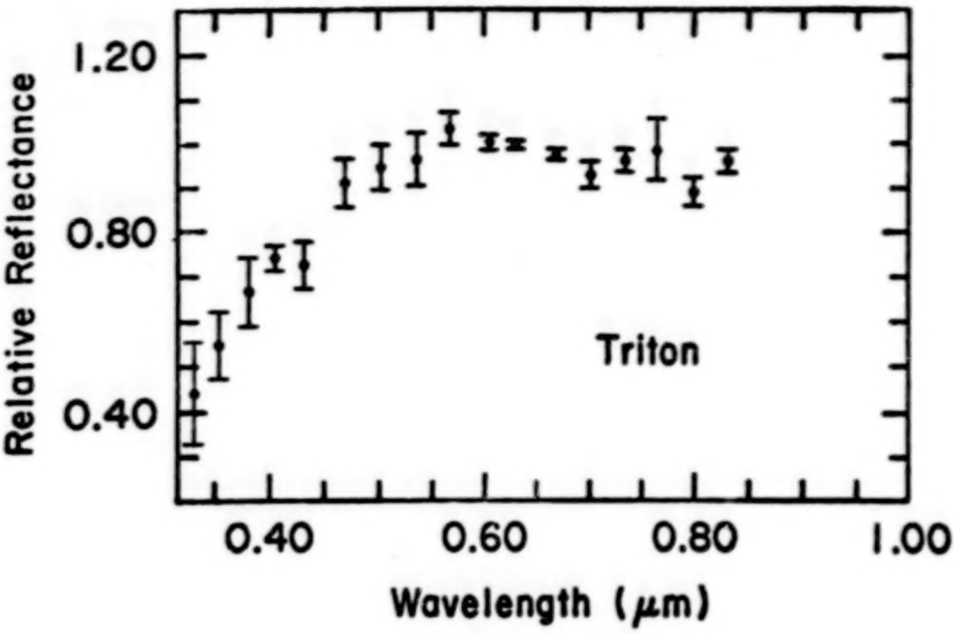

Fig. 1. Reflectance of Triton from multifilter photometry. The data are normalized to reflectance 1.0 at 0.6 μm. From Bell et al. (1979).

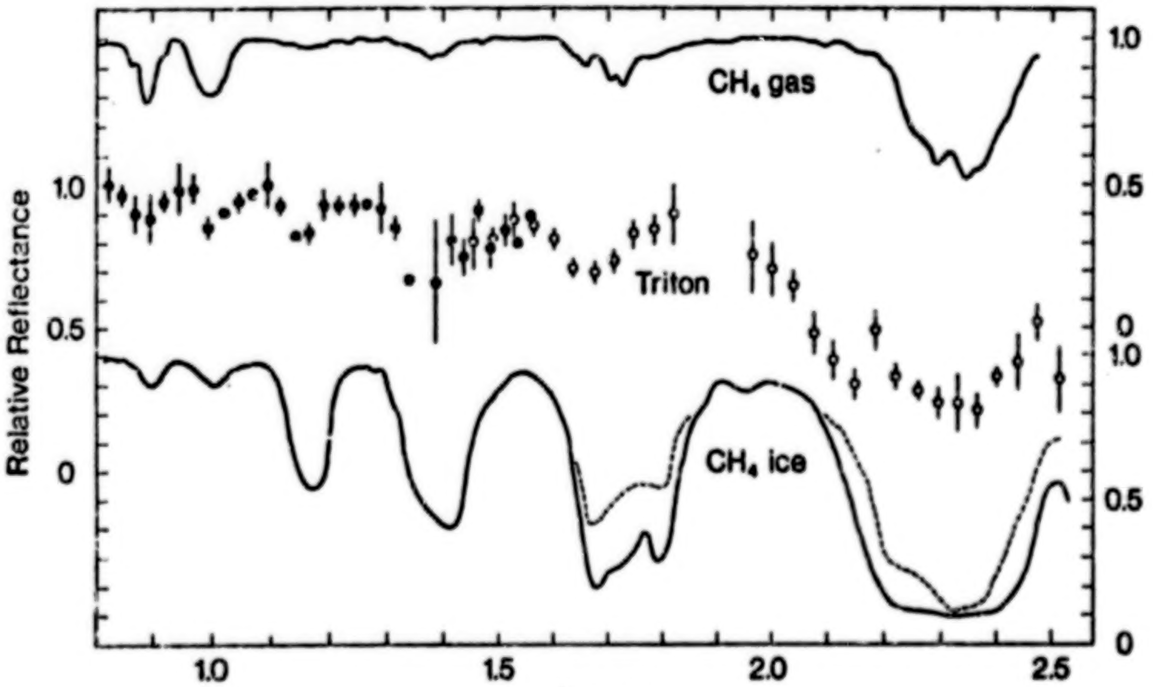

Fig. 2. Composite spectrum of Triton. Solid dots represent data obtained on 18.6 May 1982; open circles are from 2.4 June 1980. The synthetic methane gas spectrum at the top of the figure was calculated for T = 55K and 50 m-Am density at 0.001 bar pressure. The bottom traces are laboratory spectra of methane ice in diffuse reflection. From Cruikshank and Apt (1984).

in the composite spectrum of Triton in Figure 2, in which the 0.8-2.5 μm data are from Cruikshank and Apt (1984)[3] and Cruikshank et al. (1984).[4] The majority of these bands are identified as due to methane on the basis of comparisons with synthetic laboratory spectra of gaseous methane calculated for the low-temperature conditions on Triton (Cruikshank and Apt 1984)[3] and with laboratory spectra of methane ice. The 2.3-μm absorption band was first identified as methane by Cruikshank and Silvaggio (1979)[5] on the basis of spectra of lower resolution. In high-resolution spectra, Apt et al. (1983)[6] have found the 0.89-μm band of methane and have noted that it is weaker than the same band in the spectrum of Pluto.

In addition to the six bands in the Triton spectrum that match the methane spectrum, there is an additional feature centered at 2.16 μm located on the steep slope of the 2.3-μm methane band that cannot itself be attributed to methane either in the gaseous or solid state. Cruikshank et al. (1984)[4] have tentatively identified this band as the density-induced (2-0) absorption band of molecular nitrogen. The identification is regarded as tentative because it is based upon the presence of one band alone, and the apparent coincidence of the central wavelengths of N_2 observed in the laboratory and the band on Triton. From a consideration of the expected temperature of Triton's surface and the phase equilibrium of nitrogen, Cruikshank et al. (1983, 1984)[7,4] showed that in order for the observed spectral band to be produced in gaseous nitrogen, the surface pressure would exceed that at which condensation would occur at the relevant temperature. Thus, the nitrogen should exist as a liquid or solid, depending upon the exact temperature. Laboratory observations show that the 2.16-μm feature also occurs in liquid nitrogen. From a determination of the absorption coefficient in the band, Cruikshank et al. calculated that the spectral feature on Triton is produced by absorption through a few tens of centimeters of liquid nitrogen on the surface of the satellite.

This result raises interesting possibilities about the atmosphere of Triton, its interaction with the liquid nitrogen and the solid methane, and the nature of the red color of the satellite. Estimates of the temperature of Triton are also complicated because of the unknown effects of the atmosphere. It is probable that the atmosphere itself has not yet been observed because it is mostly nitrogen at a surface pressure regulated by the temperature of the liquid; the equilibrium vapor pressure of nitrogen at $T = 64°K$ is 0.13 atm. The vapor pressure of methane is less by about 10^3, so that this gas is likely a minor constituent of the satellite's atmosphere.

Additional observational results show that the strengths of the methane bands on Triton vary with its orbital position (Cruikshank and Apt 1984).[3] Because Triton is in locked synchronous rotation in its orbit around Neptune, the orbital variability reflects a nonuniform distribution of methane on the surface of the satellite. There are presently no conclusions about the possible variability of the strength of the nitrogen band. Triton does not show a pronounced photometric variability with its orbital position. Franz (1981)[8] found an amplitude of about 0.06 mag (at $\lambda = 0.56$ μm), with the maximum at western elongation (leading hemisphere). The variability of the methane band strength appears to be in the sense that the strongest bands are also found near western elongation, though this requires confirmation.

Methane is highly soluble in liquid nitrogen and has the effect of raising the freezing point of the mixture. The implications of this for Triton have been explored in a very preliminary way in the paper by Cruikshank et al. (1984),[4] from which it appears that the colder portions of the satellite, particularly those near the pole in extended darkness at the present season, are sufficiently cold to permit the nitrogen sea to freeze. Whether or not there is a diurnal freeze-thaw cycle depends on the heat capacity of the sea and its global extent, as well as the possibility that other materials are dissolved in it, which may lower the freezing point.

In attempts to model the infrared spectrum of Triton with laboratory observations of methane ice and liquid nitrogen, Cruikshank *et al.* (1983, 1984)[7,4] found that an additional component was necessary in order to match the shape of the continuum at various wavelengths. The absorption spectrum of water ice provides the additional component needed to fit the Triton spectrum to a precision commensurate with the quality of the telescopic data for the satellite. The best-fit model for Triton's spectrum, together with the individual components shown separately, is given in Figure 3.

While a detailed study of the short wavelength end of the spectrum where Triton shows a distinct reddish color has not yet been accomplished, interesting possibilities arise from a consideration of the fact that other methane-bearing bodies in the outer solar system also have reddish hues. In the case of Saturn's Titan, the red color is probably that of the aerosol photochemically produced from the methane in the upper atmosphere. Pluto is also red. Photochemistry on Triton may produce reddish organic solid matter from the methane and nitrogen. If there is methane dissolved in the liquid nitrogen, red organic matter may be suspended in the liquid. Delitsky (1983)[9] has given some consideration to the complex organic chemistry that may occur in a nitrogen sea of Triton.

The equilibrium temperature of the subsolar point on Triton can be calculated from

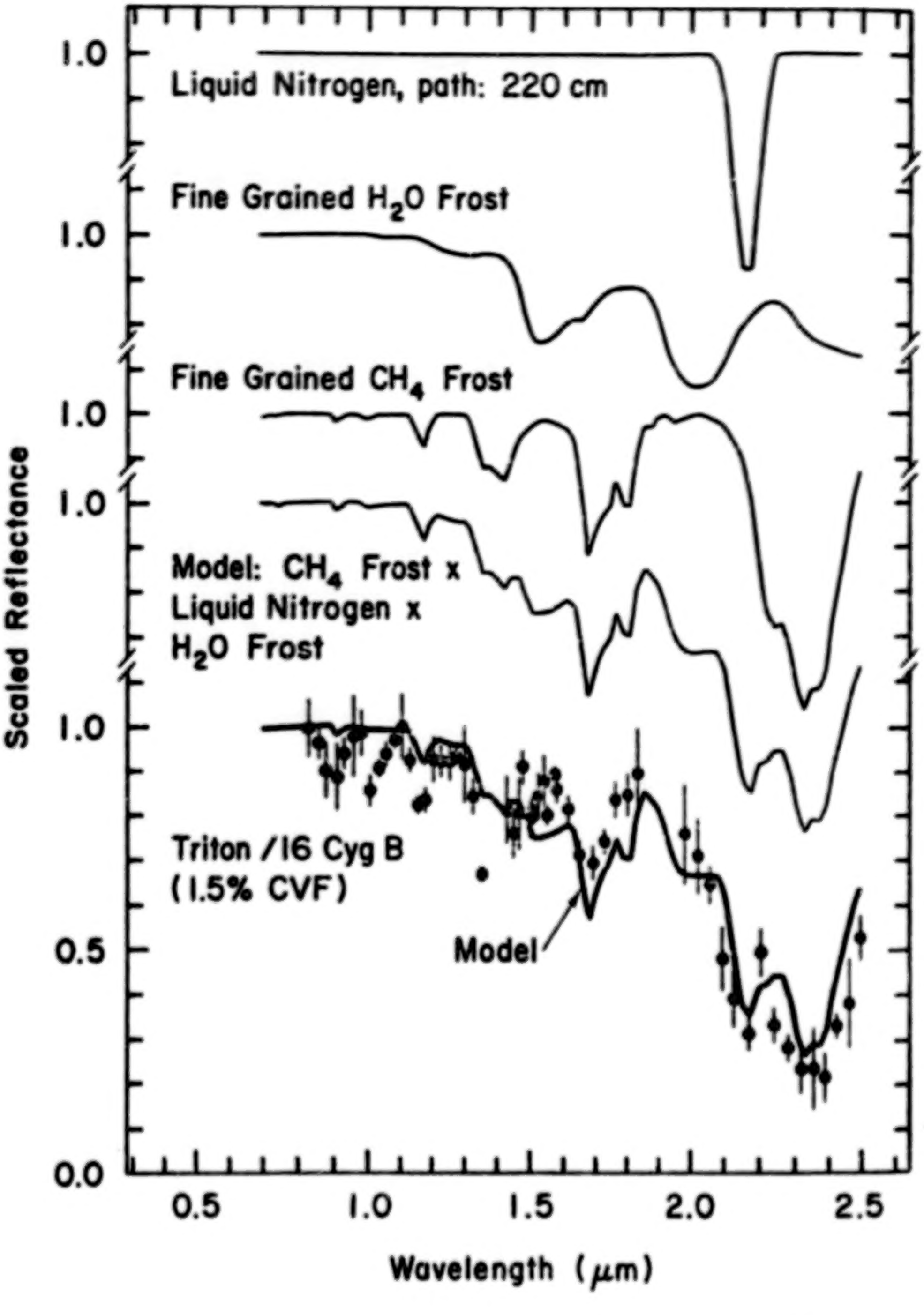

Fig. 3. The model of the Triton spectrum with resolution 1.5%, together with the individual components used in the calculation (made by Dr. R. N. Clark). The methane contribution was computed using "scaled absorption coefficients" derived from laboratory spectra. The nitrogen contribution was derived from a laboratory spectrum of LN_2. The water frost contribution was computed from extensive laboratory data from R. N. Clark and colleagues. From Cruikshank et al. (1984).

$$T_{ss} = 1.523 \times 10^9 \left(\frac{1 - A}{R^2 \ \varepsilon_b}\right)^{1/4}$$

where A is the bolometric Bond albedo, R is the heliocentric distance in centimeters, and ε_b is the bolometric emissivity. Estimates of A, as we note below, give $A \sim 0.4$. For unit emissivity, $\varepsilon_b = 1$, $T_{ss} = 60°K$. The disk-averaged temperature, assuming a temperature distribution proportional to $\cos^{1/4}$ of the angle between the insolation and surface normal, is

$$T_{avg} = \left(\frac{2}{\pi}\right)^{1/4} T_{ss} = 57°K$$

As noted, however, the actual temperature near the subsolar point may be moderated by the heat capacity of the atmosphere and the possible shallow liquid nitrogen sea covering some fraction of the surface.

In summary, the surface of Triton is characterized by solid methane, either as a continuous surface or as icebergs floating in a sea of unknown depth of liquid nitrogen. Reddish photochemical products may give the surface a slight coloration, and water ice may occur as crystals suspended in the liquid nitrogen or as a solid mixed with the methane frost on expanses of solid surface (spectral modeling favors a suspension of fine crystals in the liquid). In this scenario, the satellite has an atmosphere of nitrogen with other possible minor constituents; the surface pressure may be regulated by the vapor pressure at the local temperature, but strong diurnal and seasonal effects are probable (see also Trafton 1983).[10]

This model is subject to test by the planned occultation of the Voyager 2 spacecraft by Triton in 1989.

2. Radius and Mass of Triton. Lebofsky et al. (1982)[11] obtained a weak detection of the 22.5-μm thermal radiation of Triton, thus permitting a deter-

mination of the radius and bolometric geometric albedo through the photometric/radiometric technique widely used for determinations of these parameters for asteroids and planetary satellites (Morrison and Lebofsky 1979).[12] Nearly simultaneously, Morrison _et al._ (1982)[13] attempted the same measurement but derived only an upper limit to the thermal flux. Both groups of investigators obtained essentially the same result: The radius of Triton is 1750 ± 250 km, and the bolometric geometric albedo is ~0.4.

It is important to inject a cautionary note before these results are taken as certain, however. The thermal model upon which the radius and albedo are calculated from the infrared flux assumes that the surface of the satellite is in instantaneous thermal equilibrium with the solar insolation and that thermal radiation from surface areas not in sunlight is negligible. For a liquid surface, the large heat capacity of the fluid would probably violate the assumption of instantaneous thermal equilibrium. In the case of Triton, the degree of validity of the model, hence the quality of the calculated radius and albedo, depends on the true nature of the surface, in particular, how much is solid and how much might be covered by liquid. In the extreme, it is possible that the radius given above is underestimated by √2 and that the albedo is a factor of 2 too high (Cruikshank _et al._ 1984).[4]

As an historical aside, it is interesting to recall Kuiper's (1954)[14] direct measurement of the diameter of Triton with a diskmeter attached to the Hale 5-m telescope. He found the diameter to be 0.173 arcsec (Triton was 30.1 AU from the sun), corresponding to a radius of 1900 km, or within the errors in the determination discussed above. Large systematic errors in Kuiper's technique, especially for the smaller objects he measured (such as Pluto), show that this agreement is fortuitous.

For comparison, the largest planetary satellite is Ganymede with r = 2631; for Titan, r = 2575 km; for Io, r = 1815 km; and for the moon, r = 1738 km.

The mass of Triton has been estimated from its effect on the motion of Neptune in separate studies by Nicholson _et al._ (1931)[15] and Alden (1940, 1943).[16,17] The values obtained are, respectively $(3.5 \pm 1.4) \times 10^{-2}\ M_N$ and $(1.34 \pm 0.3) \times 10^{-3}\ M_N$. Alden's mass value is based upon observations during a three-year period with a telescope of astrometic precision, while the observations made by Nicholson _et al._[15] were much less extensive and were obtained with a reflecting telescope. On these bases, the mass value by Alden appears preferable. The errors quoted for Alden's mass is a probable error in the weighted mean of three separate determinations in successive years. An updated determination reported by T. C. Van Flandern (private communication, 1982) gives $1.7 \times 10^{-3}\ M_N$, consistent with the Alden determinations. The mass value often quoted (e.g., Morrison and Cruikshank 1974)[18] is that given in the compilation by Duncombe _et al._ (1974),[19] which is equally weighted mean of the Nicholson _et al._ [15] and Alden (1940, 1943)[16,17] determinations. This mean value, when taken with r = 1750 km, as discussed above, gives a mean density that is completely unrealistic. Even the Alden determination alone, which is much smaller than that of Nicholson, gives a mean density on the order of 6 g cm^{-3} and should be viewed with caution. Our experience with other bodies in the outer solar system suggests that for these volatile-dominated objects the mean densities should lie in the range 1-3 g cm^{-3}.

In a sense, anguish over the mass and radius of Triton is an idle exercise, because the planned flyby of Voyager 2 through the Neptune system in 1989 will yield these quantities with far greater precision than can be achieved by ground-based observations.

NEREID

Nereid is a 19th magnitude satellite of Neptune discovered in 1948 by Kuiper. It lies in a mean distance of 0.037 AU from Neptune in an orbit of high eccentricity (0.76) and high inclination (27.5°), with a period of 359.4 days. The most recent study of the orbit, based on new observations, is that by Veillet (1982).[20]

There is virtually no physical information on Nereid apart from the photographically determined brightness. From plausible assumptions about color (the difference between the V magnitude and the photographic magnitude), Morrison and Cruikshank (1974)[18] found V(1,0) = +4.0. If the geometric albedo is 0.04, the radius is 525 km; if it is 0.4, the radius if 165 km.

The inclined, eccentric (direct) orbit suggests an origin by capture, in which case Nereid could be representative of the small, icy satellites, or could be a dark asteroid of mainly silicate composition. There is no information to support either interpretation, but Nereid will soon be within reach of multicolor photometric systems, and observations at a range of wavelengths will help discern between the ices and a surface predominantly composed of rocky or carbonaceous material.

A THIRD SATELLITE OF NEPTUNE?

Neptune was monitored photometrically from two locations separated by 6 km during the close approach of the planet to a star in May 1981. Both stations recorded a drop in signal lasting 8.1 sec. Reitsema et al. (1982)[21] have interpreted their observations as the occultation of the star by a previously unknown satellite of Neptune. If the object lies in Neptune's orbital plane, it orbits at a distance of 3 Neptune radii from the planet's center and has a minimum radius of 90 km. Attempts to image this suspected object have thus far not succeeded.

This work was supported in part by NASA grant NGL 12-001-057. It is a particular pleasure to acknowledge the important contributions of Drs. R. N. Clark and R. H. Brown to the Triton work. I thank Dr. J. F. Bell for permission to reproduce the Triton data in Figure 1 in advance of publication.

REFERENCES

1. Cruikshank, D. P., A. Stockton, H. M. Dyck, E. E. Becklin, and W. Macy, Jr. (1979). The diameter and reflectance of Triton. Icarus 40, 104-114.

2. Bell, J. F., R. N. Clark, T. B. McCord, and D. P. Cruikshank (1979). Reflection spectra of Pluto and three distant satellites. Bull. Amer. Astron. Soc. 11, 570 (Abstract).

3. Cruikshank, D. P., and J. Apt (1984). Methane on Triton: Physical state and distribution. Icarus (in press).

4. Cruikshank, D. P., R. H. Brown, and R. N. Clark (1984). Nitrogen on Triton. Icarus (in press).

5. Cruikshank, D. P., and P. M. Silvaggio (1979). Triton: A satellite with an atmosphere. Astrophys. J. 233, 1016-1020.

6. Apt, J., N. P. Carleton, C. D. Mackay (1983). Methane on Triton and Pluto: New CCD spectra. Astrophys. J. 270, 342-350.

7. Cruikshank, D. P., R. H. Brown, and R. N. Clark (1983). Nitrogen on Triton. Bull. Amer. Astron. Soc. 15, 857 (Abstract).

8. Franz, O. G. (1981). UBV photometry of Triton. Icarus 45, 602-606.

9. Delitsky, M. L. (1983). Chemistry of Triton's ocean. Bull. Amer. Astron. Soc. 15, 857 (Abstract).

10. Trafton, L. (1983). Does Triton's atmosphere undergo large seasonal variations? Paper presented at IAU Colloquium 77, Natural Satellites, Ithaca, NY, July 5-9.

11. Lebofsky, L. A., G. H. Rieke, and M. J. Lebofsky (1982). The radii and albedos of Triton and Pluto. Bull. Amer. Astron. Soc. 14, 766 (Abstract).

12. Morrison, D., and L. A. Lebofsky (1979). Asteroid radiometry. In

Asteroids (T. Gehrels, Ed.) Univ. Arizona Press, Tucson, pp. 184-205.

13. Morrison, D., Cruikshank, D. P., and R. H. Brown (1982). Diameters of Triton and Pluto. Nature 300, 425-427.

14. Kuiper, G. P. (1954). Report of the Commission for Physical Observations of Planets and Satellites. Trans. Int. Astr. Union 9, 250.

15. Nicholson, S. B., A. van Maanen, and H. C. Wills (1931). A preliminary determination of the mass of Neptune's satellite. Pub. Astron. Soc. Pacific 43, 261-262.

16. Alden, H. L. (1940). Mass of the satellite of Neptune. Astron. J. 49, 71.

17. Alden, H. L. (1943). Observations of the satellite of Neptune. Astron. J. 50, 110-111.

18. Morrison, D., and D. P. Cruikshank (1974). Physical properties of the natural satellites. Space Sci. Rev. 15, 641-739.

19. Duncombe, R. L., W. J. Klepczynski, and P. K. Seidelmann (1974). The masses of the planets, satellites, and asteroids. Fundamentals Cosmic Phys. 1, 119-165.

20. Veillet, C. (1982). Orbital elements of Nereid from new observations. Astron. Astrophys. 112, 277-280.

21. Reitsema, H. J., W. B. Hubbard, L. A. Lebofsky, and D. J. Tholen (1982). Occultation by a possible third satellite of Neptune. Science 215, 289-291.

PHYSICAL PROPERTIES OF THE URANIAN SATELLITES

Robert Hamilton Brown

Planetary Geosciences Division
Hawaii Institute of Geophysics
University of Hawaii
2525 Correa Road
Honolulu, Hawaii 96822

Abstract

Recent work on the satellites of Uranus has revealed many of their basic physical properties. Radiometric measurements have shown that the Ariel, Umbriel, Titania and Oberon have diameters which range from 1630 to 1110 km and albedos which range from 0.30 to 0.18. Spectrophotometric observations of Miranda suggest that it may have the highest albedo of the known Uranian satellites and a diameter of about 500 km. Near-infrared measurements show that Ariel, Titania and Oberon have the largest known opposition surges. All five known satellites of Uranus have surfaces which are composed of water ice contaminated with small amounts of dark material. The dark material on the surfaces of Ariel, Umbriel, Titania and Oberon is spectrally bland and has spectral similarities to carbon black, charcoal, carbonaceous chondritic material and other dark, spectrally neutral materials. Recent density determinations suggest that there may be large density differences among Ariel, Umbriel, Titania and Oberon, with density increasing with distance from Uranus.

INTRODUCTION

Rapid advancement in the technology of electro-optical detector systems, especially detectors optimized for the near-infrared, have resulted in useful, groundbased studies of the physical properties of the satellites of Uranus. The Uranian satellite system is an interesting system for many reasons, not the least of which being the unusual orientation of its angular momentum and the regularity of the orbits of the five known satellites. The satellites of Uranus also comprise the most distant of the regular satellite systems and as such may have formed under much different conditions than their warmer counterparts in the Jovian and Saturnian systems. All five known satellites have orbits that fit the criteria for a regular system. In order of distance from Uranus, the five satellites are U5 Miranda, U1 Ariel, U2 Umbriel, U3 Titania and U4 Oberon.

One dynamical aspect of the Uranian system is particularly interesting, that being the inclination of the rotation axis of Uranus with respect to the plane of its orbit (and also to the plane of the ecliptic). Uranus' axial inclination of 98° with respect to the ecliptic pole is the one of the most extreme examples of axial tilt among the planets. It has been suggested that the origin and evolution of the Uranian satellites may have been strongly affected by the events which are responsible for the observed axial tilt[1]. The 1984 aspect of the Uranian system as seen from the Earth is essentially polar and this has simplified the derivation of some orbital parameters from astrometric observations, as well as simplifying other observations such as photometry. The polar aspect does, however, frustrate groundbased observations which would search for such properties as albedo asymmetries with respect to the leading and trailing sides of the Uranian satellites.

Because the initial groundbased reconnaissance of the Uranian satellite system is reasonably mature, a review of their physical properties is timely. Specific topics discussed for the bodies in this paper will be size, surface compositions, photometric properties and densities, as well as problems for further study from both the ground and spacecraft. A compilation of the known properties of the satellites of Uranus prior to 1982 has been published by Cruikshank[2], so this paper will concentrate primarily on work done since the Cruikshank review.

SURFACE COMPOSITIONS

Most of what is known about the surface compositions of satellites in the outer solar system is derived from observations of their reflectance spectra. Absorption features characteristic of the surface mineralogy of a planetary body can be observed in the entire region of the solar spectrum where there is detectable reflected light (~0.1 to 5 µm). Observations of the reflectance of icy bodies are particularly diagnostic of surface composition in the near infrared where several cosmochemically important molecules (e.g. H_2O, NH_3 and CH_4) have vibrational transitions which result in absorptions seen in spectra of their diffuse reflectance. This technique has been applied to the Uranian satellites by many researchers and has resulted in a reasonable characterization of their surface compositions.

The first study of the near-infrared spectral reflectance of Titania and Oberon was published by Cruikshank[3]. In his spectra appear absorptions at 1.5 and 2.0 µm characteristic of the presence of water ice or frost on the surfaces of Titania and Oberon. In a follow-up study of Ariel and Umbriel, Cruikshank and Brown[4] also found water-ice absorptions in the near-infrared reflectance spectra of these satellites. Due to its faintness and proximity to Uranus, reflectance spectra of Miranda in the near-infrared have been extremely difficult to obtain using available telescopes and detector systems. Nevertheless, Brown and Clark[5] succeeded in obtaining a spectrum of Miranda in the 1.6-2.4 µm spectral region which clearly shows a deep absorption at 2.0 µm characteristic of water ice. The spectrum of Miranda from Brown and Clark overlaid with a spectrum of water frost from Clark[6] is displayed in Figure 1. It is now clear that all five Uranian satellites have water-ice surfaces.

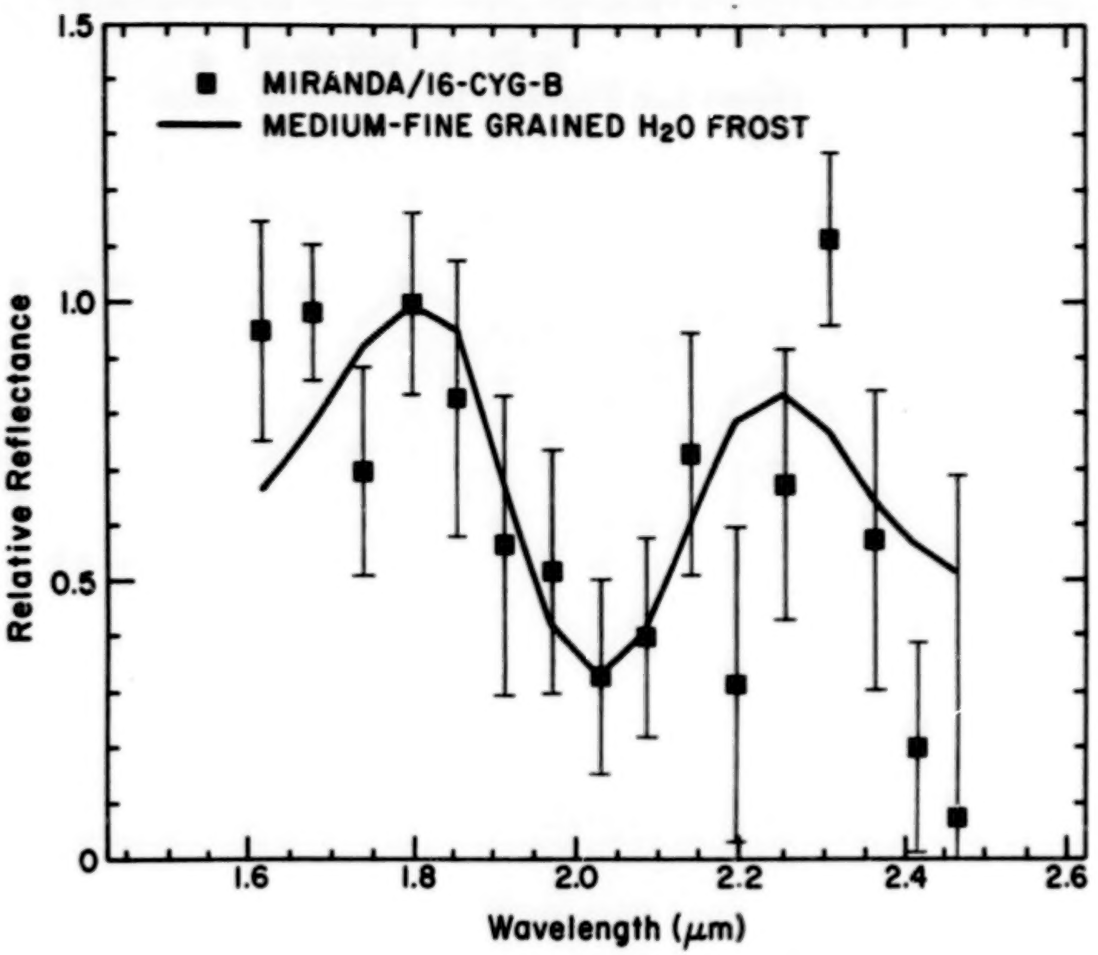

Figure 1: Plotted is the reflectance spectrum of Miranda from Brown and Clark[5]. The Miranda spectrum is normalized to 1.0 at 1.79 μm and is overlaid with a spectrum of fine-grained water frost from Clark[6]. The laboratory frost spectrum has been convolved to the resolution of the Miranda spectrum and normalized to 1.0 at 1.79 μm.

Soifer _et al._[7] obtained reflectance spectra of Umbriel, Titania and Oberon which confirmed the discovery of water ice and raised the possibility that these satellites had lower albedo than are characteristic of pure water-ice surfaces heavily gardened by meteoritic infall. That some of the Uranian satellites have relatively low albedos was firmly established by the radiometric measurements of Brown _et al._[8] who found the visual geometric albedos of Ariel, Umbriel, Titania and Oberon to be roughly intermediate to the visual geometric albedo range for most solar system bodies (~0.03 to 0.7). This does not seem to be the case for Miranda, however, because the depth of the 2.0 µm absorption in its reflectance spectrum implies that the water ice on its surface is relatively pure[5]. This suggests that Miranda's albedo is near the upper end of the range (Table I) and that its surface may be similar to those of some of the icy satellites of Saturn. With their p_v range of 0.2 to 0.3, the nearest albedo analogs for the large Uranian satellites among other icy satellites are Callisto and Hyperion whose p_v are 0.19 and 0.28 respectively[9,10]. As we shall see below, Hyperion may be similar to Ariel in surface composition as well as albedo.

Because the relatively low albedos of the Uranian satellites suggest the presence of a dark contaminant either on or in their surfaces, some recent studies of the near-infrared reflectance of the Uranian satellites have concentrated on its identification. Brown and Cruikshank[11] and Brown[12,19] have obtained reflectance spectra of Ariel, Umbriel, Titania and Oberon in the 0.8- to 2.6-µm spectral region which indicate that the non-water component of the surfaces of these satellites has a relatively bland reflectance spectrum. They have further noted that the non-water component has spectral similarities to substances such as charcoal, carbon black, carbonaceous chondritic material and other neutrally colored, low-reflectance materials. Composite spectra of the Uranian satellites are displayed in Figure 2. All spectra in Fig. 2 show the strong H_2O absorption at 2.0 µm and some show the 1.5 µm absorption as well. A laboratory spectrum of a sample of fine-grained water frost obtained by Clark[6] is displayed in Figure 3 to illustrate this point.

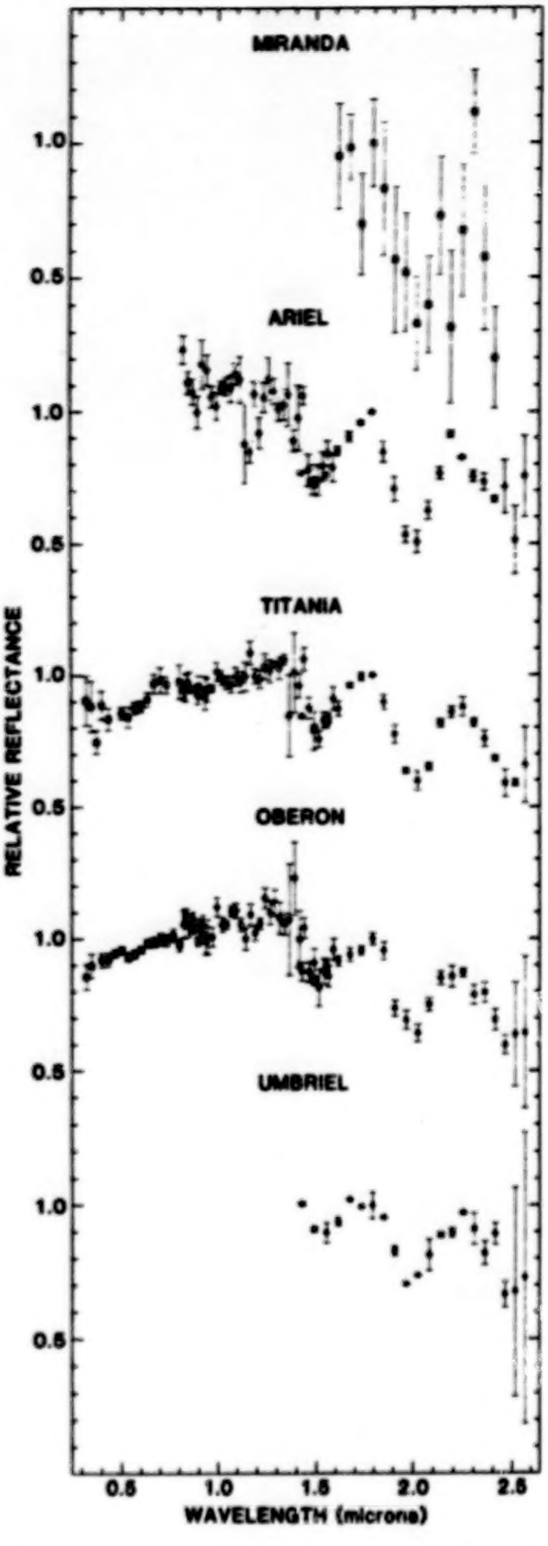

Figure 2: Plotted are composite spectra, from several sources, of the five satellites of Uranus[5,11,12,32]. All spectra are normalized to 1.0 near 1.8 μm.

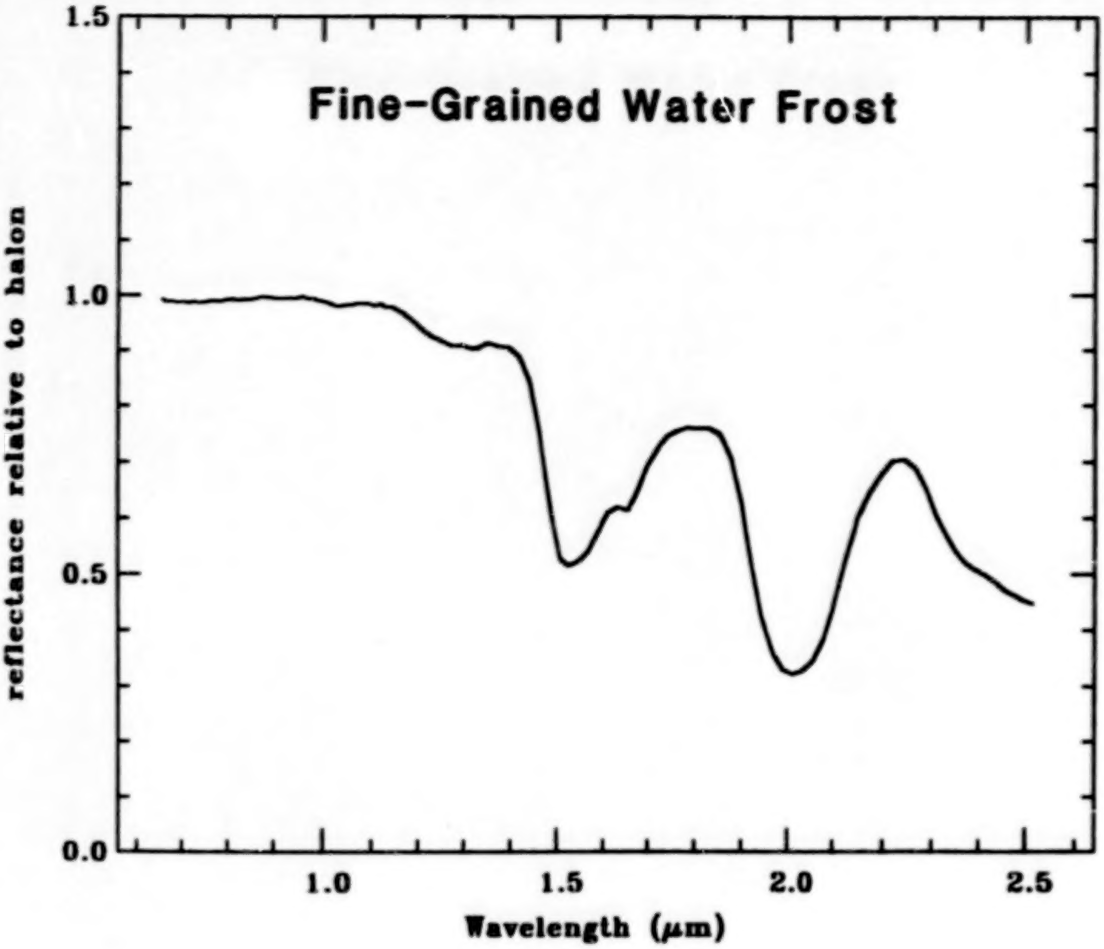

Figure 3: Plotted is a spectrum of fine-grained water frost from Clark (1981).

Brown[12] has investigated areal mixtures of water frost with isolated patches of dark, opaque, spectrally neutral material as potential analogs for the surfaces of Ariel, Umbriel, Titania, Oberon and Hyperion, and some of his results are displayed in Figure 4. The simulated spectra were constructed by the linear superposition of two laboratory spectra: that of fine-grained water frost, and that of an intimate mixture of 30 wt % charcoal and 70 wt % water ice.

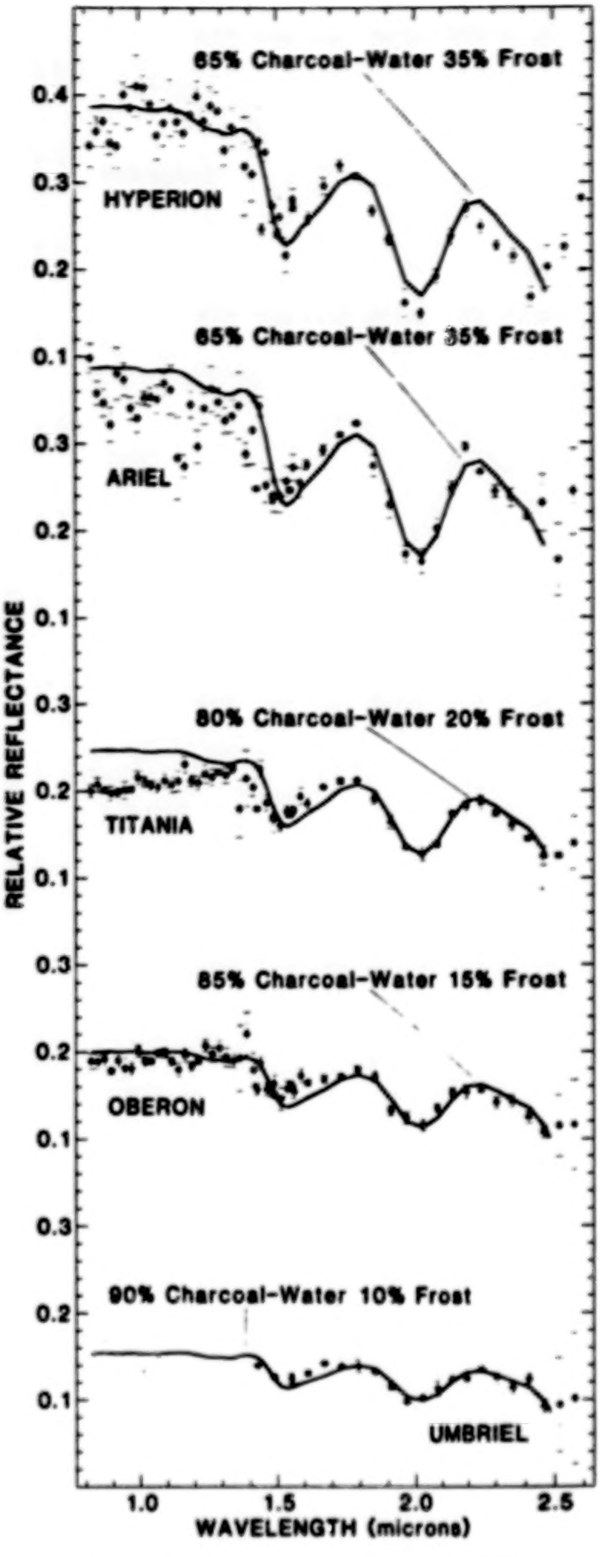

Figure 4: The spectra of Hyperion, Ariel, Titania and Oberon overlaid with spectra constructed from a linear superposition of lab spectra[12] (see text). Note that the normal reflectances of the laboratory spectra approximately match the satellites geometric albedos.

BEST COPY AVAILABLE

Reasonable matches constructed using this method demonstrate the consistency of the Uranian satellite spectra with areal mixtures of water frost and isolated patches of dark spectrally neutral materials. The spectral matches shown in Fig. 4 are, of course, not unique, but serve to demonstrate a large class of spectral analogs capable of approximately reproducing the depths of the absorption bands and the overall reflectance level of the Uranian satellite spectra. It is not possible, however, to determine conclusively using available data whether the dominant state of dispersal of the dark component of the Uranian satellite surfaces is voluminal or areal.

While looking for spectral analogs for the surfaces of the Uranian satellites, Brown and Cruikshank[11] noticed that the 0.8- to 2.6-μm reflectance spectrum of Saturn's satellite Hyperion[10] was very similar to that of Ariel. This is demonstrated in Figure 5 where the 1.5- to 2.6-μm spectra of Ariel and Hyperion have been normalized to 1.0 at 1.79 μm and overlaid. The spectral similarity extends to shorter wavelengths as well (Fig. 4) and is supported by the similarity of the two bodies visual geometric albedos (0.30 for Ariel and 0.28 for Hyperion). The exact reason for this spectral similarity is not clear, but it may result from a similarity in the distribution and spectral characteristics of the dark components contaminating the water ice on their surfaces[12]. A problem with this interpretation is the fact that the spectrum of Hyperion is redder than those of Titania and Oberon in the spectral region 0.3 to 0.8 μm. This would suggest that the dark component of Hyperion's surface is different from that of Ariel, or that Ariel's dark surface component is different from that of the other Uranian satellites.

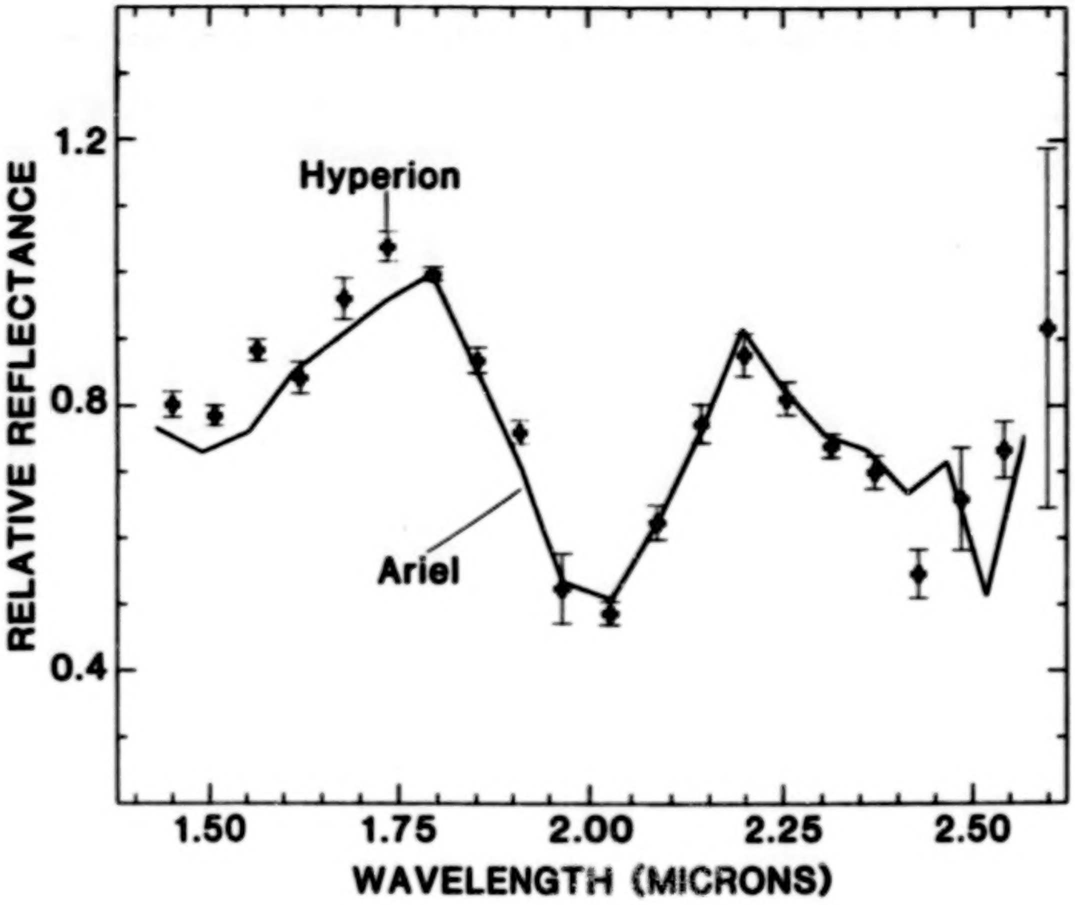

Figure 5: Plotted are the spectra of Ariel and Hyperion, both normalized to 1.0 at 1.79 µm. The data are from Brown and Cruikshank[11]. To facilitate comparison, no error bars are shown for the Ariel spectrum though they are comparable in size to those of the Hyperion spectrum.

Many theories of the formation of bodies in the outer solar system predict the incorporation of volatiles such as ammonia, methane and carbon monoxide into the surfaces of the Uranian satellites[13-18,31]. Conclusive evidence for the presence of such volatiles in the Uranian satellite surfaces has not yet been uncovered, but there are some interesting features of the reflectance spectra of Ariel and Hyperion which might result from the presence of NH_3, CH_4 or CO. The spectral feature in question is subtle, but amounts to a depression of the continuum at 2.25 µm in the Ariel and Hyperion spectra relative to that of pure water frost (see Figures 3, 4 and 5). The effect results in the spectra of Ariel and Hyperion peaking at 2.19 µm instead of at 2.25 µm as is normal for pure water ice or a mixture of water ice and small amounts of spectrally neutral material. Spectra of Ariel obtained during the 1983 apparition of Uranus (Brown and Clark, unpublished) confirm the spectral feature seen in the data of Brown and Cruikshank[11]. Ammonia, methane and carbon monoxide all have strong absorptions in the 2.2- to 2.3-µm region, but the low-resolution and precision of the existing data prevents a positive identification of which of these compounds, if any, is present on the surfaces of Ariel or Hyperion.

OPPOSITION SURGES

A non-linear increase in logarithmic brightness approaching zero-degrees solar phase angle (opposition surge) has been observed to exist for many solar system bodies, but recent observations indicate that the Uranian satellites opposition surges are unusual. The near-infrared opposition brightness surges of the Uranian satellites are the largest known over the 3° of solar phase angle which can be observed from Earth[11,19]. In Figure 6 are displayed the near-infrared brightness verses solar phase angle of Ariel, Umbriel, Titania and Oberon as well as broadband visual data on Saturn's rings, which, until recently, had the largest known opposition surges. As can be seen from Figure 6, the opposition surges of at least three of the Uranian satellites is 0.5 mag or more.

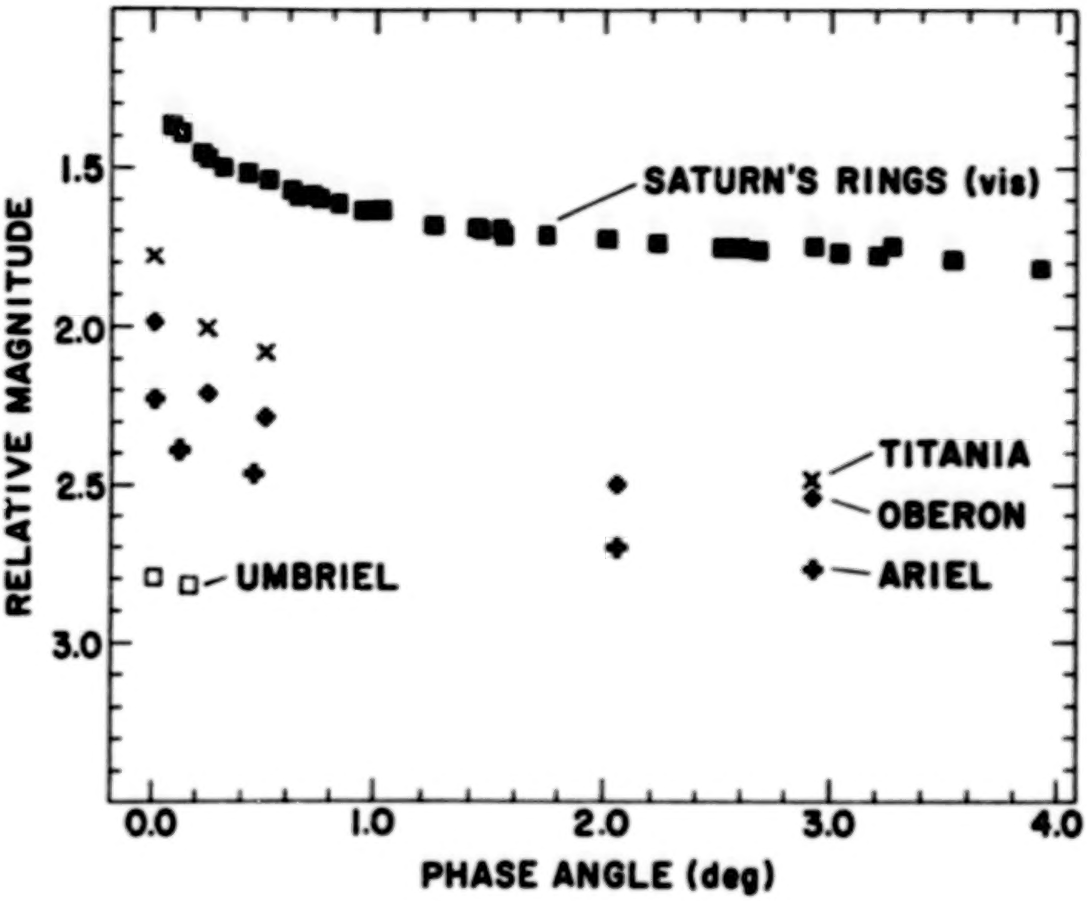

Figure 6: Near-infrared opposition brightness surges of Ariel, Umbriel, Titania and Oberon. The data are from Brown and Cruikshank[11]. Also plotted are the visual opposition surge data for Saturn's rings from Franklin and Cook[30]. The data for the Uranian satellites contain an arbitrary offset to facilitate comparison to the data for Saturn's rings.

A follow-up study of the broadband visual (V) opposition surges of the Uranian satellites[20] tentatively shows comparable results, but more observations are required to fully characterize the visual phase curves. It is not clear what surface properties of the Uranian satellites might be responsible for the large opposition surges, but some work points to surfaces composed of particles with highly back-scattering phase functions[21]. Hapke[22] has been able to model the very large and narrow opposition surges of the Uranian satellites by requiring that the density of the surface layer of scattering particles increase with depth from near zero to close packed over a distance of about 30 times the mean particle size. Veverka and Gradie[23] argue that grain size distribution, grain shape and packing texture are some of the several mechanisms that can be invoked to explain why the surfaces of icy satellites, in general, are not lambert scatterers.

RADII AND DENSITIES

Mean density deduced from measurements of mass and radius is an important physical property to determine in the study of the origin of a satellite system. Until recently, however, this quantity could only be estimated for the satellites of Uranus. The distance from Earth and faintness of the Uranian satellites makes direct determination of their radii nearly impossible using groundbased techniques. For the same reasons, observations from which accurate masses of the Uranian satellites can be derived are very difficult. Nevertheless, recent studies by Brown et al.[8], Brown and Clark[5], and Veillet[24] have made considerable progress in the determination of the densities of the satellites of Uranus. Brown et al.[8] have determined the radii of Ariel, Umbriel, Titania and Oberon by measuring the 20-μm thermal fluxes from the satellites and combining them with measurements of the satellites' broadband visual fluxes. These measurements were then incorporated into a version of the standard radiometric model[25-27], from which were deduced the radius and albedo for each satellite (Table I).

Table I: Radii, Masses, Densities and Albedos				
	radius (km)	mass (10^{23}g)	density (g cm^{-3})	p_v
Miranda	250 ± 110	1.7 ± 1.7	~ 3	~ 0.5
Ariel	665 ± 65	15.6 ± 3.5	1.3 ± 0.5	0.30 ± 0.06
Umbriel	555 ± 50	10.0 ± 4.2	1.4 ± 0.6	0.19 ± 0.04
Titania	800 ± 60	59.0 ± 7.0	2.7 ± 0.6	0.23 ± 0.04
Oberon	815 ± 70	60.0 ± 7.0	2.6 ± 0.6	0.18 ± 0.04

Table I: Masses and densities are drawn from Veillet[24], radius and visual geometric albedo (p_v) are drawn from Brown *et al.*[8], except the radius and albedo of Miranda which are drawn from Brown and Clark[5].

Because the photometric/radiometric technique is a model dependent determination, it is useful to digress slightly to discuss the limits of validity of the Brown *et al.*[8] measurements. The radiometric technique is model dependent in general and, for the specific case of the Uranian satellite diameter measurements, values were assumed for some of their photometric properties. The phase integrals of the Uranian satellites have never been determined because only ± 3° of solar phase angle can be covered by observations from the ground. Therefore, Brown *et al.* assumed phase integrals for each of the four large Uranian satellites by analogy with other icy satellites whose phase integrals are known and have similar geometric albedos. Fortunately, the effect of a rather large uncertainty in the phase integral on the derived radius is quite small for the case of the Uranian satellites (e.g. the assumption of 0.8 ± 0.1 for the phase integral of Ariel results in a change in the derived radius of ± 3%[8]). Brown et al. also found it necessary to assume a value of V(1,0) for each of the Uranian satellites from measurements of their brightness made at a solar phase angle of 0.01° (V(1,0) is a linear extrapolation of visual magnitude to 0° solar phase angle from phase angles greater than 6° with normalization to a distance of 1 AU from Earth and Sun). This was necessary because the standard linear extrapolation to zero-phase brightness can not be made from groundbased measurements. The uncertainty in V(1,0) of ± 0.2 mag specifically used by Brown et al., translates into about a ± 5% uncertainty in derived radius. This is not the case for the derived albedos because they depend almost entirely on the amount of light reflected by the body being measured. Therefore, rather large systematic errors in V(1,0) can translate into equally large errors in derived albedo. An additional uncertainty in the radiometric radii of the Uranian satellites derives from the fact that the model is based on monochromatic fluxes derived from broadband measurements. The derivation of monochromatic fluxes requires a knowledge of the atmospheric transmission function above the observing site as well as the convolved filter transmission and instrument response function. For the Brown et al. measurements, atmospheric transmission was determined from measurements of the column density of H_2O derived from observations of the 1.4-μm telluric absorption obtained contemporaneously with the 20-μm thermal measurements. Uncertainties of ± 0.1 mag in the correction of broadband fluxes to monochromatic fluxes were folded into the results of Brown et al. to maintain conservative error estimates.

Perhaps the greatest potential problem with any radius derived using the radiometric technique is one basic assumption--that the surface of the body is in instantaneous thermal equilibrium with absorbed insolation. If that assumption is seriously violated (i.e. the entire surface of the body is isothermal), it is possible to underestimate the radius of the body by as much as a factor of root two. This is not likely to be a problem with the Brown _et al_. measurements because the Uranian satellites are essentially pole-on with respect to the Sun (unless, of course, the bulk composition of the satellites is a material with very high thermal conductivity or they all have substantial atmospheres--neither of which are likely). Though it is possible that there may be some residual systematic errors in the Brown _et al_. radii, they are not likely to be larger than the quoted random errors unless the surfaces of the Uranian satellites have highly unusual thermal properties.

As can be seen from Table I, the satellites of Uranus are comparable in size to the largest of Saturn's icy satellites Dione, Iapetus and Rhea which have diameters of 1120, 1460 and 1530 km respectively[28]. They are therefore among the largest satellites in the solar system, but are considerably smaller than the giant satellites Ganymede, Callisto, and Titan whose diameters are approximately 5000 km.

As was mentioned previously, Veillet[24] has derived masses for all the Uranian satellites from observations of their mutual orbital perturbations. He has combined six years of his own observations of the Uranian satellites with all other astrometric observations made since the discoveries of the satellites, redetermining all their orbital parameters and mutual perturbations. Combining his mass measurements with the radii measured by Brown _et al_.[8], Veillet has derived densities for Ariel, Umbriel, Titania and Oberon. The masses of all the Uranian satellites as well as their densities and albedos are listed in Table I (The density of Miranda listed in Table I was derived from the diameter estimate of Brown and Clark[5] and the mass estimate from Veillet). As can be seen from Table I, the Uranian satellites seem to form two distinct density groups. Given that all the Uranian satellites are known to have water-ice surfaces, and that the densities of Ariel and Umbriel are comparable to those of several of Saturn's satellites whose bulk compositions are thought to be about 40% silicates and 60% water ice by weight, one can conclude that the bulk compositions of Ariel and Umbriel may be similar. In contrast, Titania and Oberon have densities which indicate that much larger fractions of their bulk compositions are of high density materials such as silicates. Since they are large enough to have undergone melting and at least partial differentiation[29], densities of 2.6 to 2.7 g cm^{-3} for Titania and Oberon suggest that they may have a large core which is mostly rock with a skin of water ice composing their crusts and mantles. If the apparent density variations are real, then we have a system whose density gradient is opposite to that which one would expect if primordial heat from the accretion and contraction of Uranus determined what materials were available for incorporation into the satellites. This might be seen to favor origins of the Uranian satellites which are closely connected to the catastrophic events hypothesized to be responsible for the present axial orientation of the Uranian system[1]. Nevertheless, large uncertainties in the densities of the Uranian satellites council restraint with regard to speculations about the satellites' origins based on their apparent density differences. Further thoughts regarding the origins of the Uranian satellites can be found in Stevenson _et al_.[18].

SUMMARY

The Uranian satellites comprise a system of five regular satellites, all having water-ice surfaces of varying degrees of purity. Ariel, Umbriel, Titania and Oberon have opposition surges which are among the largest in the solar system and have low albedos relative to those typical of relatively pure, heavily gardened water-ice surfaces. Present with the water ice on the surfaces of Ariel, Umbriel, Titania and Oberon is a dark spectrally neutral component which has spectral characteristics similar to those of carbon black, charcoal, carbonaceous chondritic material, and other neutrally colored, low-reflectance materials. Compounds more volatile than water ice (e.g. methane, ammonia and carbon monoxide) have not yet been conclusively shown to exist on any surfaces in the Uranian system, though there are as yet unidentified spectral features in the spectrum of Ariel which might be the result of the presence of the hydrate of one of these compounds. The Uranian satellites are comparable in size to the largest of Saturn's icy satellites while density measurements suggest that the bulk compositions of Ariel and Umbriel are quite different than those of Titania and Oberon. Ariel and Umbriel have densities which are similar to the icy Saturnian satellites and may have similar bulk compositions. Titania and Oberon have densities which suggest that they have a much higher proportion of silicates or other high-density materials than do Ariel and Umbriel. If the apparent increase in satellite density with increase in distance from Uranus is real, it may perhaps result from catastrophic events hypothesized to be responsible for Uranus' axial orientation.

PROSPECTS FOR FURTHER STUDY

Certainly some of the most important data on the Uranian satellites will be obtained when Voyager 2 arrives in January, 1986. As the trajectory is now planned, Voyager's closest satellite encounter in the Uranian system will be with Miranda, resulting in the highest resolution imaging of the five satellites, and, despite the non-ideal trajectory (the spacecraft will pass through the Uranian system on a trajectory roughly perpendicular to Uranus' equatorial plane), good imaging should also be obtained for Ariel, Umbriel, Titania and Oberon. High-quality images will likely yield clues to the relative importance of endogenic and exogenic processes in the modification of the surfaces of the Uranian satellites and may also help determine the source of the satellites' low albedos. The prospects are encouraging for measurement by Voyager of all five satellites' radii and masses, with reasonably accurate density measurements being an important result. The Voyager 2 spacecraft, however, is not well equipped for detailed remote sensing of the surface compositions of satellites and, until another spacecraft arrives at Uranus with the proper instrumentation, groundbased research will be the primary source of further information of the composition of the Uranian satellite surfaces. Groundbased studies of the surface compositions of the Uranian satellites have been difficult in the past, but the new technology of infrared array detectors promises to allow significant further progress. As was mentioned in the section on surface compositions, a particularly interesting problem with regard to the surface compositions of the Uranian satellites, as well as other icy satellites, concerns the presence or absence of hydrated and anhydrous ammonia (NH_3), methane (CH_4), nitrogen and carbon monoxide (CO). A search for these compounds in the surfaces of the Uranian satellites is important, because the result has profound consequences for our understanding of the origins of icy bodies within the context of currently accepted theories.

REFERENCES

(1) Singer, S. F. (1975). When and where were the satellites of Uranus formed? *Icarus* 25, 484-488.

(2) Cruikshank, D. P. (1982). The satellites of Uranus. In *Uranus and the Outer Planets* (G. E. Hunt, ed.), pp. 193-216, Cambridge University Press.

(3) Cruikshank, D. P. (1980). Near-infrared studies of the satellites of Saturn and Uranus. *Icarus* 41, 246-258.

(4) Cruikshank, D. P. and R. H. Brown (1981). The Uranian satellites: Water ice on Ariel and Umbriel. *Icarus* 45, 607-611.

(5) Brown, R. H. and R. N. Clark (1984). Surface of Miranda: Identification of water ice. *Icarus*, in press.

(6) Clark, R. N. (1980). Water frost and ice: The near-infrared spectral reflectance 0.65-2.5 microns. *JGR* 86, 3087-3096.

(7) Soifer. B. T., G. Neugebauer and K. Matthews (1981). Near-infrared spectrophotometry of the satellites and rings of Uranus. *Icarus* 45, 612-617.

(8) Brown, R. H., D. P. Cruikshank and D. Morrison (1982). Diameters and albedos of satellites of Uranus. *Nature* 300, 423-425.

(9) Squyres, S. W. and J. Veverka (1981). Voyager photometry of surface features on Ganymede and Callisto. Icarus 46, 137-155.

(10) Cruikshank, D. P. and R. H. Brown (1982). Surface composition and radius of Hyperion. Icarus 50, 82-87.

(11) Brown, R. H. and D. P. Cruikshank (1983). The Uranian satellites: Surface compositions and opposition brightness surges. Icarus 55, 83-92.

(12) Brown, R. H. (1983). The Uranian satellites and Hyperion: New spectrophotometry and compositional implications. Icarus 56, 414-425.

(13) Cameron, A. G. W. (1973). Formation of the outer planets. Space Sci. Rev. 14, 392-400.

(14) Cameron, A. G. W. (1973). Elemental and isotopic abundances of the volatile elements in the outer planets. Space Sci. Rev. 14, 392-400.

(15) Lewis, J. S. (1971a). Satellites of the outer planets: Their physical and chemical nature. Icarus 15, 174.

(16) Lewis, J. S. (1972). Low temperature condensation from the solar nebula. Icarus 16, 241-252.

(17) Lewis, J. S. (1973). Chemistry of the outer solar system. Space Sci. Rev. 14, 401-411.

(18) Stevenson, D. J., A. W. Harris and J. I. Lunine (1984). Origins of satellites. In Natural Satellites, Chapter 2. University of Arizona Press, Tucson, Arizona. In preparation.

(19) Brown, R. H. (1982). The satellites of Uranus: Spectrophotometric and radiometric studies of their surface properties and diameters. Ph.D. dissertation, University of Hawaii, Honolulu, Hawaii.

(20) Brown, R. H. and J. Goguen (1984). Opposition surges of the Uranian satellites. Icarus, to be submitted.

(21) Pang, K. D. and J. W. Rhoads (1983). Interpretation of disk integrated photometry of the Uranian satellites. Paper presented at the IAU Colloquium 77, Natural Satellites, July 5-9, 1983 at Cornell University, Ithaca New York.

(22) Hapke, B. (1983). The opposition effect. Bull. Amer. Astron. Soc. 15, 856-857 (Abstract).

(23) Veverka, J. and J. Gradie (1983). Why don't icy satellites scatter like model snow-covered planets? Bull. Amer. Astron. Soc. 15, 853 (Abstract).

(24) Veillet, Ch. (1983). De l'observation et du mouvement des satellites d'Uranus. Ph.D. dissertation, University of Paris, Paris, France.

(25) Morrison, D. (1973). Determination of radii of satellites and asteroids from radiometry and photmetry. Icarus 19, 1-14.

(26) Morrison, D. and L. A. Lebofsky (1979). Radiometry of asteroids. In Asteroids (T. Gehrels, Ed.), University of Arizona Press, pp. 184-205.

(27) Brown, R. H, D. Morrison, C. M. Telesco and W. E. Brunk (1982). Calibration of the radiometric asteroid scale using occultation diameters. Icarus 52, 188-195.

(28) Smith, B. A. et al. (1982). A new look at the Saturn system: The Voyager 2 images. Science 215, 504-536.

(29) Lewis, J. S. (1971b). Satellites of the outer planets: Thermal models. Science 172, 1127.

(30) Franklin, F. A. and A. F. Cook (1965). Optical properties of Saturn's rings II. Two-color phase curves of the two bright rings. Astron. J. 70, 704-720.

(31) Lunine, J. I. and D. J. Stevenson (1983). The role of clathrates in the formation and evolution of icy satellites. Paper presented at the IAU Colloquium No. 77, Natural Satellites, Cornell University, July 5-9, 1983.

(32) Bell, J. F., R. N. Clark, T. B. McCord and D. P. Cruikshank (1979). Reflection spectra of Pluto and three distant satellites. Bull. Amer. Astron. Soc. 11, 572 (Abstract).

BLANK PAGE

462.

Satellite Masses in the Uranus and Neptune Systems

Richard Greenberg
Planetary Science Institute, Tucson, Arizona

Abstract

Our knowledge of satellite masses, and how they are derived, is reviewed with emphasis on implications for bulk densities and albedos. In general for the Uranian system, the inner satellites have lower densities and/or higher albedos than the outer ones. However, uncertainties are great enough that all five satellites may have nearly equal densities (~ 2 gm/cm^3). In that case, albedo would generally (but not monotonically) decrease with semi-major axis. A more severe constraint than previously published is here placed on Miranda's mass, and hence on its density and albedo. The recent radiometric value for Triton's diameter, combined with now-rather-old mass determinations, yields a density greater than 4 gm/cm^3, but systematic errors are possible in both mass and diameter.

INTRODUCTION

Until spacecraft fly reasonably close to planetary satellites, we can evaluate the satellites' masses only from their effects on one another or on the motion of their planet. In general, satellites are so small and so far from the Earth that their periodic effects on one another are too small to be useful in determining masses. What made reasonably precise mass determinations possible for several of the satellites of Jupiter and Saturn, even before the arrival of Voyager spacecraft, were the commensurable orbital periods that gave enhanced, resonant (and hence measurable) responses of other satellites.

In the case of the Uranian satellites, several fortuitous circumstances combine to permit meaningful mass determinations. First, there is a three-way near commensurability among the satellites Miranda, Ariel, and Umbriel which, although it doesn't give masses directly, does permit determination of products of masses. Second, the inclination of the system relative to the ecliptic gives useful perspectives (alternately pole-on and edge-on views) that facilitate separation of orbital elements. And third, the presence and measurement of the ring system has allowed precise determination of the gravitational oblateness of the planet, which in turn permits mutual precessional effects of the satellites to be separated from the components of precession due to the planetary oblateness. For Triton, mass determination depends on the fact that the mass is large enough to have a significant effect on the motion of Neptune, and is facilitated by the fact that there is no other satellite of comparable mass, which would complicate the motion of the planet.

In this paper, I review the methods by which satellite masses have been determined. An historical approach is taken because, to a significant degree, the improvements in accuracy and precision have been based on the work that went before. In the case of Triton, an historical approach is the only possible one: there are no recent determinations. Throughout the paper, I emphasize the constraints on density and albedo provided by the mass constraints. For the best and most recent determinations of masses and radii, I emphasize the wide range of densities that are still admitted.

MASSES OF URANIAN SATELLITES

The Work of Harris. The first determination of the masses was by D.L. Harris[1], who combined photometric estimates of the relative masses of the satellites with measurements of the apsidal precession of Umbriel and Titania "to obtain some idea of the order of magnitude of the quantities involved." The photometric estimates were based on preliminary, unpublished magnitudes from G.P. Kuiper and on the assumption of equal albedos and densities for all five satellites. Measurement of precession (of either apsides or nodes) was potentially a very powerful tool in mass determination because the effects are secular rather than oscillatory: they represent the average effect of a satellite with its mass smeared over its orbit. Even if the mass is small and the precession induced in another satellite's orbit is slow, masses may be obtained if one only waits long enough. However, Harris had two things working against him in his efforts. First, the orbital eccentricities are so small that measurement of apsidal orientation was difficult; second, he had no way to separate the precessional effects of Uranus' oblateness from those of the satellites. The effects are qualitatively similar because oblateness is like a ring of excess mass around the planet's equator, similar to the averaged, smeared rings of satellite mass. Despite these difficulties, as shown in Table 1, Harris' estimates were fairly close to our best current values, exceeding his goal of order-of-magnitude precision.

The Work of Dunham. In 1971, Dunham used a similar method to determine masses.[2] With improved magnitudes from Harris[3] and assuming that all five satellites have the same albedos and densities, Dunham obtained $\mu_V = 0.032\mu_{III}$, $\mu_I = 0.58\mu_{III}$, $\mu_{II} = 0.17\mu_{III}$, and $\mu_{IV} = 0.77\mu_{III}$, where μ denotes a mass m divided by the planet's mass M. He obtained a value for the oblateness coefficient $J_2 = 0.013$ from the apsidal precession of Ariel, which he assumed was dominated by oblateness. (Apparently the value $J_2 = 0.034$ found by Harris was spurious.) Then, using Harris'[1] theoretical expression for Titania's apsidal precession rate,

$$\frac{d\tilde{\omega}_{III}}{dt} = (0.065J_2 + 1.2\,\mu_V + 3.2\,\mu_I + 10.1\,\mu_{II} + 22.5\,\mu_{IV}) \times 10^3 \text{ deg/yr} \qquad (1)$$

BLANK PAGE

BLANK PAGE

BLANK PAGE

TABLE I: HISTORY OF MASS DETERMINATIONS*

	Miranda (UV) $\mu_V \times 10^5$	product $\mu_V \times \mu_I \times 10^{10}$	Ariel (UI) $\mu_I \times 10^5$	product $\mu_I \times \mu_{II} \times 10^{10}$	Umbriel (UII) $\mu_{II} \times 10^5$	Titania (UIII) $\mu_{III} \times 10^5$	Oberon (UIV) $\mu_{IV} \times 10^5$
Harris (1949)	0.1	—	1	—	0.6	5	3
Dunham (1971)	0.33 ± 0.25	—	6 ± 4	—	1.8 ± 1.4	10 ± 7	8 ± 6
Greenberg** (1976, 1979)	—	≤0.05	—	≤10.	—	—	—
Veillet (1981)	—	—	—	1.10 ± 0.25	—	14.7 ± 1.0	—
Veillet (1983)	—	—	3.2 ± 0.5	1.37 ± 0.15	0.4 ± 0.1	—	—
Veillet (thesis, part IV)	—	0.36 ± 0.1	—	2.0 ± 0.12	—	—	—
Veillet Best Values (thesis, part V)	0.2 ± 0.2		1.8 ± 0.4		1.2 ± 0.5	6.8 ± 0.8	6.9 ± 0.8
This Paper	<0.1						

[*] μ is a satellite's mass divided by the mass of Uranus (8.66×10^{28} gm).

[**] Greenberg (1979) also gave mass product $\mu_V \mu_{II} \leq 0.06 \times 10^{-10}$.

and his own measurement of Titania's precession (2.9 ± 1.5)/yr, he determined the satellite masses as shown in Table 1.

According to Eq. (1), the precession rate is most strongly dependent on μ_{IV}, i.e., Oberon dominates Titania's precession. Thus, Dunham's calculation is essentially a dynamical determination of Oberon's mass μ_{IV}, and a photometric determination of the other masses, based on comparison with μ_{IV}. (This important point may have been obscured for some readers because both Dunham and Harris arbitrarily expressed satellite masses in terms of μ_{III}, giving the false impression that the determination of μ_{III} was more fundamental.) The evaluation of μ_{IV} itself was only minimally dependent on the assumption of equal densities and albedos and on the adopted value of J_2. We now know (see below) that Dunham's J_2 value was a few times too large; this introduces an error of only ~10% in the determination, small compared with Dunham's ±75% error brackets. On the other hand, as I pointed out,[4] if μ_I or μ_{II} were a few times larger than the assumed value relative to μ_{IV}, then Dunham's lower limit to Oberon's mass would break down. Nevertheless, the best current value for μ_{IV} (discussed below) fits well within Dunham's range.

Motion of Miranda. In 1973 E. Whitaker and I remeasured all known images of Miranda in order to determine whether or not any gross error had been made in the determination of Miranda's orbital period, and in particular to confirm Harris'[1] observation that the periods of the three inner satellites are in a near commensurability, but not an exact one.[5,6,7,8] While the study did confirm the orbital period, there were also useful systematic residuals in the analysis. For images made in 1948-49 when the orbits were viewed pole-on from Earth, the residuals varied sinusoidally with position angle. Since inclination errors have negligible effect when the system is viewed pole-on, the residuals were attributed to a previously undetected eccentricity ~0.01. Furthermore, in order to fit residuals at later epochs, a model with inclination and with precession of apsides and nodes was introduced. We obtained the surprisingly large inclination of 4° (surprising because such large inclinations were unheard-of well inside a regular satellite system) and precession rates just over 20°/yr. For comparison, the most recent orbital analysis (by Veillet[9], discussed more below) gives $e \approx 0.003$, $i = 4^\circ$, and precession of 20°/yr.

The precession rates for Miranda yielded an estimate of the oblateness parameter J_2. Assuming the precession to be due to the oblateness alone, I obtained $J_2 \approx 0.005 \pm 10\%$ (Greenberg, 1975). However, at the same time, I estimated that the effect of the masses of the other satellites on Miranda's precession would depress the inferred value of J_2 by ~20%. Thus, my estimate of J_2 was quite close to the value 0.00335 now obtained with great precision from studies of the precession of Uranus' rings.[10]

The Laplace Resonance. In our analysis of Miranda's motion, we were careful to point out that we had not taken account of possible variations in the motion due to enhanced resonant perturbations associated with the near-commensurability of orbital periods. The inner three satellites of Uranus have a commensurability relationship similar to the one between the inner three Galilean satellites of Jupiter. In the latter case, the stable resonance relation (known as the "Laplace relation") is described by the expression

$$\lambda_1 - 3\lambda_2 + 2\lambda_3 = 180^\circ, \qquad (2)$$

where λ is the mean longitude and subscripts 1, 2, and 3 refer to Io, Europa, and Ganymede, respectively. This expression implies that whenever Europa and Ganymede are in conjunction with respect to Jupiter (i.e., whenever $\lambda_2 = \lambda_3$), Io is 180° away. The three satellites are prevented from lining up on the same side of Jupiter. The commensurability relation between mean motions n is obtained by differentiation yielding

$$n_1 - 3n_2 + 2n_3 = 0. \tag{3}$$

In the case of Miranda, Ariel, and Umbriel (Uranus V, I, and II, respectively), the equivalent expression is small but not zero:

$$n_V - 3n_I + 2n_{II} = 0.08 \text{ day}^{-1}. \tag{4}$$

Thus, $\lambda_V - 3\lambda_I + 2\lambda_{II}$ circulates through 360° in 12.5 yr. This slight deviation from the Laplace relation motivated our[5,6,7] investigation into the remote possibility that this commensurability appears inexact due to some error in the determination of Miranda's orbital period. The addition of one revolution of Miranda in the 12-year gap between the bulk of the observations available then (late 40's and early 60's) would have given exactly the commensurate period. But, as mentioned above, no such error was discovered. The Uranus system also differs from the Galilean satellites in that, taken by pairs, the mean motions are not near ratios of small whole numbers.

The four outer satellites have a combination of mean motions even closer to zero than (4):

$$n_I - n_{II} - 2n_{III} + n_{IV} = 0.0034 \text{ day}^{-1}. \qquad (5)$$

However, this is not the type of relation associated with stable resonances. For a resonant interaction, the sum of the integer coefficients in a commensurability relation must be zero. Otherwise, the interaction would depend on the choice of reference longitude. The sum here is not zero, so relation (5) simply represents a numerologically intriguing distribution of orbits, not a resonance relation per se.

Limits On Mass Products. In our work on Miranda's motion, the near Laplace commensurability (Eq. 4) provided first a motivation for the work, and then a caveat that our orbital fit had not included resonance effects. As it turns out the resonance effects were not great enough to affect our orbital determinaton. However, I realized that the study of resonance effects might be exploited to get some handle on satellite masses. First I developed the theory of the effects of Ariel and Umbriel on Miranda,[11,12] assuming that these would be most readily observable. In the case of the Laplace-type near-commensurability, the dominant effect is a 12.5 yr oscillation in orbital longitude relative to uniform motion. The amplitude is proportional to the product of the two perturbing satellite masses. Comparison with the observational record available at that time showed no discernable effects in Miranda's motion. Thus, I was able to set an upper limit to the mass product $\mu_I \mu_{II}$ of 10^{-9} which was the first dynamical constraint on the masses of those two satellites[12] and was somewhat more restrictive than the earlier photometric estimates (see Table 1).

An interesting sidelight of this research was that if $\mu_I \mu_{II}$ were larger than 3.5×10^{-9}, as was quite plausible from the photometric estimates, then the resonance would have been strong enough to have restored the system to exact commensurability from its only nearly commensurable condition of the late 1940's. The resonant argument shown as the left side of Eq. (2) would librate about 180°. Harris[1] was premature, though fortuitously correct, in discounting the possibility of an exact commensurability.

A mass constraint based on the product of masses is sufficiently unconventional that extra care should be used in its interpretation. Soifer et al.[13] provide some examples of how not to interpret this result. They say that my analysis suggests $\mu_{II} \sim 10^{-4.5}$. In fact, my analysis said nothing about any individual mass, and it gave only an upper limit for the mass product. Those authors also said my result was based on the effect of Ariel and Umbriel on the formation of Miranda. In fact, it is based on ongoing gravitational perturbations.

In 1978, I extended the theoretical analysis to include effects on Ariel and Umbriel (proportional to $\mu_V\mu_{II}$ and $\mu_V\mu_I$, respectively).[14,15] Again no resonant variations in longitude were detected. That negative result yielded the limits $\mu_V\mu_I \leq 5 \times 10^{-12}$ and $\mu_V\mu_{II} \leq 6 \times 10^{-12}$, again constraints more restrictive than the photometric estimates. In reporting those results, I stressed the importance of getting a more complete data set with good longitudinal coverage each year over a dozen years (the period for resonant oscillations), in order to evaluate these mass products more precisely. As I discuss later below, such improvements have now been made.[9]

Density-Albedo Limits. These mass constraints can be related to bulk physical properties of the satellites by consideration of an albedo vs. density diagram (Fig. 1). If a body's mass and visual magnitude (but not its radius r) are known, it is confined to a line of slope 2/3 on the log-log plot, because the density ρ is given by

$$\rho = \frac{3}{4\pi}\, mr^{-3} \tag{6}$$

and albedo p_V is given by

$$2.5 \log p_V = -26.77 - V(1,0) - 5 \log(r/1\ \mathrm{AU}). \tag{7}$$

Constraints on radius reduce this locus to a segment of the line of slope 2/3. Also uncertainties in mass can spread the area of possible values in the ±ρ direction.

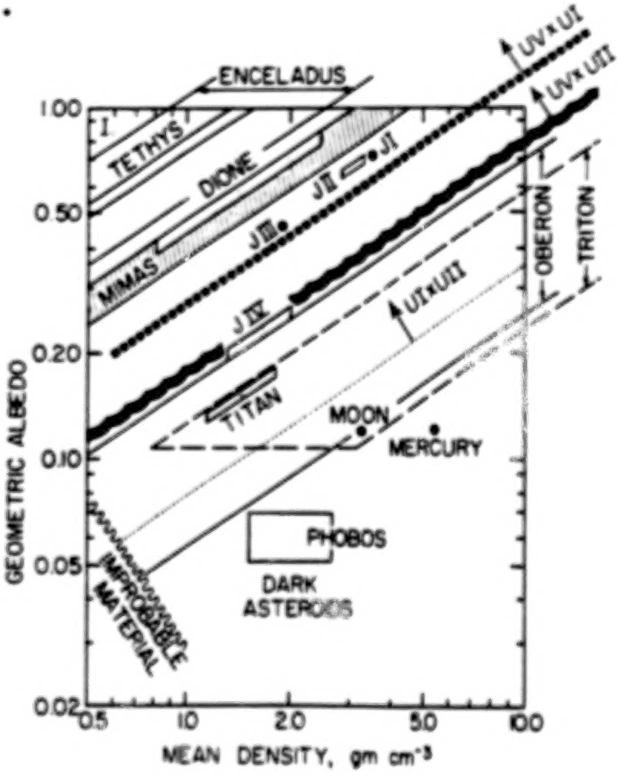

Figure 1: Density vs. Albedo diagram showing the state of knowledge in 1978. Dotted line labelled UI x UII shows region defined by limit on mass product $\mu_I \mu_{II}$. The midpoint between the position of Ariel and Umbriel must lie above this line. Similar interpretations apply for UV x UI and UV x UII. Masses for all Jovian, Saturnian, and Uranian satellites are based on resonant effects.

Figure 1 shows the status of density vs. albedo constraints in 1978.[14] Among the satellites of Saturn, the masses of the resonant satellites Mimas, Enceladus, Dione, Tethys, and Titan were reasonably well constrained, yielding the bands of 2/3 slope shown; at that time, only Titan had a radius determination available to limit the length of the band. These satellites seemed certain to be fairly icy. Densities and albedos of the Galilean satellites were already well known. The constraints on Triton will be discussed in a separate section below. For the Uranian satellites, we had the limits on Oberon due to Dunham's mass determination (with ±75% uncertainty). The range of density and albedo was quite wide, but clearly ruled out an extremely low density and bright surface, such as the inner Saturnian satellites had. For Ariel and Umbriel, the limit is shown (labeled UI x UII) assuming each has the same density and albedo. Because the limit is on the mass product, one satellite might lie below this limiting boundary, but in that case the other must lie above it such that the mid-point of the two satellites lies above the boundary. Similar limits are shown for the pairs UV-UI and UV-UII. These limits allowed one to make some meaningful (but complicated and conditional) statements about the physical properties, p_V, ρ, and r. The most direct was "the inner satellites are much brighter material than the rings and significantly brighter and/or less dense than Oberon",[14] a statement that has survived subsequent reevaluation of the masses and measurement of radii.

The Work of Veillet. The task of continuing to improve mass determination was taken up by C. Veillet, based on new data obtained by himself and earlier by Walker et al.[16] Veillet and Ratier[17] published residuals in Miranda's longitude that indicated a periodicity consistent with the 12.5

yr commensurability period. Veillet[18] reported the value $\mu_I \mu_{II} = (1.10 \pm 0.25) \times 10^{-10}$ based on his measurements of Miranda's motion, combined with my orbital theory for the resonant variations. Veillet also gave the value shown in Table 1 for Titania, based on Miranda's apsidal precession and on the improved value of J_2 from ring studies. (Incidentally, the reader is cautioned that Veillet follows my notational lead[12] in designating Miranda with subscript 1, Ariel with 2, etc. That notation facilitates orbital theory, but in this review I am using conventional notation: Miranda = UV, Ariel = UI, etc.)

The analysis was improved still further based on additional observations of Miranda in 1980-81. Veillet[19] obtained $\mu_I \mu_{II} = (1.37 \pm 0.15) \times 10^{-10}$. He also obtained a rather precise value for the precession of Miranda's nodes, which is dominated by the effects of J_2, μ_I, and μ_{II}. Since J_2 is now known, he was able to solve (with the value of $\mu_I \mu_{II}$) for the separate values of μ_I and μ_{II} shown in Table 1.

Most recently, Veillet[9] has extended the study to include more data. From Miranda's orbit, he now obtains $\mu_I \mu_{II} = (2.0 \pm 0.12) \times 10^{-10}$. From consideration of the resonant effects of Miranda and Ariel on Umbriel, he finds $\mu_V \mu_I = (0.36 \pm 0.10) \times 10^{-10}$. These new limits on the mass products are plotted in the density-albedo diagram of Fig. 2. Remember, the midpoint between the positions of two satellites must lie in the range shown for that pair. Note that the magnitudes V(1,0) used here are from Cruikshank,[20] based on photometry by Reitsema _et al_.[21] and Degewij _et al_.[22] Figure 1 had been based on magnitudes from Harris (1961). The boundary shown in Fig. 2 for UV x UII is still based on my 1979 mass limit as in Fig. 1, but is moved upward due to the brighter improved magnitude for Umbriel.

The astute reader will note that Veillet's range for $\mu_V \mu_I$ is outside the limits I had established earlier (see Table 1, and compare Fig. 2 and Fig. 1). According to Veillet,[9] this discrepancy is due to an error on my part in determining a dominant coefficient in the expression for variation of Umbriel's longitude. I have not yet found any error in my complicated algebraic analysis, but Veillet quotes Aksnes,[23] Lazzaro and Ferraz-Mello,[24] and his own numerical integrations as giving an effect 1/6 as strong. Thus, my old upper limit on $\mu_V \mu_I$ was apparently 6 times too small (i.e., the boundary in Fig. 1 should have been more to the right by a factor $6^{1/2}$ in density).

In Veillet's thesis,[9] he made use of improved apsidal precession rates

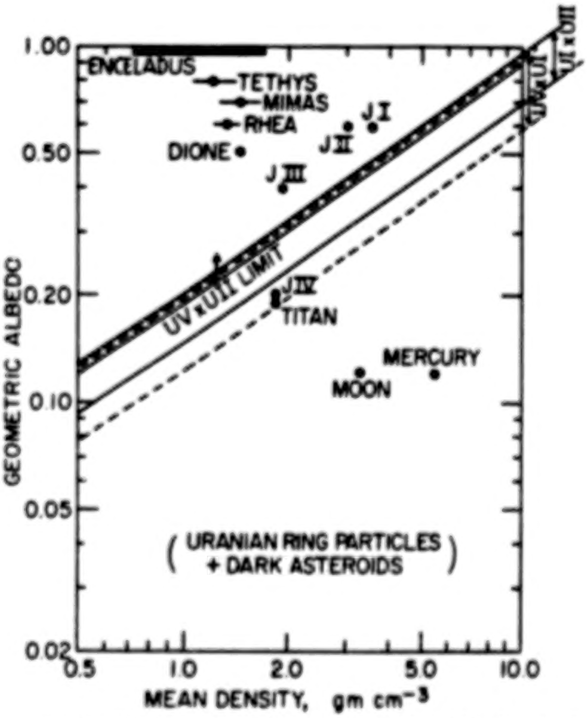

Figure 2: Improved constraints on density and albedo (cf. Fig. 1). Limits for Uranian satellites are based on more precise mass product determinations by Veillet.[9] Midpoint between Miranda and Ariel values of density and albedo must be between dashed lines labelled "UV x UI"; midpoint between Ariel and Umbriel must be within narrow band labelled "UI x UII"; midpoint between Miranda and Umbriel must lie above line labelled "UV x UI limit". Note post-Voyager values for other satellites.

for Umbriel, Titania, and Oberon, combined with his two mass-product determinations, to obtain the individual masses. Each of the three precession rates depends on the masses of all four other satellites and on J_2. Since J_2 is known from the rings, and since $\mu_V \mu_I$ and $\mu_I \mu_{II}$ are known, there are five equations and five unknowns, the masses. The solution is shown as Veillet's bottom line on Table 1.

Updated Density-Albedo Limits. In Fig. 3, I have combined the latest mass determinations by Veillet,[9] the magnitudes from Cruikshank,[20], and determinations of radii and albedo by Brown et al.[25] I show for each satellite the greatest region consistent with published error brackets. The horizontal limit lines are from the albedo limits, the diagonal limits are from the masses, and the vertical limits are from direct calculation of

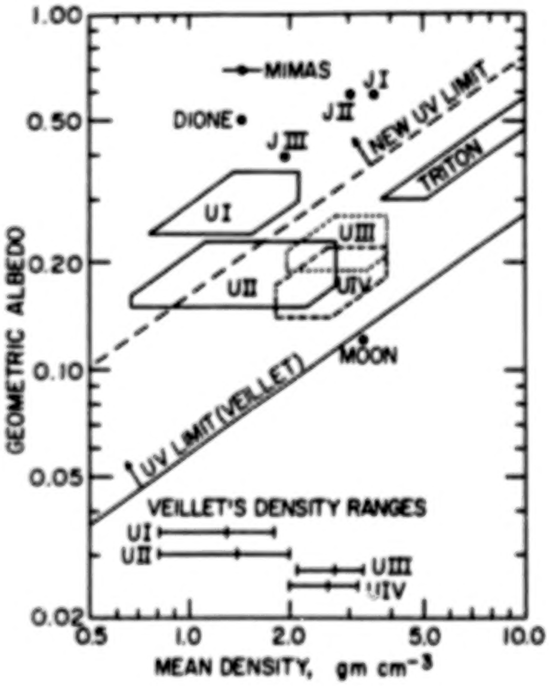

Figure 3: Recent constraints on density and albedo from Veillet's[9] masses and Brown et al.'s[25] radii. Contrast overlapping density ranges with more restricted ranges quoted by Veillet,[9] shown near the bottom. Note also the new restriction on Miranda (UV) discussed in the text, and the range for Triton based on Morrison et al.[31] and Alden.[27]

density ranges from radii and masses. Note that Veillet's value for μ_V has uncertainty as large as the value; it only provides an upper limit to the mass of Miranda.

In fact, it may be possible to constrain Miranda's mass even more than Veillet has dared. Recall my constraint $\mu_V \mu_U < 6 \times 10^{-12}$. If we combine that limit with Veillet's mass for Umbriel, $\mu_U = (1.2 \pm 0.5) \times 10^{-5}$, we obtain $\mu_V < 10^{-6}$, a more restrictive value than Veillet's $\mu_V < 4 \times 10^{-6}$. This new limit is also shown in Fig. 3. Note from Fig. 3 that this additional constraint is significant in terms of density and albedo: Miranda is moved in the direction of ice. Like Ariel, it is brighter and/or less dense than Titania and Oberon. Veillet's limit, in contrast, would have permitted Miranda to be as dark and dense as the Moon, for example.

At the bottom of Fig. 2 are shown the possible density ranges computed by Veillet[9] on the basis of his mass determinations and Brown et al.'s[25] radii. These ranges suggest that the inner satellites Ariel and Umbriel may be significantly less dense than the outer ones Titania and Oberon, perhaps an ice/rock dichotomy. Veillet has emphasized this distinction between pairs.[9,26] This result could be significant for considerations of the origin of the system. It is opposite to the case of Jupiter's Galilean satellites where the inner two are rocky and the outer two icy. However, my own computation of the ranges of uncertainty yields significantly wider ranges than indicated by Veillet. The extremes in density that I show in Fig. 3 are even wider; to emphasize the uncertainty, the ranges shown are based on extreme values of both Veillet's masses and Brown et al.'s radii.

It is important to recognize that rather large ranges of density are possible. It might be premature to get too excited at present about interpreting any particular apparent trend in density with semi-major axis. The data are still consistent will all five satellites having the same density of about 2 gm/cm^3. However, Miranda and Ariel are, as was already apparent several years ago, brighter and/or less dense than the satellites farther from Uranus. All the satellites are much brighter than the ring particles.

MASS OF TRITON

The most recent determination of Triton's mass, by Alden in 1943,[27] was based on the satellite's effect on the motion of Neptune. Alden found $\mu_T = (1.34 \pm 0.23) \times 10^{-3}$. With Neptune's mass of 1.03×10^{29} gm, we find $m_T = (1.38 \pm 0.24) \times 10^{26}$ gm. However, Duncombe et al.[28] assigned significant weight to an earlier determination by Nicholson et al.[29] which had yielded $\mu_T = 5.26 \times 10^{-3}$. On that basis, the USNO group[28] assigned the value $\mu_T = (3.30 \pm 1.96) \times 10^{-3}$ to cover the range between Alden's and Nicholson's values. The range of densities and albedos possible for Triton is shown in Fig. 1, based on the mass range given by Duncombe et al.,[28] with a lower cut-off in albedo from the upper radius limit given by Morrison and Cruikshank.[30]

In Fig. 3, I show a more restricted albedo-and-density range for Triton based on Alden's[27] mass determination and on Morrison et al.'s[31] recent radius values. A larger mass value, such as Nicholson et al.'s,[29] would shift the position in Fig. 3 toward higher densities, but even the density range shown seems surprisingly high for an outer solar system body. There are reasons to be suspicious of the density and albedo shown in Fig. 3. First, Triton's atmosphere may introduce systematic errors in the radiometric radius determination,[31] and, second, there remains the possibility of a systematic error in Alden's mass determination.[32] It seems time now, after more than forty years and with a spacecraft visit to Neptune ahead, for someone to re-determine the mass of Triton. Similarly, it would be useful if, with a couple of additional years of astrometric data on the Uranian satellites, the mass values of those objects can be narrowed down further in time to help interpret upcoming Voyager data.

Acknowledgments

C.R. Chapman, D.R. Davis, A.W. Harris, W.K. Hartmann, and S.J. Weidenschilling provided information and suggestions that helped with preparation of this review. P.K. Watson-McBride prepared the manuscript for publication. This work was supported by NASA Contract NASW-3134. This is PSI Contribution #198. PSI is a division of Science Applications, Inc.

References

1. Harris, D.L. (1949). Ph.D. Thesis, University of Chicago.
2. Dunham, D.W. (1971). Ph.D. Thesis, Yale University
3. Harris, D.L. (1961). In Planets and Satellites, G.P. Kuiper and B.M. Middlehurst, eds. (University of Chicago Press), pp. 272-342.
4. Greenberg, R. (1976). Icarus **29**, 427.
5. Whitaker, E.A., and R. Greenberg (1973). Mon. Not. Roy. Astron. Soc. **155**, 15P.
6. Whitaker, E.A., and R. Greenberg (1973). Comm. Lunar Planet. Lab. **10**, 70.
7. Greenberg, R., and E.A. Whitaker (1974). Bull. Amer. Astron. Soc. **6**, 207.
8. Greenberg, R. (1975). Icarus **24**, 325.
9. Veillet, C. (1983). These de Doctorat d'Etat, University de Paris 6.
10. Elliot, J.L., et al. (1981). Astron. J. **86**, 444.

References (continued)

11. Greenberg, R. (1975). Mon. Not. Roy. Astron. Soc. **173**, 121-129.
12. Greenberg, R. (1976). Icarus **29**, 427.
13. Soifer, B.T., et al. (1981). Icarus **45**, 612.
14. Greenberg, R. (1979). In Dynamics of the Solar System, R.L. Duncombe, ed. (Reidel), pp. 177-180.
15. Greenberg R. (1979). In Natural and Artificial Satellite Motion, P.E. Nacozy and S. Ferraz-Mello, eds. (University of Texas Press).
16. Walker, R.L., et al. (1978). Astron. J. **83**, 838.
17. Veillet, C. and G. Ratier (1980). Astron. Astrophys. **89**, 342.
18. Veillet, C. (1981). Astron. Astrophys. **98**, 218.
19. Veillet, C. (1983). Astron. Astrophys. **118**, 211.
20. Cruikshank, D. (1982). In Uranus and the Outer Planets, G. Hunt, ed., (Cambridge University Press), pp. 193-210.
21. Reitsema, H.J. (1978). Bull. Amer. Astron. Soc. **10**, 585.
22. Degewij, J., et al. (1980). Icarus **44**, 520.
23. Aksnes, K. (1984). In Comptes-Rendus du Colloque sur les Anneaux Planetaires, A. Brahic, ed., (IAU Colloq. 75).
24. Lazzaro, D., and S. Ferraz-Mello (1983). Private communication with C. Veillet.
25. Brown, R.H., et al. (1982). Nature **300**, 423.
26. Veillet, C. (1983). Presentation and abstract for IAU Colloq. 77, "Natural Satellites".
27. Alden, H.L. (1943). Astron. J. **50**, 110.
28. Duncombe, R.L., et al. (1973). Fund. Cosmic Phys. **1**, 119.
29. Nicholson, S.B., et al. (1931). Pub. Astron. Soc. Pacific **43**, 261.
30. Morrison, D., and D.P. Crukshank (1974). Space Sci. Rev. **15**, 641.
31. Morrison, D., et al. (1982). Nature **300**, 425.
32. Harris, A.W. (1984). Private communication.

SEASONAL VARIATIONS IN TRITON'S ATMOSPHERIC MASS AND COMPOSITION

L. M. Trafton

McDonald Observatory
The University of Texas at Austin
Austin, Texas 78712

Abstract

Condensed phases of gases making up the bulk of Triton's atmosphere are likely to exist on Triton's surface in the form of solid or liquid "polar caps" which extend as far as 55° from the poles. The mass of Triton's atmosphere is governed by the energy balance between the sunlight these caps absorb and the heat they radiate to space. The polar cap temperatures should be approximately equal and uniform over their surfaces. Because of the rapid precession of Triton's orbit about Neptune's pole, the insolation and, therefore, the temperature of the polar caps must vary in a complex fashion. This will cause the mass of Triton's atmosphere to undergo a sinusoidally seasonal variation with an amplitude which ranges sinusoidally from mild to extreme in extent. The variations in the temperature of the polar caps will also cause seasonal variations in the mixing ratio of the volatile atmospheric gases owing to the different behaviors of their saturation vapor pressures with temperature. Triton's visible hemisphere is currently approaching a major southern summer with solstice scheduled to occur in ~ 2006 A.D. If the polar caps are not too thin, we should witness a dramatic increase in the CH_4 column abundance before then. As well as serving to test the basis of our reasoning, this increase and its behavior will provide further information on Triton's atmosphere and surface volatiles. We propose some important measurements for Voyager to make of Triton.

INTRODUCTION

Reasons for expecting an atmosphere on Triton center on Triton's near infrared spectrum, 0.8 - 2.5 μ, which shows absorption at the wavelengths of the bands of CH_4. Cruikshank and Silvaggio[1] detected an absorption feature at the wavelength of the 2.3μ CH_4 band in Triton's spectrum. They also saw a hint of absorption at the wavelength of the 1.7μ CH_4 band. Apt, Carleton, and Mackay[2] succeeded in detecting an absorption feature at the wavelength of the 8900A CH_4 band which matches laboratory spectra of both CH_4 gas and CH_4 ice.

Fitting a synthetic spectrum for CH_4 gas using a random band model, they derived a column abundance of 1.7 ± 0.7 m-Am CH_4. This is consistent with the ~1 m-Am upper limit set among other observers (Spinrad[3] [> 8 m-Am]; Martin[4] [<8 m-Am]; Benner et al.[5] [<50 m-Am]; Johnson et al.[6] [< 1 m-Am]; and Combes et al.[7] [< 3.5 m-Am]. Because this gas abundance is too small to explain the strength of the 2.3μ feature, Apt et al. believe that both the 8900A and 2.3μ features can be explained as CH_4 ice. They claim a good match occurs for each feature with the CH_4 ice spectrum of Kieffer and Smythe.

However, the presence of CH_4 ice implies that CH_4 gas is present. This is because of the tendency of the solid and gas phases of CH_4 to reach an equilibrium in closed systems for temperatures below the freezing point of CH_4 (90 K). The atmospheric column abundance of CH_4 in units of cm-Am will be given by

$$[CH_4] = P_s(T)\ H\ \frac{273}{T} \tag{1}$$

where $P_s(T)$ is the saturation vapor pressure of CH_4 at the surface in units of atm, H is the scale height in units of cm,

$$H = \frac{k}{\mu}\frac{T}{m_p}\ g^{-1} \tag{2}$$

T is the temperature, g is the surface gravity, μ is the atmospheric mean molecular weight, k is Boltzmann's constant, and m_p is the proton mass. These expressions neglect the spherical geometry; this is O.K. because the scale height is small compared to Triton's radius. For example, if $\mu=16$, $T=60K$, Triton's radius is 2100 km, and Triton's mass is 1.4 x 10^{26} g, then H = 14.6 km.

TABLE I

ADOPTED PARAMETERS OF TRITON

Mass	$M = 1.4 \times 10^{26}$g
Radius	$R = 2100$ km
g	212 cm s^{-2}
H	$14.6\ (\frac{16}{\mu})\ (\frac{T}{60})$ km
Orbital period	5.88 days (synchronous)
Orbital radius	3.56×10^{5} km
Orbital inclination	160°
Period of precession of orbit	637 ± 40 yrs
Neptune's sidered period	165 yrs
Neptune's obliquity	30°

The quantity H (273/T) is independent of temperature and equals 66.4 km for a CH_4 atmosphere on Triton assuming the parameters listed in Table 1. The saturation vapor pressure $P_s(T)$ is very sensitive to temperature; a 2K change for the CH_4 on Triton's surface is enough to double the vapor pressure of CH_4 gas lying over the ice assuming temperatures in the range expected for the outer solar system (65K > T > 40K). This would double the mass of CH_4 in Triton's atmosphere.

These conclusions are likely to hold for Triton's atmosphere as a whole, not just for the CH_4 component, because at these cold temperatures, most gases made up of cosmogonically abundant elements are below their freezing points. The main exceptions, H_2 and He have probably escaped. It is likely that condensed phases of other gases made up of ices of the abundant elements exist on Triton's surface. Therefore, we may expect Triton (like Pluto[8]) to have an atmosphere composed of N_2, CO_2, O_2, Ar and CH_4, in decreasing order of mixing ratio. Ne could also be present but its saturation vapor pressure is too high for saturation. If Ne is present, we expect its column abundance to remain constant as the surface temperature changes. We therefore conclude that Triton should have an atmosphere and, except for Ne, the composition of that atmosphere should be governed by the temperature of the surface ices through the saturation vapor pressure relations rather than by the bulk composition of Triton. The abundance of surface elements will have no bearing on the mixing ratios of the gases except that in the extreme case where no ice or liquid state of a gas exists anywhere on the surface, or in communication with the surface, then that gas will not occur in Triton's atmosphere. We further conclude that, except for Ne, an increase in the temperature of Triton's surface ices (and liquids) by 2K will approximately double the mass of Triton's whole atmosphere. A change in the mixing ratios can also be expected to occur with a change in temperature because of the various dependences upon temperature of the saturation vapor pressure of the various gases.

CONTRASTS BETWEEN TRITON AND PLUTO

Triton contrasts with Pluto in several ways. First, Triton's mass is an order of magnitude greater so that Triton can retain lighter gases in its atmosphere over a cosmogonic time scale. Second, the scale height is 20% of Pluto's so that the column abundances of volatile gases are expected to be significantly smaller even though the surface temperatures may be the same (Triton and Pluto are currently about equal distances from the Sun). Third, Neptune's orbit is nearly circular while Pluto's orbit is highly elliptic for a planet (eccentricity = 0.25). Therefore, no significant seasonal drives occur for Triton as a result of insolation changes due to changing distance between Triton and the Sun. Fourth, Pluto has a very high obliquity which causes its solstices to occur nearly over its poles, while Triton's solstices have an amplitude which is not constant but varies sinusoidally as a result of the rapid precession of Triton's inclined orbit about Neptune's oblique pole[9,10]. Table 1 gives the appropriate periods. While Pluto's seasons are extreme and are somewhat distorted by the elliptically of Pluto's orbit, Triton's seasons are complicated by solstices varying between latitudes of 9° and 52°. Figure 1 shows Harris'[9] calculation of the seasonally variable solar latitude for Triton. The summers and winters vary from being mild to being severe. The mass of Triton's atmosphere undergoes a similar variation, leveraged by the sensitivity of vapor pressure to temperature.

A fifth essential difference between Triton and Pluto pertains to the distribution of surface volatiles. Pluto's high obliquity causes surface volatiles to migrate (via sublimation and condensation) from pole to pole so that deposits at even low latitudes are periodically replenished. Essentially all of Pluto's surface is regulated in temperature by the atmospheric surface pressure[11,8]. The surface temperature is globally constant but varies seasonally with the insolation. By contrast, Triton's smaller obliquity results in the net transport of surface volatiles to latitudes further than 35° from the equator[12]. Triton, therefore, should have polar caps of solid and/or liquid volatiles. Volatiles may exist transiently at lower latitudes but they are quickly sublimated as the seasonal changes warm them. Consequently, Triton's atmosphere is not saturated at lower latitudes; that is, the lower latitudes may be warmer than the polar latitudes. In this respect, Triton is more like Mars than Pluto. The temperature of the polar caps regulates the mass of the atmosphere.

TRITON'S SEASONAL VARIATION

If surface volatiles were to cover Triton, then no seasonal variation in the mass of Triton's atmosphere would occur at all because the surface temperature would remain constant in time and over Triton's surface (neglecting topography). This would be a consequence of Neptune's circular orbit and the regulation of the local surface temperature by the globally uniform surface pressure through the saturation vapor pressure relation. The atmospheric mass

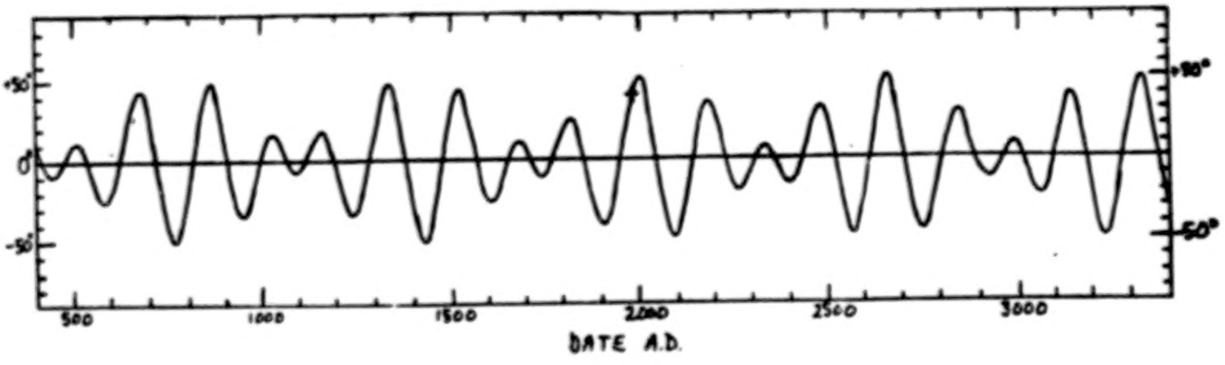

Fig. 1 - Latitude of the subsolar point on Triton vs date (from Harris[9]).

would be regulated by this globally uniform surface temperature which, in turn would be determined by the total insolation absorbed by Triton. This is be unaffected by the latitude of the Sun when ices cover the planet and no latitudinal variation of albedo or thermal emissivity occur. The surface temperature would be given by the condition that the flux absorbed by the disk is radiated uniformly by the sphere.

However, this condition could not persist because of the net transport of tropical surface volatiles to the polar regions which would occur as a result of the greater mean insolation that obtains in the tropics. This would cause a net sublimation to occur in the tropics and a net freezing to occur in the polar regions as the atmosphere flows towards the poles to achieve global hydrostatic equilibrium. The tropical volatiles would soon become depleted. Then the tropics would heat up and the polar regions would cool down. As the polar regions cooled, the mass of the atmosphere would decline to a value given by the scale height and the saturation vapor pressure relation (see Equation 1) for the temperature of the polar caps. This must be the present state of Triton's atmosphere.

The temperature of Triton's winter polar cap must be as warm as the summer cap, even for the extreme solstices. This is because the surface pressures over the two poles are equal and the surface temperature is specified by the surface pressure when the gases are saturated. The temperature of the poles governs the mass of the atmosphere and is derived by the condition that the sunlight absorbed by both poles must equal the heat radiated by both poles. For an extreme solstice, and for modest equally-sized polar caps, sunlight absorbed by the summer cap is radiated equally by both caps. More generally, the polar cap temperature depends on the seasonally varying insolation of the polar caps, their sizes, albedos and thermal emissivities. Triton's atmosphere can be expected to vary strongly with season, especially for small polar caps, for which the insolation changes sharply with season. Trafton[12] has computed the seasonal changes of Triton's atmospheric mass for several cases of these parameters. Figure 2 shows the variation in column abundance of CH_4 for two extreme cases, (1) cap albedo = 0.50 with polar cap radius

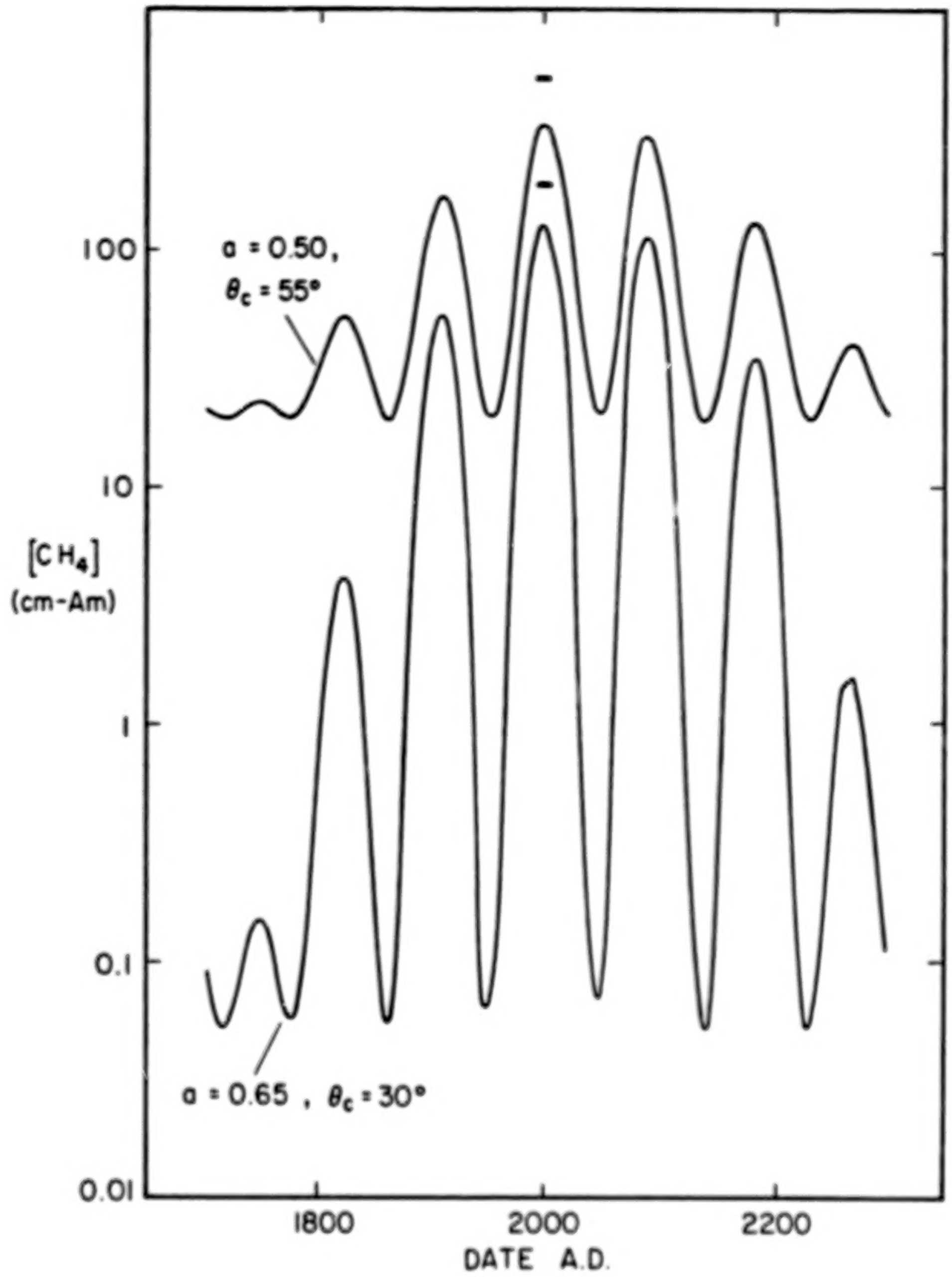

Fig. 2 - Predicted CH_4 column abundance vs date for Triton neglecting the thermal conductivity and capacity of the surface. θ_C denotes the angular size of the polar caps (assumed equal for the two poles) and a denotes the plane albedo of the polar caps. The values of a are representative for icy materials and the values of θ_C should bracket their present size. If Triton's radius is 2600 km instead of 2100 km, these curves would be raised to the fiducials indicated at 2000 A.D. Triton's atmospheric bulk is currently approaching a major maximum. At the time of the Voyager flyby, it should be significantly greater than it is now. Note that the presently observed upper limits ~ 100 cm-Am CH_4 do not effectively constrain the polar cap size or albedo.

55°and (2) cap albedo = 0.65 with polar cap radius 30°. A planetary radius of 2100 km is assumed; it enters through the scale height (see Equation 1). The variation in the column abundance is smaller for larger polar cap sizes. The thermal capacity and conductivity of the surface have been ignored in these calculations, as have the effects of advection. They would tend to partially smooth out the variations and to introduce a time lag.

As Figure 2 shows, Triton is currently approaching an extreme solstice, which is due in 2006 A.D. The mass of Triton's atmosphere should increase substantially between now and then. Methane absorption should increase to levels which permit a more accurate measurement of the column abundance. Such an increase would confirm the presence of CH_4 gas and allow a separation of the solid and gaseous contributions to the absorption. The thermal conductivity between the surface and atmosphere and the heat capacity of the surface are not known but information on these may be derived by observing the phase lag between the actual CH_4 absorption and these curves. Because of this lag, the abscissa for Fig. 2 should be shifted to the left by some unknown amount (but less than 90° in phase) to better represent the column abundance now and at the time of the Voyager flyby. Consequently, the potential for atmospheric growth in the next couple of decades is great. At the time of the Voyager flyby of Neptune, Triton's atmosphere may well be appreciably denser than it is now.

POTENTIAL ATMOSPHERIC COLLAPSE

One important difference between Triton and Mars is the much greater length of Triton's seasons. If Triton's summer polar cap is sufficiently thin to sublimate entirely during the major summer, the source maintaining Triton's atmosphere would disappear. The sink, however, would still remain; namely, the condensation over the winter polar cap which provides the latent heat to replace the radiation lost to space. Consequently, Triton's atmosphere would commence to freeze out over the winter cap. The extent to which this occurs depends on the volume of the "volatiles" constituting the cap, as well as on the duration of the seasons. The Martian seasons, for example, are too short for appreciable freezing out of its atmosphere to occur. Such an event could be detected observationally if the atmosphere first grows to a size where the CH_4 absorption is strong enough that changes in it can be detected above the instrumental noise. This should be the case if the absorption approaches that for Pluto or stronger. Measuring such a phenomenon would provide more information about Triton's atmosphere and surface volatiles.

The volatility of surface materials is a relative thing. In our discussion of a polar cap or "surface volatiles", we have neglected all materials with vapor pressures small compared to Triton's surface pressure. These result in negligible latent heat transfer compared to the latent heat flow from CH_4 and other bulk gases in Triton atmosphere.

VOYAGER FLYBY EXPERIMENTS

General Science. A Voyager flyby of Triton could provide important information for understanding the nature of Triton's atmosphere and its relation to Triton's surface volatiles. First, a radio occultation experiment would pin down the radius, now uncertain ($1800 \text{ km} < R < 2600 \text{ km}$), so that the mean density of the body could be accurately determined. This will reveal the degree of ice or rock in the body as a whole. This ratio bears on Triton's origin and on the probable atmospheric composition. Comparison with Pluto will then shed more light on the formation of these bodies and provide an important datum for understanding the conditions in the outer protosolar nebula at the time of the formation of the outer planets. The radius also determines (along with the temperature and molecular weight) how deeply bound an atmosphere is to the planet. Other things being equal, a planet with a smaller radius can hold an atmosphere longer. It is more likely to contain lighter gases.

An occultation experiment can also establish the presence of an atmosphere and determine its scale height. From observations of the temperature, or from temperature estimates, the mean molecular weight of the atmosphere can then be obtained. This bears on the bulk composition of the atmosphere. The surface density might also be determined.

The Infrared Spectrometer may identify gases in Triton's atmosphere and determine column abundances and vibrational-rotational temperatures. The spectral energy distributions may yield effective temperatures of various surface regions. It can also yield information on the composition of surface ices and other surface materials.

Tests of our model. Our model of Triton's atmosphere and surface volatiles is amenable to a number of tests by Voyager. It predicts an atmosphere which will be more substantial at the time of the voyager flyby than now. It predicts the presence of two polar caps of essentially equal and uniform temperatures. The strength of the 2.3μ feature in Triton's spectrum implies that the summer polar cap is still large and so is likely to still be there in 1990. Our model predicts an absence of all but transitory surface volatiles below a latitude of 35°. It further predicts a warmer surface there. It predicts that the bulk atmosphere will be made up of CH_4 and some gases from the group N_2, Ne, Ar, CO_2 and O_2. Nitrogen is probably the dominant gas. Diurnal effects on the column abundance will be negligible. Both polar caps should show evidence of shrinking around their borders. Finally, our model predicts that for regions covered by surface volatiles, elevated areas are cooler and depressed areas are warmer. The low lying areas should have the thickest deposits of surface volatiles because they radiate more heat to space by virtue of their higher temperatures. This cooling tendency causes a greater freezing rate (or, in summer, a smaller sublimation rate) than average.

CONCLUSIONS

In conclusion, much can be learned about Triton's atmosphere and its seasonal tendencies from Voyager observations. Critical experiments are an occultation, spectrometer observations with good spatial resolutions and imaging observations. Critical objectives are the detection of an atmosphere, identification of its major gases, and measurement of their abundances.

Planetary radius and atmospheric scale height, temperature and mean molecular weight are important objectives. Also critical are the location, size, albedo, composition and effective temperature of the surface volatiles. Do polar caps exist? Are elevated regions devoid of volatiles? Is the surface temperature the same for all volatiles? The latter may have to be inferred from measurements of the effective temperature (flux) by assuming composition or emissivity. Alternatively, if the constancy of surface temperature is assumed, then variations in effective temperature may be used to locate regions of different thermal emissivity in order to study the distribution of different surface ices. Finally, if polar caps are indeed found, how warm is the equatorial band of non-volatiles? What is their composition? Is there "fossilized" evidence of variable-solstice seasonal activity in the images? If so, what conclusions can be drawn about the magnitude and nature of this activity? Does the atmosphere seasonally collapse? How thick are the volatile deposits? The Voyager flyby of Neptune will provide an excellent opportunity to learn much of significance about Triton - an object with a seasonal behavior unique in the solar system.

Acknowledgements: This research was supported by NASA Grant NGR 44-012-152

REFERENCES

1. Cruikshank, D.P., and P.M. Silvaggio (1978). The surface and atmosphere of Pluto. Icarus 41, 96-102.

2. Apt, J., N.P. Carleton, and C.D. Mackay (1983). Methane on Triton and Pluto: New CCD spectra. Astrophys. J. 270, 342-350.

3. Spinrad, H. (1969). The lack of a noticeable methane atmosphere on Triton. Publ. Astron. Soc. Pac. 81, 895-896.

4. Martin, T.Z. (1975). Saturn and Jupiter: A study of atmospheric constituents. Ph.D. thesis, Univ. Hawaii, Honolulu.

5. Benner, D.C., U. Fink, and R.H. Cromwell (1978). Image tube spectra of Pluto and Triton from 6800 to 9000A. Icarus 36, 82-91.

6. Johnson, J.R., U. Fink, B.A. Smith, and H.J. Reitsema (1981). Spectrophotometry and upper limit of gaseous CH_4 for Triton. Icarus 46, 288-291.

7. Combes, M., T. Encrenaz, J. Lecacheux, and C. Perrier, (1981). Upper limit of the gaseous CH_4 abundance on Triton. Icarus 47, 139-141.

8. Stern, S.A., and L.M. Trafton (1984). Constraints on bulk composition, seasonal variation, and global dynamics of Pluto's atmosphere. Icarus, in press.

9. Harris, A.W. (1983). Physical characteristics of Neptune and Triton inferred from the obital motion of Triton. Icarus, in press.

10. Dobrovolskis, A.R. (1980). Where are the rings of Neptune? Icarus 43, 222-226.

11. Trafton, L.M., and S.A. Stern (1983). On the global distribution of Pluto's atmosphere. Astrophys. J. 267, 872-881.

12. Trafton, L.M. (1984). Large seasonal variations in Triton's atmosphere. Icarus, in press.

BLANK PAGE

PART V

Magnetospheres And Solar Wind

BLANK PAGE

496

MAGNETOSPHERIC STRUCTURES: URANUS AND NEPTUNE

T. W. Hill

Space Physics and Astronomy Department
Rice University
Houston, TX 77251

Abstract

Although the existence of magnetospheres at Uranus and Neptune has not been established, the available statistics indicate a sufficiently high probability to warrant consideration of their likely properties in advance of the Voyager encounters. Because the spin axis of Uranus lies nearly in the ecliptic and presently points approximately sunward, Voyager is likely to encounter the unique "pole-on" configuration that has special theoretical significance. Corotation in the magnetospheres of Uranus and Neptune would probably exclude solar-wind-driven convection as an important driver of global magnetospheric dynamics, as it does at Jupiter and Saturn. Unlike at Jupiter and Saturn, however, the magnetospheres of Uranus and Neptune probably lack sufficient internal sources of plasma (with the possible exception of Neptune's satellite Triton) to produce significant levels of rotationally-driven convection. The reported observation of auroral emission from Uranus has therefore motivated the development of an alternative model in which solar-wind motion is coupled directly to the rotation of the ionosphere to establish a dynamo circuit which generates Birkeland currents and polar-cap aurora. This model predicts the strength and configuration of the aurora as functions of the magnitude and polarity, respectively, of the planetary magnetic moment.

INTRODUCTION

The purpose of this paper is to describe magnetospheric structures that Voyager might reasonably be expected to encounter at Uranus (1986) and Neptune (1989). The known properties of the magnetospheres of Jupiter and Saturn (established in large part by past successful Voyager encounters) are well documented; I will therefore not attempt to review these properties but will refer to them by analogy where appropriate. (By way of introduction to the literature, I would recommend, in the case of Jupiter's magnetosphere, the book edited by Dessler[1] and, in the case of Saturn's magnetosphere, the

Voyager encounter issue of Journal of Geophysical Research [November, 1983]. I also recommend the interesting discourse on comparative magnetospherology by Siscoe[2].)

It is useful, first of all, to review the conditions for which a given planet may be expected to have a magnetosphere. The solar wind is now observed[3] to extend past the orbit of Neptune, its dynamic pressure decreasing roughly as the inverse square of heliocentric distance. It is then straightforward[2] to calculate the minimum planetary magnetic dipole moment for which the surface magnetic-field pressure would just balance the typical solar-wind dynamic pressure, thus (marginally) creating a magnetosphere. This critical magnetic moment is of the order of 3×10^{-5} G-$R_U{}^3$ for Uranus and 2×10^{-5} G-$R_N{}^3$ for Neptune, where R_U and R_N are the radii of Uranus and Neptune, respectively (the unit of magnetic moment is chosen such that the magnetic moment is numerically equal to the surface equatorial dipole field strength in Gauss). In order for the magnetosphere to be encountered by a spacecraft at a planet-centered distance of n planetary radii, the magnetic moment would have to exceed this critical value by a factor n^3.

There is, to my knowledge, no theory that has demonstrated success at predicting a priori the magnetic moment of a planet given its interior structure and composition (which are, in any case, not exactly "given" in the cases of Uranus and Neptune). (This should be taken as an indication of the enormous complexity of the problem, not as an indictment of the considerable work that has been done on it.) There is, however, a quasi-empirical rule of thumb known (appropriately) as the magnetic Bode's law[4], whereby the magnetic dipole moment is taken to be proportional to the spin angular momentum, the constant of proportionality being inferred from the terrestrial ratio or from some combination of known planetary ratios. This linear relationship works reasonably well, in an order-of-magnitude sense, for Earth, Jupiter, and Saturn, although it has some difficulty with Mercury, Venus, and Mars (Figure 1). If, for example, Uranus and Neptune were to follow the same linear relationship, their

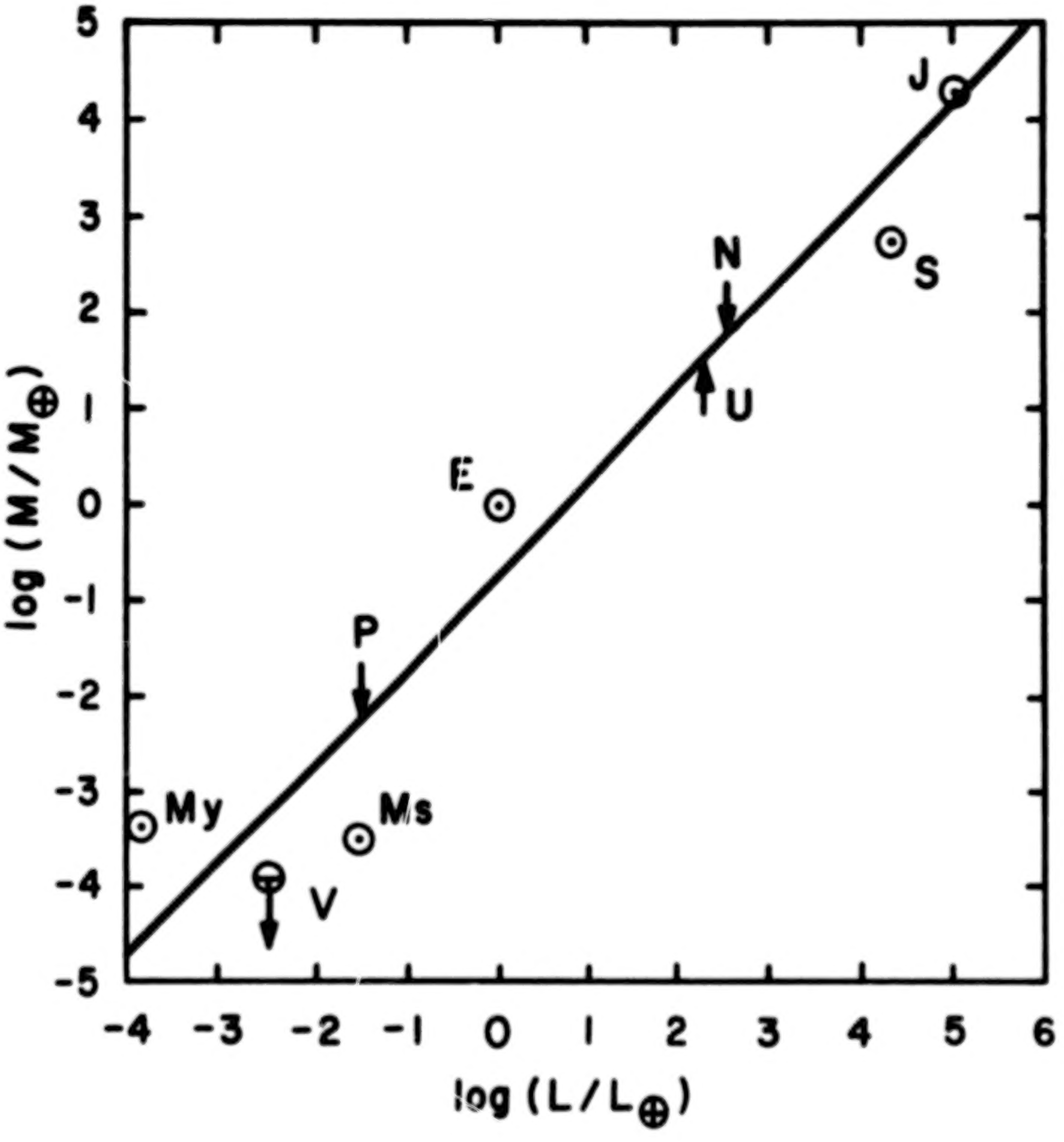

Figure 1. The magnetic Bode's law: planetary magnetic moment vs. spin angular momentum (both normalized to terrestrial values). [Adapted from ref. 4]

BEST COPY AVAILABLE

magnetic moments would exceed the respective critical values by factors of several times 10^4, producing magnetospheres a few tens of planetary radii in extent. While these "margins of error" may lend credibility to the supposition that magnetospheres exist at Uranus and Neptune, they certainly provide no firm basis for prediction (e.g., of magnetopause standoff distances). It is perhaps more compelling simply to note that Uranus and Neptune are not too dissimilar to Jupiter and Saturn in size, density, and spin rate, and presumably therefore in composition and interior structure, and that there is no obvious reason why they should not also have significant magnetic moments.

There is one set of observations that may be interpreted as evidence for the existence of a magnetosphere at Uranus. Observations of Uranus from the IUE spacecraft[5] have revealed Lyα and H_2 emissions that are difficult to explain quantitatively in terms of scattered sunlight, and have therefore been attributed to aurora. If such auroral emissions are confirmed by Voyager UVS observations during the approach to Uranus, they may provide an early warning of an impending magnetosphere encounter.

For the sake for further discussion, let us assume that Voyager will discover magnetospheres at Uranus and Neptune.

THE POLE-ON CONFIGURATION

The most interesting property of Uranus, at least from the viewpoint of magnetospheric physics, is the 98° inclination of its spin equator to its orbital plane. Virtually every point of the surface becomes the subsolar point at some time during each orbit; by the same token, the magnetosphere samples virtually all angles of solar-wind incidence relative to the planetary dipole moment. Moreover, if the dipole moment is roughly aligned with the spin axis (as it has been found to be in four out of four cases so far), then the 1986 Voyager encounter will sample the special "pole-on" configuration (angle of incidence near 0° or 180°) as sketched in Figure 2.

Siscoe[2,6,7] has drawn attention to several curious features of this pole-on configuration that have no apparent analog in the "normal-incidence" configuration that characterizes all other known planetary magnetospheres. The most obvious is a single funnel-shaped cusp that directly faces the solar-wind flow. This cusp is bound to be more symmetrical than that observed in Earth's magnetosphere (and those inferred, but not yet observed, in Jupiter's and Saturn's); any aurora resulting from particle precipitation therein should

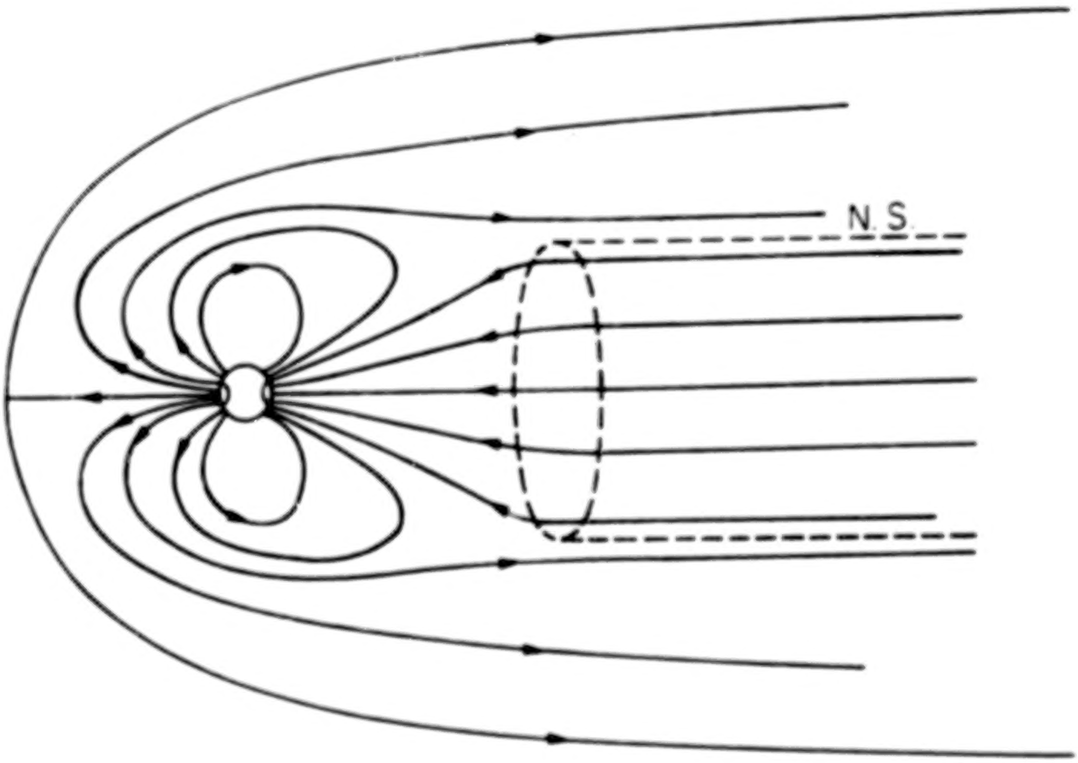

Figure 2. The pole-on configuration anticipated for the magnetosphere of Uranus. [ref. 6]

likewise occupy a circular spot near the pole in contrast to the longitudinally-extended features of Earth's day side aurora. Other differences may be expected to arise from the fact that the cusp of the pole-on configuration occurs near the subsolar stagnation point of the magnetosheath flow. One possibility is that the cusp region fills with hot, weakly-magnetized plasma of magnetosheath origin that is compressed until it balances the stagnation pressure of the solar wind; in this case a spacecraft entering the magnetosphere near the subsolar point may have greater than usual difficulty identifying an unambiguous magnetopause crossing.

A second curious property of the pole-on configuration is that the tail current sheet separating the two magnetotail lobes has the shape of a cylinder rather than a plane. The topology of the tail current system is that of two opposed *coaxial* solenoids rather than that of two opposed *adjacent* solenoids as in the case of normal incidence. This may have important physical consequences because the tail current sheet separating the two lobes closes on itself rather than on the magnetopause, and it seems likely therefore that the current-carrying particles (if any) derive from internal sources rather than from the solar wind[8].

It is also quite likely that the tail magnetic field has a helical twist[6,9] associated with the transmission of torque between a conducting ionosphere, which tends to enforce corotation at the feet of the field lines, and the solar wind, which tends to resist corotation either through magnetic interconnection or some other quasi-viscous process. (This effect was proposed nearly twenty years ago[10] for Earth's magnetosphere, where it undoubtedly occurs although the resulting field-line twist is unobservably small because the tendency to corotation is swamped by the solar-wind-driven convection in the polar caps.) The maximum pitch of the helix, occurring in the limit of high ionospheric conductivity, is just the arctangent of the ratio of the corotation speed in the tail to the solar-wind speed, and this ratio is of order unity if the magnetosphere attains Bode's-law dimensions[9]. The absence of a detectable twist could thus be taken as evidence of an unusually low ionospheric conductivity and/or an unusually weak solar-wind coupling. The requisite Birkeland (magnetic-field-aligned) currents are likely to have auroral effects as described below.

A further interesting consequence of the pole-on configuration is that the subsolar magnetopause presents magnetic fields of all orientations to the solar wind, thus allowing merging with and interconnection to the interplanetary magnetic field (IMF) with equal probability and equal effect irrespective of the orientation of the latter. (A similar magnetic-field geometry occurs at the cusps of Earth's magnetosphere, but there the consequences are quite sensitive to IMF orientation[11,12] because the magnetic cusp is far removed from the symmetry axis of magnetosheath flow, and because both polar cusps are exposed to the magnetosheath.) Were it not for the rotation of Uranus, one might thus expect an omnipresent and vigorous system of solar-wind-driven convection in the pole-on magnetosphere, merely rotating its symmetry meridian to follow the IMF orientation. The rapid rotation of Uranus, however, probably prevents the establishment of such a convection system (see below), and the primary result of day side merging would then presumably be to drive highly variable, perhaps even turbulent, localized flows in the cusp region.

Neptune's equator is inclined by 29° to its orbital plane; its magnetosphere would therefore presumably resemble more nearly the conventional normal-incidence configuration.

SATELLITES

The satellite Io is known to be the dominant source of plasma in Jupiter's magnetosphere[13]. The satellite Titan, and perhaps certain of the icy satellites and rings, are likely to be significant, if not dominant, sources of plasma in Saturn's magnetosphere[14]. The outward transport of this plasma, in turn, provides the principal means of extraction of planetary rotational energy to power the aurora and other magnetospheric phenomena[15]. Moreover, the satellites or their ionospheres may excite dynamo interactions with the planetary ionosphere, giving rise to auroral and/or radio emissions[13].

The presence or absence of sizable satellites can thus have a decisive effect on the plasma population and dynamics of a magnetosphere, especially a rapidly-rotating magnetosphere. There is, unfortunately, no established theory to predict the plasma source arising from a given satellite, and hence its potential effect on the magnetosphere. In the case of Uranus, the situation is considerably simplified by the absence of any satellites of the Galilean size class and of any extensive ring system comparable to that of Saturn. What satellities there are probably have no sensible atmospheres and no significant tidal stresses (hence no volcanoes[16]), and one may thus expect their magnetospheric effects to be insignificant[8].

Neptune has one sizable satellite (Triton), and its orbit would indeed be enclosed by a magnetosphere approaching Bode's-law dimensions[2]. The lack of large neighboring satellites probably rules out tidally-induced vulcanism and the associated Io-like plasma source, but the presence of an atmosphere[17] leaves open the possibility of a Titan-like plasma source and associated magnetospheric perturbations.

OTHER PLASMA SOURCES

The other two sources of plasma that are known to be important in planetary magnetospheres are the solar wind and the ionosphere of the planet. From either source, the resulting magnetospheric plasma content can be expressed as the product of two factors, the first being the total source rate (ion-electron pairs/sec) and the second being the mean residence lifetime of particles in the magnetosphere. The source rate can be scaled more-or-less plausibly from terrestrial and/or Jovian values (more plausibly for the ionospheric source than for the solar-wind source), but the lifetime cannot. Thus there is no apparent way to predict the total plasma content arising from either source, but the relative importance of the two sources can be assessed plausibly by comparing their respective source rates.

The source rate of photoelectrons (and accompanying "polar-wind" ions) escaping the planetary ionosphere can be written, for order-of-magnitude purposes, as

$$S_p \sim \epsilon_p f_p (\pi R_p{}^2) \qquad (1)$$

where f_p is the flux of solar photons at ionizing wavelengths, ϵ_p is the efficiency with which they are converted to escaping photoelectrons, and R_p is the planetary radius. Likewise, the solar-wind injection rate can be written

$$S_m \sim \epsilon_m f_m (\pi R_m{}^2) \qquad (2)$$

where f_m is the flux of solar-wind particles, ϵ_m is the efficiency with which they are captured by the magnetosphere, and R_m is the effective radius of the magnetosphere cross-section. Dividing (2) by (1) gives the ratio of solar-wind to ionospheric source rates:

$$S_m/S_p \sim (\epsilon_m/\epsilon_p)\ (f_m/f_p)\ (R_m/R_p)^2 \qquad (3)$$

It is interesting to consider how this ratio depends on heliocentric distance. The solar-wind particle flux f_m and the solar ionizing photon flux f_p both conform closely to the inverse-square law; thus, their ratio ($\sim 5 \times 10^{-3}$), although variable in time, has no systematic variation with heliocentric distance. The photoelectron emission efficiency ϵ_p depends on atmospheric composition and structure, but the value ($\sim 10^{-2}$) calculated for Jupiter[18] is closer to the terrestrial value than one might expect, and probably applies as well to the other Jovian planets. The solar-wind capture efficiency ϵ_m is not well established even for Earth, but a value $\sim 2 \times 10^{-3}$ seems plausible[19], and may as well be adopted for other planets in the absence of any evidence to the contrary. One then obtains

$$S_m/S_p \sim (R_m/30\ R_p)^2 \qquad (4)$$

with no explicit dependence on heliocentric distance. In other words, if the mechanisms of the solar-wind and ionospheric sources remain the same, then the ratio of their source rates simply scales as the ratio of the areas over which they operate. For Earth, Jupiter, and Saturn, the indicated ratios are of the order of 1/4, 10, and 1, respectively (taking R_m to be 1.5 times the average subsolar standoff distance). The value for Earth appears reasonable inasmuch as both sources are known to be significant and neither is known to be clearly dominant[20]. For Jupiter and Saturn the evidence regarding solar-wind vs. ionospheric sources is clouded by the overwhelming presence of satellite sources, although both (solar-wind and ionospheric) sources are evident at both planets in certain Voyager observations of energetic-ion composition[13,21]. For the sake of illustration, the implied ratio of solar-wind to ionospheric source rates for both Uranus and Neptune would be of the order of 5 for a magnetosphere of Bode's-law dimensions. This is not to be taken as a quantitative prediction (it is unlikely that any such prediction could be adequately tested by Voyager in any case), but simply as an indication that neither source can be ruled out _a priori_.

It is, however, reasonably safe to predict[8] that all plasma sources are weaker at Uranus than at Jupiter and Saturn, and weaker still at Neptune, with the remotely possible exception of a Triton source at Neptune. This expectation follows primarily from the inverse-square scaling with heliocentric distance, and secondarily also from the lesser dimensions of the planets themselves and (presumably) of their magnetospheres.

An interesting exception to this rule is the potential plasma source resulting from _in situ_ ionization of ambient interstellar gas (mainly hydrogen) within the magnetosphere[2]. Plasma from this source would be distinguished, not by its composition, but by its uniform rate of production throughout the magnetosphere. Evidence of such an interstellar plasma source has not yet been detected in a planetary magnetosphere, but its relative importance must increase with increasing heliocentric distance: the interstellar gas becomes more accessible while the other competing sources become less potent[2].

A plasma population that is produced by local ionization of interstellar gas might have a particularly interesting first-order effect on magnetospheric structure, namely, none at all. Electric currents are associated with gradients of plasma pressure, not with plasma pressure per se. The interstellar gas, being uniformly distributed throughout the magnetosphere, might conceivably give rise to a plasma whose pressure, however large, has no significant gradients and hence no significant effect on the field configuration. For example, Figure 3 shows quantitative magnetostatic solutions of the pole-on configuration anticipated for Uranus, for three assumed distributions of plasma pressure in the tail[8]. The top panel shows the "vacuum" (zero-current) configuration, appropriate to any uniform plasma pressure distribution (of which the vacuum is merely a special case). The bottom panel shows the opposite limiting case (insofar as the magnetic-field distortion is concerned) in which the plasma pressure is assumed to vary with distance from the tail axis (thus producing a cylindrical current sheet as described above), but to be independent of distance as measured along the tail axis. The middle panel shows an intermediate case in which the pressure is allowed to vary in both dimensions (along, and transverse to, the tail axis). Similar solutions for the "normal-incidence" configuration have been developed for Earth's magnetosphere[22] and would presumably apply as well to Neptune's magnetosphere.

Such models can often be combined with magnetic-field measurements to infer global properties of the plasma distribution in regions far removed from the site of measurement. For example, numerous such efforts, based largely on Voyager observations, have been applied with varying degrees of success to the Jovian magnetosphere[23]. The complementary nature of particle and field measurements is particularly evident in this case — particle measurements can uniquely provide (among other things) information on the magnitude of the

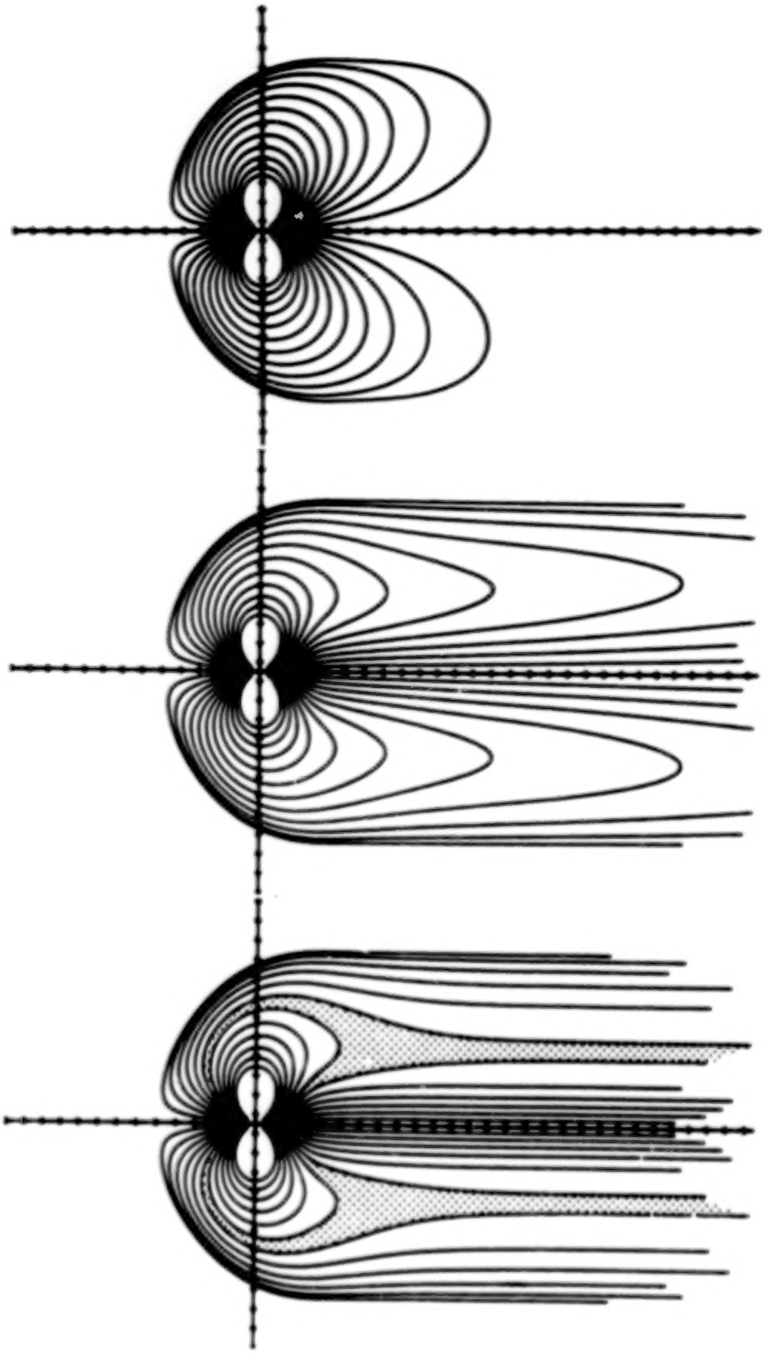

Figure 3. Magnetostatic solutions of the pole-on configuration illustrating the effect of the plasma pressure gradient. [ref. 8]

plasma pressure along a given spacecraft trajectory, while magnetic-field measurements, when carefully interpreted in the context of appropriate physical arguments, can uniquely provide (among other things) information on the gradient of that pressure transverse to the spacecraft trajectory.

EXTERNALLY DRIVEN CONVECTION

It is known that the solar-wind interaction produces a system of plasma convection in Earth's magnetosphere, and that this convection system is the controlling factor in magnetospheric dynamics. A global measure of the strength of the solar-wind/magnetosphere coupling at any given time is provided by the total voltage developed across the polar cap by the convection ($-\underline{v} \times \underline{B}$) electric field. Predicting the magnitude of this voltage, even qualitatively, is a fundamental unsolved theoretical problem[24]. Its magnitude is known empirically[25] to vary within the range 20-200 kV in response to solar-wind variations, being most sensitive to the north-south component of the IMF.

This and numerous other observations[26] indicate that the polar-cap convection electric field is a projection of the solar-wind ($-\underline{v} \times \underline{B}$) electric field along interconnected magnetic field lines[27]. In that case, the polar-cap convection voltage could hardly be expected to exceed that developed by the upstream solar-wind electric field across the diameter of the magnetosphere cross section. The ratio of the actual convection voltage to the maximum available voltage (as thus defined) can be taken to represent the efficiency of the magnetic coupling between the magnetosphere and the IMF (often referred to as the "reconnection efficiency"). Terrestrial observations[25] indicate a value ~0.1 for this ratio, consistent with the model requirement that it be $<$ 1.

We have neither theoretical nor empirical guidance for scaling this result to other planets — the coupling efficiency, as noted above, has not been derived from first principles, and planetary probes have not yet explored the regions of high magnetic latitude where the effects of solar-wind-driven convection, if any, would be apparent. In the absence of any such guidance, it is customary to assume[7,9,13,28-30] that the terrestrial coupling efficiency (~0.1) applies to all planets; it is then straightforward[2] to estimate the voltage associated with solar-wind-driven convection, given the planetary dipole magnetic moment and heliocentric distance. Given this hypothetical convection voltage, one can estimate the magnetospheric convection electric field and compare it with the corotation electric field to obtain the nominal radius of the "plasmasphere" within which, by definition, the latter is dominant[2,28,31]. If the nominal plasmasphere radius is significantly less than that of the magnetosphere (as in the terrestrial case), then solar-wind-driven convection may be considered a potentially important driver of internal magnetospheric dynamics; if not, it may be anticipated that the effects of solar-wind-driven convection, if any, are largely restricted to the polar caps.

For a coupling efficiency of 0.1, the resulting nominal plasmasphere radius is roughly half the magnetosphere radius for Earth, and roughly three times the magnetosphere radius for both Jupiter and Saturn. This comparison was the basis of the successful prediction[28] of the dominant role of corotation in Jupiter's magnetosphere (and, by obvious extension, in Saturn's). It should be noted, however, that the success of this prediction implies nothing about the validity of the scaling hypothesis with respect to the magnetic coupling efficiency — even the smallest nominal plasmasphere radius, corresponding to the maximum (unit) coupling efficiency, would exceed the characteristic magnetosphere radius (although marginally) at Jupiter and Saturn.

For a given set of solar-wind and IMF parameters, and a given planetary radius and spin rate, the ratio of nominal plasmasphere radius to day side magnetosphere radius scales as the 1/6 power of the magnetic moment and the -1/2 power of the magnetic coupling efficiency. Even for unit coupling efficiency, this ratio would be about 2 for both Uranus and Neptune if their magnetic moments were to have Bode's-law values, and would exceed unity for any magnetic moment larger than about 3×10^{-2} times the Bode's-law value. If the coupling efficiency has its commonly-assumed terrestrial value (~0.1), the nominal plasmapause radius would exceed the magnetosphere radius for virtually any magnetic moment large enough to produce a magnetosphere.

Our inability to predict the magnetic coupling efficiency does not impose a severe practical limitation in this context; it appears that only a rare combination of circumstances could conspire to invalidate the conclusion that externally-driven convection should be unimportant in the internal dynamics of the magnetospheres of Uranus and Neptune.

One cannot, however, rule out the possibility of solar-wind effects within the polar caps. The anticipated pole-on configuration at Uranus (Figure 2 above) has two interesting consequences insofar as solar-wind-driven convection is concerned. The first is that a spacecraft approaching the planet along the Sun-planet axis (as Voyager is obliged to do) would access very high magnetic latitudes, precisely the region where the effects of solar-wind-driven convection, if any, should be most apparent. (The constraints of orbital mechanics have precluded the probing of such high magnetic latitudes in the magnetospheres of Jupiter and Saturn.) The second consequence is that any polar-cap convection driven by the solar wind through magnetic interconnection should be closely aligned with the IMF direction[6], the polar-cap flow being (parallel/antiparallel) to the IMF direction if the (north/south) magnetic pole of the planet faces the Sun. The analogous effect is observed in Earth's magnetosphere[26] where it constitutes, so to speak, a first-order modification of the zero-order antisunward flow across the polar cap. In the pole-on geometry, the IMF alignment would become the zero-order effect; its observation would provide important confirmation not only that the polar-cap flow is driven by the solar-wind interaction, but also that the mechanism of that interaction is magnetic interconnection. To the extent that it occurs, this IMF-aligned convection would tend to destroy the cylindrical symmetry of the tail structure[6,8], although it is unlikely that any realistic Voyager encounter trajectory would permit the identification of any such asymmetry.

INTERNALLY DRIVEN CONVECTION

The above arguments indicate that corotation would probably prevent the establishment of a large-scale system of solar-wind-driven convection in a magnetosphere having Bode's-law dimensions at Uranus or Neptune. On the other hand, corotation itself may give rise to an entirely different kind of convection system, powered not by the solar wind but by the rotation of the planet. The necessary conditions for a rotationally-driven convection system are (1) that the magnetosphere contain a significant, localized, internal source of plasma, and (2) that this plasma source be located outside the synchronous orbital distance so that the centrifugal force of corotation exceeds the centripetal force of gravity. Both conditions are well met in Jupiter's magnetosphere (thanks to Io), where rotationally-driven convection provides the essential mechanism whereby the magnetosphere rids itself of the plasma that is continually injected by Io. It is not clear whether this convection occurs in the form of a large-scale systematic pattern that corotates with Jupiter[32] or in the form of small-scale eddy diffusion[33], but there can be little doubt that it occurs[34], and that it extracts rotational energy from Jupiter at a rate proportional to the mass injection rate at Io[15,32,35]. The conditions for rotationally-driven convection are apparently also satisfied at Saturn, although there remains some considerable uncertainty as to the magnitude(s) and location(s) of the relevant plasma source(s).

On the basis of arguments presented earlier, it appears doubtful that the magnetosphere of Uranus contains any significant, localized, internal source of plasma. Thus, there is no apparent reason to expect a significant system of rotationally-driven convection, in spite of the fact that corotation is expected to prevail over solar-wind-driven convection throughout. The same conclusion applies to Neptune with one reservation: if Triton should prove to be a significant source of magnetospheric plasma, then rotationally-driven convection may well result because Triton is well outside the synchronous orbital distance.

THE DISC DYNAMO INTERACTION

From all the above arguments one might well conclude that the magnetospheres of Uranus and Neptune, if indeed they exist, are rather boring places. On the one hand, it has been argued that solar-wind-driven convection may be largely excluded by the omnipresent corotation; on the other hand, it has been argued that rotationally-driven convection, the obvious alternative, may also fail to materialize for lack of an internal plasma source. Does this mean that the magnetosphere just sits there and corotates?

Not necessarily. There is a third alternative, namely, that the motion of the solar wind and the rotation of the planet are coupled so as to produce dynamic effects that neither of them alone could produce. The coupling mechanism is analogous to a Faraday disc dynamo, in which rotational energy is extracted from a rotating disc (the ionosphere) to drive a current through an electrical load (the solar wind). Such coupling was originally proposed as a source of auroral energy for Earth's magnetosphere[10], and more recently for Jupiter's magnetosphere[36]. Subsequent observations have shown that the effects of the disc dynamo interaction, if any, are insignificant at Earth and Jupiter compared to those of convection (driven externally and internally, respectively). However, the likelihood that both types of convection are ineffective at Uranus, according to the above arguments, has led to the proposal[9] that the disc dynamo mechanism operates effectively at Uranus and, indeed, that it is capable of powering the aurora whose existence has been inferred from the IUE measurements cited above. The same argument would apply to Neptune[37], unless Triton were to furnish a plasma source sufficient to produce rotationally-driven convection.

Figure 4 illustrates the disc dynamo process in the pole-on configuration anticipated for Uranus. The tail is assumed to be coupled to the adjacent magnetosheath flow, most likely through magnetic interconnection. The planet exerts a torque on the ionosphere through ion/neutral collisional coupling, and the torque is transmitted by the magnetic field to the tail and magnetosheath. The frictional coupling in the ionosphere requires that the ions rotate more slowly than the neutral atmosphere, the extent of the difference

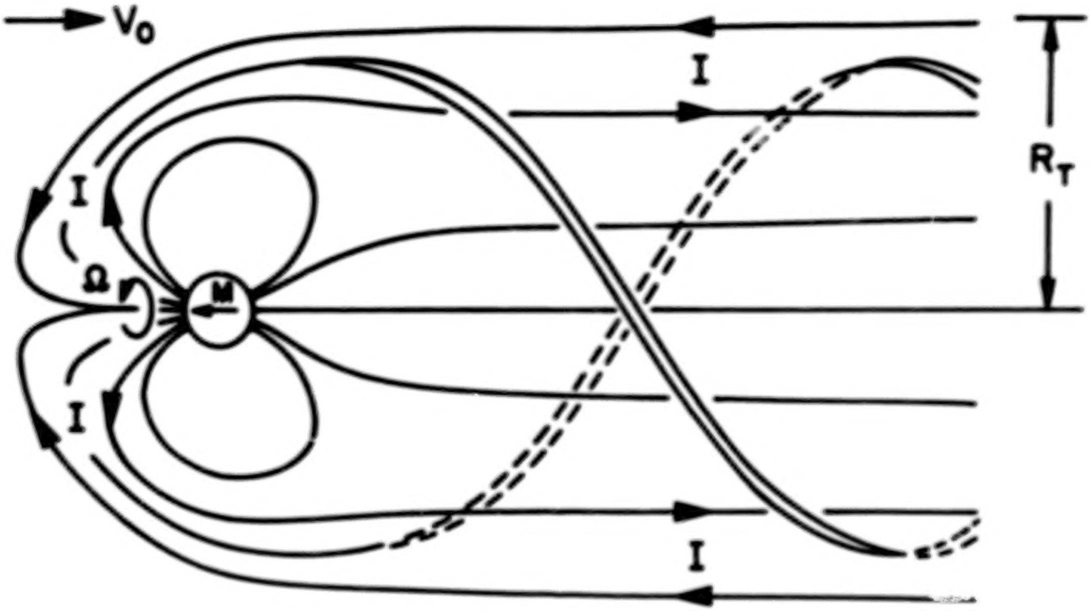

Figure 4. Birkeland currents and associated helical magnetic field configuration for the disc dynamo interaction. [ref. 9]

being proportional to the torque that is required to maintain the coupling between the tail and the magnetosheath. This departure from corotation in turn requires an electric field in the corotating frame of reference, and the resulting Pedersen current is connected by Birkeland (magnetic-field-aligned) currents to the acceleration current associated with the tail/magnetosheath coupling. The ionospheric $\underline{j} \times \underline{B}$ force balances the ion/neutral drag force, and the magnetopause $\underline{j} \times \underline{B}$ force tends to spin up the magnetosheath; the entire circuit thus has the effect of transferring planetary rotational energy and angular momentum from the atmosphere to the surrounding magnetosheath. The planetary ionosphere constitutes the disc dynamo, and the magnetosheath constitutes the load. The power drain (perhaps needless to say) is of no great consequence either to the planetary rotation or to the magnetosheath flow, but the magnetospheric consequences may be considerable[9].

The essential ingredients of this disc dynamo interaction are (1) a rapidly rotating planet with (2) a sufficiently conducting ionosphere, connected magnetically to (3) a non-corotating external medium such as the solar wind. These ingredients are not unique to Uranus; they are probably common to all four Jovian planets[37]. Uranus is, however, uniquely suited to the study of the mechanism for two reasons: (1) its magnetosphere, more than that of any other planet, is expected to be relatively free of competing convection processes that would contaminate any observational signature of the disc dynamo process, and (2) the symmetry of the anticipated pole-on configuration lends itself to theoretical analysis with a minimum of restrictive simplifying assumptions.

By virtue of this axial symmetry one can, in fact, develop a complete analytic solution for a realistic first-order model of the disc dynamo process[9]. The power extracted from planetary rotation is found to be proportional to, among other things, the first power of the solar-wind speed and the second power of the planetary rotation frequency; the disc-dynamo mechanism is thus clearly distinguished from both externally-driven convection, which operates independently of planetary rotation, and internally-driven convection, which operates independently of the solar wind.

The power generated by the disc dynamo model is also proportional to the 4/3 power of the planetary magnetic dipole moment, and depends on ionospheric conductivity through a function whose algebraic expression is tedious but whose behavior is predictable: the dynamo efficiency varies monotonically between zero and one as a function of the ratio between the disc conductance (represented by the height-integrated ionospheric conductivity) and the load conductance (represented by the quantity $1/\mu_o v_{sw} = 2$ mho, where v_{sw} is the solar-wind speed). Given an assumed (or independently calculated) value for the ionospheric conductance, the power generated by the disc dynamo model is given as a function of the magnetic moment.

The intermediate case (ionospheric conductance = $1/u_o v_{sw}$ = 2 mho, dynamo efficiency = 2/9) is illustrative, and not implausible for Uranus; the resulting relationship between magnetic moment and power output is shown in Figure 5. The scale of the abscissa indicates, not the total dynamo power output, but only the portion thereof that is available to maintain an auroral primary particle flux, assumed to be a fixed fraction (0.1) of the total dynamo power

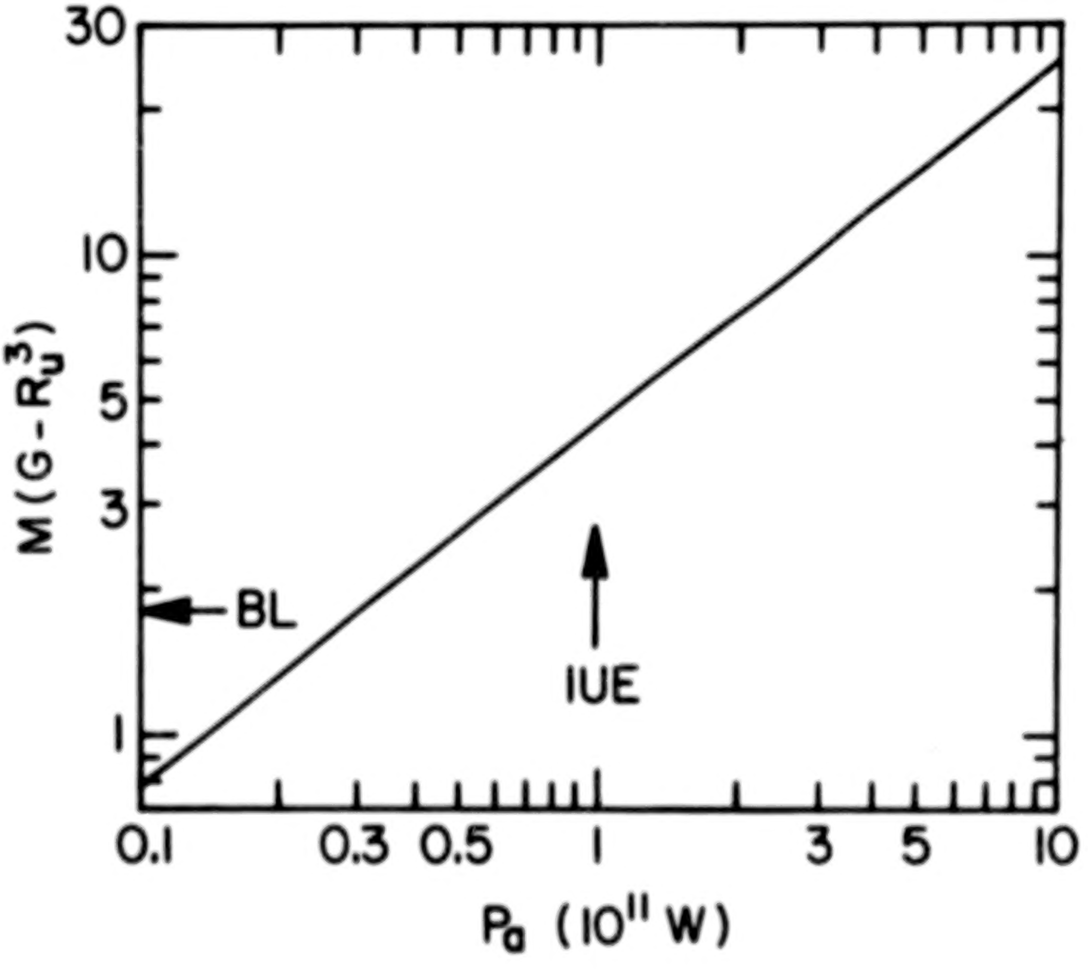

Figure 5. Magnetic moment required to produce a given global energy deposition rate in the form of auroral primary particle precipitation (assumed to be one-tenth of the total dynamo power output) within the disc dynamo model. [ref. 9]

output. The arrow labeled "IUE" reflects a preliminary analysis[38] of the reported auroral emissions observed from the IUE spacecraft, suggesting that a total power ~10^{11} W in the form of precipitating primary electrons may be required to produce the observed emissions, assuming a 5% efficiency of conversion of incident electron energy to escaping Lyα photon energy. The arrow labeled "BL" indicates the Bode's-law value of the magnetic moment. Although the power requirement inferred from the IUE observations is subject to order-of-magnitude uncertainty[38], it is worth noting that the disc dynamo model readily satisfies such a requirement if the magnetic moment is comparable to the Bode's-law value.

As Voyager approaches Uranus, UVS observations should provide a more definitive estimate of the auroral power requirement (provided that the existence of auroral emissions is confirmed). Meanwhile, a realistic calculation of the ionospheric conductivity is feasible and worthwhile, including the (probably dominant) effect of auroral impact ionization. To the extent that the ionospheric conductivity and auroral power output can be established, the disc dynamo model provides a means for remote sensing of the magnitude of the planetary magnetic moment.

If the polar-cap auroral form can be resolved spatially, then the direction of the magnetic moment can also be deduced remotely in the context of the disc dynamo model. The model predicts a broadly distributed Birkeland current of one sign over the polar cap, and a thin return-current sheet of opposite sign at the edge of the polar cap. If the north magnetic pole faces the Sun, as in Figure 4, the distributed polar-cap current is downward and the return sheet current is upward; if the south magnetic pole faces the Sun, these current directions are reversed. The brightest auroral emissions are expected to occur primarily in association with upward, rather than downward, Birkeland currents[9]. Thus a thin bright auroral ring centered on the pole is expected if the north pole faces the Sun, as compared to a relatively diffuse polar-cap glow in the opposite case.

CONCLUSION

Before Jupiter's magnetosphere was explored by Pioneers 10 and 11 and Voyagers 1 and 2, it was anticipated that solar-wind-driven convection, the prime mover of terrestrial magnetospheric phenomena, might be eclipsed in Jupiter's magnetosphere by the effects of rotation. There was, however, no clear idea of just what those rotational effects might be. In situ observations were essential to the identification of rotationally-driven convection as the alternative mechanism that replaces solar-wind-driven convection as the prime mover in the Jovian magnetosphere. The detailed behavior of this rotationally-driven convection is by no means understood (nor, for that matter, is the solar-wind-driven convection system in Earth's magnetosphere understood in full detail), but rotationally-driven convection is, at least, now recognized as a real and distinct alternative to the solar-wind-driven convection process that governs the behavior of Earth's magnetosphere.

The Voyager observations at Saturn were full of surprises, particularly in relation to ring structure, and some of these novel features may well prove to be related to unanticipated magnetospheric effects. The global structure and dynamics of Saturn's magnetosphere, however, appear to be consistent with the concepts of rotationally-driven convection as developed for the Jovian magnetosphere, combined with a certain element of inferred solar-wind control at high latitudes.

For the magnetospheres of Uranus and Neptune, a third, qualitatively different, mode of behavior is anticipated. Solar-wind-driven convection is expected to be ineffective for the same reason that it was expected to be ineffective at Jupiter and Saturn. Rotationally-driven convection is also expected to be ineffective owing to the lack of internal plasma sources. In the absence of either externally- or internally-driven convection, it is proposed that direct electrodynamic coupling between the solar wind and the planetary ionosphere establishes a disc dynamo interaction whereby planetary rotational energy is extracted to power polar-cap auroral phenomena.

I have attempted to give a fair account of the various known options that might be anticipated for magnetospheric structure and behavior at Uranus and Neptune. These are based on past experience and whatever tools of extrapolation are available to us. I have also given tentative conclusions as to the relative likelihood of the various options; these conclusions are necessarily conjectural and would no doubt differ from author to author. (This is why we need Voyager.) There is, however, one prediction that I can make without fear of contradiction, namely, that no preconceived scenario, including the one presented above, will fully anticipate the discoveries that await the arrival of Voyager.

Acknowledgments. This work was supported in part by the National Science Foundation, Division of Atmospheric Sciences, under Grant ATM-8311146, and by the National Aeronautics and Space Administration, Outer Planets Data Analysis Program, under Grant NAGW-168.

REFERENCES

1. Dessler, A. J. (ed.), Physics of the Jovian Magnetosphere, Cambridge University Press, New York, 1983.
2. Siscoe, G. L., Towards a comparative theory of magnetospheres, in Solar-System Plasma Physics — A Twentieth Anniversary Review, C. F. Kennel, L. J. Lanzerotti, and E. N. Parker, eds., North Holland, Amsterdam, 1979.
3. Barnes, A., The solar wind at 20-30 AU, this volume.
4. Hill, T. W., and F. C. Michel, Planetary magnetospheres, Rev. Geophys. Space Phys., 13, 967, 1975.
5. Durrance, S., Lyman-alpha aurora, this volume.
6. Siscoe, G. L., Two magnetic tail models for Uranus, Planet. Space Sci., 19, 483, 1971.
7. Siscoe, G. L., Particle and field environment of Uranus, Icarus, 24, 311, 1975.
8. Voigt, G.-H., T. W. Hill, and A. J. Dessler, The magnetosphere of Uranus: Plasma sources, convection, and field configuration, Astrophys. J., 266, 390, 1983.
9. Hill, T. W., A. J. Dessler, and M. E. Rassbach, Aurora on Uranus: A Faraday disc dynamo mechanism, Planet. Space Sci., 31, 1187, 1983.
10. Dessler, A. J., and R. D. Juday, Configuration of auroral radiation in space, Planet. Space Sci., 13, 63, 1965.
11. Crooker, N. U., Dayside merging and cusp geometry, J. Geophys. Res., 84, 951, 1979.
12. Crooker, N. U., The half-wave rectifier response of the magnetosphere and antiparallel merging, J. Geophys. Res., 85, 575, 1980.

13. Hill, T. W., A. J. Dessler, and C. K. Goertz, Magnetospheric models, in Physics of the Jovian Magnetosphere (Chapter 10), A. J. Dessler, ed., Cambridge Univ. Press, New York, 1983.

14. Lazarus, A. J., and R. L. McNutt, Jr., Low-energy plasma ion observations in Saturn's magnetosphere, J. Geophys. Res., 88, 8831, 1983.

15. Dessler, A. J., Mass-injection rate from Io into the Io plasma torus, Icarus, 44, 291, 1980.

16. Peale, S. J., P. Cassen, and R. T. Reynolds, Melting of Io by tidal dissipation, Science, 203, 892, 1979.

17. Trafton, L., Seasonal variation of Triton's atmosphere, this volume.

18. Swartz, W. E., R. W. Reed, and T. R. McDonough, Photoelectron escape from the ionosphere of Jupiter, J. Geophys. Res., 80, 495, 1975.

19. Hill, T. W., Origin of the plasma sheet, Rev. Geophys. Space Phys., 12, 379, 1974.

20. Hultqvist, B., Recent progress in the understanding of the ion composition in the magnetosphere and some major question marks, Rev. Geophys. Space Phys., 20, 589, 1982.

21. Hamilton, D. C., D. C. Brown, G. Gloeckler, and W. I. Axford, Energetic atomic and molecular ions in Saturn's magnetosphere, J. Geophys. Res., 88, 8905, 1983.

22. Fuchs, K., and G.-H. Voigt, Self-consistent theory of a magnetospheric B field model, in Quantitative Modeling of Magnetospheric Processes, Geophys. Monogr. Ser., 21, W. P. Olson, ed., pp. 86-95, AGU, Washington, D. C., 1979.

23. Vasyliunas, V. M., Plasma distribution and flow, in Physics of the Jovian Magnetosphere (Chapter 11), A. J. Dessler, ed., Cambridge Univ. Press, New

York, 1983.

24. Hill, T. W., Solar-wind magnetosphere coupling, in Solar-Terrestrial Physics, R. L. Carovillano and J. M. Forbes, eds., pp. 261-302, D. Reidel, Hingham, MA, 1983.

25. Reiff, P. H., R. W. Spiro, and T. W. Hill, Dependence of polar-cap potential drop on interplanetary parameters, J. Geophys. Res., 86, 7639, 1981.

26. Reiff, P. H., Evidence of magnetic merging from low-altitude spacecraft and ground-based experiments, in Magnetic Reconnection, Geophy. Monogr. Ser., E. W. Hones, ed., AGU, Washington, D. C., in press, 1984.

27. Dungey, J. W., Interplanetary magnetic field and the auroral zones, Phys. Rev. Lett., 6, 47, 1961.

28. Brice, N. M., and G. A. Ioannidis, The magnetospheres of Jupiter and Earth, Icarus, 13, 173, 1970.

29. Kennel, C. F., Magnetospheres of the planets, Space Sci. Rev., 14, 511, 1973.

30. Kennel, C. F., and F. V. Coroniti, Jupiter's magnetosphere, Ann. Rev. Astron. Astrophys., 15, 389, 1977.

31. Vasyliunas, V. M., Concepts of magnetospheric convection, in The Magnetospheres of the Earth and Jupiter, V. Formisano, ed., pp. 179-188, D. Reidel, Hingham, MA, 1975.

32. Hill, T. W., A. J. Dessler, and L. J. Maher, Corotating magnetospheric convection, J. Geophys. Res., 86, 9020, 1981.

33. Siscoe, G. L., and D. Summers, Centrifugally driven diffusion of Iogenic plasma, J. Geophys. Res., 86, 8471, 1981.

34. Hill, T. W., Rotationally-induced Birkeland current systems, in Magnetospheric Currents, Geophys. Monogr. Ser., 28, T. A. Potemra, ed., pp. 340-

349, AGU, Washington, D. C., 1983.

35. Eviatar, A., and G. L. Siscoe, Limit on rotational energy available to excite Jovian aurora, Geophys. Res. Lett., 7, 1085, 1980.

36. Gold, T., The magnetosphere of Jupiter, J. Geophys. Res., 81, 3401, 1976.

37. Dessler, A. J., private communication, 1984.

38. Atreya, S. K., private communication, 1982.

BLANK PAGE

THE SOLAR WIND AT 20-30 AU

Aaron Barnes and Paul R. Gazis

Theoretical Studies Branch

NASA, Ames Research Center

Moffett Field, CA 94035

ABSTRACT

Pioneer 10 sampled the interplanetary plasma over the range 20-30 astronomical units, during the period 1979-1983. The median flow speed is about 400 km/s, and at 20 AU the median density, proton temperature and dynamic pressure are, respectively, 0.025 cm^{-3}, 10^4 K, and $6x10^{-11}$ dyne cm^{-2}. Comparison with nearly simultaneous observations taken from Pioneer 11 in the vicinity of 10 AU shows the average solar wind flow speed does not vary significantly with increasing heliocentric distance, and the density falls off as R^{-2}, as predicted by simple solar wind models. The day-to-day variations in solar wind parameters are smaller at larger distance. However, very large shocks, probably due to one or several solar flares, have been detected beyond 25 AU. The dynamic pressure at 20 AU does vary by a factor 5 or more, which could result in >30% variation in the scale of the magnetosphere of Uranus. Comparison of Pioneer 10 and 11 observations at similar distances but different phases of the solar activity cycle shows that solar wind dynamic pressure varies over a wider range during epochs of high solar activity. In particular, the variation near 20 AU is likely to be smaller at Voyager 2 Uranus encounter than observed by Pioneer 10 in the 1979-80 period.

The solar wind plasma analyzers aboard Pioneers 10 and 11 are alive and well, and sending back data, more than a decade after launch. During 1979-83 Pioneer 10 traversed the solar wind between 20 and 30 astronomical units heliocentric distance, thus providing firm data about the interplanetary environment at the distances of Uranus and Neptune. In this paper we summarize these observations, in the hope of providing a basis for anticipating the solar wind plasma environments for the Voyager 2 encounters with Uranus in 1986 and Neptune in 1989. However, it should be borne in mind that the Pioneer observations come from a different phase of the solar activity cycle, and that Pioneer 10 is on the opposite side of the Sun (see Fig. 1). Observations from Pioneer 11, in conjunction with those from the more distant Pioneer 10, provide a means of addressing how solar wind conditions at encounter might differ from those found earlier by Pioneer 10, because of either the advance of the solar cycle or the interaction with interstellar neutral gas.

The radial variation of solar wind parameters out to 20 AU was studied by Kayser et al (1981). They reported that, on the average, the flow speed does not vary with R and that the density falls off as R^{-2}, as is expected from the simplest steady radial flow models. The proton temperature varies as R^{-a}, where a $\sim$.5-.7, much smaller than would be expected for adiabatic expansion (see also Gazis and Lazarus, 1981; Gazis, 1984). A wide range of day-to-day variations is superposed on these large-scale radial trends.

Figure 2 shows the distribution of speed, density, proton temperature and dynamic pressure measured over a 295 day period at Pioneer 10 near 20 AU. Corresponding measurements from Pioneer 11 near 10 AU are also shown (with density and dynamic pressure scaled to 20 AU). The median values of all quantities are approximately consistent with the distance scaling laws described above. Thus "typical" parameters at the orbit of Uranus are speed = 400 km/s, density = 0.025 protons/cm^3, proton temperature = 10 K^4, and dynamic pressure = 6×10^{-11} dynes/cm^2.

The day-to-day variation of velocity and temperature decreases with increasing heliocentric distance, as may be inferred from Fig. 2. To some extent this trend represents the continued erosion of the corotating stream structure (Collard et al, 1982; Burlaga, 1983). However, it should be remembered that these observations come from a period of high solar activity when it is difficult to distinguish corotating streams from transient variations due, for example, to solar flares or other mass ejection events. Fig. 3 shows two 100 day time series of velocity and density near 10 and 20 AU. The series for 10 AU shows a very large transient event, probably due to a solar flare. By contrast, the 20 AU data show only small jumps in velocity. Although large events such as in Fig. 3b are infrequent, in general the solar wind velocity is more variable at 10 than 20 AU during this period. However, the observed range of variations is far from negligible at the orbit of Uranus. The range of dynamic pressures, which determine the size of the planetary magnetosphere, is more than a factor of 5. This range would correspond to a variation of more than 30% in the magnetopause distance (assuming that the solar-wind interaction is governed by a permanent planetary field as at Earth, Jupiter and Saturn).

Voyager 2 will encounter Uranus near solar minimum. It is pertinent to ask how conditions depicted by Fig. 2 are likely to differ then. Fig. 4 shows conditions near 10 AU, at comparable latitude, for two different parts of the solar cycle. The median values and distributions are not strikingly different at the two epochs, although the dynamic pressure distribution exhibits a fairly prominent high-pressure "tail" for the period of higher solar activity. This tail is presumably reflects transient streams associated with solar flares and other solar mass-ejection events. Fig. 5 shows a 100 day time series from Pioneer 10 near solar minimum. The velocity profile is characterized by steady, recurring streams. In contrast, the same distance at solar maximum (cf. Fig. 3b) shows a disturbed, transient velocity profile.

Hence it seems likely that at the time of Uranus encounter the dynamic pressure variation, and associated variation of magnetopause size, will be diminished in comparison with what Fig. 2 would imply. It is possible that during the encounter period the ecliptic solar wind will consist mainly of high speed streams from coronal holes, as was the case in 1973-4 (Zirker, 1977). Under these conditions magnetic activity occurs at Earth, repeating with the solar rotation period. We would expect similar phenomena to be diminished or absent at Uranus, because of the general and strong erosion of corotating stream structure at large heliocentic distance.

Fig. 4 summarizes conditions between 25 and 30 AU recently observed by Pioneer 10. Density and dynamic pressure are normalized to the orbit of Neptune. At these distances the situation is much as at Uranus, although there was an extended period of very high speed in 1982, when Pioneer 10 was beyond 27.8 AU. The disturbance is thought to have originated in a solar flare (or, perhaps more likely, a series of several flares), and appears to rise and fall with roughly the solar rotation period. The disturbed period lastfed for several solar rotations and clearly represents a widespread disruption of the outer heliosphere. This period is presently being studied in detail; for the present purpose we only note that it is a clear indication that major solar wind disturbances, though rare, can reach the orbits of Uranus and Neptune.

REFERENCES

Burlaga, L.F., Corotating pressure wave without fast streams in the solar wind, *J. Geophys. Res.*, *88*, 6085-6094, 1983.

Collard, H.R., J.D. Mihalov, and J.H. Wolfe, Radial variation of the solar wind speed between 1 and 15 AU, *J. Geophys. Res.*, *87*, 2203-2214, 1982.

Gazis, P.R., Observations of plasma bulk parameters and the energy balance of the solar wind between 1 and 10 AU, *J. Geophys. Res.*, *89*, 775-785, 1984.

Gazis, P.R., and A.J. Lazarus, Voyager observations of solar wind proton temperature: 1-10 AU, *Geophys. Res. Lett.*, *9*, 431-434, 1982.

Kayser, S.E., A. Barnes, and J.D. Mihalov, The far reaches of the solar wind: Pioneer 10 and Pioneer 11 plasma results, submitted for publication, 1981.

Zirker, J.B., Coronal holes and high-speed wind streams, *Rev. Geophys. Space Phys.*, *15*, 257-269, 1977.

FIGURE CAPTIONS

Fig. 1. Ecliptic plane projections of the trajectories of Pioneers 10 and 11 and Voyagers 1 and 2.

Fig. 2. Histograms of relative frequency of velocity, density, proton temperature and dynamic pressure observed at 10 and 20 astronomical units. The observed periods at each spacecraft are 295 days, lagged to allow for corotation and for the transit time between 10 and 20 A.U. Density and dynamic pressure are normalized to the distance of Uranus.

Fig. 3. Time series of velocity and density (normalized to 1 AU) for 100 day intervals from the period corresponding to Fig. 2. There were no large velocity jumps near 20 AU, although smaller jumps (of order > 20 km/s) are frequently associated with shocks. In contrast, an enormous shock was observed near 10 AU during this period.

Fig. 4. Histograms of relative frequency of solar wind parameters 10 AU near solar minimum (Pioneer 10) and near solar maximum (Pioneer 11). Density and dynamic pressure are normalized to the distance of Uranus.

Fig. 5. Time series of velocity and density at Pioneer 10 for a 100 day interval near solar minimum. This period is characterized by the regularity of the stream structure, and may be contrasted with the transient character of the streams near solar maximum (Fig. 3b).

Fig. 6. Histograms of relative frequency of solar wind parameters between 25 and 30 AU. Density is normalized to the orbit of Uranus.

Fig. 7. Time series of velocity and density for a 100 day period that includes the first stages of the giant disturbance of the outer heliosphere that occurred in late 1982.

533

BEST COPY AVAILABLE

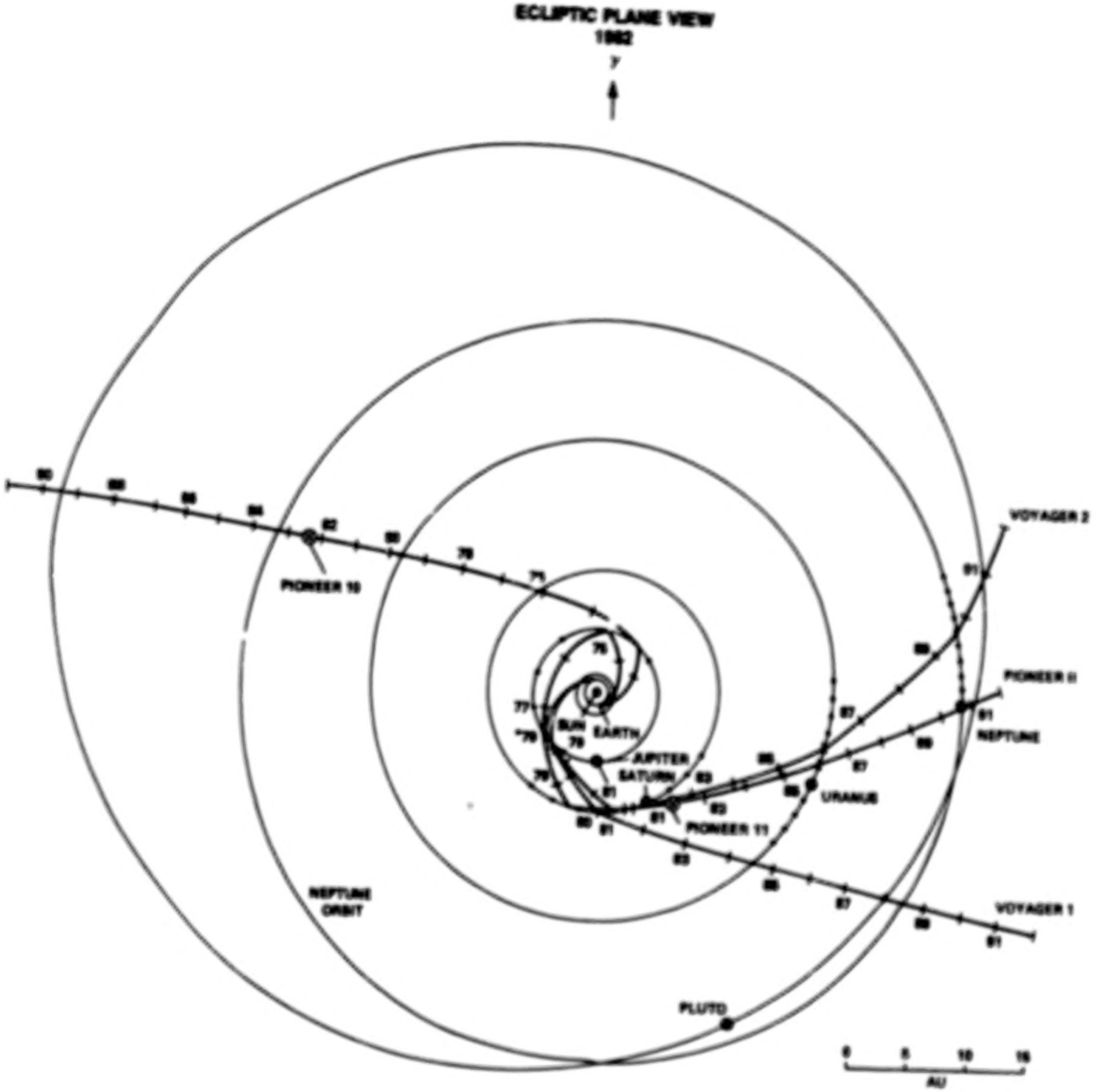

ECLIPTIC PLANE VIEW
1982
γ
VOYAGER 2
PIONEER 10
PIONEER II
NEPTUNE
SUN
EARTH
JUPITER
SATURN
URANUS
PIONEER 11
VOYAGER 1
NEPTUNE ORBIT
PLUTO
0
5
10
15
AU

Fig. 1

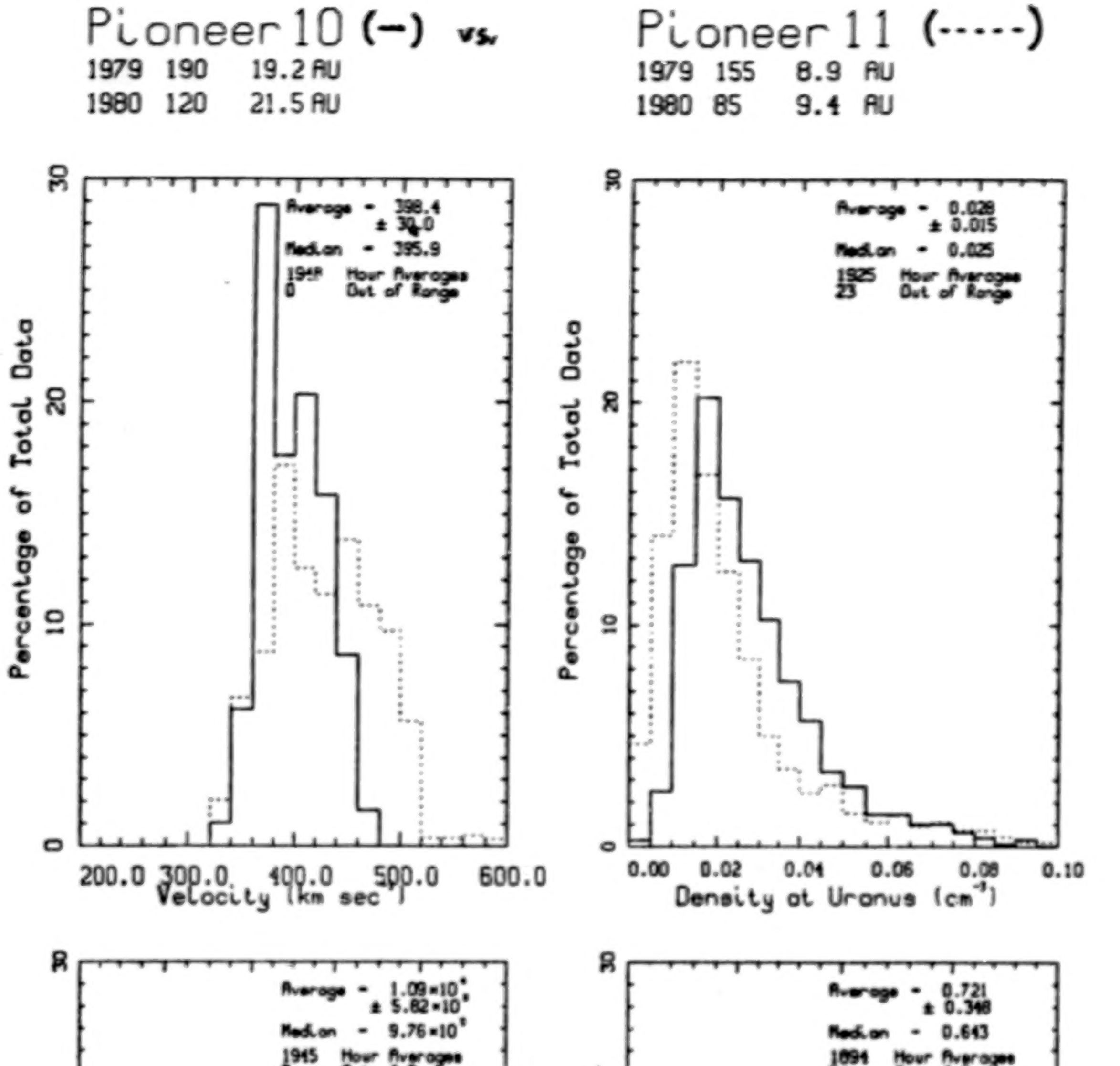
Pioneer 10 (—) vs. Pioneer 11 (-----)
1979 190 19.2 AU
1980 120 21.5 AU
1979 155 8.9 AU
1980 85 9.4 AU
Average - 398.4 ± 30.0
Median - 395.9
1948 Hour Averages
0 Out of Range
Percentage of Total Data
0
10
20
30
200.0 300.0 400.0 500.0 600.0
Velocity (km sec^{-1})
Average - 0.028 ± 0.015
Median - 0.025
1925 Hour Averages
23 Out of Range
0.00 0.02 0.04 0.06 0.08 0.10
Density at Uranus (cm^{-3})
Average - 1.09×10^{4} ± 5.82×10^{3}
Median - 9.76×10^{3}
1945 Hour Averages
3 Out of Range
0.0 1.0 2.0 3.0 4.0 5.0
Proton Temperature (10^4 °K)
Average - 0.721 ± 0.348
Median - 0.643
1894 Hour Averages
54 Out of Range
0.0 0.5 1.0 1.5 2.0
Dynamic Pressure at Uranus (10^{-10} dynes cm^{-2})

Fig. 2

PLOT 2 09.50.15 FRI 27 JAN, 1984 JOB=ROTTCH , NASA AMES DISSPLA 9.0

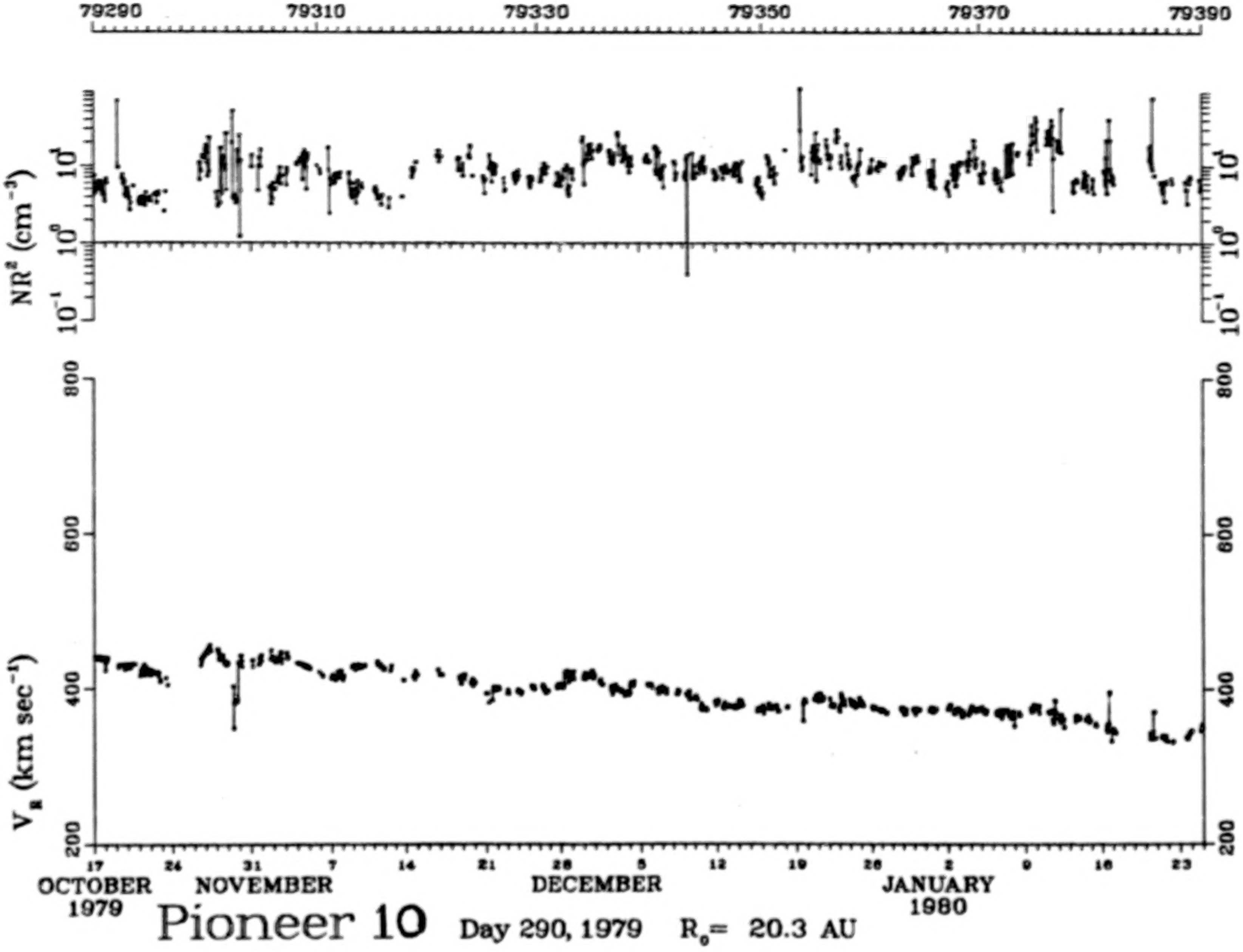

Fig. 3a

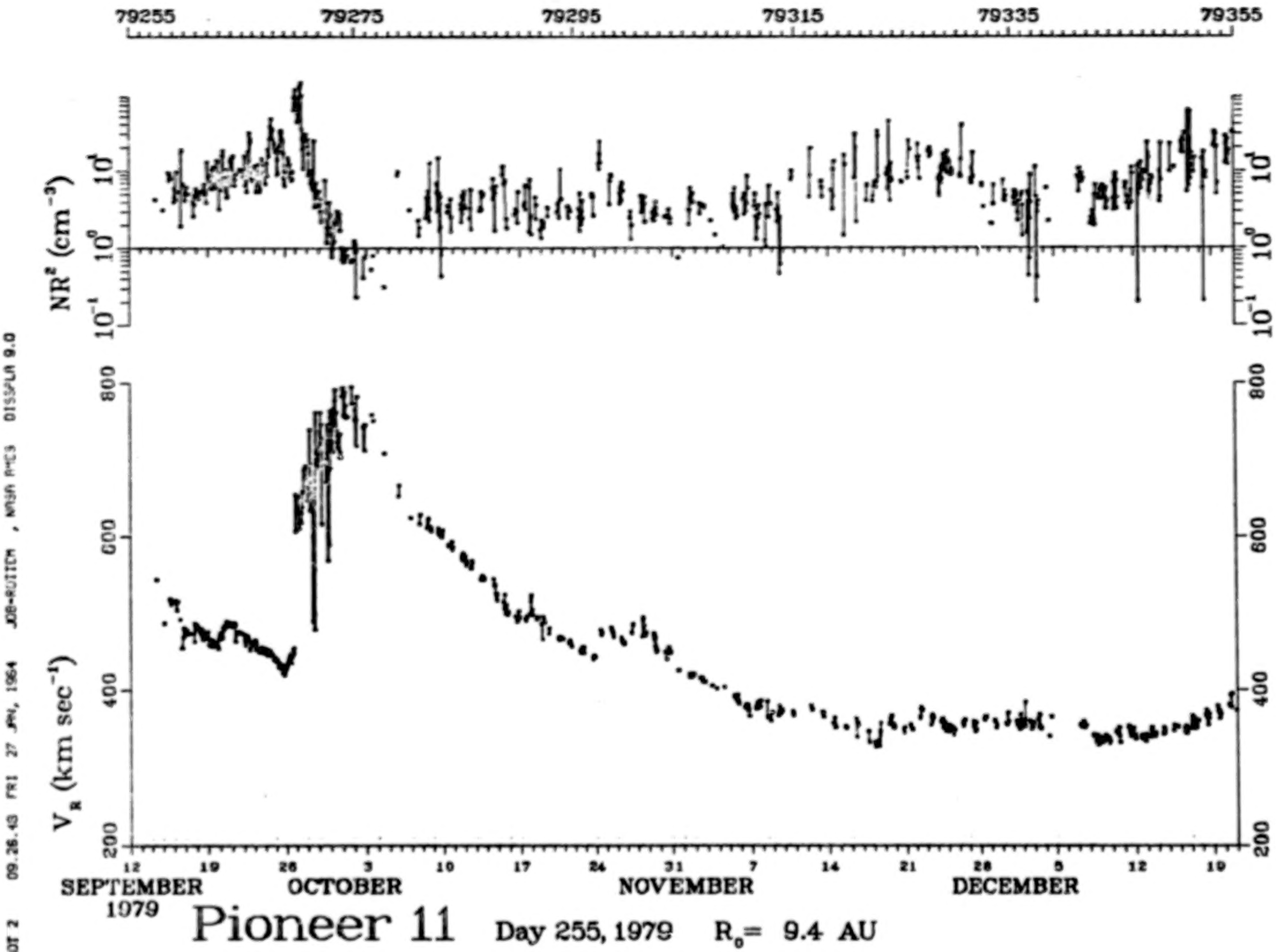
79255
79275
79295
79315
79335
79355
NR^2 (cm^{-3})
10^1
10^0
10^{-1}
V_R (km sec^{-1})
800
600
400
200
12
19
26
3
10
17
24
31
7
14
21
28
5
12
19
SEPTEMBER
1979
OCTOBER
NOVEMBER
DECEMBER
Pioneer 11 Day 255, 1979 R_0= 9.4 AU
PLOT 2 09.26.43 FRI 27 JAN, 1984 JOB=ROTTEM , NASA AMES DISSPLA 9.0

Fig. 3b

536

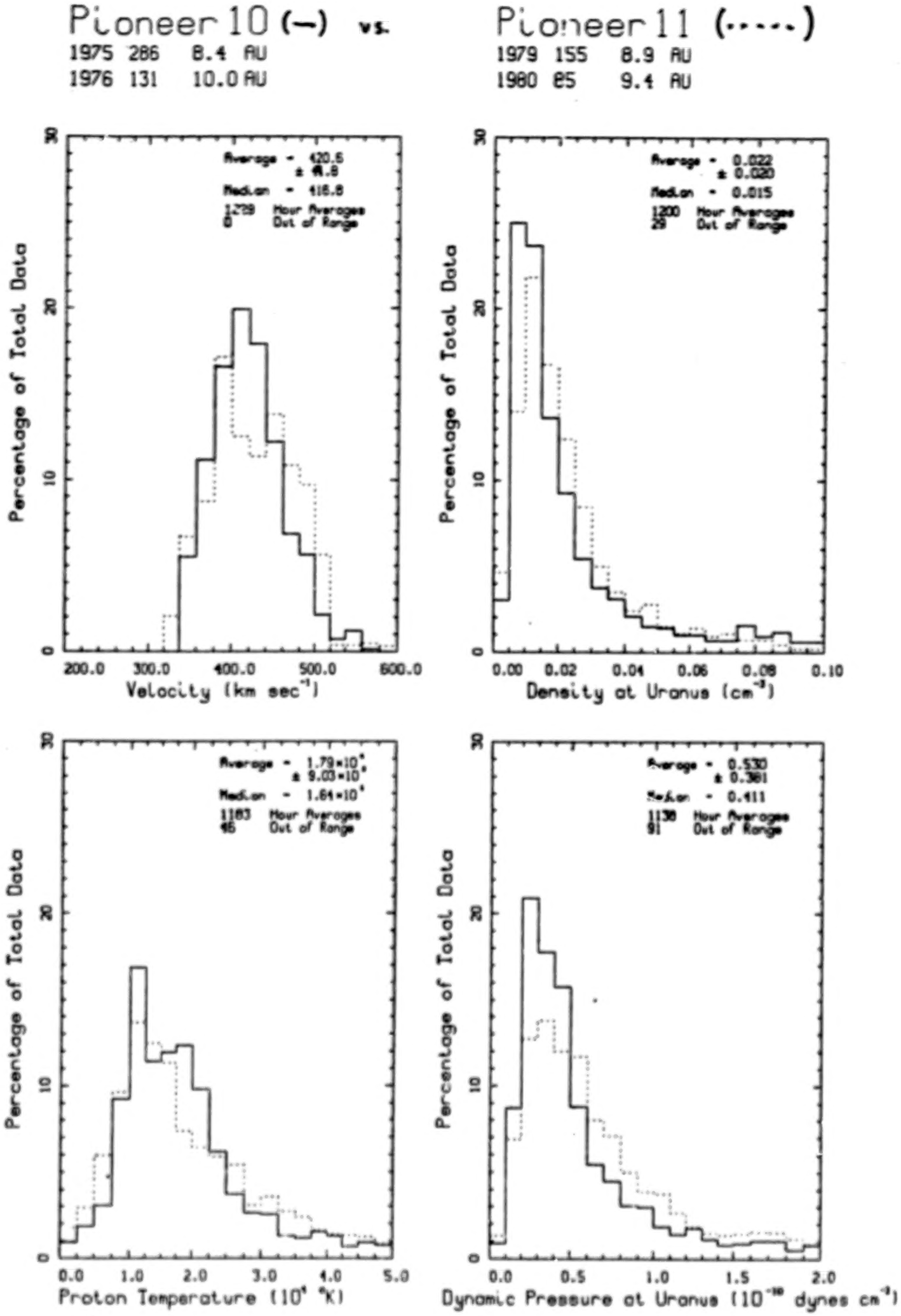
Pioneer 10 (—) vs. Pioneer 11 (·····)
1975 286 8.4 AU
1976 131 10.0 AU
1979 155 8.9 AU
1980 85 9.4 AU
Average - 420.6 ± 41.8
Median - 416.8
1229 Hour Averages
0 Out of Range
Percentage of Total Data
0
10
20
30
200.0
300.0
400.0
500.0
600.0
Velocity (km sec^{-1})
Average - 0.022 ± 0.020
Median - 0.015
1200 Hour Averages
29 Out of Range
Percentage of Total Data
0.00
0.02
0.04
0.06
0.08
0.10
Density at Uranus (cm^{-3})
Average - 1.79×10^{5} ± 9.03×10^{4}
Median - 1.64×10^{5}
1183 Hour Averages
46 Out of Range
Percentage of Total Data
0.0
1.0
2.0
3.0
4.0
5.0
Proton Temperature (10^{5} °K)
Average - 0.530 ± 0.381
Median - 0.411
1138 Hour Averages
91 Out of Range
Percentage of Total Data
0.0
0.5
1.0
1.5
2.0
Dynamic Pressure at Uranus (10^{-10} dynes cm^{-2})

Fig. 4

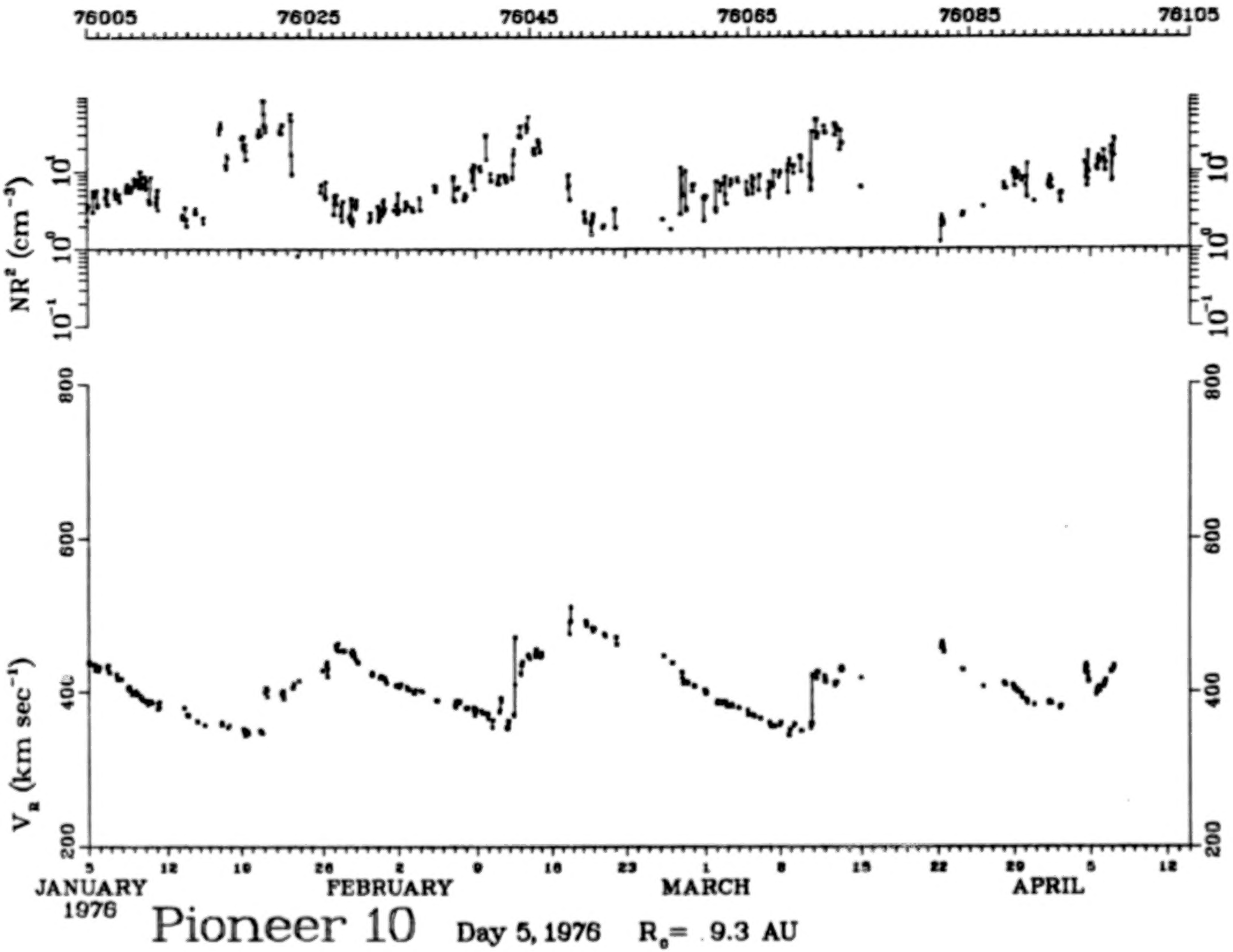
76005
76025
76045
76065
76085
76105
NR^2 (cm^{-3})
10^1
10^0
10^{-1}
V_R (km sec^{-1})
800
600
400
200
5
12
19
26
2
9
16
23
1
8
15
22
29
5
12
JANUARY
1976
FEBRUARY
MARCH
APRIL
Pioneer 10
Day 5, 1976 R_0= 9.3 AU
PLOT 2 19.27.12 THUR 26 JAN, 1984 JOB-ROTTCM , NASA AMES DISSPLA 9.0

Fig. 5

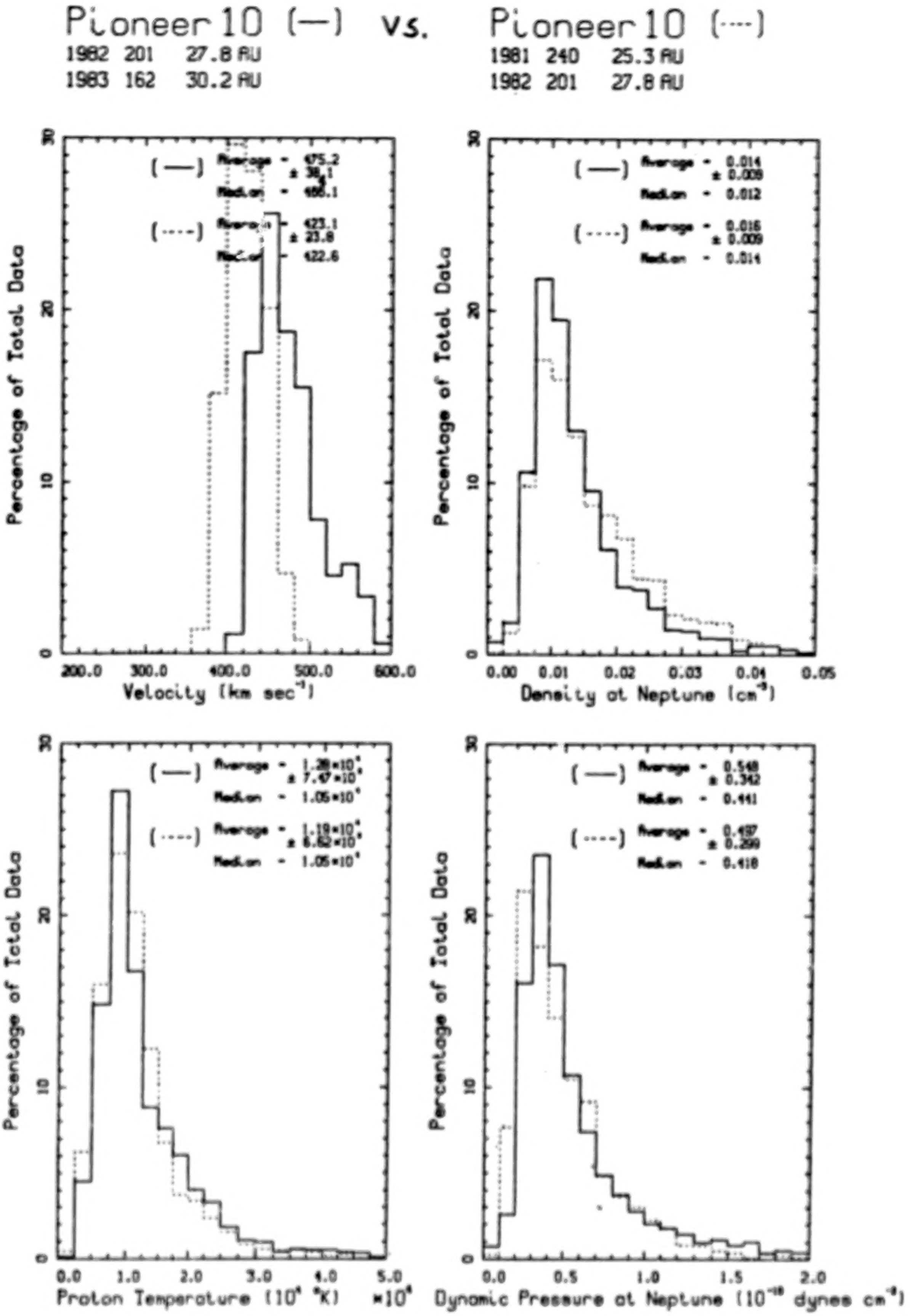
Pioneer 10 (—) vs. Pioneer 10 (···)
1982 201 27.8 AU
1983 162 30.2 AU
1981 240 25.3 AU
1982 201 27.8 AU
(—) Average = 475.2 ± 38.1
Median = 466.1
(----) Average = 423.1 ± 23.8
Median = 422.6
Percentage of Total Data
0
10
20
30
200.0
300.0
400.0
500.0
600.0
Velocity (km sec^{-1})
(—) Average = 0.014 ± 0.009
Median = 0.012
(----) Average = 0.016 ± 0.009
Median = 0.014
0.00
0.01
0.02
0.03
0.04
0.05
Density at Neptune (cm^{-3})
(—) Average = 1.28×10^{4} ± 7.47×10^{3}
Median = 1.05×10^{4}
(----) Average = 1.19×10^{4} ± 6.62×10^{3}
Median = 1.05×10^{4}
0.0
1.0
2.0
3.0
4.0
5.0
Proton Temperature (10^{4} °K) $\times 10^{4}$
(—) Average = 0.548 ± 0.342
Median = 0.441
(----) Average = 0.497 ± 0.299
Median = 0.418
0.0
0.5
1.0
1.5
2.0
Dynamic Pressure at Neptune (10^{-10} dynes cm^{-2})

Fig. 6

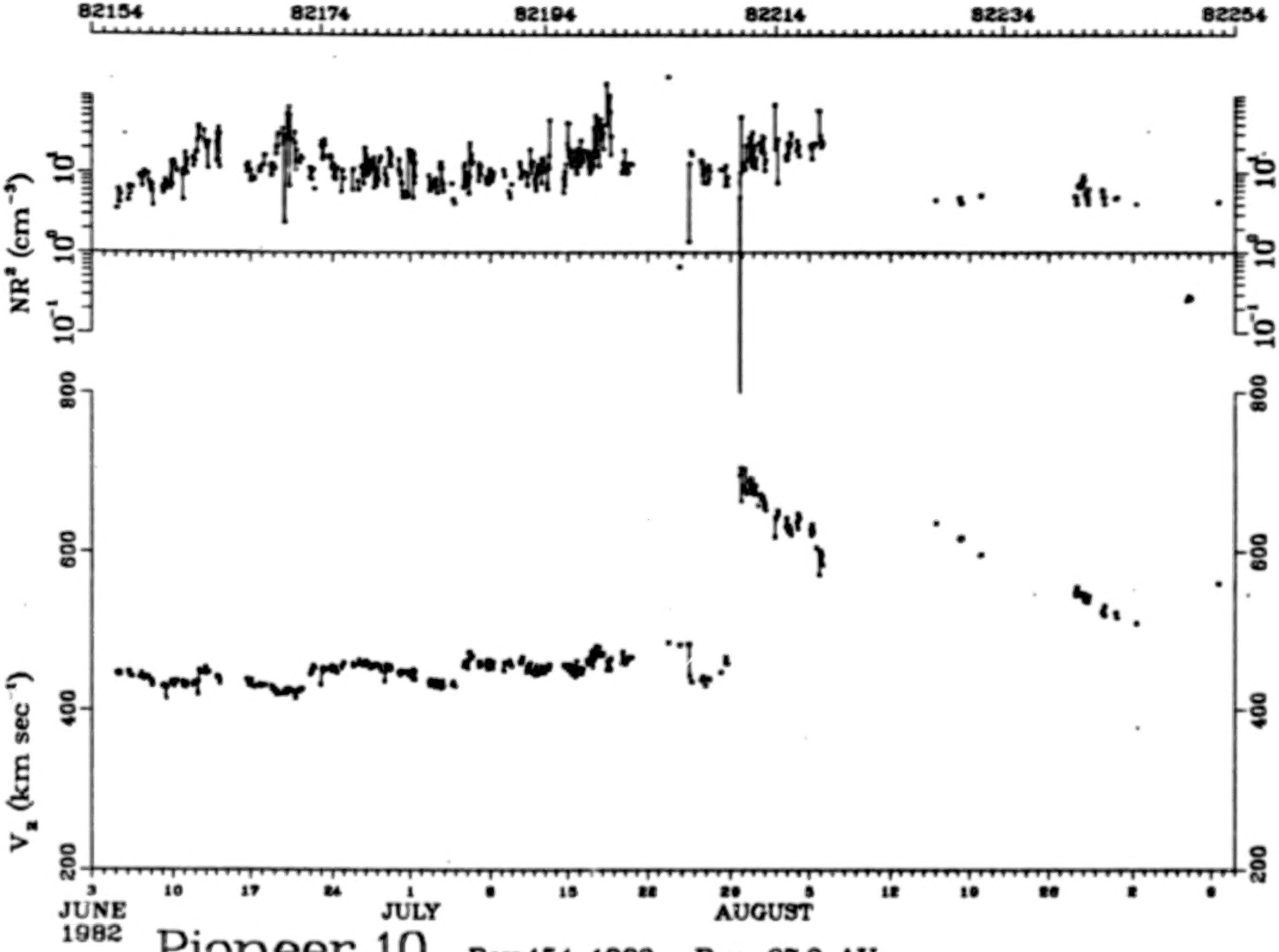

Pioneer 10 Day 154, 1982 R_o = 27.8 AU

Fig. 7

540

MAGNETOSPHERE, RINGS, AND MOONS OF URANUS

Andrew F. Cheng

Johns Hopkins University
Applied Physics Laboratory
Laurel, Maryland 20707

Abstract

The observation of an ultraviolet aurora on Uranus implies the existence of a magnetosphere. It is suggested here that the magnetospheres of Uranus and Saturn may be very similar. Charged particle sputtering of water ice surfaces on the Uranian moons may maintain an oxygen ion plasma torus similar to the heavy ion plasma torus at Saturn. Atmospheric cosmic ray albedo neutron decay may sustain an inner radiation belt with omnidirectional proton fluxes ~ 300 cm^{-2}s^{-1} above 80 MeV near 2.7 R_U. If the $\gtrsim 100$ keV ion fluxes near 7 R_U are similar to Saturnian ion fluxes at such energies, the Uranian aurora may be maintained by ion precipitation from the radiation belts at nearly the strong diffusion rate. This mechanism would predict comparable aurorae over both magnetic poles of Uranus, in contrast with the Faraday disc dynamo mechanism, which powers an aurora only over the sunlit pole of Uranus. Furthermore, if the $\gtrsim 100$ keV ion fluxes at Uranus are comparable to those at Saturn, any exposed methane ice surfaces on the moons and rings of Uranus would be quickly transformed by ion impacts to a black, carbonaceous polymer.

INTRODUCTION

The International Ultraviolet Explorer (IUE) spacecraft has recently detected intense H Lyman-α and H_2 1600 Å emissions from Uranus.[1-3] These are interpreted as auroral emissions implying the existence of a magnetosphere. A power input $\sim 2 \times 10^{11}$ W is required to maintain the H_2 emissions from Uranus, nearly equal to the power required to maintain the H_2 Lyman and Werner band emissions from Saturn's aurora.[3,4] The Faraday disc dynamo model[5] for a field-aligned current system in the Uranian magnetosphere suggests that a power input of $\sim 2 \times 10^{11}$ W to the sunlit pole of Uranus would require a Uranian magnetic moment ~ 7 G - R_U.[3] In this model, the field lines in the Uranian magnetotail are twisted into a spiral owing to the planetary spin and the solar wind interaction. The magnetosphere is assumed to be pole-on.[7] A field-aligned current system then flows into and out of the sunlit pole only.

In the Faraday disc model, the Uranian magnetosphere is considered to be uniquely different from the magnetospheres of Earth and Jupiter, in that both the solar wind interaction and the planetary rotation are important for the magnetospheric energy budget. Furthermore, the Uranian magnetosphere is viewed in this model as lacking significant internal sources of plasma when compared with Earth, Jupiter or Saturn, so that convection will be relatively unimportant.[5,6]

This paper will develop a different view which emphasizes possible similarities between the magnetospheres of Uranus and Saturn. It is proposed that the five known icy moons of Uranus lie within the magnetosphere, and that the resulting satellite source of plasma may be comparable to that at Saturn. It is also proposed that energetic ion fluxes above 100 keV at Uranus may be comparable to those at Saturn. If so, the Uranian aurora may be powered by ion precipitation, and ion bombardment of methane ice surfaces may account for the absence of methane ice spectral features on the Uranian moons and the very low albedo of the Uranian ring particles.[8,9,10]

PLASMA SOURCES

Voigt et al.[6] have already shown that the solar wind source and the ionospheric plasma source per unit volume of the magnetosphere should be weaker on the average at Uranus than at Saturn, using conventional scaling laws. These same scaling laws, however, indicate that all five known Uranian moons should lie within the magnetosphere. If the planetary dipole magnetic field, augmented by magnetopause currents, balances the solar wind dynamic pressure, then the magnetopause radius scales as $r^{1/3}B^{1/3}$, where r is distance to the sun and B is surface field. If L_M is magnetopause radius divided by planetary radius, then

$$\frac{L_M\ (\text{Uranus})}{L_M\ (\text{Earth})} \simeq \left[\frac{r_U}{r_E}\right]^{1/3} \left[\frac{B_U}{B_E}\right]^{1/3} \sim 4 \text{ to } 6, \tag{1}$$

for a Uranian surface field of 1 to 4 G. Since L_M (Earth) ≃ 10, the Uranian magnetosphere may have $L_M \sim 40$ to 60, approaching Jovian values.

The five known Uranian moons lie within 22.6 R_U, so all five should be within the magnetosphere. Recent spectroscopic observations show that all of these moons are covered with water ice mixed with an unknown dark material, and that three of the moons have a diameter larger than Dione, while two are larger than Rhea.[8] It is therefore natural to suggest that the satellite source of plasma at Uranus may be comparable to that at Saturn.

If the five large, icy moons of Uranus are exposed to magnetospheric charged particle fluxes, then sputtering of water ice surfaces would occur. For low temperature water ice, the sputter ejecta are primarily H_2O molecules. Nearly all the sputtered H_2O would be able to escape the gravity of the Uranian moons, as is the case at Saturn.[11] The escaping H_2O remains gravitationally bound to Uranus and forms a large neutral cloud in the magnetosphere.

Ionization and dissociation of this H_2O leads to injection of protons and oxygen ions. Very similar processes appear to maintain the heavy ion plasma torus near Tethys and Dione in the inner Saturnian magnetosphere.[12] A recent review of laboratory sputtering data and consequences for satellite-magnetosphere interactions is given by Cheng et al.[13]

At the icy moons of Saturn, sputtering by the corotating heavy ions is at least comparable to sputtering by more energetic ions $\gtrsim$ 100 keV. If the same is true at Uranus, a simple comparison can be made between satellite sources at Uranus and Saturn. For a Uranus rotation period of $16^h\ 10^m$ and a radius 2.6×10^9 cm, the plasma corotation velocity is 2.8 L km s^{-1}, with L in planetary radii. If R_i denotes the radius[8] of moon i, n_i the ion density, and Y_i the sputtering yield[13], then the source of H_2O from corotating ion sputtering would be from Ariel and Umbriel only

$$\dot{N}(H_2O) = \sum_i n_i\, Y_i\, \pi R_i^{\,2}\ (2.8\ L_i - 15\ L_i^{\,-0.5}) \qquad (2)$$

$$= 4.4\ \overline{nY} \times 10^{22}\ s^{-1},\ \text{Uranus.}$$

The analogous procedure for Tethys and Dione at Saturn yields

$$\dot{N}(H_2O) = 8.3\ \overline{nY} \times 10^{22}\ s^{-1},\ \text{Saturn.} \qquad (3)$$

Thus the H_2O supply rates from corotating ion sputtering would be comparable at Saturn and Uranus, given comparable average ion densities. Indeed, for

$\bar{n} \approx 30$ heavy ions cm^{-3} and $\bar{Y} = 10$ the source of H_2O is $\dot{N}_c\,(H_2O) \approx 2.5 \times 10^{25} s^{-1}$ at Saturn and $1.3 \times 10^{25}\ s^{-1}$ at Uranus. Each H_2O injected into the neutral cloud eventually yields roughly one O+, so the heavy ion source is $\dot{N}_c$ (O+) $\approx \dot{N}_c(H_2O)$.

The rate of energetic ion sputtering at Saturn is evaluated from Voyager 1 outbound data[14] which were taken at low magnetic latitude. The H_2O escape fluxes at Tethys and Dione are $\sim 1 \times 10^8\ cm^{-2}\ s^{-1}$ and $\sim 2 \times 10^8\ cm^{-2}\ s^{-1}$ respectively, assuming escape fractions[11] of ~ 0.8 and sputtering yields[13] of ~ 100 for oxygen ions on water ice. Energetic ion sputtering at Tethys and Dione then yields a source $\dot{N}_E(H_2O) \sim 10^{25}\ s^{-1}$. If energetic ion sputtering drives H_2O escape fluxes $\sim 10^8 cm^{-2} s^{-1}$ at Ariel and Umbriel, the source at Uranus would be $\dot{N}_E\ (H_2O) \sim 0.9 \times 10^{25}\ s^{-1}$.

These arguments suggest the presence of a substantial neutral H_2O cloud and oxygen ion plasma torus near 8 R_U. The sources of H_2O and O+ can each be comparable to those at Saturn, and the lifetimes may even be longer at Uranus than at Saturn. This is because photoionization and photodissociation rates will be reduced by about a factor of 4 at Uranus compared with Saturn. However, electron impact and charge exchange rates (for H_2O and O+) and radial diffusion (for O+) may be comparable at Uranus and Saturn.

With a substantial neutral cloud and plasma torus, efficient mechanisms exist for generation of energetic ion fluxes at Uranus. Charge exchange and electron impacts can yield fast oxygen atoms which escape to the outer Uranian magnetosphere. If these atoms are ionized there, they are "picked up" by the rotating magnetic field and achieve a gyrovelocity comparable to the local corotation velocity. An oxygen atom ionized at 40 R_U achieves ~ 1 keV. With inward radial diffusion conserving the first invariant, the oxygen ion achieves ~ 130 keV at 8 R_U. Similar mechanisms may operate at Jupiter[15,16] to maintain energetic ion fluxes there.

The solar wind source of protons also contributes to energetic ion fluxes. With a magnetopause radius of 50 R_U and a conventional capture efficiency of 10^{-3}, roughly 3×10^{25} protons s^{-1} enter the magnetosphere. This source is comparable to or greater than the anticipated satellite source of oxygen ions. Solar wind protons would enter the outer magnetosphere with energies ~ 0.8 keV, and inward radial diffusion would energize these protons to $\gtrsim$ 100 keV at 8 R_U.

Finally the ionospheric source of cold protons can be scaled as $(R/r)^2$ from Jupiter. For a Jovian source ~ 10^{28} s^{-1}, the Uranus ionospheric source is ~ 8×10^{25} s^{-1} of cold protons, much of which may escape as a polar wind. Uranus may have an Earth-like inner plasmasphere.

CRAND SOURCE

Cosmic ray impacts on the Uranian atmosphere create nuclear cascades there, from which energetic neutrons can escape into the magnetosphere. Beta decay of these neutrons yields energetic protons and electrons in the inner Uranian magnetosphere. Conventional scaling arguments[17-19] can be used to estimate the strength of this cosmic ray albedo neutron decay (CRAND) source at

Uranus. These scaling laws have been reasonably successful in characterizing the CRAND belts at Saturn based on knowledge of the Earth.

At Saturn, the dominant CRAND source is the main A and B ring system, which dominates atmospheric CRAND. At Uranus, the atmosphere will be dominant, as at Earth.

The Uranus atmospheric CRAND source is now scaled from the energetic albedo neutron flux at $L = 2.7$ above 80 MeV escaping the Earth's atmosphere, ~ 0.2 $cm^{-2}s^{-1}$. This flux is multiplied by 0.2 to take account of the mainly H_2 and He composition, and multiplied by 0.1 to take account of the higher Stoermer cutoff momentum $pc \propto BR \cos^4 \lambda$, where λ is latitude. Finally, an injection efficiency[19] of 0.05 is assumed near $L \sim 2.7$; this arises from the mismatch in phase space between outward streaming neutrons and gyrating protons. The proton source rate at $L \sim 2.7$ is then estimated as $\sim 2 \times 10^{-7}$ $cm^{-2}s^{-2}$ above 80 MeV. For a proton lifetime at Uranus of 40 yr., similar to that at Saturn[19], the proton flux would be ~ 300 $cm^{-2}s^{-1}$ above 80 MeV at 2.7 R_U. The CRAND source scales very roughly as the inverse fourth power of the radius, from two factors of solid angle (one for neutron flux, one for injection efficiency). The CRAND belt fluxes would decrease more rapidly with radius.

AURORA

It is now supposed, for the sake of argument, that the electron and ion fluxes at Uranus are generally similar to those at Saturn. The question is now whether precipitation of either ions or electrons from the radiation belts or plasma torus could then maintain the UV aurora of Uranus. At Earth, both ions and electrons are precipitated from various regions of the plasmasphere and radiation belts by interactions with electromagnetic and electrostatic ion and electron cyclotron waves. Pitch angle scattering at nearly the strong diffusion rate can occur for ring current ions, relativistic electrons, and auroral electrons, particularly during substorms. At Jupiter[20], the UV aurora may be powered by precipitation of energetic ions $\gtrsim$ 100 keV near $L = 7$ at nearly the strong diffusion rate. Significant precipitation of electrons ~ 1 keV and $\gtrsim$ 100 keV also occurs there.

The precipitating particle intensity j_P averaged over the loss cone can be estimated from the trapped particle intensity $j_T\ (E,\alpha)$ by[20]

$$j_P \approx \frac{\tau_{SD}}{\tau_L} \int_0^{\sim 1} j_T\ (E,\alpha)\ d \cos \alpha \tag{4}$$

where τ_L is the scattering lifetime and τ_{SD} the strong diffusion lifetime. It is now supposed that trapped electron and ion fluxes at Uranus are generally similar to those at Saturn, so measured Saturnian trapped fluxes can be used to estimate possible precipitation fluxes at Uranus.

Analyses of Voyager plasma wave data[22] and suprathermal electron data[23] at Saturn have already shown that wave particle interactions there produce only weak diffusion and negligible precipitation of $\gtrsim$ keV electrons. The same is true for electrons $\gtrsim$ 100 keV. It therefore remains to consider precipitation

BEST COPY AVAILABLE

of energetic ions $\gtrsim$ 100 keV. The scan averaged intensities of these ions as measured by Voyager 1 outbound near L = 7 at low latitude were[14]

$$j = 700\ (E/200)^{-5.3},\ E > 200$$

$$j = 700\ (E/200)^{-1.5},\ 40 < E < 200 \qquad (5)$$

where j is in $cm^{-2}s^{-1}sr^{-1}keV^{-1}$, E is in keV, and protons were assumed. On the other hand, if oxygens are assumed,

$$j = 60\ (E/550)^{-7.0},\ E > 550$$

$$j = 60\ (E/550)^{-3.0},\ 84 < E < 550 \qquad (6)$$

The oxygen value may be more appropriate, since oxygen apparently dominated the energetic ion fluxes within the inner magnetosphere.[14] This was inferred from the ratio of PLO5 ion rates to channel 32 proton rates at similar proton passbands.

If it is now assumed that energetic ion scattering occurs at nearly the strong diffusion rate, then the precipitation flux integrated over the loss cone is estimated by $2\pi j$, and the precipitation energy flux $\varepsilon = 2\pi \int j\, E\, dE$ above 40 keV for protons or 110 keV for oxygens becomes

$$\varepsilon = 0.4 \text{ erg cm}^{-2}\text{s}^{-1}, \text{ protons}$$

$$\text{or } \varepsilon = 0.8 \text{ erg cm}^{-2}\text{s}^{-1}, \text{ oxygens} \qquad (7)$$

This provides a reasonable upper limit to the energy flux deposited near L = 7 in Saturn's atmosphere. Indeed, intense ion cyclotron waves have been detected near the Dione L-shell.[24]

An upper limit $\varepsilon \sim 0.8$ erg $\text{cm}^{-2}\text{s}^{-1}$ is assumed for energetic ion precipitation in the Uranus auroral region. A total power input ~ 2×10^{11} W is required for 10 keV electron precipitation[4], and a greater power input ~ 4×10^{11} W would be required assuming energetic ion precipitation. The area of Uranus' sunlit auroral zone would then be at least $\gtrsim 5 \times 10^{18}\text{cm}^2$. This area would correspond to all latitudes above 62° on the sunlit hemisphere, which is not unreasonable. If the observed aurora on Uranus turns out to have a smaller area than $5 \times 10^{18}\text{cm}^2$, or if energetic ion scattering does not occur at the strong diffusion rate, then the required energetic ion fluxes at Uranus would be even greater than those at L = 7 for Saturn. Alternatively, of course, the Uranus aurora may be powered by an entirely different mechanism.

Finally, if the Uranian aurora is powered by energetic ion precipitation, then comparable UV aurora should exist over both poles of Uranus, with differences arising from the field line mapping to the two poles, the absence of solar Lyman α, and the different atmospheric structure. On the other hand, the Faraday disc dynamo mechanism[5] powers an aurora over the sunlit pole only.

The question of whether comparable aurorae exist over both poles of Uranus will be resolved by Voyager.

SPUTTERING AND DECOMPOSITION OF METHANE

The previous section suggested that if energetic ion fluxes at Uranus and Saturn are comparable, then the Uranus aurora could be powered by energetic ion precipitation. This section will show that Uranian energetic ion fluxes comparable to Saturnian fluxes may account for the absence of methane ice spectral features on the Uranian moons and the very low albedo of the Uranian rings. Blackening of the Uranian ring particles by ion impacts has already been considered[10]. Of course, absence of methane ice on the moons of Uranus can also be attributed to a high temperature at the time of their formation, which may have prevented condensation of methane.

Recent laboratory experiments[25] have shown that energetic ion bombardment of thin methane ice films causes decomposition of the methane as well as sputtering, with formation of a black carbonaceous residue. For 500 keV proton and 1.5 MeV alpha bombardment[25], a fluence of $\sim 10^{16}\mathrm{cm}^{-2}$ will transform CH_4 ice to CH_n with $n \approx 2$. Laboratory irradiation of benzene ice films with 0.1 - 1 MeV protons shows that fluences of $\sim 10^{16}\mathrm{cm}^{-2}$ cause substantial polymerization of the benzene[26]. Decomposition and polymerization of ices by ion impacts have important astrophysical implications.[25,26]

For definiteness, proton impacts are considered for energies $\gtrsim$ 100 keV. A fluence of $\sim 10^{16}\mathrm{cm}^{-2}$ suffices to blacken and polymerize any exposed methane ice surface to a depth $\gtrsim 10^{-4}$ gm cm^{-2}. More energetic protons would polymerize the methane to a greater depth. An incident energetic proton flux of $9 \times 10^5 cm^{-2}s^{-1}$, similar to the value observed by Voyager 1 outbound near Dione above 80 keV, would yield a fluence of $10^{16}cm^{-2}$ in ~ 400 yr. The incident flux above 80 keV measured by Voyager 2 at Saturn L = 2.75 was 3×10^5 cm^{-2} s^{-1}, which would yield $10^{16}cm^{-2}$ in ~ 1000 yr.

Thus any exposed methane ice surface at Uranus would be blackened and polymerized within 10^3 yr, if energetic ion fluxes there are comparable to those at Saturn. No such phenomenon would occur for H_2O ice surfaces there. Energetic ion bombardment of water ice[13] does create dissociation products O_2 and H_2, but these escape and leave behind a surface which is still H_2O ice. A water ice surface exposed to an incident energetic ion flux ~ $10^6cm^{-2}s^{-1}$ would thus be eroded at a rate ~ 1 m per 10^9 yr. A pristine methane ice surface would initially be eroded at a roughly comparable rate, but would also be decomposed and transformed within 10^3 yr to a black, carbonaceous polymer. In addition, methane ice sputtering would imply injection of carbon ions to the magnetosphere. These processes may well be important if fresh methane ice surfaces can be exposed at the Uranian moons and rings, for example, by micrometeroid impacts.

CONCLUSIONS

The arguments presented above are clearly speculative. If the five large, icy moons of Uranus are within the magnetosphere, it is natural to draw an analogy with the magnetosphere of Saturn. It is proposed that energetic ion fluxes $\gtrsim$

100 keV may be roughly comparable at Uranus and Saturn. If so, the Uranus aurora may be powered by energetic ion precipitation at nearly the strong diffusion rate, and intense UV aurora would be predicted over both poles of Uranus. With energetic ion fluxes approaching Saturnian values, any exposed methane ice surface in the Uranian magnetosphere would be blackened and polymerized within 10^3 yr by energetic ion impacts. The blackened surface layer is opaque in the visible and near IR, but becomes transparent in the far IR. A heavy ion plasma torus is predicted at Uranus, containing oxygens and perhaps also carbons. A CRAND belt and a proton plasmasphere may exist in the inner magnetosphere.

ACKNOWLEDGEMENTS

I am happy to thank S. M. Krimigis and L. J. Lanzerotti for providing data in advance of publication and for numerous useful discussions. This work was supported by NASA under Task I of Contract N00024-78-C-5384 between the Johns Hopkins University and the Department of the Navy.

REFERENCES

1. Durrance, S. T. and Moos, H. W., Nature, 299, 428 (1982).
2. Clarke, J. T., Ap. J., 299, L105, (1982).
3. Caldwell, J., Wagener, R., Owen, T, Combes, M. and Encrenaz, T., Tentative confirmation of an aurora on Uranus, Nature, 303, 310 (1983).
4. Sandel, B. R. and Broadfoot, A. L., Morphology of Saturn's Aurora, Nature, 292, 679 (1981).

5. Hill, T. W., Dessler, A. J. and Rassbach, M. E., Aurora on Uranus: A Faraday disk dynamo mechanism, Planet. Sp. Sci., 31, 1187 (1983).

6. Voigt, G. H., Hill, T. W., Dessler, A. J., The magnetosphere of Uranus: Plasma sources, convection, and field configuration, Ap. J., 266, 390 (1983).

7. Siscoe, G. L., Two magnetic tail models for Uranus, Planet. Sp. Sci., 19, 483, (1971).

8. Brown, R. H., Cruikshank, D. and Morrison, D., Diameters and albedoes of satellites of Uranus, Nature, 300, 423 (1982).

9. Sinton, W. M., Uranus: The rings are black, Science, 198, 503 (1977).

10. Cheng, A. F. and Lanzerotti, L. J., Ice sputtering by radiation belt protons and the rings of Saturn and Uranus, J.G.R., 83, 2597 (1978).

11. Lanzerotti, L. J., Maclennan, C. G., Brown, W. L., Johnson, R. E., Barton, L. A., Reimann, C., Garrett, J. and Boring, Jr., Implications of Voyager data for energetic ion erosion of the icy satellites of Saturn, J.G.R., 88, 8765

12. Cheng, A. F., Lanzerotti, L. J. and Pironelio, V., Charged particle sputtering of ice surfaces in Saturn's magnetosphere, J.G.R., 87, 4567 (1982).

13. Cheng, A. F., Haff, P. K., Johnson, R. E., and Lanzerotti, L. J., Interactions of magnetospheres with icy satellite surfaces, in Natural Satellites, ed. J. Burns and D. Morrison, in preparation (1984).

14. Krimigis, S. M., Carbary, J. F., Keath, E. P., Armstrong, T. P., Lanzerotti, L. J., and Gloeckler, G., General characteristics of hot plasma and energetic particles in the Saturnian magnetosphere: Results from the Voyager spacecraft, J.G.R., 88, 8871 (1983).

15. Cheng, A. F., Effects of Io's volcanoes on the plasma torus and Jupiter's magnetosphere, *Ap. J*, *242*, 812 (1980).

16. Eviatar, A. and D. Barbosa, Jovian magnetospheric neutral wind and auroral precipitation, *EOS*, *64*, 795 (1983).

17. Van Allen, J. A., Randall, B. A., and Thomsen, M. F., Sources and sinks of energetic electrons and protons in Saturn's magnetosphere, *J.G.R.*, *85*, 5679 (1980).

18. Fillius, W. and C. McIlwain, Very energetic protons in Saturn's radiation belt, *J.G.R.*, *85*, 5803, (1980).

19. Cooper, J. F., Nuclear cascades in Saturn's rings: Cosmic ray albedo neutron decay and origins of trapped protons in the inner magnetosphere, *J.G.R.*, *88*, 3945 (1983).

20. Thorne, R. M., Microscopic plasma processes in the Jovian magnetosphere, in *Physics of the Jovian Magnetosphere*, ed. A. J. Dessler, Cambridge Univ. Press (1984).

21. Cheng, A. F., Maclennan, C. G., Lanzerotti, L. J., Paonessa, M. T., and Armstrong, T. P., Energetic ion losses near Io's orbit, *J.G.R.*, *88*, 3936 (1983).

22. Scarf, F. L., Gurnett, D. A., Kurth, W. S., and Poynter, R. L., Voyager plasma wave measurements at Saturn, *J.G.R.*, *88*, 8971 (1983).

23. Sittler, E. C., Ogilvie, K. W., and Scudder, J. D., Survey of low energy plasma electrons in Saturn's magnetosphere: Voyagers 1 and 2, *J.G.R.*, *88*, 8847 (1983).

24. Smith, E. J. and Tsurutani, B. T., Saturn's magnetosphere: Observations of ion cyclotron waves near the Dione L-shell, *J.G.R.*, *88*, 7831 (1983).

25. Lanzerotti, L. J. and Brown, W. L., Ion bombardment of methane ice, *Proc. NATO Advanced Research Workshop on Ices in the Solar System*, Nice, France (1984).

26. Strazzulla, G., Calcagno, L., Foti, G., Polymerization induced on interstellar grains by low energy cosmic rays, *M.N.R.A.S.*, *204*, 59P (1983).

DO THE SATELLITES OF URANUS CONTROL ITS MAGNETOSPHERE?

A. F. Cheng[1] and T. W. Hill[2]

1 Johns Hopkins University
2 Rice University

In our separate contributions above, we have presented widely divergent views on the expected importance of the satellites of Uranus as sources of magnetospheric plasma. The purpose of this note is to elucidate this fundamental question and the ways in which it can be effectively addressed by Voyager.

We agree that neither an Io-like plasma source (associated with tidally-induced vulcanism) nor a Titan-like source (associated with a dense satellite atmosphere) is likely at Uranus. We have diverged on the question of the likely presence (Cheng) or absence (Hill) of a heavy-ion plasma torus maintained by charged particle sputtering of the icy satellites. Sputtering of Saturn's icy satellites (e.g., Tethys and Dione) is considered an important source of heavy-ion (oxygen) plasma in Saturn's inner magnetosphere. A major unresolved question is whether this sputtering process does (Hill) or does not (Cheng) depend on the pre-existence of magnetospheric heavy ions derived from another source, namely Titan.

This question can be resolved at Uranus, which has analogs to the small icy satellites of Saturn, but no analog to Titan. Our separate arguments presented above suggest two critical observations that Voyager can perform at Uranus to resolve this question: (1) a search for a heavy-ion torus in the inner magnetosphere (within about 20 planetary radii), and (2) a comparison of UV auroral emissions between the day side and the night side. A significant internal plasma source would produce a magnetically conjugate Jovian-type aurora on closed, internal magnetospheric field lines, whereas in the absence of a significant internal plasma source the aurora would be largely restricted to the day side polar cap.

Voyager observations at Uranus can thus close a major gap in our understanding of the plasma source mechanisms operating at Saturn. The resolution of this question will, in turn, determine whether the magnetosphere of Uranus represents a third example of the Jupiter-Saturn type dominated by internally-driven convection (Cheng) or the first example of a new class of magnetosphere dominated by the proposed disc dynamo interaction (Hill).

LYMAN-ALPHA AURORA

Samuel T. Durrance

Department of Physics, Johns Hopkins University
Baltimore, Maryland 21218

and

John T. Clarke

Space Sciences Laboratory
University of California, Berkeley

Abstract

The existence of intense and variable H Ly a emission from Uranus is demonstrated utilizing the monochromatic imaging capabilities of the International Ultraviolet Explorer satellite. A series of 14 observations, using the IUE short wavelength spectrograph in low dispersion and covering the period from 3 March 1982 through 2 September 1983, shows the disk averaged Ly a brightness of Uranus to vary between 690 and 2230 Rayleighs. Model calculations indicates that < 400 R of this emission can be attributed to resonant scattering of solar Ly a radiation. An upper limit of 100 R is obtained for the Raman scattering of solar Ly a by H_2 (1280 A). This implies that < 300 R is contributed to the planetary Ly a emission by Rayleigh scattering. In addition to being unexpectedly strong, the Uranian Ly a emission has been observed to vary by a factor of two in one 24 hr period and by about 50% in one 5 hr period. These data thus

offer the first strong evidence for the presence of aurora and therefore a magnetic field on Uranus.

Introduction

Spectroscopy of the outer planets at far ultraviolet wavelengths has progressed rapidly over the past few years with the advent of the International Ultraviolet Explorer satellite and the Voyager flybys of Jupiter and Saturn. Measurements of H Ly a emission (1216 A) from these planets has been a particularly useful tool to understand the physical conditions in their upper atmospheres and magnetospheres. The three principal excitation mechanisms to produce H Ly a emission from the outer planets are (a) resonant scattering of solar Ly a radiation, (b) Rayleigh scattering of solar Ly a radiation, and (c) charged particle excitation of atmospheric H and H_2. Each of these mechanisms provides complementary information on the physical state of the atmosphere.

Resonant scattering of solar Ly a photons by atmospheric H provides a direct measure of the atomic hydrogen column abundance above the lower UV absorbing layers. Atomic hydrogen is produced in the upper atmosphere by photodissociative processes and mixed downward by eddy diffusion. Methane is also produced photochemically in the upper atmosphere and mixed downward. The column abundance of H above an absorbing CH_4 layer can thus be used, in conjunction with model calculations, to determine the eddy diffusion coefficient and the level of the homopause in the atmosphere. Resonant scattering of solar Ly a photons has been observed from both Jupetir and Saturn.

Rayleigh scattering of solar Ly a photons by atmospheric H_2 is another plausible mechanism to produce planetary Ly a emission. At low spectral resolution (>2 A) this emission is indistinguishable from that produced by resonant scattering. Rayleigh scattering will, however, produce a Raman-shifted line at 1280 A with about 1/3 the intensity of the Rayleigh scattered line (Dalgarno and Williams, 1962, and Brandt, 1963). This Raman-shifted line can be used to determine the amount of Rayleigh scattering present at 1216 A. The Rayleigh scattering cross section is low (~ 10^{-24} cm^2), so it requires a large H^2 column density (~ 10^{24} cm^{-2}) above the absorbing CH_4 layer. Such large H^2 columns are not present on Jupiter of Saturn and the Raman-shifted emission at 1280 A has not been detected.

Charged particle excitation can produce Ly a emission by direct excitation of H or by dissociative excitatio of H^2. On Jupiter and Saturn this type of emission has been observed in both the polar aurorae and in the equatorial regions. Its presence is indicated by H_2 band emission and by the more varriable nature of particle precipation. This emission is a usefull indicator the level of magnetospheric activity and as a tool to study the dynamics of the magnetosphere.

Recently H Ly a emission from Uranus has been detected by three independent groups (Frike and Dauius, 1982, Durrance and Moos, 1982 and Clarke, 1982). Frike and Darius interpret their measurements as most likely due to resonant scattering of solar Ly a by H. The Hopkins and Berkely grogps, however, interpret their data as most likely due to auroral excitation. These data will be reviewed and newer observations will be presented in a hope to clarify the situation.

Observations

In the spring of 1982 two research groups, one at Johns Hopkins University and one at the University of California Berkely, began observational programs to search for H Ly a emission from Uranus and Neptune. The observational techniques used take advantage of the monochromatic imaging capabilities of the IUE short wavelength spectrograph. The large entrance aperture of the spectrograph has a projection onto the sky of about 10 x 20 arc sec as indicated in the upper portion of figure 1. The disk of Uranus, which has a diameter of about 3.8 arc sec, was imaged into the center of this aperture as is also indicated in figure 1. The background geocoronal and interplanetary Ly a emissions are varriable on both short and long time scales; however, they are spatially uniform over scale lengths comparable to that of the aperture so it should be possible to resolve the planetary Ly a emission from that of the background. The file with line by line spectra from the standard NASA/IUE data package (in which a data point corresponds to an area 1.1 arc sec in the dispersion direction and 2.1 arc sec high) was used to obtain a two-dimensional plot of the focal plane flux. A projection of the resulting data set at Ly a is shown in figure 1. The dispersion direction is parallel to the axes pointing downward and to the right. Figure 1a shows an exposure taken about 3 arc min south-west of the planet and thus contains background Ly a emission only. Figure 1b shows an exposure with Uranus centered in the aperture, so it contains both planetary and background Ly a emissions. The planetary emission is clearly resolved from the background emission. There are curently about 30 Uranus observations of

564

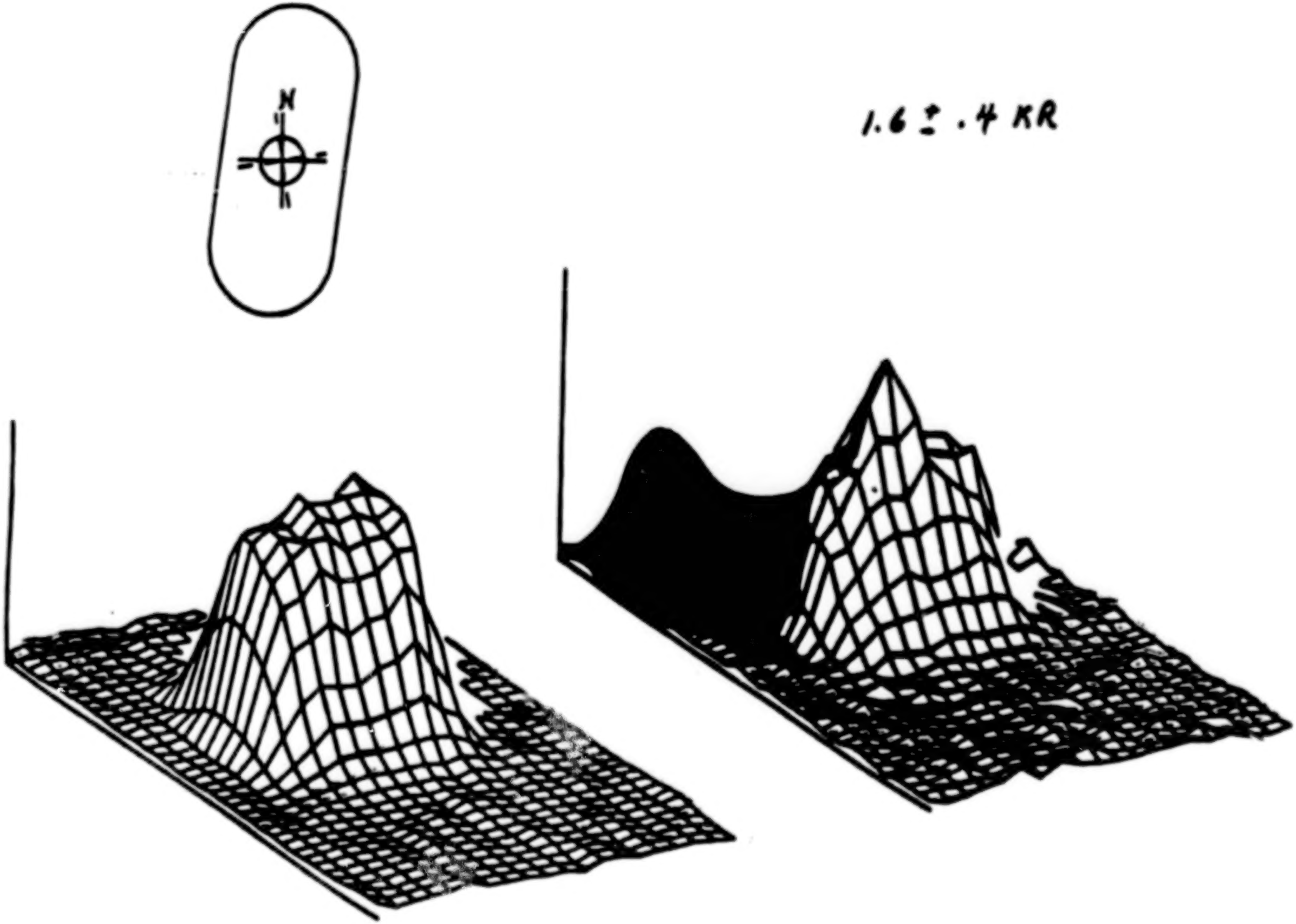

1.6 ± .4 KR

this type scattered throughout the period from 3 March 1982 to 2 september.

The Uranian Ly a brightness is obtained from these data by the following process. The two or three uranus exposures obtained in a given 8 hr IUE shift are combined into one. The exposure with background emission only is scaled to match the background contribution to this combined exposure and the two data sets are subtracted. The resulting array is summed over a region about 9 arc sec diameter, which is centered on the planetary emission, to give the total measured planetary Ly a signal in IUE flux numbers. This summing region is chosen to include all of the flux from the ~ 4 arc sec planetary disk after convolution with the ~ 5 arc sec point spread function of the instrument. This is converted to a disk averaged brightness using the absolute calibration of the SWP camera given by Bolin et al (1980) and the size of the Uranian disk at the time of the observations as given in the Astronomical Almanac.

The data from Clarke (1982) were analized in a somewhat different manner. The photometrically corrected image segment from the standard NASA/IUE data package was used instead of the line by line file. This file should provide somewhat better spatial resolution. There is, however, a transformation necessary to convert the photometrically corrected image data into the IUE flux numbers in which the absolute calibration is given. When the IUE image processing system was changed in 1980 to increace the digitation of the low dispersion spectra by a factor of 2 this transformation was normalized by a factor of 2 (Turnrose, 1980) so that the same calibration could be used. The Ly a brightnesses of Uranus given by Clarke (1982) should thus be increaced by a factor of 2 to account for this.

The Ly a brightness of Uranus from the above analysis plotted as a function of time in figure 2. The data shown as squares are from Durrance and Moos (1982) and several subsequent observations analyzed using the same technique. The data shown as diamonds are from Clarke (1982) but they have been increaced by a factor of 2 to account for the propper normalization. Two additional observations by Clarke are also shown as diamonds. The largest uncertianty in these measurements is a systematic error introduced by the background subtraction and is estimated to be + 20%. However, it is estimated that extracting different images by this method introduces a relative error of < 10%. The quoted uncertainty in the IUE calibration is 2s = 15% in a 25 A band at 1216 A (Bolin, et al. 1980), and the instrument has been determined to be stable in time to within this uncertainty by observing standard stars. The systematic error in the background subtraction and the uncertainty in absolute calibration are not shown in figure 2; only the relative error between different observations is shown. A variability by as much as a factor of 3 on relativly short time scales is clearly indicated by these data.

BEST COPY AVAILABLE

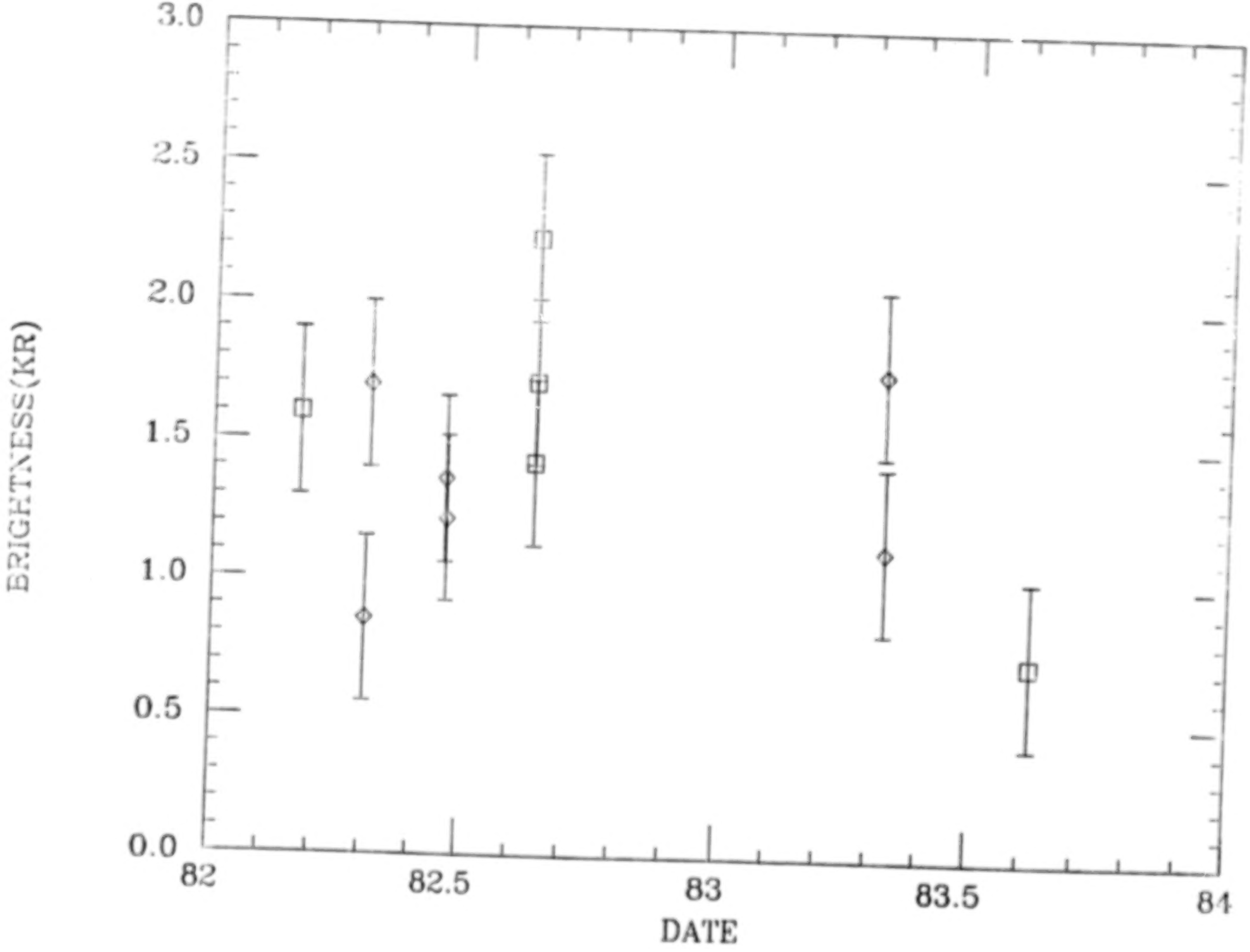

Discussion

The data presented here clearly show Uranus to be an intense and highly variable source of H Ly a radiation. To understand this emmision we will now address the three most plausable excitation mechanisms. First consider the resonant scattering of solar H Ly a photons by an optically thick layer of atomic hydrogen in the upper atmosphere. There is evidence that CH_4 is condensed out of the atmosphere on Uranus at the temperature minimum (danielson, 1977). This could provide a larger column of H than one would expect based on analogy with Jupiter and Saturn. However, since both H and CH_4 are produced photochemically in the upper atmosphere and mixed downward and since the solar flux at Uranus is relatively weaker, it is difficult to produce the large H column required to explain the high Ly a brightness by resonant scattering. Detailed model calculations by Atreya and Ponthieu (1983) and by Atreya (this volumn) show that for a range of model parameters the expected H column density above an absorbing CH_4 layer is ~ 5×10^{15} cm^2. A simple model for the resonantly scattered emission was presented by Clarke (1982). The two curves of growth from that model are presented in figure 3; this model assumes monochromatic scattering in a plane-parallel isothermal layer with a completely absorbing lower boundry. This is an idealization but should b adaquate for our purposes here. For the lower temperature model, which appears more reasonable, the above column of H would produce a Ly a brightness of ~ 100 R considerably less than the 2.1 KR of the highest brightness observed. To produce this level of Ly a emission via resonant scattering would require an H column density in excess of 10^{18} cm^2 which seems unlikely.

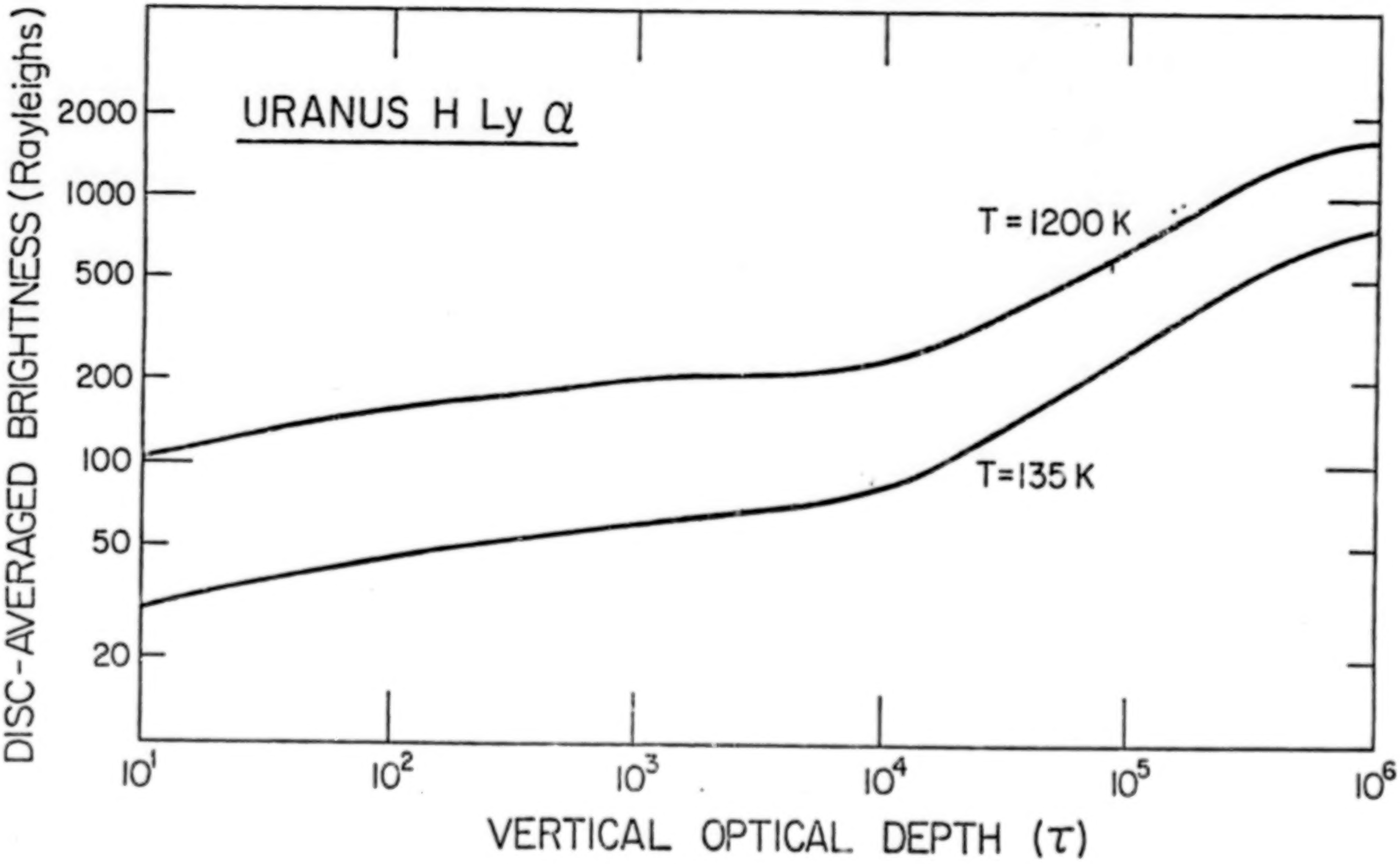
URANUS H Ly α
T = 1200 K
T = 135 K
DISC-AVERAGED BRIGHTNESS (Rayleighs)
2000
1000
500
200
100
50
20
10^1
10^2
10^3
10^4
10^5
10^6
VERTICAL OPTICAL DEPTH (τ)

If an extended H atmosphere existed, as a result of a hot hydrogen corona for example, then our conversion of the measured flux to a disk averaged brightness would be an over estimate. Two things argue against this. First, the size of Uranus' image in these observations is ~ 5 arc sec which is the same size as the point spread function of the telescope. If Uranus were emitting over an area much larger than the visible disk then it would show up as a more extended image. Second, calculations using a 60,000 K hydrogen corona (Shemansky and Smith, private communication) show that the optically thick H column would extend out to $< 1.1\ R_u$. This would reduce the derived disk averaged brightness by only about 15%.

If CH_4 is condensed out of the atmosphere, Uranus may have a deep H_2 atmosphere and thus Rayleigh scattering could be an important contributer to the Ly a brightness. However, the Rayleigh scattering cross section is $\sim 10^{-24}\ cm^2$ (Dalgarno and Williams, 1962) and the model calculations of Atreya (this volumn) give $N(H_2) \sim 10^{15}\ cm^{-2}$ so this mechanism is probably not important. Also, in a sum of several long low dispersion IUE exposures using the small aperture an upper limit to the Raman-shifted emission of < 30 R is set (Frike and Darius, 1982). This sets an upper limit to the Rayleigh scattered Ly a emission of < 100 R.

Charged particle excitation by direct impact of solar wind particles on the Uranian disk could also produce H Ly a emission. If one assumes an average velocity of 400 Km/sec for solar wind protons and an average excitation energy of 12 eV per emitted photon and in addition that the entire disk captures and converts these protons to UV photons with 100% efficiency, then the resulting Ly a bribhtness would be < 50 R. There does not appear to be enough energy available for this process to be important.

An auroral emission from a zone between 80 and 90 degrees latitude and centered on the Earth facing pole would be able to produce the observed Ly a emission if the average surface brightness of this aurora were ~ 15 KR. This is comparable in brightness to the aurora observed on Jupiter and Saturn. Recent theoretical calculations by Hill, Dessler and Rassbach (1983) indicate that, if Uranus has a magnetic field, it will have an aurora that is highly variable in response to variations in the solar wind velocity. The highly variable nature of the Uranian emission is indicative of this type of emission. If the brightest emission observed is interpreted as intitely due to auroral particle precipatation, the required power is estimated to be ~ 3 x 10^{11} W using a 5% conversion efficiency (Gerard and Sing, 1981). This amount of power could be supplied by a magnetospheric interaction with the solar wind (Hill, Dessler, and Rassbach).

Conclusions

Intense and highly variable H Ly a emission has been observed fron Uranus. The disk averaged brightness is seen to vary between 717 R and 2.1 KR. Resonant scattering of solar Ly a by atmospheric H appears insufficient to explain this emission; model calculations limit this contribution to the Uranian Ly a brightness to < 400 R. Rayleigh scattering also is insufficient and an upper limit to this contrabution was derived to be < 100 R. Auroral precipatation of charged particles is the most likely cause of this emission. This implys that Uranus has a magnetic field and thus a magnetosphere. The required input power to the aurora is about 3×10^{11} W.

PART VI

Ring Systems

BLANK PAGE

THE STRUCTURE OF THE URANIAN RINGS AND THE SEARCH FOR RINGS AROUND NEPTUNE

James L. Elliot
Department of Earth, Atmospheric, and Planetary Sciences
Department of Physics
Massachusetts Institute of Technology
Cambridge, MA 02139

Abstract

The nine narrow rings of Uranus, presently the only confirmed features of this system, have been observed with the diffraction-limited resolution (3.5 km) of ground-based occultations since their discovery in 1977. These data have been used to establish an orbit model, from which the five Keplerian orbit parameters for each ring, the pole of the mean ring plane, and the gravitational harmonic coefficients J_2 and J_4 have been determined. The rings are typically a few kilometers wide with eccentricities of about 10^{-3} and inclinations of a few hundredths of a degree, although a few have no measurable eccentricity or inclination. Interesting Voyager investigations would include probing the structure of the rings at higher spatial resolution, searching for new rings in the system (including inter-ring material), locating the postulated shepherd satellites, and searching for satellites inside the orbit of Miranda that might have dynamical influence on the rings. The high precision (~2 km) of the ring orbits might prove useful for spacecraft navigation. For Neptune, occultation searches have revealed no rings to a limit of a few hundredths optical depth, within a few hundred kilometers from the top of the planet's atmosphere (for equatorial rings).

INTRODUCTION

Virtually all of our knowledge about the kinematics of the Uranian rings has been derived from observations of 13 stellar occultations during the past seven years. These data have a limiting sensitivty of a few hundredths in optical depth and can resolve structural features separated by 3.5 kilometers. The location of a ring feature can be established with a precision of about 0.1 kilometer. Within these sensitivity limitations, the confirmed features of the Urnaian system are nine sharp-edged, narrow ringlets; some are elliptical and/or inclined. The general appearance of this system contrasts markedly with the elaborate rings of Saturn and the tenuous ring of Jupiter.

This review presents an overview of our present understanding of the structure and kinematics of the system, with an emphasis on current problems that hold promise of successful attack by Voyager investigations. The photometric properties of the rings are being reviewed at this conference by Phil Nicholson. Together we have written a complete review of the Uranian rings[1], soon to be published. For the kinematics, our earlier review remains current qualitatively and presents a much more exhaustive description of the system than I am giving here. To keep abreast of the most recent numerical values of the parameters describing the Uranian system, one should obtain current and future publications of the three groups actively working in the field: the Cornell-Caltech consortium (Nicholson, Matthews et al.); the group at the Observatory of Paris (Sicardy, Brahic et al.); and my group at M.I.T. (Elliot, French et al.).

These same groups, along with Bill Hubbard's group at the University of Arizona, have also been active in using occultation techniques to search for rings around Neptune. These seaches have been extensive, but have revealed no rings.

STRUCTURE

An overview of the Uranian ring system is shown in the diagram of Fig. 1, where we can see that all the known rings lie within the synchronous orbit and the Roche limit for a body of density 2.0 gm cm^{-3}. The widths and optical depths of the rings are summarized in Table I. The α, β and ϵ rings have widths proportional to their local radii, which is strong evidence that all particle orbits in these rings precess as a unit--a phenomenon known and "uniform precession". Unless they are presently disrupting, the other

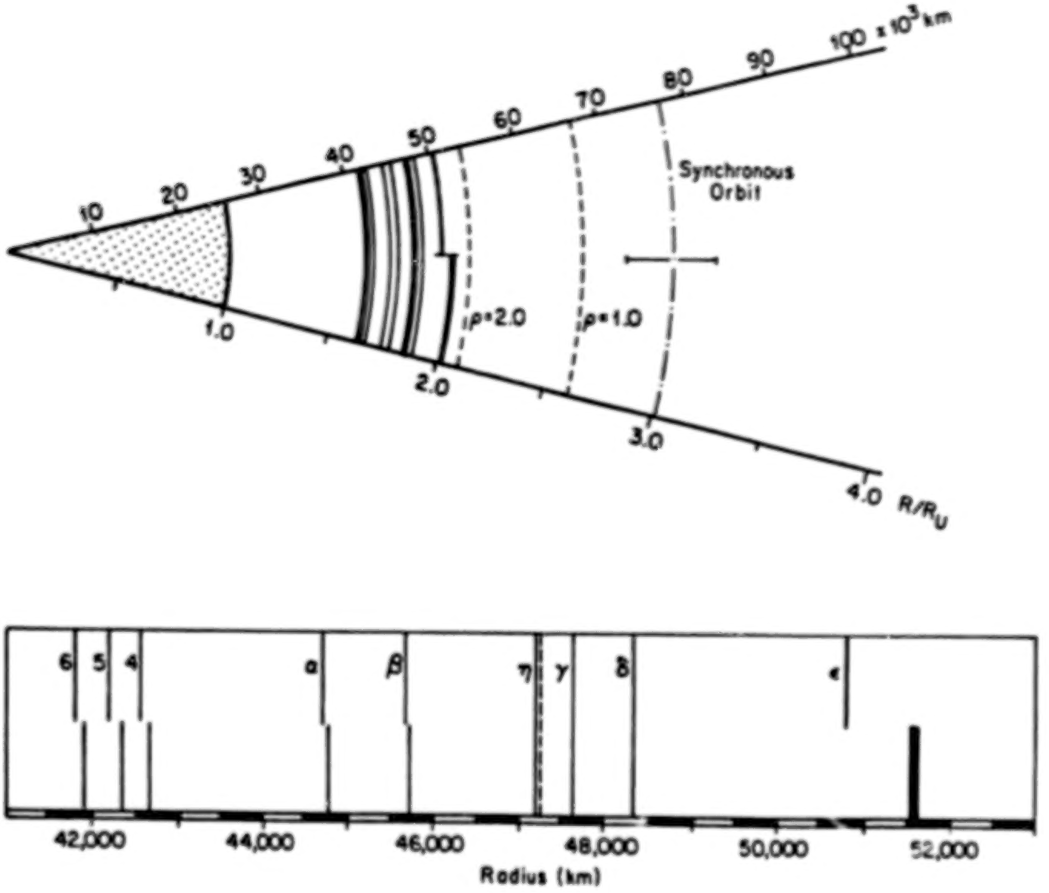
10
20
30
40
50
60
70
80
90
100 × 10³ km
Synchronous Orbit
ρ=2.0
ρ=1.0
1.0
2.0
3.0
4.0 R/R_U
6
5
4
α
β
η
γ
δ
ε
42,000
44,000
46,000
48,000
50,000
52,000
Radius (km)

Fig. 1. Schematic diagram showing the locations of the nine confirmed rings of Uranus. The dashed arcs represent the Roche limits for satellite densities of 1.0 and 2.0 g cm^{-3}, while the dot-dashed arc corresponds to the synchronous orbit distance for a planetary rotation period of 15.6 ± 1.4 hr. The lower portion of the diagram shows the radial region which spans the known rings, enlarged by a factor of 10. For each of the 6 definitely eccentric rings both the minimum (periapse) and maximum (apoapse) radii are indicated. The width of the ε ring, which varies markedly from periapse to apoapse, is plotted to scale: the other rings all have widths of <10 km, below the resolution of this figure. The outer boundary of the η ring's broad component is indicated by a dashed line. (Figure from reference 1.)

TABLE I

Ring Structures

Ring	Radial Width[1] (km)	Normal Optical Depth	Confirmed Structural Features
6	0.4 - 2	>0.5	---
5	0.8 - 2	>1.0	---
4	0.7 - 2	>0.8	---
α	5 → 10	~1.4 → 0.7	"Double-dip" structure at widest part.
β	5 → 11	~1.5 → 0.35	---
η	0.5 - 2[2]	>0.6	Broad component terminated by a 2nd narrow ringlet ~55 km outside principal component.
γ	~3	>1.5	---
δ	2 - 3	>1.5	2nd Component ~12 km inside.
ε	20 → 96	? → 1.2[3]	Consistent internal structure, sharp edges.

Notes

[1] → indicates established width variation, otherwise a range of possible widths is given.

[2] Narrow component.

[3] Optical depth of narrowest part of the ε ring is too high to be reliably measured.

(Table from reference 1.)

elliptical rings also precess uniformly (and the nodes of the inclined rings regress uniformly), but no width-radius relations have yet been established for rings other than α, β and ϵ. Several mechanisms that could produce the uniform precession were investigated by Goldreich and Tremaine[2], who conclude that self-gravity is the most likely cause--an explanation not universally accepted[3]. If self-gravity is the mechanism producing the uniform precession, then masses can be derived from the observed orbital parameters of the rings. The masses given in reference 1 are: α ring, 2.6×10^{16} gm; β ring, 1.4×10^{16} gm; ϵ ring, 4.9×10^{18} gm.

Within the diffraction limited resolution of our present data, the occultation profiles of the rings can be described to a good approximation by a "square-well" model, which has abrupt edges and transmits a fraction of light that remains constant across the width of the ring. As can be seen in Figs. 4-8 of reference 1, several of the rings have occultation profiles that exhibit structure beyond that of the square-well approximation. The ϵ ring has an undulating optical depth structure that becomes apparent at the widest part of the ring, and it also shows several features at the limit of our present spatial resolution. Also at its widest part, the α ring profile exhibits two peaks separated by 4 km, perhaps indicating two components. The η ring has two components--broad and narrow--that produce an occultation profile that closely resembles, in both optical depth and spatial extent, that obtained by the PPS for Saturn's F ring[4]. The inner edge of the β ring may not be as abrupt as its outer edge, and the δ ring has a second component of lower optical depth located about 12 kilometers closer to Uranus than the main ring.

The occultation profiles observed at optical and infrared wavelengths show no obvious difference, which indicates that the ring opacities are not dominated by micron-sized particles.

ORBITS

For each occultation event we obtain precise relative positions of the occulting segments for each of the nine rings. Our orbit model allows each ring to be an ellipse, which may be inclined to the equatorial plane of Uranus, and the rings precess due to the harmonics of the Uranian gravity potential. This model has been fit by least squares to our occultaiton data set; the free parameters of the model are:

- a, e, and i for each ring.
- The longitude of periapse (ω_0) and the longitude of the ascending node (Ω_0) for each ring at a specified epoch (10 March 1977 at 20^h UT).
- The right ascension and declination (α_p and δ_p) for the rotation pole of Uranus.
- J_2 and J_4 for Uranus.
- Corrections in right ascension and declination ($\Delta\alpha$ and $\Delta\delta$) to the coordinates of each occulted star.

The results of the latest published fit[1,5] are given in Table II. The precision of the model has been continually increasing as the model has been improved. However, the rms residual of 0.1 seconds of the ring occultation midtimes from the model exceeds the precision with which we can determine the midtimes from a ring occultation profile by an order of magnitude. This large discrepancy indicates that our model for the ring orbits is not yet complete. The missing effect(s) could prove as interesting as yet unmodeled perturbations on the ring orbits, or as uninteresting as timing errors in some

BLANK PAGE

BLANK PAGE

BLANK PAGE

TABLE II

Fitted Model Parameters[1,2]

(a) Orbital Elements

Ring	Semi-Major Axis a (km)	Eccentricity $e \times 10^3$	Azimuth of Periapse ω_0 (degrees)[3]	Inclination i (degrees)	Azimuth of the Ascending Node Ω_0 (degrees)[3]
6	41877.3 ± 16.6	1.01 ± 0.10	243.6 ± 3.6	0.066 ± 0.012	15.7 ± 4.4
5	42275.2 ± 16.6	1.85 ± 0.08	170.1 ± 2.5	0.050 ± 0.010	288.5 ± 9.1
4	42609.6 ± 16.8	1.15 ± 0.04	125.3 ± 3.0	0.022 ± 0.005	117.2 ± 24.7
α	44758.3 ± 16.4	0.78 ± 0.02	329.4 ± 2.3	0.017 ± 0.003	65.4 ± 13.6
β	45701.0 ± 16.5	0.43 ± 0.02	223.9 ± 2.8	0.006 ± 0.002	296.3 ± 41.0
η	47214.9 ± 16.5	(0.03 ± 0.04)	(129.0 ± 58.0)	(0.003 ± 0.004)	(263.0 ± 117.7)
γ	47666.3 ± 16.4	(0.04 ± 0.02)	(84.0 ± 22.3)	0.006 ± 0.002	100.2 ± 31.1
δ	48338.7 ± 16.5	0.06 ± 0.02	135.1 ± 15.8	0.012 ± 0.003	299.0 ± 11.5
ε	51188.1 ± 17.0	7.94 ± 0.02	214.9 ± 0.4	(0.003 ± 0.003)	(242.9 ± 29.5)

(b) Harmonic Coefficients of the Gravity Potential[4]

$$J_2 = (3.349 \pm 0.005) \times 10^{-3}$$
$$J_4 = (-3.8 \pm 0.9) \times 10^{-5}$$

(c) Pole of the Ring Plane

$$\alpha_{1950.0} = 5^h\ 06^m\ 29\overset{s}{.}4 \pm 5\overset{s}{.}3$$
$$\delta_{1950.0} = +15^\circ\ 14'\ 10'' \pm 1'31''$$

[1] For $M_U = 8.669 \times 10^{28}$ gm and $G = 6.670 \times 10^{-8}$ dyn cm^2 gm^{-2}.
[2] This tabulation is for the model of French *et al*. (1982).
[3] At 20:00 UT on 10 March 1977.
[4] For a reference radius, R = 26,200 km.

(Table from reference 1.)

of the data.

A plot of the eccentricities and inclinations of the rings versus their semi-major axes is shown in Fig. 2. With the exception of the ε ring, the inclination of each ring (in radians) is nearly equal to its eccentricity, and these quantities follow a decreasing trend with semi-major axis. No explanation for this trend has yet been offered. Also, no convincing relation between the semi-major axes of the rings and resonances with the five known satellites has been established[6].

PROBES OF URANUS

As part of the orbit solution, we obtain the coordinates of the Uranian pole and values for the coefficients, J_2 and J_4, of the Uranian gravity potential (see Table II). Also, the rings serve as a fiducial "target" that we use for obtaining the equatorial radius and oblateness of Uranus. As discussed by Dick French at this conference and in reference 1, the oblateness and the harmonic coefficients can be used to derive the rotation period of Uranus under the assumption of hydrostatic equilibrium. Although this assumption is not strictly valid, we expect the derived rotation period to be reliable in view of the close agreement of the rotation periods derived in this manner with those directly measured for Jupiter and Saturn[1].

CURRENT WORK

With the ultimate goal of learning the origin of the rings and how they evolved to their present state, our current work is aimed at the more immediate task of confronting dynamical models with our continually increasing set of occultation data. Progress along these lines should lead to an understanding of their present dynamics, which might allow enough extrapolation into the past to make an educated guess about their origin.

The most widely accepted model for the Uranian ringlets is the shepherd satellite model of Goldreich and Tremaine[7], which has been developed to explain the eccentricities[8], inclinations[9], and sharp edges[10] of narrow rings. To account for the uniform precession of narrow rings, the self-gravity model[2], along with some effects of collisional dissipation near periapse[3], has become our working hypothesis.

The effects of shepherd satellites could show up in occultation data in three ways. First, a shepherd satellite could occult a star. To estimate the likelihood of detecting such an occultation, we postulate the minimum of ten shepherds to confine the nine rings and assume that each satellite is about ten kilometers in diameter. Then for a given event, a single station would have a probability of about 1.5×10^{-3} of detecting an occultation by a shepherd satellite. Considering all observations to date[1], the probability of having detected a shepherd is about 0.04. Two less direct (but more likely) ways to confirm the existence of the shepherd satellites would be to observe their perturbing effects on the shapes and precession rates of the rings[6]. In fact, the unaccountably large residuals of the occultation timings from our orbit model could be caused by perturbations of the ring orbits by shepherd satellites. However, before we can conclude that perturbations are causing the large residuals, we must carefully eliminate all other possible effects. Eventually, the perturbing effects of the shepherds (if they exist) should be detectable, since the precision of the precession rates improves even faster than in inverse proportion to the time interval spanned by the occultation

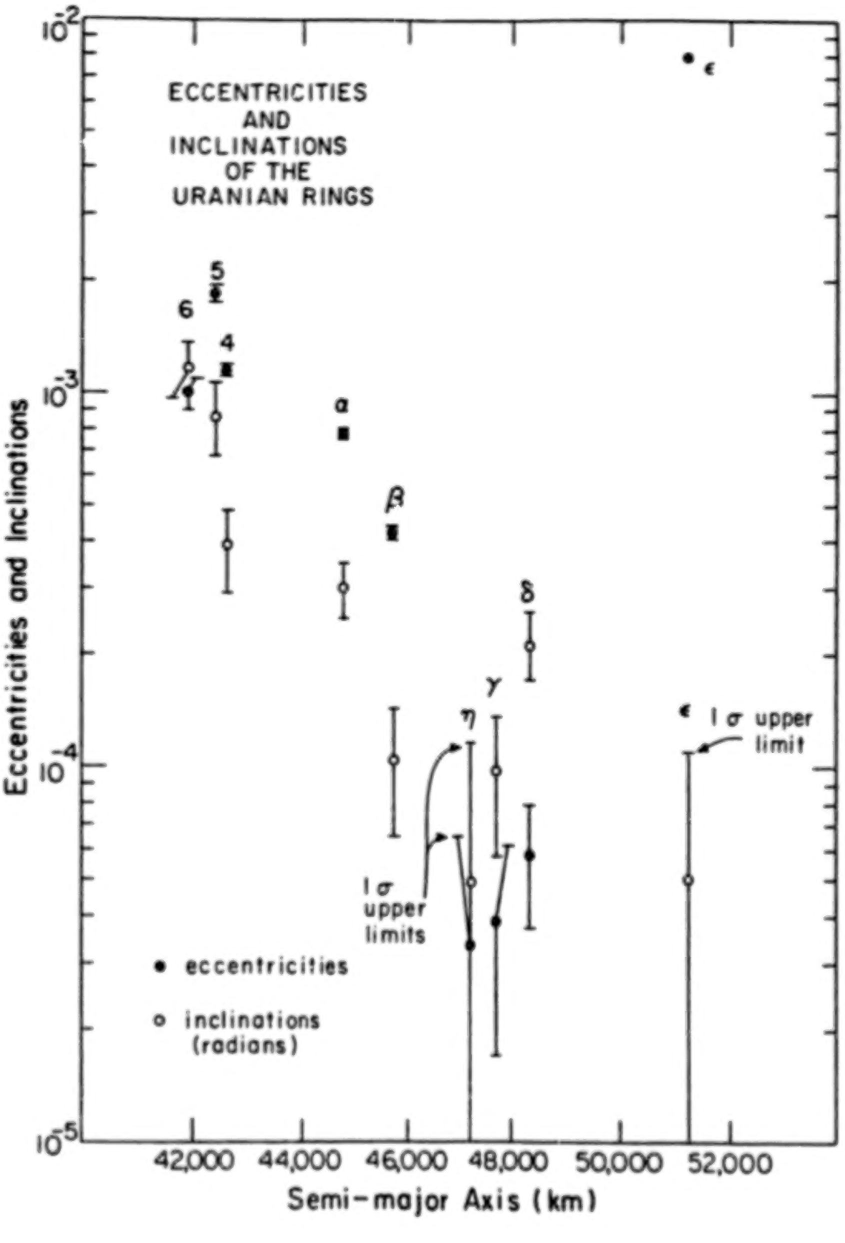

Fig. 2. Eccentricities (●) and inclinations (○) of the Uranian rings. The eccentricity and inclination (in radians) for each of the nine presently known rings is plotted against the semimajor axis. Except for the eccentricity of the ε ring, the e's and i's show a decreasing trend with increasing semimajor axis. The eccentricities of the η and γ ring, as well as the inclinations of the η and ε rings, are not large enough to be statistically significant (Figure from reference 5.)

data.

In addition to improving the orbit model, we are working on several problems involving the structure of the rings. At the DPS meeting last fall, Phil Nicholson reported on his search for a difference between the periapse of a ring and the orbital longitude of its minimum width. Finding a definite difference could provide information about dissipative processes within a ring. We have been also interested in testing the self-gravity model for the ε ring by comparing the shapes of the occultation profiles observed at different orbital longitudes against predictions of the model[2]. Dick French described his results[12] on this project, which are not yet conclusive. Right now, Dick and I are fitting a square-well model to the ring profiles by least squares, from which we expect to obtain more accurately determined ring widths, transmissions, and occultation midtimes--along with their errors. These results will allow us to establish more rigorous constraints on the optical depth of the rings as a function of wavelength; to investigate the widths of the rings as a function of their orbital longitudes; and to determine whether the particles producing most of the ring opacity form a monolayer. The square-well model also provides a first-order approximation to the ring structure, which can be used as a basis for establishing more sophisticated descriptions of the ring structure.

SUGGESTED VOYAGER INVESTIGATIONS

With the notable exception of the interval of time coverage, which provides the basis for our orbit model (see Table II), the capabilities of the Voyager instruments for observing the rings are substantially superior to what has been available from Earth. Hence we can anticipate some exciting discoveries that will produce significant strides in our understanding of this unique ring system. Several investigations come to mind:

1. Search for additional rings and inter-ring material. The much greater sensitivity of imaging observations to rings of low optical depth, compared with occultations, suggests the need for a survey of the system with moderately long exposures. Inter-ring material must exist, at some level, since dissipative forces--proportional to particle area--will cause the smallest particles to overcome the confining gravitational force, which is proportional to the particle volume.

2. Observe all rings with high spatial resolution. The occultation profiles of the rings show diffraction effects, indicating structure on scales below the 3.5 km resolution limit of Earth-based occultations. The widths and structure of the α and ϵ rings, as well as the width of the β ring, varies with orbital longitude; at higher spatial resolution, the orbital longitude variation may hold for all rings.

3. Test the self-gravity model for the ϵ and other rings. According to the self-gravity model, knowledge of the radial mass distribution at one orbital longitude can be used to predict the radial mass distribution at any other orbital longitude. The change in shape of the mass distribution is greatest near periapse; a minimum of two profiles would be necessary to test the model^{2}.

4. Investigation of the particle size distributions. As was done for Saturn's rings, the phase function of the ring particles and their occultation profiles observed over a range of wavelengths can be used to constrain the distribution of particle sizes for each ring.

5. Tying together the ring orbit and satellite orbit reference systems. The satellite orbits and ring orbits have been determined by different methods, so that their relation is not well known. In fact, the rotation pole of Uranus determined form the satellite orbits^{13} and that determined from the ring orbits differ by several standard deviations.

6. Search for inner satellites. The rings may be influenced by small satellites that have orbits between Miranda and the ϵ ring. Their discovery would add to our understanding of the ring dynamics.

7. Search for shepherd satellites. Location of the shepherd satellites would confirm this model for the Uranian rings; an extensive, unsuccessful search would require a new explanation for the narrowness of the rings.

The reference system defined by the ring geometry might prove useful for spacecraft navigation or determining the trajectory after the encounter.

Although our present values for J_2 and J_4 (obtained from the ring orbit solution) are already more precise than can be determined from analysis of the spacecraft trajectory[14], the accuracy of these quantities could be improved with the more accurate value of GM that will be obtained from the trajectory analysis.

RINGS AROUND NEPTUNE?

Following the discovery of rings around Uranus and Juptier, the a priori likelihood of rings around Neptune increased--on the basis of Neptune's similarity with the other three ringed planets. If one believes, however, that rings are associated with regular satellites systems, then Neptune would not be expected to have rings. Occultation searches for rings in 1981[15] and 1983[16,17] revealed no rings to a limit of a few hundredths in optical depth. For equatorial rings, the 1983 occultation probed within a few hundred kilometers from the top of Neptune's atmosphere. The occultation work has been extensive enough that even unusual configurations[18] of rings would have been detected. Infrared images of Neptune taken by David Allen have also revealed no rings[19].

REFERENCES

[1] Elliot, J.L., and Nicholson, P.D. (1984). In *Planetary Rings*, ed. by A. Brahic and R. Greenberg (Tucson: University of Arizona Press), in press.

[2] Goldreich, P., and Tremaine, S. (1979). *Astron. J. 84*, 1638.

[3] Dermott, S.F., and Murray, C.D. (1980). *Icarus 43*, 338.

[4] Lane, A.L., Hord, C.W., West, R.A., Esposito, L.W., Coffeen, D.L., Sato, M., Simmons, K., Pomphrey, R.B., and Morris, R.B. (1982). *Science 215*, 537.

[5] French, R.G., Elliot, J.L., and Allen, D.A. (1982). *Nature 298*, 827.

[6] Freedman, A., Tremaine, S.D., and Elliot, J.L. (1983). *Astron. J. 88*, 1053.

[7] Goldreich, P., and Tremaine, S. (1979b). *Nature 277*, 97.

[8] Goldreich, P., and Tremaine, S. (1981). *Astrophys. J. 243.*, 1062.

[9] Borderies, N., Goldreich, P., and Tremaine, S. (1983). *Astron. J. 88*, 226.

[10] Borderies, N., Goldreich, P., and Tremaine, S. (1982). *Nature 299*, 209.

[11] Nicholson, P.D. (1983). *B.A.A.S. 15*, 816.

[12] French, R.G. (1983). *B.A.A.S. 15*, 816.

[13] Dunham, D.W. (1971). Ph.D. thesis, Yale University.

[14] Stone, E.C. (1982). In *Uranus and the Outer Planets*, ed. by G. Hunt (Cambridge: Cambridge University Press), 275.

[15] Elliot, J.L., Mink, D.J., Elias, J.H., Baron, R.L., Dunham, E., Pingree, J.E., French, R.G., Liller, W., Nicholson, P.D., Jones, T.J., and Franz, O.G. (1981). *Nature 294*, 526.

[16] Elliot, J.L., Dunham, E., Mink, D.J., Meech, K.J., Goguen, J., Hammel, H.B., and Erickson, E.F. (1983). *B.A.A.S. 15*, 817.

[17] Vilas, F., Hubbard, W.B., Frecker, J.E., Hunten, D.M., Gehrels, T., Lebofsky, L.A., Smith, B.A., Tholen, D.J., Zellner, B.H., Wisniewski, W., Gehrels, J.A., Capron, B. (1983). *B.A.A.S. 15*, 816.

[18] Dobrovolskis, A.R. (1980). *Icarus 43*, 222.

[19] Allen, D.A. (1983). *Sky and Telescope 65*, 110.

INFRARED IMAGES OF THE URANIAN RINGS

Philip D. Nicholson

Cornell University
Space Sciences Building
Ithaca, NY 14853

Abstract

Images of the Uranian rings at a wavelength of 2.2 μm, chosen to reduce the problem of scattered light from the planet, have been acquired on several occasions spanning the period 1978-1983. Although individual rings are not resolved in these images, the integrated brightness of the system is observed to vary with azimuth. The phase and amplitude of this variation is found to be consistent with the precession rate and variable width of the ε ring, as deduced from stellar occultation data. Quantitative analyses of the brightness variations permit an upper limit of ~ 0.0015 to be placed on the average normal optical depth of any diffuse inter-ring material. Preliminary absolute calibration of the 1983 data yields an average ring geometric albedo, at 2.2 μm, of 0.022 ± 0.002, consistent with previous estimates. Lastly, the potential use of near-infrared images in searches for faint inner satellites of Uranus is discussed.

INTRODUCTION

Following the discovery of a system of five (later increased to nine) narrow rings encircling Uranus, several unsuccessful attempts were made to identify their presence in previously obtained images of the planet. Based on a photograph taken in March 1972, obtained with an image-intensifying tube and an interference filter centered at a wavelength of 0.888 μm, W. Sinton[1] obtained an upper limit on the average geometric albedo of all five rings of ~ 0.09.* Using a CCD image obtained in May 1976, at a similar effective wavelength of 0.886 μm, B. A. Smith[2] was able to set an even lower upper limit on the average geometric albedo of ~ 0.01.* For each of these observations, the wavelength was chosen to match that of the strongest methane absorption band in Uranus' visible spectrum, in order to reduce scattered light from the disk of the planet.

---

*The original published values are here corrected to a uniform value of 85 km for the integrated width of all nine rings, as determined from stellar occultation analyses.[8]

In addition to these direct searches for reflected light from the rings, Sinton[1] noted the possible appearance of the silhouette and/or shadow of the rings across the disk of Uranus in a high-resolution photograph obtained in March 1970 by the balloon-borne telescope, Stratoscope II.[3] The presence of this feature has been confirmed in further enhancements of the original data by C. C. Avis and coworkers,[4] although its interpretation as a shadow remains uncertain.

In March 1978, Thomsen et al.,[5] again using a CCD detector at a wavelength of 0.890 μm, detected an elliptical component in the halo of scattered light around Uranus which they attributed to the rings. The derived average geometric albedo was 0.02 ± 0.01 (uncorrected, as the width assumed was not given), consistent with the above upper limits.

In each of the observations described above, the principal difficulty was posed not by the intrinsic faintness of the rings, but rather by their close proximity (1-2") to the planet's limb and the resulting high level of scattered radiation from the planetary disk. This problem can most readily be avoided by making observations in the near-infrared region, where the absorption bands are in general much

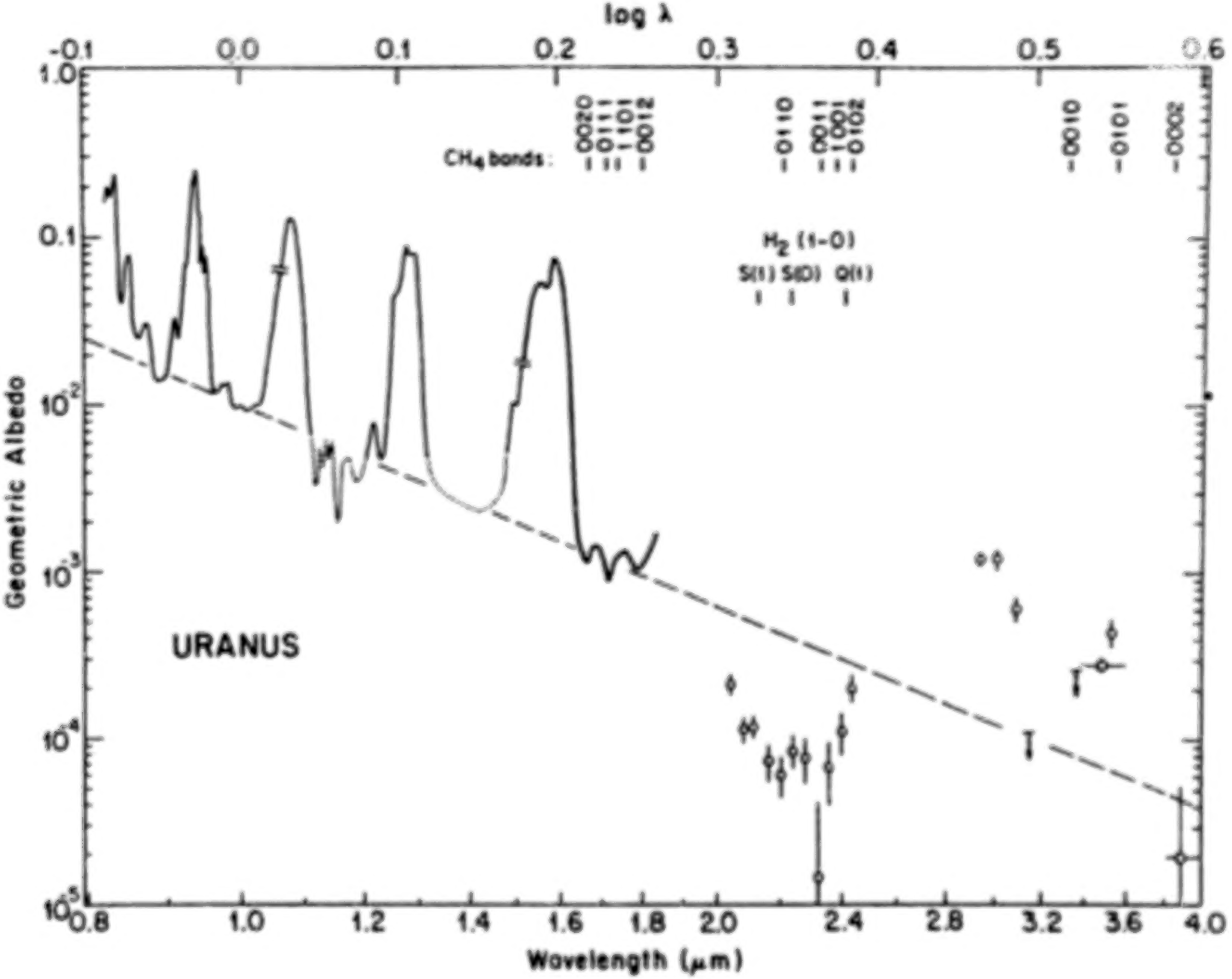

Fig. 1. Near-infrared geometric albedo spectrum of Uranus, for an equatorial radius of 25,600 km. Data from Trafton[6] (0.8 - 1.05 μm), Fink and Larson[7] (1.05 - 1.50 μm), and unpublished observations by Nicholson, Jones, and Gatley (1.5 - 4.0 μm). The dashed line is a Rayleigh scattering spectrum fitted throught the bottoms of strong CH$_4$ bands.[7] Regions of the spectrum near 1.9 and 2.7 μm have not been observed, because of strong telluric absorption at these wavelengths.

stronger than those at wavelengths shortward of 1μm (see Fig. 1). Particularly suitable for this purpose are the bands centered at 2.2 μm (due to a combination of methane and pressure-induced hydrogen absorption), and at 3.3 μm (the ν_3 fundamental of methane). In each of these two bands, Uranus' geometric albedo is $\leq 1 \times 10^{-4}$, as compared with albedos of ~ 0.015 and ~ 0.010 in the 0.89 μm and 1.01 μm bands accessible to CCD observations.

At the time of writing, all reported infrared imaging observations of the Uranian rings have utilized the 2.2 μm band, partly because of the close match between this band and the passband of the standard broadband K filter (λ_0 = 2.20 μm, $\Delta\lambda$ = 0.40 μm), and partly because of the higher thermal background at 3.3 μm.

OBSERVATIONS

As yet, sensitive imaging systems which operate at wavelengths longward of the CCD cutoff at ~ 1.1 μm are not generally available for astronomical work. In consequence, all infrared "images" of Uranus and its ring system published to date have been generated from sets of raster scans made with a single InSb detector looking out through a small aperture in the telescope's focal plane. As is standard practice in infrared photometry, an oscillating or rotating mirror is used to alternately sample radiation from the planet or rings, and background radiation from a nearby area of sky; the output signal represents the difference "planet + sky" - "sky". The data so obtained, suitably averaged and binned, are then converted into either

TABLE I. Summary of imaging observations of the Uranian rings at a wavelength of 2.2 μm.

Date	Phase angle	B	P	ε ring periapse	Earth-Uranus distance (AU)	Ref.
5/19/78	0.76°	55.8°	274.3°	6.4°	17.667	9
7/06/79	2.62	58.9	272.1	206.4	18.127	9
5/09/82	0.77	74.0	253.0	179.7	17.900	11
3/26/83	2.71	78.8	236.8	256.3	18.473	unpubl.
5/26/83	0.14	77.3	243.0	339.3	17.934	"
7/25/83	2.56	75.7	248.3	61.5	18.377	"

Notes: B is the Uranocentric declination of the Earth with respect to the ring plane, while P is the position angle of superior conjunction in the ring plane, measured towards the East from North. Column 5 gives the position angle of the ε ring's periapse. The ring pole position and ε ring orbital elements are from reference (8).

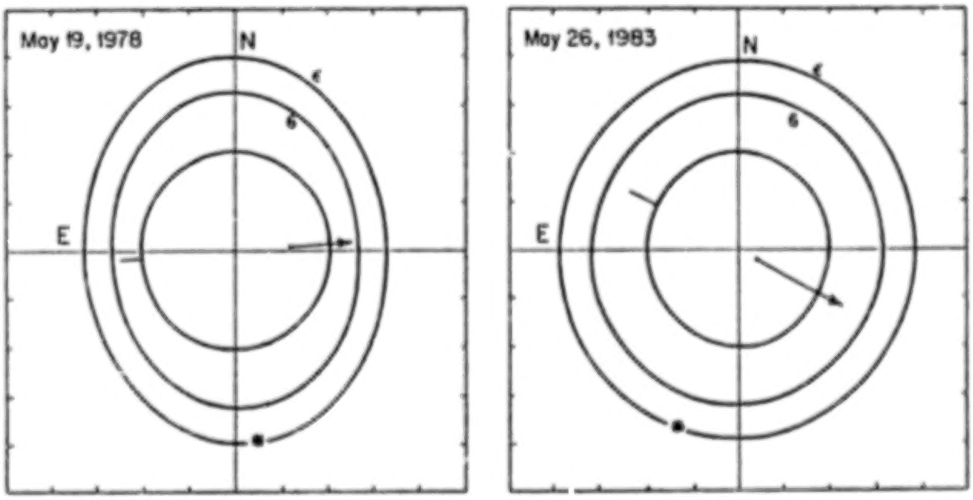

Fig. 2. Viewing geometry for Uranus and its ring system at the times of imaging observations in 1978 and 1983. The arrow indicates the direction of the planet's north pole. Only the innermost (6) and outermost (ε) rings are plotted. The apoapse, i.e., broadest part, of the precessing ε ring is indicated by an asterisk. Tick marks on the axes are at intervals of 1.0".

a contour map or a television image, whose resolution depends on the aperture size, atmospheric seeing, and possibly the response time of the recording system.

Near-infrared images of Uranus and its rings have been acquired during four oppositions -- 1978, 1979, 1982, and 1983. Table I lists dates, distances, and phase angles for all these observations, together with the ring plane orientation and the location of the apsidal line of the eccentric ε ring. Fig. 2 illustrates the aspect of the system in May 1978 and in May 1983, based on information derived from stellar occultation studies.[8] At a mean-opposition distance of 18.18 AU, the disk of Uranus subtends a diameter of 3.88", while the major axis of the ε ring subtends 7.76". The innermost ring, ring 6, subtends 6.36", so that the maximum projected width of the ring system is only 0.70".

Before discussing the interpretations of, and conclusions to be drawn from, these images, the individual observations are briefly described below.

1978-1979. The first infrared maps of the rings were obtained in May 1978 by K. Matthews et al. using the Hale 5-m telescope, and were followed by similar observations in July 1979.[9] A rather oversized aperture of 4" diameter was employed for these observations, and data were recorded simultaneously at effective wavelengths of ~ 1.55 and 2.2 μm. The former wavelength corresponds to a continuum region in Uranus' spectrum (see Fig. 1), and was used to monitor the planetary component of the total flux.

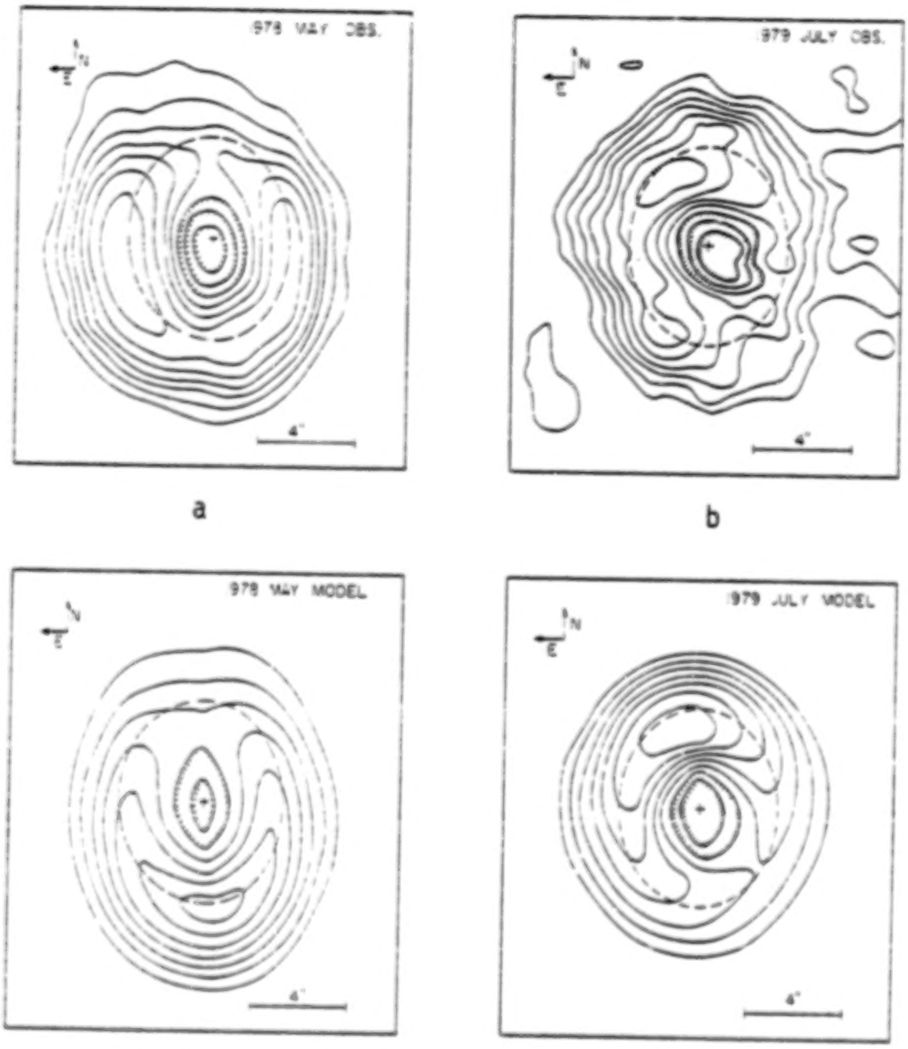

a b

c d

Fig. 3. Contour maps of the Uranian rings at a wavelength of 2.2 μm, constructed from scanning observations on (a) May 19, 1978 and (b) July 6/7, 1979. Also shown are synthetic maps (c,d) based on a simple model of the rings derived from stellar occultation observations (see text for further details). The center of Uranus is indicated by a cross, and a dashed ellipse represents the ε ring. Figure from Matthews, et al..[9]

The final contour maps (Figs. 3(a,b)) were generated by subtracting the (appropriately scaled) 1.55 μm signal from the 2.2 μm signal, and show the rings without the planet. Examination of the raw scans indicated that, at 2.2 μm, the peak flux recorded from the rings was approximately equal to that measured when the aperture was centered on Uranus. When the aperture diameter is taken into account, this result is consistent with the multi-aperture photometry of Nicholson and Jones,[10] which indicated that the total flux from the rings at 2.2 μm is ~ 3 times the total planetary flux at that wavelength.

Each of the 1978 and 1979 maps represents an average of several sets of raster scans, individually smoothed and then digitized at intervals of 0.67". The scan spacing was ~ 1.2", in an east-west direction. A total of four hours of observing time was required to produce the map in Fig. 3(a), and two hours for the somewhat noisier map in Fig. 3(b). For further details the reader is referred to reference (9).

1982. In May 1982, D. A. Allen observed Uranus with the 4-m Anglo-Australian Telescope, again at 2.2 μm, and produced an image which shows the rings clearly separated from the planet.[11] The resolution of this map is ~ 1.5", and the pixel size is 0.5" x 0.5". The total observing time was only ~ 30 minutes, indicating both the efficiency of this modern, fully computer-controlled telescope, and the rapid improvement in sensitivity of infrared detector systems over the intervening period of 3 or 4 years. This image is also reproduced, by permission, in reference (8).

1983. The Hale telescope was again used to observe Uranus at 2.2 μm on three occasions during the 1983 opposition (see Table I for details). On March 26 and May 26, an aperture of diameter 1.5" was used, and the scan spacing was 1.0"; on July 25 the aperture was reduced to 1.0", and the scan spacing to 0.5". In each case, the measured fluxes were averaged into 0.5" bins, and then interpolated (if necessary) between scans to produce an array of 0.5" x 0.5" pixels. Several sets of data were obtained on each night, and were subsequently co-added to improve the signal-to-noise ratio of the final images. The total observing time involved on each of the three nights was approximately 60 minutes.

In addition, a single set of scans at a continuum wavelength of ~ 1.6 μm was obtained on May 26, and used to generate an image of the planet alone, for comparison with the 2.2 μm data.

DISCUSSION

As is noted above, the entire width of the system of 9 rings, viz., 9300 km, subtends an angle of only 0.7" at the Earth. Ground-based observations, with the exception of occultations, are thus incapable of distinguishing the individual rings. It is, however, possible to study the radial and azimuthal brightness distributions of the integrated ring system. Such investigations are greatly facilitated by Uranus' obliquity of 98° and its current, almost pole-on, orientation (see Fig. 2). (The latitude of the

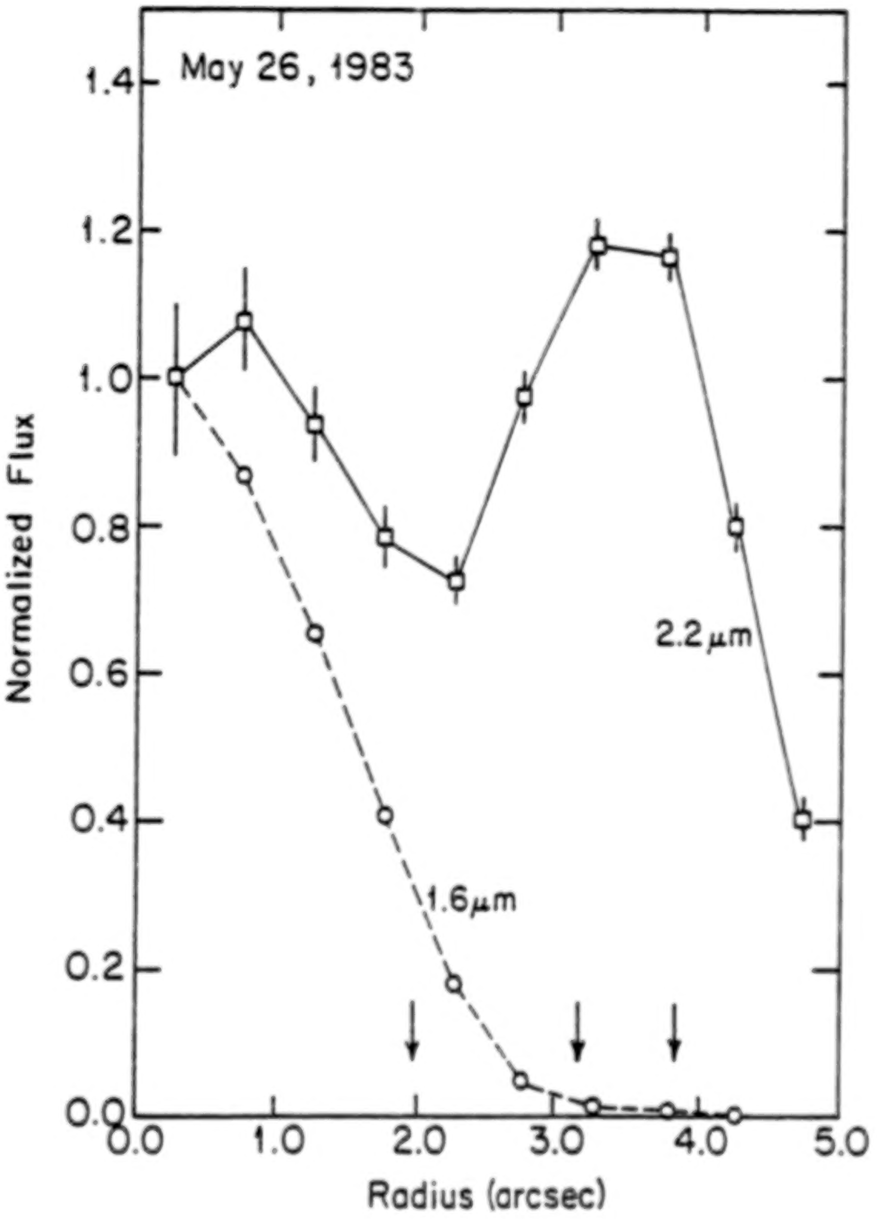

Fig. 4. Azimuthally-averaged radial brightness profiles of the Uranian system at wavelengths of 1.6 and 2.2 μm, from images obtained on May 26, 1983. Each point represents the mean flux per pixel in an annulus of width 0.5", centered on the planet. Arrows indicate the mean projected radii of Uranus' limb, ring 6, and the ε ring.

sub-solar point on Uranus will reach its maximum value of ~ 82°N in late 1985, shortly before the Voyager encounter.)

Radial brightness distribution. Fig. 4 shows the mean radial brightness profile of the Uranian system at wavelengths of 1.6 and 2.2 μm, derived from the observations of May 26, 1983. These data were obtained under conditions of ~ 1" seeing, and are limited in resolution primarily by the 1.5" diameter scanning aperture. Each point represents the average flux measured in a circular annulus of width 0.5", centered on the planet. (The deviations of the projected ellipses of the rings from circularity amounted to < 0.12" at the time of these observations, and may be neglected.)

The peak 2.2 μm flux occurs at a radius of 3.5", with the mean brightness decreasing rapidly both inside 3.0" and outside 4.0". This is consistent with the locations of the narrow, optically thick rings observed during stellar occultations, whose mean projected radii ranged from 3.22" (ring 6) to 3.90" (ε ring) in May 1983. Detailed modelling of these data should yield upper limits on the optical depth of any tenuous material which may extend beyond the radial limits of the known rings.

At 1.6 μm, as expected, the radial brightness profile is dominated by scattered light from the disk of Uranus, and there is no obvious signal attributable to the rings. Uranus itself appears to be quite limb-darkened at 1.6 μm, although the profile in Fig. 4 is significantly influenced by both seeing and the finite aperture size. At 2.2 μm, on the other hand, the limb-darkening is considerably weaker, and perhaps non-existent. This behavior is consistent with that observed in at least some methane bands and nearby continuum regions at shorter wavelengths.[12]

Geometric albedos. The measured fluxes, integrated over suitable ranges of radius, may also be used to estimate the geometric albedos of both Uranus and the rings. All measurements at radii less than 2.5" are assigned to the planet, while those between radii of 2.5" and 5.0" are assigned to the rings. A preliminary absolute calibration of the 1983 data yields the following results, calculated for a planetary equatorial radius of 25,600 km and a total ring surface area[13] of 2.64×10^7 km^2:

Uranus: $p\ (1.65\ \mu m) = 0.024 \pm 0.002$

$p\ (2.20\ \mu m) = (1.06 \pm 0.15) \times 10^{-4}$

Rings: $p\ (1.65\ \mu m) < 0.13$

$p\ (2.20\ \mu m) = 0.022 \pm 0.002$

(Filter passbands at 1.65 and 2.2 μm are 0.30 μm and 0.40 μm, respectively.)

The results for Uranus are in good agreement with previous broadband photometric observations.[9,10] The upper limit obtained for the ring albedo at 1.65 μm is not particularly interesting, most of the measured flux between 2.5" and 5.0" radius at this wavelength being due to scattered light from the planet (see Fig. 4). At 2.2 μm, the ring albedo obtained here is somewhat lower than the value of

0.032 ± 0.005 obtained from broadband photometric observations in 1978/79,[9] but in excellent agreement with the mean albedo of 0.023 ± 0.002 derived by Nicholson et al.[14] from spectroscopic observations made in 1980/81. The latter covered a spectral range of 2.04 to 2.40 μm, almost identical with the passband of the K filter used for the imaging observations.

Azimuthal brightness distribution. The most striking feature in each of the near-infrared images and maps is the strong azimuthal variation in ring brightness. This effect was attributed by Matthews et al.[9] to the known variation in width of the eccentric ε ring, and this interpretation is supported by the observations of 1982 and 1983. This ring, which alone accounts for 70% of the total surface area of the ring system, ranges in width from a minimum of 20 km at periapse to a maximum of 96 km at apoapse.[8] (Similar width variations, of somewhat smaller fractional amplitude, are exhibited by the α and β rings, and perhaps by rings 6, 5, and 4 as well.)

Due to the oblate figure of Uranus, the apsidal line of the ε ring precesses in a counter-clockwise direction (as viewed from Uranus' northern hemisphere) at a rate of 1.363 degrees per day, completing one circuit in 264 days. This rapid precession accounts for the varying appearance of the ring system; in every instance the minimum in ring brightness is found to coincide closely with the predicted position angle of the ε ring's periapse (see Table I). Generally, although not invariably, the brightness maximum is located approximately 180° from the minimum, and thus coincides with the apoapse of this ring.

Matthews et al. generated model maps for comparison with the May 1978 and July 1979 data, employing a simple description of the ε ring's width variation. These model maps, shown in Figs. 3(c,d), provide quite a good fit to the observations, the principal discrepancy being an east-west asymmetry in the May 1978 map which does not appear in the model. We shall return to this point below. From a quantitative comparison of observed and model maps, Matthews et al. derived an upper limit of ~ 0.003 on the optical depth of any uniformly distributed inter-ring material with the same single particle albedo as the narrow rings. (The hypothetical inter-ring material was assumed to have a radial extent of 5000 km.)

Fig. 5 shows the azimuthal ring brightness distribution observed on May 26, 1983, binned into 30° segments. As in the geometric albedo calculation above, only measured fluxes in the radial range 2.5" to 5.0" were used. Superimposed on the observations is a theoretical brightness distribution, based on a rather more sophisticated ring model than that used by Matthews et al. The model treats each of the nine rings as a flat Lambertian surface, lying in the mean ring plane, with a reflectivity proportional to $1 - e^{-\tau}$, where τ is the local line-of-sight optical depth of the ring. Known width variations for the α, β, and ε rings are incorporated in the model, with the normal optical depth of each ring assumed to vary inversely with its radial width. The remaining six rings are assigned constant widths, and

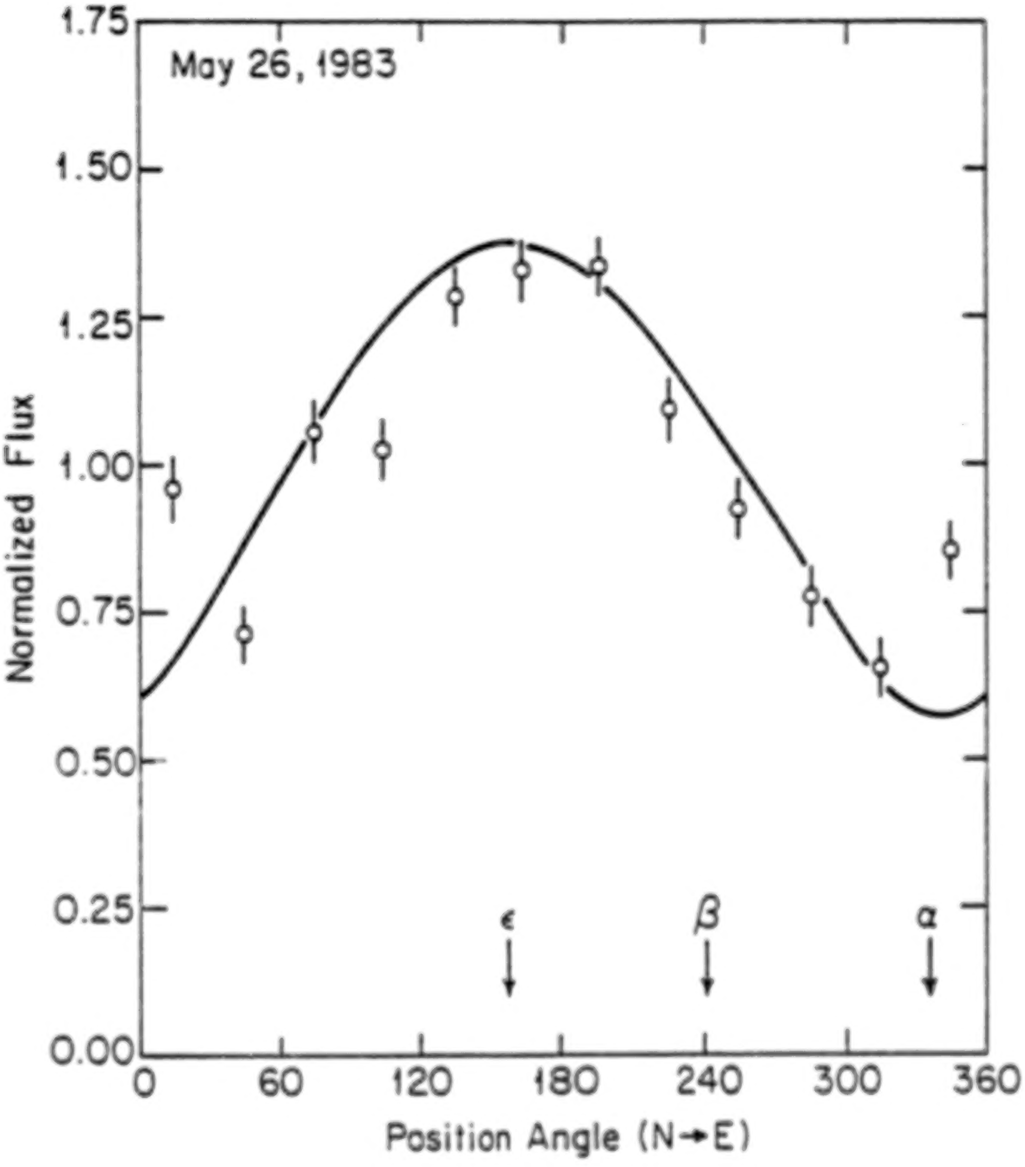

Fig. 5. Azimuthal brightness profile of the ring system at a wavelength of 2.2 μm, from an image obtained on May 26, 1983. Each point represents the mean flux per pixel in a 30° segment, between radii of 2.5" and 5.0", while the solid curve shows the predicted brightness variation based on a model described in the text. Arrows indicate the apoapse locations for the α, β, and ε rings, whose variable widths are incorporated in the model.

nominal optical depths of 2. All ring parameters are taken from Tables V and VI of reference (8). Note that the model has not been adjusted in any way to improve the match with the observations.

Apart from the two neighboring points at position angles of 345° and 15°, the observed azimuthal brightness distribution is in excellent agreement with the occultation-derived model. In particular, the fit to the observed (normalized) distribution of brightness would be significantly impaired by the addition of any azimuthally symmetric inter-ring material which increased the total cross-section of the system by as much as 20%. The corresponding upper limit on the optical depth of a diffuse sheet of material, spread uniformly over the 9300 km radial range of the rings, is ~ 0.0015. This limit, which will be refined in a more complete analysis of the 1983 observations, is comparable with that derived by Matthews et al. from the 1978/79 maps, and at least an order of magnitude lower than the limiting sensitivity of ground-based stellar occultation observations.

Although the larger-scale features of the images may be interpreted in terms of the known properties of the Uranian ring system, there remain several anomalies in the data. For example, at least three of the six available images show the integrated ring brightness to be significantly greater in the two quadrants leading the ϵ ring's periapse than in the two trailing quadrants. (In this context, 'leading' refers to the direction of apsidal precession; a ring particle's orbital motion carries it through periapse from the 'trailing' to the 'leading' quadrants.) This asymmetry is most noticeable in the map of May 1978, where the difference in integrated brightness is ~ 30% (see Fig. 3(a)), but it also appears in the May 1982 image published by Allen,[11] and in the data obtained in March and, less certainly, July of 1983. The May 1983 image, however, for which the ϵ ring's periapse lies in almost the same direction as in May 1978, shows no evidence of any leading/trailing asymmetry. This image does, on the other hand, exhibit an anomalous brightening at a position angle of ~ 0°, within 20° of periapse.

The occultation model predicts a brightness distribution which is symmetric about the apsidal line of the ϵ ring (see Figs. 3(c,d) and Fig. 5), subject only to small modifications due to the α and β rings, and to projection effects. In an attempt to explain the May 1978 results, Matthews, et al. considered several hypotheses, including localized clumping of ring particles, inter-ring satellites, and the chance superposition of a star. Each of these possibilities could be eliminated, either because of orbital motion of the putative clumps or satellites during the course of the observations, or because of the motion of Uranus relative to the stellar background. In the case of tne 1982 and 1983 observations, the reduced time intervals involved (an hour or less, as opposed to four hours in 1978) make it difficult to rule out the first two possibilities, as the orbital periods of objects in or near the rings range from 6.2 to 8.4 hours.

Satellite searches. Near-infrared images of the Uranian system may also prove useful in searches for any previously undiscovered satellites lying between Miranda (mean distance 9.9", or 130,000 km) and the ε ring. In the images obtained in March and May 1983, the 3σ noise level in one pixel corresponds to a mean-opposition K magnitude of 16.3. A satellite of this magnitude, with a geometric albedo of 0.25, typical of the four large satellites of Uranus,[15] would have a diameter of 250 km. Although no objects brighter than this appear in the 1983 data, these images cover only a small region of sky, about 12" square. Similar observations, but extending out to the orbit of Miranda, are presently planned for 1984 or 1985.

ACKNOWLEDGMENTS

The 1983 observations of Uranus described herein were carried out in collaboration with K. Matthews of Caltech, and with the assistance of several staff members of Palomar Observatory. This research has been supported, in part, by NASA.

REFERENCES

(1) Sinton W. (1977). Uranus: the rings are black. Science 198, 503.

(2) Smith, B. A. (1977). Uranus rings: an optical search. Nature 268, 32.

(3) Danielson, R. E., Tomasko, M.G., and Savage, B.D. (1972) High-resolution imagery of Uranus obtained by Stratoscope II. Astrophys. J. 178, 887.

(4) Franklin, F.A., Avis, C.C., Colombo, G., and Shapiro, I.I. (1980) The geometric oblateness of Uranus. Astrophys. J. 236, 1031.

(5) Thomsen, B., Baum, W. A., Wilkinson, D. T., and Loh, E. (1978). New results on the albedo of the rings around Uranus. B.A.A.S. 10, 581.

(6) Trafton, L. (1976). The aerosol distribution in Uranus' atmosphere: interpretation of the hydrogen spectrum. Astrophys. J. 207, 1007.

(7) Fink, U. and Larson, H. P. (1979). The infrared spectra of Uranus, Neptune, and Titan from 0.8 to 2.5 microns. Astrophys. J. 233, 1021.

(8) Elliot, J. L. and Nicholson, P. D. (1984). The rings of Uranus. In Planetary Rings, R. Greenberg and A. Brahic, Eds. Univ. of Arizona Press.

(9) Matthews, K., Neugebauer, G., and Nicholson, P. D. (1982) Maps of the rings of Uranus at a wavelength of 2.2 microns. Icarus 52, 126.

(10) Nicholson, P. D., and Jones, T. J. (1980). Two-micron spectrophotometry of Uranus and its rings. Icarus 42, 54.

(11) Allen, D. A. (1983). Infrared views of the giant planets. Sky and Telescope 65, 110.

(12) Trafton, L. (1981). The atmospheres of the outer planets and satellites. Rev. Geophys. and Space Phys. 19, 43.

(13) Nicholson, P. D., Matthews, K., and Goldreich, P. (1982). Radial widths, optical depths, and eccentricities of the Uranian rings. Astron. J. 87, 433.

(14) Nicholson. P. D., Jones, T. J., and Matthews, K. (1983). Infrared observations of the Uranian rings. In Planetary Rings, I.A.U. Colloquium No.75, A. Brahic, Ed.

(15) Brown, R. H., Cruikshank, D. P., and Morrison, D. (1982). Diameters and albedos of satellites of Uranus. Nature 300, 423.

DYNAMICS OF THE URANIAN RINGS

Stanley F. Dermott
Center for Radiophysics and Space Research
Cornell University
Ithaca, NY 14853

Abstract

I describe some of the problems of the shepherding satellite model of Goldreich and Tremaine. We need to understand how waves on rings are damped. Damping of excited eccentricities results in ring confinement, but we do not understand why all the observed narrow rings have optical depths near unity. In some circumstances sharp edges may be associated with Lindblad resonances. However, wavelength variation across a ring can lead to shock formation between consecutive encounters of the particles and the shepherding satellites. If this results in complete wave damping, and this is the case for the waves observed on the edges of the Encke gap, then resonance has no meaning and cannot be invoked.If the surface mass density of the ϵ-ring is as high as 36 g cm^{-2}, which must be the case if self-gravity is responsible for the observed apse alignment, then the separation timescales of the satellites may be short (~ 4 10^8 years). Perhaps the rings are young? Close-packing of particles at pericenter has been suggested as a mechanism for apse alignment. However, this cannot account for node alignment. This may not be a problem for the ϵ-ring, which appears to be coplanar with the planet's equator, but all the other Uranian rings, except the η-ring, have small inclinations. The existence of small satellites may account for some of the observed discrepancies in the MIT ring-fitting model. I emphasize that the observed discrepancies must be related. In particular, if the discrepancies in the apse rates of ~ 0.005°/day are real, then we must expect waves on the rings of amplitude ~ 2 km and these waves should result in observable variations in ring width and radial displacement. However, the satellite masses needed to produce these putative discrepancies are not particularly small. If the separations of the rings and satellites are > 300 km, then we need mass ratios ~ 6 10^{-10} with satellites of diameter $\gtrsim$ 40 km.

INTRODUCTION

The Voyager 2 image of the Saturnian F ring showing the two "shepherding" satellites, 1980S26 and 1980S27, leaves little doubt that the theory of shepherding satellites proposed by Goldreich and Tremaine[1] is essentially correct. There is no direct evidence that satellites confine the nine Uranian rings, but this must be regarded as very likely. The horseshoe-orbit model of Dermott et al.,[2] postulates that each narrow ring contains a small satellite. While viable, this model cannot account for some of the observed features of the Uranian rings, in particular, the asymmetric occultation profiles. However, the model can be applied to the narrow rings from which the co-orbital Saturnian satellites presumably formed.

Recent reviews of this subject include those of Goldreich and Tremaine[3] and Dermott.[4] Numerous other reviews and papers are to appear in the books edited by Greenberg and Brahic[5] and Brahic.[6] Given the existence of these recent and comprehensive articles, I do not attempt to review the subject in this short report. Rather, I focus on a number of unresolved problems. I discuss the following questions:

1. Why are the optical depths of all the observed narrow rings close to unity?
2. Why are the satellite and ring separation timescales so short?
3. Why are the ring edges sharp?
4. How important is shock formation in narrow rings?
5. Do we have any evidence for the existence of small satellites near the Uranian rings? What are the probable sizes of these satellites?
6. How are the apse and node alignments of the eccentric and inclined rings maintained?

SHEPHERDING SATELLITES

In the shepherding satellite model of Goldreich and Tremaine,[1] particle confinement is achieved by tidal torques exerted on the rings by small nearby satellites. The torques arise from the second-order change in semimajor axis that each ring particle experiences at each close encounter with a shepherding satellite. However, for the cumulative change in semimajor axis to be finite, the ring particle must lose some orbital energy between consecutive encounters. This loss is achieved either by collisions, which result in eccentricity damping (see Fig. 1), or by energy transfer to other ring particles through the excitation of spiral density waves.

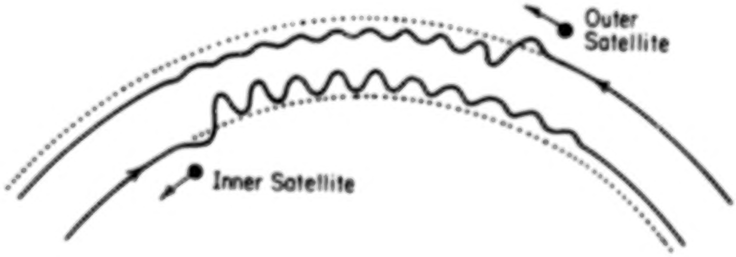

Fig. 1. Schematic diagram showing the action of the shepherding satellites. Arrows on the ring particle paths show the direction of motion of the particles with respect to the perturbing satellite. At conjunction, the satellite changes the eccentricity and the semimajor axis of each ring particle. Eccentricity damping by particle collisions results in a further change in the semimajor axis, but this change is usually negligible in comparison with that produced by the satellite interaction. (Copyright University of Arizona Press).

If a ring is bounded by two satellites, then its width will be reduced until the confining torques just counteract the tendency of the ring to spread. The predicted[1] equilibrium width of the ring is

$$W \approx \left(\frac{15}{4}\right)^{1/2} \tau^{1/2} \frac{M}{m} \left(\frac{x}{a}\right)^{5/2} d, \qquad (1)$$

where τ is the optical depth and a the radius of the ring, m/M is the mass ratio of the satellites and the planet, x is the separation of the satellites from the ring, and d is the "characteristic" size of the ring particles. (In this heuristic argument, we assume that the satellites have equal masses and equal separations from the ring and that the ring is narrow, i.e., $W \ll x$.)

Equation (1) gives no hint as to why τ should be close to unity. The mean widths of the Uranian rings are observed to vary from < 4 km to 60 km. The separation of the rings varies from ~ 300 km to ~ 3000 km and we should expect a corresponding variation in x and an even greater variation in $x^{5/2}$, and there is, of course, no reason why the satellite masses should be similar. I conclude that some essential step in the dynamics describing the confinement of ring particles has been overlooked in the derivation of equation (1). This step is likely to involve the relation between the mean optical depth and the magnitudes of the various torques in the problem.

Borderies et al.[7] have also criticized the original version of the shepherding satellite model. As discussed by Goldreich at this meeting, each satellite exerts a torque Γ on the ring and energy is dissipated in the ring at a rate

$$\dot{E} = -U\Gamma, \qquad (2)$$

where U is the relative angular velocity of the satellite and the ring particles. Borderies et al. calculate that this input of energy increases the velocity dispersion and the associated viscosity of the ring particles to such an extent that the satellites can no longer confine the ring particles.

A further and, perhaps, a related problem of the shepherding satellite model is that of the short satellite-ring separation timescales. The confining satellites also experience a torque Γ exerted on them by the ring and this pushes the satellites away from the ring at rates given by $x/\dot{x} = T_{sep}$, where

$$T_{sep} = \frac{5}{8\pi}\frac{M^2}{mm_r}\left(\frac{x}{a}\right)^5 T, \tag{3}$$

m_r is the mass of the ring and T is the orbital period of the ring particles. If we accept the validity of eqn. (1), then we can eliminate m/M and write

$$T_{sep} = 3\ 10^{14}\tau^{1/2}\,\frac{\rho_r}{\Sigma}\left(\frac{x}{a}\right)^{5/2}\ \mathrm{yr} \tag{4}$$

where ρ_r is the density of the ring particles and Σ is the surface mass density of the ring (both in cgs units). If the apse alignment of the Uranian ε-ring is maintained by self-gravitation,[8] then $\Sigma \approx 36$ g cm^{-2} (see Table 2). Hence, if we allow that x is as large as 1000 km, then $T_{sep} \approx$ 4 10^8 yr. Goldreich and Tremaine have suggested that the shepherding satellites could be anchored by stable resonances,[3] but I calculate[4] that none of the candidate resonances are strong enough. Goldreich, at this meeting, suggested that previous calculations may have overestimated the probable masses of the confining satellites and that the separation timescales are larger than those given by equation (4). This may help in the case of the Uranian rings, but a more drastic problem exists for the small satellites close to the Saturnian A ring and in that case we have good estimates of the satellite masses. Perhaps we should allow for both the Uranian and the Saturnian systems that either the rings or the confining satellites or both are young.

SHOCK FORMATION

Each shepherding satellite raises a near-sinusoidal wave on a ring of particles. These waves have wavelengths

$$\lambda = 3\pi x \tag{5}$$

and amplitudes[9,10]

$$A = 2.24 \frac{m}{M} \left(\frac{a}{x}\right)^2 a. \tag{6}$$

Here, I assume that the satellites and the ring particles have near-circular, near-coplanar orbits. A nice illustration of equation (5) and the concept of both wave generation and damping has been discussed by Cuzzi.[11] Although no satellite has actually been observed in the Encke gap, waves have been detected on each side of the gap with wavelengths λ_1 and λ_2 that satisfy

$$\lambda_1 + \lambda_2 = 3\pi(x_1 + x_2) = 3\pi D, \tag{7}$$

where x_1 and x_2 are the separations of the putative satellite from the inner and outer edges of the gap and D is the gap width.

In any narrow section of a ring, the perturbations of the ring particle orbits are highly coherent, and, although particle collisions will act to damp the waves, the process may be slow. If the waves survive from one encounter with the perturbing or shepherding satellite to the next, then a Lindblad resonance will be excited at those locations in the ring where the local ring circumference is an integral number of wavelengths, that is, wherever, $2\pi a/\lambda = p + 1$, where p is an integer ≥ 0. Consecutive perturbations will then be in phase and a wave with amplitude significantly $> A$ may result.[4]

Borderies et al.[12] consider that the sharp edges of rings are probably associated with Lindblad resonances. This is the case for the sharp outer edges of the Saturnian A and B rings, but there are other cases of sharp-edged rings for which Lindblad resonance cannot be invoked and some of the Uranian rings may be in that category.

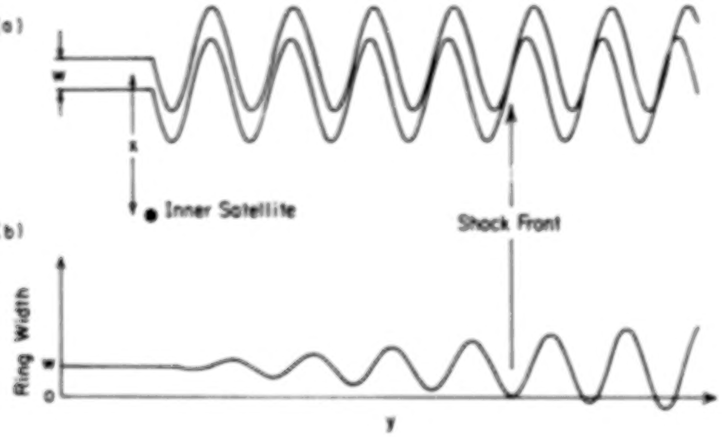

Fig. 2. (a) The length of the wave generated on a ring depends on the distance x of the satellite from the ring; hence there is always a small variation in wavelength across a ring of finite width. The resultant particle path pattern could lead to the formation of shocks and, if the ring contains gaps, loops. This could account for some of the features seen in the Saturnian F-ring, but in the latter case the eccentricities of the satellite and the ring orbits are also important. (b) Radial variation of ring width associated with the wave pattern shown in (a). (Copyright University of Arizona Press).

For a ring of finite width W, there is a variation of x and wavelength across the ring and this can result in large variations in ring width downstream from the perturbing satellite[4,13]--see Fig. 2. For most of the Uranian rings it is probable that $W > 2A$, hence the largest variation in width due to one of the satellites is 2A. It is now well-established that the widths of the α and β rings of Uranus vary harmonically with true anomaly.[14,15] The widths of both of these rings increase from a minimum $\approx$ 5 km near pericenter to a maximum $\approx$ 10 km near apocenter. Over and above these regular width variations, Nicholson and Matthews[15] consider that there is evidence for irregular variations of magnitude > 2 km. If these observations are substantiated, then I should consider that we have clear evidence for the existence of shepherding satellites--this is discussed further in the next section.

The shock front shown in Fig. 2 will form at a distance

$$y = \frac{3x^2}{2A} \tag{8}$$

downstream from the perturbing satellite. For this distance to be less than the ring circumference, we require that

$$x < 200 \left(\frac{m/M}{10^{-12}}\right)^{1/4} \text{ km} \tag{9}$$

for the case of a satellite in the Encke gap, and that

$$x < 300 \left(\frac{m/M}{10^{-10}}\right)^{1/4} \text{ km} \tag{10}$$

for the case of the Uranian rings. Shock front formation probably has a major role in the wave damping process, although the physics of this phenomenon has yet to be described. It is probable that eqn. (10) is satisfied by at least the shepherding satellites of the closely-spaced, inner Uranian rings. The waves on the edges of the Encke gap are not observed at all longitudes, and in that case we can be certain that the waves are damped between consecutive satellite encounters. Hence, resonance cannot be invoked to account for the sharp edges of the gap.

Shock fronts are likely sites for the formation of temporary particle clumps; thus I would expect these to have a mean longitudinal separation of one wavelength, λ. These shocks and the associated variations of ring width may also contribute to the marked periodic variations in brightness observed in the F ring and in the narrow rings in Encke's gap.[16,17,18]

The lines drawn in Fig. 2 represent the boundaries of a narrow ring, but they could equally well represent the boundaries of a narrow gap within a ring. In that case, near the shock front the gap would degenerate into a series of loops or braids of length λ. The gap would be expunged at the shock front and would have to be regenerated by some agency. This could be achieved by small satellites in the ring. I consider[4] that this is a likely explanation for the braided appearance of the Saturnian F ring--see Fig. 3.

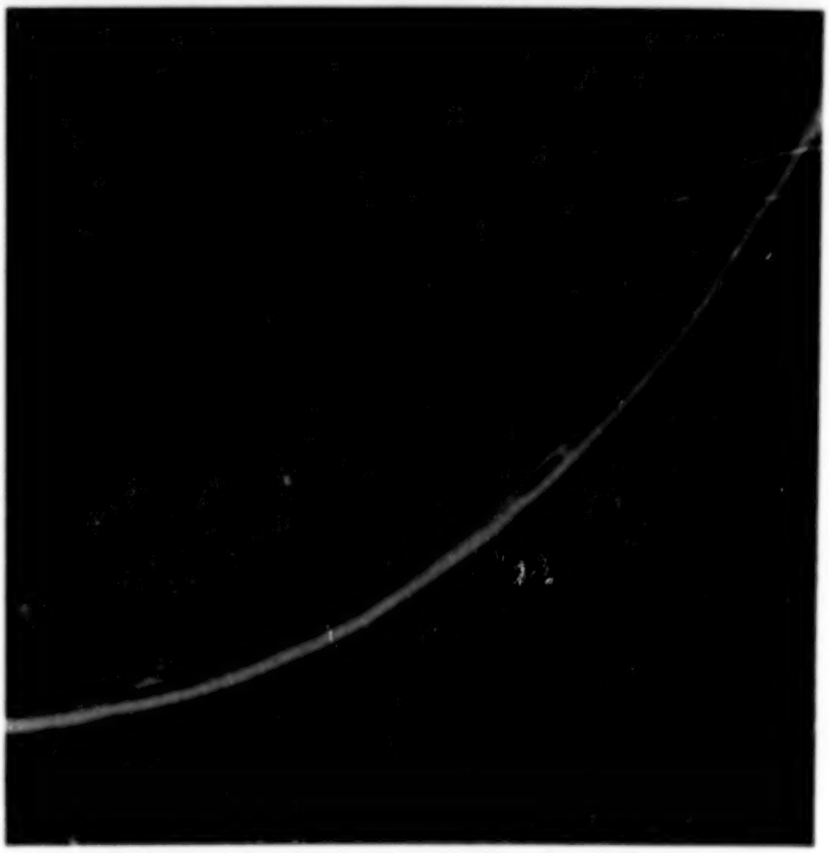

Fig. 3. In this Voyager 1 image of Saturn's F Ring, two prominent bright strands appear twisted and kinked, giving a braided appearance to the ring. (Image couresty of JPL/NASA.)

J_2 AND J_4 OF URANUS

The shepherding satellites may make appreciable contributions to the observed precession rates of the Uranian rings.[19] The pericenter precession rate, $\dot{\omega}$, due to the gravitational field of an oblate planet, can be written as

$$c\dot{\omega} = J_2 - \frac{5}{2} J_4 \left(\frac{R_r}{a}\right)^2 \tag{11}$$

where

$$c = \frac{2a^{7/2}}{3(GM)^{1/2}R_r^2} \tag{12}$$

a is now the geometrical semimajor axis of the best-fitting ellipse traced by the ring particles[14] and R_r is the normalizing radius in the spherical harmonic expansion of the potential. A plot of $c\dot{\omega}$ against $5/2\ (R_r/a)^2$ should be a straight line of slope - J_4 and intercept J_2. Fig. 4 shows such a plot for data from the 1981 MIT Uranian ring model.[20] The points represent the individually fitted precession rates, whereas the quoted values of J_2 and J_4 were determined from the data set as a whole. Fig. 4 not only shows that J_4 was then poorly determined, but also suggests that some of the discrepancies in the observed precession rates may be real.

French et al. [21] have since shown that some of the Uranian rings are not only eccentric but are also inclined to the equatorial plane of the planet. The inclusion of the inclinations in the best-fit model reduces the residuals. However, discrepancies in $\dot{\omega}$, ~ 0.005 deg/day, still remain[14,19] and it is worth asking if these could be due to the shepherding satellites and how that hypothesis could be tested.

Freedman et al.[19] have discussed a number of the effects that small

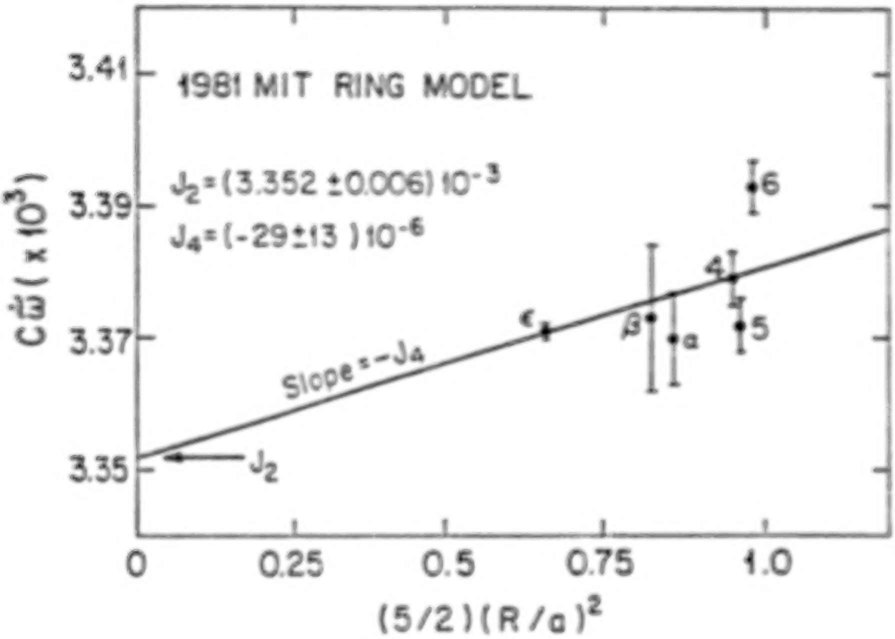

Fig. 4. The individual precession rates $\dot{\omega}$ are compared with those predicted from the best-fit values of J_2 and J_4 as calculated by Elliot et al. It would appear from these results that the shepherding satellites may make significant contributions to the precession rates. (Copyright of Phil. Trans. Roy. Soc. Lond.).

satellites would have on the rings, but I consider[4] that confirmation of the existence of small satellites could probably be most directly achieved by detection of the irregular ring-width variations discussed in the previous section, that is, the width variations not associated with the regular harmonic variation of ring width with true anomaly.

Regardless of whether a shepherding satellite orbits inside or outside the ring, the radial gravitational forces that it exerts on the ring act to increase the ring's pericenter precession rate by

$$\delta\dot{\omega} = \frac{n}{2\pi}\frac{m}{M}\left(\frac{a}{x}\right)^2 \tag{13}$$

where n is the mean motion of the ring particles. Since the net external torque on a ring confined by two satellites and in equilibrium must be zero,

$$\frac{m_1}{x_1^2} = \frac{m_2}{x_2^2} \tag{14}$$

where the subscripts refer to the two satellites. It follows that the magnitudes of $\delta\dot{\bar{\omega}}$ and of the wave amplitude A associated with each satellite are equal.[10] Hence, we can write

$$\delta\dot{\bar{\omega}}_t = \frac{n}{2.24\pi}\frac{A}{a}, \tag{15}$$

where $\delta\dot{\bar{\omega}}_t$ is the total increase in the precession rate due to both satellites. If $\delta\dot{\bar{\omega}}_t = 0.005$ deg/day, then each satellite must raise a wave on the ring of amplitude $A \sim 1.3$ km. These waves can interfere constructively to produce waves of amplitude 2A[10]. Thus, the discrepancies in $\dot{\bar{\omega}}$ would appear to be consistent with the irregular width variations found by Nicholson and Matthews. Progress is expected with this problem in the very near future (French, private communication).

A discrepancy $\delta\dot{\bar{\omega}} \sim 0.005$ deg/day could be produced by satellites, for example, of mass ratios $m/M \sim 6\ 10^{-10}$ or diameters ~ 40 km separated from the ring by ~ 300 km. (Note, the necessary masses increase as x^2.) Since the contributions to $\dot{\bar{\omega}}$ of the J_4 term in eqn. (10) are ~ 0.02 deg/day, it follows that the contributions due to the shepherding satellites may have to be determined before J_4 is known with useful accuracy.

APSE AND NODE ALIGNMENT

Goldreich and Tremaine[1,8] consider that the apse alignment of the eccentric Uranian rings is maintained by the self-gravitation of the ring particles. The contribution of the self-gravitation of the ring to the differential precession rate, $d\dot{\tilde{\omega}}/da$, across the ring arises from the variation with true anomaly of the radial forces acting on the ring particles. The average value of the radial forces is only finite if the width of the ring varies with true anomaly and this requires that an eccentricity gradient, a de/da, exists across the ring. For the average radial force to counteract the differential precession due to the oblateness of the planet, the eccentricity gradient must be positive and this in turn implies that the ring must be narrowest at pericenter. Quantitatively, we require that

$$a \frac{de}{da} \approx +2.3e \langle W \rangle J_2 \left(\frac{B}{a}\right)^5 \frac{\rho}{\Sigma} , \qquad (16)$$

where e is the mean eccentricity, <W> the mean width and Σ the mean surface mass density of the ring, and ρ is the mean density and B the radius of the planet.

The self-gravitation model of apse alignment has now been extended to node alignment.[22,23] The analysis predicts that if the self-gravitation of the ring alone acts to align the apses and the nodes, then we must have

$$\frac{\Delta i}{i} = \frac{\Delta e}{e} \qquad (17)$$

where Δi and Δe are the variations of inclination and eccentricity across the ring. Yoder[23] has also shown that the configuration of aligned pericenters and nodes is stable against small displacements. An eccentric ring is stable even if its inclination is zero, but a ring with an appreciable inclination is only stable if it is also eccentric.[23]

Dermott and Murray[24] pointed out that, by itself, self-gravitation does not explain why all the observed values of a de/da are close to unity. If a de/da is determined by three presumably independent parameters of the ring (e, <W> and Σ), then it is unreasonable to expect those quantities to be always such that a de/da ≈ 0.5 (see Table 1). They argued that the ring particles are probably close-packed at pericenter and that close-packing may prevent differential precession.

The only alternative to this argument is to allow that e, <W>, Σ and a de/da are not independent parameters.[24] The coupled evolution of these parameters has now been solved by Borderies et al.[25] In their model, self-gravitation is always responsible for the alignment of the pericenters, and evolution of the parameters only ceases when close-packing of the particles at pericenter limits the growth of the mean eccentricity e.

In the equilibrium configuration as described by Borderies et al.[25], the differential precession of the pericenters is zero, but the pericenters are not exactly aligned: a small shift, $\Delta\tilde{\omega}$, exists across the rings. Since $\Delta\tilde{\omega}$ is not zero, the radial gravitational forces act to increase the eccentricity gradient of the ring. The magnitude of $\Delta\tilde{\omega}$ is such that the radial forces just counteract the effects of interparticle collisions which act to decrease the eccentricity gradient. An outward manifestation of the small shift $\Delta\tilde{\omega}$ is a comparatively large shift, γ, in the location of that part of the ring for which the radial width is a minimum. The variation of the radial ring width with true anomaly is determined by the quantity

$$q = \left(\left(a\,\frac{\Delta e}{\Delta a}\right)^2 + \left(a\,\frac{\Delta\tilde{\omega}}{\Delta a}\right)^2\right)^{1/2} \qquad (18)$$

TABLE 1

Eccentric rings of nonuniform width

Planet	Ring	$\langle W \rangle$ km	$\langle e \rangle$ $\times 10^4$	$J_2(B/a)^5$ $\times 10^4$	a de/da
Uranus	α	7.4	7.2	2.3	0.39
Uranus	β	8.2	4.5	2.1	0.30
Uranus	ε	58.6	79.2	1.2	0.65
Saturn	1.29B	25	2.7	46.9	0.35
Saturn	1.45B	69	3.9	26.1	0.55

TABLE 2

Surface densities and velocity dispersions of the Uranian rings

Ring	α	β	ε
Δa (km)	7.4 ± 0.2	8.2 ± 0.3	58.6 ± 0.3
q	0.42 ± 0.05	0.32 ± 0.06	0.65 ± 0.01
γ	22° ± 8°	20° ± 12°	< 0°.9
$\Delta\tilde{\omega}$	-1°.9 ± 0.5	-2.6 ± 1.2	< 0°.08
Σ(g cm^{-2})	2.8 ± 0.3	1.8 ± 0.2	36.0 ± 0.4
τ/Σ (cm^2 g^{-1})	0.4	0.3	0.06
σ (cm s^{-1})	0.19 ± 0.03	0.13 ± 0.03	< 0.4
H (cm)	800	500	< 2000

where Δa is the variation of semimajor axis across the ring. The predicted shift, γ, has now been observed by Nicholson and Matthews.[15] Their observations for the α, β and ε Uranian rings are shown above the dashed line in Table 2. The quantities that can be derived from the observations, using the theory of Borderies et al.[25] are shown below the dashed line: σ is the velocity dispersion of the particles and H is the associated scale height.

Since the ε-ring appears to have zero inclination, I still maintain that close-packing of particles at pericenter may be sufficient to maintain the observed apse alignment. However, in the case of the other, inclined rings, that hypothesis is no longer tenable. Since the ring particle nodes circulate with respect to the pericenters, close-packing of particles at pericenter would not act to maintain node alignment as well. Thus, the detection by French et al.[21] of ring inclinations convinces me that the apse and the node alignment of the inclined rings at least are maintained by self-gravitation. The detection of finite values of γ by Nicholson and Matthews[15] provides further strong support for Goldreich and Tremaine's model.

ACKNOWLEDGEMENTS

This work was supported by NASA Grant NAGW-392.

REFERENCES

1. Goldreich, P. and Tremaine, S. (1979). Towards a theory for the uranian rings. Nature, 277, 97-99.
2. Dermott, S. F., Gold, T., and Sinclair, A. T. (1979). The rings of Uranus: Nature and origin. Astron. J. 84, 1225-1234.
3. Goldreich, P. and Tremaine, S. (1982). The dynamics of planetary rings. Ann. Rev. Astron. Astrophys. 20, 249-283.
4. Dermott, S. F. (1984). Dynamics of narrow rings. In Planetary Rings, (eds. R. Greenberg and A. Brahic), University of Arizona Press (in press).
5. Greenberg, R., and Brahic, A. (eds.). (1984). Planetary Rings, University of Arizona Press (in press).
6. Brahic, A. (ed.). (1984). Proceedings of I.A.U. Colloquium 75 Planetary Rings, Toulouse, France, Aug. 1982 (in press).
7. Borderies, N. Goldreich, P., and Tremaine, S. (1984). Unsolved problems in planetary ring dynamics. In Planetary Rings, (eds. Greenberg, R., and Brahic, A.), University of Arizona Press (in press).
8. Goldreich, P., and Tremaine, S. (1979). Precession of the ε ring of Uranus. Astron. J. 84, 1638-1641.
9. Julian, W. H., and Toomre, A. (1966). Non-axisymmetric responses of differentially rotating disk of stars, Astrophys. J. 146, 810-832.
10. Dermott, S. F. (1981), The "braided" F-ring of Saturn, Nature 290, 454-457.

11. Cuzzi, J. N. (1984), (in preparation).

12. Borderies, N., Goldreich, P., and Tremaine, S. (1982). Sharp edges of planetary rings. Nature 299, 209-211.

13. Dermott, S. F. (1984). Rotation and the internal structures of the major planets and their inner satellites. Phil. Trans. R. Soc. Lond. A. (in press).

14. Elliot, J. L., and Nicholson, P. D. (1984). The rings of Uranus. In Planetary Rings (eds. Greenberg, R., and Brahic, A.), University of Arizona Press (in press).

15. Nicholson, P. D., and Matthews, K. (1984). (in preparation).

16. Gehrels, T., et al. (1980), Imaging photopolarimeter on Pioneer Saturn, Science 207, 434-439.

17. Smith, B. A. et al. (1981). Encounter with Saturn: Voyager 1 imaging science results. Science 212, 163-191.

18. Smith, B. A. et al. (1982). A new look at the Saturn system: the Voyager 2 images. Science 215, 504-537.

19. Freedman, A. P., Tremaine, S., and Elliot, J. L. (1983). Weak dynamical effects in the Uranian ring system. Astron. J. 88, 1052-1059.

20. Elliot, J. L., French, R. G., Frogel, J. A., Elias, J. H., Mink, D. J., and Liller, W. (1981). Orbits of nine Uranian rings. Astron. J. 86, 127-134.

21. French, R. G., Elliot, J. L., and Allen, D. A. (1982). Inclinations of the Uranian rings. Nature 298, 827-829.

22. Borderies, N., Goldreich, P., and Tremaine, S. (1983). Precession of inclined rings. Astron. J. 88, 226-228.

23. Yoder, C. F. (1984). The gravitational interaction between inclined, elliptical rings. Proceedings of I.A.U. Colloquium 75 Planetary Rings, (ed., Brahic, A.), Toulouse, France, Aug. 1982.

24. Dermott, S. F., and Murray, C. D. (1981). Origin of the eccentricity gradient and the apse alignment of the ϵ ring of Uranus. Icarus 43, 338-349.

25. Borderies, N., Goldreich, P., and Tremaine, S. (1983). The dynamics of elliptical rings. Astron. J. 88, 1560-1568.

1. Report No. NASA CP-2330	2. Government Accession No.	3. Recipient's Catalog No.

4. Title and Subtitle URANUS AND NEPTUNE	5. Report Date October 1984
	6. Performing Organization Code EL
7. Author(s) Jay T. Bergstralh, Editor	8. Performing Organization Report No.
	10. Work Unit No.
9. Performing Organization Name and Address Earth and Space Sciences Division Jet Propulsion Laboratory Pasadena, California 91109	11. Contract or Grant No.
	13. Type of Report and Period Covered Conference Publication
12. Sponsoring Agency Name and Address National Aeronautics and Space Administration Washington, D.C. 20546	14. Sponsoring Agency Code

15. Supplementary Notes

16. Abstract

This volume contains the papers presented to a workshop sponsored by the Voyager project. The principal goal of the workshop was to establish a scientific framework within which to plan the Voyager encounters with Uranus and Neptune. Nearly thirty invited papers summarize the current state of knowledge of Uranus and Neptune, their atmospheres, their magnetospheres, and their respective systems of satellites and rings (if any). The workshop was held February 6 through 8, 1984, in Pasadena, California.

17. Key Words (Suggested by Author(s)) Uranus, Neptune, Planetary Atmospheres, Planetary Interiors, Magnetospheres, Planetary Satellites, Planetary Rings	18. Distribution Statement Unclassified - Unlimited Subject Category 91

19. Security Classif. (of this report) Unclassified	20. Security Classif. (of this page) Unclassified	21. No. of Pages 636	22. Price A99

N-305

For sale by the National Technical Information Service, Springfield, Virginia 22161

628

BEST COPY AVAILABLE

END

12-19-84